UNIVERSITY OF SOUTHERN QUEENSLAND

Modelling the Environmental and Anatomical Solar Ultraviolet Distribution in a School Playground

A dissertation submitted by

Nathan James Downs
BEd, BEng(Hons), MPhil

for the award of Doctor of Philosophy

2009

Abstract

The causative association between exposure to sunlight and the development of melanoma and non-melanoma skin cancer is well recognised. Intermittent sunburning episodes and chronic exposure to solar ultraviolet radiation significantly increase the risk of developing skin cancer. A large proportion of the solar ultraviolet received during childhood can be attributed to exposures received in the school playground. School playgrounds are essentially controlled environments. Increasing awareness and providing accurate predictions of ultraviolet exposure unique to individual school environments is an essential step that needs to be taken to educate children, teachers and school administrators of the risks faced in the playground and will contribute toward reducing unnecessary exposures. This is the first research to provide detailed maps of the ultraviolet exposure received in the school playground and upon the three dimensional skin surfaces of the body based on high density miniaturised polysulphone dosimeter measurements and environmental surveying of the playground environment. In this research, measurements of playground sky view were taken at 822 playground locations and UV exposure ratios were measured at 1453 body sites to map playground exposures and the three dimensional ultraviolet hot spots occurring on the face, neck, arm, hand and leg as a result of using that environment. Predictions of ultraviolet exposure were tested against measurements of erythemally effective ultraviolet exposure received by a cohort of school children using the modelled school playground. Effective shade, playground surface albedo, sky view and sunburning ultraviolet are provided for the modelled school and the suitability of the developed technique to provide estimates of personal ultraviolet exposure in the playground are discussed relative to the solar health risks experienced in Queensland.

Certification of Dissertation

I certify that the ideas, experimental work, results, analyses, software and conclusions reported in this dissertation are entirely my own effort, except where otherwise acknowledged. I also certify that the work is original and has not been previously submitted for any other award, except where otherwise acknowledged.

________________________ __________

Signature of Candidate Date

ENDORSEMENT

Signature of Supervisor Date

Signature of Supervisor Date

Signature of Supervisor Date

Acknowledgements

In the four years required to produce this work a small but significant number of people have made valuable contributions essential to its completion. Associate Professor Alfio Parisi, as principle supervisor has provided not only the assistance required to develop and progress this current research, through advice, suggestion and ongoing editing assistance but has also played a significant mentoring role since my beginning a postgraduate career in science. The value with which Alfio's assistance has been appreciated is reflected in the fact that every research paper I have worked on or co-authored, including those not specifically related to this research topic has included Alfio. I therefore thank particularly Alfio for his assistance over the years for not only this work but those works which have preceded that which is presented here. Particular thanks must also be given to Dr David Turnbull and Dr Brad Carter for their assistance and suggestions that have enabled the production of this dissertation. Of the other USQ staff that have made valuable contributions, thanks must also be given to Graham Holmes and Oliver Kinder for providing the loans and assembly of necessary equipment. Grateful acknowledgment is given to the former school principal of Hervey Bay State High School, Glenn Vaughan, for providing the necessary permission to conduct a number of studies, including this research in the school. I appreciate also the support of interested teachers and the many students involved over the years in research conducted at the school. I also give my thanks to the readers of this work and hope that the ideas and techniques presented are found to be of some value. Lastly, I acknowledge and thank my family for their support and assistance with this work, particularly in regards to the making of dosimeters which I at times have asked for assistance with, given that many thousands have had to be made over the years. Perhaps most importantly however I thank my grandfather for his early encouragement in the sciences. Without such support, it seems unlikely to me that any one of my interests in either my former engineering career or current scientific studies would ever have been attempted, including this little endeavour.

Table of Contents

CHAPTER 1 INTRODUCTION

1.1 Research focus and objectives 1
1.2 Review of the literature 2
1.2.1 Origins of sunlight 2
1.2.2 Definition and classification of ultraviolet 4
1.2.3 Terrestrial ultraviolet radiation 4
1.2.3.1 Spectral UV irradiance 5
1.2.4 Ozone as a moderator of ultraviolet 7
1.2.5 Dobson Units 11
1.2.6 Scattering mechanisms 11
1.2.6.1 Rayleigh scattering by air 12
1.2.6.2 Mie scattering by aerosols 13
1.2.7 Ultraviolet incident on the local playground environment 14
1.2.7.1 Surface condition 14
1.2.7.2 Altitude and aspect 14
1.2.7.3 Latitude 15
1.2.7.4 Time of day 16
1.2.7.5 Cloud 17
1.2.8 Humans and ultraviolet radiation 18
1.2.8.1 Human skin 19
1.2.8.1.1 Skin type 19
1.2.8.1.2 Ultraviolet penetration of the skin 21
1.2.8.2 Erythema 22
1.2.8.3 Actinic exposure 23
1.2.8.4 Vitamin D 24
1.2.8.5 Lifestyle and behaviour 26
1.2.9 Skin Cancer 27
1.2.9.1 Non-melanoma skin cancer 28
1.2.9.2 Melanoma skin cancer 29
1.2.10 Personal measurements of UV radiation with polysulphone dosimeters 30
1.2.11 Ultraviolet exposure models 31
1.2.11.1 Variation in UV irradiance due to orientation 32
1.2.11.2 Modelling personal biologically damaging ultraviolet 33
1.2.12 Trends in school practices and the ultraviolet environment 34
1.2.12.1 Sun protection policy 34
1.2.12.2 Behavioural attitudes and practices of school children 35
1.3 Methodology 36

CHAPTER 2 MATERIALS AND METHODS

2.1 Instrumentation 39
2.1.1 Scanning spectroradiometer 39
2.1.2 Broadband meter 40
2.2 Miniaturised polysulphone dosimetry and measurements of body site exposure 40
2.2.1 Mannequin measurements of exposure ratio 42
2.2.1.1 Mannequin body surface measurement sites 43
2.2.2 Calibrated measurements of personal UV exposure 45
2.3 Modelling the horizontal plane ultraviolet irradiance 47
2.3.1 The ultraviolet irradiance model 47
2.3.1.1 Extra-Terrestrial spectral irradiance 48
2.3.1.2 Earth-Sun distance 49
2.3.1.3 The direct irradiance modelled at the earth's surface 50
2.3.1.3.1 Standing surface contributions to the direct ultraviolet irradiance 51
2.3.1.4 The diffuse UV irradiance modelled at the earth's surface 52
2.3.1.4.1 Modification of the diffuse ultraviolet irradiance with sky view 55
2.3.1.5 Erythemally effective ultraviolet irradiance 55
2.3.2 The ultraviolet exposure model 56
2.4 Survey work and image processing 56
2.4.1 Measurement of playground sky view 56
2.4.1.1 Sky view image area 57
2.4.1.2 Image processing 61
2.4.2 Ground and standing surface albedo contributions 63
2.4.2.1 Ground surface albedo contribution to the diffuse ultraviolet 63
2.4.2.2 Standing surface albedo contribution to the direct ultraviolet 63
2.5 Integrating playground ultraviolet exposure and body site exposure ratio 64
2.6 Measurements of exposure to the student population 65
2.7 Summary of methods 65

CHAPTER 3 MEASUREMENTS OF BODY SURFACE EXPOSURE

3.1 Measured patterns in facial exposure under low cloud cover 67
3.2 Measured pattern in facial exposure under high cloud cover 69
3.3 Measured pattern in facial exposure with changing sky view 76
3.4 Polynomial representation of facial exposure 78
3.5 Patterns in body surface exposure 81
3.5.1 Surface exposure received by the back of the neck 81
3.5.2 Surface exposure received by the arm 83
3.5.3 Surface exposure received by the hand 87
3.5.4 Surface exposure received by the leg 90

3.6 Summary of headform and body surface exposures 94
3.7 Conclusions 97

CHAPTER 4 MODELLING THE PLAYGROUND UV EXPOSURE
4.1 The playground 98
4.2 School children and behaviour 98
4.3 Classification of school playground regions 99
4.4 The albedo of building and playground surfaces 102
4.4.1 Uncertainties in albedo measurement 104
4.4.2 Total albedo contribution to ambient UV in the playground 106
4.5 Playground sky view 108
4.6 Solar zenith angle and playground shade 110
4.7 Modelling seasonal variation in playground ultraviolet exposure 114
4.8 Playground model summary statistics 117
4.9 Significance of the playground model 121

CHAPTER 5 STUDENT EXPOSURE IN THE PLAYGROUND
5.1 Measurements of student body surface exposure in the playground 122
5.1.1 Swimming carnival exposure 126
5.1.2 Incidental playground exposures 127
5.1.3 Variation in UVE playground exposure with cloud cover 129
5.1.4 Variation in UVE playground exposure with season 131
5.1.5 Variation in exposure with body measurement site 133
5.1.6 Student movement in the playground 134
5.1.6.1 Playground Activity Index 137
5.2 Modelling body surface exposures in the playground environment 139
5.2.1 Comparison with measured body site exposure 139
5.2.2 Estimates of body surface exposure by playground region 140
5.2.2.1 Swimming carnival schedule 143
5.2.2.1.1 Non-melanoma skin cancer risk 145
5.2.2.2 Open and protected playground regions 148
5.2.3 Estimates of annual exposure 151
5.3 Reduction in NMSC risk by wearing a hat 153
5.3.1 Measured hat use among the student population 155
5.4 Summarising student playground exposure 156

CHAPTER 6 APPLICATIONS OF THE SOLAR UV MODEL
6.1 Activity scheduling in the playground and variation in exposure with SZA 157
6.1.1 Variation in yearly SZA 157
6.1.2 Implications for the use of hats in the school playground 159
6.1.2.1 Reduction in facial exposure with increasing SZA 160
6.2 Scheduling by playground region 161
6.3 Reducing playground and playground region exposure 161

6.3.1 Assessment of playground tree cover 162
6.3.2 Playground shade structures and their effectiveness 164
6.3.2.1 Additional notes on playground shade cloth structures 166
6.4 Vitamin D deficiency 167
6.5 UV distribution of body surface exposure 168
6.5.1 Comparison of measured exposure with sites of melanoma skin cancer incidence 168
6.5.2 Comparison of measured exposure with sites of NMSC incidence 169
6.5.2.1 BCC facial incidence 169
6.5.2.2 SCC facial incidence 171
6.5.2.3 The anatomical distribution of BCC and SCC 172
6.6 Future work and extension of the research project 175
6.6.1 Model applications in different environments 175
6.6.2 Model limitations 177
6.6.3 Increasing awareness in school populations 179

CHAPTER 7 CONCLUSIONS
7.1 Annual playground exposure 181
7.2 Playground exposure ranges 181
7.3 Tree shade and shading structures 182
7.4 Measurement of playground surface albedo 182
7.5 SZA ranges of body surface UV distribution 182
7.6 Comparison of measured body ER and sites of skin cancer incidence 183
7.7 Measured student exposure 183
7.8 Activity Index 183
7.9 Hat use 184
7.10 NMSC risk 184
7.11 Recommendations of playground exposure limits 184

REFERENCES 186

APPENDICES

Appendix A. Manufacturing polysulphone film dosimeters A1
A.1 Mixing the polysulphone film solution A1
A.2 Casting the polysulphone film solution A1
A.3 Film inspection and storage A2
A.4 Attaching polysulphone film to dosimeter frames A2

Appendix B. Calibration and uncertainty in polysulphone dosimeters B1
B.1 Polysulphone dosimeter calibration B1

	B.2	Measurements of uncertainty in polysulphone dosimeters	B3
Appendix C.		Colouring body surface wireframes	C1
Appendix D.		Developed software and algorithms	D1
	D.1	The horizontal plane UV exposure package	D2
		D.1.1 Horizontal plane UV exposure model interface	D4
	D.2	Horizontal plane UV exposure model code	D6
		D.2.1 UV irradiance model subroutine	D6
	D.3	Three dimensional wireframe exposure models	D14
	D.4	Playground exposure model	D50
	D.5	Playground sky view image processing algorithm	D62
Appendix E.		Measured UV transmission of playground shade cloths	E1
Appendix F.		Student diaries	F1
Appendix G.		Measurments of body surface exposure ratio listed by individual trial	G1
	G.1	Facial exposure ratios	G1
	G.2	Neck exposure ratios	G15
	G.3	Arm exposure ratios	G17
	G.4	Hand exposure ratios	G23
	G.5	Leg exposure ratios	G25
Appendix H.		Surface model contour assignments	H1
Appendix I.		Polynomial coefficients for facial horizontal contours	I1
Appendix J.		Photographs of ground and standing surfaces located in the model playground	J1
Appendix K.		Playground buildings	K1
Appendix L.		Playground sky view image set	L1
	L.1	Processed sky view	L1
	L.2	Playground sky view site locations	L10
	L.3	Sky view survey images	L11
Appendix M.		Shade density templates	M1
Appendix N.		Ozone concentrations for Hervey Bay	N1
Appendix O.		Playground site albedo, shade and UV exposure data	O1
Appendix P.		Additional facial UV exposures measured in the student population	P1

Appendix Q. Comparison of facial site incidence of BCC and SK to ER Q1

Appendix R. Comparison of mannequin to human facial site measurements of ER R1

Appendix S. Publications resulting from this research S1

List of Figures

Figure 1.1: Radiation intensity curves for perfect blackbody emitters. The peak emission of radiation for the sun at approximately 6000 K is in the visible region of the electromagnetic spectrum……………………………………………………….. 3

Figure 1.2: Terrestrial UV irradiance recorded during a clear day at the University of Southern Queensland, Toowoomba campus……………………………………..5

Figure 1.3: Rayleigh scattering of incident radiation in the UV and visible waveband……………………………………………………………………... 13

Figure 1.4: Increase in UV spectral irradiance distributions recorded at the University of Southern Queensland on a clear day during mid morning (blue line) and at midday (red line)……………………………………………………………………. 17

Figure 1.5: UV penetration and the layers of the skin (Bruls et al. 1984, cited in WHO 1994, pp. 46-47; Parrish et al. 1982, cited in WHO 1994, pp. 46-47)……………... 21

Figure 1.6: The erythemal action spectrum (CIE 1987)…………………………… 23

Figure 1.7: The actinic action spectrum (IRPA 1989)……………………………... 24

Figure 1.8: Action spectrum for the synthesis of vitamin D_3 in human skin (CIE 2006)…………………………………………………………………… 25

Figure 1.9: Weighted UV exposure of vitamin D (blue line), erythema (red line) and actinic response (black line) for a typical terrestrial UV irradiance……………….. 26

Figure 2.1: Life sized headform mannequin model photographed at a school playground measurement site. Horizontal plane exposures were recorded in proximity to the mannequin. Horizontal plane dosimeters can be seen in the figure foreground (green arrow) for this experiment which measured facial UV exposure distribution in a low sky view environment……………………………………………………………………41

Figure 2.2: Life sized mannequin model dressed in school uniform. The photograph was taken in an open field measurement site at the USQ, Toowoomba campus (28^{o}S, 152^{o}E). This site was used to measure the three dimensional surface exposures presented in Chapter 3……………………………………………………………………………….42

Figure 2.3: Optical bench assembly. (a) Marking the mannequin headform (b) Marking the leg of the body mannequin……………………………………………………...44

Figure 2.4: Mannequin headform and its wireframe mesh model. Marked dosimeter placement sites (a) correspond with horizontal and vertical contour mesh intersections (b) Mesh colouring was used to highlight the measured ER pattern. Colour interpolation between measurement sites (wireframe intersections) is detailed in Appendix C….44

Figure 2.5: Extra-terrestrial UV spectrum modelled over the 280 nm to 400 nm waveband……………………………………………………………………………49

Figure 2.6: Direct albedo UV contribution (A_{dir}) to a horizontal plane (ground) surface due to the influence of a nearby standing vertical surface…………………………52

Figure 2.7: An example of image overlap in a panoramic composite image of the horizon. The overlap of 103 pixels is highlighted in green in the figure……………58

Figure 2.8: Calculating the lower ZA limit for images taken with the mounted camera orientated in a horizontal plane. The green arrow in (b) marks the approximate height of the camera lens (840 mm) and the horizon limit……………………………………59

Figure 2.9: Calculating the lower ZA limit for images taken with the mounted camera orientated at its greatest elevation. The green arrow in (b) marks the top of the vertically standing pole with the camera 7 m away…………………………………………... 59

Figure 2.10: ZA limits of composite images measured with the camera in the horizontal plane and at maximum elevation. The limits listed in the figure were determined from trigonometric tangent ratios of the stand and pole height to camera distance………60

Figure 2.11: (a) Composite site sky view image divided into horizontal plane images (bottom series) and images taken at maximum elevation (top series); (b) fish eye lens view of the approximate regions of the sky imaged at each respective facing. The limits of the imaged area are from 32.3^o to 90^o in ZA……………………………………..61

Figure 2.12: A composite playground site image (top) and the respective sky view processed image of the same site (bottom). The image of the solar disk was removed before processing…………………………………………………………………62

Figure 2.13: Standing surface albedo contribution estimate for a site located near the school's library. The total site standing surface albedo contribution of $A_S = 0.0425$ was estimated from the average of 0 for a clear south facing region (image left), 0.11 for painted brickwork west facing (mid left image), 0 for the predominately clear north facing region (mid right) and 0.06 for east facing standing vegetation (image right)…………………………………………………………………………………64

Figure 3.1: Facial ER measured with changing SZA for low cloud cover cases (a) SZA 0^o-30^o; (b) SZA 30^o-50^o; (c) SZA 50^o-80^o…………………………………………. 68

Figure 3.2: Facial ER with changing SZA for high cloud cover cases (a) SZA 0^o-30^o; (b) SZA 30^o-50^o…………………………………………………………………………73

Figure 3.3: Location of dosimeters for examining the influence of sky view on facial ER……………………………………………………………………………………76

Figure 3.4: Variation in measured facial site ER with sky view (red data points were measured across the forehead, green data points were measured across the nose, eye and temple, and blue data points were measured across the lower proximities of the face (Figure 3.3). Square points in this figure represent measurements made through the center of the face, crosses were measured through the outer side of the face and triangular points represent measurements made between the centre and outer proximities of the facial region extending through the eye of the mannequin headform. Error bars show the maximum ER uncertainty of ±32% for the SZA range 50^o-80^o. Data points were separated for clarity in the figure but represent sky view exposures of 19%, 30%, 35% and 48%………………………………………………………………………… 77

Figure 3.5: Horizontal facial contour ER for high (square point) and low (circular point) cloud cover cases in the SZA ranges 0^o-30^o (black), 30^o-50^o (green) and 50^o-80^o (red)…………………………………………………………………………………80

Figure 3.6: Variation in ER measured to the back of the neck (a) SZA 0^o-30^o, < 4 oktas; (b) SZA 30^o-50^o, > 4 oktas; (c) SZA 50^o-80^o, < 4 oktas……………………………81

Figure 3.7: Variation in ER measured to the forearm with SZA for low cloud cover cases (a) SZA 0^o-30^o; (b) SZA 30^o-50^o; (c) SZA 50^o-80^o. The shirt used on the mannequin covers the upper arm……………………………………………………………..84

Figure 3.8: Variation in ER measured to the hand (a) SZA 0^o-30^o, < 4 okta; (b) SZA 30^o-50^o, < 4 okta; (c) SZA 50^o-80^o, > 4 okta……………………………………………88

Figure 3.9: Hand orientation with respect to the arm used on the full body mannequin……………………………………………………………………………..88

Figure 3.10: Variation in ER measured to the left leg with SZA for low cloud cover cases (a) SZA 0^o-30^o; (b) SZA 30^o-50^o; (c) SZA 50^o-80^o…………………………..91

Figure 4.1: Buildings and structures located in the HBSHS playground (red: covered pathways; light green: shade structures; dark green: large tree sites)……………….100

Figure 4.2: Ground surfaces located in the HBSHS playground (light green: grass surfaces; dark green: garden beds; cyan: bitumen surfaces; grey: concrete surfaces; yellow: blue metal paving dust; orange: light coloured paving; dark brown: dark coloured paving)…………………………………………………………………101

Figure 4.3: Subdivided playground regions. Each region contains similar surfaces and structure density………………………………………………………………..102

Figure 4.4: Estimated standing and ground surface contribution to the direct UV irradiance. Playground albedo in the figure is weighted to sky view (Section 4.5) to give an indication of the relative effectiveness of playground surface contributions to the sunburning ambient UV…………………………………………………………..107

Figure 4.5: Location of sky-view survey sites in the playground…………………..109

Figure 4.6: Contour map of playground sky view. The influence of covered pathways (Figure 4.1) can be clearly seen as can the influence of shading structures located in the playground…………………………………………………………………..110

Figure 4.7: Daily playground shade density experienced on 21 June 2008 (winter solstice)…………………………………………………………………….. 112

Figure 4.8: Daily playground shade density experienced on 21 December 2008 (summer solstice) ……………………………………………………………………….113

Figure 4.9: Determining shade density at playground site 86 for 26 June 2008 (Figure L.1). For this example, the playground site experiences shade at 2:30pm (white arrow – right of figure), giving a total shade density level between 8:30am and 3:05pm of 1……………………………………………………………………………………..114

Figure 4.10: Total erythemal UV exposure received on a horizontal plane for 21 June 2008……………………………………………………………………………………116

Figure 4.11: Total erythemal UV exposure received on a horizontal plane for 21 December 2008…………………………………………………………………………117

Figure 4.12: Column chart of mean erythemally effective UV exposure modelled for 21 June 2008 (dark blue columns) and 21 December 2008 (light blue columns). Error bars show the standard deviation in region exposure…………………………………….120

Figure 4.13: Measured site sky view versus modelled summer solstice UV_{ery}……..121

Figure 5.1: Frequency distribution of personal UVE exposure measured between February and June 2008…………………………………………………………..128

Figure 5.2: Mean UVE exposure plotted for students spending time indoors (region 1), near buildings in outdoor environments (regions 2-20), and in open outdoor environments (regions 21-25). Exposures are given for low (0-2 okta), middle (0-5 okta) and high (0-8 okta) cloud cover days and were averaged across all body sites measured in the respective cloud cover ranges. Error bars show the full range of daily UVE exposure for each respective environment and cloud cover range. Only one measurement point was taken for a student using an indoor environment on a high cloud cover day.………………………………………………………………………..........130

Figure 5.3: Mean UVE exposure plotted for students spending time indoors (region 1), near buildings in outdoor environments (regions 2-20), and in open outdoor environments (regions 21-25). Exposures are given for the late summer period (5 February to 30 March), autumn (1 April to 30 April) and early winter (1 May to 4 June) and were averaged across all body sites measured in the respective season. Error bars show the full range of daily UVE exposure for each respective environment and season. Only one student measurement point was taken in Autumn-Winter near buildings.…………………………………………………………………………..132

Figure 5.4: Mean UVE exposure plotted with respect to body measurement site. Exposures are given for facial, neck, arm, hand and leg sites and were averaged across all cloud cover conditions. Error bars indicate the full range of exposure measured at each body site. No indoor or winter leg data was measured in the study period…….133

Figure 5.5: Mean outdoor activity index of student behaviour observed relative to time spent in sunlit areas of the school playground. Error bars show the standard deviation in outdoor activity index in the sample population……………………………………..138

Figure 5.6: Comparison of measured and model body site UV exposure in the HBSHS playground. Swimming carnival data was ignored in determining the correlation coefficient ……………………………………………………………………………140

Figure 5.7: The HBSHS pool environment photographed from the eastern end of the region………………………………………………………………………………141

Figure 5.8: (a) The HBSHS oval photographed from the northern end of the region, and Region 18 photographed from a site located in the middle of the region (b)………...142

Figure 5.9: Modelled pool region exposure on 15 February 2008 (a) and 15 April 2008 (b). Body parts from top to bottom are the face, back of the neck, arm, hand, and leg.……………………………………………………………………………….145

Figure 5.10: Cumulative meal break exposure modelled for region 22 (a) and region 18 (b), 12 December 2008. Body parts from top to bottom are the face, back of the neck, arm, hand, and leg.……………………………………………………………………151

Figure 5.11: Measuring the protection offered by a broad-brimmed hat at seven different facial sites. Protected and unprotected exposures were recorded simultaneously…..153

Figure 6.1: Daily variation in SZA plotted between 9:00am and 3:00pm (light curve) and between 9:00am to 10:00am and 2:00pm to 3:00pm (dark curve) at latitude 25.3^{o} S…………………………………………………………………………………..158

Figure 6.2: Examples of sparse tree cover. North facing view of cover located in the north western corner of the playground (left), shade in the pool region (middle), and cover behind the school canteen (right)……………………………………………..163

Figure 6.4: Examples of thick tree cover. North facing view of thick tree shade located between 90 m and 130 m on the school's western fence line (left), thick canopy cover in the eastern end of the school's main carpark (middle), thick cover on the school oval (right)…………………………………………………………………………..163

Figure 6.4: The playground bus shelter PF can be calculated by comparing model UV_{ery} at sites located underneath the shelter to sites located in proximity to the shelter but not located directly underneath it. The bus shelter shade cloth measured approximately 3 m x 12 m and was located approximately 3 m from the ground surface……………….. 165

Figure 6.5: Facial BCC tumour density (Brodkin et al. 1969) and UV exposure per lesion site. The Brodkin et al. (1969) facial tumour densities are expressed relative to the facial measurements of SZA in the ranges: (0^{o}-30^{o}) open circles; (30^{o}-50^{o}) closed circles; and (50^{o}-80^{o}) crosses……………………………………………………..171

Figure 6.6: Facial SK incidence (Nguyen et al. 1998) and UV exposure per lesion site in the SZA 0^o-30^o (open circles); 30^o-50^o (closed circles); and 50^o-80^o (crosses) range…………………………………………………………………………...172

Figure B.1.1: Polysulphone dosimeter calibration for 23 February 2008…………. B1

Figure B.1.2: Polysulphone dosimeter calibration for 18 April 2007……………... B2

Figure B.1.3: Polysulphone dosimeter calibration for 8 May 2008……………….. B2

Figure C.1: Exposure contours and representative colour ER segment divisions interpolated between two adjacent measurement sites, A and B highlighted in the figure. For the case shown here, points A and B are separated by approximately 5 mm and represent ERs to the forehead. Each segment between A and B is given a specific colour level……………………………………………………………………………C1

Figure C.2: Photographed manikin arm dosimeter sites (left) and three dimensional model exposure contours (right). The ERs were measured for the arm in a vertical position alongside the manikin as photographed…………………………………...C2

Figure E.1: Bus shelter shade cloth structure…………………………………….E2.

Figure E.2: Oval steps shade cloth structure……………………………………...E2

Figure E.3: Quadrangle plastic shelter structure……………………………………E2

Figure E.4: H Block shade cloth sails (light green)…………………………………E2

Figure E.5: H block shade cloth sails (dark green)…………………………………E2

Figure E.6: M Block shade cloth sail………………………………………………E2

Figure E.7: C Block shade cloth sail……………………………………………..E3

Figure E.8: Art block shade cloth sail………………………………………………E3

Figure H.1: Horizontal (Cx) and vertical (Cn) facial contour assignments…………H1

Figure H.2: Horizontal (Cx) and vertical (Cn) neck contour assignments………….H2

Figure H.3: View of three dimensional arm surface from behind the shoulder. Contours marked Cn1 through Cn23 are oriented along the arm's longitudinal axis. Contours Cn1, Cn5 and Cn10 are shown. Contours marked Cx10, Cx14 and Cx20 are also shown in the diagram. These contours formed complete bands around the arm surface and were numbered from the shoulder (figure right) to the wrist (figure left)……………………………………………………………………………H3

Figure H.4: Contours marked Cn1 through Cn23 represent the longitudinal contours extending from the wrist to the finger tips of the three dimensional hand surface. These contours start and end on the thumb. Contours banded about the hand surface and individual fingers start from the wrist and extend to the finger tip bands. Contours Cx5 and Cx8 are shown in the figure…………………………………………………… H4

Figure H.5: Longitudinal leg contours extending from the upper thigh to the ankle start at Cn0 and end at Cn16. Contours Cn11 through Cn13 are shown in the figure for a forward facing view of the leg model showing the knee positioned to the upper right. Banded contours Cx1, Cx10, Cx20 and Cx30 show the thigh to ankle order in which these contours were labeled………………………………………………………H5

Figure L.1: Hervey Bay State High School identifier codes for sky view survey sites……………………………………………………………………………… L10

Figure M.1.1: Shade template for 21 June 2008 (arrows show solar position)……. M1

Figure M.1.2: Shade template for 21 December 2008 (arrow show solar position, lines show azimuth position only at the respective times)....................................M1

List of Tables

Table 1.1: Sun reactive skin types (Diffey 1991, p.314)……………………………20

Table 3.1(a): Facial site exposure ratio expressed as a percentage for the SZA range 0^o-30^o and cloud cover less than 4 oktas……………………………………………….70

Table 3.1(b): Facial site exposure ratio expressed as a percentage for the SZA range 30^o-50^o and cloud cover less than 4 oktas. ER ratio is expressed as a percentage of the ambient horizontal plane exposure………………………………………………….71

Table 3.1(c): Facial site exposure ratio expressed as a percentage for the SZA range 50^o-80^o and cloud cover less than 4 oktas……………………………………………….72

Table 3.2: Comparison of facial site ER data made under high and low cloud cover conditions. ER is expressed as a percentage of the ambient horizontal plane exposure……………………………………………………………………………..74

Table 3.3: ER of facial site dosimeters measured in sites of varying sky view…….76

Table 3.4(a): Site exposure ratio measured to the back of the neck and expressed as a percentage for the SZA range 0^o-30^o and cloud cover less than 4 oktas……………82

Table 3.4(b): Site exposure ratio measured to the back of the neck and expressed as a percentage for the SZA range 30^o-50^o and cloud cover greater than 4 oktas……….82

Table 3.4(b): Site exposure ratio measured to the back of the neck and expressed as a percentage for the SZA range 50^o-80^o and cloud cover less than 4 oktas…………..82

Table 3.5(a): Site exposure ratio measured to the arm and expressed as a percentage for the SZA range 0^o-30^o and cloud cover less than 4 oktas……………………………85

Table 3.5(b): Site exposure ratio measured to the arm and expressed as a percentage for the SZA range 30^o-50^o and cloud cover less than 4 oktas…………………………..86

Table 3.5(c): Site exposure ratio measured to the arm and expressed as a percentage for the SZA range 50^o-80^o and cloud cover less than 4 oktas…………………………. 87

Table 3.6(a): Site exposure ratio measured to the hand and expressed as a percentage for the SZA range 0^o-30^o and cloud cover less than 4 oktas…………………………... 89

Table 3.6(b): Site exposure ratio measured to the hand and expressed as a percentage for the SZA range 30^o-50^o and cloud cover less than 4 oktas…………………………..89

Table 3.6(c): Site exposure ratio measured to the hand and expressed as a percentage for the SZA range 50^o-80^o and cloud cover greater than 4 oktas……………………….90

Table 3.7(a): Site exposure ratio measured to the leg and expressed as a percentage for the SZA range 0^o-30^o and cloud cover less than 4 oktas……………………………92

Table 3.7(b): Site exposure ratio measured to the leg and expressed as a percentage for the SZA range 30^o-50^o and cloud cover less than 4 oktas…………………………..93

Table 3.7(c): Site exposure ratio measured to the leg and expressed as a percentage for the SZA range 50^o-80^o and cloud cover less than 4 oktas…………………………. 94

Table 3.8: Exposure ratio statistics listed for the face, back of the neck, forearm, hand and leg in the SZA ranges 0^o-30^o, 30^o-50^o and 50^o-80^o……………………………95

Table 4.1: Ground surface erythemal UV albedo. Uncertainty is stated as ±17% of the measured albedo…………………………………………………………………103

Table 4.2: Vertical standing surface erythemal UV albedo. Uncertainties include meter measurement uncertainty of ±17% for each listed aspect added to an additional standing surface uncertainty estimate calculated as the difference in maximum and minimum measured albedo for aspects measured on north, east, south and west facing surfaces ……………………………………………………………………………………104

Table 4.3: Arithmetic mean, median and range statistics for site surface erythemal UV albedo, sky view, and erythemal UV exposure subdivided by playground regions 2 through 24...118

Table 5.1: Personal UVE measured in the school population between 5 February and 4 June 2008. Data in the table is subdivided by body site and playground region……123

Table 5.2: School playground regions………………………………………………125

Table 5.3: Personal UVE exposure sorted by student movement in the playground………………………………………………………………………..136

Table 5.4: Mean mannequin facial ER (%) measured in region 24 (basketball courts) and region 22 (oval). ERs are given relative to ambient UV_{ery} horizontal plane exposure. Measurements of exposure to the temple, mandible and ear lobe were averaged and given as a single "side" measurement in the table…………………………………..154

Table 5.5: Relative increase in NMSC risk by not wearing a broad-brimmed hat for a student observing the normal school routine (activity index 0.2). Biological amplification factors used to determine the relative risk for BCC and SCC were implemented as specified in section 5.2.2.1.1…………………………………... 155

Table 6.1: Survey line variation in UV_{ery} exposure modelled about the bus shelter for the respective winter and summer solstice. Estimated PF was calculated using the ratio of average unprotected modelled UV_{ery} to average protected modelled UV_{ery}………..166

Table 6.2(a): Comparison of the anatomical distribution of BCC site localisation in Geraldton (Kricker et al. 1990) and Townsville (Raasch et al. 1998) to median ER…………………………………………………………………………………173

Table 6.2(b): Comparison of the anatomical distribution of SCC site localisation in Geraldton (Kricker et al. 1990) and Townsville (Raasch et al. 1998) to median ER…………………………………………………………………………………174

Table B.2.1: Variation in ΔA for sets of miniaturised polysulphone dosimeters exposed to equivalent solar UV exposures. Sets are organized into separate rows in the table…………………………………………………………………………………B3

Table B.2.2: Change in absorbency measured on a horizontal plane in the SZA ranges 0^o-30^o, 30^o-50^o and 50^o to 80^o……………………………………………………………B5

Table E.1: Percentage UV transmission measured under playground shade cloth structures. Protected measurements were made approximately 0.5 m underneath the shade cloth using a broadband meter (Solar Light Co., model 3D, Philadelphia, PA 19126). UV transmission estimates include the meter measurement uncertainty of ±17%. Protection Factors for shade cloth structures were calculated as the ratio of unprotected modelled UV_{ery} exposure located at sites in proximity to each respective structure for both the winter solstice (21 June 2008) and summer solstice (21 December 2008). Figures E.1 through to E.8 depict each shade cloth structure found in the HBSHS playground…………………………………………………………………………..E1

Table G.1.1: 18 February 2006, SZA 0^o-30^o, 4/8 cumulus…………………………G1

Table G.1.2: 12 March 2007, SZA 0^o-30^o, 1/8 cirrus……………………………..G2

Table G.1.3: 21 February 2008, SZA 0^o-30^o, 4/8-2/8 cumulus………………….. G3

Table G.1.4: 25 January 2008, SZA 0^o-30^o, 2/8-5/8 cumulus / altocumulus……..G4

Table G.1.5: 14 November 2007, SZA 0^o-30^o, 1/8-3/8 cumulus…………………G5

Table G.1.6: 19 June 2006, SZA 30^o-50^o, 8/8 cumulonimbus / altocumulus…….G6

Table G.1.7: 22 June 2006, SZA 30^o-50^o, 7/8-8/8 cumulonimbus………………. G7

Table G.1.8: 16 September 2005, SZA 30^o-50^o…………………………………..G8

Table G.1.9: 5 October 2006, SZA 30^o-50^o, 3/8 cumulus……………………….. G9

Table G.1.10: 18 December 2007, SZA 30^o-50^o, 7/8-8/8 cumulonimbus / stratus..……………………………………….......G10

Table G.1.11: 16 October 2007, SZA 30^o-50^o, clear……………………………… G11

Table G.1.12: 16 October 2007, SZA 50^o-80^o, clear……………………………… G12

Table G.1.13: 27 May 2005, SZA 50^o-80^o………………………………………G13

Table G.1.14: 27 August 2007, SZA 50^o-80^o, 1/8 cumulus………………………..G14

Table G.2.1: 14 November 2007, 0^o-30^o, 1/8-3/8 cumulus………………………G15

Table G.2.3: 25 January 2008, 0^o-30^o, 2/8-5/8 cumulus / altocumulus………….. G15

Table G.2.4: 18 December 2007, 30^o-50^o, 7/8-8/8 cumulonimbus / stratus………G15

Table G.2.5: 27 August 2007, 50^o-80^o, 1/8 cumulus…………………………….. G16

Table G.3.1: 13 December 2007, 0^o-30^o, 5/8-7/8 cumulonimbus / altocumulus / cirrus……………………………………………………………………….. G17

Table G.3.2: 1 February 2008, 0^o-30^o, 3/8-5/8 cumulus…………………………G18

Table G.3.3: 30 April 2007, 30^o-50^o, clear……………………………………. G19

Table G.3.4: 2 April 2008, 30^o-50^o, 1/8-2/8 cumulus……………………………..G20

Table G.3.5: 18 July 2007, 50^o-80^o, clear………………………………………G21

Table G.3.6: 12 July 2007, 50^o-80^o, clear……………………………………... G22

Table G.4.1: 21 November 2007, 0^o-30^o, 2/8-3/8 cumulus………………………G23

Table G.4.2: 1 February 2008, 0^o-30^o, 3/8-5/8 cumulus…………………………G23

Table G.4.3: 2 April 2008, 30^o-50^o, 1/8-2/8 cumulus……………………………G24

Table G.4.4: 28 August 2007, 50^o-80^o, 4/8-5/8 cirrus…………………………… G24

Table G.5.1: 13 November 2007, 0^o-30^o, 2/8 cumulus…………………………...G25

Table G.5.2: 1 February 2008, 0^o-30^o, 3/8-5/8 cumulus…………………………G26

Table G.5.3: 4 March 2008, 30^o-50^o, 3/8-2/8 cumulus…………………………...G27

Table G.5.4: 6 August 2007, 50^o-80^o, clear……………………………………… G28

Table G.5.5: 2 August 2008, 50^o-80^o, clear……………………………………… G29

Table I.1: Equation 3.1 Coefficients β_1 through β_9 for the SZA range 0^o-30^o……...I1

Table I.2: Equation 3.1 Coefficients β_8 through β_{14} for the SZA range 0^o-30^o……. I1

Table I.3: Equation 3.1 Coefficients β_{15} through β_{19} for the SZA range 0^o-30^o…..... I2

Table I.4: Equation 3.1 Coefficients β_1 through β_9 for the SZA range 30^o-50^o…….I3

Table I.5: Equation 3.1 Coefficients β_8 through β_{14} for the SZA range 30^o-50^o…... I3

Table I.6: Equation 3.1 Coefficients β_{15} through β_{19} for the SZA range 30^o-50^o….. I4

Table I.7: Equation 3.1 Coefficients β_1 through β_9 for the SZA range 50^o-80^o…….I5

Table I.8: Equation 3.1 Coefficients β_8 through β_{14} for the SZA range 50^o-80^o…... I5

Table I.9: Equation 3.1 Coefficients β_{15} through β_{19} for the SZA range 50^o-80^o….. I6

Table J.1: Sample ground surface images………………………………………..J1

Table J.2: Sample vertical standing surface images……………………………….. J3

Table K.1: School buildings in the model school playground………………………K1

Table L.1: Hervey Bay State High School playground sky view site locations, sky/cloud threshold (blue-red pixel threshold), and site sky view estimate listed as a percentage. Site sky view was determined from each site location processed image up to 32.3^o in SZA and estimated by ground observation above 32.3^o in SZA. Estimates of sky view for playground sites covered by shade cloths were determined from the measured UV transmission of each playground shade cloth (Appendix E). Site locations listed in the table refer to playground locations where the sky view was surveyed (Figure L.1). Site locations were sorted into survey (traverse) lines according to position from the western fence. Each survey line was separated by 5 m when located near buildings and 20 m over the school's open playground environment. Each site location listed in each survey line starts from the northern fence and ends at the southern fence with site locations being separated by approximately 5 m and 20 m. Variations in site locations from separations of 5 m and 20 m were due to playground obstructions and are shown in Figure L.1…………………………………………………………………………L1

Table L.2: Unprocessed images (upper part) and processed sky view (lower part) listed according to site identifier codes (Figure L.1). Processed images include the horizon mask (black)………………………………………………………………...L11

Table M.1.1: SZA, azimuth and pixel positions used to develop 21 June 2008 shade template……………………………………………………………………………..M2

Table M.1.2: SZA, azimuth and pixel positions used to develop 21 December 2008 shade template……………………………………………………………………M2

Table N.1: OMI (TOMS 2008) ozone concentrations listed for Hervey Bay (25^{o}S, 153^{o}E), June 2007 and December 2007……………………………………………N1

Table O.1: The table presents playground site data used to produce Figures 4.4, 4.7, 4.8, 4.9 and 4.10 for playground survey lines 1 through 37. Data is arranged in each survey line from sites located on the playground northern fenceline to sites located on the southern fenceline. Figure L.1 gives playground site codes referred to in the table………………………………………………………………………………O1

Table P.1: Facial site exposure (SED) measured to students wearing (protected) and not wearing (unprotected) broad brimmed hats in region 24 (basketball courts) and region 22 (school oval) (Downs & Parisi 2008). The error given in the Table, t, is the 95% C.I…………………………………………………………………………….. P1

Table Q.1: Measurements of facial exposure ratio and the density of facial basal cell carcinoma (BCC) and solar keratosis (SK)………………………………………....Q1

Table R.1. A comparison of mannequin and human ER (%) measured in the HBSHS population (Downs & Parisi 2008)……………………………………………….... R1

Glossary and Acronyms

AACR: Australasian Association of Cancer Registries.

ACCV: Anti-Cancer Council of Victoria (Australia).

Action Spectra: The normalised response of a specified action, typically biological, including for example the human erythema reaction, measured at set wavelengths.

AEST: Australian eastern standard time.

AIHW: Australian Institute of Health and Welfare.

ARPANSA: Australian Radiation Protection and Nuclear Safety Agency.

Basal Cell Carcinoma (BCC): The most frequent non-melanoma human skin cancer originating in the basal cell layer of the epidermis occurring on both chronically exposed and infrequently exposed skin surfaces.

CIE: International Commission on Illumination.

Cutaneous Malignant Melanoma (CMM): The least common but most frequent metastasising skin cancer in humans. CMM develop from the DNA mutation of melanocytic (pigmented) skin cells.

Deoxyribonucleic Acid (DNA): Contains the genetic instructions for living cells. DNA resides as an acid in the nucleus of skin cells.

Dobson Unit (DU): A unit of measure of ozone concentration representing total column ozone at STP (0^{o}C and 1 atm) over a given surface area. One DU is the equivalent of 0.01 mm ozone column thickness at STP.

Education Queensland (EQ): The Department of Education, Training and the Arts (Queensland, Australia).

Erythema: The perceptive reddening of fair skin caused by the dilation of epidermal blood vessels following exposure to UV radiation (Sunburn). Human erythema is most effective in the UVB wavelengths.

Exposure Ratio (ER): The exposure ratio is defined as the exposure measured to a specific body site expressed relative to the ambient horizontal plane exposure.

HBSHS: Hervey Bay state high school.

ICNIRP: International Commission on Non-Ionizing Radiation Protection.

IRPA: International Radiation Protection Association.

Minimal Erythema Dose (MED): The ultraviolet exposure required to produce a mildly perceptible erythema or sunburn reaction.

NHMRC: National Health and Medical Research Council (Australia).

Non-Melanoma Skin Cancer (NMSC): Non-melanoma cancerous lesions of a low metastasising nature. These incorporate both basal and squamous cell carcinomas.

Ozone Monitoring Instrument (OMI): A satellite ozone mapping spectrometer (NASA).

Protection Factor (PF): Sometimes also referred to as the UPF (Ultraviolet Protection Factor). The ratio of the ultraviolet exposure in a location to the ultraviolet exposure received at the same location but with some form of protection in place. The PF is commonly used to rate the ultraviolet protection of shade cloths, trees and forms of personal protective clothing and hats.

QTH: Quartz tungsten halogen. Specifically the type of lamp used to calibrate the USQ's scanning spectroradiometer.

Shade density: The total level of shade at a given location occurring within a set period of time. The longer a location is covered by shade, the greater the shade density in the period. For this research, seven shade levels are defined for each school period in the 8:30 am to 3:05 pm school day.

Standard Erythema Dose (SED): A common unit of measure of the erythemally effective UV radiation. One SED represents 100 Jm^{-2} of erythemally effective UV radiation.

Squamous Cell
Carcinoma (SCC): Non-melanoma skin cancer affecting the stratified squamous epithelium. These cancers occur less frequently than BCC but are more prevalent on the frequently exposed surfaces of the human body.

Solar Zenith Angle
(SZA): The angle subtending the zenith and the position of the solar disc.

TOMS: Total Ozone Mapping Spectrometer (NASA).

Ultraviolet (UV): Electromagnetic radiation specifically modelled in this research between the 280 nm to 400 nm waveband.

Ultraviolet A (UVA): Ultraviolet radiation in the 290 nm to 320 nm waveband.

Ultraviolet B (UVB): Ultraviolet radiation in the 320 nm to 400 nm waveband.

Ultraviolet C (UVC): Ultraviolet radiation defined in this research to lie below 290 nm.

UVE: Personal erythemally effective ultraviolet measured using polysulphone dosimeters.

UV_{ery}: Erythemally effective ultraviolet defined for this research to be the modelled erythemally effective ultraviolet.

Zenith Angle (ZA): The angle subtended from the zenith.

CHAPTER 1 INTRODUCTION

1.1 Research focus and objectives

School playgrounds present a significant health risk to children in Australia for the development of environmental solar ultraviolet (UV) induced disease. The risk is most significant in Queensland, enhanced by a proportionately fair skinned population, high solar altitudes due to geographical latitude, a high number of sunshine days and low aerosol concentrations (Armstrong 1994; Roy et al. 1995). These risks contribute to Queensland having the highest incidence rates of NMSC (non-melanoma skin cancer) and cutaneous malignant melanoma (CMM) in the world (Lowe et al. 1993). Children, having unacclimatised skin and being potentially placed in the sun during school hours at times of peak UV intensity increase their risk of receiving acute and long term damage associated with excessive exposure to UV. Furthermore, the risk of developing skin cancer is potentially greater for school aged children, with some studies indicating an increased risk of melanoma and other skin cancers associated with a past history of severe sunburn during childhood and adolescence (Armstrong 1988; Diffey 1991; Longstreth et al. 1998).

The National Health and Medical Research Council's (NHMRC) Sun Protection Programs Working Party (NHMRC 1996) recommended the undertaking of further research for developing more effective measures of population sun exposure. This project addresses this recommendation directly through measurements designed to build up a scientifically collected database of UV exposures to humans that take the physical playground environment into account. Specifically this will be achieved by integrating measurements of UV exposures received by school children during normal school activities with physical modelling of the ambient UV exposure within a school playground. The development of a computer model utilising personal exposure and playground survey measurements will provide a technique for assessing the UV exposure within individual school environments and provide a tool for the analysis of risks associated with UV exposure to children placed within those environments.

The computer model developed for this research incorporates the ambient UV and the distribution of solar UV exposures to the face and exposed parts of the human body for a large range of solar zenith angles (SZA) in three dimensional space. The influence of buildings, surfaces, trees and other materials that are commonly found within school playgrounds has also been investigated. The influence of the modelled environment will be examined with respect to human measurements of exposure and these results will be discussed relative to the development of sun-safe strategies for schools. The outcomes from this project have the potential to contribute to the reduction of solar UV exposures leading to a reduction in skin cancers and associated cost of treatment for these cancers.

This study will aid the development of better sun-safe practices in schools through:

1. The development of a model for the calculation of solar UV exposures in three dimensional space that takes into account the physical playground environment;
2. The collection of detailed quantitative data on the distribution of solar ultraviolet radiation to the face and other uncovered parts of the human body over a large range of solar zenith angles and under varying atmospheric conditions;
3. The development of computer software that produces UV hazard charts that highlight the UV hot spots within school environments to assess the potential risk associated with exposure to uncovered parts of the body for seasonal and daily (AEST) periods.

1.2 Review of the literature

1.2.1 Origins of sunlight

The sun may be considered a perfect blackbody, absorbing and reemitting all radiation that falls upon it across the electromagnetic spectrum. The intensity of electromagnetic radiation emitted by any blackbody, including the earth's sun varies with wavelength. The peak intensity of radiation emitted by a blackbody is dependent upon the temperature of the body. All bodies with temperatures above absolute zero emit electromagnetic radiation, with their peak emission being shifted toward shorter wavelengths the higher the temperature of the body. Figure 1.1 shows the variation in peak radiation intensity for perfect black body emitters of different temperatures (Cutnell & Johnson 1998). The sun has a surface temperature of approximately 6000 K. Its peak emission lies in the visible spectrum at approximately 500 nm, giving the sun a yellowish appearance.

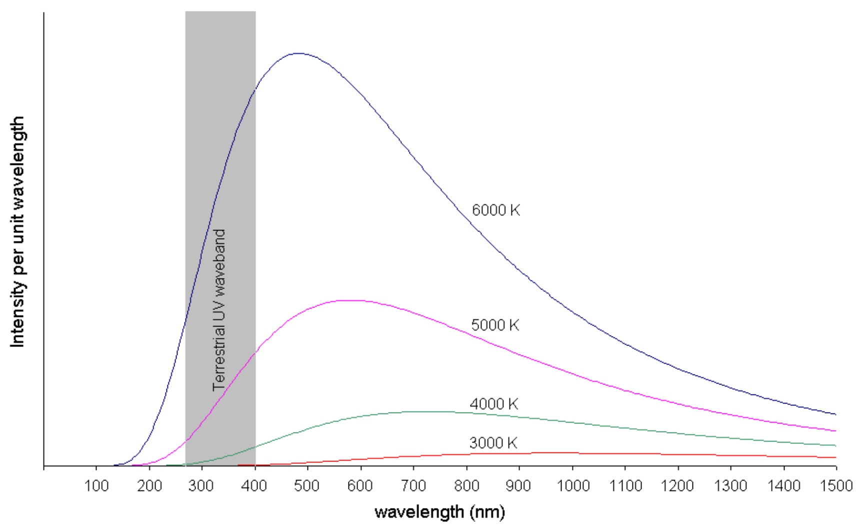

Figure 1.1: Radiation intensity curves for perfect blackbody emitters. The peak emission of radiation for the sun at approximately 6000 K is in the visible region of the electromagnetic spectrum (Cutnell & Johnson 1998).

The sun does not however emit radiation consistently across the electromagnetic spectrum. Absorption of radiation in the continuum, particularly by elements in the sun's photosphere results in noticeable drops in the emitted intensity. These drops are observed as Fraunhofer absorption lines in the visible spectrum, having a notable effect also in the UV waveband that eventually reaches the earth's surface following further absorption by the earth's atmosphere. Therefore, although the intensity of solar radiation may be noted to increase from lower to higher wavelengths in the UV waveband (Figure 1.1), the spectrum is not continuous. Furthermore, the changing position of the sun relative to the earth's atmosphere, variation in ozone concentration and other aerosols including particulates, local pollutants and cloud cover will also affect the intensity of UV radiation that reaches the surface of the earth. Each of these factors play a role in influencing the UV that is eventually incident upon the exposed skin surfaces of children using a playground environment.

1.2.2 Definition and classification of ultraviolet

Ultraviolet radiation (UV) is defined as those wavelengths of the electromagnetic spectrum that lie immediately below 400 nm. This region lies just below the visible region of the electromagnetic spectrum, defined as those wavelengths that lie between 400 nm (violet) to 700 nm (red). UV is further classified into three separate bands, UVA, UVB, and UVC. A general classification of the near to middle UV wavebands is as follows: UVA - 400 nm to 320 nm; UVB - 320 nm to 290 nm; UVC – 200 nm to 290 nm (Campbell et al. 1993). In this classification, the UVB region represents those wavelengths to which human skin is most sensitive under natural sunlight which does not readily penetrate the earth’s atmosphere below 290 nm. The transmission of wavelengths through the earth's atmosphere decreases rapidly across the UVB region. Of the UV received from the sun, the UVC region represents that region in which no radiation is detected at the earth's surface, except at high altitudes (Diffey 2002). Terrestrial UVA is more readily transmitted through the atmosphere and is therefore the most prominent UV waveband detected at the earth’s surface.

1.2.3 Terrestrial ultraviolet radiation

Human exposure to UV most commonly occurs from exposure to the sun. As mentioned previously, solar UV however, is not distributed continuously. The sun's energy output is also variable. This variability is often linked to the solar cycle and can significantly influence the extra-terrestrial spectral irradiance distribution. Depletions, and increases in ozone content, related to UV flux, have been linked to the variable energy output of the sun and the solar cycle (McKenzie 1991; Schindell et al. 1999). The seasonal variation in the distance between the earth and the sun is another effect that influences the intensity of the extra-terrestrial spectral irradiance. The sun's elliptical orbit increases terrestrial UV in the southern hemisphere summer during the earth's closest approach to the sun in early January.

1.2.3.1 Spectral UV irradiance

A number of Fraunhofer absorption lines are prominent in the extra-terrestrial UV spectrum which are also noted following transmission through the earth’s atmosphere in the terrestrial UV waveband. The Ca II Fraunhofer absorption line is one such line prominent between 390 nm and 400 nm (Rottman 2000). Strong Fraunhofer absorption lines are also found in the ultraviolet region of the extra-terrestrial spectrum below 290 nm, however these lines are less noticeable in terrestrial spectra as wavelengths below 290 nm are strongly absorbed by atmospheric oxygen and ozone. The terrestrial UV spectrum, as measured on the ground differs from the extra-terrestrial UV spectrum. Figure 1.2 shows a typical terrestrial UV spectrum following transmission through the atmosphere recorded at the University of Southern Queensland, Toowoomba (152^{o}E, 28^{o}S) for a SZA of 50^{o}. The spectral irradiance is strongly moderated below 320 nm due to the presence of stratospheric ozone.

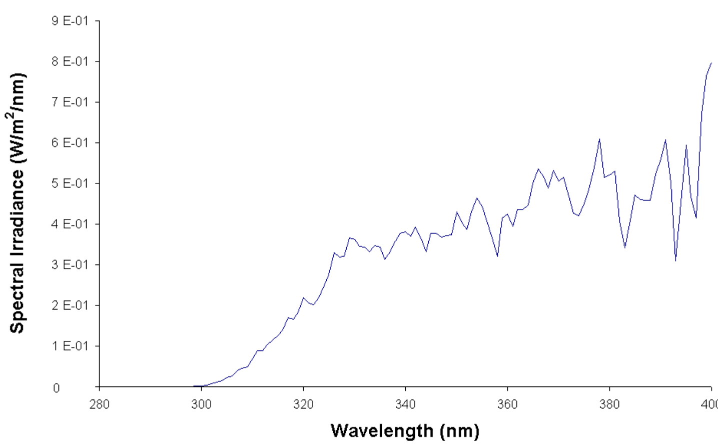

Figure 1.2: Terrestrial UV irradiance recorded during a clear winter day at the University of Southern Queensland, Toowoomba campus.

The earth's atmosphere contains a number of atmospheric windows across the entire range of the electromagnetic spectrum in which the atmosphere is almost completely transparent (visible region), partially opaque, or completely opaque. The degree to which the atmosphere absorbs certain wavelengths and obscures others depends on its chemical composition and particulate or aerosol concentration. As with the Fraunhofer absorption lines observed due to solar photospheric absorption, the earth's atmosphere contains a number of elements that absorb discrete wavelengths of incident solar eltromagnetic radiation. Examples of elements in the atmosphere known to absorb extra-terrestrial radiation at UV wavelengths include molecular and diatomic oxygen, nitrogen and ozone (Huffman 1992). Sunlight is absorbed by ozone across the entire UV and visible region (Orphal & Chance 2003). Absorption by ozone is particularly efficient in the Hartley absorption band between wavelengths of 200 nm to 320 nm with the peak efficiency being around 250 nm (Huffman 1992; Orphal & Chance 2003).

Photons covering a broad range of the electromagnetic spectrum are scattered by the re-emission of atmospheric constituents making up a proportion of the diffuse radiation, or blue skylight, received during the day that are not directly incident from the solar beam. The UV radiation incident directly from the sun is therefore not always the dominant component of the solar UV received at the earth’s surface. Direct solar radiation is also predominantly scattered into diffuse radiation by Mie and Rayleigh scattering mechanisms. The total or global terrestrial UV spectral irradiance distribution such as that depicted in Figure 1.2 is made up of the vertical component of the direct solar beam and the diffuse radiation received at the earth’s surface. In a standard solar radiation measuring system, the global UV irradiance is measured with the input sensor of the measuring instrument oriented in a horizontal plane measuring both the direct UV and diffuse skylight UV from the whole sky (Webb et al. 1999).

Terrestrial UV spectral distributions are not constant, nor are the relative proportions of direct and diffuse UV. The UV spectral irradiance changes depending on the local surroundings, atmospheric conditions and the position of the sun in the sky. The spectral irradiance received at the earth’s surface changes with the position of the sun because of the angle over which the incoming sunlight is spread and because of the changing degree of atmospheric interference. Variable atmospheric conditions, including cloud, aerosol distributions, turbidity, ozone and other atmospheric gases influence the way solar UV is distributed at the earth's surface. Reflections from ground surfaces influencing atmospheric backscatter, local altitude and the local surroundings also play an important role in altering the terrestrial UV spectral intensity that is incident upon a horizontal surface. UV exposures received by the human body are further influenced by the orientation and inclination of the receiving surface topography and the position of the body relative to the reflecting ground surface.

The path that solar UV takes as it travels through the atmosphere and reaches the surface of the earth can be explained in a number of stages, namely:

- Ozone absorption;
- Rayleigh scattering by air;
- Mie scattering by aerosols; and
- Local environment.

1.2.4 Ozone as a moderator of ultraviolet

UVC is most readily absorbed by nitrogen (N_2) and molecular and diatomic oxygen, (O) and (O_2), at the shorter UV wavelengths that extend into the far (typically < 200 nm) and extreme (< 100 nm) regions of the UV range (Huffman 1992). Absorption of these more harmful wavelengths of UV radiation occurs in the upper layers of the earth's atmosphere, typically at altitudes above 100 kilometers. Stratospheric concentrations of ozone (O_3), between 18 to 50 kilometers in altitude, additionally limit the levels of UVC across the Hartley absorption band such that wavelengths below 290 nm and extending to the far UV are absorbed almost completely. The combined molecular absorption of oxygen, ozone and nitrogen, results in negligible UV wavelengths below 290 nm being recorded at sea level. The level of UVB detected at the earth's surface is regulated by the higher concentration of O_3 molecules in the stratosphere between an altitude of approximately 20 km to 30 km. Stratospheric ozone is responsible for the absorption of most UV that enters the earth's atmosphere and its absorption of wavelengths in the UVB is of particular importance to the regulating of ambient levels of UV detected at the earth's surface (Barton & Paltridge 1979; Diffey 1991; Madronich 1993). Increasing UVB intensities at ground level have been linked to depleted ozone concentrations (Kerr & McElroy 1993). By contrast, the absorption of UVA wavelengths by ozone is quite weak. Ozone concentration is however an important factor to consider when modelling or making predictions of future terrestrial UV exposures, particularly biologically effective exposures which have a tendency to be strongly weighted toward the UVB wavelengths.

In the natural atmosphere, undisturbed by the effects of pollutants and in the absence of global warming, concentrations of stratospheric ozone are regulated by a series of photo-sensitive reactions. Namely, absorption by UV wavelengths results in the photo-disassociation of oxygen and ozone molecules. An O_2 molecule is dissociated by the absorption of UV wavelengths below 242 nm into free atomic oxygen (Diffey 1991). Similarly, the absorption of wavelengths up to approximately 320 nm by O_3 molecules results in their conversion into a single free O atom and diatomic O_2 (Chapman 1930, cited in Diffey 1991, p.301). Free atmospheric oxygen atoms will combine to form either molecular oxygen or ozone. Alternatively, an ozone molecule can be destroyed by reaction with atomic oxygen (Huffman 1992). The reactions that control concentrations of stratospheric ozone are delicately balanced. Spread thinly throughout the stratosphere at low, high altitude pressures, UV levels detected at ground level are particularly sensitive to changes in ozone concentration.

Concentrations of ozone in the stratosphere and therefore terrestrial distributions of UVB are different at different locations on earth. Production of ozone is greatest around the earth’s equatorial regions due to the stronger diurnal levels of UV compared to the available levels of UV received at higher latitudes. Global ozone concentrations tend to be higher toward polar regions but are subject to large variations in concentration as distributions change throughout the year due to the seasonal variation of global atmospheric circulation patterns (Van Heuklon 1979; Huffman 1992). The distribution of ozone is also influenced by pollution often associated with human activity. Atmospheric pollutants such as chlorofluorocarbons (CFC's) exposed to sunlight experience a photochemical breakdown into chlorine, which subsequently reacts with O_3 to reduce it to O_2. The chlorine released by CFC's acts as a catalyst in the breakdown of stratospheric ozone, and following the destruction of O_3 is free to continue with the process following the initial reaction (WMO 1994):

$$Cl + O_3 \longrightarrow ClO + O_2$$

$$ClO + O \longrightarrow Cl + O_2$$

Bromine species may also be implicated in destructive ozone processes (Huffman 1992). Other halons, CFCs, nitrous oxide (NO_2), methane (CH_4) and carbon dioxide (CO_2) also affect stratospheric ozone concentrations (WMO 1994). Although efforts are being made to reduce CFC emissions, levels of CH_4 and NO_2 have been reported to be on the rise (Isaksen & Stordal 1986). The catalytically active reaction of pollutants including CFCs and NO_2, have the potential to greatly influence future ozone concentrations (Isaksen & Stordal 1986; WMO 1994). Ozone concentrations are further influenced by increasing levels of CH_4, and the absorption of UV by ozone molecules resulting in stratospheric heating which may in turn increase reaction rates (Isasken & Stordal 1986). Although the combined effect that these pollutants will have on ozone levels is uncertain, ozone levels have been recorded and shown to fall since the 1970s (Isaksen & Stordal 1986; NASA 1988; Sze et al. 1989; McKenzie 1991). More recent evidence seems to suggest that ozone levels may be on the increase, though further uncertainties remain as to whether ozone concentrations will reach levels observed before the declines which have resulted in current concentrations (McKenzie et al. 2007).

Depleted ozone levels over Antarctica, first reported by Farman et al. (1985) are likely to be one potential consequence of atmospheric pollutants. The reduction of ozone concentration over Antarctica changes with the season, with the lowest concentrations being recorded during the Southern Hemisphere spring (Parisi & Kimlin 1997a). Recent observations of the total daily ozone concentration over Antarctica are approximately one third of the concentrations measured 35 years ago (Parisi & Kimlin 1997a). Variations in the ozone concentration similarly occur over populated regions of the world. There is a strong relationship in the latitudinal variation in ozone concentration in both hemispheres, with the Southern Hemisphere having consistently less ozone than the Northern Hemisphere (Van Heuklon 1979; McKenzie 1991). There are further suggestions that the reduction in ozone over the Southern Hemisphere is related to depleted ozone concentrations over Antarctica (Sze et al. 1989; Atkinson et al. 1989, McKenzie 1991; Parisi & Kimlin 1997a).

Seasonal variations in latitudinal ozone occur in both hemispheres. Seasonal variations are greatest in the respective spring months of each hemisphere at mid to sub polar latitudes of around 70^o North and 70^o South (Van Heuklon 1979; McKenzie 1991). These latitudes experience the highest level of seasonal fluctuation in ozone concentration and experience the greatest ozone losses in the upper stratosphere (Randel et al. 1999), while the equatorial regions experience the least influence in seasonal fluctuation (Van Heuklon 1979; McKenzie 1991). Fluctuations in ozone can also occur daily with some evidence suggesting daily changes in concentration in the mid latitudes of $\pm 20\%$; however, changes observed in the tropics are more subtle (McKenzie 1991). Ozone fluctuations over mid latitudes are of greater concern than fluctuations observed near the poles due to average UV irradiance levels being considerably lower toward the polar regions (McKenzie 1991), and the increased number of people living in the mid latitudes.

In addition to stratospheric ozone there are many local concentrations of tropospheric ozone produced in urban areas as a result of pollutants. Car exhausts being the main cause of photochemical smog, produce NO_2 which is photochemically disassociated by the absorption of UV photons into NO and O which subsequently forms O_3 when a free O atom combines with diatomic O_2 (Van Heuklon 1979). Ozone is a toxic gas, so that the potential benefits of higher concentrations of ozone found in urban areas are offset somewhat by the health risk to the population. Typically 90% of the ozone found in a vertical column that regulates the levels of UV detected at the earth's surface is concentrated in the stratosphere rather than the troposphere (Huffman 1992). The distribution of terrestrial UV is inextricably linked to the climatology of atmospheric ozone. A 1% decrease in stratospheric ozone concentration is estimated to increase the incidence of non-melanoma skin cancer by 2 to 3% (Hofmann 1987; Urbach 1997). Recently, increasing UV irradiances at Northern Hemisphere sites have been linked to long term changes in cloud, aerosol and ozone concentrations (WMO 2007).

1.2.5 Dobson Units

Concentrations of ozone are typically measured in a vertical column toward the zenith above the surface of the earth. Most commonly, ozone concentrations are expressed in *Dobson units*, or alternatively, as molecular densities. Dobson units (DU) provide the number of milliatmosphere centimeters of ozone that would extend in a 1 metre square vertical column if held at standard temperature and pressure (STP). Standard temperature and pressure is defined as $0^{o}C$ and 1 atmosphere. In these conditions, a typical level of ozone concentration of 300 DU would be the equivalent of a 1 metre square column density of ozone of 0.3 cm height if measured at sea level and at $0^{o}C$.

1.2.6 Scattering mechanisms

Scattering by air and aerosols contributes to the production of an isotropic distribution of diffuse radiation. The radiation is however, not evenly distributed near the zenith or the horizon and there is an increased amount of forward scattered radiation near the position of the sun on a clear day (Barton & Paltridge 1979). Diffuse radiation is not distributed evenly because the atmosphere is spherical. Scattered light is less likely to reach an observer from a line of sight along the horizon as air and aerosol concentrations are highest toward the earth's surface. Similarly, there is little scattered light at all toward the zenith, as air and aerosol concentrations are least in a vertical column. Variation in atmospheric scattering and the changing diurnal position of the sun results in changes in the distribution of UV incident on a horizontal plane and on vertically inclined surfaces, so that distributions to both surfaces are not proportional and depend upon surface orientation, solar position and wavelength (Webb et al. 1999).

1.2.6.1 Rayleigh scattering by air

Rayleigh scattering has a significant effect on the relative skylight distributions of wavelengths observed at the earth's surface. Shown below is Rayleigh's equation describing the relative degree of light scattering depending on the wavelength of the incident light (Meyer-Arendt 1995):

$$i \propto 1/\lambda^4 \qquad (1.1)$$

where i is the intensity of the light scattered out of the direct line of sight and λ is the wavelength.

The intensity of UV light scattered according to equation 1.1 and normalised at 280 nm is plotted in Figure 1.3. The figure shows that the degree of Rayleigh scattering is inversely proportional to the fourth power of the wavelength. The differential degree of scattering by air molecules in the lower atmosphere accounts for the blue appearance of the sky as seen in the visible region of the electromagnetic spectrum. More importantly, scattering at shorter UV wavelengths that are able to penetrate the earth's ozone layer is much greater than scattering at longer wavelengths. Rayleigh scattering results in a higher diffuse component of UV than the perceived diffuse visible radiation. Scattered UV is of a similar intensity to direct UV; however the direct visible beam is usually five times greater than the diffuse visible radiation (Barton & Paltridge 1979). The potentially harmful effects of a high level diffuse component of UV are therefore not immediately noticeable in conditions that may protect an individual from the direct solar beam, namely shaded locations. In addition, the level of scattering at UVB wavelengths is higher than the level of scattering at UVA wavelengths, increasing the UVB component of diffuse skylight and further increasing the risk of over exposure to UV in shaded environments.

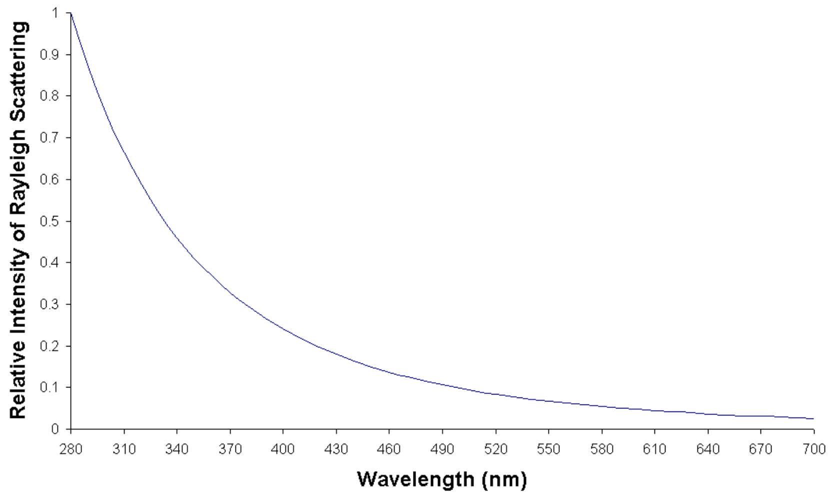

Figure 1.3: Rayleigh scattering of incident radiation in the UV and visible waveband.

1.2.6.2 Mie scattering by aerosols

Mie scattering, like Rayleigh scattering is another scattering mechanism that scatters the light depending on the scattering particle size; however this mechanism scatters incoming light independently of the wavelength. Mie scattering is responsible for the scattering of light by larger sized particles found in the troposphere as opposed to Rayleigh scattering by atomic sized particles. Mie scattering therefore occurs in the lowest region of the earth's atmosphere extending to an altitude of approximately 30 km. Scattering by larger sized aerosol particles includes scattering by water droplets (clouds), dust, and smoke particles. Unlike the scattering of UV by air molecules, scattering by aerosols is constant across the entire UV spectrum. Additionally, the degree of aerosol scattering is not overly significant unless there is a noticeable amount of smog or smoke (Barton & Paltridge 1979). Scattering by aerosols, including clouds has the effect of reducing the overall intensity of the direct UV radiation received on the ground (Diffey 1991). However, partial cloud cover not directly covering the sun can enhance the level of UV received at ground level due to the extra reflection of direct radiation (Estupinan et al. 1996).

1.2.7 Ultraviolet incident on the local playground environment

1.2.7.1 Surface condition

The condition of the earth's surface influences the UV intensity received at ground level. Reflection over the entire earth's surface, including the ocean is normally less than 7% (Diffey 1991). Reflection of radiation from the surface of the earth is defined as the surface albedo. UV surface albedo is expressed as the ratio of incident to reflected UV and is measured along the reflecting surface normal. Examples of surfaces that have a high albedo include snow, ice, sand, and water, making locations such as the beach and snow covered mountains, regions of particular high risk to UV exposure, particularly in the UVA waveband which typically has a higher surface albedo than in the UVB (Blumthaler & Ambach 1988; Fiester & Grewe 1995; McKenzie et al. 1996). Different surfaces reflect different wavelengths differently, depending on the surface colour, texture and chemical composition. Surfaces that seem to be poor reflectors of visible radiation may not necessarily be poor reflectors of UV. Similarly, materials found in an urban environment may be good reflectors of visible radiation but poor reflectors of UV radiation (Grant & Heisler 1996). In a school environment, typically high reflectors of UV radiation include bitumen and concrete surfaces, and common building materials, especially galvanized metal surfaces (Lester & Parisi 2002). The UV reflectivity of a surface also depends upon solar incidence angles. Glass surfaces for example are extremely efficient reflectors at near grazing angles of incidence (Heisler & Grant 2000). The extent to which surface orientations of reflective building surfaces influence ambient UV has been investigated in previous research, showing daily increases of several hundred Jm^{-2} of sun-burning effective UV in different situations (Parisi et al. 2003), and increased UV contributions from vertically inclined reflecting building surfaces compared to horizontal surfaces (Turner et al. 2008).

1.2.7.2 Altitude and aspect

Altitude can have a significant effect on the UV irradiance. Lower air densities result in cooler, less humid conditions at altitude, reducing turbidity and decreasing attenuation by aerosols (McKenzie 1991). Locations at higher altitude can also often be higher than particulate altitudes produced from smoke, smog or other pollutants, increasing the intensity of UV not scattered or absorbed by a thick aerosol layer. Of the UV that is transmitted through the ozone layer, approximately half is backscattered into space and the other half contributes to diffuse skylight (McKenzie 1991). At higher altitudes, lower air densities reduce the amount of Rayleigh scattering, reducing the level of UV backscattered into space and increasing the direct component of UV radiation. Calculations by Barton and Paltridge (1979) found that an increase in height of 1 km above sea level resulted in a 15% increase in the erythemal (sunburn) dose. Similar results by McKenzie (1991) predict a 10% increase in the UV irradiance due to a loss of air pressure affecting Rayleigh scattering at a height of 2 km. At extreme altitudes, reductions in ozone concentrations can also have an effect on the UV irradiance.

Aspect plays an important role in the levels of UV exposure received. Surfaces that face toward their respective poles (south in Southern Hemisphere, north in Northern Hemisphere) receive less direct exposure to sunlight on vertical surfaces than surfaces facing the opposite direction (Grifoni et al. 2005). Tilted surfaces receive varying amounts of UV radiation depending on their orientation. If the tilted surface faces the direction of the sun in azimuth and the sun is not directly overhead, it will receive more direct radiation than a horizontal surface or a surface tilted away from the sun (Barton & Paltridge 1979). Similarly any object, including the human form, located on a tilted surface receives an increased exposure due to reflected radiation from the ground (Barton & Paltridge 1979; Schauberger 1990; Grifoni et al. 2006). Diffuse radiation is the more significant component of UV when the sun is at low elevations (McKenzie 1991), therefore the influence of surface orientation with respect to the horizontal plane is less at lower solar elevations compared to when the sun is located higher in the sky.

1.2.7.3 Latitude

Surface environments and playgrounds located in higher latitudes receive a lower UV irradiance than those located in latitudes closer to the equator on a daily and yearly basis due to the highest elevation angle that the sun can reach in those locations. This is the most significant factor influencing the UV irradiance received at the earth's surface. In the polar regions of the earth the sun doesn't rise above the horizon in winter and in summer can only reach low elevations compared to the equatorial regions in which the sun always reaches the zenith. The season, as mentioned previously, also affects the distance the earth is to the sun. The UV irradiance in the Southern Hemisphere mid summer is approximately 6.6% greater at all wavelengths than in the Northern Hemisphere mid summer (McKenzie 1991). Hemispherical differences in the UV latitudinal distribution are greatest at shorter wavelengths in the UV waveband and these differences are further amplified by differences in atmospheric turbidity and lower ozone levels in southerly latitudes (McKenzie 1991). Consequently summertime sunburning UV irradiances can be up to 40% greater in the Southern Hemisphere compared to latitudes located in the Northern Hemisphere (Madronich et al. 1998). Tropical latitudes tend to have a higher humidity than other latitudes, increasing turbidity and therefore increasing the efficiency of absorption of UV by aerosols, offsetting somewhat lower tropical ozone levels and higher UV irradiances, however there remains a significant UV irradiance latitude gradient in both hemispheres (McKenzie 1991). Many locations, especially in northern latitudes tend to have increased levels of aerosols as the result of population induced pollutants, influencing the levels of UV irradiance at ground level (Van Heuklon 1979). Furthermore, tropospheric ozone levels are higher in northern latitudes compared to southern latitudes (Fishman et al. 1990).

1.2.7.4 Time of day

The UV irradiance recorded at the earth's surface changes with the position of the sun in the sky. At solar noon, when the sun is at its highest point in the sky, the path the sunlight has to take through the atmosphere is its shortest, resulting in less particulate and atmospheric scattering, and less absorption by ozone. A larger vertical component of direct solar radiation is also received at solar noon, resulting in a higher irradiance than would be received when the sun is lower in the sky. At lower solar elevations, the received UV irradiance is reduced by a larger horizontal component of the direct solar UV beam and an increased atmospheric path through which the sunlight must travel. In addition to atmospheric absorption, atmospheric scattering differentially alters the distribution of solar UV throughout the day. As has been previously discussed, scattering of UV radiation is greatest at shorter wavelengths. This tends to shift the relative degree of scattering at different wavelengths as the sun moves across the sky (Parisi & Kimlin 1997b). This differential degree of UV scattering further increases the risk of exposure during midday when the sun is at its highest elevation and scattering of shorter wavelengths is less than the scattering of those same wavelengths at lower solar elevation angles, particularly for individuals including school children that use open outdoor playground environments during lunch breaks. Measurements of the increase in the spectral UV irradiance are shown in Figure 1.4 for a day in which little or no cloud cover was observed. It can be noted from the figure, that increases are particularly high in the biologically significant shorter wavelengths of the measured spectrum.

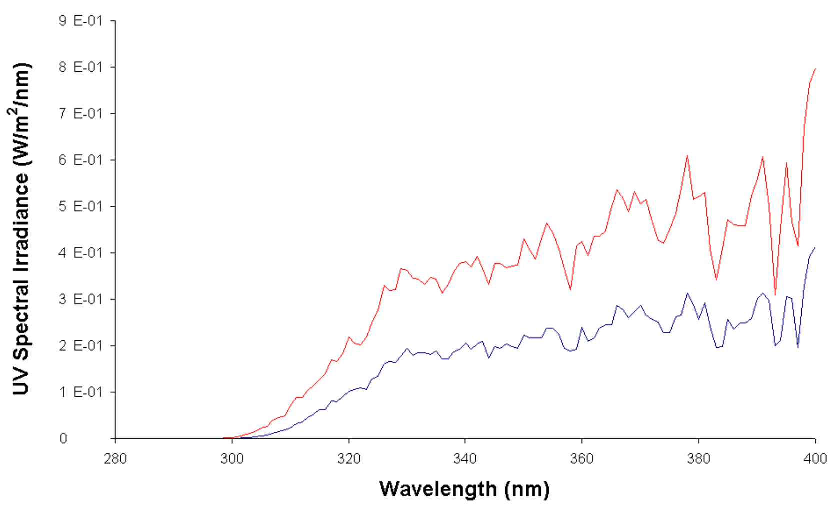

Figure 1.4: Increase in UV spectral irradiance distributions recorded at the University of Southern Queensland on a clear winter day during mid morning (blue line) and at midday (red line).

1.2.7.5 Cloud

The influence of cloud on terrestrial UV varies depending on the type of cloud and the degree of cover. Light, sparsely distributed clouds have little effect on the received UV irradiance. Total cloud cover can reduce terrestrial UV by one half of its clear sky value (Diffey 1991). Attenuation of solar electromagnetic radiation by clouds is greater in the visible region of the electromagnetic spectrum than at UV wavelengths. Furthermore, attenuation of solar infrared radiation by water droplets in clouds is greater than attenuation at UV wavelengths, reducing the sensation of heat on human skin, increasing the behavioural risk of overexposure to UV (Diffey 1991). Cloud cover has little influence on the diffuse component of solar UV radiation received at the earth's surface, reducing the total diffuse component by levels often less than 10% of levels measured under a clear sky (Paltridge & Barton 1979). Cloud cover can therefore not be considered an adequate form of protection from excessive UV exposure. The active use of sunscreens, hats and other forms of sun protection should be employed in cloudy conditions to avoid the risks associated with long term chronic and short term acute exposures to environmental UV radiation.

Furthermore, the type of cloud cover plays an important role in determining levels of terrestrial UV. Sparse cumulus cloud cover for example can enhance the UV irradiance above the nominal clear sky UV irradiance received at the earth's surface when not located directly in front of the solar disk (Estupinan et al. 1996; Sabburg et al. 2003; Parisi et al. 2004). This can enhance the UV irradiance by up to 25% (WMO 2007). Temporal variations in cloud cover resulting in significant variations in the UV irradiance received in the playground environment between 9:00am and 3:00pm often occur over short time periods. This effectively results in changing UV conditions in a real playground environment varying from cases of UV enhancement to UV reductions in short, random time frames.

1.2.8 Humans and ultraviolet radiation

Personal UV exposure depends on the activity or orientation of the individual, the environment in which the individual is exposed, the altitude of the sun, the season and atmospheric and weather conditions. Typically, humans experience between 5% to 10% of the ambient UV, with this fraction increasing for outdoor workers to between 20%

and 30% (WHO 2006). Personal sensitivity to UV is additionally dependent on the skin type or degree of pigmentation in the skin and on individual phenotypes. Unlike many other forms of radiation hazardous to humans, UV has a low penetrating ability, limiting potential damage to the skin and eyes. Human skin is least sensitive to wavelengths in the UVA region, however biological damage to deeper layers of the skin is likely to be due to UVA being able to penetrate human skin further than the shorter UVB wavelengths. Photoageing caused by UV penetration of the skin affects underlying structural macromolecules of dermal connective skin tissue resulting in skin wrinkling and loss of elasticity (Wlaschek et al. 2008). UVB is also the primary cause of sunburn or erythema in human skin. The relationship between exposure and UV and the development of non-melanoma skin cancer (NMSC) later in life including in particular the development of Basal Cell Carconimas (BCC) and Squamous Cell Carcinomas (SCC) are generally well accepted (Urbach 1997; deGruijl 1999) although this is largely based on indirect epidemiological evidence including higher incidence rates observed in low latitudes and high rates of incidence observed in populations exposed to high ambient levels of UV (Kricker et al. 1994). The links between UV and malignant melanoma are less well defined although exposure during childhood and intense intermittent exposure to solar UV are likely to be the most significant environmental risk factors for the development of the disease (Armstrong 1988; Longstreth et al. 1998; Walter et al. 1999; Gilchrest et al. 1999). Some exposure to solar UV is however essential for human health. Indeed, the reported disease burden due to no UV exposure exceeds the disease burden caused by excessive exposure to UV (WHO 2006).

1.2.8.1 Human skin

1.2.8.1.1 Skin type

The single most important factor influencing the effect of UV on humans is skin type. Different types of skin offer differing degrees of protection from UV. Melanin, a chemical compound that exists in the upper layers of the skin is responsible for the primary absorption of UV. Melanin is also responsible for variation in skin pigmentation. Concentrations of melanin are strongly correlated with population origin with darker pigmentations typically being observed in populations originating from low latitudes and lighter skin pigmentations being observed in individuals originating from higher latitudes. As a result, darkly pigmented populations do not burn or suffer the incidence of skin cancer observed in lightly pigmented populations. Australia, as a consequence of its geographical location is placed at significant risk due to the high number of fair skin types observed in the current population. The relative health risk to a population associated with exposure to UV must take into consideration the differences in skin type. Six sun reactive skin types have since been defined following an experiment based on the personal history of exposure to the sun (Fitzpatrick 1975). The six reactive human skin types are listed in Table 1.1.

Table 1.1: Sun reactive skin types (Diffey 1991, p.314).

Skin Type	Skin reaction to UV	Examples
I	Always burns easily and severely (painful burn); tans little or none and peels.	People most often with fair skin, blue eyes, freckles; unexposed skin is white.
II	Usually burns easily and severely (painful burn); tans minimally or lightly, also peels.	People most often with fair skin, red or blond hair, blue, hazel or even brown eyes; unexposed skin is white.
III	Burns moderately and tans about average.	Unexposed skin is white.
IV	Burns minimally; tans easily and above average with each exposure; exhibits immediate pigment darkening reaction (rapid tanning).	People with white or light brown skin, dark brown hair, and dark eyes; unexposed skin is white or light brown.
V	Rarely burns; tans easily and substantially; always exhibits immediate pigment darkening reaction.	Unexposed skin is brown.
VI	Never burns and tans profusely; shows immediate pigment darkening.	Unexposed skin is black.

1.2.8.1.2 Ultraviolet penetration of the skin

Ultraviolet radiation can penetrate up to no more than 1 mm of skin (Bruls et al. 1984). Scattering by surface follicles, glands, absorption and reflection of the skin at the surface and within deeper layers of higher refractive index, account for the varying degree of penetration with depth (WHO 1994). In addition to this, melanin in darker skin types reduces the effectiveness of the incoming UV (Kollias et al. 1991). Figure 1.5 indicates the degree of penetration by radiation of 365 nm and 313 nm which lie in the UVA and UVB bands respectively. It can be seen that 50% of the incident UVA and 33% of the UVB penetrates to a depth of 30 μm. Similarly, only 9.5% of the UVB reaches 70 μm while to the same depth, 19% of the incident UVA is still effective (WHO 1994). Approximately 1% of the UVA radiation reaches the subcutaneous tissue (Parrish et al. 1982). The increased proportion of UVA that is able to penetrate the atmosphere and the increased depth of the skin reachable in this waveband places significant importance on the prevention of penetration of UVA wavelengths.

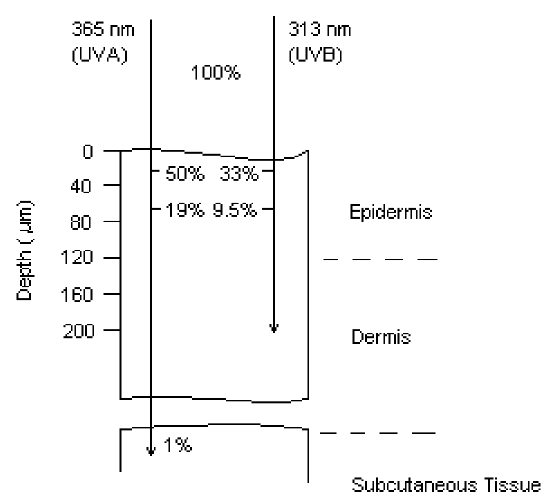

Figure 1.5: UV penetration and the layers of the skin (Bruls et al. 1984, cited in WHO 1994, pp. 46-47; Parrish et al. 1982, cited in WHO 1994, pp. 46-47).

1.2.8.2 Erythema

There are a number of reactions that human skin can exhibit as a result of exposure to ultraviolet radiation. The most noticeable acute effects are sunburn and tanning. Sunburn, or erythema is defined as the reddening of the skin that results from excessive exposure to UV. The reddening is the result of increased blood flow caused by the dilation of superficial blood vessels in the dermal layer of the skin. The reddening of the skin takes several hours to appear with the maximum effect becoming noticeable 8 to 12 hours after exposure, eventually fading entirely within 2 days (Olson et al. 1966; Farr et al. 1988). High levels of exposure to UV often result in severe pain, blistering and eventually peeling of the dermal skin layer. Erythemal intensities are typically measured in units of MED or SED. An MED (minimal erythema dose) represents the UV exposure required to produce mildly perceptible erythema with a definite border, measured typically 24 hours following the exposure event (Harrison & Young 2002). The MED is a measure of an individual's susceptibility to sunburn and varies with individual skin type with higher exposures typically being required in individuals of increasingly higher skin type number (Harrison & Young 2002). The SED (standard erythema dose) is referred to in this research work and represents 100 Jm^{-2} of erythemally effective UV (Diffey et al. 1997). In determining the SED, the erythemally effective action spectrum (CIE 1987) is weighted to the global ultraviolet of the source which for this research is global solar UV in the 280 nm to 400 nm waveband.

The relative effectiveness of UV wavelengths at causing an erythemal reaction in type I human skin is given in Figure 1.6. Type I skin is used for the reference action spectrum as it represents the worst possible case of the erythema response. The relative effectiveness of the UV wavelengths at causing an erythemal reaction in other types of human skin are progressively lower for each darker skin type, however the general trend of shorter wavelengths being more effective than longer wavelengths in the UV waveband is preserved. Although the erythema action spectrum is low at UVA wavelengths, higher UVA levels in terrestrial sunlight mean UVA contributes around 15% to 20% of the sunburn reaction (Diffey 1991).

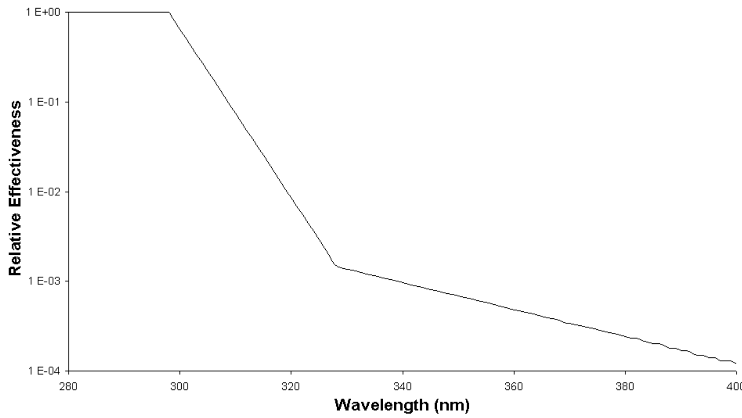

Figure 1.6: The erythemal action spectrum (CIE 1987).

The relative response of the erythemal action spectrum is determined by measuring the narrowband UV exposure required to produce perceptible erythema in human skin. It is considerably more difficult to determine an action spectrum for skin cancers as such effects have a longer period of latency before they are noticed and are likely to be produced through chronic exposure rather than a single exposure to UV radiation. Action spectra for skin cancers are therefore often inferred from animal experiments that can be performed in controlled environments (Setlow et al. 1993). The actinic and vitamin D_3 action spectra are included in this review below to demonstrate their response similarities particularly at the shorter UV wavelengths.

1.2.8.3 Actinic exposure

The actinic exposure represents the adopted international occupational and public safety standard of the limiting UV exposure that may be received by humans to both the skin and the eye. The relative effectiveness of the actinic spectrum is not normalised to any particular wavelength. The greatest relative effectiveness of the actinic action spectrum peaks at 270 nm. The weighted actinic UV in the range 280 nm to 400 nm can be integrated over a given exposure interval to determine the effective actinic exposure. The occupational standard for outdoor workers is chosen to reflect the average biologically damaging UV to the eyes and the skin such that received exposures do not exceed 30 Jm^{-2} over an 8 hour day (NHMRC 1989; ARPANSA 2006). Although the erythema and actinic weighted UV exposure cannot be directly compared due to variations in each respective spectral response, the occupational limit of exposure represents approximately 1.2 SED under most conditions, with the comparison changing for different periods of the day due to solar position and variations in the resulting atmospheric path (Gies & Wright 2003).

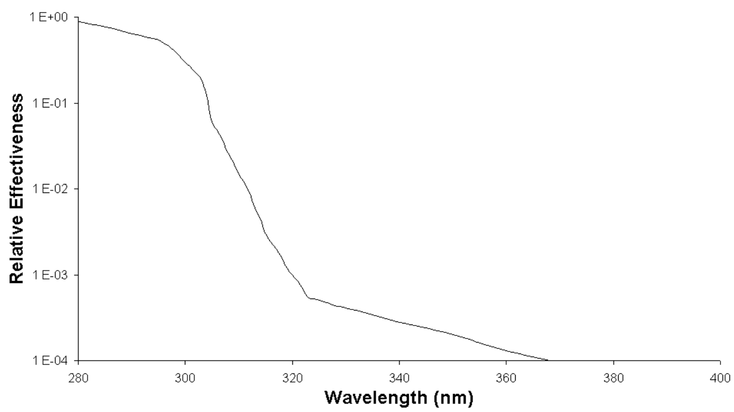

Figure 1.7: The actinic action spectrum (IRPA 1989).

1.2.8.4 Vitamin D

One potentially beneficial consequence of exposure to sunlight is the production of vitamin D. Exposure to solar UVB radiation photochemically converts 7-dehydrocholesterol in the epidermis to pre-vitamin D_3. No more than 5 to 15% of the 7-dehydrocholesterol content in the skin is converted into pre-vitamin D_3 due to excessive exposure reducing the pre-vitamin D_3 into biologically inert photoproducts regardless of the duration of the exposure (Diffey 1991). In two to three days, the pre-vitamin D_3 is completely converted to vitamin D_3 by a reaction controlled by skin temperature (Diffey 1991). The reference action spectrum for the production of vitamin D_3 is given in Figure 1.8. The spectrum shows the relative production of the vitamin D_3 that would be produced following an initial UV exposure. Vitamin D_3 produced in the skin is taken by the bloodstream to the liver to be metabolised to 25-hydroxyvitamin D (Webb & Holick 1988). As vitamin D is found in limited food sources including some fish and other fortified products, the dietary intake of Vitamin D can be limited such that most humans obtain the body's requirement from casual exposure to sunlight (Holick 2004).

Vitamin D deficiency has been linked to rickets (Meulmeester et al. 1990; Holick 2003), calcium imbalances in the elderly (Preece et al. 1975), type I diabetes (Hypponen et al. 2001), multiple sclerosis (Hayes et al. 1997) and the possible development of some cancers (Gorham et al. 1990; Garland et al. 2002; Grant 2002). Darker skin types, having an increased melanin pigmentation (Clemens et al. 1982) and older age groups (MacLaughlin & Holick 1985) are more likely to be deficient in vitamin D_3, especially when the sun is at lower elevations, as might occur at higher latitudes or depending on the season (Holick 1997). This does not mean however, that vitamin D deficiency is constrained to those latitudes and environments that experience low ambient levels of UV. Vitamin D deficiency has also been reported in sub tropical latitudes (McGrath et al. 2001) and can be linked to a number of factors that might alter the received UV exposure. The efficiency of sunscreens (Matsuoka et al. 1988), certain clothing (Matsuoka et al. 1992), and glass at reducing the UVB irradiance can significantly reduce if not eliminate the ability of the skin to produce vitamin D_3 (Holick 1997). These factors in addition to lifestyle factors may limit the effective vitamin D_3 produced by exposure to natural sunlight, even in high ambient UV climates such as those experienced in Australia.

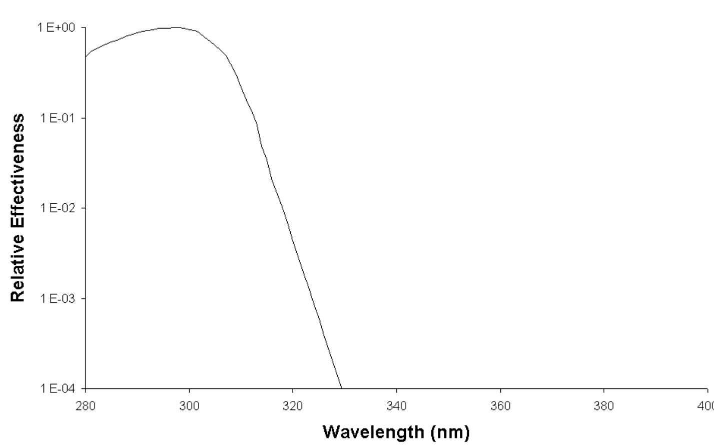

Figure 1.8: Action spectrum for the synthesis of vitamin D_3 in human skin (CIE 2006).

The effective response of the vitamin D (CIE 2006), actinic (IRPA 1989) and erythemal action spectra (CIE 1987) when weighted to a typical terrestrial UV spectrum is shown in Figure 1.9. It can be seen from the figure that the relative response of vitamin D is greater than the erythema response which in turn is greater than the actinic exposure when weighted with the global UV that occurs naturally in the playground environment. The erythemal response of human skin has been employed extensively in the research undertaken in this project.

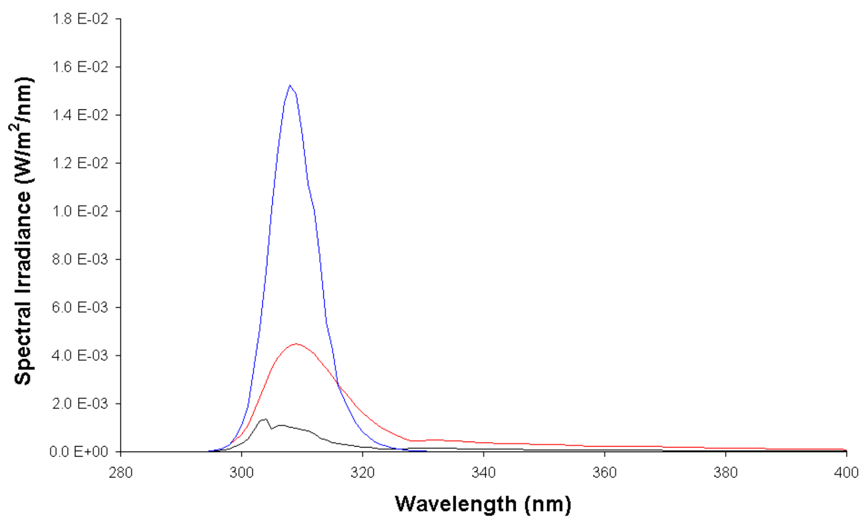

Figure 1.9: Weighted UV exposure of vitamin D (blue line), erythema (red line) and actinic response (black line) for a winter UV spectrum measured at SZA 50^o.

1.2.8.5 Lifestyle and behaviour

Potentially the most significant consequence of exposure to terrestrial UV is the risk of developing skin cancer and sun related eye diseases. Increasing rates of the incidence of malignant melanoma and corresponding mortality rates may be due to changing lifestyle or behavioural patterns in humans (Diffey 1991; McKenzie 1991). The rate of increase in skin cancer is therefore not necessarily related to increases in UV irradiance at ground level. Changes in lifestyle have been suggested for increases in malignant melanoma. In New Zealand, a 7.5% increase per year in malignant melanoma (Cooke et al. 1983) precedes predicted levels of ozone depletion (McKenzie 1991). Such reports come despite the fact that there have been significant increases in the survival rate of melanoma over the past few decades (Rigel et al. 1987), suggesting an outdoor lifestyle and sun-safe attitudes play an important role in increasing melanoma skin cancer rates which cannot be attributed to changes in the environment alone. This point is particularly significant for a school environment. Controlling the outdoor behaviour patterns of children in a school environment could effectively reduce incidence rates of skin cancer.

The risk of developing chronic UV induced skin damage is reduced provided effective sun protective strategies are implemented on a daily basis (Gasparro et al. 1998). The correct use of sunscreens, hats, protective clothing, exposure avoidance and the sustained development of effective sun safe strategies is an important factor in reducing the risk of overexposure to UV and reducing the risks of overexposure incurred during childhood.

1.2.9 Skin Cancer

It is well recognised that exposure to UV radiation is the primary cause of all types of skin cancer. Skin cancer, as a consequence of exposure to terrestrial UV radiation is the most common type of cancer observed in humans, particularly in high ambient UV climates (Diffey 1991; deGruijl 1999). Most skin cancers occur as a result of solar exposure during childhood (Leyden 1990; Katsambas & Nicolaidou 1996; Weinstock 1996; Longstreth et al. 1998; Walter et al. 1999; Gilchrest et al. 1999), however, as previously mentioned this may also be due to higher exposure rates at a young age and outdoor behavioural activity rather than environmental factors.

Skin cancer results in the mutation of normal skin cells into either benign or malignant tumours. The frequency with which skin cancers develop depend on the skin's melanin synthesis capability as levels of cutaneous melanin absorb and act as a filter to UV radiation (Hussein 2005). Skin cancer itself is not a fatal disease, however the metastasizing nature of many skin cancers, particularly malignant melanoma often results in the spreading of cancerous growth to other organs which can result in death. It is estimated that skin cancer costs the Australian community an estimated $400 million per year (Girgis et al. 1994). The high incidence of skin cancers in the Australian population and the rising incidence of skin cancer in risk population groups (Longstreth et al. 1998) highlight the need for further research to develop effective sun-safe strategies.

1.2.9.1 Non-melanoma skin cancer

NMSC is the most common type of cancer observed in fair skinned populations (Diepgen and Mahler 2002). NMSC does not readily metastasize. The risk factors associated with the development of NMSC are similar to the observed risks commonly associated with erythema. Lightly coloured individuals with poor tanning ability and high sunburn susceptibility, especially those with light eye and hair colour are more likely to develop NMSC than darker pigmented individuals (Urbach et al. 1974; Kollias et al. 1991). While darker skin pigmentation reduces the risk of the development of NMSC, they can still occur in areas of lighter pigmentation including the palms of the hand or the lips (Diffey 1991). Areas of the body that are often exposed to solar UV such as the head and neck are common sites for NMSC (Urbach 1982). Experiments derived from animals have shown that the UVB wavelengths are more effective than UVA wavelengths in producing NMSC (Sterenborg & van der Leun 1987).

Of the types of NMSC, BCC occurs more frequently, originating in the basal cell layer of the epidermis varying in depth from between 40 μm for the head, 50 μm for the arms and legs and 150 μm for the dorsal sides of the hand (Konishi and Yoshizawa 1985). SCC, affecting the stratified squamous epithelium occur frequently to exposed areas of human skin. SCC and the nodular form of BCC show an increasing rate of incidence with age (Scrivener et al. 2002; Staples et al. 1999) and are strongly correlated in fair skinned populations living in risk climates. The ambient UV incident upon skin surfaces of the human body is strongly dependent on geographical latitude, having a significantly greater intensity in lower latitudes due to higher solar elevation. Low geographical latitude and the predominately northern European ethnocentric origin of the current Australian population contribute to Australia having the largest incidence rates of both NMSC and melanoma skin cancer in the world, displaying a distinct latitudinal gradient for both forms of the disease (Staples et al. 1999; McCarthy 2004).

1.2.9.2 Melanoma skin cancer

Cutaneous malignant melanoma occurs less frequently but metastasises at a higher rate than NMSC. The development of benign or malignant skin cell tumors is linked to the absorption of UV radiation causing mutation in the DNA of skin cells (deGruijl 1999). A malignant melanoma is a tumour that develops from the pigmented cells of the skin. The pigmented cells, known as melanocytes contain melanin, a chemical that absorbs radiation over all UV wavelengths (Setlow et al. 1993). The absorption of radiation by the melanin in melanocytes may be responsible for the mutation of DNA, a symptom that may lead to the development of skin cancer (Selow et al. 1993). The direct absorption of UV by DNA is stronger in the UVB than the UVA (Setlow et al. 1993), however the complexity of the processes involved in the mutation of DNA and the long latent time period between exposure and the development of melanoma makes it difficult to determine an action spectrum. The absorption of UV by melanin and the difficulties associated with determining the effectiveness of UV absorption by DNA have led to suggestions that wavelengths other than those concentrated in the UVB region may be responsible for the onset of malignant melanoma. The visible, UVA and infrared regions of the electromagnetic spectrum may be responsible for the development of malignant melanoma (Loggie & Eddy 1988; Setlow et al. 1993) with the deeper skin penetrating ability of UVA photons likely being responsible for acute DNA damage (Agar et al. 2004). While research from other groups has placed a significant importance on the UVB regions (Sober 1987; Koh et al. 1990), there is general agreement that the development of melanoma is related strongly to exposure to sunlight (Armstrong & Kricker 1996; Setlow et al. 1993; Diffey 1991; Gasparro et al. 1998).

The ability of skin cell DNA to repair itself is a significant contributing factor toward preventing the development of skin cancer (Kraemer et al. 1994; Wei et al. 2003). Individuals afflicted with the DNA repair deficient skin disorder, xeroderma pigmentosum are hyper-sensitive to UV and readily develop both cutaneous malignant melanoma and NMSC, supporting the links between DNA repair deficiency and the likelihood of developing skin cancer (Kraemer et al. 1994; Taylor 1995). Like NMSC, certain phenotypic characteristics including fair skin type, eye and hair colour contribute to the likelihood of developing melanoma (Evans et al. 1988; Lock-Anderson, et al. 1998; Harris & Alberts 2004) with the most significant phenotypic risk associated with melanoma being the number of moles larger than 2 mm on the skin (MacKie et al. 1989). Melanoma occurs more frequently on unacclimatised skin surfaces including the body trunk and legs and unlike NMSC is not always a prevalent condition on areas of the skin that receive high ambient UV exposures. Approximately 800 Australians die annually from melanoma and 200 annually from NMSC (NHMRC 1996). More recent data indicate increases in these figures with 390 deaths attributed to NMSC and 1146 deaths attributed to cutaneous malignant melanoma in the year 2003 (AIHW and AACR 2007).

In children, the sensitivity of unacclimatised skin may be an important risk factor influencing the later development of melanoma. Research on human personal characteristics and sun related beliefs has shown that the number of sunburns, and therefore total human UV exposure, is related to human behaviour (Hill et al. 1993). The behaviour of children in a potentially unsafe environment warrants the necessity to develop protective strategies based on a detailed investigation of the school environment.

1.2.10 Personal measurements of UV radiation with polysulphone dosimeters

Polysulphone dosimeters originally developed for use in UV exposure studies by Davis et al. (1976) have a response to UV radiation similar to human skin. This type of thin film polysulphone dosimeter has been constructed and implemented previously to measure personal UV exposures to school children (Diffey et al. 1996; Gies et al. 1998; Milne et al. 1999a). Studies involving mannequins have also made extensive use of polysulphone dosimeters to determine the erythemally effective UV to specific anatomical sites under various atmospheric and physical conditions (Diffey et al. 1977; Diffey et al. 1979; Kimlin et al. 1998). Previous polysulphone dosimeter studies using mannequin and human subjects are however limited by the total number of anatomical sites assessed and have been developed primarily to examine the influence of the local environment (Lester & Parisi 2002; Turnbull & Parisi 2006; Turner et al. 2008) and occupation or activity (Holman et al. 1983; Herlihy et al. 1994; Gies et al. 1995; Vishvakarman et al. 2001; Gies & Wright 2003; Siani et al. 2008; Siani et al. 2009) on anatomical sunlight distributions and relative environmental exposures, or to determine protection factors for subjects using various forms of personal sun protective clothing and hat wear (Parisi et al. 2000; Gies et al. 2006). Polysulphone dosimetry has been used extensively in this research to determine body surface exposure distributions in the school playground environment. The methods and techniques used to measure UV exposure with polysulphone dosimeters are discussed in the following chapter.

1.2.11 Ultraviolet exposure models

Terrestrial UV radiation models have been developed by a number of researchers to predict the horizontal plane spectral UV irradiance. Computer models developed to predict the horizontal plane UV irradiance list the direct UV component and the diffuse or scattered UV component. Typically, as the mechanisms that affect the transmission of the direct and diffuse UV at the earth's surface are different, different methods are used to model their influence. The levels of diffuse and direct UV reaching the earth's surface depend on the sunlight's optical path through the atmosphere and atmospheric concentrations of ozone, aerosols, and particulates. Semi-empirical models such as that used for this research, model the UV irradiance as the product of the extra-terrestrial UV irradiance and the total attenuation due to transmission through ozone, aerosol and particulate atmospheric layers. Modelled direct and diffuse spectral UV depends strongly on the incident sunlight angle and the incident atmospheric path. Following atmospheric attenuation for a given SZA, the global UV irradiance can be modelled for any particular time of day providing results comparative to spectroradiometeric measurements. UV exposure models have been applied to predict exposure risks to humans and employed to investigate variations in environmental UV (Jokela et al. 1993; Feister 1994; Kimlin et al. 2003; Downs et al. 2001). Furthermore, the biologically effective UV has been measured and modelled extensively under tree shade indicating that perceived shady locations can present a significant risk of exposure in the biologically effective UVB (Grant 1997; Grant et al. 2002; Heisler et al. 2003). For this research, a hybrid UV exposure model was developed for predicting the horizontal plane UV exposure in a school playground environment. This model is discussed in detail in the following chapter.

1.2.11.1Variation in UV irradiance due to orientation

Surfaces orientated away from a horizontal plane receive varying amounts of UV radiation depending on their orientation with respect to the sun and the local environment influencing the total biologically damaging UV received by human subjects. The surrounding surface and ground objects can also influence the UV reflected back into the atmosphere. The Australian UV index predicts the maximum ambient UV on a horizontal plane. However, no mechanism exists for the prediction of human UV exposure based on scientifically measured human exposure data taking into account human activities, the complex shape of the human body, geographic factors and local climatic and physical conditions.

The influence of the environment and variation in UV exposure due to orientation has been investigated by a handful of researchers. Mech and Koepke (2004) developed a model for the computation of UV on arbitrarily orientated surfaces. The influence of albedo contribution to the total UV irradiance incident on surfaces orientated away from the horizontal plane has also been investigated (Schauberger 1990). Hoeppe et al. (2004) measured the UV irradiance at 27 differently inclined surfaces with radiometers and interpolated the results in two dimensions to visualise the whole body UV exposure.

Recently, Hess and Koepke (2008) developed a model to calculate the UV irradiance on arbitrarily orientated surfaces taking into account surface obstructions which influence the effective sky view. This approach required modelling the complete hemispheric UV radiance field including the influence of the regional albedo. This work extended the model of Mech and Koepke (2004) by positioning sky obstructions in the radiance field, whereby the influence of incident UV on the modelled obstruction included the UV transmission and reflection properties of the obstructing structure. The effectiveness of this model was demonstrated by modelling UV in an urban environment and a mountain skyline.

1.2.11.2 Modelling personal biologically damaging ultraviolet

Mannequins and human dosimeter experiments have been used to model human exposures in different physical environments and situations. In a comparative study using mannequin and human subjects, Airey et al. (1995) found that the orientation of human subjects can be modelled by mannequin headforms tilted at various angles with respect to the environment to represent the postures of standing, sitting, bending and kneeling respectively. Previous research has emphasised the use of rotating mannequins and headforms to determine the UV exposure to specific sites of the human body as human volunteers wearing dosimeters may not always represent a feasible or practical approach. Alternatively, predictions not involving the direct measurement of human exposure to UV have been modelled directly onto three dimensional representations of the human form through the use of ray tracing and UV irradiance algorithms (Streicher et al. 2004).

Research conducted by Kimlin et al. (1998) utilising polysulphone dosimeters located on different mannequin facial sites found the relative exposure to the nose varied by a factor of approximately three due to seasonal variation in SZA from winter to summer. These findings were supported by Downs et al. (2001) following the development of a UV exposure model highlighting variation in erythemally effective UV to the face with variation in SZA. The model developed by Downs et al. (2001) was later integrated into studies to investigate UVA facial exposure distributions and to investigate variation in facial UV exposure distribution with latitude (Kimlin et al. 2003a; Kimlin et al. 2003b). For this work, a three dimensional high density headform exposure network was developed from measurements of UV exposure improving the resolution of modelled facial exposure distributions over existing polysulphone mannequin model measurements. This extends the work of others by representing UV exposure distributions in high detail and in three dimensional space by assessing hundreds of exposure measurements rather than assessing a handful of anatomical sites. Furthermore, as this work is based on measured exposures, the unique shading effects caused by the body itself in the natural UV environment can be examined.

1.2.12 Trends in school practices and the ultraviolet environment

1.2.12.1 Sun protection policy

The extent to which UV modelling and prediction can be transferred to sun safe practice is dependent on the attitudes and resulting behaviours of individuals. Schools, being directly responsible for the behaviour of students under their care have the opportunity to modify and control playground practice. Protective strategies aimed at reducing exposure to solar UV in schools include the active use of suitable clothing, hat and eyewear, the application of sunscreens, appropriate role modeling and education by teachers, timetabling and planning to avoid periods of peak daily UV intensity, and the use of physical shade structures designed to minimise direct exposure to the sun in a variety of playground environments.

SunSmart campaigning by the Anti-Cancer Council of Victoria has resulted in the development of safer practice in schools and the broader community in Australia through markedly influencing the behaviour and subsequent exposure of individuals to environmental UV (Montague et al. 2001). A national program for the accreditation of SunSmart early childhood centers, primary and secondary schools was launched in 1998 by the Anti-Cancer Council of Victoria to formalise participation in sun-safe practice by child care providers (ACCV 1999). Adoption of sun-safe practice in schools, such as those formalised by the SunSmart campaign, has generally been well accepted in both early childhood and primary schools, however, policy acceptance by high schools is less frequent (ACCV 1999). While it has been well documented that childhood exposure to UV is crucial to the potential development of skin cancers later in life, behavioural trends among school aged children show a decrease in sun safe practices with age, particularly among adolescents (Broadstock et al. 1996; Dixon et al. 1999; Balanda et al. 1999; Lowe et al. 2000) and a reluctance from high schools compared with the early childhood and primary school sectors to formalize safe sun policies (ACCV 1999).

1.2.12.2 Behavioural attitudes and practices of school children

Due to school hours coinciding with periods of peak UV intensity, school children can potentially be exposured to significant levels of biologically damaging UV. Dosimeter experiments have shown exposures to the shoulders of school children range from between 34% (Gies et al. 1998) to 15% (Milne et al. 1999b) of the daily available ambient UV. Poor sun-safe practices noted by Milne et al. (1999a) in a study conducted across 33 primary schools located in Perth showed that use of hats affording quality protection worn by school children was often less than 30%. Giles-Corti et al. (2004) showed that this figure could be increased in schools that implemented intensive intervention policies, namely SunSmart accreditation and strict “no hat no play” policies. Kimlin and Parisi (2001) determined that the ambient UV exposure received by primary school children could further be reduced provided school children were aware of the daytime risk to ambient UV and its potential to increase facial exposure without hat protection while at school. Further research has shown that sun-protective practices however, are reduced markedly as children age. This behavioural trend has been reported to increase in high school children as they progress in year level and is especially noticeable as children move from primary to high school (Broadstock 1996; Lowe et al. 2000). Strategic approaches aimed at reducing UV exposure to children in high schools are needed to develop safer school environments.

1.3 Methodology

The research program developed to achieve the objectives introduced at the beginning of this introduction will be described as follows:

- Chapter 2 (Materials and Methods) will present a brief introduction of the instrumentation required to measure the three dimensional UV anatomical surface exposure. The horizontal plane UV exposure model, required to make predictions of the erythemally effective exposure incident in the playground environment is discussed in detail. The method used to survey a playground environment is introduced and the techniques needed to weight the horizontal plane playground exposure to the three dimensional surfaces of the body are discussed. The chapter concludes by discussing the measurement of personal UV exposure in a cohort of the school population. These measurements were taken to compare to model predictions of personal playground exposure.

- Chapter 3 (Measurements of body surface exposure) is the first results chapter. Measured patterns in body surface exposure for each of the face, neck, arm, hand and leg are discussed relative to the SZA ranges of 0^o-30^o, 30^o-50^o, and 50^o-80^o.

- Chapter 4 (Modelling the playground UV exposure) presents the results developed for the model school playground environment. Specifically, playground sky view, surface albedo, shade density and erythemally effective UV exposure are presented from playground measurements. Summary statistics for various regions of the model school playground are also presented. UV exposures and subsequent playground hot spots found in the real playground environment are detailed.

- Chapter 5 (Student exposure in the playground) is the third results chapter. This chapter details the exposure distribution measured in the school population. The influence of the local playground environment is discussed in relation to cloud cover, season, and measured face, neck, arm, hand, and leg body site exposures. Comparisons of measured body site erythemally effective exposures are presented relative to modelled erythemally effective body surface exposures. The risks associated with the development of non-melanoma skin cancer are discussed in relation to modelled body surfaces and measured hat use in the student population. Estimates of the annual erythemally effective UV exposure received by a school child using the model school environment are provided for each of the face, neck, arm, hand, and leg surfaces.

- Chapter 6 (Discussion) discusses the value of playground activity scheduling in regards to reducing skin cancer risks incurred by students using the model school playground environment. The value of playground tree cover and shading structures are assessed by application of the techniques developed to modelled school playground exposure. The techniques developed for this research are presented with respect to their potential use in different outdoor environments and the playground model limitations are also presented.

- Chapter 7 (Conclusions) summarizes the effective outcomes of this research.

In review of the topics discussed thus far, the origins of sunlight and UV radiation have been presented with respect to the total path of UV radiation that is eventually incident upon the exposed skin surfaces of individuals using the playground environment. This has involved the discussion of solar photospheric and terrestrial atmospheric absorption of UV radiation, reflection and transmission influenced by well recognised atmospheric mechanisms. Incident radiation at the earth’s surface has been discussed in relation to surface orientation, aspect and the albedo properties of materials common in the school environment. The potentially harmful effects of solar UV radiation and the techniques used to measure and model some of the commonly observed human responses to UV exposure have been presented. This provides a foundation upon which the discussion presented in this work now moves toward detailing the techniques developed to model the UV radiation to children using the school environment.

CHAPTER 2 MATERIALS AND METHODS

Modelling the UV received at the skin's surface in a school playground requires consideration of the playground location, the physical playground environment itself, the atmospheric parameters that affect the UV irradiance, and the orientation of exposed skin surfaces relative to the irradiating source. The methodology applied to this work considers each of these factors by application and modification of existing horizontal plane UV irradiance modelling techniques, measurement of personal UV exposure, and assessing the influence of the school playground environment. Specifically this has involved:

- Modelling the influence of the direct and diffuse component of solar UV radiation incident on a horizontal plane at the earth's surface with variation in atmospheric parameters including ozone and aerosol species;
- Modifying the modelled horizontal plane irradiance to account for the influence of the playground including shading and surface reflections in the UV waveband;
- Applying the modelled horizontal plane playground irradiance to make accurate predictions of the exposure received to human skin surfaces by application of measured exposure ratios received by body surfaces, and
- Validating the predictions made by measurement of the UV exposure received by a school population.

The modelled UV exposure affecting the skin surfaces of the face, neck, arm, hand and leg are presented for an Australian school playground situated in a sub-tropical latitude. The techniques presented can however be applied to other schools for predictions of exposure in the 0^{o} to 80^{o} SZA range. Measurements of the playground sky view and surface reflections were applied to the horizontal plane UV irradiance calculated for the playground's altitude and latitude. Ratios of UV exposure measured using mannequin field subjects and expressed relative to the horizontal plane were used to weight the modelled horizontal plane playground exposure providing estimates of the UV exposure received by unprotected skin surfaces of the body. The work is innovative as it provides a model that can predict day to day playground and body surface UV exposures which can be used to assist schools and students in understanding their local UV environment.

2.1 Instrumentation

2.1.1 Scanning spectroradiometer

Measurements of UV exposure made over the surface of the human body are critical toward understanding exposure risk in a student population. The distributions of cancerous squamous cell carcinoma are greatest on frequently exposed parts of the body including the dorsa of the arms and hands, and the face (Pearl and Scott 1986; Kricker et al. 1990; Raasch et al. 1998). By developing a technique to map realistic UV exposure distributions over the surface of the body, distributions of pre-cancerous and cancerous lesions resulting from exposure to sunlight may be better understood. In this research a polysulpone dosimeter technique has been further developed to map detailed UV exposure distributions over the human body. Additionally, UV exposures measured to the student population in the school playground have been measured using polysulphone dosimeters. UV exposures measured to the student population were calibrated to the University of Southern Queensland's scanning spectroradiometer (model DTM300, Bentham Instruments, Reading UK). This instrument is a double grating monchromator which measures the UV spectrum incident on a horizontal plane on each 10 minute interval between 5:00am and 7:00pm, Australian Eastern Standard Time (AEST) daily. The spectroradiometer is located on a roof top site at the USQ Toowoomba campus and has a virtually unobstructed view of the horizon, with some tree canopies covering the south-western region of the sky up to an elevation of approximately 5^{o}. The accuracy of the irradiance measured by this instrument is quoted at ±10% (Parisi & Downs 2004), including ±5.2% uncertainty in temporal stability measured against the output of the instrument's 150 W quartz tungsten halogen (QTH) lamp, ±1.1% uncertainty due to variation in wavelength response, ±0.8% uncertainty in the cosine response of the instrument diffuser, ±0.1% dark count variability and ±3% uncertainty in the traceability of the QTH lamp calibrated to the National Physical Laboratory, UK standard.

2.1.2 Broadband meter

Field measurements of UV radiation were made using a portable broadband UV meter (Solar Light Co., model 3D, Philadelphia, PA 19126). The broadband UV meter was used to measure the UV transmission through various playground shade cloths and to determine the UV reflected from various playground surfaces. This meter has a measured uncertainty of ±17% including a ±12% uncertainty in temporal stability measured against a constant UV emitting source (Solar Light Co. Xenon arc lamp) and ±5% variation in cosine response for incident radiation received at angles up to 80^{o} from the input diffuser. Additional uncertainties resulting from the measurement of reflected radiation of surfaces oriented in the horizontal and vertical plane are discussed in Chapter 4.

2.2 Miniaturised polysulphone dosimetry and measurements of body site exposure

The UV exposure received by the body was measured so that modelled horizontal plane playground exposures could be weighted to the UV surface distributions of frequently exposed regions of the body, namely the face, neck, arms, hand and leg. This technique was initially employed by Davis et al. (1976), however for this research the dosimeters were miniaturised to allow for high density placement. Measurements of ultraviolet exposure were made using miniaturised polysulphone dosimeters which exhibit changes in optical absorbance when exposed to UVB radiation. The miniaturised flexible dosimeters were attached to the surface topography of a life sized mannequin headform model (Figure 2.1) and life sized body mannequin (Figure 2.2). The body mannequin has a height of 178 cm and was taken to represent the height of a high school aged student. Measurements of personal exposure were also made by attaching dosimeters to the exposed skin surfaces of school students. Each miniaturised dosimeter was made from flexible card frame measuring approximately 10 mm by 15 mm with a clear circular aperture of 6 mm over which polysulphone film of an approximate thickness of 40 μm was adhered. (The manufacturing process of the polysulphone film used in this research is detailed in Appendix A). Pre- and post- exposure measurements of polysulphone film absorbance were made at four locations over the dosimeter aperture and averaged to minimise inconsistencies in the measurement of the film. The change in absorbance is defined as:

$$\Delta A = A_{post} - A_{pre} \qquad (2.1)$$

Measurements of the polysulphone absorbance, *ΔA* were made at 330 nm using a spectrophotometer (model 1601, Shimadzu Co., Kyoto, Japan). This wavelength represents the approximate maximum change in optical absorbance for 40 μm thick polysulphone film which has a strong spectral response in the UVB (CIE 1992) that can further be calibrated to the erythemal response of human skin.

Figure 2.1: Life sized headform mannequin model photographed at a school playground measurement site. Horizontal plane exposures were recorded in proximity to the mannequin. Horizontal plane dosimeters can be seen in the figure foreground (green arrow) for this experiment which measured facial UV exposure distribution in a low sky view environment.

Figure 2.2: Life sized mannequin model dressed in school uniform. The photograph was taken in an open field measurement site at the USQ, Toowoomba campus (28^{o}S, 152^{o}E). This site was used to measure the three dimensional surface exposures presented in Chapter 3.

2.2.1 Mannequin measurements of exposure ratio

Exposures measured by dosimeters placed on the headform and body mannequin were expressed relative to the horizontal plane exposure which was measured in proximity to both mannequins. For the results presented here, the exposure measured at any mannequin body site and expressed relative to the horizontal plane exposure was given by:

$$ER = \frac{E_{site}}{E_{hor}} \qquad (2.2)$$

where *ER* is the exposure ratio of the UV exposure measured by the polysulphone dosimeters at any given body site, E_{site}, and expressed relative to the maximum received exposure measured on a horizontal plane, E_{hor}. The erythemally effective exposures, *E* were calculated using the third order polynomial approximation to the calibrated erythemally effective exposure given with increasing change in optical absorbency measured at 330 nm (Diffey 1989):

$$E = K(9\Delta A^3 + \Delta A^2 + \Delta A) \qquad (2.3)$$

In the equation, ΔA is the change in polysulphone film absorbance measured at 330 nm and K (Jm^{-2}) is a constant that is eliminated in the ratio, ER. The mean uncertainty of the miniaturised dosimeters calculated as the range in measured ΔA over a series of 46 dosimeter sets which received identical UV exposures was determined to be ±6% of the recorded horizontal plane exposure in the 0^o to 30^o SZA range, ±9% in the 30^o-50^o SZA range and ±16% in the 50^o-80^o SZA range. Uncertainty in the measured exposure ratio, ER is therefore taken to be in the order of ±12%, ±18% and ±32% for the 0^o-30^o, 30^o-50^o and 50^o-80^o SZA ranges respectively. The uncertainty in the measured ER increases with SZA due to increases in the ratio between the measured ranges of ΔA and decreasing horizontal plane exposure experienced at increasing SZA (Measurements of ΔA for the 46 sets of dosimeters used to determine the stated uncertainty in ER are provided in Appendix B.2).

2.2.1.1 Mannequin body surface measurement sites

Measurements of ER were taken on up to 1453 body sites including the mannequin face (709 sites), neck (98 sites), forearm (166 sites), hand (247 sites) and leg (233 sites). Sites on each of the body parts were organised into horizontal and vertical contours. Contours on the face and hand were separated by 5 mm, 10 mm on the arm and neck, and 20 mm on the leg. To visualise measured patterns in the ER for the UV a three dimensional wireframe mesh of each of the face, neck, arm, hand and leg was developed from measurements of body surface sites. The developed body surface meshes were built to the measured spatial contour resolutions of the face, neck, arm, hand and leg models. Wireframe representations of body exposure patterns show the positions of horizontal and vertical contours in which the intersection of a horizontal and vertical contour shows the measured position in three dimensional space of the body site which was also marked on the respective mannequin model. These sites were measured and marked onto the mannequin models by application of a laser mounted to an optical bench and jig assembly (Figure 2.3). Exposures measured by polysulphone dosimeters placed at marked body sites on each mannequin were represented by colour levels on the developed wireframe mesh of each respective body part expressing the UV exposure relative to the horizontal plane exposure measured in proximity to the mannequin in the ER range 0 to 100%. Figure 2.4 is a comparison of the mannequin headform model and wireframe mesh developed in three dimensional space.

(a) (b)

Figure 2.3: Optical bench assembly. (a) Marking the mannequin headform (b) Marking the leg of the body mannequin.

(a) (b)

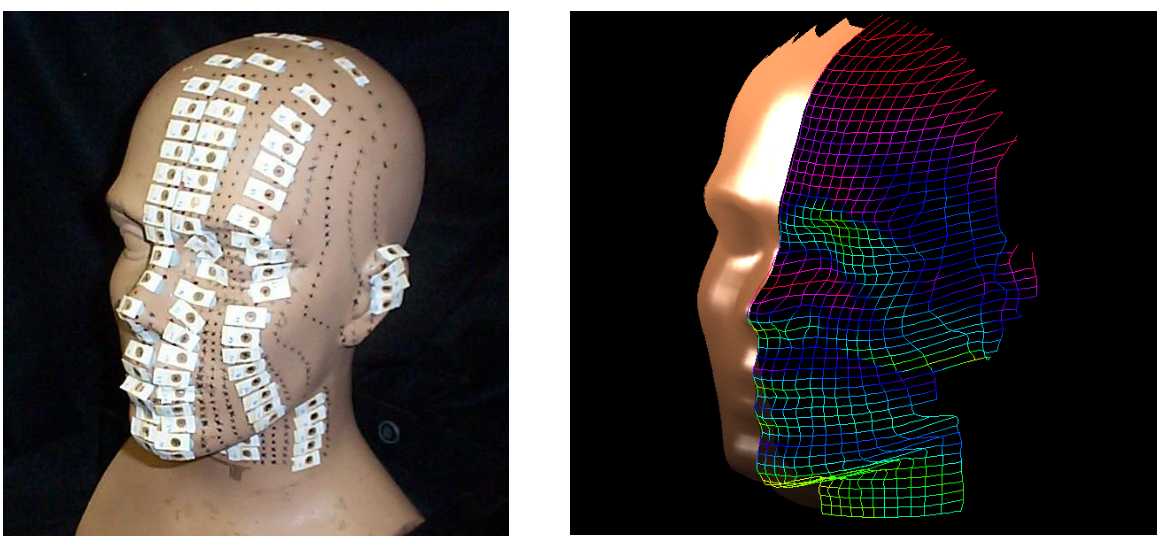

Figure 2.4: Mannequin headform and its wireframe mesh model. Marked dosimeter placement sites (a) correspond with horizontal and vertical contour mesh intersections (b) Mesh colouring was used to highlight the measured ER pattern. Colour interpolation between measurement sites (wireframe intersections) is detailed in Appendix C.

For field measurements of UV exposure, both mannequins were placed on rotating platforms that completed approximately two revolutions per minute. As the movement of a mannequin placed on the rotating platform was fast compared to the changing SZA in the field, the influence of mannequin aspect relative to the environment was negated and measured exposures were taken to represent the random movements of an upright human subject. The rotating platform and mannequins were placed in an open environment which was located at least 30 m from the nearest buildings inside the grounds of the University of Southern Queensland's Toowoomba campus (28^{o}S, 152^{o}E). The field measurement site has a sky view of 95% and was covered by grass for most of the field experiments with the degree of grass cover being sparse in 2007 due to drought conditions. Measurements of the ER were made over a four year period between 2005 and 2008. Measurements of ER were taken under various cloud cover conditions during periods when the SZA varied from 0^{o}-30^{o}, 30^{o}-50^{o} and 50^{o}-80^{o}. These SZA ranges were chosen to represent three periods of the summer day in a low latitude location, namely the highest UV irradiance period of the day either side of midday, 0^{o}-30^{o}, the period following the highest irradiance period and leading into the lowest UV irradiance period of the day, 30^{o}-50^{o} and the lowest UV irradiance period of the day, 50^{o}-80^{o}. The SZA ranges cover the most significant range of SZA that have a biologically effective influence on exposure and can be applied at any latitude to show patterns in human exposure with daily and seasonal variation.

2.2.2 Calibrated measurements of personal UV exposure

Miniaturised polysulphone dosimeters used to measure personal UV exposures were calibrated to the erythemally effective UV, represented by the equation:

$$UVE = \int_{0}^{t} \int_{280nm}^{400nm} S(\lambda,t)A(\lambda)d\lambda dt \qquad (2.4)$$

where *UVE* represents the measured erythemally effective UV exposure, $A(\lambda)$ is the erythemal action spectrum (CIE 1987), and $S(\lambda,t)$ is the measured horizontal plane UV irradiance integrated over the biologically effective UV waveband, λ from 280 nm to 400 nm, and over the exposure time interval, *t*.

Dosimeters that were utilised in measuring personal UVE were kept in light proof containers prior to field exposure. The measured change in dosimeter absorbance, ΔA was determined at least 24 hours following field exposure of the dosimeters to allow for the polysulphone dark reaction following exposure to solar UV (Davis et al. 1976). Given the possibility for seasonal variation in polysulphone film exposure response (Wong et al. 1995), the measured change in dosimeter absorbance was calibrated to the erythemally effective UV during cloud free days for the months of February, April and May. These dates were chosen as they roughly divide the 5 month period between February and June into three periods, namely, late summer early autumn (summer-autumn), mid autumn, and late autumn early winter (autumn-winter). The calibrated response of the polysulphone film dosimeters employed in measuring personal UV exposures for this work are listed in Appendix B.1. The measured change in dosimeter absorbance at 330 nm was calibrated to the horizontal plane erythemally effective UV measured by the USQ's scanning spectroradiometer to determine personal UVE. The summertime dosimeter saturation limit was measured at a ΔA of 0.7 and represents an exposure period of 5 hours. Calibrated polysulphone dosimeter exposures were used to measure personal exposures to children using the model school playground between February and June 2008. Erythemally weighted UVE exposures measured by calibrated polysulphone dosimeters were expressed in units of standard erythema dose (SED) where 1 SED represents 100 Jm^{-2} of erythemally effective UV (Diffey et al. 1997) and 2 SED represents the approximate exposure required to produce mildly perceptible erythema in fair skinned (type I) individuals 12 to 24 hours following an exposure event.

The total maximum uncertainty in the measurement of the personal UVE was determined to be in the order of $\pm 26\%$ including the uncertainty estimate of $\pm 10\%$ based on the spectroradiometer measurement of the horizontal plane irradiance and $\pm 16\%$ maximum uncertainty in measured polysulphone film absorbance measured in the 50^{o} to 80^{o} SZA range. The uncertainty estimate of the dosimeters quoted here exceeds the coefficient of variation of 10% determined by Diffey (1987) for polysulphone dosimeters not exceeding a ΔA of 0.3, however is within the upper limit of 30% further specified by Diffey (1987) for a ΔA less than 0.4.

2.3 Modelling the horizontal plane ultraviolet irradiance

Measured UV exposure distributions for each of the face, neck, arm, hand and leg expressed as a ratio of the horizontal plane UV exposure in each of the three SZA ranges were used to weight the modelled horizontal plane playground exposure. The horizontal plane playground UV exposure was determined by weighting the direct and diffuse components of the horizontal plane UV modelled in an open environment to the measured sky view and albedo of various playground structures surveyed at 822 playground sites located within the grounds of the model school. The horizontal plane playground UV exposure was determined for the winter and summer solstice over the entire area of the selected school playground. In this way the extremes in UV exposure received within the playground environment could be assessed for the playground environment itself and for the students using that environment.

2.3.1 The ultraviolet irradiance model

The radiative transfer of UV through the atmosphere is affected by the refraction and absorption of air, and aerosols including ozone, cloud and particulate matter. The processes that govern the absorption and refraction of the direct solar beam by each of these atmospheric constituents are quantified in this research by the use of semi-empirical equations. The diffuse component of the UV that reaches the earth's surface which needs to account for the random scattering and reflection of UV in a turbid atmosphere is estimated through the use of radiative transfer equations. The direct UV irradiance modelled at the earth’s surface in this research was based on Rundel’s (1986) formulation of the Green, Cross and Smith (1980) and Schippnick and Green (1982) improvement to the original Green, Sawada and Shettle (1974) semi-empirical model. The horizontal plane diffuse UV irradiance model is based on the equations of Green, Cross and Smith (1980). These equations employ the radiatve transfer calculations of Braslau and Dave (1973) and Dave and Halpern (1976) for diffuse UV reaching the terrestrial surface. The diffuse UV model was found to overestimate the received surface irradiance being the greater proportion of the total modelled UV, however for this research this overestimate resulted in better predictions of the modelled horizontal plane UV compared to measurements made in Toowoomba which represent a higher UV irradiance environment than the environment in which the original model was developed (Northern Hemisphere).

2.3.1.1 Extra-terrestrial spectral irradiance

The extra-terrestrial spectral UV irradiance incident on the earth's atmosphere was modelled over the biologically significant 280 nm to 400 nm waveband using the following estimate (Schippnick and Green 1982):

$$H(\lambda) = H_b(\lambda)(1 + \sum_i A_i \exp - (\lambda - \lambda_i)^2 / 2\sigma_i^2) \qquad (2.5)$$

$$\text{where } H_b(\lambda) = K\left(\frac{\lambda_o}{\lambda}\right)^5 \frac{\exp(p) - 1}{\exp(p\lambda_o / \lambda) - 1}$$

$H(\lambda)$ is the extra-terrestrial irradiance at wavelength λ, K = 0.582 $Wm^{-2}nm^{-1}$, p = 9.102, λ_o = 300 nm,

And:

λ_i	A_i	σ_i
279.5	- 0.738	2.96
286.1	- 0.485	1.57
300.4	- 0.243	1.80
333.2	+0.192	4.26
358.5	-0.167	2.01
368.0	+0.097	2.43

Figure 2.5 displays the resultant extra-terrestrial spectrum of equation 2.5. The N Fraunhoffer line caused by solar photospheric absorption of iron at 358 nm and a Magnesium absorption line at 285 nm are prominent in the figure.

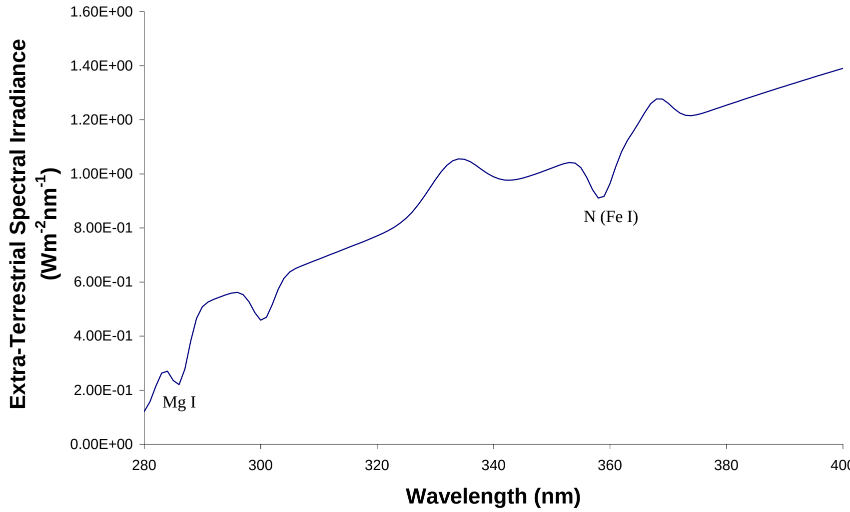

Figure 2.5: Extra-terrestrial UV spectrum modelled over the 280 nm to 400 nm waveband.

2.3.1.2 Earth-Sun distance

Variation in the extra-terrestrial UV irradiance incident on the earth's atmosphere due to the elliptical orbit of the earth was accounted for in the model. Equation 2.6 (Josefsson 1986) represents the factor by which the spectral extra-terrestrial irradiance was multiplied to account for the seasonal variation in the earth-sun distance which is closest during January and greatest in June. The extra-terrestrial irradiance varies by approximately 6.7% throughout the year (Björn 1989).

$$f = 1 + 0.033\cos(2\pi D_n / 365.25) \qquad (2.6)$$

where f is the seasonal extra-terrestrial intensity variation factor, and D_n is the day number of the year.

2.3.1.3 The direct UV irradiance modelled at the earth's surface

The direct component of the UV irradiance varies with altitude above sea level. This variation was considered by the direct application of Rundel's (1986) algorithm formulated from the improvements of Green, Cross and Smith (1980) and Schippnick and Green (1982). The sequence required to determine the direct UV irradiance at sea level and at altitude is given by equation 2.7 (Green, Cross & Smith 1980):

$$U_{dir}(\lambda, \theta, y) = \mu H(\lambda) e^{-A_t} \qquad (2.7)$$

where $U_{dir}(\lambda, \theta, y)$ is the local direct spectral irradiance ($Wm^{-2}nm^{-1}$) at a given wavelength, SZA, and altitude. A_t is the attenuating thickness of the atmosphere along the path of the direct solar beam, $H(\lambda)$ is the extra-terrestrial spectral irradiance (equation 2.4), and μ is the cosine response, $\cos(\theta)$, such that U_{dir} is the modelled direct UV that is incident on a horizontal plane,

$$\text{where, } A_t = \sum_j \frac{\tau_j}{\mu_j}$$

and where τ_1, τ_2, τ_3 are the resultant product of the wavelength dependent species optical depth and altitude dependent concentrations of air, ozone and aerosols respectively, and μ_1, μ_2, μ_3 are geometric cosine functions that describe each of the aforementioned species relative to a spherical earth.

$$\text{And, } \mu_j = \left(\frac{\mu^2 + t_j}{1 + t_j} \right)^{1/2}$$

where t_1, t_2, t_3 are constants that depend on the altitude distribution of the air, ozone, and aerosol species.

2.3.1.3.1 Standing surfaces contributions to the direct ultraviolet irradiance

Contributions to the direct UV were further modified depending on the measured albedo of standing surfaces located in proximity to the modelled site. In this way vertically incident contributions to the horizontal plane direct UV irradiance were increased depending on the location of nearby buildings and other playground structures:

$$U_{dir}(\lambda,\theta,y,A_s) = \mu H(\lambda)e^{-A_t} + A_{dir} \qquad (2.8)$$

Here, U_{dir} is the modelled direct UV component of the global UV irradiance (direct vertical component), and A_{dir} is the vertical cosine component of direct UV due to the standing surface albedo of a nearby vertical surface which is dependent on A_s, the measured standing surface albedo (equation 2.9). The global direct component of the UV irradiance (U_{dir}) was formulated in this instance as the cosine of the sun normal direct UV (Figure 2.6). The direct component of standing surface albedo, A_{dir}, takes the same value as the product of the standing surface albedo (A_s) and the cosine of the sun normal UV, U_{sn}, giving an equation dependent on U_{dir}, the direct UV irradiance and the standing surface albedo:

$$\begin{aligned} A_{dir} &= A_s U_{sn}\cos(SZA) \\ A_{dir} &= A_s \frac{U_{dir}}{\cos(SZA)}\cos(SZA) \\ A_{dir} &= A_s U_{dir} \end{aligned} \qquad (2.9)$$

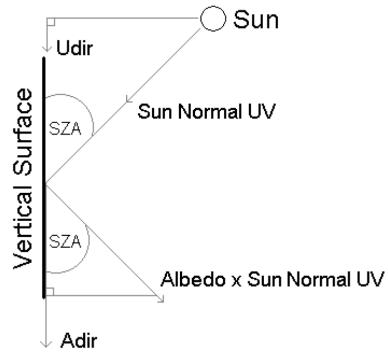

Figure 2.6: Direct albedo UV contribution (A_{dir}) to a horizontal plane (ground) surface due to the influence of a nearby standing vertical surface.

2.3.1.4 The diffuse UV irradiance modelled at the earth's surface

Contributions to the diffuse irradiance due to surface reflection (albedo) were implemented originally by application of Rundel's (1986) formulation of the Green, Cross and Smith (1980) and Schippnick and Green (1982) modifications to Green, Sawada and Shettle's (1974) algorithm for modelling the diffuse UV irradiance contribution at the earth's surface. The diffuse component of the total UV irradiance determined by Schippnick and Green (1982) that was implemented in Rundel's (1986) algorithm was found to be less than the diffuse irradiance calculated in the original Green, Sawada and Shettle (1974) algorithm. The original modification to the diffuse irradiance reduced the predicted global UV irradiance when compared with measurements of the horizontal plane UV irradiance made with the USQ's scanning spectroradiometer. This discrepancy was overcome by reverting to a modification of the older Green, Sawada and Shettle (1974) diffuse component equation. The modification to the Green, Sawada & Shettle (1974) diffuse irradiance was included to account for variation in the diffuse horizontal plane UV irradiance with altitude and surface albedo (equation 2.10).

The modifications suggested by Green, Sawada and Shettle (1974, p.257) alter the parameters K_{ap} and q_2 respectively, to account for variation in altitude. The modified parameters are listed under equation 2.10, the semi-empirical parameterisation of the diffuse irradiance, $U_{diff}(\lambda,\theta,y)$ ($Wm^{-2}nm^{-1}$) listed by Green, Sawada and Shettle (1974):

$$U_{diff}(\lambda,\theta,y) = H(\lambda)e^{-D_t(\theta,\lambda)} \qquad (2.10)$$

$$\text{where } D_t(\theta,\lambda) = K_{oz}(e^{\kappa k_0 w_{oz} - (\lambda-\lambda_0)/(\delta speq\theta)})seq(\theta,q_1) + K_{ap}seq(\theta,q_2)$$

$$speq\theta = \frac{1}{\left(1-\frac{\sin p_\theta}{q}\right)^{1/p}}$$

$$seq_i(\theta,q_i) = \left(1-\left(\frac{\sin^2\theta}{q_i}\right)\right)^{-1/2}$$

$K_{ap} = 1.255$ at sea level, $q_2 = 1.32$ at sea level, $K_{oz} = 1.62$, $\kappa = 2.40$, $\delta = 7.48$,

$q_1 = 1.10$, $q = 1.148$, and $p = 4$

and at altitude, $K_{ap} = 0.872(1+0.179y+0.0487(\tau_p - 0.538)^2)$

$$q_2 = 1.06(1+0.106y)$$

where y is the altitude above sea level expressed in kilometers, and τ_p is a wavelength and altitude dependent atmospheric parameter (product of the aerosol optical depth and aerosol species concentration). The modification of K_{ap} for variation in altitude was used for diffuse calculations of the UV irradiance incident in a playground environment.

Equation 2.10 was further modified by adding the surface albedo contribution formulated by Schippnick and Green (1982, p.96). The surface albedo contribution added to equation 2.11 and used by the final algorithm was originally intended for use with the omitted diffuse equation used by Rundel's (1986) algorithm and has been included here as an improvement to the Green, Sawada, and Shettle (1974) diffuse equation amended for altitude.

$$U_{diff}(\lambda,\theta,y,A_g) = H(\lambda)e^{-D_t(\theta,\lambda)} + A_{diff} \tag{2.11}$$

$$\text{where, } A_{diff} = r(\lambda)S_u$$

S_u is the upward irradiance resulting from the local ground surface albedo, and $r(\lambda)$ is the air reflectivity function describing the spectral reflectivity of the above atmosphere such that A_{diff} is the total downward albedo contribution of the diffuse irradiance resulting from downward atmospheric backscatter.

$$\text{Furthermore, } S_u = \frac{A_g G_s E_d}{1 - r(\lambda)A_g}$$

where A_g is the site ground surface albedo measured 0.3 m from the playground surface, G_s is the global ultraviolet irradiance at sea level without an albedo contribution and, E_d is the normalised altitude dependence defined as the ratio of the albedo contribution at altitude to the albedo contribution at sea level.

The modified formula (equation 2.11) increases the diffuse component of the total UV irradiance over most of the day such that the greatest increases are calculated near solar noon. By utilising equation 2.11, it was found that total daily exposures were more closely matched to the erythemally effective exposure measured by the scanning spectroradiometer. The calculated component of the diffuse irradiance is typically less at SZAs near sunrise and sunset than the calculated diffuse irradiance found using Green, Sawada & Shettle's, (1974) unmodified formula (equation 2.10). However, because the erythemally effective exposure falls significantly at large SZA, equation 2.11 was selected as the preferred representation of the diffuse UV irradiance. For applications that require accurate modelling of the ratio of diffuse to direct UV, either the original Green, Sawada and Shettle (1974) or Rundel's (1986) algorithm are recommended. For Northern Hemisphere model applications, Rundel's (1986) algorithm may provide better estimates of the horizontal plane UV irradiance than the hybrid employed for this work.

2.3.1.4.1 Modification of the diffuse ultraviolet irradiance with sky view

The resultant diffuse representation of the UV irradiance was further modified to account for variation in site sky view (equation 2.12):

$$U_{diff}(\lambda, \theta, y, A_g, V) = V(H(\lambda)e^{-D_t(\theta,\lambda)} + A_{diff}) \qquad (2.12)$$

where *V* is the site sky view expressed as a value between 0 and 1. For sites located in the playground that had an unobstructed horizon (100% sky view) *V=1*. This modification to the diffuse UV irradiance incident on a horizontal plane was applied to a total of 822 playground sites in which the sky view was measured using the photographic technique detailed in Section 2.4.

2.3.1.5 Erythemally effective ultraviolet irradiance

The total or global UV irradiance was determined by summing the direct and diffuse components formulated by the above semi-empirical equations 2.8 and 2.12. The result is equation 2.13:

$$G_t(\lambda, \theta, y, A_g, A_s, V) = U_{dir}(\lambda, \theta, y, A_s) + U_{diff}(\lambda, \theta, y, A_g, V) \qquad (2.13)$$

The global UV irradiance was weighted to the erythemally effective action spectrum (CIE 1987) (equation 2.14):

$$E_t(\lambda, \theta, y, A_g, A_s, V) = G_t(\lambda, \theta, y, A_g, A_s, V)A(\lambda) \qquad (2.14)$$

where $E_t(\lambda, \theta, y, A_g, A_s, V)$ is the erythemal weighted UV irradiance expressed in Wm^{-2} specified for a given wavelength, SZA, altitude, site ground surface albedo, site standing surface albedo and site sky view, $A(\lambda)$ is the erythemal action spectrum (CIE 1987), and $G_t(\lambda, \theta, y, A_g, A_s, V)$ is the global UV irradiance (equation 2.13).

2.3.2 The ultraviolet exposure model

The horizontal plane spectral erythemally effective UV irradiance modelled over the 280 nm to 400 nm range was integrated to provide the erythemally effective UV irradiance in Wm^{-2} at each 5 minute interval in the modelled exposure period. UV_{ery}, the erythemally effective UV exposure was determined by integrating the erythemally effective UV irradiance with respect to the modelled exposure period, *t*, using a trapezoidal integration technique to determine the erythemally effective UV exposure in Jm^{-2}:

$$UV_{ery} = \int_{0}^{t} \int_{280nm}^{400nm} E_t(\lambda, \theta, y, A_g, A_s, V) d\lambda dt \qquad (2.15)$$

Appendix D lists the principle component of the horizontal plane UV exposure model code which was developed using Microsoft Visual Basic (version 6).

2.4 Survey work and image processing

Albedo contributions from ground and vertical standing surfaces to the modelled direct and diffuse UV exposure were determined at each of the series of 822 playground survey sites. Additionally, the sky view weighted diffuse UV irradiance modelled over the playground environment was measured at each of the playground survey sites. Both the albedo and site sky view were determined by employing a photographic technique to survey the school playground being modelled.

2.4.1 Measurement of playground sky view

Measurements of the sky view were taken by application of an image processing algorithm to classify sky regions from the local surface environment for a ground observer. A series of 16 images were taken at each of 822 sites located in the model school playground to form single composite site images. Images were taken with a Digital SLR camera (50 mm lens) at f11 (Canon EOS 350D). The composite sky view image developed from 16 images taken at each of the model school playground site locations covers 32^o to 90^o in zenith angle (ZA) and 0^o to 360^o in azimuth. The camera used to take each site image set was fitted to a tripod, levelled and positioned with respect to north. The height of the mounted camera objective lens was approximately 840 mm above the playground surface. This technique was preferred as hemispherical lenses were not available at the time the survey work was commenced resulting in parrallax error associated with imaging the sky at different orientations to complete composite site images, and not imaging regions of the sky above 32^o in ZA.

The panoramic composite site image developed for this research was found to be the most convenient for plotting the position of the solar disk to determine patterns in playground shade density. The sky view less than 32^o in ZA that was not photographed was predominately clear of surface obstructions for most playground sites. The area not represented in site composite images makes up 36% of the total sky view. Sites that were covered by surface objects above this range were noted upon survey of the study site and estimates of the unmeasured sky view less than 32^o in ZA were included to determine the total sky view. For measurements of the sky view presented in this research, several shade structures were found to cover the sky above 32^o in ZA and for these cases the percentage of cover less than 32^o was estimated from UV transmission measurements of each playground shade cloth used by respective shade structures (Appendix E).

2.4.1.1 Sky view image area

To develop a composite site image of the sky view, photographs were taken orientated with respect to N, NE, E, SE, S, SW, W, NW and repeated with the camera tilted at approximately 30^o to the horizon. The first north facing image in each composite sky view image was orientated with respect to the facings of the playground boundary fence which had a north-south aspect. The location of true north was corrected for by comparison of photographed solar positions to the expected azimuth of the sun for the respective date and time at which the sun was photographed. The azimuth image limits for each of the N, NE, E, SE, S, SW, W, and NW facings were set at 243 pixels each. This was determined by comparing the overlap between respective image facings. Figure 2.7 highlights the overlap in three survey site sky views of the horizon facing SW, W and NW. The highlighted length between overlapping images shown in the example of Figure 2.7 is 103 pixels. Site image facings were photographed to a horizontal resolution of 346 pixels each which were cut down to a horizontal width of 243 pixels to produce the 360^{o} panoramic site view of the horizon.

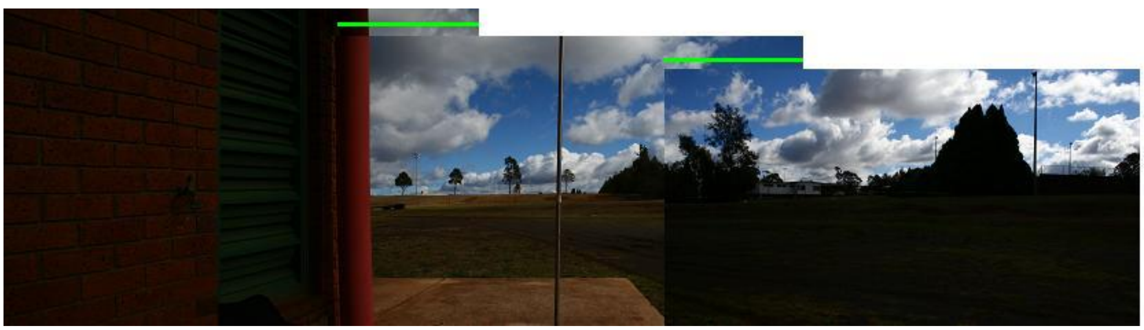

Figure 2.7: An example of image overlap in a panoramic composite image of the horizon. The overlap of 103 pixels is highlighted in green in the figure.

The ZA limits of the image field of view were determined by simple trigonometric measurements of a stand of known height set at various distances from the camera lens. Figure 2.8 shows how the upper and lower ZA limit of images were determined with the camera orientated parallel to the horizon. The height of the camera lens when placed on the field tripod was measured at 840 mm. This height was also marked on a vertical standing pole. The image in Figure 2.8(b) shows the position of this height marked on the standing pole with white tape. This position marks the horizon limit (ZA 90^{o}). As the bottom limit of the image captured by the camera lens marks the bottom of the pole which is 840 mm from the central axis of the horizontally orientated camera, the top of the pole in the image was determined to be 840 mm from the camera's horizon axis. The limit of elevation measured by the lens which was positioned 2000 mm from the stand and pole was determined to be 22.8^o (67.2^o in ZA).

(a)

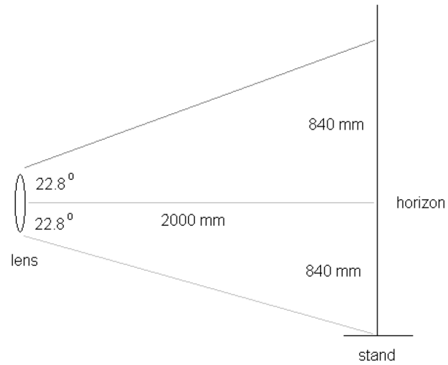

(b)

Figure 2.8: Calculating the lower ZA limit for images taken with the mounted camera orientated in a horizontal plane. The green arrow in (b) marks the approximate height of the camera lens (840 mm) and the horizon limit.

The calculation of the lower ZA limit for images taken with the camera orientated at approximately 30^o to the horizontal plane is illustrated in Figure 2.9. Here, images of the vertical stand and pole were taken with the camera orientated at its greatest tripod elevation (approximately 30^o) at increasingly further distances from the vertically standing pole until its top could just be imaged in the resulting photograph. This limit was determined to be 9.5^o (ZA 80.5^o).

(a)

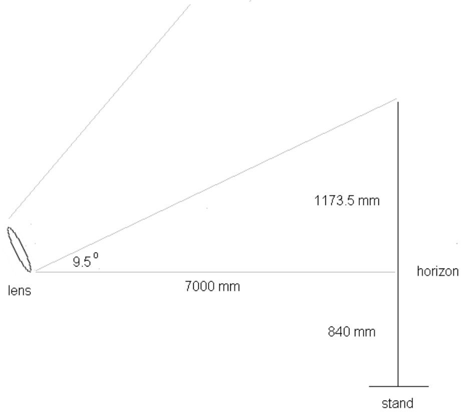

(b)

Figure 2.9: Calculating the lower ZA limit for images taken with the mounted camera orientated at its greatest elevation. The green arrow in (b) marks the top of the vertically standing pole with the camera 7 m away.

Measurements of the top of the stand and pole taken at a series of distances from 1 m to 12 m away were used to determine ZA limits in composite image facings whereby images taken at maximum tripod elevation were overlaid onto images taken with the camera orientated in the horizontal plane. Matching the visible horizon between images taken at maximum elevation and images taken with the camera orientated in the horizontal plane determined the vertical height of composite images to be 383 pixels. Figure 2.10 shows the calculated ZA limits measured from the top of the vertical stand and pole assembly. The extreme ZA limit of the camera when orientated to its maximum elevation and determined by extrapolating the limits in Figure 2.10 was estimated to be 32.3^{o} in ZA for the top pixel in the 383 pixel height limit of the composite image area.

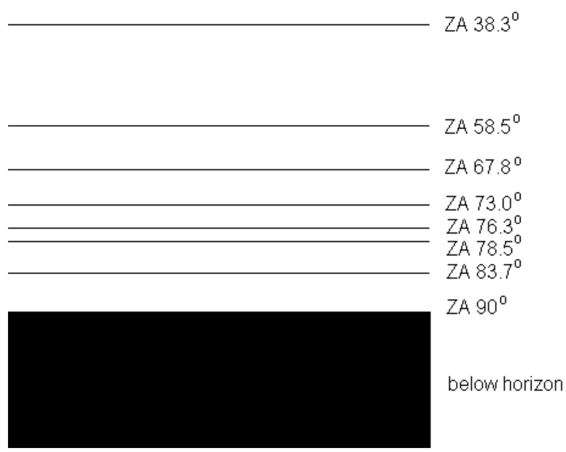

Figure 2.10: ZA limits of composite images measured with the camera in the horizontal plane and at maximum elevation. The limits listed in the figure were determined from trigonometric tangent ratios of the stand and pole height to camera distance.

The complete composite sky view template made from N, NE, E, SE, S, SW, W, NW images taken with the camera oriented parallel to the horizontal plane and same respective images with the camera orientated to its maximum elevation are shown in Figure 2.11(a). The approximate area of the sky photographed in the 16 images of each sky view composite image is given in Figure 2.11(b). Some overlapping of regions in the sky occur closer toward the zenith. Sky view was determined at each playground site under clear sky conditions as the percentage of blue pixels available in the composite image sky view.

(a)

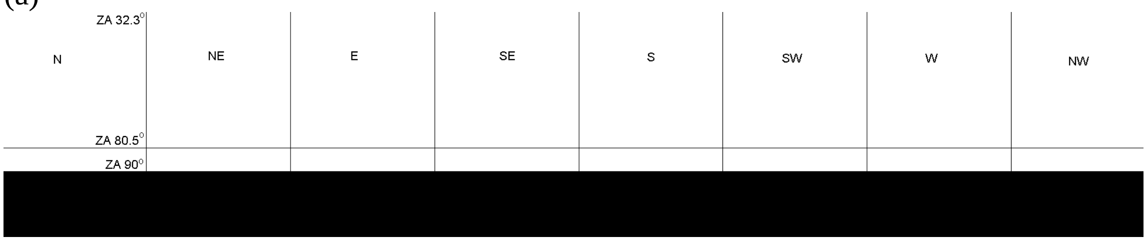

(b)

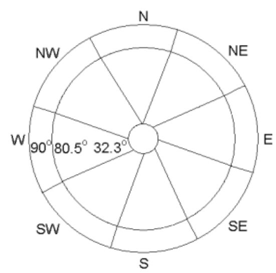

Figure 2.11: (a) Composite site sky view image divided into horizontal plane images (bottom series) and images taken at maximum elevation (top series); (b) fish eye lens view of the approximate regions of the sky imaged at each respective facing. The limits of the imaged area are from 32.3^o to 90^o in ZA.

2.4.1.2 Image processing

The image processed sky view was determined as the percentage of pixels classified as "sky" in each site composite image and included the sky view estimate for a ZA less than 32^o. For the image processing algorithm, the difference between the blue and red (B-R) RGB colour level of each pixel in the unprocessed photograph of each composite playground site was used to determine if an image pixel would be classified as "sky" or surface obstruction. Pixels having a higher blue RGB level in unprocessed photographs produce a positive B-R difference. For an unprocessed image pixel to be classified as a "sky" pixel by the image processing algorithm used here, the RGB blue level needed to be significantly higher than the respective RGB red pixel level. For this research, the threshold B-R value was set at 0.8 for most site images, which classified the majority of sky pixels correctly. The threshold B-R value was varied from 0.8 to accomodate changes in image brightness between site image sets. Changes in the B-R threshold were made following comparison between the unprocessed and “sky” pixel processed site image whereby increases in the threshold level were made to increase the classification of “sky” pixels and decreases in the thresold value were made to increase the processed level of surface obstructions. Due to atmospheric scattering, particularly at low solar elevations, the red component of unprocessed RGB pixel levels made the classification of “sky” pixels difficult if a B-R threshold of 1 was used (pixels containing no RGB red colour level), therefore the maximum B-R threshold was set at 0.95. The image processing algorithm used to classify “sky” pixels from playground surface obstructions was written using MATLAB version 7 (The MathWorks, Inc. 2004) and is listed in Appendix D.5. Figure 2.12 compares a processed playground site composite image to the original playground site composite photograph. In the figure, pixels classified as “sky” were given the false colour blue, remaining pixels were classified as surface obstructions and coloured white. The site sky view was determined as:

$$\text{sky view (\%)} = \text{blue pixel count (\%)} + \text{estimate above } 32^{o} \text{ in ZA (\%)} \qquad (2.16)$$

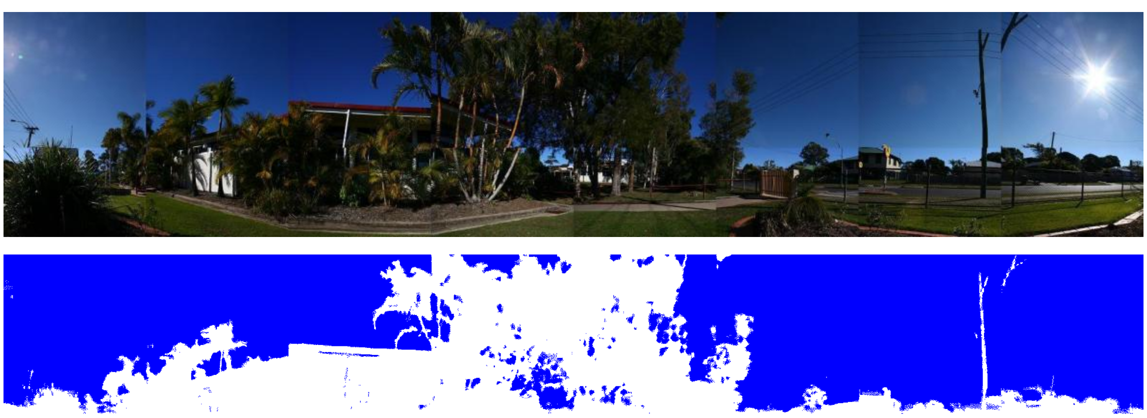

Figure 2.12: A composite playground site image (top) and the respective sky view processed image of the same site (bottom). The image of the solar disk was removed before processing.

It should be noted that the technique used to classify sky view does not distinguish between white cloud, the solar disk and surface objects in the unprocessed photograph and is similarly limited if blue surface objects are photographed. Blue surface structures and the solar disk were manually edited from the image before determining the site sky view percentage. Photographed playground site images were taken on days with no cloud cover where possible. For sites photographed that included sparse regions of cloud cover, the cloud was manually edited from the image before determining the site sky view percentage. An alternative method of removing heavy cloud cover was developed in which the number of colours in the composite image were reduced to 16 and areas of cloud were manually coloured blue. The sky view of the processed figure above, determined as the percentage of pixels classified as "sky" relative to the unobstructed sky view was calculated in this case to be 76% which was determined from the processed site image of 40% and the estimated unobstructed 36% sky view above the image limit of 32.8^{o} in ZA.

2.4.2 Ground and standing surface albedo contributions

2.4.2.1 Ground surface albedo contribution to the diffuse ultraviolet

The albedo of playground ground surfaces was measured using a portable broadband UV meter. Surface contributions to the modelled diffuse atmospheric backscatter (equation 2.11) were included at each survey site depending on the measured albedo of the site ground surface. The albedo of each site ground surface was determined by examining each survey site image to determine the playground site surface and was measured as the ratio of reflected UV to incident UV along the ground surface normal. Standing surface albedo was also measured in this research with respect to the surface normal.

2.4.2.2 Standing surface albedo contribution to the direct ultraviolet

Composite site images were examined to determine the relative area of vertical standing surfaces orientated with respect to North, East, South and West. Composite images were divided into four segments to approximate regions of surface orientation. Each region was classified as either clear (no albedo contribution), or was assigned the measured surface albedo of the various playground standing surfaces and an average standing surface albedo value was calculated for each playground site. Figure 2.13 shows how site standing albedo contributions were calculated for a site located near the school's library. Vertical standing structures, including both vegetation and buildings that were further than 2 m from the playground composite image site location were classified as "clear" for the calculation of standing site albedo. This was based on the assumption that surfaces further than 2 m from the site survey location made no significant direct albedo contribution to the surveyed site.

Figure 2.13: Standing surface albedo contribution estimate for a site located near the school's library. The total site standing surface albedo contribution of $A_S = 0.0425$ *was estimated from the average of 0 for a clear south facing region (image left), 0.11 for painted brickwork west facing (mid left image), 0 for the predominately clear north facing region (mid right) and 0.06 for east facing standing vegetation (image right).*

2.5 Integrating playground ultraviolet exposure and body site exposure ratio

The weighted albedo and sky view influence on the playground site horizontal plane UV exposure was determined at each of the 822 survey sites measured in the school playground. Estimates of erythemally effective exposure to the surfaces of the face, neck, arm, hand and leg were calculated by weighting individual site horizontal plane exposures to the measured exposure ratios of each respective body part for each of the 1453 sites measured on the mannequin headform and body models. The modelled erythemally effective UV exposure to any body site was calculated as:

$$UV_{site} = ER(UV_{ery}) \qquad (2.17)$$

where UV_{site} is the erythemally effective exposure at any given body site, ER is the body site exposure ratio and UV_{ery} the erythemally effective exposure calculated over the desired exposure period at a given playground site (equation 2.15).

2.6 Measurements of exposure to the student population

Modelled estimates of UV_{site} for each respective body part were compared with measurements of the erythemally effective exposure received by school children using the school playground. Ethics clearance was given by the USQ human ethics committee to measure a total of 147 personal UV exposures to school children in the period between February and June 2008 at the school playground. During the personal exposure measurement period, children were instructed in the proper handling of the polysulphone film badges and asked to apply them to the skin normally exposed to solar UV. This included application of the badge frames using medical tape onto regions classified as the face, neck, arm, hand or leg. Badges were attached at 8.30am (AEST) on each trial day under a covered area in the school playground and retrieved at 3.05pm (AEST) at the same location. Participating students were asked to complete a daily diary of the school playground locations they attended during each period and meal break of the day (Appendix F). Students were asked to complete their diaries for those areas where they spent the majority of each period or break time. Data on the degree of cloud cover, estimated in eighths (oktas) was measured by an observer on each trial day in the February through June period and the type of hat (voluntary at the study school) used by each participant was also recorded in the daily diary.

2.7 Summary of methods

The methodology presented details a technique to model the UV exposure received by the skin surface of students using a school environment. This involves modelling the horizontal plane UV exposure; modifying the horizontal plane exposure due to structural and other surface objects located in the playground influencing the sky view and albedo; and weighting the modelled playground exposure to the surface topography of the human form. Chapters 3, 4, and 5 detail exposure patterns measured to the mannequin headform and body models, highlight variations in the modelled playground UV exposure, and validate modelled values of personal body surface exposures with respect to measurements made over the student population.

CHAPTER 3 MEASUREMENT OF BODY SURFACE EXPOSURE

The pattern in UV exposure received by specific body sites, being dependent upon solar zenith angle is critical toward understanding frequency of incidence and anatomical distribution of NMSC present in worldwide populations. This chapter presents the measured UV exposure distribution received by surfaces of a headform and full body mannequin with variation in SZA to a spatial resolution of between 5 mm and 20 mm to the face, neck, forearm, hand and leg. The effect of cloud cover and variation in measurement site sky view on patterns in UV surface exposures are also investigated.

3.1 Measured patterns in facial exposure under low cloud cover

Of the parts of the human body that are exposed to the sun regularly, the human face receives a significant proportion of ambient ultraviolet. This significance is increased considering that the face is not regularly protected by clothing as are other regions of the body that receive high exposures to solar UV. Correspondingly, non-melanoma skin cancers are highly prevalent on the face followed by other regions of the body that receive high solar UV exposures including the arms, hands and legs (Pearl and Scott 1986; Kricker et al. 1990; Raasch et al. 1998). Within the human facial region, the nose, ears and cheeks receive the highest proportions of ambient UV (Diffey et al. 1979; Urbach 1993). Of these facial regions, the nose often receives the greatest proportion of ambient UV over a wide SZA range (Kimlin et al. 1998; Downs et al. 2001; Downs and Parisi 2007). Figure 3.1 illustrates the variation in facial ER measured under low cloud cover conditions (less than 4 okta or eighths) with changing SZA. A clear spreading of the exposure relative to the horizontal plane toward the lower proximities and outer extremities of the face is evident in the figure for lower solar elevations (larger SZA). These findings are due to the increased proportion of direct UV incident to a greater area of the face at lower solar elevations (larger SZA). A greater distribution of diffuse UV at low solar elevations also contributes to a greater distribution of facial UV exposure.

Apart from the vertex and forehead, measurements of facial ER were consistently high on the bridge of the nose which receives a high proportion of incident UV at both small and large SZA as the nose protrudes from the face receiving less shading by other facial features. The angle of inclination of the nose bridge, being orientated at an angle of approximately 45^{o} to the vertical, results in direct UV radiation incident at 30^{o}-50^{o} and 50^{o}-80^{o} in SZA having more influence on the exposure patterns observed in Figure 3.1 than UV radiation incident at 0^{o}-30^{o}. The effect is high nose bridge ER observed in the 30^{o}-50^{o} and 50^{o}-80^{o} SZA ranges.

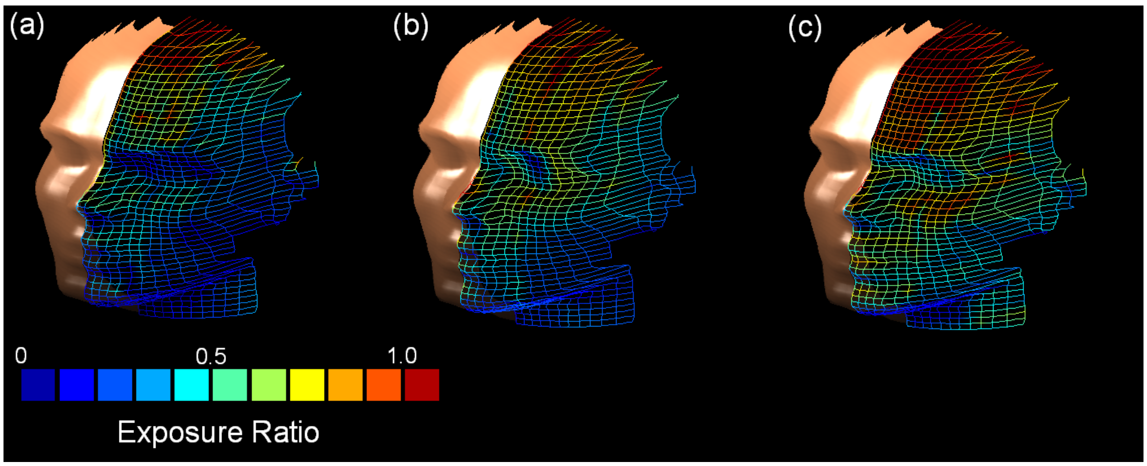

Figure 3.1: Facial ER measured with changing SZA for low cloud cover cases (a) SZA 0^{o}-30^{o}; (b) SZA 30^{o}-50^{o}; (c) SZA 50^{o}-80^{o}.

Measurements of ER to facial sites are listed in Tables 3.1(a), 3.1(b) and 3.1(c). The Tables are organised into contours, listing individual ER measurements made over the measurement period between 2005 and 2008. Data provided in the tables are the measured ER recorded over several measurement trials in each SZA range. Where more than one measurement has been recorded at a specific site, mean ER is listed. Individual table columns represent vertical facial contours and rows represent horizontal facial contours. The facial wireframe exposure model is made up of 18 vertical contours ranging from Cn1 (the middle of the face) to Cn18 (the ear) and 49 horizontal contours ranging from Cx1 (the top of the head) to Cx49 (the bottom of the neck). Table data is listed for each intersection of the wireframe model where a measurement has been made. Note that in each of the tables, the first horizontal contour starts at the second vertical position and is labelled Cx1. The first contour, Cx1 can be clearly seen in Figure 3.1 at the top of the head as the first horizontal red contour. (Facial ER data recorded over each trial in the 2005 to 2008 measurement period is listed in Appendix G.1. The positions of vertical and horizontal contour labels for the face, neck, arm, hand and leg are shown on their respective three dimensional wireframe models in Appendix H).

3.2 Measured pattern in facial exposure under high cloud cover

Figure 3.2 shows the variation in facial exposure for SZA ranges 0^o-30^o and 30^o-50^o for cloud cover conditions greater than 4 okta. Exposures represented in the figure were interpolated from measurements taken under high cloud cover cases (Appendix G.1) and do not include the 50^o-80^o range due to low levels of ambient UV received under high cloud cover conditions and large SZA ranges. Comparison between Figure 3.1 and Figure 3.2 shows little obvious variation in facial exposure. Greater cloud cover conditions reduce the influence of the direct solar UV incident on the face, effectively increasing the incident diffuse UV that affects the facial exposure pattern. It is therefore reasonable to expect that a slightly broader exposure pattern affecting the outer extremities and lower proximities of the face would result as the influence of the direct UV which changes significantly with SZA would be negated. High ratios of UV exposure can be observed in Figure 3.2(b) toward the side of the face, neck and ear which are notably higher than the ER observed at the same sites in low cloud cover conditions (Figure 3.1). However, the observed increases in facial ER are not significantly greater than the ER uncertainty of ±18% quoted for the 30^o-50^o SZA range.

Table 3.1(a): Facial site exposure ratio expressed as a percentage for the SZA range 0^o-30^o and cloud cover less than 4 oktas.

	Cn1	Cn2	Cn3	Cn4	Cn5	Cn6	Cn7	Cn8	Cn9	Cn10	Cn11	Cn12	Cn13	Cn14	Cn15	Cn16	Cn17	Cn18
	100	100	82	85	77	96												
Cx1	67	100	84	95	95		85	58										
Cx2		100	80	77	85		64		70	86								
Cx3	87	80	84		76		88	68	71	81	72							
Cx4		78	74		89				46	94	74	69						
Cx5					56		79			41		79	65					
Cx6		70	53								28		40	55				
Cx7					49			56	49	67		46		53				
Cx8		38	58										38	48	42			
Cx9					58		45			62	42				47			
Cx10		51	52		50				54					36	29			
Cx11					88			84		45				45		36		
Cx12		30	45				49				29	33	29	27	29	26		
Cx13					50				54	69					46	40		
Cx14		56	34						69	60		29			22	17		
Cx15					51		42			43		48		25		22		
Cx16		32	27						4			23	35		13	23		
Cx17					4					7		14		22	29	18		
Cx18		17	6		8		10							27	17	22		
Cx19					8					16	9	9	15	26				
Cx20	59	23	11		7									25	19	19		
Cx21					7			15		21	8	8		25	14		65	
Cx22	70	55	42		17										18	31	75	
Cx23	59	40	32			31		35		31	40	21	29	25	21			
Cx24		55	34		54			34		40				17		19	22	31
Cx25	27	19	47		44			48			47	34	22					
Cx26				40						29				26	20	7	13	25
Cx27		5	8		30			35			29	18	24	14	28			9
Cx28					25					24				16	12	20	26	
Cx29		12	19					27			17	9	14	15			8	
Cx30	28		37		38		36		19	15	14	12	17	15		20		
Cx31		40	46					26			10	9		15		17		
Cx32					33					20		13		8		10		
Cx33		5	8					21			14	12	13	6				
Cx34					26					19		16						
Cx35		25	28					14			18	15	15					
Cx36					16	12				21								
Cx37		7	7					26	16		19	14						
Cx38					19		27	19		18		10						
Cx39		33	29								12	13						
Cx40					38			19		15	7							
Cx41		21	16						11	5		19						
Cx42					6	10	8	7	3	11								
Cx43		4	5			4	3	8				25						
Cx44	1	1	1		3		5			23								
Cx45			3	2								28						
Cx46					7		9	15		18								
Cx47			7									29						
Cx48					13		14			17								
Cx49			9		11			18				29						

Table 3.1(b): Facial site exposure ratio expressed as a percentage for the SZA range 30^o-50^o and cloud cover less than 4 oktas.

	Cn1	Cn2	Cn3	Cn4	Cn5	Cn6	Cn7	Cn8	Cn9	Cn10	Cn11	Cn12	Cn13	Cn14	Cn15	Cn16	Cn17	Cn18
			69															
Cx1	100		97					70										
Cx2							100											
Cx3			69					63										
Cx4							100											
Cx5	71	66		70		70		64		75	66	75	57					
Cx6			61				90											
Cx7	65												56	88				
Cx8			45				79	55										
Cx9	62													70	46			
Cx10							58						10					
Cx11	66							60						53	46			
Cx12							77											
Cx13	69												32	51				
Cx14		16		48		54	82	57		59		47	33	29	33	32		
Cx15	66							49						40				
Cx16							12						37		32			
Cx17	35													42				
Cx18							13	9										
Cx19	38												26	48				
Cx20							21	16										
Cx21	82		27											42				
Cx22							33						44					
Cx23	98		46					37						60				
Cx24		47		53		57	83	58		58		52	43	36	28		20	24
Cx25	56		36					49					38	47	17			
Cx26							51											
Cx27	9													32	31			
Cx28			16				39	34										
Cx29	31												22	32				
Cx30							54								30			
Cx31	67	44	35	45		39		30		19		18	20	25		20		
Cx32							40						21					
Cx33	12		8											6				
Cx34							31	24					15					
Cx35	50		37															
Cx36							26						18					
Cx37	11							19										
Cx38			18				42											
Cx39	54							21										
Cx40			35				38											
Cx41	34	16		16		41		14										
Cx42			17					8										
Cx43	8																	
Cx44							13	11										
Cx45																		
Cx46	8						24	21										
Cx47																		
Cx48	12						25											
Cx49								26										

Table 3.1(c): Facial site exposure ratio expressed as a percentage for the SZA range 50^o-80^o and cloud cover less than 4 oktas.

	Cn1	Cn2	Cn3	Cn4	Cn5	Cn6	Cn7	Cn8	Cn9	Cn10	Cn11	Cn12	Cn13	Cn14	Cn15	Cn16	Cn17	Cn18
	100	100	81	83	100													
Cx1		100		100			73	74										
Cx2	100	96							100									
Cx3							100		79									
Cx4	100	94									63	77						
Cx5							84		92			88	97					
Cx6	78	73												83				
Cx7							80		94				72	72				
Cx8	94	73									66		78	63				
Cx9							90		86									
Cx10	88	78						39					62	100	66			
Cx11							75		79		74					68		
Cx12	88	65						55						61				
Cx13							83		66		60		56			61		
Cx14	92	77						54					52	53	53			
Cx15							82		77							54		
Cx16	56	58						18				53	45	34		57		
Cx17							11		28					43		26		
Cx18	41	29											45	94	31			
Cx19							34		39	18			54			36		
Cx20	67	61											11	43				
Cx21							42	25	39						23	52		
Cx22	100	53	30							38		58		77				
Cx23							59							49	49			65
Cx24	33	75						83	64			83	52	44		31		
Cx25			46				79	51			82						16	47
Cx26	25	26							73					47				
Cx27							56	37					51		49			37
Cx28	21	15									47	23		51				
Cx29							52		51				22		34		25	
Cx30	65	63						40			33			30				
Cx31							59						28	27		37		
Cx32	39	39						56	44		33	33		34				
Cx33							45						24	8				
Cx34	64	72									22							
Cx35							39	39	30			38	41					
Cx36	22										45							
Cx37		15					41	37										
Cx38	36								35		36	29						
Cx39		66				45	63					23						
Cx40	62							24			18	44						
Cx41		33				43	25		22			38						
Cx42	29																	
Cx43		10					8		28	43		36						
Cx44	7	0																
Cx45	1	1					14		40	35		27						
Cx46																		
Cx47	13						15			46		58						
Cx48									52									
Cx49	28	16					35			33		43						

Previous research has determined UV exposures measured to anatomical sites to be independent of cloud cover (Diffey et al. 1977). Table 3.2 compares measurements of facial site ER made under high and low cloud cover conditions in the 0^o-30^o and 30^o-50^o SZA range. A total of 66 identical facial sites were measured under both high and low cloud cover conditions in the 2005 to 2008 measurement period. Variations, measured as the difference between high cloud cover ER cases and low cloud cover ER cases observed at identical facial sites are given in the table. The mean variation, measured as the difference between high and low cloud cover ER sites was -3% and -2% for the SZA ranges 0^o-30^o and 30^o-50^o respectively, indicating the ER was greater under low cloud cover conditions. The difference is expressed relative to the horizontal plane ambient UV.

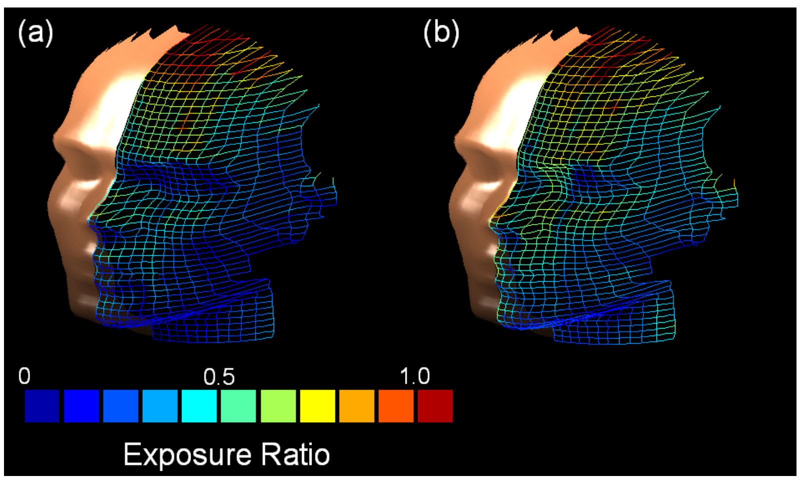

Figure 3.2: Facial ER with changing SZA for high cloud cover cases (a) SZA 0^o-30^o; (b) SZA 30^o-50^o.

Table 3.2: Comparison of facial site ER data made under high and low cloud cover conditions. ER is expressed as a percentage of the ambient horizontal plane exposure.

SZA 0^{o}-30^{o}				SZA 30^{o}-50^{o}			
Site	Low Cloud ER (< 4 okta)	High Cloud ER (> 4 okta)	High cloud ER % – Low cloud ER %	Site	Low Cloud ER (< 4 okta)	High Cloud ER (> 4 okta)	High cloud ER % – Low cloud ER %
Cn1 / Cx0	100%	100%	0%	Cn1 / Cx19	38%	34%	-4%
Cn1 / Cx30	28%	29%	+1%	Cn1 / Cx25	56%	51%	-4%
Cn1 / Cx44	1%	2%	+1%	Cn1 / Cx31	67%	48%	-19%
Cn5 / Cx0	77%	100%	+23%	Cn1 / Cx41	34%	54%	+20%
Cn5 / Cx2	85%	98%	+13%	Cn1 / Cx41	34%	52%	+18%
Cn5 / Cx4	100%	78%	-22%	Cn1 / Cx46	8%	7%	-1%
Cn5 / Cx4	78%	78%	0%	Cn2 / Cx24	47%	73%	+26%
Cn5 / Cx10	50%	54%	+4%	Cn7 / Cx4	100%	100%	0%
Cn5 / Cx18	8%	5%	-3%	Cn7 / Cx6	90%	48%	-42%
Cn5 / Cx20	7%	5%	-2%	Cn7 / Cx34	31%	33%	+2%
Cn5 / Cx24	55%	42%	-13%	Cn10 / Cx14	59%	75%	+16%
Cn5 / Cx24	52%	42%	-10%	Cn10 / Cx24	58%	44%	-14%
Cn5 / Cx28	25%	24%	-1%	Cn12 / Cx5	75%	63%	-12%
Cn5 / Cx30	45%	36%	-9%	Cn12 / Cx14	47%	34%	-13%
Cn5 / Cx30	36%	36%	0%	Cn12 / Cx31	18%	18%	0%
Cn5 / Cx30	32%	36%	+4%	Cn14 / Cx7	88%	51%	-37%
Cn5 / Cx32	33%	23%	-10%	Cn14 / Cx9	70%	35%	-35%
Cn5/ Cx34	25%	25%	0%	Cn14 / Cx14	29%	27%	-2%
Cn5 / Cx34	27%	25%	-2%	Cn14 / Cx24	36%	34%	-2%
Cn5 / Cx36	16%	10%	-6%	Cn14 / Cx29	32%	25%	-7%
Cn5 / Cx38	23%	25%	+2%	Cn16 / Cx14	32%	31%	-1%
Cn5 / Cx38	15%	25%	+10%			Mean difference	-2%
Cn5 / Cx42	6%	9%	+3%				
Cn5 / Cx46	7%	8%	+1%				
Cn5 / Cx48	13%	11%	-2%				
Cn11 / Cx3	89%	66%	-23%				
Cn11 / Cx3	55%	66%	-11%				
Cn11 / Cx9	42%	34%	-8%				
Cn11 / Cx19	9%	7%	-2%				

Cn11 / Cx21	8%	10%	+2%
Cn11 / Cx23	40%	34%	-6%
Cn11 / Cx25	47%	45%	-2%
Cn11/ Cx27	29%	24%	-5%
Cn11 / Cx29	17%	13%	-4%
Cn11 / Cx31	10%	12%	+2%
Cn11 / Cx33	14%	13%	-1%
Cn11 / Cx35	18%	12%	-6%
Cn11 / Cx37	19%	16%	-3%
Cn11 / Cx39	12%	12%	0%
Cn17 / Cx21	69%	58%	-11%
Cn17 / Cx21	60%	58%	-2%
Cn17 / Cx24	22%	18%	-4%
Cn17 / Cx26	12%	11%	-1%
Cn17 / Cx26	13%	11%	-2%
Cn17 / Cx28	26%	17%	-9%
		Mean difference	-3%

Large ER site differences were observed in the 30^o-50^o SZA range at facial sites (Cn7, Cx6) and (Cn14, Cx7). The ER at these two facial sites were higher under low cloud cover conditions than the ER recorded under high cloud cover conditions at their respective (Cn7, Cx6) and (Cn14, Cx7) sites showing an ER difference between high and low cloud cover of -42% and -37% expressed relative to ambient horizontal plane exposure. If the effect of cloud cover were to broaden the pattern in exposure observed across the face the ER would be expected to be higher under high cloud cover conditions, especially at sites located further from the centre of the face. Given the two sites (Cn7, Cx6) and (Cn14, Cx7) located on the forehead at the middle to further extremities of the face have a lower ER measured under high cloud cover conditions and given the mean variation in high to low cloud cover ER (Table 3.2) shows that the ER was higher under low cloud cover conditions, it can be reasoned that the influence of cloud cover does not broaden the facial exposure pattern.

3.3 Measured pattern in facial exposure with changing sky view

A total of five trials were run to determine the influence of sky view on facial ER. Measurements of exposure were recorded to the face during each of these trials at the facial sites illustrated in Figure 3.3 for playground locations that had sky views varying from 19% to 48%. The measured ER results are listed in Table 3.3 and plotted in Figure 3.4.

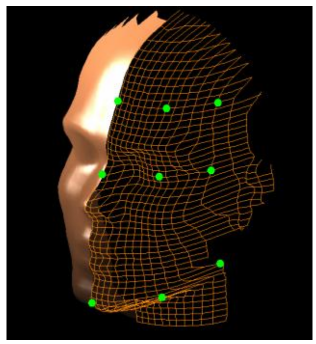

Figure 3.3: Location of dosimeters for examining the influence of sky view on facial ER.

Table 3.3: ER of facial site dosimeters measured in sites of varying sky view.

Facial site location	Location A (48% sky view)	Location B (19% sky view)	Location C (48% sky view)	Location D (30% sky view)	Location E (35% sky view)
Upper face					
Cn1, Cx10	66	52	40	69	75
Cn9, Cx8	61	63	63	71	66
Cn14, Cx4	49	47	54	65	55
Middle face					
Cn1, Cx24	91	65	75	78	64
Cn9, Cx24	72	78	60	62	58
Cn14, Cx20	47	50	40	43	52
Lower face					
Cn1, Cx42	29	34	36	30	35
Cn9, Cx40	25	39	26	20	28
Cn12, Cx45	23	28	25	23	23

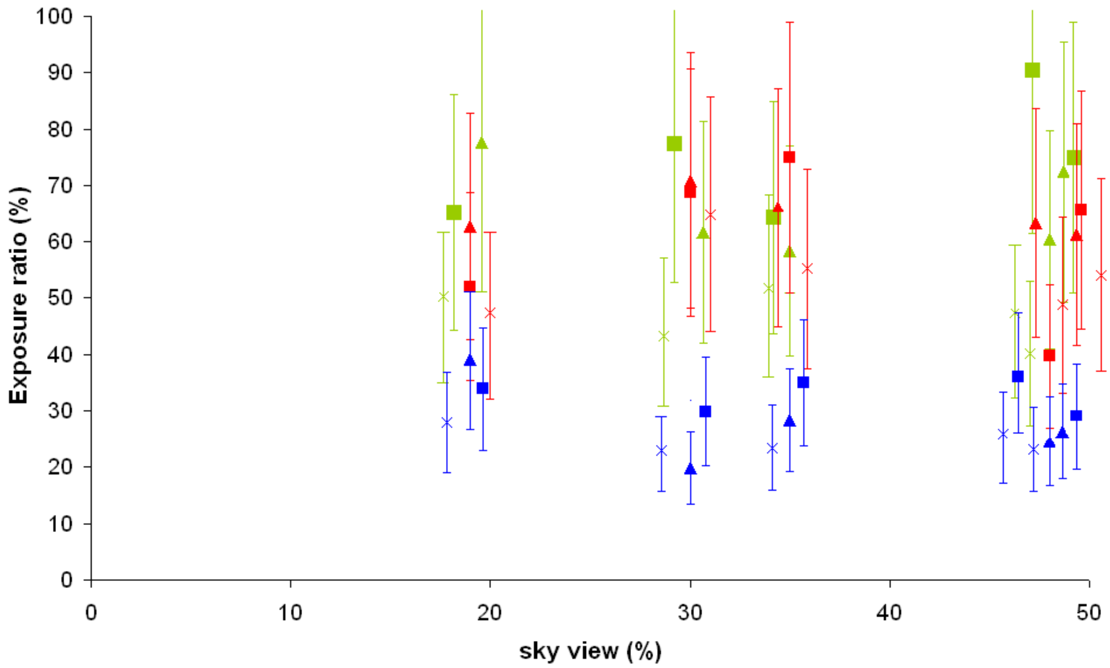

Figure 3.4: Variation in measured facial site ER with sky view (red data points were measured across the forehead, green data points were measured across the nose, eye and temple, and blue data points were measured across the lower proximities of the face (Figure 3.3). Square points in this figure represent measurements made through the centre of the face, crosses were measured through the outer side of the face and triangular points represent measurements made between the centre and outer proximities of the facial region extending through the eye of the mannequin headform. Error bars show the maximum ER uncertainty of ±32% for the SZA range 50^o-80^o. Data points were separated for clarity in the figure but represent sky view exposures of 19%, 30%, 35% and 48%.

As observed from the data presented in Figure 3.4, no obvious trend in facial site ER could be found for variations with sky view. It is likely that if variations in facial ER are present they are less than the stated uncertainty in dosimeters used for this research. A handful of facial site locations did however show a statistically significant increase in ER ($P<0.05$). These sites included the side of the forehead, the nose, the eye and the jaw. Of the six sites that showed a significant increase in ER, five where determined at locations in which the sky view was 30% or 19% and one was measured in a location that had a sky view of 48%. A reasonable explanation for these significant results at lower sky view locations is the level of ambient UV recorded over the 7 hour period in which the ER was measured, in this instance out of direct sunlight, whereby increases in the ER are possible when the ambient UV is lower due to the increased error introduced in measuring exposure relative to lower ambient UV incident on a horizontal plane. Increased uncertainty due to measurement of ER in low sky view environments is similar to increased error discussed in the pervious chapter for measurements taken over high SZA ranges during which the measurements of ambient horizontal plane UV were also low.

3.4 Polynomial representation of facial exposure

Figure 3.5 is a polynomial representation of the facial ER with variation in horizontal position measured from the centre of the face for each of the horizontal contours, Cx1 through Cx49. Horizontal contour ER plotted with respect to the facial position measured from the centre of the face is given for SZA ranges of 0^o-30^o, 30^o-50^o and 50^o-80^o for low and high cloud cover cases. The polynomial fits to the data presented in the figure were derived from the low cloud cover facial ER data listed in Tables 3.1(a), 3.1(b) and 3.1(c) where the data presented in these tables represents the mean ER measured for each specific site for each SZA range. The polynomials plotted as solid lines in Figure 3.5 for each horizontal facial contour Cx1 through Cx49 are of the general form:

$$ER(x_i) = \beta_n x_i^n + \beta_{n-1} x_i^{n-1} ... \beta_o x_i^o \qquad (3.1)$$

where $ER(x_i)$ is the exposure ratio for the horizontal facial contour, β_n is a constant polynomial parameter for a polynomial of degree *n*, where in this case *n* is 18 for each contour and x_i is the distance from the centre of the face. All polynomials represented in the figure were chosen to be 18^{th} order polynomials to provide the best fits through measured ER data. A least squares polynomial regression fitting technique was chosen as the best fit for the measured data due to the high degree of variability in the data over closely spaced horizontal facial distances between measurement points. The polynomial parameters, β_n are listed for each horizontal facial contour Cx1, through Cx49 in each SZA range in Appendix I.

As is evident in Figures 3.1 and 3.2, Figure 3.5 clearly identifies that higher UV exposures relative to the horizontal plane are received by contours located in the upper regions of the face with the highest exposures occurring at the vertex. Horizontal contours Cx1 through Cx16 located above the eyebrows show a decreasing trend in ER moving toward the outer facial proximities (increasing distance from the centre of the face). Contours Cx17 through Cx22 show the effect of the eye socket reducing ER between 25 mm and 50 mm measured from the centre of the face. Contours Cx23 through Cx29 highlight increases in exposure over the same 25 mm to 50 mm range. The increase in ER over this range is likely to be due to the protruding influence of the upper cheek. Horizontal contours show decreasing exposure moving toward the outer facial proximities from underneath the nose to the lower lip (Cx30 through to Cx35) and then show an increasing trend in exposure moving toward the outer facial proximities for contours located underneath the bottom lip. The influence of the chin (Cx38 through to Cx41), results in higher exposure at the centre of the face. The ER is shown to clearly increase moving toward the side of the neck in contours Cx42 through to Cx49 showing the strong influence of the chin and jaw shading sites located directly underneath the neck. The figure, being produced by measurements made on a mannequin headform shows clearly the advantage of using polysulphone dosimeter measurements as the effects of shading and surface orientation at individually located sites are taken into account. All measurements show that greater ERs are received with increasing SZA. Cloud affected data, provided in the figure as square points do not show consistent variations from the plotted facial exposure polynomials. The lower high cloud cover affected ER compared to the low cloud cover ER measured in the 30^o-50^o SZA range discussed previously can be seen in the figure at approximately 30 mm (Cx6) and 70 mm (Cx7).

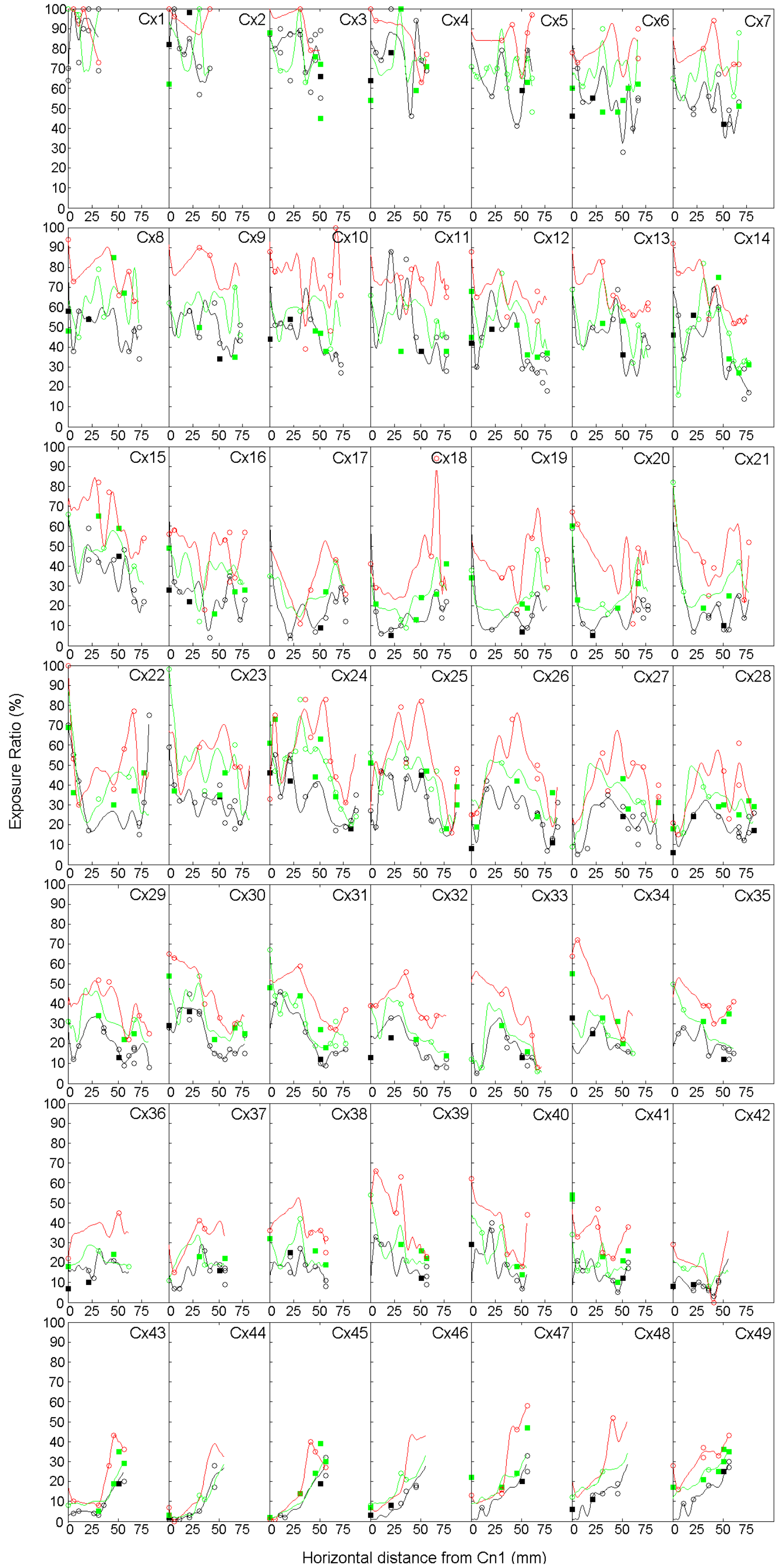

Figure 3.5: Horizontal facial contour ER for high (square point) and low (circular point) cloud cover cases in the SZA ranges 0^o-30^o (black), 30^o-50^o (green) and 50^o-80^o (red).

3.5 Patterns in body surface exposure

Measurements of exposure in the SZA ranges 0^o-30^o, 30^o-50^o and 50^o-80^o taken over the four year study period are given for the back of the neck, arm, hand and leg in Figures 3.6, 3.7, 3.8 and 3.10 respectively. Where possible, data presented in the figures were measured under low cloud cover conditions (less than 4 okta). The three dimensional wireframe models represented in each figure are orientated to highlight surfaces that received the maximum ER. Each of the body parts represented in the figures show clearly the variation in UV exposure resulting from changing SZA. ER data measured under low and high cloud cover conditions for each of the neck, arm, hand and leg models are listed in Appendix G. The mean site ER data used to produce each of the body ER figures are listed in tabular form under each of the respective body part sub headings.

3.5.1 Surface exposure received by the back of the neck

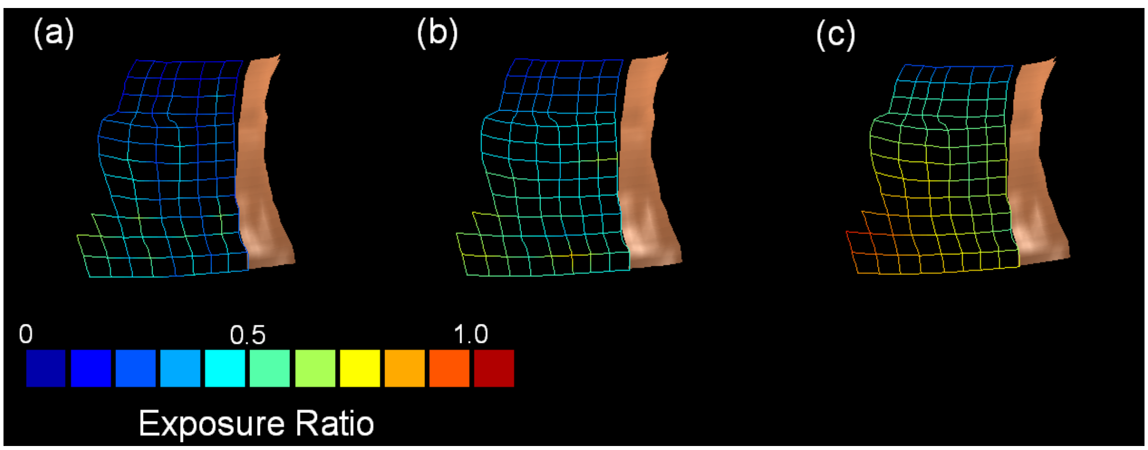

Figure 3.6: Variation in ER measured to the back of the neck (a) SZA 0^o-30^o, < 4 oktas; (b) SZA 30^o-50^o, > 4 oktas; (c) SZA 50^o-80^o, < 4 oktas.

Table 3.4(a): Site exposure ratio measured to the back of the neck and expressed as a percentage for the SZA range 0^o-30^o and cloud cover less than 4 oktas.

	Cn1	Cn2	Cn3	Cn4	Cn5	Cn6	Cn7	Cn8	Cn9
Cx1	6		6	17	7	16	8		
Cx2	10		9		12		12		
Cx3	13		14		14		12		
Cx4	14		18		17		15		
Cx5	20		15	20	20	24	19		
Cx6	19		17		21	23	19		
Cx7	20		18		17	26	23		
Cx8	21		22		23	34	27		
Cx9	17		22	28	21	18	32		
Cx10	20		22		29		32	50	
Cx11	23		23		32		37	52	50
Cx12	19		20		26		30	38	48
Cx13	24		28		20	39	34	36	40

Table 3.4(b): Site exposure ratio measured to the back of the neck and expressed as a percentage for the SZA range 30^o-50^o and cloud cover greater than 4 oktas.

	Cn1	Cn2	Cn3	Cn4	Cn5	Cn6	Cn7	Cn8	Cn9
Cx1		14		13		13			
Cx2		21		21		16			
Cx3		24		23		23			
Cx4		32		30		27			
Cx5		38		35		32			
Cx6		33		37		35			
Cx7		56		33		35			
Cx8		35		32		47			
Cx9		37		38		44			
Cx10		33		44		44		62	
Cx11		40		30		40		49	53
Cx12		43		69		42		59	
Cx13		38		42		44		48	

Table 3.4(b): Site exposure ratio measured to the back of the neck and expressed as a percentage for the SZA range 50^o-80^o and cloud cover less than 4 oktas.

	Cn1	Cn2	Cn3	Cn4	Cn5	Cn6	Cn7	Cn8	Cn9
Cx1	19								
Cx2									
Cx3	43								
Cx4									
Cx5	49				47		48		
Cx6			49						
Cx7	59				62		57		
Cx8			48						
Cx9	58				66		69		
Cx10			56						
Cx11	45				63		77		86
Cx12			60						
Cx13	62				68		68		73

Exposures represented in Figure 3.6 show the left side of the back of the neck of the headform model. Measurements of the UV ER were made from the shoulder to the middle of the neck under high and low cloud cover conditons. Tables 3.4(a), 3.4(b) and 3.4(c) show the data used to produce Figure 3.6. Tables 3.4(a) and 3.4(c) give neck site ER recorded under low cloud cover conditons (< 4 okta). Table 3.4(b) was measured under high cloud cover conditions. Each table is organised into vertical and horizontal contours. Vertical contour, Cn1 is located along the centreline of the mannequin neck model, vertical contour Cn9 is located on the shoulder. Horizontal contours are positioned from the base of the headform skull (Cx1) to the bottom of the neck (Cx13). The effects of headform shading are most evident in Figure 3.6 at the top of the neck having the lowest ER. The highest exposures measured on the back of the neck of the upright headform were located on the shoulder. Like exposures measured to the face, surfaces on the neck model that are more closely oriented toward the horizontal plane received the greatest ER.

3.5.2 Surface exposure received by the arm

Measurements of surface UV ER to the arm were made with the body mannequin wearing a school uniform (Figure 2.2). Dosimeters placed underneath the cotton polo shirt worn by the mannequin recorded no appreciable ER resulting in the low ER evident in the upper arm (Figure 3.7). Exposure ratios measured to the forearm were shown to increase with increasing SZA. These increases are attributed to solar UV incident at lower elevations with increasing SZA affecting a larger area of the arm which was orientated in a vertical position during the measurement campaign.

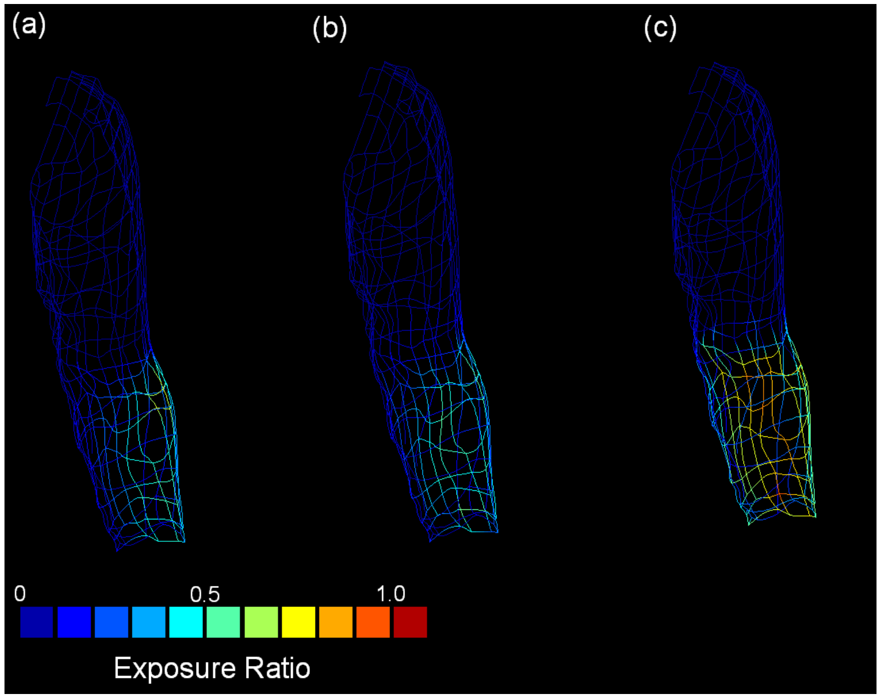

Figure 3.7: Variation in ER measured to the forearm with SZA for low cloud cover cases (a) SZA 0^o-30^o; (b) SZA 30^o-50^o; (c) SZA 50^o-80^o. The shirt used on the mannequin covers the upper arm.

Tables 3.5(a), 3.5(b) and 3.5(c) give the mean site ER data recorded under low cloud cover conditions (< 4 okta). Vertical contours start from the top of the shoulder and end at the wrist of the mannequin arm model. Horizontal contours are banded around the arm starting from the top of the shoulder and finishing in a band circling the wrist. Appendix H shows the position of vertical and horizontal contours on the three dimensional arm model. Vertical contours Cn16, Cn17, Cn18, and Cn19 were located on the underside of the upper arm. As these contours received no exposure they have not been included in Tables 3.5(a), 3.5(b) and 3.5(c).

Table 3.5(a): Site exposure ratio measured to the arm and expressed as a percentage for the SZA range 0^o-30^o and cloud cover less than 4 oktas.

	Cn1	Cn2	Cn3	Cn4	Cn5	Cn6	Cn7	Cn8	Cn9	Cn10	Cn11	Cn12	Cn13	Cn14	Cn15	Cn20	Cn21	Cn22	Cn23
Cx1																			
Cx2																			
Cx3																			
Cx4																			
Cx5																			
Cx6																			
Cx7																			
Cx8																			
Cx9																			
Cx10																			
Cx11																			
Cx12																			
Cx13																		5	9
Cx14	18	9	6	7	21	5	20	15		8								8	13
Cx15	25	43	43	31	54	23	35	31	13	17	13					3	4	9	10
Cx16	13	23	38	39	61	49	37	32	20	23	17				3		3	6	7
Cx17	12	19	29	30	54	60	40		27	21	19	8	4	3					7
Cx18	8	13	19	27	38	36	44	42	23	22	13	13			3			5	6
Cx19	6	10	19	29	31	40	43	36	25	23		11	8	5			3	5	
Cx20	5	9	13	23	30	41	39					10	6	4	4				
Cx21				18	29	43			40				6	3	4				
Cx22						35							5	4	4				
Cx23						27							5		6				
Cx24													7	3	4				
Cx25															3				
Cx26														4					
Cx27													8		3				
Cx28														4					

Table 3.5(b): Site exposure ratio measured to the arm and expressed as a percentage for the SZA range 30^o-50^o and cloud cover less than 4 oktas.

	Cn1	Cn2	Cn3	Cn4	Cn5	Cn6	Cn7	Cn8	Cn9	Cn10	Cn11	Cn12	Cn13	Cn14	Cn15	Cn20	Cn21	Cn22	Cn23
Cx1																			
Cx2					0														
Cx3							0			0									
Cx4												0							
Cx5					0		0												
Cx6	0									0					0				
Cx7					0														
Cx8										0		0				0		0	
Cx9	0		0		0		0												
Cx10								0	0					0				0	
Cx11	0		0		0	0						0				0			
Cx12							9		1									3	1
Cx13	10	0	1	1	7		14	8	7	4				0				8	13
Cx14	18	1	20	8	38	5	13	24	11	6	5	0					6		14
Cx15	22	28	30	44	49	31	39	40	25	25	17	5		2	3	0	7	15	10
Cx16	18	25	29	51	46	47	45	46	29	28	25	9	5		4			8	9
Cx17	17	23	19	40	43	33	49	43	36	32	20			3	4		6	6	8
Cx18	7	17	33	41	45	45	37	35	34	22	17	22	11					2	8
Cx19	8	20	29	33	48	49	37	55	41	28		16	13	7	3		6	7	
Cx20	4		20	24	42	42	45		17			14	10	5					
Cx21				23	39	47	19		38				9	5	6				
Cx22						39							7	3					
Cx23						30									7				
Cx24															6				
Cx25													11	4					
Cx26																			
Cx27													11	4	5				
Cx28													15						

Table 3.5(c): Site exposure ratio measured to the arm and expressed as a percentage for the SZA range 50^o-80^o and cloud cover less than 4 oktas.

	Cn1	Cn2	Cn3	Cn4	Cn5	Cn6	Cn7	Cn8	Cn9	Cn10	Cn11	Cn12	Cn13	Cn14	Cn15	Cn20	Cn21	Cn22	Cn23
Cx1																			
Cx2																			
Cx3																			
Cx4																			
Cx5																			
Cx6																			
Cx7																			
Cx8																			
Cx9																			
Cx10																			
Cx11														2					
Cx12								11											20
Cx13						6				25					4				24
Cx14	27	20	39	31			66	64	43		46		13						23
Cx15	32	27				61		71		49	65				13	12		14	
Cx16		41	47	62	67			87	76	66	49		23						
Cx17	19	26		55	51	58	72	61	63	54		24		16				11	19
Cx18	19	23	41	55	54		71	69		60	49	41	37		13				
Cx19	12	14	32	47	52	60	63	82	57	44		43		26					
Cx20	11	22		36		55	58	56	66			48	29	18					
Cx21				29	43	54	65						30						
Cx22													19	12					
Cx23						45													
Cx24														12					
Cx25													29						
Cx26														20					
Cx27																			
Cx28													46	21					

3.5.3 Surface exposure received by the hand

The surface ERs received by the mannequin hand for low cloud cover conditions in the SZA ranges 0^o-30^o, and 30^o-50^o are illustrated in Figure 3.8. ERs measured in the 50^o-80^o SZA range were made under conditions in which the cloud cover increased over 4 oktas. Tables 3.6(a), 3.6(b) and 3.6(c) give the ERs used to produce the three dimensional wireframe exposure plots given in the figure. Vertical contours start at the wrist and move toward the finger tips for both the dorsal and palm surfaces of the hand. UV exposures received by the palm of the mannequin hand were less than 10% of the horizontal plane UV exposure. The greatest exposures were received by the dorsal surface of the hand. Figure 3.8 clearly illustrates changes in the received UV ER with variation in SZA showing that a greater area of the hand receives a higher ER with increasing SZA. The ERs received by the hand were typically higher than the exposure ratios received by the arm surface. This was due to the orientation of the hand model with respect to the attached arm model. The hand was orientated with a greater surface being exposed to vertically incident UV (Figure 3.9).

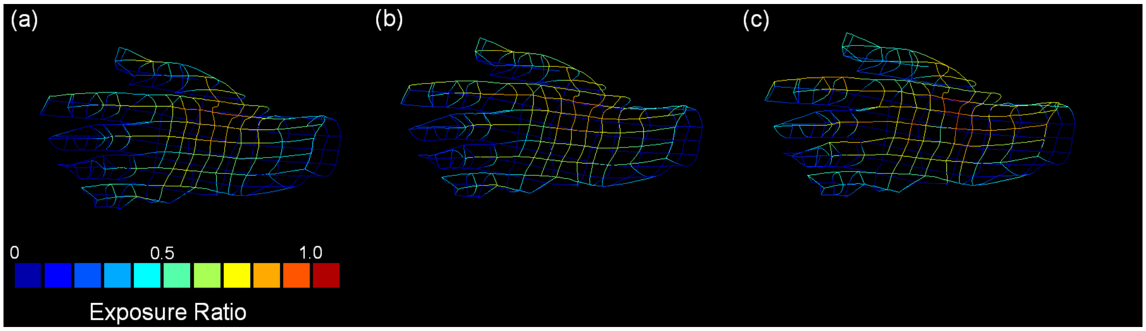

Figure 3.8: Variation in ER measured to the hand (a) SZA 0°-30°, < 4 okta; (b) SZA 30°-50°, < 4 okta; (c) SZA 50°-80°, > 4 okta.

Figure 3.9: Hand orientation with respect to the arm used on the full body mannequin.

Table 3.6(a): Site exposure ratio measured to the hand and expressed as a percentage for the SZA range 0^o-30^o and cloud cover less than 4 oktas.

	Cn1	Cn2	Cn3	Cn4	Cn5	Cn6	Cn7	Cn8	Cn9	C10	C11	C12	C13	C14	C15	C16	C17	C18	C19	C20	C21	C22	C23
Cx1																	4			4			
Cx2						22													4				
Cx3							42									8		3			13		
Cx4					11	31	45									6			3				
Cx5					37	49	48	37	35	30	27					7			3		14		
Cx6						65		35	34	24	15					5							
Cx7					52	76		62		44	26					2							
Cx8				20	69			52		46	30	11				2					3		
Cx9			16		76	73		73		50	42	34		2	5							5	
C10		29		57	66	75		72		48	52	53	6	2	2		1			2		3	10
C11		42	69	51	57	75		71		61	56	53				1				2	1		6
C12			31	63	47	65		63		56		38						2				1	6
C13	32		29	10	42		33	70		40		23				3			2				3
C14		26	22		37	67	9	62		61	8				2			5		8			
C15			17		30	65			10							5							
C16					41	54	3	58		29	28							8	3				
C17					37	17		41		14													
C18					46			11		7													
C19					41			11		9													
C20								9															

Table 3.6(b): Site exposure ratio measured to the hand and expressed as a percentage for the SZA range 30^o-50^o and cloud cover less than 4 oktas.

	Cn1	Cn2	Cn3	Cn4	Cn5	Cn6	Cn7	Cn8	Cn9	C10	C11	C12	C13	C14	C15	C16	C17	C18	C19	C20	C21	C22	C23
Cx1																		6			15		
Cx2						31										12			6				
Cx3																		5		12	20		
Cx4					21	46	57									10	5				22		
Cx5					50			45	42	44	33							5					
Cx6					61	62	70	53	45		18								6				
Cx7					64	74			56		32					5	4			6			
Cx8				35				61	55	53	41	25	10		20			2					
Cx9			34		52	76	70	70		58		34		3	7	2		1				10	
C10		47		61	67	66			58		52								3		3		20
C11			66					71		51	53	58				3		3					13
C12	39		64	67	53	70	60	46	53	56				4						11		5	
C13		69	31	10			37			51	32	33											9
C14		47			52	72		60	10							8				15			
C15			16		48	68				60					4			17					
C16						60	15	61	11														
C17					51	31		45		20													
C18					60			24															
C19					57			15		14													
C20								15															

Table 3.6(c): Site exposure ratio measured to the hand and expressed as a percentage for the SZA range 50^o-80^o and cloud cover greater than 4 oktas.

	Cn1	Cn2	Cn3	Cn4	Cn5	Cn6	Cn7	Cn8	Cn9	C10	C11	C12	C13	C14	C15	C16	C17	C18	C19	C20	C21	C22	C23
Cx1																							
Cx2																			3				
Cx3						60											3						
Cx4							60									17			7		39		
Cx5					58		71		60		41												
Cx6						57			53		27						7		10				
Cx7								71		45											0		
Cx8					53	84				68		35	17		17	0		0					
Cx9						75		80		58				0			0		0		3		
C10				58		73		42		59					0		0		0				41
C11			67			60		66		56				5		2				6			
C12				70	52	58		78		63													20
C13				10		68		62		53		34								20			
C14		42	31		40	72	7	77								15		12					
C15						60		73		60													
C16					76	67	20																
C17						34		61										26					
C18					65					8													
C19								36															
C20																							

3.5.4 Surface exposure received by the leg

Surface UV exposures measured under low cloud cover conditions are shown in Figure 3.10 for the SZA ranges 0^o-30^o, 30^o-50^o and 50^o-80^o. The figure represents UV ER measured to the left leg and is orientated so that the anterior and calf muscle of the left leg is to the front of the figure (the knee cap faces away from the viewer). Clothing worn by the mannequin protected the upper thigh as is evident in the figure. Measurements of exposure were not made below the ankle as it was assumed that students in a playground environment would be wearing shoes and socks. The greatest exposures were received over the calf muscle region of the leg. Lower solar elevations account for increases in surface exposure ratio observed with increasing SZA in parts (b) and (c) of the figure.

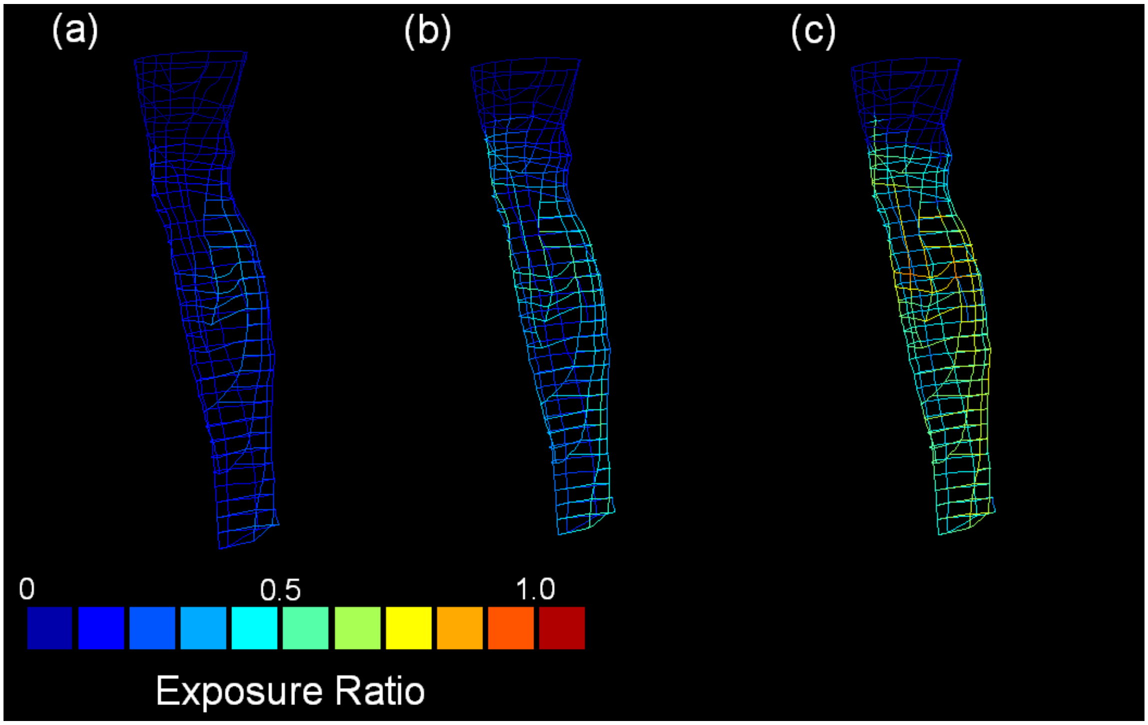

Figure 3.10: Variation in ER measured to the left leg with SZA for low cloud cover cases (a) SZA 0^o-30^o; (b) SZA 30^o-50^o; (c) SZA 50^o-80^o.

Tables 3.7(a), 3.7(b) and 3.7(c) give the mean ER data used to produce Figure 3.10. Vertical contours Cn0, Cn1, Cn2 and Cn16 are not included in the tables as these contours were located high on the mannequin leg and were well protected by clothing. These contours were small and did not extend beyond 20 cm from the upper thigh and were therefore well protected by clothing for this work.

Table 3.7(a): Site exposure ratio measured to the leg and expressed as a percentage for the SZA range 0^o-30^o and cloud cover less than 4 oktas.

	Cn3	Cn4	Cn5	Cn6	Cn7	Cn8	Cn9	Cn10	Cn11	Cn12	Cn13	Cn14	Cn15
Cx1						7	6	9					
Cx2						6	6	22					
Cx3					1	9	5						
Cx4		0	0	1	3	10	5		0	0	0	0	0
Cx5	0	3	2	2	4	11				0	0	0	0
Cx6	1	6	4	4	5	10			0	0	0	0	0
Cx7	6	8	8	6	8	9			7	12	13	9	1
Cx8		11	12	10	11	9			10	13	16	13	7
Cx9		13	15	14	15	10			10	10	15	12	9
Cx10		15	19	17	18	9			8	8	11	11	19
Cx11		14	19	19	19	10			8	6	7	11	17
Cx12		20	23	19	16	7			7	6	6	13	15
Cx13		23	20	21	16	12			6	8	8	15	15
Cx14		21	21	20	14	12			7	7	9	16	13
Cx15		20	20	19	14	14			9	8	9	14	16
Cx16		20	19	18	14	13			9	8	9	13	
Cx17			16	16	14	16			11	10	9	12	
Cx18			16	18	15	17			9	9	9	12	
Cx19			15	15	15	24			8	10	9	11	
Cx20			13	15	15				7	8	9	10	
Cx21			15	16	17				6	10	9	8	
Cx22				16	17				7	9	10	11	
Cx23				17	16				7	9	10	11	
Cx24				18	17				6	10	9	12	
Cx25				14	16				8	9	10	13	
Cx26				14	19				8	10	11	14	
Cx27					24				8	11	10	13	
Cx28					16				7	11	11	12	
Cx29									9	10	12		
Cx30									10	10	12		
Cx31									10	11	16		
Cx32									9	10	13		
Cx33										10	12		

Table 3.7(b): Site exposure ratio measured to the leg and expressed as a percentage for the SZA range 30^o-50^o and cloud cover less than 4 oktas.

	Cn3	Cn4	Cn5	Cn6	Cn7	Cn8	Cn9	Cn10	Cn11	Cn12	Cn13	Cn14	Cn15
Cx1						17	13	18					
Cx2					4	21	11	35					
Cx3		4	5	6	9	23	11						
Cx4	6	11	9	8	12	25	10						
Cx5	13	15	13	13	13	31			14	20	17		9
Cx6	21	22	18	15	20	25			16	22	25	37	19
Cx7	25	28	29	21	25	21			17	22	28	38	30
Cx8		34	33	18	38	22			17	20	26	22	29
Cx9		37	34	29	43	23			14	17	25	44	30
Cx10		52	29	38	38	23			14	10	24	44	42
Cx11		43	45	31	42	22			11	12	22	42	45
Cx12		44	44	38	33	27			13	13	21	43	31
Cx13		37	47	36	33	28			10	13	21	48	35
Cx14		33	39	44	36	35			12	12	21	46	33
Cx15		39	32	28	33	30			18	15	21	40	33
Cx16		36	32	32	30	40			14	14	21	36	
Cx17			27	31	34	35			14	14	21	35	
Cx18			29	35	35	46			14	14	20	22	
Cx19			34	31	45	41			13	14	15	26	
Cx20			21	28	41				12	13	16	27	
Cx21			32	38	48				11	15	16	26	
Cx22				38	39				11	14	17	23	
Cx23				32	36				14	16	18	29	
Cx24				26	36				11	15	19	32	
Cx25				33	37				13	15	24	29	
Cx26				26	39				16	16	19	33	
Cx27					43				13	18	23	26	
Cx28					44				15	17	25	25	
Cx29									15	18	23		
Cx30									16	19	23		
Cx31									14	21	22		
Cx32									15	19	28		
Cx33										14	25		

Table 3.7(c): Site exposure ratio measured to the leg and expressed as a percentage for the SZA range 50^o-80^o and cloud cover less than 4 oktas.

	Cn3	Cn4	Cn5	Cn6	Cn7	Cn8	Cn9	Cn10	Cn11	Cn12	Cn13	Cn14	Cn15
Cx1						33	24						
Cx2					12								
Cx3					19	36							
Cx4					22								
Cx5		35		35							47		
Cx6	43		42		40								
Cx7	50		38	36					32		50	36	51
Cx8		45	15		58								38
Cx9		63	70	41					34	37	51	56	
Cx10		62	42	58	65						37		77
Cx11		64	62	65	55				24	25		40	
Cx12		71	70		52						31		48
Cx13		62	75		46				27	25			
Cx14		60	53		56						35		47
Cx15		43	59	59	40				39	25		61	52
Cx16		62	60		45						27		
Cx17			53		44					27		57	
Cx18			56	59	51						41		
Cx19			55		57					33		42	
Cx20			46	51							45		
Cx21			49		57					24			
Cx22				58							32		
Cx23				54	60					33		37	
Cx24				51							26		
Cx25				52	58							53	
Cx26				51	53						42		
Cx27					61							45	
Cx28					50						49		
Cx29													
Cx30											41		
Cx31													
Cx32											40		
Cx33													

3.6 Summary of headform and body surface exposures

Table 3.8 represents the variation in measured ER for each of the face, neck, arm, hand and leg models. The minimum, maximum, median and first and third inter-quartile ranges are listed in the table. The highest measured exposure relative to the horizontal plane UV was received by the face at the vertex in each SZA range. Of each of the body parts studied in the 0^o-30^o SZA range, the dorsum of the hand received the highest exposure relative to the horizontal plane UV, followed by the face, the back of the neck, the forearm and legs. ERs measured within the 0^o-30^o SZA range received the strongest UV irradiance. This is due to high solar elevation and reduced atmospheric absorption caused by incident sunlight moving through a shorter atmospheric path than occurs at greater SZA. The measured pattern of exposure in the 0^o-30^o SZA range would commonly be observed in sub-tropical to low latitudes during the summer months either side of midday. At greater SZA ranges, the face and neck were found to receive the highest ER for the 30^o-50^o and 50^o-80^o SZA ranges with the hand and leg receiving higher exposures than the forearm (Table 3.8). This is due to UV radiation incident in the greater SZA ranges having a more significant influence on vertically orientated body surfaces.

Exposures to all body parts measured in this study showed an increase in ER with increasing SZA range. Apart from the ER measured in the 0^o-30^o SZA range for the back of the neck, all body parts showed a further increase in the inter-quartile range (IQR) of exposures. These findings indicate that the UV exposure received over the body surface increases relative to the horizontal plane exposure and affects a larger surface area of the body with increasing SZA.

Table 3.8: Exposure ratio statistics listed for the face, back of the neck, forearm, hand and leg in the SZA ranges 0^o-30^o, 30^o-50^o and 50^o-80^o.

	Face		
	0^o-30^o	30^o-50^o	50^o-80^o
Range	1-100%	6-100%	0-100%
IQR	15-47%	24-58%	33-70%
Median	26%	39%	48%
Total measurements	391	154	229
	Neck		
	0^o-30^o	30^o-50^o	50^o-80^o
Range	4-67%	13-69%	19-86%
IQR	16-33%	30-44%	49-67%
Median	23%	36%	59%
Total measurements	170	44	23

	Forearm		
	0^o-30^o	30^o-50^o	50^o-80^o
Range	3-61%	0-55%	2-88%
IQR	5-29%	7-35%	21-57%
Median	13%	17%	41%
Total measurements	140	175	109
	Hand		
	0^o-30^o	30^o-50^o	50^o-80^o
Range	1-76%	1-76%	0-84%
IQR	8-51%	12-57%	10-61%
Median	30%	35%	42%
Total measurements	264	119	82
	Leg		
	0^o-30^o	30^o-50^o	50^o-80^o
Range	1-39%	4-52%	12-82%
IQR	9-16%	15-33%	37-57%
Median	12%	23%	47%
Total measurements	248	231	112

While there is a clear spreading in the received exposure over a larger surface area with increasing SZA, exposures measured in the larger SZA ranges were received during periods of the day that receive a lower UV irradiance. The ER measured at sites in the 0^o-30^o SZA range, though affecting a smaller surface area receive a significant level of the ambient UV due to the higher UV irradiances that are incident at the earth's surface when the sun is located in the 0^o-30^o SZA range. The measured ranges of exposure listed in Table 3.8 provide an indication of the areas of each body part at risk of receiving high levels of solar UV radiation. Of the areas of the body surface shown to receive high exposures relative to the measured horizontal plane UV in the 50^o-80^o SZA range, those at greater risk of receiving higher exposures are reduced to the areas measured in the respective 30^o-50^o and 0^o-30^o SZA range and are clearly seen in Figures 3.1, 3.6, 3.7, 3.8 and 3.10. For populations located in sub-tropical to low latitudes that experience high solar elevations, and subsequently all of the SZA ranges studied in this research, the areas of the body surface that receive the highest UV exposure are the vertex, the nose, the cheeks, the top of the ear, the dorsa of the forearms and hand, the lower back of the neck located near the shoulder, and the calf muscle and anterior region of the leg.

3.7 Conclusions

Measurements of mannequin facial exposure were highest toward the upper facial proximities. Facial exposures measured to human subjects also show an increasing trend in ER for sites located closer to the vertex (Downs & Parisi 2008). However, exposures measured to the vertex and forehead are often protected by hair cover and hat use. Hats also offer more protection to the upper proximities of the face (Gies et al. 2006; Downs & Parisi 2008). The nose and cheek represent the highest exposure regions of the face that are positioned toward the lower limits of protection offered by hats. Measurements of high ER to the nose and cheek show that these regions of the face are likely to be at high risk of the development of solar induced disease. Measurements of body surface UV exposure patterns have been presented with respect to changing SZA. These measurements improve upon previously available data which is often limited to fewer isolated body sites. The presented collection of measured UV exposure data is of further importance in detailing the solar exposures that affect human skin surfaces which are influenced by shading caused by the body itself and surface orientation with respect to the diffuse skylight and the direct solar beam. A total of 2491 measurements of ER to the face, neck, forearm and leg have confirmed that exposures received by the face and back of the neck are greater than exposures received by both the upper and lower limbs. Of each of the studied body parts, the anatomical distribution of BCC and SCC is greatest to the face and upper limbs, particularly the dorsum of the hand and forearm (Pearl and Scott 1986; Kricker et al. 1990; Raasch et al. 1998; Giles et al. 1988). Incidence rates of both types of NMSC cancer are particularly high at the nose (Pearl and Scott 1986; Brodkin et al. 1969) and correlate with the facial ER measurements taken in this research across all SZA ranges.

CHAPTER 4 MODELLING THE PLAYGROUND UV EXPOSURE

4.1 The playground

Public schools funded by the Queensland state and Australian commonwealth governments make up approximately 70% of primary and secondary schools in Queensland (EQ 2008). These schools share a distinctive architecture common in public buildings and are often built and furnished from the same materials depending upon when they were established. A public school playground was chosen for this research as the Queensland school population is made up of predominately public students and similarities in architecture and building materials were likely to reduce errors in comparisons made between other public school playgrounds. Public schools in Queensland are commonly made up of double story weatherboard buildings, temporary demountables or single storey brick buildings, although there is some variation between schools. These buildings are typically painted with white or cream coloured paint and are often connected by a series of covered concrete pathways. Long rectangular shaped buildings are orientated East-West to minimise morning and afternoon sunlight entering classrooms.

Hervey Bay State High School (HBSHS) (25^{o}S, 153^{o}E) was chosen as the study playground. This school neighbours the University of Southern Queensland's Fraser Coast campus and experiences a yearly SZA range of between 3^o and 46^o over the summer months and 67^o and 34^o over the winter months (Michalsky 1988) during school hours from 9:00am to 3:00pm.

4.2 School children and behaviour

Open areas typically make up a significant proportion of school playgrounds, however these areas are not always proportionately occupied by children in the school population leading to overcrowding in more stimulating playground regions (Malone & Tranter 2003). During the HBSHS school playground survey, smaller numbers of children were observed using the open oval space during lunchtime breaks compared with children occupying medium and high density playground environments. This behaviour is likely to result in lower playground exposures to UV experienced during lunch breaks compared with activities that require children to be placed in an open environment, such as scheduled sporting activities.

4.3 Classification of school playground regions

The HBSHS playground covers an area of 6.5 ha, excluding the school's neighbouring agricultural plots. Approximately 16% of the playground surface area is covered by hard surfaces including concrete, paving dust, brick pavers and asphalt surfaces with another 4% of the playground surface area being covered by garden beds. The remainder of the playground surface area is covered with grass. Grass surfaces were found predominately in two large open areas or 'ovals' which consisted of the school running track and a soccer field. These two large open areas cover approximately 46% of the surveyed school playground. Hard playground surfaces were located near buildings and in high traffic areas and included pathways and school carparks. School buildings were located in proximity to one another, typically no more than 30 m apart at the western end of the playground.

The three largest school buildings were double storey rectangular shaped structures. These buildings, referred to as B, C, and D blocks have classrooms running the length of their upper level, and have classrooms and large undercover spaces accessed by students during lunch breaks on the lower level. A large school assembly hall is located in the playground's south-western corner. There were eleven large single storey buildings located in the playground. These were the administration building, the school library, the manual arts classrooms and manufacturing workshops, the art building, the canteen, the toilet block, and classroom buildings E, G, H, L and M blocks. There were several other smaller structures located in the playground, including three steel storage sheds, the pool storage building, pool canteen and pool toilet block, a large plastic shade structure, the school bus shelter, and several shade-cloth covered areas. The position of these structures and large shade providing trees are given in Figure 4.1. The figure also provides the location of the school's covered pathways that link each of the main school buildings. The types and locations of playground surfaces are provided in Figure 4.2.

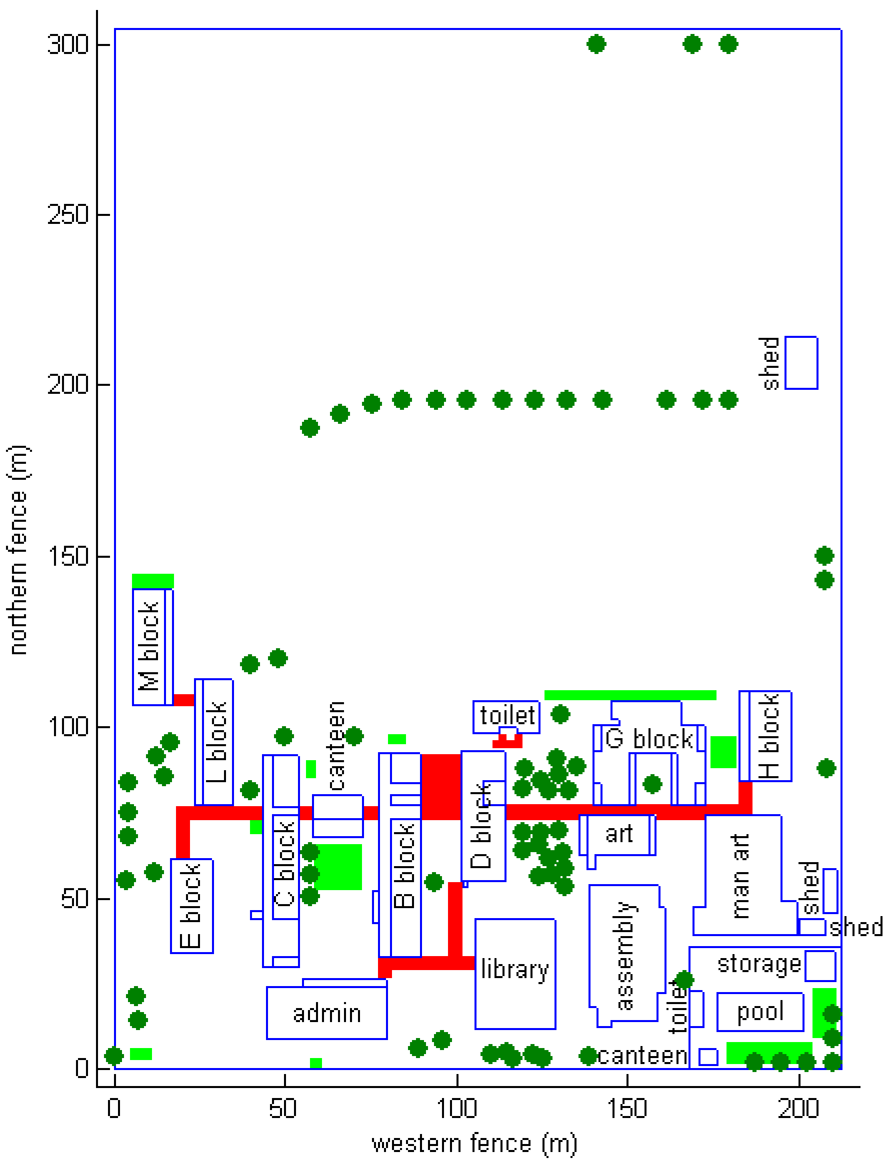

Figure 4.1: Buildings and structures located in the HBSHS playground (red: covered pathways; light green: shade structures; dark green: large tree sites).

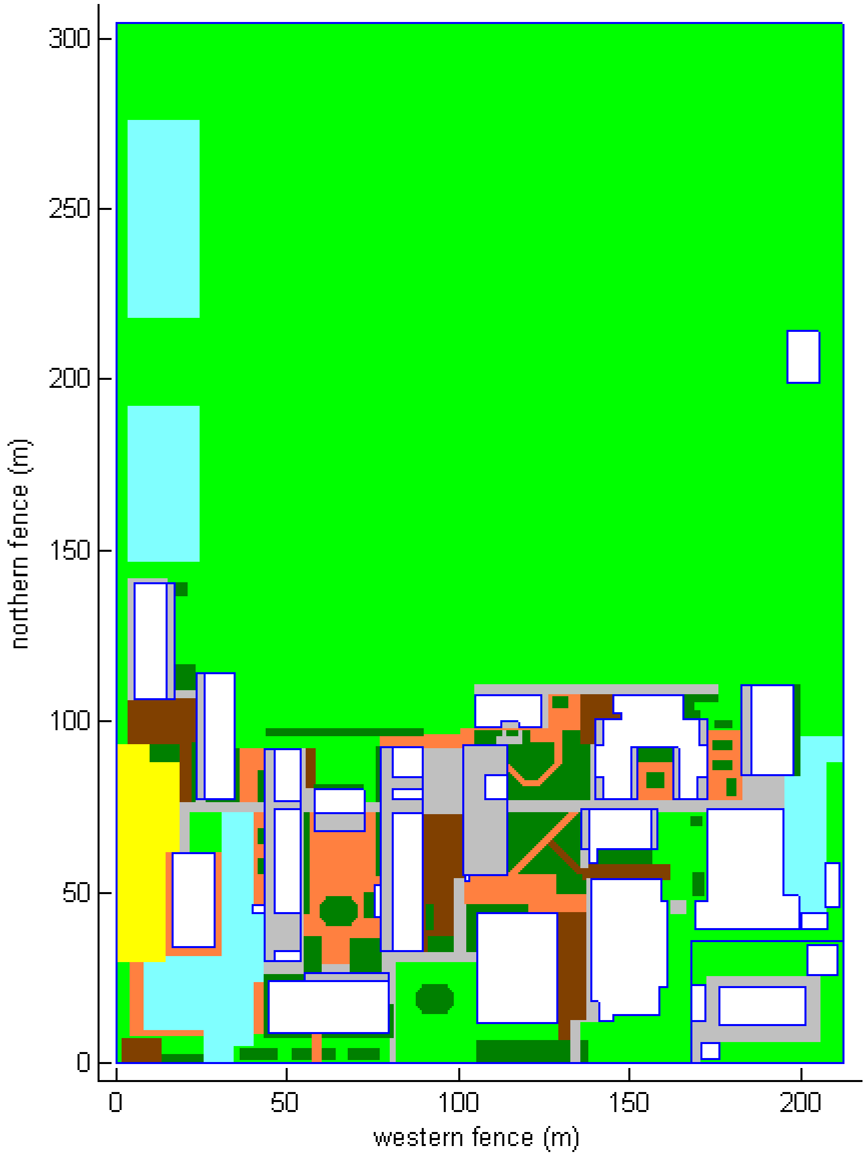

Figure 4.2: Ground surfaces located in the HBSHS playground (light green: grass surfaces; dark green: garden beds; cyan: bitumen surfaces; grey: concrete surfaces; yellow: blue metal paving dust; orange: light coloured paving; dark brown: dark coloured paving).

The playground was subdivided into 25 regions based on similarities in ground surface and surface structure (building and tree) density. Figure 4.3 is included as a reference to the numbered outdoor regions. Additional regions not given in the figure included covered areas and verandas specific to each building.

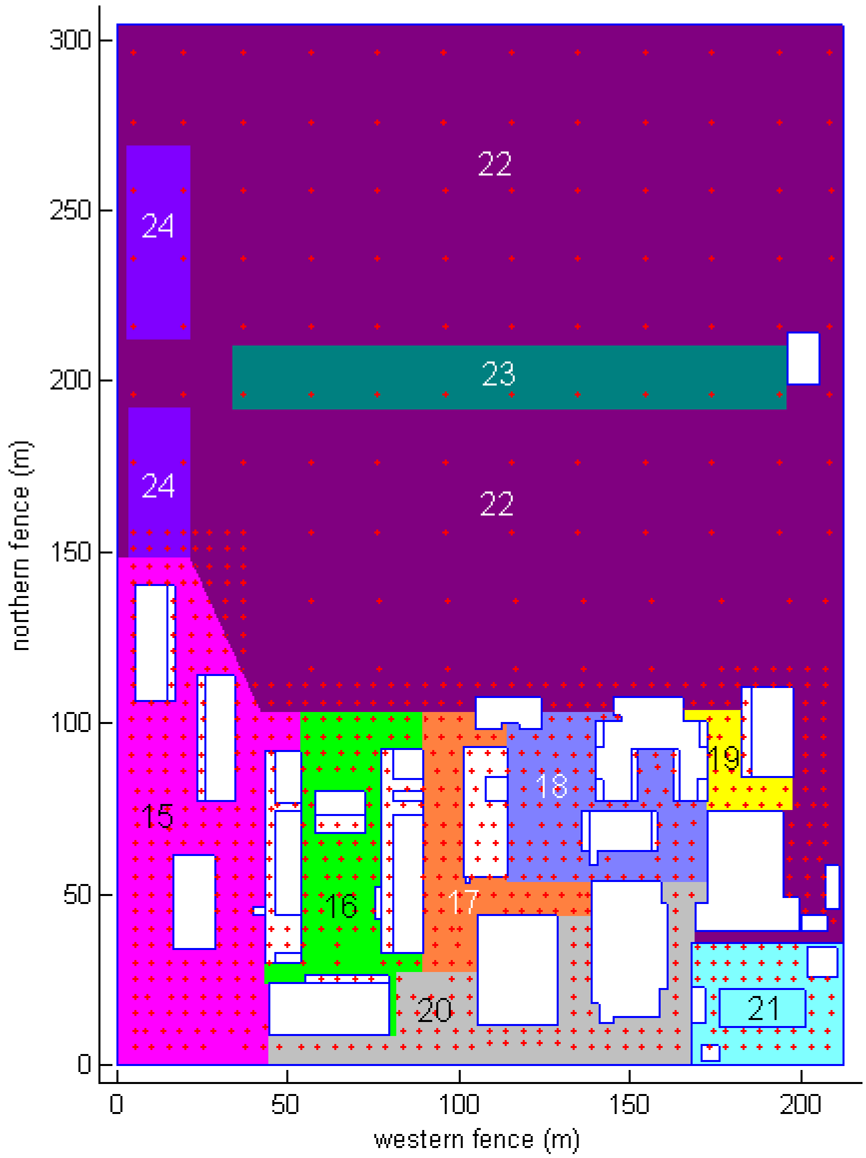

Figure 4.3: Subdivided playground regions. Each region contains similar surfaces and structure density.

4.4 The albedo of building and playground surfaces

Tables 4.1 and 4.2 list the surface materials visible in the playground and their measured UV albedo. Surface materials visible on each school building and playground surface have been provided in the appendices (Appendix J). Photographs of each of the school buildings are also provided in Appendix K. The erythemal UV albedo of ground and vertical standing surfaces given in each of the tables below was calculated as the ratio of incident to reflected UV measured along the surface normal.

The reflectivity of each surface will vary with the incident angle of the UV radiation field. For this research the diffuse UV modelled on a horizontal plane considers the vertical up-welling UV albedo of ground surfaces, influencing atmospheric backscatter. Furthermore, the direct contribution resulting from standing surface UV reflections was considered for nearby playground structures as that component of the reflected UV radiation that is vertically incident upon a horizontal plane. Reflections from highly anisotropic surfaces such as glass windows will result in variations to the albedo stated in Table 4.2 which was measured along the surface normal, resulting in increased surface reflections depending upon solar position. To minimise this uncertainty, measurements of glass window albedo were performed on windows which were protected by building awnings and were therefore measured under full shade conditions. Modelled albedo contributions from glass window surfaces are however subject to some error depending upon the time of the day playground exposures are modelled. To simplify this uncertainty, glass window surfaces are assumed to be shaded for playground surface exposure models presented in this chapter.

Table 4.1: Ground surface erythemal UV albedo. Uncertainty is stated as ±17% of the measured albedo.

Ground surface	Erythemal UV albedo (%)
Light coloured pavers	7 ± 1
Dark coloured pavers	6 ± 1
Concrete	10 ± 2
Bitumen	7 ± 1
Blue metal paving dust	8 ± 1
Grass	4 ± 1

Table 4.2: Vertical standing surface erythemal UV albedo. Uncertainties include meter measurement uncertainty of ±17% for each listed aspect added to an additional standing surface uncertainty estimate calculated as the difference in maximum and minimum measured albedo for aspects measured on north, east, south and west facing surfaces.

Standing surface	Erythemal UV albedo of standing surfaces with aspect (%)			
	North facing	East facing	South facing	West facing
White fibreboard	6 ± 8	8 ± 8	3 ± 8	1 ± 7
Light coloured brick	5 ± 6	6 ± 6	2 ± 5	7 ± 6
Dark coloured brick	4 ± 7	6 ± 7	3 ± 7	9 ± 8
White painted brick	6 ± 8	8 ± 8	1 ± 7	na
Brown painted paling	7 ± 3	6 ± 3	6 ± 3	8 ± 3
White painted paling	na	6 ± 7	1 ± 6	7 ± 7
Glass	4 ±3	2 ± 2	2 ± 2	2 ± 2
White painted blocks	7 ± 9	8 ± 9	3 ± 9	11 ± 10
White painted weatherboard	7 ± 7	1 ± 6	3 ± 7	1 ± 6
Yellow painted sleepers	6 ± 11	1 ± 10	2 ± 10	11 ± 12
Stone work	11 ± 10	12 ± 10	4 ± 9	na
Light coloured garden block	11 ± 13	6 ±12	2 ± 11	13 ± 13
Dark coloured garden block	3 ± 14	3 ± 14	2 ± 13	15 ± 16
Thick vegetation	7 ± 9	6 ± 9	2 ± 8	9 ± 10

4.4.1 Uncertainties in albedo measurement

Measurements of the UV albedo were taken using a broadband UV meter (Solar Light Co., model 3D, Philadelphia, PA 19126) and measured perpendicular to and 0.3 m from the reflecting surface. The accuracy of the broadband UV meter was determined to be in the order of ±17% for UV radiation incident at angles up to 80^{o}. Errors in albedo measurement due to hand held positioning of the broadband UV meter orientated along the approximate surface normal of all measured surfaces are estimated at ±17%. Additional uncertainties in stated albedo measurements were due to body shading reducing the sky view and therefore incident diffuse UV reflected by the measured surface, SZA at the time of measurement affecting instrument cosine response sensitivity, and variation in atmospheric parameters occurring between incident and reflected measurements. To minimise these errors measurements of surface albedo were taken in full sun conditions during cloud free periods near midday and the meter was held as far from the body as possible during measurement.

The stated albedo provided for vertical standing surfaces were subject to greater uncertainty than measurements of ground surfaces. This was due to additional factors influencing surface normal measurements that require the measuring instrument to be exposed to a greater proportion of the diffuse UV when held parallel to the horizon whereby the total surface area of the measured reflecting surface directly influences the proportion of diffuse skylight received by the measuring broadband UV meter. The albedo measured along the vertical standing surface normal and given as the ratio of incident to reflected UV experiences further variation due to meter cosine response sensitivity with SZA if direct UV radiation is incident on the meter sensor. To minimise the effect of exposure to diffuse UV when the meter was held parallel to the horizon, measurements of standing vertical surfaces were taken where possible on large surfaces in positions located well away from surface edges. Measurements of standing surface albedo were also repeated for north, south, east and west facing surfaces for each material found in the school that covered a large vertical standing area. Albedo measurements of south facing surfaces were taken in full shade, east facing surfaces were measured in the morning and west facing surfaces were measured in the afternoon to minimise the likelihood of stray direct UV contributions affecting reflected surface measurements. A surface with either a north, south, east or west aspect experiences a variation in the received UV irradiance (Webb et al. 1999). As the UV albedo is a property of the material and not the incident UV irradiance, variation in measurements indicated in Table 4.2 give some indication of the measuring meter's uncertainty when orientated parallel to the horizon. The additional uncertainty in standing surface albedo was estimated for each vertical standing surface as the maximum variation in measured standing surface albedo measured over each of the north, south, east and west facing aspects (Table 4.2). The additional uncertainty in standing surface albedo measured as the maximum range in variation with aspect, varied from between 13% listed for dark coloured garden edges and 2% listed for glass. The greater uncertainty in the albedo of surfaces such as garden beds were likely due to increased diffuse radiation affecting the albedo measurements of surfaces that have a relatively small surface area. As an approximation to the true vertical standing surface albedo, the measured albedo of standing surfaces orientated with respect to north, south, east and west were used to model the influence of the reflecting surface on the incident horizontal plane UV irradiance.

4.4.2 Total albedo contribution to ambient UV in the playground

Estimates of the direct increase in playground UV irradiance due to both standing and ground surfaces are given in Figure 4.4. The albedo plotted in the figure is the direct albedo playground estimate calculated from measurements of each ground and vertical standing surface (Tables 4.1 and 4.2) affecting each of the 822 playground survey sites. Standing surface contributions to each site albedo estimate were only included if a vertical standing surface was within 2 m of a playground survey site. For the figure, the total direct albedo contribution at each playground site was determined by adding ground surface albedo and mean standing surface albedo determined by the method outlined in Section 2.4.2.2. The total albedo contribution at each playground site shown in Figure 4.4 was further weighted to site sky view (Section 4.5), providing an estimate of those regions in the playground that make the most significant contribution to the ambient playground UV. It should be noted here that the direct albedo contribution to playground ambient UV shown in Figure 4.4 is the total albedo contribution from reflecting ground surfaces and vertical standing surfaces, not the vertically incident components of the diffuse and direct UV discussed in Chapter 2. Figure 4.4 was developed as the cumulative sum of direct measurements of the up-welling ground surface albedo for ground surfaces and the mean horizontally incident reflected UV measured parallel to the horizon for standing surfaces based on the contribution of each standing surface affecting each particular playground site. Figure 4.4 is the calculated UV albedo contribution based on the sampled surface albedo measurements for each ground and standing surface listed in Tables 4.1 and 4.2. The contributions, while not directly affecting the down-welling UV irradiance will contribute to student exposures. Figure 4.4 is provided as a reference to playground albedo contributions not modelled directly onto a horizontal plane or weighted to ER body surface measurements.

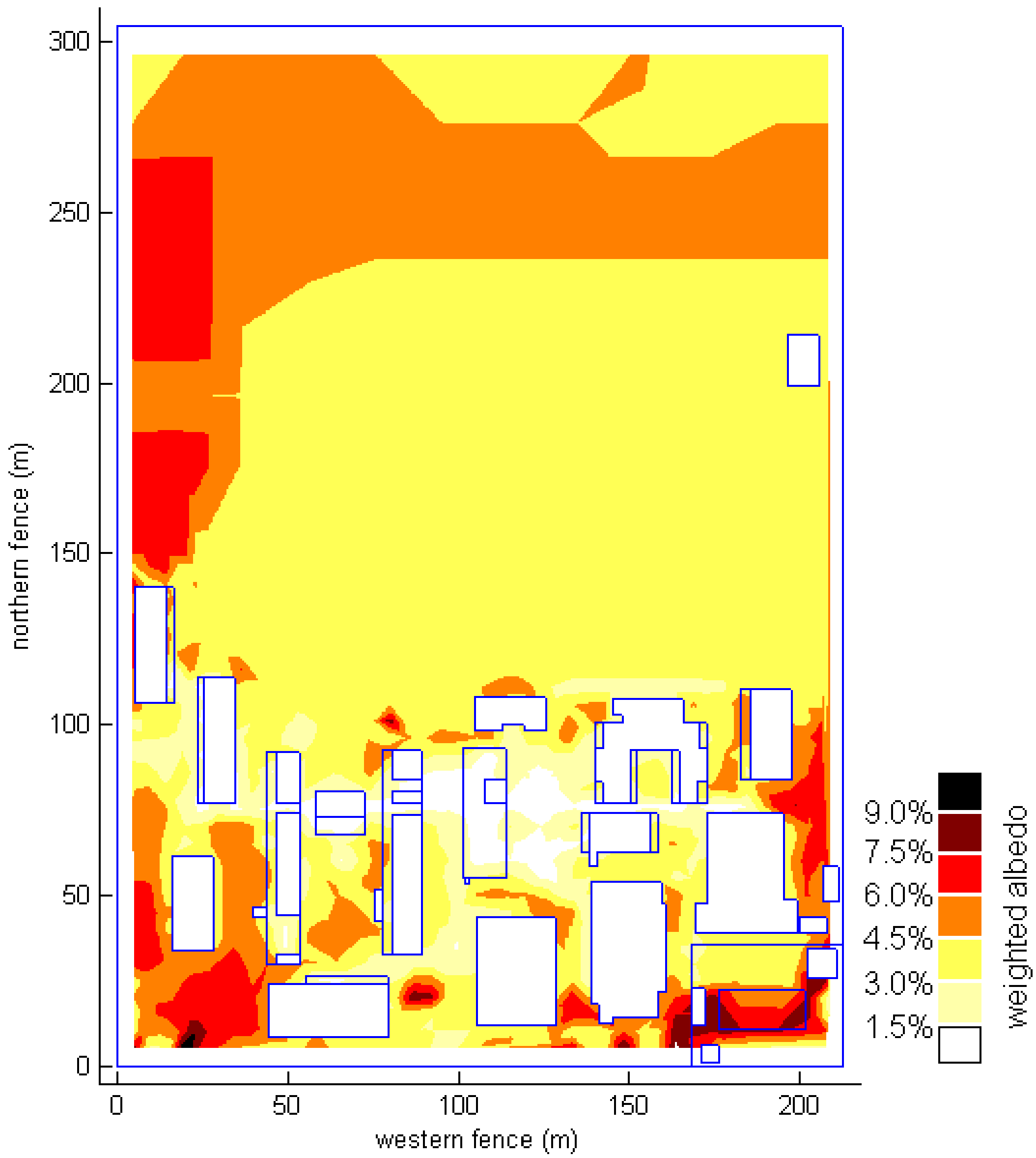

Figure 4.4: Estimated standing and ground surface contribution to the direct UV irradiance. Playground albedo in the figure is weighted to sky view (Section 4.5) to give an indication of the relative effectiveness of playground surface contributions to the sunburning ambient UV.

4.5 Playground sky view

A significant proportion of the ambient UV received at the earth's surface can be attributed to skylight with the relative proportion of UVA and UVB attributed to diffuse skylight being dependent upon the SZA. Rayleigh scattering of UV increases the proportion of UVB in diffuse skylight before and after peak daily solar elevation, while diffuse UVA is generally lower than the direct sun UVA for most of the day. Although methods for modelling the relative proportions of diffuse UV have already been discussed (Chapter 2), the additional dependence of site sky view needs to be taken into account in order to develop a playground specific model of the diffuse UV irradiance. Modelling of the diffuse UV dependence on SZA and site sky view was considered for each period and break time of the school day from 8:30am to 3:05pm observed at HBSHS for 21 June 2008 and 21 December 2008. These dates represent the winter solstice (lowest daily solar elevation) and summer solstice respectively (highest daily solar elevation).

The influence and quality of UV protection afforded by playground surface structures was assessed by measurements of playground sky view. The playground sky view was developed from measurements taken at each of the 822 survey sites located inside HBSHS (Figure 4.5). Figure 4.6 is a coloured contour map of the playground sky view measured using the survey technique described in Chapter 2. Measurements of site sky view are included in Appendix L.

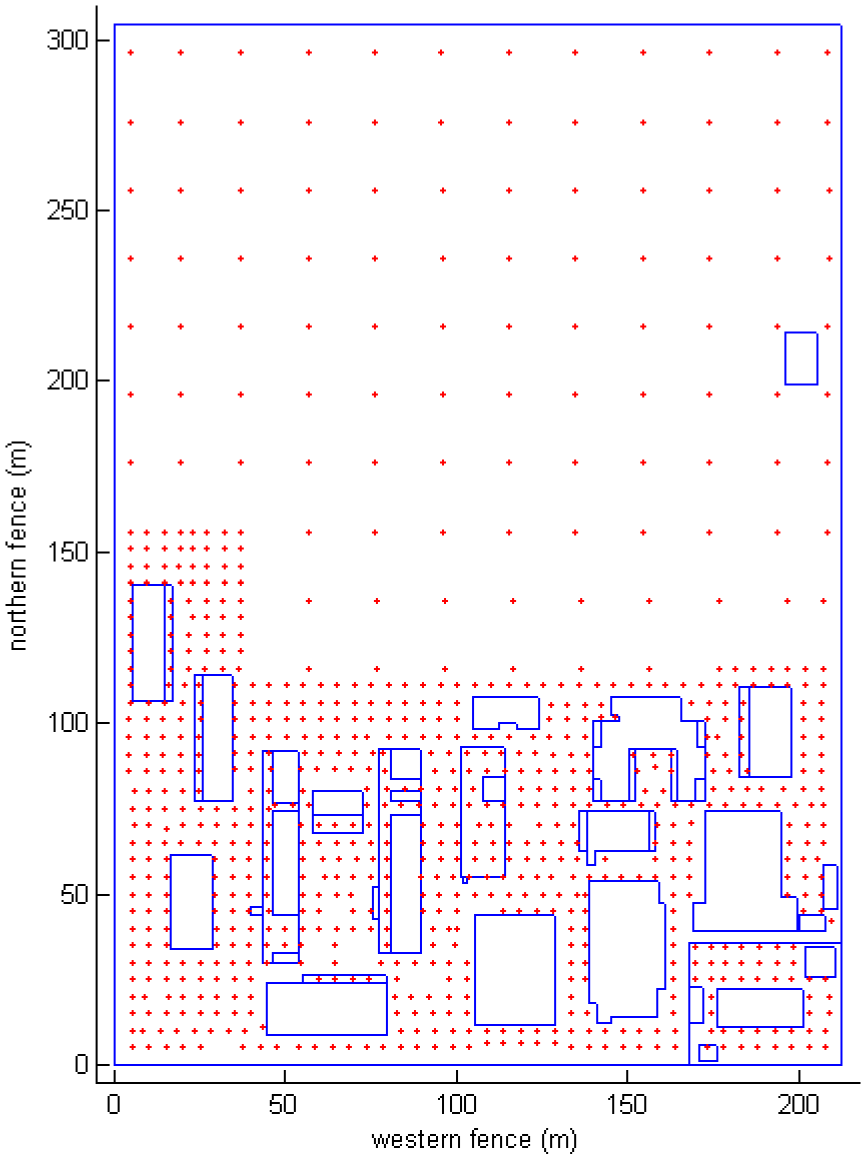

Figure 4.5: Location of sky view survey sites in the playground.

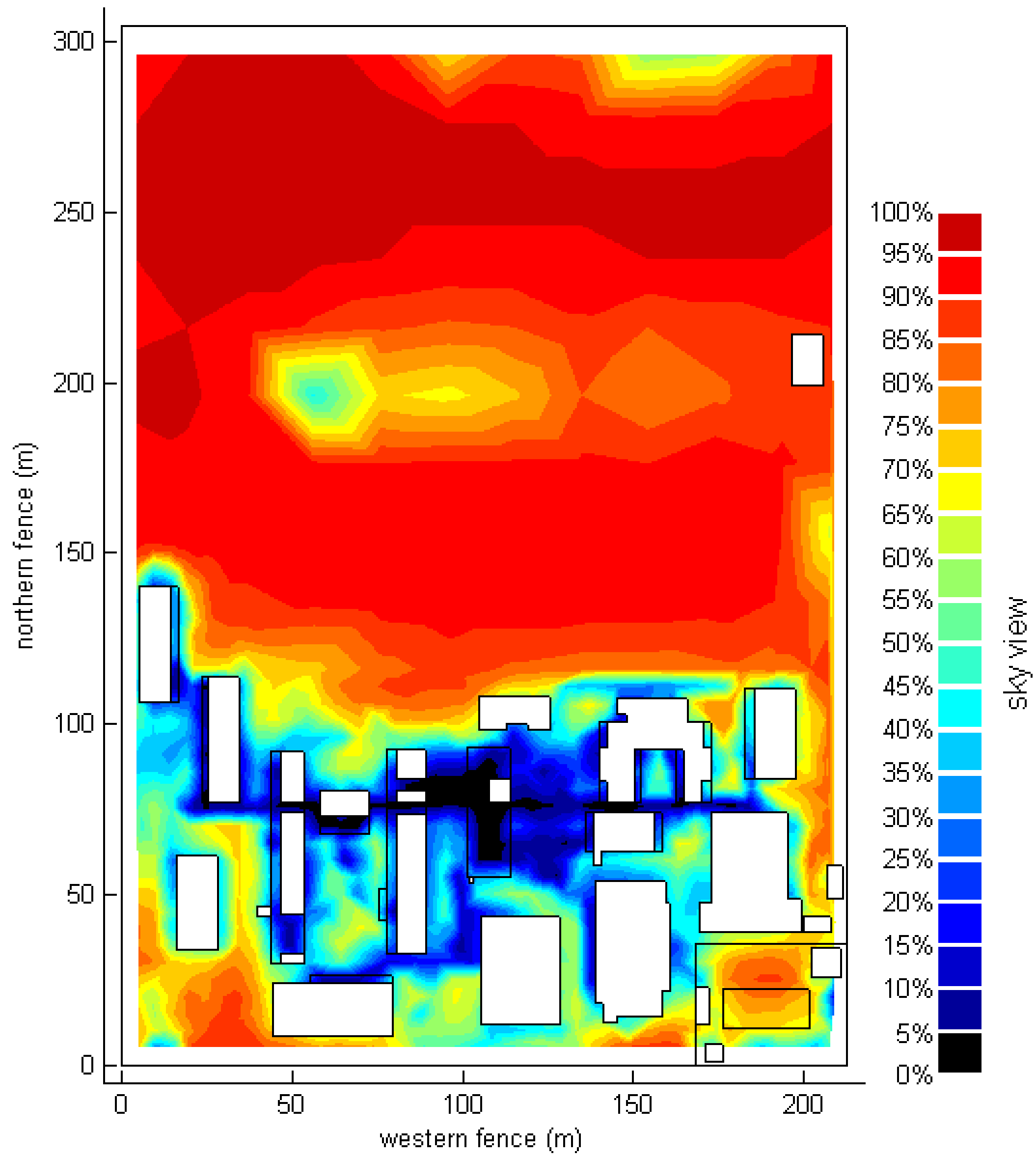

Figure 4.6: Contour map of playground sky view. The influence of covered pathways (Figure 4.1) can be clearly seen as can the influence of shading structures located in the playground.

4.6 Solar zenith angle and playground shade

The influence of shade in the playground was examined for the winter and summer solstice, 21 June and 21 December 2008 respectively. The influence of playground surface structures on shade density were examined on each of these dates during each school period and break time at 8:30am (before school), 9:35am (first school period), 10:50am (second school period), 11:45am (first lunch break), 12:40pm (third school period), 1:35pm (second lunch break), and 2:30pm (fourth school period). Apart from 8:30am, these times represent the middle of each 70 minute teaching and 40 minute break period between 9:00am and 3.05pm observed at the school. Figure 4.7 and Figure 4.8 highlight regions of shade density in the playground on 21 June and 21 December 2008 respectively where shade density (either shaded or not shaded for each of the above times) was determined by comparing the predicted position of the solar disc to playground site photographs to determine whether or not playground obstructions would cause shading at each of the 822 playground sites. Shade density was measured as one of seven shade levels illustrated in the figures below. These figures show the approximate regions of shade protection offered by playground surface structures. These regions were calculated by comparing the solar position at 8:30am, 9:35am, 10:50am, 11:45am, 12:40pm, 1:35pm and 2:30pm on 21 June and 21 December respectively to playground survey site images. Figure 4.9 shows an example of the plotted solar position on 21 June 2008. The solar position templates calculated from the SZA and azimuth position of the sun (Michalsky 1988) for 21 June and 21 December 2008 are given in Appendix M. In Figures 4.7 and 4.8, regions showing the darkest shade levels were found to be in shade for each of the seven school period and break sample times (shade density level 7) with the lightest shade level showing those regions that were in shade for only one of the seven sample times. Those playground sites that were not located in the shade were given a shade density level of 0. It is clear from the figures that there is a significant variation in shade density between the winter and summer solstice periods. The increased solar elevation during the summer solstice shows clearly the reduction in playground shade density due to the solar disc moving beyond the limiting obstruction of playground surface objects.

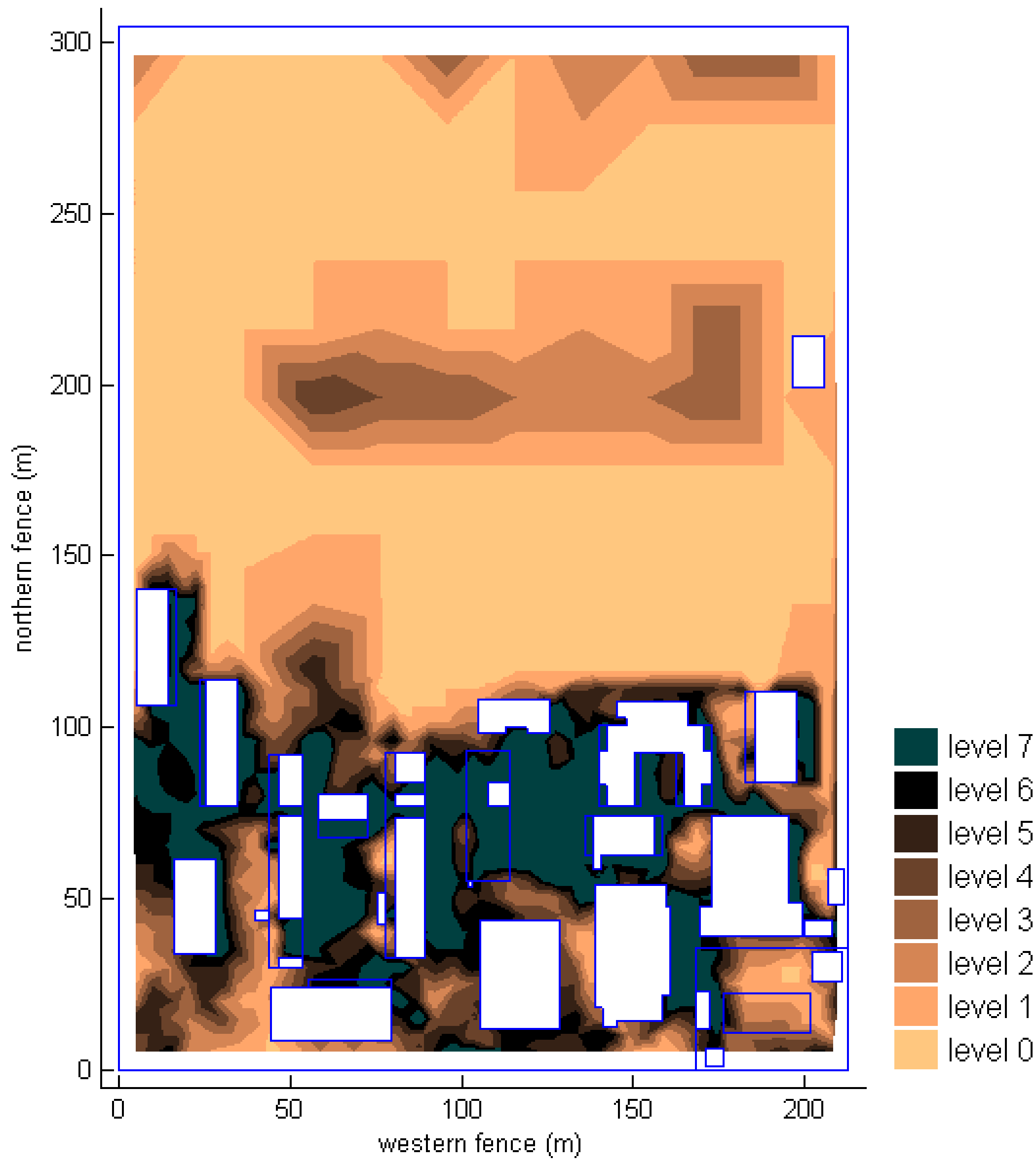

Figure 4.7: Daily playground shade density experienced on 21 June 2008 (winter solstice).

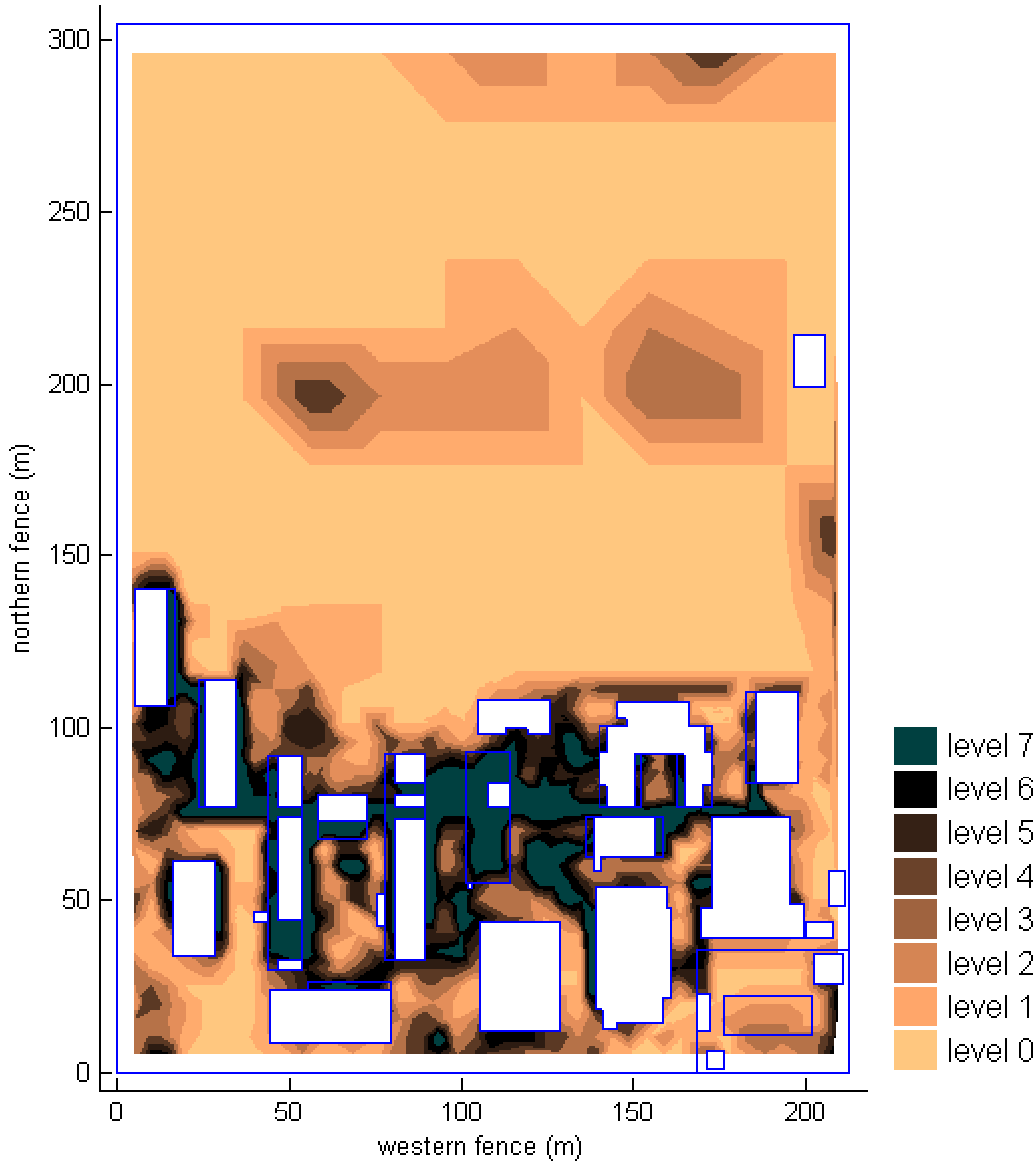

Figure 4.8: Daily playground shade density experienced on 21 December 2008 (summer solstice).

Figure 4.9: Determining shade density at playground site 86 for 21 June 2008 (Figure L.1). For this example, the playground site experiences shade at 2:30pm (white arrow – right of figure), giving a total shade density level between 8:30am and 3:05pm of 1.

4.7 Modelling seasonal variation in playground ultraviolet exposure

Both the diurnal and seasonal variation in playground ultraviolet exposure in any school environment is dependent upon the SZA, local atmospheric conditions, local geography, the positioning of shading structures in the playground such as buildings and trees, and the albedo of ground and vertical standing surfaces located in the school environment. The modelled school playground is located at sea level in a regional city of approximately 40 000 residents, local anthropogenic influences to air quality were minimal. The highest Ozone Monitoring Instrument (OMI) ozone concentrations measured over the site varied from between 303 DU and 297 DU over the respective June and December months of 2007 (TOMS 2008). The lowest ozone concentrations recorded over the same June and December period in 2007 were 250 DU and 256 DU respectively. (Appendix N lists the ozone concentrations for Hervey Bay (25^{o}S, 153^{o}E) for June and December in the year 2007).

An ozone concentration of 300 DU was input into the UV irradiance model employed in this work and was taken to be a reasonable estimate of the highest ozone concentration experienced at the study site during the winter and summer solstice period. Estimated values of the playground erythemal UV exposure received on 21 June (Figure 4.10) and 21 December (Figure 4.11) therefore represent the minimal threshold of the possible daily exposure. These figures represent the cloud free UV_{ery} exposure. Shading by playground surface structures including shade cloths, playground sky view and the influence of surface albedo contributions to the horizontal plane UV exposure were used to develop Figures 4.10 and 4.11. Additional UV irradiance model inputs used to calculate the daily exposures represented in these figures included air, aerosol and ozone species concentration with altitude, specified in this instance at sea level, and air, aerosol and ozone optical depths. These were calculated across the 280 nm to 400 nm range and are specified by the Rundel (1986) modification to the Green, Sawada and Shettle (1974), Green, Cross and Smith (1980), and Schippnick and Greeen (1982) UV irradiance equations employed by the horizontal plane UV irradiance model discussed previously. (The complete code listing of the UV irradiance model is included as supplementary material to this work. A partial code listing is provided in Appendix D). The surface albedo contributions to the UV exposures modelled in Figures 4.10 and 4.11 affect the horizontal plane only and are caused by vertically incident atmospheric backscatter from ground surface albedo and the direct vertically incident contribution due to vertical standing surfaces (equations 2.8 and 2.11). Ground and standing surface albedo contributions however (Figure 4.4.), affect the reflected direct UV irradiance which is not necessarily vertically incident upon a horizontal plane and are therefore not included in the Figure 4.10 and Figure 4.11 playground exposure representations. Essentially, the radiation that is vertically incident on a horizontal plane was considered by the horizontal plane UV irradiance model employed for this research (a 1-sided plane). Direct contributions to the UV irradiance due to reflections from playground surfaces did not influence the horizontal plane exposure model but will however influence estimates of human body surface exposure in the playground as stray reflections which have been estimated in Figure 4.4.

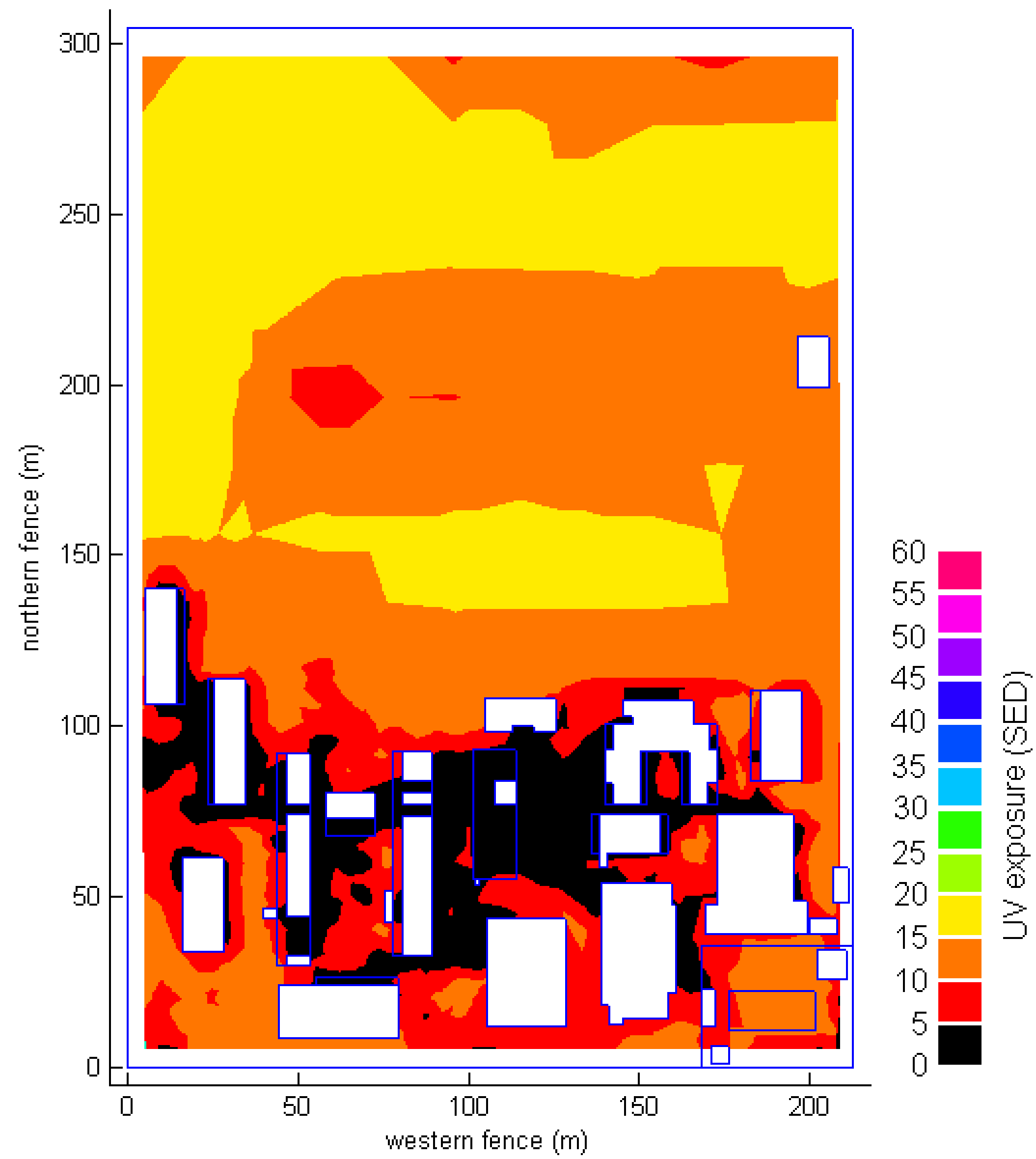

Figure 4.10: Total erythemal UV exposure received on a horizontal plane for 21 June 2008.

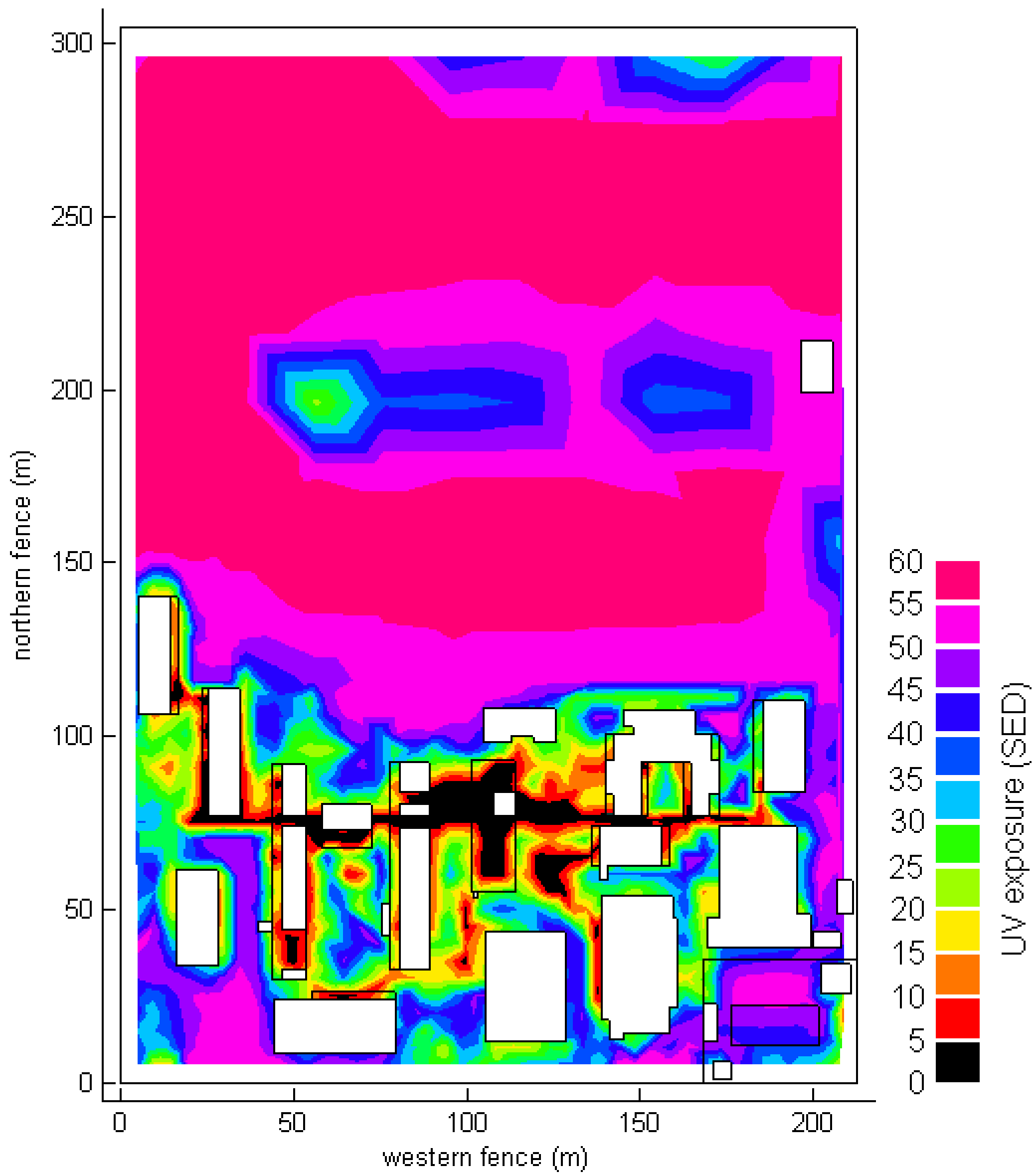

Figure 4.11: Total erythemal UV exposure received on a horizontal plane for 21 December 2008.

4.8 Playground model summary statistics

Table 4.3 summarizes the albedo, shade density, and modelled UV exposure determined at each of the 822 playground study sites by region categories, 2 to 24 (Figure 4.3). In the table, regions 2 through 14, not shown in Figure 4.3 represent covered areas and verandas associated with each school building (Figure 4.1). Specifically, regions 2 through 14 include under building and covered areas accessible to students including M block (region 2), L block (region 3), C block (region 4), B block (region 5), D block (region 6), G block (region 7), Art (region 8), H block (region 10), the canteen (region 12) and the office administration building (region 14). The complete surface and vertical standing erythemal UV albedo contribution, shade density and erythemal UV exposure model data for both the summer and winter solstice is listed for each of the 822 playground survey sites in Appendix O.

Table 4.3: Arithmetic mean, median and range statistics for site surface erythemal UV albedo, sky view, and erythemal UV exposure subdivided by playground regions 2 through 24.

Mean

Playground region	Erythemal UV surface albedo (%)	Erythemal UV standing surface albedo (%)	Shade density 21 June (level: 0-7)	Shade density 21 Dec (level: 0-7)	Sky view (%)	Erythemal UV exposure 8:30am to 3:05pm 21 June (SED)	Erythemal UV exposure 8:30am to 3:05pm 21 Dec (SED)
Region 2	10	4	7	7	24	2.4	8.2
Region 3	10	6	7	7	7	1.1	4.2
Region 4	10	4	4	6	18	4.4	9.9
Region 5	10	5	4	6	19	4.5	12.5
Region 6	10	2	7	7	5	0.8	2.7
Region 7	10	3	5	6	11	2.9	7.7
Region 8	10	3	7	7	29	3.0	10.2
Region 10	10	5	2	4	33	7.8	24.6
Region 12	10	0	7	7	1	0.1	0.2
Region 14	6	3	6	5	38	4.8	25.1
Region 15	7	2	4	2	60	8.8	41.1
Region 16	7	2	5	3	44	5.9	31.4
Region 17	8	2	5	4	33	4.9	22.9
Region 18	7	3	6	5	25	3.4	19.2
Region 19	7	1	4	3	49	7.1	33.7
Region 20	6	2	4	2	57	8.5	40.1
Region 21	6	2	3	2	64	9.7	44.4
Region 22	5	0	1	1	81	12.7	54.0
Region 23	4	1	2	2	76	11.5	46.5
Region 24	7	0	0	0	93	15.0	61.0

Median

Playground region	Erythemal UV surface albedo (%)	Erythemal UV standing surface albedo (%)	Shade density 21 June (level: 0-7)	Shade density 21 Dec (level: 0-7)	Sky view (%)	Erythemal UV exposure 8:30am to 3:05pm 21 June (SED)	Erythemal UV exposure 8:30am to 3:05pm 21 Dec (SED)
Region 2	10	3	7	7	31	3.2	10.9
Region 3	10	6	7	7	5	1.5	1.8
Region 4	10	5	4	6	14	3.2	8.3
Region 5	10	6	3	6	19	5.0	15.1
Region 6	10	0	7	7	3	0.4	1.1
Region 7	10	4	5	6	13	3.8	10.1
Region 8	10	2.5	7	7	29	3.0	10.2
Region 10	10	6	1	3.9	37	8.0	25.0
Region 12	10	0	7	7	1	0.1	0.4
Region 14	6	2	6	4.5	39	4.8	25.0

Region 15	7	0	4	1	64	9.6	45.7
Region 16	7	0	6	3	48	5.5	31.6
Region 17	7	0	6	4	30	3.9	23.0
Region 18	6	1.5	7	5	23	2.6	18.1
Region 19	7	0	5	2.4	58	8.2	38.9
Region 20	4	0	4	2	58	8.4	43.9
Region 21	4	0	2.8	1	68	10.6	48.7
Region 22	4	0	0	0	85	14.1	57.5
Region 23	4	0	2	2	80	11.6	44.2
Region 24	7	0	0	0	94	15.2	61.3

Range

Playground region	Erythemal UV surface albedo (%)	Erythemal UV standing surface albedo (%)	Shade density 21 June (level: 0-7)	Shade density 21 Dec (level: 0-7)	Sky view (%)	Erythemal UV exposure 8:30am to 3:05pm 21 June (SED)	Erythemal UV exposure 8:30am to 3:05pm 21 Dec (SED)
Region 2	10-10	6-3	7-7	7-7	34-5	3.5-0.5	11.9-1.8
Region 3	10-10	7-3	7-6	7-6	14-3	2.1-0.3	10.6-1.1
Region 4	10-10	7-0	7-0	7-4	37-2	9.1-0.3	26.1-0.7
Region 5	10-10	9.5-0	7-0	7-3	45-1	9.2-0.1	36.0-0.4
Region 6	10-10	8-0	7-5	7-4	24-0	3.6-0.0	22.6-0.0
Region 7	10-10	4-2	7-4	7-6	14-7	4.1-0.7	10.4-2.5
Region 8	10-10	3-2	7-7	7-7	32-26	3.3-2.7	11.2-9.1
Region 10	10-10	6-4	5.7-0	7-3	43-17	10.3-3.4	35.7-6.0
Region 12	10-10	0-0	7-7	7-7	1-0	0.1-0.0	0.4-0.0
Region 14	7-4	7-0	7-5	5-4	41-33	5.5-4.2	29.9-20.4
Region 15	10-4	11-0	7-0	7-0	90-4	14.5-0.4	60.2-1.4
Region 16	10-4	9-0	7-0	7-0	76-0	13.1-0.0	55.3-0.0
Region 17	10-4	9-0	7-1	7-0	76-2	13.1-0.2	54.8-0.7
Region 18	10-4	9-0	7-0	7-0	66-0	12.1-0.0	51.5-0.0
Region 19	10-4	8-0	7-0	7-0	80-1	13.7-0.1	56.2-0.4
Region 20	10-4	11-0	7-0	7-0	88-13	14.5-2.5	59.2-4.6
Region 21	10-4	11-0	7-0	6.2-0	86-17	14.3-3.6	58.2-9.2
Region 22	10-4	9-0	7-0	5-0	97-30	15.4-3.4	62.0-22.6
Region 23	4-4	9-0	4-0	4-0	92-44	14.9-6.3	60.3-23.5
Region 24	7-7	0-0	1.9-0	0-0	96-88	15.4-14.1	62.0-59.2

The mean UV_{ery} playground exposure determined for each region 2 through 24 is given also in Figure 4.12. From the data presented in the table and Figure 4.12 it can be seen that region 24, the bitumen basketball courts had the highest UV exposure during both the winter and summer solstice periods. The lowest playground UV exposures were modelled for region 12 (underneath the canteen veranda). This site although surfaced by concrete has very low sky views ranging from between 0% and 1%. The lowest modelled exposure determined for a playground region not located underneath a building or veranda was found to occur at region 18, which is predominately covered with trees. From the data presented in Table 4.3, it can be seen that sky view plays the most important role in influencing the modelled playground UV exposure. Figure 4.13 plots the mean sky view versus the modelled horizontal plane UV_{ery} exposure for 21 December 2008 at each of the 822 playground sites. The high correlation between sky view and modelled exposure (R^2 = 0.93) indicates further that playground sky view is a significant factor influencing playground exposures.

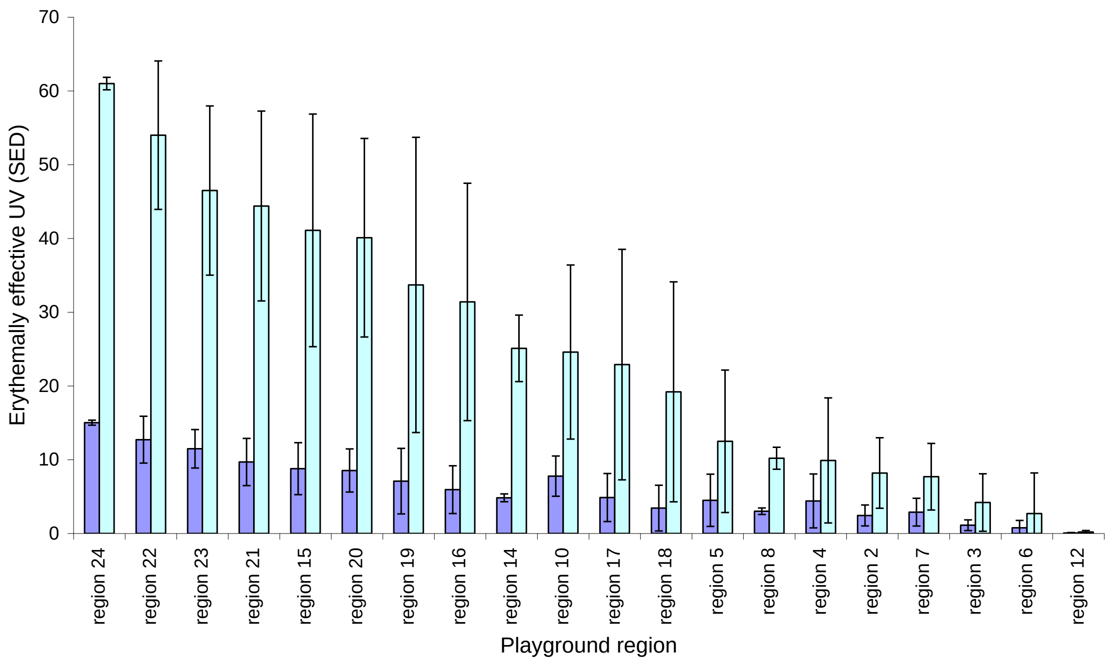

Figure 4.12: Column chart of mean erythemally effective UV exposure modelled for 21 June 2008 (dark blue columns) and 21 December 2008 (light blue columns). Error bars show the standard deviation in region exposure.

From Figure 4.13, a broader range in modelled UV exposure can be observed in middle sky view ranges. A plausible explanation for this is due to the increasingly variable nature of middle sky view environments compared to those with either high or low sky views. High sky view environments for example are open environments that are less likely to be affected by changing shade patterns throughout the day. Low sky view environments are those surrounded by a higher density of buildings and playground surface objects and are therefore those environments more likely to be in full shade during the day and therefore those environments that experience little variation in modelled UV exposure.

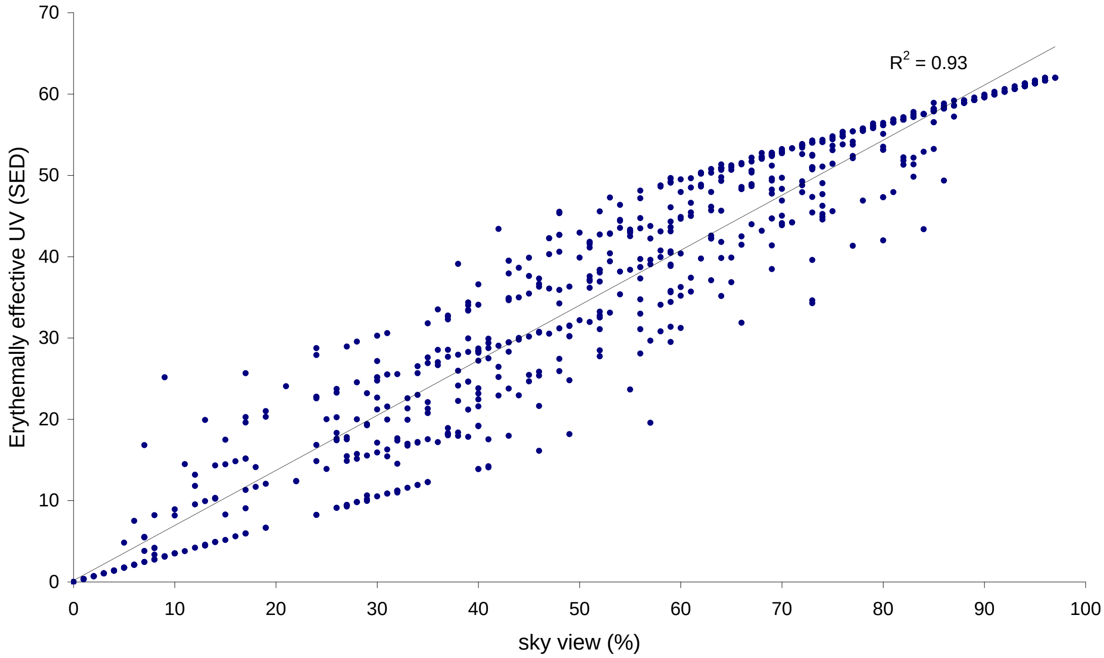

Figure 4.13: Measured site sky view versus modelled summer solstice UV_{ery}.

4.9 Significance of the playground model

The horizontal plane UV irradiance modelled for the HBSHS school playground demonstrates that variations in the incident UV irradiance are affected by sky view, shading by playground surface structures and the albedo of playground structures and surfaces. The techniques presented to model these influences presented here have been based on measurements of each of these factors. The techniques discussed, when applied to other playgrounds and outdoor environments may be used to provide an assessment of variations in the incident horizontal plane UV. Models of the horizontal plane playground UV may be further extended by weighting to body surface exposures. In this way an assessment of human exposure to UV due to influences in the playground environment can be made.

CHAPTER 5 STUDENT EXPOSURE IN THE PLAYGROUND

The modelled erythemally effective UV exposure incident in the playground environment provides a valuable tool that can be used to asses the protective influence of playground structures with daily and seasonal variation in solar elevation. Playground exposures weighted to unprotected skin surfaces of the body extend the value of the playground exposure model in assessing the risks placed upon students using the playground environment. In this chapter the risks of exposure to potentially harmful solar UV to students using the playground environment are assessed over the short term for different regions of the playground and over the long term to provide an estimate of the body surfaces that are likely to receive the greatest proportion of incident solar UV due to incidental exposures received while at school. Measurements of exposure to children using the model school environment are provided to asses the suitability of the approaches applied to model body surface exposures. The movements of children about the school environment recorded over a five month survey period are used to estimate incidental daily exposures that occur due to the outdoor behavioural patterns observed in the measured school population.

5.1 Measurements of student body surface exposure in the playground

A total of 147 measurements of personal erythemally effective UV exposures (UVE) were taken using miniaturised polysulphone dosimeters in a small cohort of the student population at HBSHS. Details of personal movements about the school playground and the measured UVE for each of the face, neck, arm, hand and leg body sites are given in Table 5.1 for the February to June measurement period. Dosimeters placed by children on the skin were located in a variety of places within each of the classified face, neck, arm, hand and leg areas but were limited to the forehead, nose, cheek, and chin for the face, the thigh just above the knee, the shin and upper foot for the leg, the outer surfaces of the upper arm and lower forearm, the back of the hand and the side and center of the back of the neck. Playground sites, noted by student participants for each measurement day were coded according to the playground regions specified in Figure 4.3. Playground regions were further subdivided into one of four categories including, indoors; shaded outdoor locations located near buildings; unshaded outdoor locations located near buildings; and open unshaded locations (Table 5.2). The calibrated UVE listed in Table 5.1 was determined using the dosimeter calibration curves (Appendix B) whereby exposure measured between 5 February and 31 March used calibration curve B.1, exposures measured between 1 April and 30 April used calibration curve B.2, and exposures measured between 1 May and 4 June used calibration curve B.3. Daily exposures include the calibrated dosimeter uncertainty of ±26%. Given exposures were calibrated under clear sky conditions, there is an increased uncertainty in the calibrated personal exposures presented for high cloud cover ranges due to the increased proportion of UVB present under such conditions. Aerosol, particulate density and the time of day during which students were exposed will also influence the calibrated exposures presented which were determined in this case from the clear sky calibration curves presented in Appendix B.1.

Table 5.1: Personal UVE measured in the school population between 5 February and 4 June 2008. Data in the table is subdivided by body site and playground region.

Summer calibration 5 February 2008 to 31 March 2008

Body site	Date	Mean cloud cover (okta)	Hat type	Region location in the School Playground Before school 8:30 to 9:00	Per. 1 9:00 to 10:10	Per. 2 10:15 to 11:25	First break 11:25 to 12:05	Per. 3 12:05 to 13:15	Second break 13:15 to 13:55	Per. 4 13:55 to 15:05	Total Exposure (SED)
arm	5/02	8/8	none	12	1	1	6,17	1	6	1	0.5 ± 0.1
arm	5/02	8/8	none	12	1	1	6	1	6	1	0.5 ± 0.1
arm	5/02	8/8	none	12	1	1	1	1	3	1	NA
arm	5/02	8/8	none	12	1	1	3	1	3	1	0.5 ± 0.1
arm	5/02	8/8	none	12,17	1	1	17	1	17	1	0.6 ± 0.1
arm	6/02	7/8	none	12	1	1	18,1	1	18	1	0.9 ± 0.2
arm	6/02	7/8	none	12	1	1	6	1	22	1	1.3 ± 0.3
arm	6/02	7/8	none	12,3	1	1	2	1	2	1	1.7 ± 0.4
arm	6/02	7/8	none	12,2	1	1	16,17,22	1	16,17,22,23,24,15	1	3.1 ± 0.8
arm	6/02	7/8	cap	12	1	1	1	1	12	1	0.9 ± 0.2
arm	6/02	7/8	none	12,20	1	25	20	1	20	1	2.6 ± 0.7
arm	6/02	7/8	none	12	1	1	3	1	1	1	1.0 ± 0.3
arm	6/02	7/8	none	12	1	1	9	11	9	1	5.2 ± 1.4
arm	6/02	7/8	none	12	1	1	22	1	12	1	1.5 ± 0.4
arm	6/02	7/8	none	12	1	1	12,22	1	12,22	1	2.9 ± 0.8
arm	6/02	7/8	none	12	1	1	10,19	1	10,19	1	5.0 ± 1.3
arm	6/02	7/8	none	12,1	1	1	3	1	1,14,8	1	0.7 ± 0.2
arm	6/02	7/8	none	12	1	1	16	1	22	1	2.7 ± 0.7
arm	6/02	7/8	NA	12	1	1	16	1	16	1	1.4 ± 0.4
arm	6/02	7/8	none	12,18	1	1	1	1	1	1	0.5 ± 0.1
arm	6/02	7/8	none	12	1	1	6	1	6	1	1.2 ± 0.3
arm	6/02	7/8	none	1	22,1	1	1,18	1	1,18	1,18	0.1 ± 0.0
upper arm	7/02	0	none	16,12	1	1	1	1	1	1	0.2 ± 0.0
upper arm	8/02	0	none	19,18,17,12	1	1	17,18	1	1	1	1.2 ± 0.3
upper arm	15/02	0	NA	21	21	21	21	21	21		15.8 ± 4.1
face vertex	15/02	0	NA	21	21	21	21	21	21		39.7 ± 10.3
face vertex	15/02	0	NA	21	21	21	21	21	21		39.6 ± 10.3
face vertex	15/02	0	NA	21	21	21	21	21	21		32.0 ± 8.3
upper arm	15/02	0	NA	21	21	21	21	21	21		12.3 ± 3.2
face vertex	15/02	0	NA	21	21	21	21	21	21		49.8 ± 12.9

arm	15/02	0	none	21	21	21	21	21	21		4.9 ± 1.3
upper arm	15/02	0	NA	21	21	21	21	21	21		38.7 ± 10.1
face cheek	21/02	0-4/8	none	12	11	1	16	1	1	22	3.5 ± 0.9
face	21/02	0-4/8	NA	12,15	25	1	18	1	18	22	5.0 ± 1.3
neck front	21/02	0-4/8	none	12	1	1	6	1	6	1	1.6 ± 0.4
face	21/02	0-4/8	none	12	22,2	11	22,23	1	23	1	2.5 ± 0.7
face cheek	21/02	0-4/8	none	12	1	1	12	1	1,12	22	3.2 ± 0.8
face cheek	21/02	0-4/8	none	12	1	1	1	1	1	1	0.5 ± 0.1
face cheek	21/02	0-4/8	none	12	1	1	1	1	1	1	0.4 ± 0.1
face cheek	21/02	0-4/8	none	12	1	1	1	1	19	1	1.5 ± 0.4
face	21/02	0-4/8	NA	12	1	11	15,16,17	1	19	1	6.9 ± 1.8
neck front	21/02	0-4/8	none	12	1	1	10	1	NA	NA	0.4 ± 0.1
face cheek	21/02	0-4/8	none	12	1	1	22	1	NA	22	7.2 ± 1.9
forearm	27/02	0	none	12,17	1	22	17	1	1	1	5.6 ± 1.5
forearm	27/02	0	none	12	1	1	1	1	1	1	0.5 ± 0.1
upper arm	27/02	0	cap	12,18,6	1	1	19	25	19	1	6.6 ± 1.7
forearm	27/02	0	none	12,6	1	1	8	1	5	1	2.4 ± 0.6
arm	27/02	0	none	12	1	1	16	1	1,22,16	1	2.5 ± 0.7
arm	27/02	0	none	12	1	1	NA	1	1	1	1.5 ± 0.4
hand back	28/02	7/8	cap	12,17	1	25,22	1	1	1	NA	8.8 ± 2.3
hand back	28/02	7/8	none	12	1	1,22	1	1	1	NA	2.9 ± 0.8
hand back	28/02	7/8	none	12,3	1	1,22	1	1	1	1	2.9 ± 0.8
hand back	28/02	7/8	none	12,16	1	1,22	2	1	10	1	2.9 ± 0.7
hand back	28/02	7/8	none	12	25,1	1,22	12	1	12	1	2.0 ± 0.5
hand back	28/02	7/8	none	12	25,1	1,22	12	1	12	1	4.0 ± 1.1
hand back	28/02	7/8	NA	12	1	1,22	12	1	12	21	5.9 ± 1.5
hand back	28/02	7/8	none	12,16	1	1,22	2	1	10	25	6.2 ± 1.6
forearm	6/03	4/8	none	12,15	1	1	12,16	1	12,16	1	2.5 ± 0.7
Leg shin	6/03	4/8	wide	12	25	1	22	1	12,16	22	4.2 ± 1.1
Leg shin	6/03	4/8	none	12,16	1	1	1	1	1	22	5.8 ± 1.5
Leg foot	6/03	4/8	none	12,6	1	1	1	1	19	1	2.7 ± 0.7
Leg thigh	6/03	4/8	cap	12	25	1	22	1	12,22	22	5.1 ± 1.3
Leg foot	6/03	4/8	none	12	1	1	1	1	1	22	4.6 ± 1.2
Leg	6/03	4/8	NA	12	25,1	1	12	1	12	1	3.3 ± 0.9
Leg shin	6/03	4/8	none	12,24	1	1	24	1	24	22	3.1 ± 0.8
Leg	6/03	4/8	NA	12	1	1	15	1	1	1	1.0 ± 0.3
Leg shin	6/03	4/8	none	12,6	1	1	16	1	19	1	3.7 ± 1.0
Leg shin	6/03	4/8	none	12,6	1	1	1	1	19	25	4.5 ± 1.2
forearm	6/03	4/8	none	12,1	1	1	16	1	1	1	3.4 ± 0.9
Leg thigh	6/03	4/8	none	12	25	1	22	1	1	1	4.2 ± 1.1
forearm	6/03	4/8	NA	12	1	1	16	1	16	1	2.3 ± 0.6
hand back	7/03	4/8	none	12	1	1	9	1	9	1	1.2 ± 0.3
Leg shin	7/03	4/8	none	12	1	1	9	1	9	1	1.7 ± 0.5
hand	7/03	4/8	none	12	1	1	15	1	1	1	1.9 ± 0.5
Leg shin	7/03	4/8	none	12,15	1	1	16	1	22	22	7.2 ± 1.9
forearm	13/03	NA	none	12,15	1	1	16	1	16,23	1	3.9 ± 1.0
forearm	13/03	NA	none	12	1	1	NA	1	7	1	4.1 ± 1.1
forearm	13/03	NA	none	12	25,11	1	18	1	18	22	11.7 ± 3.0
arm	13/03	NA	none	12	1	1	12	1	1	1	2.7 ± 0.7
arm	13/03	NA	none	12	25	1	22	1	22	22	9.0 ± 2.4
arm	13/03	NA	NA	12	1	1	23	1	23	1	3.3 ± 0.9
forearm	13/03	NA	none	12	1	1	1	1	1	25	4.4 ± 1.1
arm	13/03	NA	none	12	1	1	16	1	1	1	2.5 ± 0.6
neck	26/03	NA	NA	12,7	1	1	7	1	7	1	2.9 ± 0.7
neck	26/03	NA	none	12	1	1	7	1	7	1	3.8 ± 1.0
neck	26/03	NA	none	12,16	1	1	23	1	1	1	2.2 ± 0.6
neck	26/03	NA	none	12,6	1	25	19	1	1	1	4.6 ± 1.2

Autumn calibration 1 April 2008 to 30 April 2008

Body site	Date	Mean cloud cover (okta)	Hat type	Region location in the School Playground							Total Exposure (SED)
				Before school 8:30 to 9:00	Period 1 9:00 to 10:10	Period 2 10:15 to 11:25	First break 11:25 to 12:05	Period 3 12:05 to 13:15	Second break 13:15 to 13:55	Period 4 13:55 to 15:05	
neck	3/04	NA	NA	12	NA	NA	NA	NA	NA	NA	1.1 ± 0.3
neck	3/04	NA	NA	12	NA	NA	NA	NA	NA	NA	1.4 ± 0.4
forearm	3/04	NA	NA	12	1	25					3.1 ± 0.8
forearm	3/04	NA	NA	12	1	25					2.9 ± 0.7
lower arm	3/04	NA	NA	12	1	1	NA	1	NA	1	1.2 ± 0.3
lower arm	3/04	NA	NA	12	1	1	NA	1	NA	1	0.8 ± 0.2
upper arm	3/04	NA	none	12	1	1	3	1	3	1	0.8 ± 0.2
forearm	3/04	NA	none	12	1	1	3	1	3	1	0.8 ± 0.2
forearm	16/04	1/8-5/8	NA	12	1	1	22	25	22	1	4.3 ± 1.1
forearm	16/04	1/8-5/8	NA	12	1	1	18	1	18	1	1.2 ± 0.3
face vertex	16/04	1/8-5/8	none	12	1	1	1	25	1	1	6.8 ± 1.8
Leg shin	16/04	1/8-5/8	none	12	1	1	1	25	1	1	1.7 ± 0.4
hand back	16/04	1/8-5/8	none	12	1	1	7	1	7	1	1.1 ± 0.3
Leg shin	16/04	1/8-5/8	none	12	1	1	7	1	7	1	1.2 ± 0.3
arm	16/04	1/8-5/8	cap	12,16	1	1	2	11			4.6 ± 1.2
hand back	16/04	1/8-5/8	none	12	1	25	19	1	19	1	4.2 ± 1.1
forehead	16/04	1/8-5/8	none	12	1	25	19	1	19	1	3.4 ± 0.9
hand back	17/04	7/8-2/8	none	12,15	1	1	15	1	1	1	0.4 ± 0.1
hand back	17/04	7/8-2/8	none	12,15	1	1	15	1	1	1	0.9 ± 0.2
hand back	17/04	7/8-2/8	NA	12	NA	NA	NA	NA	NA	NA	0.8 ± 0.2
hand back	17/04	7/8-2/8	NA	12	NA	NA	NA	NA	NA	NA	0.8 ± 0.2
hand back	17/04	7/8-2/8	none	12	1	25	18	1	17		3.7 ± 1.0
Leg shin	17/04	7/8-2/8	none	12	1	25	18	1	17		2.0 ± 0.5
hand back	17/04	7/8-2/8	none	12	1	1	2	1	6	1	0.9 ± 0.2
hand back	17/04	7/8-2/8	none	12,6	1	1	1	1	1	25	0.5 ± 0.1
hand wrist	23/04	4/8	NA			22	22	22	22	22	1.1 ± 0.3
forearm	23/04	4/8	NA			1	18	22	22	22	1.1 ± 0.3

forearm	23/04	4/8	NA			1	18	22	22	22	1.6 ± 0.4
forearm	23/04	4/8	NA			25	1	22	22	22	2.5 ± 0.7
forearm	23/04	4/8	NA			1	18	22	22	22	1.4 ± 0.4
forearm	23/04	4/8	NA			1	18	22	22	22	1.4 ± 0.4
forearm	23/04	4/8	NA			1	15	22	22	22	1.3 ± 0.3
face cheek	30/04	4-2/8	none	12	1	25	1	1	1	1	0.6 ± 0.2
face cheek	30/04	4-2/8	none	12	1	25	1	1	1	1	0.7 ± 0.2
neck side	30/04	4-2/8	none	12	1	1	1	1	1	1	1.2 ± 0.3
forearm	30/04	4-2/8	none	12	1	1	1	1	1	1	0.3 ± 0.1
neck side	30/04	4-2/8	none	12,16	1	1	20	1	20	1	3.0 ± 0.8

Autumn calibration 1 May 2008 to 4 June 2008

Body site	Date	Mean cloud cover (okta)	Hat type	Region location in the School Playground							Total Exposure (SED)
				Before school 8:30 to 9:00	Period 1 9:00 to 10:10	Period 2 10:15 to 11:25	First break 11:25 to 12:05	Period 3 12:05 to 13:15	Second break 13:15 to 13:55	Period 4 13:55 to 15:05	
hand back	1/05	0-5/8	none	12,16	1	1	2	1	7	NA	0.1 ± 0.0
neck side	1/05	0-5/8	none	12,1	1	1	1	1	1	1	0.1 ± 0.0
neck side	1/05	0-5/8	none	12,1	1	1	1	1	1	1	0.4 ± 0.1
hand back	1/05	0-5/8	none	12	1	1	1	1	1	NA	0.2 ± 0.1
hand back	1/05	0-5/8	none	12	1	1	1	1	1	NA	0.2 ± 0.0
hand back	1/05	0-5/8	none	12	1	1	1	1	1	1	0.4 ± 0.1
forehead	1/05	0-5/8	none	12	1	1	1	1	1	1	0.1 ± 0.0
arm	15/05	4/8	none	12	25,1	1	22	1	1	1	2.0 ± 0.5
arm	15/05	4/8	cap	12	1	1	1	25	16	1	1.7 ± 0.4
arm	15/05	4/8	cap	12	1	1	1	25	16	1	1.0 ± 0.3
arm	15/05	4/8	none	12	1	1	22	1	22	1	1.6 ± 0.4
forearm	15/05	4/8	none	12	1	1	22	1	22	1	1.6 ± 0.4
hand back	15/05	4/8	none	12,16	1	1	1	1	17	NA	0.2 ± 0.1
hand back	15/05	4/8	none	12,16	1	1	1	1	17	NA	0.3 ± 0.1
hand back	15/05	4/8	none	12	1	1	1	1	1	NA	0.0 ± 0.0
hand back	15/05	4/8	none	12	1	1	1	1	1	NA	0.3 ± 0.1
hand back	21/05	0	none	12	1	1	19	1	19	1	1.3 ± 0.3
hand back	21/05	0	none	12	1	1	1	NA	NA	NA	2.6 ± 0.7
hand back	21/05	0	NA	12	1	1	1	1	1	1	0.8 ± 0.2
hand back	21/05	0	none	12	1	1	10	22	10	1	0.2 ± 0.1
hand back	21/05	0	cap	12	1	1	2	25	2	1	0.5 ± 0.1
hand back	21/05	0	none	12,16	1	1	3	NA	NA	NA	0.3 ± 0.1
hand back	4/06	6/8-2/8	none	12	1	25	3	1	3	1	0.6 ± 0.2
hand back	4/06	6/8-2/8	none	12	1	1	1	25	15	1	1.8 ± 0.5

[1] Where data was not recorded this has been marked with an NA. Some daily measurements of exposure started later than 8:30am or finished before 3:05pm, in these cases no student movement pattern is recorded in the table and these spaces are left blank.

Table 5.2: School playground regions.

Inside	Near buildings and shaded from direct sunlight	Near buildings and not shaded from direct sunlight	open areas
Region 1 - Indoors or Classroom	Region 2 - Under Building or Covered Area – M block (Maths/Science)	Region 15 – Near Buildings Science / Music / Maths / C Block	Region 21 – Pool
	Region 3 - Under Building or Covered Area – L block (Music)	Region 16 – Near Buildings C Block / B Block / Canteen / Office	Region 22 – Oval
	Region 4 - Under Building or Covered Area – C block (Home Ec)	Region 17 – Near buildings B Block / D block / Library	Region 23 – Tree line
	Region 5 - Under Building or Covered Area – B block (Computers)	Region 18 – Near buildings Fist year Centre / Art / Toilet Block	Region 24 – Basketball / Netball courts
	Region 6 - Under Building or Covered Area – D block (Chinese)	Region 19 – Near buildings Manual Arts / Drama First /Year Centre	Region 25 – Agriculture
	Region 7 - Under Building or Covered Area – G block (First Year Centre)	Region 20 – Near buildings Library / Great Hall / Art	
	Region 8 - Under Building or Covered Area – G block (Art)		
	Region 9 - Under Building or Covered Area – F block (Manual Arts)		
	Region 10 - Under Building or Covered Area – H block (Manual Arts / Drama)		
	Region 11 - Under Building or Covered Area – Agriculture		
	Region 12 - Under Building or Covered Area – Canteen		
	Region 13 - Under Building or Covered Area – Library		
	Region 14 - Under Building or Covered Area – Office		

5.1.1 Swimming carnival exposure

From Table 5.1, the largest variation in personal UVE exposure recorded over the February to June measurement period occurred on 15 February 2008. This was the date of the school's annual swimming carnival which was run between 9:00am and 2:30pm. For this day, UVE exposures to the arm were recorded at 15.8 ± 4.1 SED, 12.3 ± 3.2 SED, 4.9 ± 1.3 SED and 38.7 ± 10.1 SED. Vertex measurements were also taken during the school swimming carnival measuring 39.7 ± 10.3 SED, 39.6 ± 10.3 SED, 32.0 ± 8.3 SED and 49.8 ± 12.9 SED. Personal UVE exposures measured during the swimming carnival were well in excess of the national occupational limit of exposure to solar UV incident upon the skin or eye which is between approximately 1.1 and 1.4 SED for an 8 hour working day (NHMRC 1989, ARPANSA 2006). Specifically, the occupational exposure limit adopted by the NHMRC (1989) and ARPANSA (2006) standards is that specified by the International Radiation Protection Association (IRPA 1989) and represents a weighted UV exposure of 30 Jm^{-2}. The weighted action spectrum for occupational exposure is different from the erythemal weighting used to derive the SED unit (Figure 1.7). As an approximation to the International Commission on Non-Ionizing Radiation Protection (ICNIRP 1999) guidelines for the specific wavelength dependent weighting of the occupational action spectrum adopted by the NHMRC (1989) and ARPANSA (2006) standards, Gies and Wright (2003) relate the CIE (1987) erythemally weighted exposure to the ICNIRP (1999) occupational weighted exposure, giving ratios of 3.5 to 4.5 at mid latitudes (30^{o}S) between 9:00am and 5:00pm. This represents between 105 Jm^{-2} (1.05 SED) and 135 Jm^{-2} (1.35 SED) of erythemally effective radiation. The lower limit of occupational exposure (105 Jm^{-2}) occurs near solar noon and is lower due to the increased relative proportion of ambient UVB at that time and the spectral differences above 300 nm in the ICNIRP (1999) and CIE (1987) weighted spectra.

Measurements of UVE exposures recorded on students placed in an outdoor environment for the entire school day show a significant increase compared to measured exposures recorded over periods during which the normal school routine was observed.

It is clearly evident from this data, that consideration and preparation by school authorities should be given to the planning of outdoor school activities that run over an entire day, particularly during summer. The active use of hats, protective clothing, sunscreen and exposure avoidance during periods of peak UV intensity need to be practiced if schools are to meet their obligations in reference to occupational UV exposure standards set out by both the NHMRC (1989) and ARPANSA (2006) standards.

The measured swimming carnival exposure results, while not typical of a student's incidental playground exposure received during a normal school day, highlight the importance of planning and scheduling outdoor events including fun runs and sports carnivals during which there is a high probability of students receiving severe sunburns which is a well recognized risk factor for the later development of melanoma and NMSC. Additional risks, including cumulative exposure to solar UV are present due to the day to day use of the school playground.

5.1.2 Incidental playground exposures

The mean incidental personal UVE playground exposure recorded over the February to June measurement period was 2.4 ± 2.1 SED (1σ). Mean personal exposures measured over the summer-autumn (5 February to 31 March), mid autumn (1 April to 31 April) and autumn-winter (1 May to 4 June) measurement periods were 3.1 ± 2.3 SED (1σ), 1.8 ± 1.5 SED (1σ) and 0.8 ± 0.7 SED (1σ) respectively. These exposures while averaged over body sites and variations in cloud coverage are significantly lower than exposures measured during the school swimming carnival. Due to the potential for students to spend various amounts of time in the sun during the school day there is also a large variation, evident in the large deviation from the mean exposures quoted above, in measured personal UVE exposure. The frequency distribution of incidental school time UVE exposures measured between February and June 2008 is plotted in Figure 5.1.

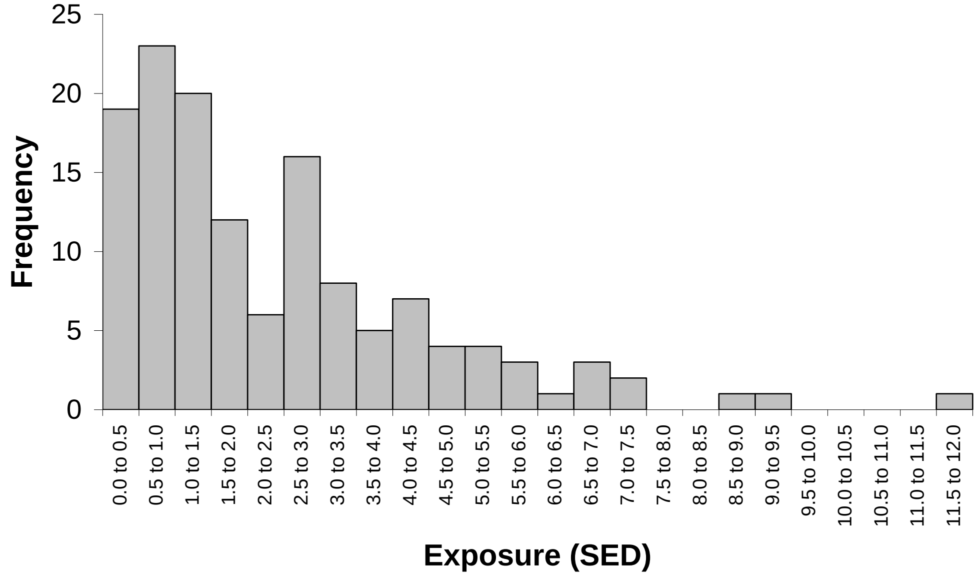

Figure 5.1: Frequency distribution of daily personal UVE exposure measured between February and June 2008.

Clearly evident in the above figure are the number of exposures skewed toward the lower daily exposure range, with the greatest number of students receiving incidental playground exposures of between 0.5 and 1.0 SED. The modelled daily horizontal plane playground UV_{ery} averaged over each of the 822 survey sites varied from between 8.3 ± 4.8 SED (1σ) and 37.3 ± 19.8 SED (1σ) for the winter and summer solstice respectively. The disparity in the comparison between personal daily UVE exposure and the modelled daily playground UV_{ery} is caused by the time students spend in classrooms reducing the total daily playground exposure. The tendency for exposures to be skewed toward the lower end of the exposure range listed in Figure 5.1 also indicates that most students do not spend a significant proportion of the day outdoors. From Table 5.1, students that received exposures ranging from 0 to 0.5 SED were found to spend the majority of the 8:30am to 3:05pm school day in indoor environments. A total of 17 out of the 19 student UVE exposures that had a recorded daily UVE exposure of < 0.5 SED were recorded on students that had spent each of the four teaching periods at the school indoors and every one of the students in this sample range had spent both meal breaks either indoors, under cover or near the school buildings.

In contrast to exposures measured on children spending most of their day indoors, significant incidental UVE exposures were observed for children that spent more than one school teaching or break period in the open outdoor playground environment. The mean personal UVE exposure measured to students spending at least one period of the day in an open environment was 2.7 ± 1.8 SED (1σ) which increased to a mean exposure of 3.3 ± 2.3 SED (1σ) for students spending more than one school class or break period in an open environment. The highest daily exposure was measured at a forearm site (11.7 ± 3.0 SED). This exposure was measured to a student that spent 2 class periods in open outdoor environments and had also spent both meal breaks near school buildings. The second highest daily personal UVE exposure (9.0 ± 2.4 SED) was measured on an arm site of a student that had spent 4 out of the 6 school class and break periods on the school oval or agricultural plot. Incidental daily exposures are presented below from the personal exposure data recorded over the February to June measurement period for variation in cloud coverage, season and body measurement site.

5.1.3 Variation in UVE playground exposure with cloud cover

UVE exposures measured with respect to variation in cloud cover are given in figure 5.2. The mean daily UVE exposure measured over the study period and plotted in the figure for variation in cloud cover was averaged across all body sites. In the figure there is a clear association between UVE exposure and school environment. For all cloud cover cases, the UVE exposure increases for students spending more time in less protected playground environments.

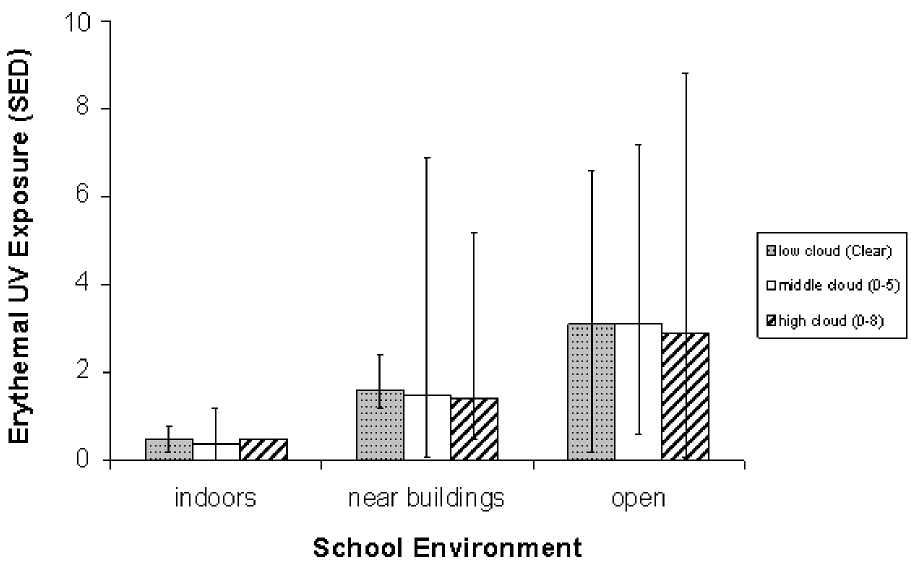

Figure 5.2: Mean UVE exposure plotted for students spending time indoors (region 1), near buildings in outdoor environments (regions 2-20), and in open outdoor environments (regions 21-25). Exposures are given for low (0-2 okta), middle (0-5 okta) and high (0-8 okta) cloud cover days and were averaged across all body sites measured in the respective cloud cover ranges. Error bars show the full range of daily UVE exposure for each respective environment and cloud cover case. Only one measurement point was taken for a student using an indoor environment on a high cloud cover day.

All cloud cover cases, averaged over all body sites show the greatest increases in UVE exposure with decreasing protection offered by the school environment. The protection offered by the school environment has a greater influence on personal exposure than cloud cover. It is possible however that increased cloud cover may reduce the influence of protection offered by the school environment as the ambient UV is reduced by absorption due to high levels of cloud cover, particularly cloud cover blocking the direct UV when in front of the solar disc. The maximum decrease in the mean UVE for students located both near buildings and in open playground environments with increasing cloud cover was 0.2 SED. The mean decrease in the personal UVE exposure is within the uncertainty of the calibrated dosimeters of ±26%. Personal UVE exposures measured in the playground environment therefore indicate that increasing cloud coverage does not reduce personal UVE exposure.

Mean daily UVE exposures exceeded 0.5 SED for students spending the day in protected indoor school environments. A likely explanation for this is due to student movement during the day, particularly at this high school when students were required to move from class to class. For this study, students were required to move between four 70 minute classes per day, meaning students would be required to be in outdoor environments at least 5 times daily, namely: before school; moving from the first class to the second; morning tea time; lunch time; and for a brief period after school. For the school studied in this research, 5 minutes of time is given to students to move from the first class ending at 10:10am to the second starting at 10:15am. Students moving to and from indoor environments at morning tea, lunch and before and after school would add to their personal time spent in an outdoor environment which may not have been necessarily recorded as the main school location noted in the daily student diary. The ARPANSA (2006) standard for occupational exposure to solar ultraviolet states that the daily exposure limit can be exceeded in 10 minutes given a UV index of 8. In summer at sub tropical latitudes the UV index readily exceeds 8 before 9.00am, the implications of which are that students moving between classes during the day may exceed the daily occupational limit even if they spend the majority of the school day in indoor environments.

The range of personal UVE exposures were also increased with increasing time spent in unprotected environments. A likely explanation for the large variation in exposure ranges for students located in outdoor environments may be attributed to students also spending some proportion of the school day in indoor environments. The large range in measured UVE exposure is also due to seasonal variation in the daily UV exposure incident in the playground environment over which the cloud classifications in the figure were produced.

5.1.4 Variation in UVE playground exposure with season

Figure 5.3 shows the variation in grouped personal UVE exposures with season. Students that spent some of their school day outdoors (near playground buildings and in open environments) received the greatest exposures during the summer-autumn (5 February to 30 March) measurement period. Furthermore, the range in personal UVE exposure was greatest during this period. This is due to the ambient playground UV being higher in summer-autumn than in the autumn-winter or mid autumn period, meaning that students spending more time in the sun receive greater exposures, especially if their time in the sun extends over several periods of the school day. Low personal UVE exposures represented in the summer-autumn exposure range are likely due to the classification of summer-autumn outdoor exposures of students that spent only one period of the school day outdoors. Further variation in the plotted exposure range was due to seasonal groupings being made regardless of the cloud coverage.

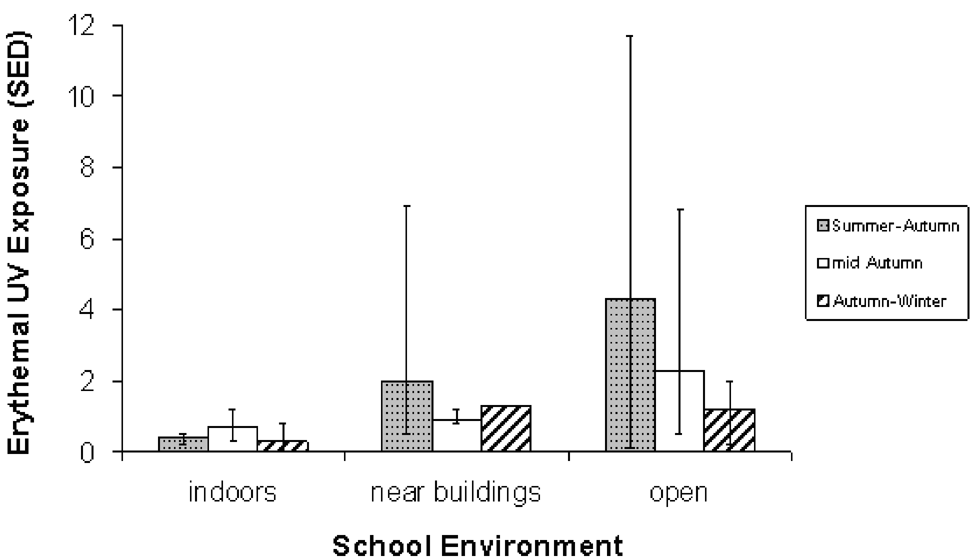

Figure 5.3: Mean UVE exposure plotted for students spending time indoors (region 1), near buildings in outdoor environments (regions 2-20), and in open outdoor environments (regions 21-25). Exposures are given for the summer-autumn period (5 February to 30 March), mid autumn (1 April to 30 April) and autumn-winter (1 May to 4 June) and were averaged across all body sites measured in each season range. Error bars show the full range of daily UVE exposure for each respective environment and season. Only one student measurement point was taken in Autumn-Winter near buildings.

Playground exposures received during the autumn-winter and mid autumn are lower than summer-autumn exposures. Mean autumn-winter exposures varied between 0.3

SED to 1.3 SED and showed the lowest variation in personal UVE exposure. As for exposures measured during the summer-autumn period which had a large range in exposure, the low autumn-winter range is due to the ambient UV received during the early winter season. Clearly, outdoor lessons and sporting events scheduled over the winter period could result in significant reductions in personal UVE exposure.

5.1.5 Variation in exposure with body measurement site

Figure 5.4 illustrates the variation in UVE exposure with respect to the body site being measured for the different school playground environments. The mean daily UVE exposure plotted in the figure was averaged over all cloud cover conditions in the study period. Like Figure 5.2 and Figure 5.3, Figure 5.4 shows a clear association between UVE exposure and school environment for each of the face, neck, arm, hand and leg sites. The full range of recorded UVE exposure for each body site is also plotted in the figure.

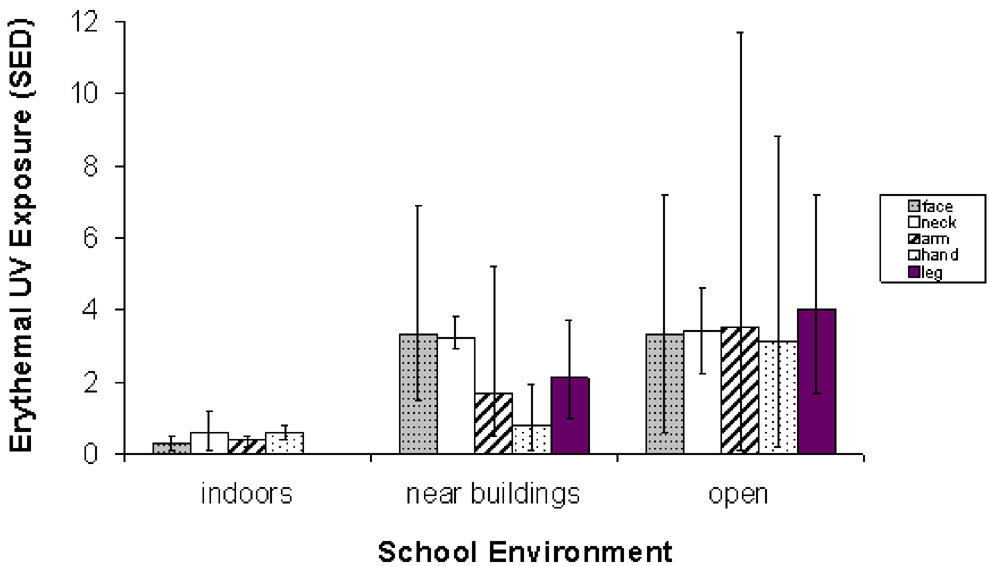

Figure 5.4: Mean UVE exposure plotted with respect to body measurement site. Exposures are given for facial, neck, arm, hand and leg sites and were averaged across all cloud cover conditions. Error bars indicate the full range of exposures measured at each body site. No indoor or winter leg data was measured in the study period.

For all body sites except the hand, the mean daily UVE exposure more than doubled for students who spent some time of the day in open outdoor environments compared with students that spent their day indoors. These results clearly show that UVE exposures increase with time spent in outdoor environments for all measured body sites. The distribution of UVE exposure to body sites however, gives no clear indication of sites that are at risk of greater exposures compared to another. This is due to the random movement and orientation of each body site with respect to the playground environment and the various activities performed by students on a day to day basis.

5.1.6 Student movement in the playground

To develop an accurate model for the prediction of skin surface exposures, the random movement of students in the playground needs to be quantified relative to the playground regions frequented by students on a daily basis. Table 5.3 details the position of students in the playground environment that were frequented on more than one occasion over the February to June personal UVE exposure measurement period. The table is organised into student groups that spent the school day in identical environments, individual students that did not show a pattern that was repeated over the measurement period are not listed in the table.

A total of 107 measurements were recorded to students between 8:30am and 3:05pm for every period of the regular school day with the remainder of measurements not being held over the full school day, not being included due to incomplete movement diaries or being recorded during the school swimming carnival (15 February 2008) or fun run day (23 April 2008) (Table 5.1). Out of the 107 personal measurements of exposure measured over regular school days, 12 were measured on students that spent the entire school day between 9:00am and 3:05pm indoors. This represents approximately 11% of the study population. A total of 23 measurements were made on students that had spent only 1 period of the school day outdoors of which 9 were required to spend time outdoors to attend agriculture or sports classes in open playground environments. These two groups make up the infrequent sun exposed school population group and comprise of approximately 32% of the study population. The majority of the measured population spent two periods outdoors. This group consisted of 44 measurements, 41% of the study population. Of these, most had spent their two periods outdoors during school meal breaks. The children that spent both meal breaks in the playground were located either near buildings or in open playground environments. Of these children, 73% chose to spend their meal breaks out of open environments with approximately half of the reminder spending both meal breaks in open outdoor playground environments. A total of 28 measurements were made on students that had spent more than 2 school periods in an outdoor playground environment (26%). All of these students had spent both meal breaks outdoors and were required to attend at least one class in an outdoor environment. This group represents the student population at most risk of overexposure to solar UV caused by attending school. Students that spent 3 or more periods outdoors were well in excess of national daily occupational limits of exposure to solar UV (ARPANSA 2006).

In a position statement of the Australian and New Zealand Bone and Mineral Society, Endocrine Society, Osteoporosis Australia, Australian College of Dermatologists and the Cancer Council Australia the recommended levels of exposure to sunlight for the adequate production of vitamin D were stated to be five minutes solar UV exposure either side of the peak UV period on most days of the week in summer and 2 to 3 hours solar UV exposure over a week in winter. These levels are exceeded by students spending two or more periods outdoors in one school day during summer and winter, affecting 68% of the sample student population and are likely to be exceeded by 89% of the student population that had spent only one school period (between 70 and 40 minutes) outdoors.

Table 5.3: Personal UVE exposure sorted by student movement in the playground.

Students predominately using indoor environments

Body site	Date	Mean cloud cover (okta)	Hat type	Region location in the School Playground: Before school 8:30 to 9:00	Per. 1 9:00 to 10:10	Per. 2 10:15 to 11:25	First break 11:25 to 12:05	Per. 3 12:05 to 13:15	Second break 13:15 to 13:55	Per. 4 13:55 to 15:05	Total Exposure (SED)
arm	6/02	7/8	none	12,18	1	1	1	1	1	1	0.5 ± 0.1
upper arm	7/02	0	none	16,12	1	1	1	1	1	1	0.2 ± 0.0
forearm	27/02	0	none	12	1	1	1	1	1	1	0.5 ± 0.1
forearm	30/04	4-2/8	none	12	1	1	1	1	1	1	0.3 ± 0.1
face cheek	21/02	0-4/8	none	12	1	1	1	1	1	1	0.5 ± 0.1
face cheek	21/02	0-4/8	none	12	1	1	1	1	1	1	0.4 ± 0.1
forehead	1/05	0-5/8	none	12	1	1	1	1	1	1	0.1 ± 0.1
neck side	30/04	4-2/8	none	12	1	1	1	1	1	1	1.2 ± 0.3
neck side	1/05	0-5/8	none	12,1	1	1	1	1	1	1	0.1 ± 0.0
neck side	1/05	0-5/8	none	12,1	1	1	1	1	1	1	0.4 ± 0.1
hand back	1/05	0-5/8	none	12	1	1	1	1	1	1	0.4 ± 0.1
hand back	21/05	NA	none	12	1	1	1	1	1	1	0.8 ± 0.2

Students located near buildings and not in direct sunlight (regions 2-14)

Body site	Date	Mean cloud cover (okta)	Hat type	Region location in the School Playground: Before school 8:30 to 9:00	Period 1 9:00 to 10:10	Period 2 10:15 to 11:25	First break 11:25 to 12:05	Period 3 12:05 to 13:15	Second break 13:15 to 13:55	Period 4 13:55 to 15:05	Total Exposure (SED)
arm	5/02	8/8	none	12	1	1	6	1	6	1	0.5 ± 0.1
arm	6/02	7/8	none	12	1	1	6	1	6	1	1.2 ± 0.3
neck front	21/02	0-4/8	none	12	1	1	6	1	6	1	1.6 ± 0.4
arm	5/02	8/8	none	12	1	1	3	1	3	1	0.5 ± 0.1
upper arm	3/04	NA	none	12	1	1	3	1	3	1	0.8 ± 0.2
forearm	3/04	NA	none	12	1	1	3	1	3	1	0.8 ± 0.2
hand back	7/03	4/8	none	12	1	1	9	1	9	1	1.2 ± 0.3
leg shin	7/03	4/8	none	12	1	1	9	1	9	1	1.7 ± 0.5
neck	26/03	NA	NA	12,7	1	1	7	1	7	1	2.9 ± 0.7
neck	26/03	NA	none	12	1	1	7	1	7	1	3.8 ± 1.0
hand back	16/04	1/8-5/8	none	12	1	1	7	1	7	1	1.1 ± 0.3
leg shin	16/04	1/8-5/8	none	12	1	1	7	1	7	1	1.2 ± 0.3

Students located near buildings and in direct sunlight (regions 15-20)

Body site	Date	Mean cloud cover (okta)	Hat type	Region location in the School Playground: Before school 8:30 to 9:00	Period 1 9:00 to 10:10	Period 2 10:15 to 11:25	First break 11:25 to 12:05	Period 3 12:05 to 13:15	Second break 13:15 to 13:55	Period 4 13:55 to 15:05	Total Exposure (SED)
hand back	7/03	4/8	none	12	1	1	15	1	1	1	1.9 ± 0.5
hand back	17/04	7/8-2/8	none	12,15	1	1	15	1	1	1	0.4 ± 0.1
hand back	17/04	7/8-2/8	none	12,15	1	1	15	1	1	1	0.9 ± 0.2
forearm	6/03	4/8	none	12,1	1	1	16	1	1	1	3.4 ± 0.9
arm	13/03	NA	none	12	1	1	16	1	1	1	2.5 ± 0.6
arm	6/02	7/8	NA	12	1	1	16	1	16	1	1.4 ± 0.4
forearm	6/03	4/8	none	12	1	1	16	1	16	1	2.3 ± 0.6

Students located in open outdoor environments (regions 21-25)

Body site	Date	Mean cloud cover (okta)	Hat type	Region location in the School Playground: Before school 8:30 to 9:00	Period 1 9:00 to 10:10	Period 2 10:15 to 11:25	First break 11:25 to 12:05	Period 3 12:05 to 13:15	Second break 13:15 to 13:55	Period 4 13:55 to 15:05	Total Exposure (SED)
forearm	3/04	NA	NA	12	1	25					3.1 ± 0.8
forearm	3/04	NA	NA	12	1	25					2.9 ± 0.7
face vertex	16/04	1/8-5/8	none	12	1	1	1	25	1	1	6.8 ± 1.8
leg shin	16/04	1/8-5/8	none	12	1	1	1	25	1	1	1.7 ± 0.4
face cheek	30/04	4/8-2/8	none	12	1	25	1	1	1	1	0.6 ± 0.2
face cheek	30/04	4/8-2/8	none	12	1	25	1	1	1	1	0.7 ± 0.2
arm	15/05	4/8	cap	12	1	1	1	25	16	1	1.7 ± 0.4
arm	15/05	4/8	cap	12	1	1	1	25	16	1	1.0 ± 0.3
hand back	16/04	1/8-5/8	none	12	1	25	19	1	19	1	4.2 ± 1.1
forehead	16/04	1/8-5/8	none	12	1	25	19	1	19	1	3.4 ± 0.9
hand back	17/04	7/8-2/8	none	12	1	25	18	1	17		3.7 ± 1.0
leg shin	17/04	7/8-2/8	none	12	1	25	18	1	17		2.0 ± 0.5
hand back	28/02	7/8	none	12	25,1	1,22	12	1	12	1	2.0 ± 0.5
hand back	28/02	7/8	none	12	25,1	1,22	12	1	12	1	4.0 ± 1.1
arm	15/05	4/8	none	12	1	1	22	1	22	1	1.6 ± 0.4
forearm	15/05	4/8	none	12	1	1	22	1	22	1	1.6 ± 0.4
forearm	23/04	4/8	NA			1	18	22	22	22	1.1 ± 0.3
forearm	23/04	4/8	NA			1	18	22	22	22	1.6 ± 0.4
forearm	23/04	4/8	NA			1	18	22	22	22	1.4 ± 0.4
forearm	23/04	4/8	NA			1	18	22	22	22	1.4 ± 0.4
upper arm	15/02	0	NA	21	21	21	21	21	21		15.8 ± 4.1
upper arm	15/02	0	NA	21	21	21	21	21	21		12.3 ± 3.2
upper arm	15/02	0	NA	21	21	21	21	21	21		38.7 ± 10.1
arm	15/02	0	none	21	21	21	21	21	21		4.9 ± 1.3
face vertex	15/02	0	NA	21	21	21	21	21	21		49.8 ± 12.9
face vertex	15/02	0	NA	21	21	21	21	21	21		32.0 ± 8.3
face vertex	15/02	0	NA	21	21	21	21	21	21		39.6 ± 10.3
face vertex	15/02	0	NA	21	21	21	21	21	21		39.7 ± 10.3

[1] Where data was not recorded this has been marked with an NA. Some daily measurements of exposure started later than 8:30am or finished before 3:05pm, in these cases no student movement pattern is recorded in the table and these spaces are left blank.

5.1.6.1 Playground Activity Index

Figure 5.5 shows the mean daily activity pattern observed in the school student population excluding the swimming carnival and fun run days. Incidental day to day playground exposures were developed from the collected student movement patterns listed in Table 5.1 where students spending time in regions 21 through 25 were assigned an outdoor activity index of 1, students located in sunlit areas but located near buildings (regions 15 through 20) were assigned an outdoor activity index of 0.75, students located under building and shading structures were assigned an outdoor activity index of 0.25, and students located indoors were assigned an outdoor activity index of 0. Here the outdoor activity index gives some indication of student exposure to the ambient UV. The data presented in Figure 5.5 therefore is not a specific measurement of student exposure but a representation of mean behavioural trends observed in the school relative to the outdoor environment.

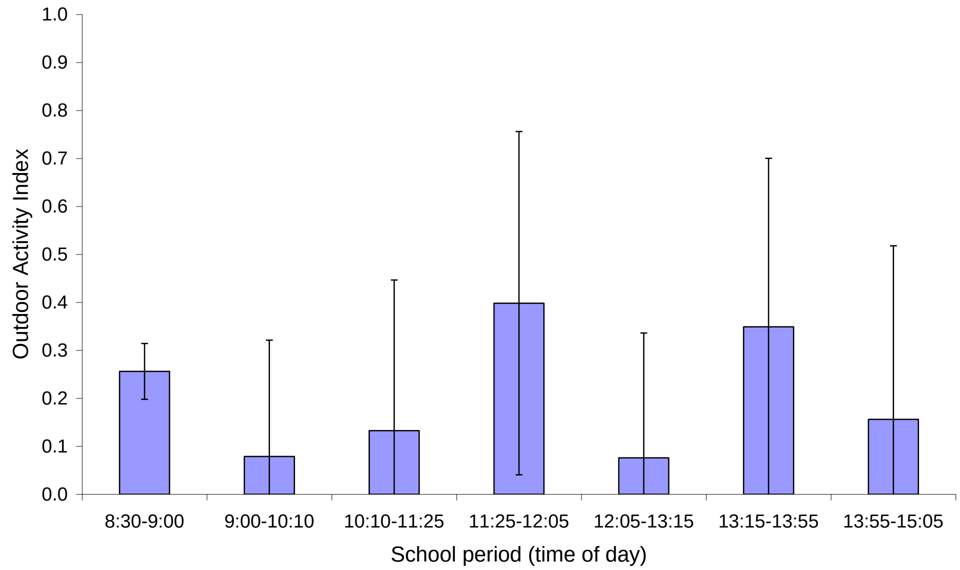

Figure 5.5: Mean outdoor activity index of student behaviour observed relative to time spent in sunlit areas of the school playground. Error bars show the standard deviation in outdoor activity index in the sample population.

From Figure 5.5, the two most significant periods of outdoor activity occur between 11:25 and 12:05, and 13:15 and 13:55. These times represent the two meal break times observed at the school. The highest mean activity index after these two time periods occurs in the period before school (8:30 to 9:00). The likely reason for the high outdoor activity index observed at these times is due to limited access to indoor environments available at these times when school classrooms are locked, and the tendency of students to seek outdoor playground regions for either sporting or leisure activity between indoor classes. Cumulative daily UV_{ery} exposure is affected most significantly by the tendency of students to be located in outdoor playground environments during meal break times, particularly as these times tend to be closest to solar noon. Reductions in cumulative daily UV_{ery} exposure brought about by active sun protection strategies held during meal breaks will have the greatest effect on reducing exposure risks to a school population.

5.2 Modelling body surface exposures in the playground environment

5.2.1 Comparison with measured body site exposure

Mean exposures for the listed movement patterns of students that had spent at least one school period outdoors were compared to modelled body surface exposures determined for students spending time in the respective playground regions. Comparisons of the modelled exposure to each body site were based on the mean statistics of each school playground region, including mean sky view, standing surface albedo contribution and shade density for the SZA range of each school period. Here, the calculated summer solstice shade density for each respective playground region was applied to modelled direct UV exposures in February and March and the winter solstice shade density determined for each playground region was applied to modelled direct UV exposures in April, May and June. Modelled horizontal plane exposures were then weighted to median mannequin ER data measured for each of the respective face, neck, arm, hand and leg body regions (Table 3.8). Modelled body site exposures were calculated according to equation 2.17 where ER was the median ER given for each body region listed in Table 3.8. Vertex body sites were the exception, and were modelled as the horizontal plane UV exposure because the measured mannequin vertex site ER was found to be 100% of the horizontal plane exposure for each SZA range. The student movement patterns listed in Table 5.3 are plotted against their respective modelled body site exposures in Figure 5.6. Modelled body site exposures were determined at sea level, for clear sky conditions and included OMI (TOMS 2008) ozone concentrations observed over Hervey Bay for each respective measurement date.

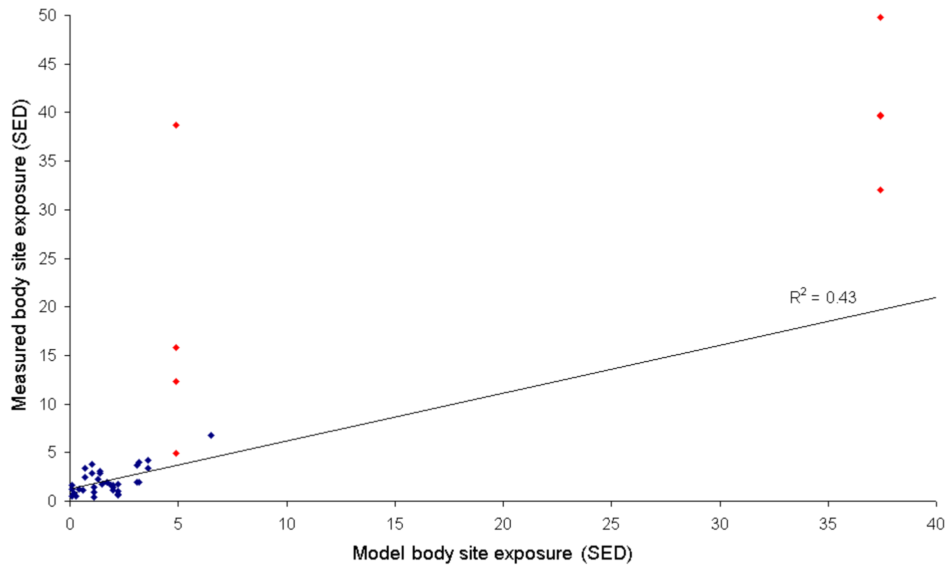

Figure 5.6: Comparison of measured and modelled body site UV exposure in the HBSHS playground. Swimming carnival data was ignored in determining the correlation coefficient. These points are coloured red in the figure.

Considering the limitations of the model predictions that will always be present due to an individual student's movement, behaviour and the subsequent details recorded in student movement diaries, the predictions given were on average within 0.9 ± 0.7 SED (1σ) of the measured exposure for all measurements excluding those taken during the swimming carnival. Modelled exposures predicted for normal school routine days were within the measured dosimeter exposure uncertainty varying from measured body site exposures by an average of 12%. Excluding the data measured during the swimming carnival, model exposures showed some correlation with measured exposures (R^2 = 0.43). In Figure 5.6, all exposures measured over 10 SED were recorded during the swimming carnival. These exposures may be taken as untypical of exposures received on a day to day basis as is further evident in the exposure distribution of Figure 5.1.

5.2.2 Estimates of body surface exposure by playground region

Playground region statistics given in the previous chapter give some indication of the overall risk associated with using different regions of the playground environment. The likelihood of overexposure to solar UV was found to increase in regions that had greater sky views. Comparison between measured UVE among the student population to the median weighted body site exposure predictions given for students using various playground sites showed that this risk could be modelled reasonably well for a student's day to day use of the school playground. To develop a more detailed assessment of the likely exposure distribution affecting unprotected skin surfaces, modelled playground exposures were weighted to the ER measurements for each of the face, neck, arm, hand and leg. Using the techniques presented in this work, detailed body surface exposure distributions can be modelled at any one of the 822 playground sites studied. A summary of exposures affecting unprotected skin surfaces is presented below for region 21 (the pool), region 22 (the oval) and region 18 (the region most covered with trees). Region 21 (Figure 5.7) was studied here as this region represents the region in which the highest student exposures were recorded during the school swimming carnival and therefore presents the most significant risk to the school population of receiving a severe sunburn. Apart from indoor environments, region 22, the school oval (Figure 5.8(a)), was the most popular region frequented by students during both meal breaks. Region 18 (Figure 5.8(b)) was the next most popular region attended during school meal breaks. Region 18 also represents an outdoor region significantly different from region 22, having a significant number of trees compared with the open oval environment.

Figure 5.7: The HBSHS pool environment photographed from the eastern end of the region.

Figure 5.8: (a) The HBSHS oval photographed from the northern end of the region, and Region 18 photographed from a site located in the middle of the region (b).

Body surface exposures were plotted between 8:30am and 2:30pm for region 21 for 15 February 2008 and 15 April 2008. These two plots show by way of example how rescheduling the swimming carnival by two months can have a significant impact on reducing UV exposure. Exposures are plotted for regions 22 and 18 over a cumulative total of two meal break times (the most popular observed pattern in student playground use) between 11:25am and 12:05pm, and 1:15pm and 1:55pm for 12 December 2008, the last day of the school year. Comparisons are made between the likely body surface exposures received by student groups spending time in these two different regions to gauge the relevant increase in risk students using open outdoor environments are placed under when using such environments for sporting or meal break activities. It should be noted that these four examples are discussed here to illustrate the value of developing a model to predict body surface exposures in a school environment. Any number of playground environments and situations can be examined at any time of the year and can be modelled using the techniques presented.

5.2.2.1 Swimming carnival schedule

Swimming carnivals, by their nature need to be held during the warmer months of the year. This has the potential to place students using such an environment at increased risk of overexposure to UV due to increased solar elevation which occurs during the warmer periods of the year. Figure 5.9(a) compares the predicted body surface exposure of a student attending a swimming carnival on 15 February between 8:30am and 2:30pm to a student attending a swimming carnival over the same time period on 15 April (Figure 5.9(b)). In producing the figure, mean ground and standing surface albedo, sky view and shade density for region 21 was applied (Table 4.3) and ozone concentration was set at 277 DU. Playground exposures were weighted to the 0^o-30^o SZA body surface ER data for part (a) of Figure 5.9 (mean 25^o SZA in the 8:30 am to 2:30 pm period), and 30^o-50^o SZA body surface ER data for part (b) (mean 45^o SZA in the 8:30 am to 2:30 pm period). In the figure, the greatest exposure was modelled for 15 February at 37.4 SED. This exposure is received by the vertex body site. High exposures are also evident in part (a) of the figure on the nose, the shoulder region of the neck, and the dorsa of the forearm and hand (> 20 SED). Exposures on 15 February were lower to the leg, but in excess of 12 SED to the calf muscle region. Exposures modelled for 15 April were lower than 20 SED to all body surface regions except the vertex (21.2 SED) as is evident by their being no blue colouration at most surface sites in the wireframe models presented in part (b). Note that in the figures, the extreme exposure range (>32 SED) was coloured purple and pink to stand out from the exposures represented in the continuum red (low) through to blue (high). The extreme exposures occur only to the vertex site for 15 February, a region of the face that is often protected by hair cover or a hat.

A broader ER pattern can also be observed between 15 February and 15 April. This is mostly evident to the side of the face. The most noticeable effect however is the reduced exposure occurring on 15 April. Comparison of the facial exposure on these two dates shows that the extreme exposure occurring toward the vertex region of the face in February is reduced considerably in April. Noticeable reductions in exposure are also evident to the lower anterior forearm and dorsa of the hand between February and April.

(a) (b)

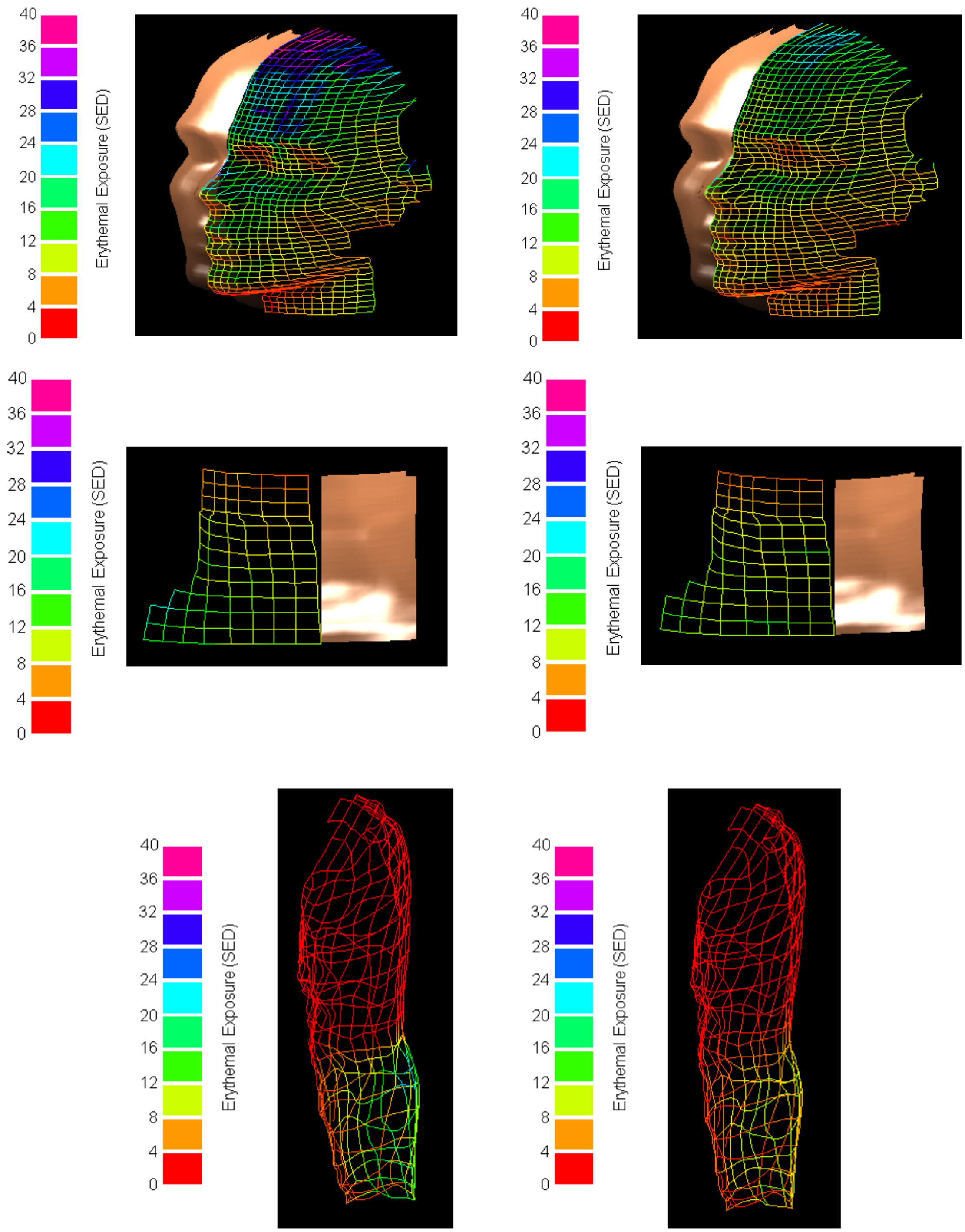

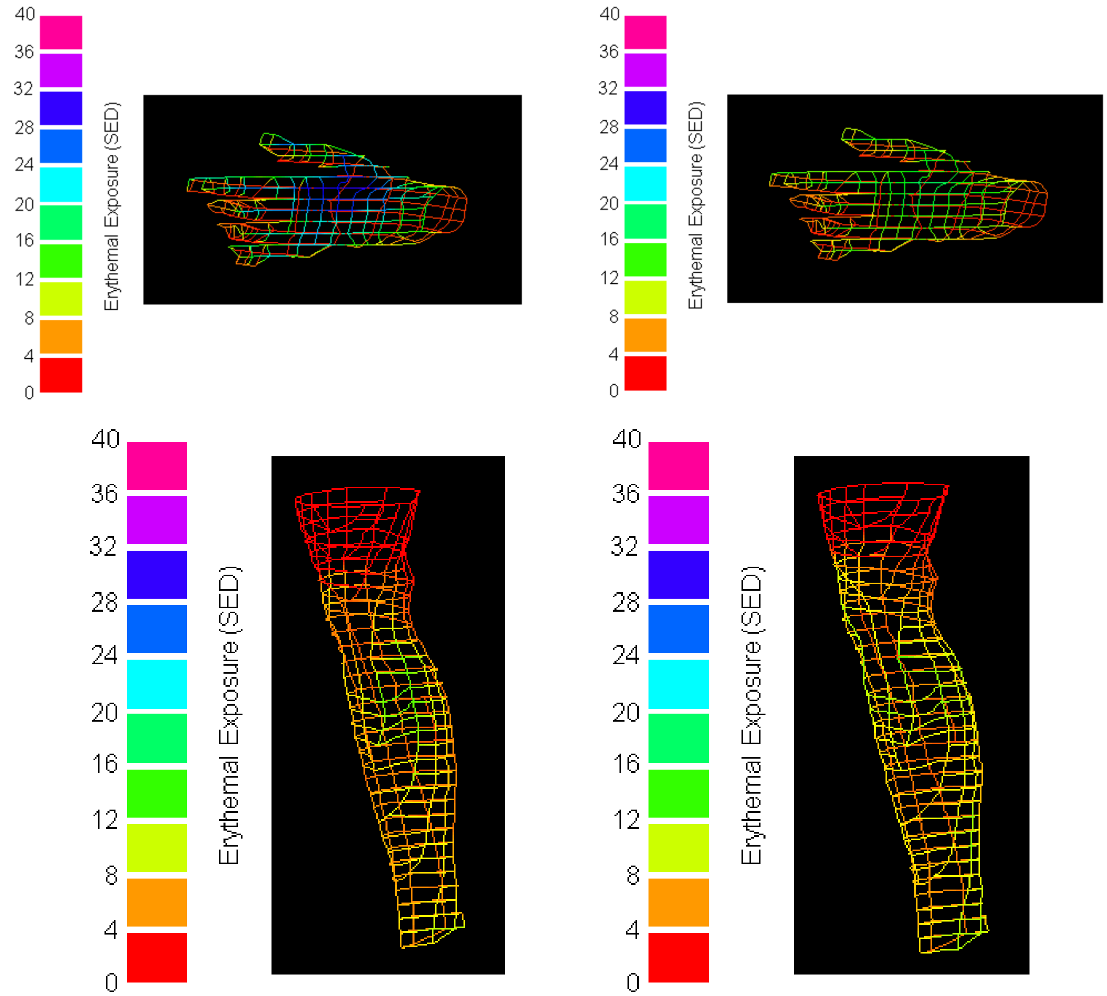

Figure 5.9: Modelled pool region exposure on 15 February 2008(a) and 15 April 2008 (b). Body parts from top to bottom are the face, back of the neck, arm, hand, and leg.

5.2.2.1.1 Non-melanoma skin cancer risk

The annual contribution to the risk of developing NMSC may be expressed as (Schothorst et al. 1985):

$$Risk = kD^{\beta} A^{\alpha} \qquad (5.1)$$

where the risk of developing NMSC is dependent upon the cumulative annual exposure, D and the age of the individual, A. In the equation, α and β are the respective age dependent and biological amplification factor constants which can be determined by epidemiological evidence. Wong et al. (1996) determined that the increase in risk by not wearing a hat could be measured at various facial sites by comparing the mean protection factors of those sites (*MPF*):

$$Risk = MPF^{\beta} \qquad (5.2)$$

Here, equation 5.2 is derived from the ratio of cumulative UV exposure of an individual not wearing a hat, D_0 to the cumulative UV exposure of an individual wearing a hat, D and the dependence on age and the constant of proportionality, k are removed in the ratio:

$$Risk = \frac{k(D_0)^{\beta} A^{\alpha}}{k(D)^{\beta} A^{\alpha}} \qquad (5.3)$$

For this research a similar method can be used to determine the risk associated with running the school swimming carnival on 15 February as opposed to 15 April. Here, the annual exposure of a child that normally spends every school day in indoor environments except the school swimming carnival spending the 8:30am to 2:30pm period in region 21 of the school playground experiences an increased risk of developing non-melanoma skin cancer. This risk was calculated by determining cumulative annual exposure received while at school. From measurements collected over the February to June 2008 period, the mean exposure of students spending the entire school day indoors was approximately 0.5 SED. From Figure 5.2, it can be seen that this mean does not vary significantly from summer to winter, nor was any significant variation measured with body site (Figure 5.4) and if applied to 201 days of the 202 day school year results in an erythemally effective exposure of 101 SED at each of the face, neck, arm, hand and leg body sites. The risk in developing BCC or SCC at a vertex site being close to the modelled horizontal plane ambient exposure is:

$$Risk_{BCC} = \frac{(101 + 37.4)^{1.7}}{(101 + 21.2)^{1.7}} = 1.2 \qquad (5.4)$$

$$Risk_{SCC} = \frac{(101+37.4)^{2.3}}{(101+21.2)^{2.3}} = 1.3 \qquad (5.5)$$

or 1.2 times greater for BCC and 1.3 times for SCC based on the epidemiological biological amplification factors, β for BCC of 1.7 (NRPB 1995, cited in Visvakarman and Wong 2003) and 2.3 for SCC, where the biological amplification factor for SCC was based on the mean result of several studies cited by Vishvakarman and Wong (2003), including Schothorst et al. (1985); DeGruijl (1982); Scotto et al. (1983); Hunter et al. (1990); Chuang et al. (1990); Levi et al. (1988); Coebergh et al. (1991); Roberts (1990); Glass and Hoover (1989); and Whitaker et al. (1979).

In the calculation, 37.4 SED was the mean modelled pool region UV exposure for 15 February and 21.2 SED was the mean modelled pool region exposure for 15 April. The risk as derived above represents a respective BCC and SCC risk of 20% and 30% due to a single daily exposure but will be reduced below 1.2 when weighted to the measured ER of other body sites and the protection of hair cover is considered for a vertex site. Furthermore, consideration needs to be given to exposure received by school students outside of school hours as this will influence the cumulative annual exposure upon which the risk is determined. In the above calculation of non-melanoma skin cancer risk, it is assumed that there is no exposure received outside of school hours. Vishvarkarmen and Wong (2003) determined an estimate for the total annual childhood UV_{ery} exposure by using the method of Diffey (1992) modified for latitudes in Central Queensland. This estimate was 1510 kJm^{-2} calculated for a total number of 4380 sunlight hours. For this research, at Hervey Bay's latitude, an annual estimate was modelled for clear skies and an ozone concentration of 300 DU, giving a total UV_{ery} exposure of 1678 kJm^{-2}. Vishvarkarmen and Wong (2003) determined that 1524 hours were spent outside annually by an Australian child in tropical weather conditions. This estimate was reduced by the estimated time spent traveling to, from and while at school estimated by Vishvarkarmen and Wong (2003) at 3.5 hours per school day giving approximately 824 annual hours spent outside of school in sunlight representing approximately 19% of the 4380 annual sunlight hours for an estimated total of 315 kJm^{-2} or 3150 SED, 19% of the annual estimate of 1687 kJm^{-2}. Including this estimate in the student's total annual exposure reduces the risk associated with attending the swimming carnival on 15 February to 1 as the difference between 15 February and 15 April (16.2 SED) is not significant compared with the estimated total annual exposure. However, the risk of developing melanoma skin cancer and BCC is also dependent upon an individual experiencing a history of severe intermittent UV exposures (Kricker et al. 1995; Rosso et al. 1998). A risk factor of 1, while indicating no apparent risk should perhaps be referred to as a low *chronic* NMSC risk, as every severe acute episode of UV exposure is likely to increase the risk of developing both BCC and melanoma skin cancer and if the school's annual swimming carnival were held on 15 April, the risk of developing skin cancer would be reduced.

5.2.2.2 Open and protected playground regions

Patterns in student behaviour observed on a day to day basis can have a more noticeable influence on the chronic skin cancer risk associated with cumulative exposure to solar UV. Figure 5.10 compares the exposure of students frequenting playground region 22 and playground region 18 on 12 December during both meal break periods. In producing the figure, mean ground and standing surface albedo, sky view and shade density for region 22 and region 18 was applied (Table 4.3), ozone concentration was set at 277 DU for the modelled horizontal plane estimate of exposure of 13.4 SED for region 22 and 4.7 SED for region 18. The modelled horizontal plane exposure estimate was calculated as the total exposure received between 11:25 am and 12:05 pm (first meal break) and 1:15 pm and 1:55 pm (second meal break) and assumed students were located indoors during other periods of the school day. Playground exposures were weighted to the 0^{o}-30^{o} SZA body surface ER data.

As for exposure modelled on 15 February and 15 April in the pool region, exposures modelled in region 22 and 18 show that the highest exposures were received by the face, the lower neck, and the dorsa of the forearm and hand. Exposures above 8 SED are not evident on the leg model. Furthermore the influence of playground tree cover affecting shade density and sky view, results in exposures less than 4 SED being represented on surface models of exposure to students using region 18.

The risk of developing BCC for students frequenting region 22 during both meal breaks on every day of the school year was calculated to be 1.8 times higher compared with students using region 18 and 2.2 times higher between the respective playground regions for the development of SCC. Essentially, the risk of using an open environment for both meal breaks doubles the risk of developing NMSC. Here these calculations were determined using the method outlined in the previous section by determining the annual exposure received between the two break periods on a horizontal plane and weighting the exposure to mean playground region sky view, and shade density where direct UV was weighted to 0.90 for the months October through to March for region 22 and 0.34 for region 18. The weighting of the modelled direct UV was determined by the mean region summer shade density. For the months April through to September, mean region winter shade densities were applied to give direct UV exposure weightings of 0.80 and 0.14 for region 22 and region 18 respectively. The total annual exposure received over the two meal break periods in the school year (subtracting holidays and weekend periods) was determined to be 2380 SED in region 22 and 740 SED in region 18, where school holidays were determined according to the 2008 school calendar year occurring after the first day of the school year, 29 January, between 21 and 24 March, 5 and 13 April, 28 June and 13 July, 20 September and 5 October, and from 13 December through to the end of the year. An additional exposure of 101 SED was added to both of these estimates to account for incidental exposures received as a consequence of student movement between indoor classes and 3150 SED was added to both region exposure estimates to account for exposure received outside of school hours, resulting in total annual exposures of 5630 SED and 3990 SED for students using the respective region 22 and region 18 playground areas every day of the school year. Biological amplification factors as required by equation 5.2 to determine NMSC risk were applied as mentioned previously (section 5.2.2.1.1) using the values of 1.7 and 2.3 to determine skin cancer risk for BCC and SCC respectively.

(a) (b)

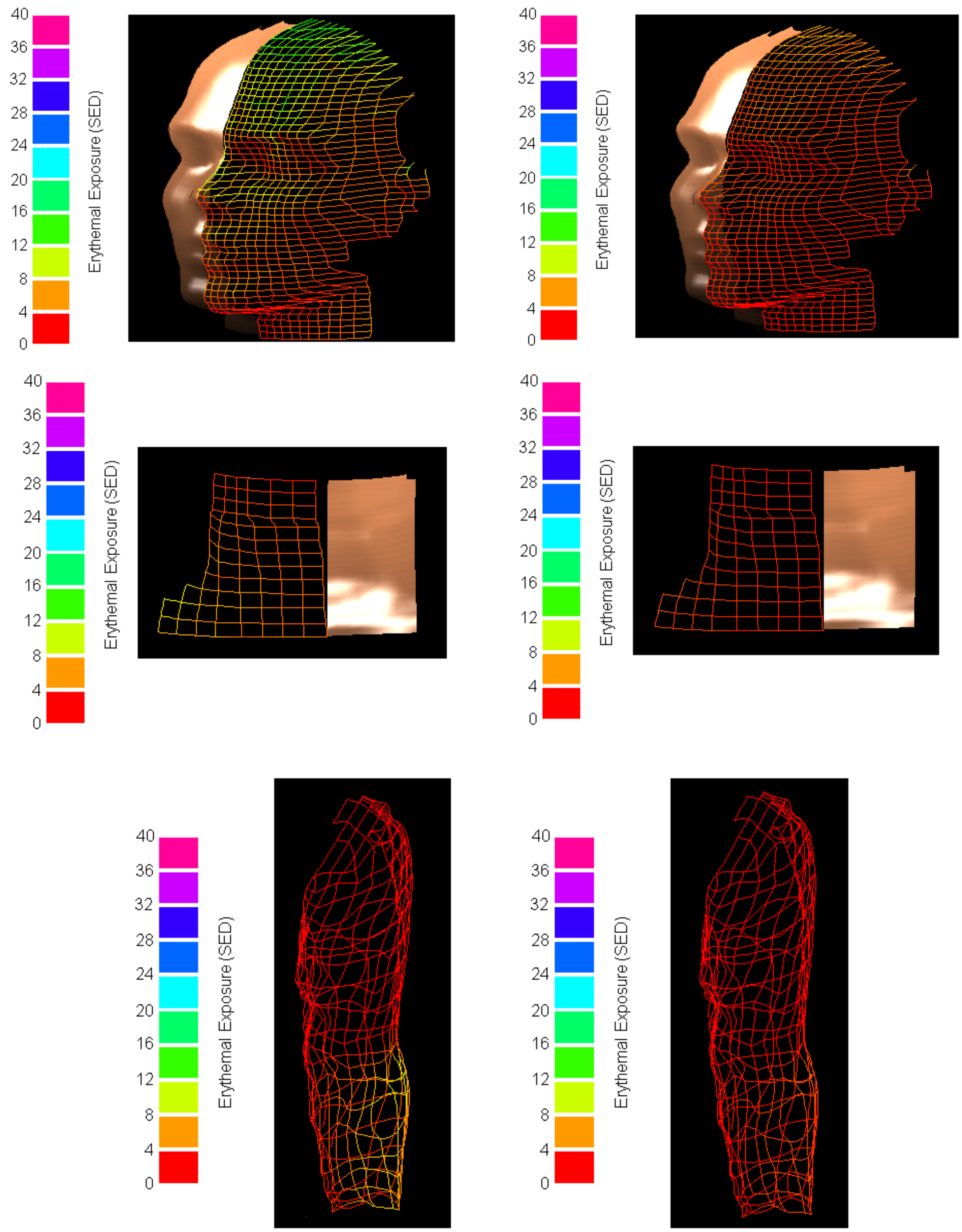

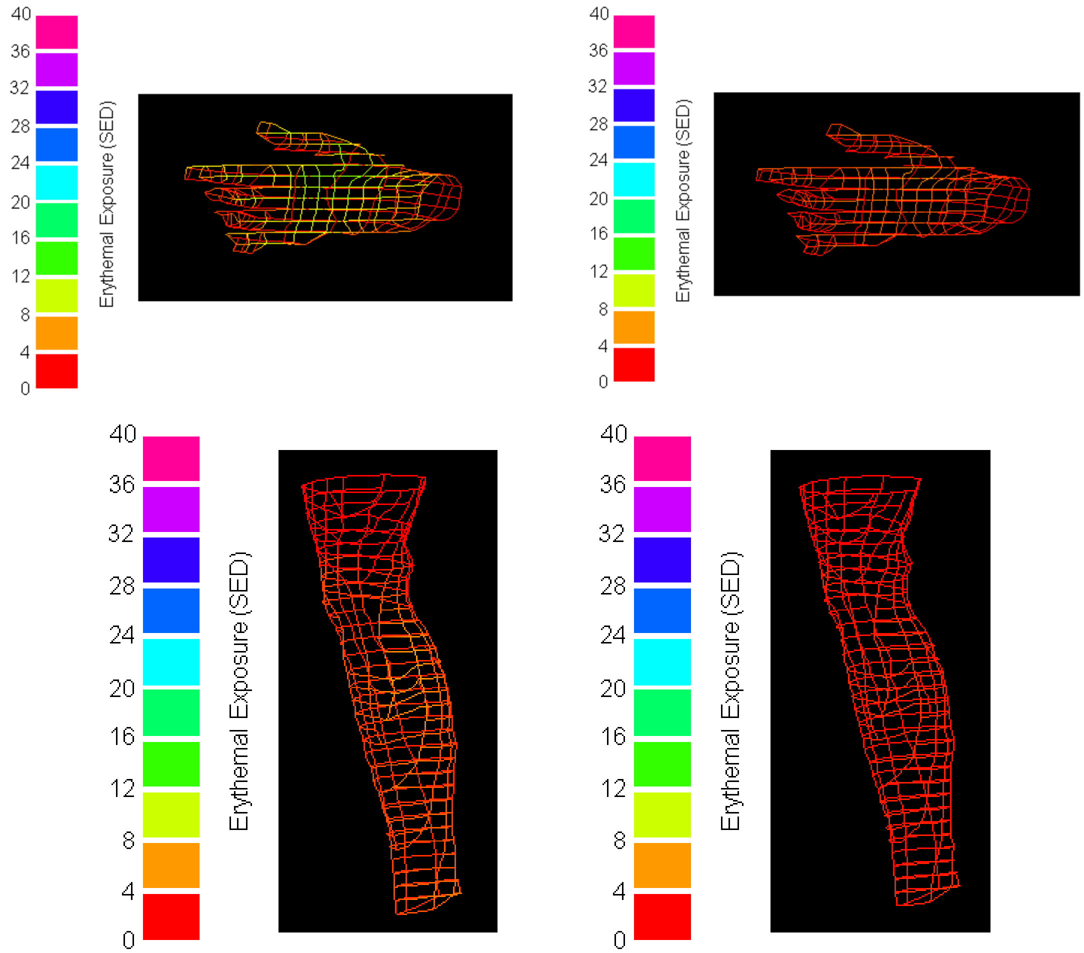

Figure 5.10: Cumulative meal break exposure modelled for region 22 (a) and region 18 (b), 12 December 2008. Body parts from top to bottom are the face, back of the neck, arm, hand, and leg.

5.2.3 Estimates of annual exposure

Mean playground sky view, shade density and albedo (Table 4.3) were used to estimate a school child's annual exposure received over the approximate 202 school days of the Queensland calendar year. The total annual exposure to erythemally effective UV received at a vertex site by a child using the HBSHS playground was estimated at 840 SED from an estimated annual playground exposure of 4210 SED. Here, the student exposure estimate was based on the calculation of a cloud free annual exposure using equation 5.6:

$$AE = \sum_{d=1}^{d=202} n(d) \sum_{h=9}^{h=15} (diff\,(h,d) \cdot S_{view} + dir(h,d) \cdot S_{density}) \cdot O_{ai} \qquad (5.6)$$

where *AE* is the estimated total annual UV_{ery} exposure, *n(d)* is the number of days in the school year (not including holidays or weekends), *h*, is the number of hours in each school day from 9:00am to 3:00pm, *diff* is the modelled horizontal plane diffuse UV_{ery} exposure modelled for each respective day, S_{view} is the mean HBSHS playground sky view of 55%, *dir* is the modelled horizontal plane direct UV_{ery} exposure modelled for each respective day, $S_{density}$ is the mean fraction of the HBSHS playground (winter and summer) not shaded in a school day which is represented by the mean shade density remainder of 57%, and O_{ai} is the mean outdoor activity index (Figure 5.5) of 0.2.

The estimated annual exposure of a child can further be subdivided by body site, where the estimated annual exposure (equation 5.6) is weighted to the median mannequin body region ER in the 30^{o}-50^{o} SZA range for each respective body part giving annual exposures of 330 SED to the face, 300 SED to the back of the neck, 140 SED to the arm, 290 SED to the hand, and 190 SED to the leg. This compares to an estimated annual erythemally effective vertex exposure of 340 ± 71 kJm^{-2} (3400 ± 710 SED) estimated for physical education school teachers in central Queensland (Vishvakarman et al. 2001), the approximate equivalent of a daily UV_{ery} exposure of 16.8 ± 3.5 SED, assuming there are approximately 202 days in a school calendar year. In this comparison, the estimated annual exposure of central Queensland physical education teachers is greater than the predicted vertex exposure of a student using the HBSHS playground (840 SED) and lower than the predicted annual playground exposure of 4210 SED. A likely explanation for this is the effective activity index of physical education teachers who are more likely to be spending a greater proportion of the day in outdoor environments than the mean activity index of 0.2 suggested from measurements of playground use patterns in the HBSHS student population. From the estimates provided in this research, annual exposures received at a vertex site are likely to be less than the mean playground exposure estimate of 4210 SED given it is unlikely that an individual would spend each hour of every school day, and each school day in the outdoor playground environment.

From this perspective, the estimates determined by Vishvakarman et al. (2001) for physical education teachers would seem to be in reasonable agreement with the annual horizontal plane playground estimate given here. Annual exposures received by teachers and students in the modelled playground environment are likely to range therefore between 101 SED to 4210 SED, where 101 SED was determined as the annual estimate from measurement of the student exposures who were exclusively located indoors and 4210 SED is the upper limit determined as the mean playground horizontal plane UV_{ery} exposure.

5.3 Reduction in NMSC risk by wearing a hat

One of the most effective types of hat that provides shading to the human facial region is the broad-brim style (Gies et al. 2006). The protection offered by this type of hat was examined by comparison of 7 unprotected (no hat) facial sites to 7 protected facial sites (hat worn) using two mannequin headforms placed in an upright position on a rotating base (Figure 5.11). Measurement of exposure recorded on both headforms which were simultaneously exposed in two open regions of the playground are provided in Table 5.4.

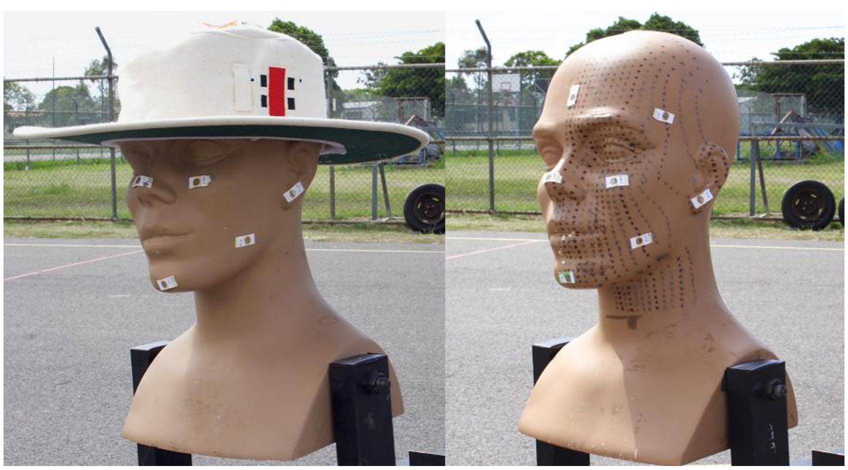

Figure 5.11: Measuring the protection offered by a broad-brimmed hat at seven different facial sites. Protected and unprotected exposures were recorded simultaneously.

Table 5.4: Mean mannequin facial ER (%) measured in region 24 (basketball courts) and region 22 (oval). ERs are given relative to ambient UV_{ery} horizontal plane exposure. Measurements of exposure to the temple, mandible and ear lobe were averaged and given as a single "side" measurement in the table.

	Region 24 ER (%) (outdoor basketball court)		Region 22 ER (%) (school oval)	
	Protected	Unprotected	Protected	Unprotected
Vertex		88		86
Forehead	2	42	24	56
Nose	22	61	17	61
Cheek	10	56	14	46
Chin	23	33	24	35
Side of face	13	26	14	28

It is clearly evident from Table 5.4 that the broad-brimmed style of hat made a significant contribution to the reduction in UV_{ery} exposure relative to the ambient horizontal plane exposure. This is evident despite the maximum ER uncertainty of ±18% present for ER measurements recorded in this case up to a maximum SZA range of 30^{o} and the movement of the broad-brimmed hat during measurement periods which accounted for the greatest ER variation at the forehead site. The broad-brimmed hat however provided greatest protection to the forehead, cheek and nose with the side and chin sites receiving less protection. Due to the forehead, cheek and nose sites being closer to the shade offered by the hat brim, better protection was provided compared to the side and chin sites. The order of increasing UV ER to specific facial sites are in agreement with broad-brimmed protection factors measured using mannequin headforms by other researchers (Diffey & Cheeseman 1992; Kimlin & Parisi 1999; Gies et al. 2006) with the exception of cheek exposure for which the dosimeters vary in position relative to those used for this work.

Not wearing a broad-brimmed hat, such as that tested for this research can be expressed relative to the increased risk of developing NMSC. As determined previously, the mean horizontal plane playground annual UV_{ery} exposure was determined at 4210 SED. When this exposure is weighted to the mean student activity index of 0.2, the mean measured ER facial site data given in Table 5.4 and the cumulative annual exposure estimate of 3150 SED received outside of school hours, the site specific contribution to the risk of developing BCC and SCC can be determined for a student not wearing a broad-brimmed hat and observing a normal school routine. The increase in risk of developing BCC and SCC to facial sites is given in Table 5.5. The risk estimates provided in the table illustrate the increased risk of developing NMSC by not wearing a hat to facial sites located toward the top half of the face (those facial regions best protected by the hat), namely the forehead, nose and cheek. The risk involved for students that spend a greater fraction of the day in outdoor environments will be higher than those quoted in Table 5.5. Similarly, teachers that spend a higher proportion of the day outside (physical education teachers for example) will be expected to have an increased risk of developing NMSC at the facial sites listed in the table provided no hat protection is used.

Table 5.5: Relative increase in NMSC risk by not wearing a broad-brimmed hat for a student observing the normal school routine (activity index 0.2). Biological amplification factors used to determine the relative risk for BCC and SCC were implemented as specified in section 5.2.2.1.1.

	Relative increase in risk	
	BCC	SCC
Forehead	1.2	1.2
Nose	1.2	1.3
Cheek	1.2	1.2
Chin	1.0	1.1
Side of face	1.1	1.1

5.3.1 Measured hat use among the student population

Of the 114 students that completed diaries on hat use during the February to June 2008 student measurement period (Table 5.1), 105 indicated that they did not wear a hat on the measurement day. Of the hats that were worn by students on the measurement days, 8 chose to wear a baseball style of cap and 1 student indicated that they wore a broad-brim style of hat. These results are comparable to the behavioural study of Milne et al. (1999a) which indicated that the use of quality hats in three Western Australian primary schools was observed to be often less than 30%. The data also supports the behavioural studies of Balanda et al. (1999) and Lowe et al. (2000) which highlight a decline in sun protection strategies used by high school aged children compared with primary school aged children and highlights the significant role school administrators can take to control the behavioural patterns of children in their care to minimise lifetime cumulative exposure to potentially harmful solar UV, particularly during meal breaks which account for most of the cumulative UV exposure received throughout the day.

5.4 Summarising student playground exposure

Playground exposures and the subsequent UV exposures predicted for unprotected body surfaces have been developed from playground site measurements and measurements of body surface UV exposure. These measurements detail the influence of shading caused by the human form and detail variation in exposure over human surface topography to a high resolution not able to be measured on living human subjects alone. This data set represents the most extensive set of body surface UV exposures available that can be applied to predict patterns in body surface exposure with seasonal and daily variation in solar elevation. Structures present in the playground such as individual trees and buildings are accounted for by survey measurements made in the playground, extending existing techniques used to model the effects of playground shading alone. The benefits of modelling the erythemally effective UV to students in a school environment include making assessments of long term UV exposure and providing added planning assistance that can be utilised to minimise UV exposures associated with school activities that use the playground environment. In the following chapter, the value of the developed body surface UV exposure model weighted to the playground environment is discussed relative to existing public health literature.

CHAPTER 6 APPLICATIONS OF THE SOLAR UV MODEL

The principal outcome of this research has been the development of a model that predicts the UV exposure in a school environment. The developed model highlights locations within a school environment that present the most risk to students using that environment, with the most significant risk being the development of NMSC and melanoma skin cancer which are essentially preventable diseases. A technique has been presented for transferring the modelled horizontal plane UV playground exposure onto three dimensional surface models of unprotected parts of the body. This is seen as an essential step for the development of better sun-safe practices in schools. Techniques used to model the effective UV exposure to students in a real school playground have been developed providing estimates of exposure that can be reliably calculated for any playground environment by region statistics or by specific playground site. An understanding of the local playground environment and how this influences the day to day UV exposure as presented in this research is essential for the reduction of skin cancer and sun-related eye disorders caused by childhood exposure to solar UV radiation. In this chapter, the specific outcomes determined from measured body surface and predicted playground exposures are discussed in relation to skin cancer, vitamin D, general public health and health education. Suggestions are given for the scheduling of activities in the current school environment and the broader use of the techniques presented thus far are discussed in relation to other school playground environments.

6.1 Activity scheduling in the playground and variation in exposure with SZA

6.1.1 Variation in yearly SZA

For Hervey Bay, the SZA ranges from between 3^o and 46^o over the summer months and between 67^o and 34^o over the winter months for the hours of 9:00am to 3:00pm (Michalsky 1988). No measurements were taken over the student exposure measurement period, 5 February 2008 to 4 June 2008 for SZA ranges greater than 63^o or less than 9^o. Students using the model school playground experience body surface distributions to UV predominately in the 0^o-30^o and 30^o-50^o SZA range for most of the year. A notable observation for the model school located in the latitude of 25^{o}S is that low solar elevation angles limited to a maximum SZA of 30^o make up the maximum range for most of the year (excepting mid spring to mid summer) that students need to be exposed to provided outdoor activities are scheduled in either the first or last hour of the school day. Roughly, these times correspond to the first teaching period (9:00am to 10:10am) and the last teaching period (1:55pm to 3:05pm). Figure 6.1 shows the complete SZA range at Hervey Bay's latitude experienced from 9:00am to 3:00pm and the SZA range experienced during the first and last hour of the 9:00am to 3:00pm range (Michalsky 1988). Provided outdoor activities are scheduled to minimise exposure to low SZA (SZA 0^o-30^o), the potential reduction in the received exposure to all body sites can be significant.

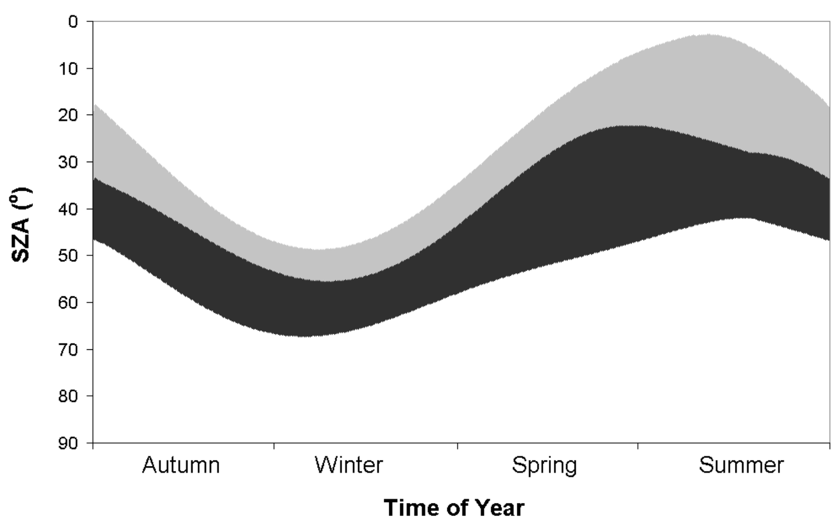

Figure 6.1: Daily variation in SZA plotted between 9:00am and 3:00pm (light curve) and between 9:00am to 10:00am and 2:00pm to 3:00pm (dark curve) at latitude 25.3^o S.

As a comparison, the modelled annual horizontal plane exposure calculated for the 202 school days in the year and determined using a mean playground sky view (55%), shade density remainder (57%), surface albedo (8%), and ozone concentration of 300 DU varies from between 3150 SED and 970 SED respectively for daily exposures received between 10:00am and 2:00pm (including the 0^o-30^o SZA range) and daily exposures received only in the first and last hours of the school day (roughly limited to the 30^o-50^o SZA range). Using the method outlined previously in section 5.2.2.1.1, the biological amplification factors also previously specified in the aforementioned section, and including an estimated 3150 SED annual UV_{ery} exposure received outside of school hours, the relative NMSC risk can be calculated. Here, a student using the playground environment between 10:00am and 2:00pm has an increased risk of developing BCC and SCC compared to a student that avoids exposure between 10:00am and 2:00pm. The increased risk is 2.1 times and 2.7 times greater for the development of BCC and SCC respectively. At first such a comparison may seem unfair considering that there are 4 hours in the period 10:00am to 2:00pm and only 2 hours in the first and last hours of the school day. However, both meal breaks occurring between 10:00am and 2:00pm are included in the risk comparison for that period. The reductions in NMSC risk therefore can be achieved provided that exposure is avoided during both meal breaks and a student is limited to exposure in the first and last hours of the school day. Sun protection strategies, including the encouragement of indoor activity, hat, protective clothing and mandatory sun screen application during meal breaks could achieve such a reduction. Where such measures cannot be implemented, timetables, particularly the timing of lunch breaks which account for the majority of the daily cumulative UV exposure (Figure 5.5) could be rescheduled to reduce exposure. Additionally consideration could be given to the hours over which a school day is held. School days could for example be lengthened to a standard 8 hour working day, starting at 8:00am and ending at 4:00pm, in which time school meal breaks could be scheduled outdoors between 9:00am and 10:00am and 2:00pm and 3:00pm and the extended two hours of the school day could be utilised as supervised indoor study or free time.

6.1.2 Implications for the use of hats in the school playground

Based on the calculated daily variation in SZA over a full year, it was found that outdoor activities run during the first and last hour of the school day could result in a maximum

SZA limit of 30^o for most of the year at 25.3^o S with the limit increasing for schools located further south and decreasing for more northerly latitudes (southern hemisphere). From the results detailed here, this has the potential to reduce the unprotected student UV_{ery} exposure from a low SZA range of 0^o-30^o to a higher SZA range of 30^o-50^o. Patterns in exposure measured to the mannequin test subjects studied in this research show a clear broadening of the surface exposure to a larger area of the body with increasing SZA. Kimlin et al. (1998) determined mannequin facial exposures would shift from horizontally inclined facial regions to vertical regions from summer to winter, attributing this to increased diffuse UV at larger SZA ranges. Previous work using the same mannequin headforms employed by Kimlin et al. (1998) has indicated similar variation in facial ER with SZA (Downs et al. 2001; Downs & Parisi 2007). The mean UV_{ery} facial exposure measured here is consistent with these findings, indicating that reductions in UV_{ery} facial exposure caused by increasing SZA range correspond with an increase in facial ER. Based on these results, it can reasonably be concluded that hat protection is particularly important at low (summer) SZA as increased ambient UV exposure can be more effectively reduced by the hat brim than at greater (winter) SZAs which affect a larger proportion of the face.

6.1.2.1 Reduction in facial exposure with increasing SZA

Measurements of human facial exposure were collected during a series of 1 hour trials in the HBSHS student population to determine the relative effectiveness of wearing broad-brimmed hats (Downs & Parisi 2008). A summary of these results is given in Appendix P. It was determined that mean UV_{ery} facial exposures received for 1 hour of the school day varied between 1.6 ± 0.5 SED (1σ) and 1.3 ± 0.2 SED (1σ) in the ranges of 0^o-30^o and 30^o-55^o respectively resulting in a yearly accumulated exposure of 320 ± 100 SED to 260 ± 40 SED taken over a 202 day school year and assuming an exposure interval of at least 1 hour per day. Both of these exposures, based on the measurement of student facial exposure agree with modelled estimates of annual facial exposure given in section 5.2.3 of 330 SED where this calculation was determined using equation 5.6 and the median mannequin facial ER of 39% (Table 3.8) for the mean annual 30^{o}-50^{o} SZA range at Hervey Bay's latitude.

6.2 Scheduling by playground region

In this research it was found that playground sky view was the most important factor influencing total playground exposure modelled on a horizontal plane. This is likely to be the case because areas of the playground that have limited sky views affecting the diffuse component of incident UV also experience higher shade densities influencing the direct component of incident UV. In the previous chapter it was determined that the risk of developing NMSC was increased for students using open playground environments compared to those located in regions that had lower sky views. Limiting student movement to regions of the playground that offer greater protection from direct and diffuse UV, particularly at times of peak solar UV irradiance, will result in lower exposures experienced by the student population.

6.3 Reducing playground and playground region exposure

UV_{ery} exposures modelled in the playground included modelling the effects of shade structures including buildings, shade structures covered by shade cloths and trees. The effect of playground surface structures combined with sky view measurements taken at each of the 822 playground sites showed some variation in the degree of protection provided as was evident in the modelled UV_{ery} variation in protected ground surface patterns observed over the playground region (Figure 4.10 and 4.11). These variations were linked strongly to site sky view and direct UV irradiance influenced by local site structures. In order to make accurate assessments of the UV_{ery} in a realistic environment such as the school playground modelled here, variation in surface UV irradiance with solar position relative to the environment was considered. Predictions of the open environment surface UV intensity such as the widely available UV index reported frequently by local forecasting agencies do not take such considerations in account, showing typically variation in UV irradiance due only to seasonal effects. While such predictions are a valuable guide to assessing the general UV risk, more detailed assessments taking the local environment into account, such as that developed here, can provide better information to the public, education and health authorities to better plan and assess for risks likely to be incurred by those using specific outdoor environments, particlarly environments such as schools that are used frequently on a day to day basis. Assesment of the risks present in any playground environment using the techniques developed for this work may include better planning of schedules for outdoor activity, the organisation of those sheduled activites, including sports days, relative to specific positions within a playground, planning for playground improvements and selecting sites for the positioning of seating, playground equipment, shade and other structures. The quality of protection unique to the studied playground environment can be examined using the survey techniques developed. The quality of tree shade and some of the shade structures present in the HBSHS playground are breifly discussed here to illustrate the value of modelling UV playground exposures using the survey technique developed for this research.

6.3.1 Assessment of playground tree cover

Apart from the shade protection offered to students located underneath buildings, trees often provide the next most reasonable form of quality cover from direct UV. Trees are also a valuable source of shade in the open playground which by necessity grow in open sunlit environments. Furthermore, shade from tree cover is relatively inexpensive to provide in a playground setting, although the quality of protection offered depends on the density of tree canopies which vary from species to species, an individual’s location relative to the canopy, and with the planted densities of the trees themselves. The protecton afforded by a tree is also very much dependent upon the total sky view covered and cannot be judged by the appearance of tree shadow alone (Heisler & Grant 2000). The image processing technique applied throughout this research adequately assesses the quality of tree shade, providing estimates of the degree of cover provided by different trees found in the playground. As expected, thicker trees were found to more likely block the direct UV irradiance and subsequently influence the modelled UV_{ery} exposure than trees that provided less cover. Comparison of solar position with composite playground site images of tree structure provided a simple and useful method of assessing tree shade quality allowing its influence to be plotted over a horizontal plane (Chapter 4). The influence of thick tree cover, and sparse tree cover is clearly evident in Figures 4.6 (sky view), 4.7, 4.8 (shade densities) and 4.11 (summer solstice UV exposure). In the figures, the influence of thick tree cover is prominent along the school's western fence between 90 m and 130 m, the upper (eastern) end of the school's carpark located between 70 m and 100 m on the northen fence line and in the middle region of the school oval. Sparse tree cover is provided in the north-western corner of the school playground, the south-western corner of the pool region and behind (east) the school canteen.

Figure 6.2: Examples of sparse tree cover. North facing view of cover located in the north western corner of the playground (left), shade in the pool region (middle), and cover behind the school canteen (right).

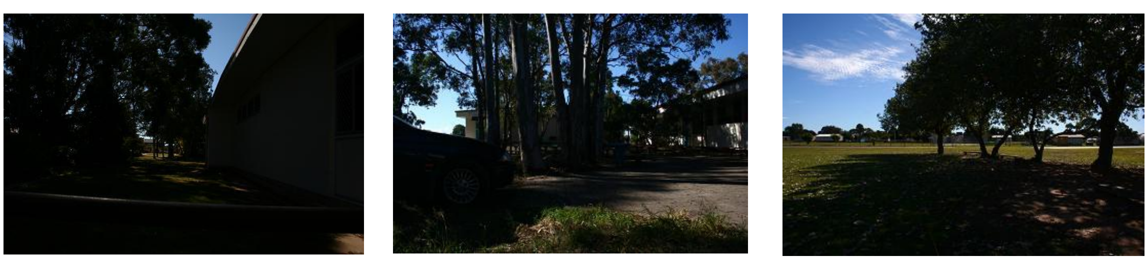

Figure 6.3: Examples of thick tree cover. North facing view of thick tree shade located between 90 m and 130 m on the school's western fence line (left), thick canopy cover in the eastern end of the school's main carpark (middle), thick cover on the school oval (right).

Measurements of the horizontal plane UVB (280 nm to 320 nm) made underneath a tree grove in previous research (Heisler et al. 2003) over the SZA range of 20^{o}-50^{o} indicates that the irradiance relative to an open sky environment varies between 0.4 and 0.6 for sky views between 40% and 60%. Similar UV shade effects have been discussed in Grant et al. (2001). Here, for tree cover between 90 m and 130 m the measured sky view examined along survey contours 1 and 2 (Appendix L) ranged between 38% and 63% which is relatively close to the sky view examined by Heisler et al. (2003). In comparison to this research, the modelled UV_{ery} playground exposure in this region expressed relative to the open environment exposure varied from between 0.41 and 0.46 for the respective winter and summer solstice periods modelled in Chapter 4 (the equivalent of an approximate Protection Factor of 2). Measurements by other researchers (Parisi & Kimlin 1999) however, indicate that tree shade protection is more effective in the UVA wavelengths (320 nm to 400 nm) and the direct comparison made to UVB estimates (Heisler at al. 2003) may better be represented if they are reduced slightly to account for the increased UVA wavelength dependence of the erythemally effective UV modelled here. Modelled predictions of the playground horizontal plane UV_{ery} exposure in the school's shaded region along the western fence line do however compare well with measurement studies (Parisi et al. 2001) for which the relative UV irradiance was determined at 0.42 in the SZA range 30^{o}-54^{o} under dense tree shade. These comparisons with the measured results of Heisler et al.(2003) and Parisi et al. (2001) indicate that the technique presented to model UV exposure in a playground environment can be used to assess the quality of tree shade in a realistic environment.

6.3.2 Playground shade structures and their effectiveness

In the summer solstice playground exposure illustrated in Figure 4.11, the influence of a small bus shelter (Figure 6.4) can be seen at approximately 10 m along the western fence line. UV_{ery} exposures modelled using the technique developed for the school bus shade structure presented in this research are comparable with subsequent Protection Factors (PF) measured for similarly built shade structures placed in an open environment (Turnbull & Parisi 2006). Here, sky view images were taken underneath the bus shade structure along the first survey line at 10 m and 15 m from the school's northern fence. The sky view at these locations was determined to be 30% and 39% respectively which included a measured 11% transmittance factor for UV penetration through the bus shelter's blue PVC shade cloth cover (Broad-band UV measurements of shade cloth UV transmission are given in Appendix E for all shade cloths found in the HBSHS playground environment). Both covered survey sites in this case were approximately centred underneath the bus shade structure shown in Figure 6.4. The reduction in modelled UV_{ery} exposure along the survey line passing through the bus shelter structure is listed in Table 6.1. The estimated PF for the shelter was determined as the ratio of mean modelled unprotected UV_{ery} to the mean protected UV_{ery} values listed in the table. The estimated PF for the structure in this school playground is similar to measured PFs of 1.8-16.1 determined for shade cloth (Toomey et al. 1995), PFs of 4-8 (Gies & Mackay 2004) determined for shade structures located in New Zealand primary schools and PFs found for small sized shade structures determined at < 3 in winter and < 8 in summer (Turnbull & Parisi 2006).

Figure 6.4: The playground bus shelter PF can be calculated by comparing model UV_{ery} at sites located underneath the shelter to sites located in proximity to the shelter but not located directly underneath it. The bus shelter shade cloth measured approximately 3 m x 12 m and was located approximately 3 m from the ground surface.

Table 6.1: Survey line variation in UV_{ery} exposure modelled about the bus shelter for the respective winter and summer solstice in the period 8:30am to 3:05pm. Estimated PF was calculated using the ratio of average unprotected modelled UV_{ery} to average protected modelled UV_{ery}.

Approx. distance from centre of shelter (m)	Winter solstice exposure (21 June 2008)	Summer solstice exposure (21 December 2008)
8 (north)	10.6 SED	45.4 SED
3 (north)*	3.7 SED	17.1 SED
2 (south)*	4.5 SED	17.8 SED
7 (south)	14.1 SED	60.2 SED
Estimated PF	3.0	3.0

Survey sites marked with an (*) were located underneath the bus shelter

6.3.2.1 Additional notes on playground shade cloth structures

The PF of shade cloth protected structures located in the HBSHS playground are given in Appendx E. The PF of shade cloth structures located in the HBSHS playgrouned were found to vary from 1.1 to 5.3 during the winter solstice and 1.1 to 16.3 during the summer solstice. The listed PFs given in the appendices were calculated in the same manner as demonstrated in Table 6.1. Additionally UV shade cloth transmissions listed in the appendix were used to weight direct UV exposure provided the sun's disc was located behind a cloth structure for the various times and sites used to determine playground shade density (Figure 4.7 and 4.8). In this way, the modelled direct UV componet was weighted to the UV transmission of the shade cloth and the diffuse UV was weighted to the site sky view which is influenced by the shade cloth attached to the shading structure and the degree to which other playground structures reduce the surrounding sky view. For playground sites located under shade structures protected by shade cloths the measured UV transmission of the respective shade cloth was used as an estimate of the sky view above 32^{o} in ZA. Using measured shade cloth UV transmissions, the model developed for this research can be applied to assess the quality of shade protection in real outdoor environments.

6.4 Vitamin D deficiency

Recently, the risks of underexposure to ambient solar UV have been linked to the development of diseases including rickets (Holick 2003), type I diabetes (Hypponen et al. 2001), multiple sclerosis (Hayes et al. 1997) and the possible development of some cancers (Gorham et al. 1990; Garland et al. 2002; Grant 2002). As has been previously mentioned, these risks are related to vitamin D deficiencies caused by limitations in diet, and the sunlight induced epidermal reaction of 7-dehydrocholesterol into pre-vitamin D_3. At the latitude examined here, the biological response of vitamin D_3 production in human skin exceeds the predicted erythemally effective UV. This is due to the vitamin D_3 response having a greater weighting at shorter UVB wavelengths than the erythemal response (Figure 1.9). Higher solar elevations observed at sub tropical latitudes result in less atmospheric scattering of the direct UV irradiance inducing a greater vitamin D_3 response than the observed erythema or sunburn reaction. Furthermore, it has been determined that at low latitudes ($< 25^o$) the effective vitamin D UV is equal during both the summer and winter seasons, meaning extended exposures to sunlight are more likely to be harmful than beneficial in sub tropical and tropical latitudes (Kimlin et al. 2006).

The research presented here, although not specifically weighted to the vitamin D_3 response, suggests outdoor playground exposures received by Queensland school children present a much more significant risk for the development of skin cancers caused by overexposure than diseases linked with underexposure to UV. Horizontal plane daily playground exposures modelled in this research were found to be in excess of 60 SED during the summer solstice and 20 SED during the winter solstice in open playround environments. Measurements of personal exposure were found to be in excess of 40 SED for students attending the school swimming carnival. These results give a clear indication of the level of risk present in a Queensland school environment relative to the risks faced by school aged children caused by underexposure and vitamin D deficiency. However, a useful technique applied using a similar method as described for this research could be used to examine the regions of low vitamin D_3 effective UV in outdoor environments by weighting the global UV spectrum to the epidermal reaction of 7-dehydrocholesterol into pre-vitamin D_3 (CIE 2006), rather than the erythemal reaction (CIE 1987).

6.5 UV distributions of body surface exposure

A significant proportion of this research work has concentrated on the detailed measurement of body surface distributions of UV exposure. This was seen as a necessary step in achieving an accurate model of human exposure to ambient UV that takes into account shading of the body itself. The face, neck, arm, hand and leg models used to represent exposure are effectively measurements of body surface exposure patterns with changing SZA rather than predictions of the surface exposure estimated for the variously inclined surfaces of the human body. In addition to this, measurements made of the surface distributions of UV exposure have been recorded to a high resolution, eliminating the uncertainty caused by interpolations made over widely spaced body surface measurement sites. A series of detailed polynomial expressions have been developed for the human facial region that can be used to express ambient UV exposure relative to facial location (Appendix I). It is intended that the surface exposure results collected here can be used in future epidemiological studies relating sites of incidence for NMSC and melanoma skin cancers and it is therefore considered relevant to dedicate some part of this discussion to this topic. Measurements of body surface exposure distribution are compared below to studies detailing sites of NMSC and melanoma skin cancer body site incidence.

6.5.1 Comparison of measured exposure with sites of melanoma skin cancer incidence

Detailed body surface incidence data for the distribution for NMSC and melanoma skin cancer is not readily available in the literature. Often, body surface incidence of a particular type of skin cancer is reported for broad regions of the body, including for example, the face, body trunk, neck, arms and legs. Measurements of ER have been performed here at 1453 body sites. The detail provided in this data set provides an opportunity to examine detailed distributions of skin cancer incidence. Where detailed skin cancer distributions could be identified in the literature these have been compared. For melanoma skin cancer, a cancer that does not necessarily occur on frequently exposed surfaces of the body (Diffey 1991), data is available indicating that the upper more frequently exposed surfaces of the body have a tendency to develop the greatest number of cancers in some populations but not others. The frequency at which melanoma is incident to heavily exposed surfaces of the body also depends on age, with less frequently exposed body surfaces having a high melanoma incidence in younger age groups, but showing a stronger correlation with heavily exposed areas in older age groups (Elwood & Gallagher 1998). Similarly, the number of nevi in individuals has been hypothesized to affect melanoma distributions between chronic and intermittent exposure patterns (Whiteman et al. 1999). Studies of melanoma skin cancer incidence in Queensland show that melanoma incidence is greater to the face and neck compared to the arms, hands and legs although it should be noted that there are differences in the distributions between males and females. (Green et al. 1993; Buettner & Raasch 1998). These results are in general agreement with ER distributions recorded for this research (Table 3.8) whereby exposure measured in the 0^{o}-30^{o} and 30^{o}-50^{o} SZA range was greatest to the face, followed by the hand, neck, leg and forearm. Measurements of body site distribution of NMSC, particularly SCC are more frequently reported on areas of the body that receive a large proportion of the ambient UV and these are discussed in more detail.

6.5.2 Comparison of measured exposure with sites of NMSC incidence

6.5.2.1 BCC facial incidence

Comparison between the detailed facial distribution of UV exposure and the localisation of BCC incidence has been reported previously (Diffey et al. 1979). The facial distribution of BCC incidence has been detailed by Brodkin et al. (1969) and more recently by Scrivener et al. (2002). Both of these studies show high rates of BCC incidence to the nose. Comparisons between the distribution of facial UV exposure and BCC incidence provide a valuable insight into the causal nature of UV exposure and the aetiology of BCC as the face is not often protected by clothing and receives a high proportion of the ambient UV.

The correlation between facial BCC tumour density (Brodkin et al. 1969) and UV expoure examined by Diffey et al. (1979) did not show a strong relationship. The facial site incidence of BCC detailed by Brodkin et al. (1969) is presented in Figure 6.5 relative to the facial UV exposure data measured in this research within each of the 0^o-30^o, 30^o-50^o and 50^o-80^o SZA ranges. In this comparison, sites of facial BCC incidence were assigned an ER for each SZA range for each specific part of the face for which BCC tumour incidence was quoted. (The Brodkin et al. (1969) BCC tumour density data is presented in Appendix Q for each of the respective measured facial site ERs). Comparisons made between the research of Diffey et al. (1979) and the facial exposure measurements made here show similarities that highlight the difficulty in establishing a relationship between UV exposure and BCC tumour density. The data presented shows a steady increase in BCC tumour density with increasing UV exposure, however consistent discontinuities in the comparison weaken the relationship with significantly higher tumour densities occurring for example, under the nose, an area of the face that does not receive a high proportion of the ambient UV. The presented comparison between BCC tumour density and exposure shows that there is no direct relationship that can be drawn between the two quantities.

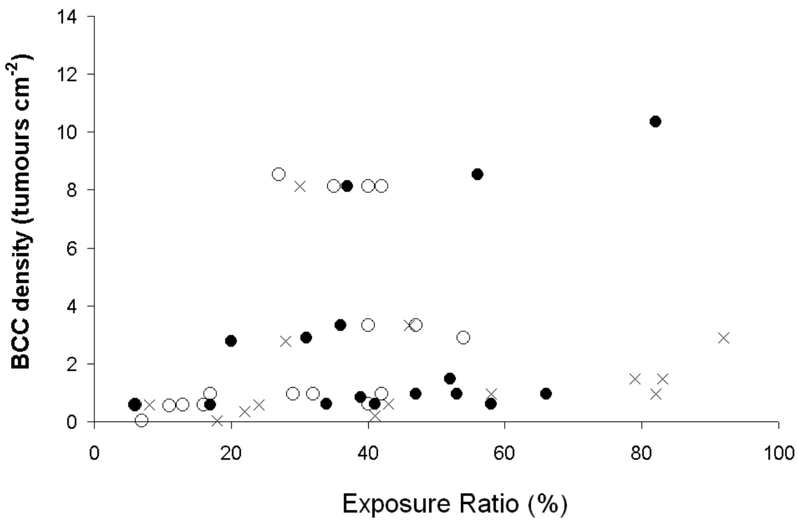

Figure 6.5: Facial BCC tumour density (Brodkin et al. 1969) and UV exposure per lesion site. The Brodkin et al. (1969) facial tumour densities are expressed relative to the facial measurements of SZA in the ranges: (0^o-30^o) open circles; (30^o-50^o) closed circles; and (50^o-80^o) crosses.

6.5.2.2 SCC facial incidence

The relationship between facial UV exposure and the distribution of solar keratoses (SK), possible markers for the later development of SCC (Marks et al. 1988), were also examined with respect to measured facial ER. Figure 6.6 compares the facial distribution of SK incidence measured in Brisbane (Latitude 27^o S) (Nguyen et al. 1998) with the facial ER data measured in each of the 0^o-30^o, 30^o-50^o and 50^o-80^o SZA ranges. (The tabular form of this data is also presented in Appendix Q). Comparisons between this data set show that SK incidence increases with facial UV exposure. The greatest incidence of observed SK for the Brisbane study (Nguyen et al. 1998) was found on the cheek, followed by the ears and the nose. Each of these regions of the face receive a consistently high UV exposure across each of the 0^o-30^o, 30^o-50^o and 50^o-80^o SZA ranges. However, as is evident in Figure 6.6, it is difficult to establish a clear relationship between UV exposure distribution and the incidence of SK.

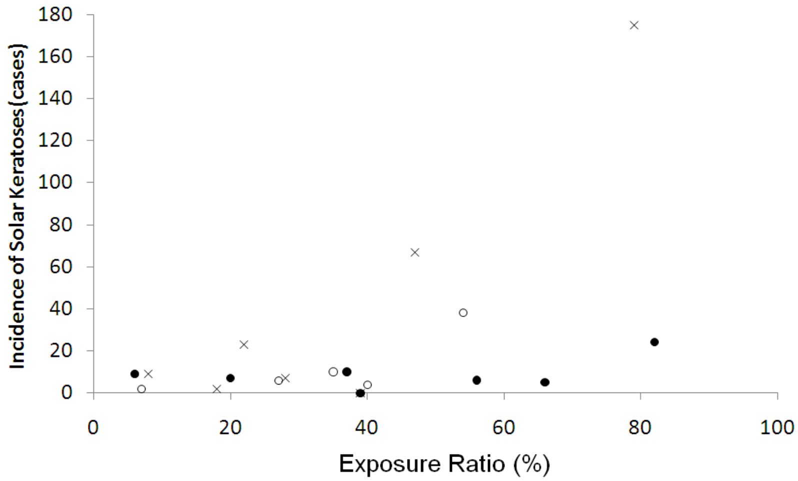

Figure 6.6: Facial SK incidence (Nguyen et al. 1998) and UV exposure per lesion site in the SZA 0^o-30^o (open circles); 30^o-50^o (closed circles); and 50^o-80^o (crosses) range.

6.5.2.3 The anatomical distribution of BCC and SCC

The incidence of SCC in men and women is lower than BCC (Staples et al. 1999; Kricker et al. 1990; Raasch et al. 1998). The proportion of SCC is however greater to the exposed surfaces of the upper limbs than BCC (Raasch et al. 1998; Giles et al. 1988). This, in part is due to the higher incidence rate of BCC localised on the body trunk, an area of the body not readily exposed to solar UV, decreasing the relative proportions of BCC incidence to frequently exposed body surfaces. Patterns in BCC incidence supported by the hypothesis that intermittent exposures affect areas of the body not readily exposed to solar UV, may account for BCC anatomical distributions that develop later in life as a result of earlier severe episodes of sunburn. In the comparisons made to exposures measured in this research, BCC incidence was most strongly correlated to UV exposures measured on the face, followed by the upper limbs.

The anatomical distribution for histologically confirmed incidences of BCC and SCC measured in Australian populations of sub-tropical and tropical latitude was compared to the median body site ER data measured in the 0^o-30^o, 30^o-50^o and 50^o-80^o SZA range for the face, neck, arm, hand and leg (Table 6.2(a) and Table 6.2(b)). The localisation of BCC and SCC data presented in the tables were measured from electoral roll populations residing in Geraldton, Western Australia (Kricker et al. 1990) and Townsville, Queensland (Raasch et al. 1998). These two regional Australian cities are located in latitudes of 29^{o}S and 19^{o}S respectively and are therefore subject to the SZA ranges studied in this research. The incidence of both BCC and SCC to the face and upper limbs were reported in these two studies to be higher than the confirmed incidences to the neck and legs, regions of the body that are better protected by clothing than the face and upper limbs, particularly in warm climates, whereby the forearms are not often protected.

Table 6.2(a): Comparison of the anatomical distribution of BCC site localisation in Geraldton (Kricker et al. 1990) and Townsville (Raasch et al. 1998) to median ER.

Body Site	Geraldton		Townsville	ER		
	men (n = 232)	women (n = 126)	men & women (n= 213)	SZA 0^{o}-30^{o}	SZA 30^{o}-50^{o}	SZA 50^{o}-80^{o}
Scalp	1%	0%	6%			
Face	17%	27%	44%	26%	39%	48%
Neck	5%	6%	7%	23%	36%	59%
Upper limbs	13%	17%	12%	*20%	*21%	*41%
Lower limbs	8%	7%	7%	12%	23%	47%

* median of forearm and hand ER

Table 6.2(b): Comparison of the anatomical distribution of SCC site localisation in Geraldton (Kricker et al. 1990) and Townsville (Raasch et al. 1998) to median ER.

Body Site	Geraldton		Townsville	ER		
	men (n = 33)	women (n = 7)	men & women (n= 121)	SZA 0^o-30^o	SZA 30^o-50^o	SZA 50^o-80^o
Scalp			4%			
Face	58%	57%	19%	26%	39%	48%
Neck	9%	0%	7%	23%	36%	59%
Upper limbs	9%	14%	49%	*20%	*21%	*41%
Lower limbs	9%	14%	18%	12%	23%	47%

* median of forearm and hand ER

It can reasonably be concluded that chronic exposure to solar UV is likely to establish an exposure pattern similar to that which has been measured in this research as chronic exposure to solar UV will affect unprotected skin surfaces of the body that receive a higher solar UV exposure. The examined incidences of SCC which were recorded in similar latitudes to the measured pattern of body surface exposure show a higher correlation with ER than the respective BCC incidence. However, the aetiological factors that influence the development of NMSC cannot be directly related to the measured anatomical distribution of UV exposure alone. The relevance of this particular point must be emphasised in relation to UV exposure distributions which were measured here using upright mannequin subjects. Additional factors including variation in skin thickness above the basal layer, the presence of hair, clothing, and personal outdoor lifestyle patterns will influence NMSC incidence rates and are difficult to quantify with respect to comparisons made using mannequin subjects.

Existing data present in the literature detailing the measured distribution of solar UV exposure to human subjects is further limited by the total number of body sites that are often measured. An approach that integrates detailed measurements of UV exposure distribution, such as the body site exposure sets provided here for mannequin subjects may improve interpolated estimates of whole body exposure measured using human subjects which in turn may improve correlations made with the anatomical distribution of NMSC and melanoma body distribution incidence data. The measured patterns in UV exposure, although not showing a strong relationship with the distribution of NMSC incidence can be applied to a variety of SZA ranges providing a detailed data set of UV exposures that may assist in future studies assessing the anatomical distribution of melanoma and NMSC incidence.

6.6 Future work and extension of the research project

6.6.1 Model applications in different environments

The main components of this research work can be summarised into three points. These include: playground specific modelling of the horizontal plane UV_{ery} exposure, measurement of body surface UV distribution relative to the horizontal plane; and modelling body surface UV exposure distributions by weighting with body site ER to predict skin surface exposures in the playground environment. The research work presented has been developed from measurements made in one specific school playground. The work presented here could similarly be extended to any outdoor playground environment or any outdoor environment in which the local ambient UV may need to be assessed including for example public parks or sporting grounds.

In order to model the UV exposure incident on human skin surfaces in the HBSHS playground measurements of sky view were taken using a photographic survey method in which 822 specific playground sites were sampled. The detail required for any other outdoor environment may be improved by sampling at higher resolutions than 5 m. Similarly, lower sampling resolutions may be used in more open environments as was demonstrated in this research whereby the sky view was sampled at 20 m in open regions of the playground.

The model developed for this research was shown to be suitable for measurements of playground shade density. This was examined during the winter and summer solstice to determine the effective range of shade that could occur in the specific playground environment. Playground shading at any time or for any particular period of the day can be determined using the methods developed to assess shade quality in any outdoor location. The effect of shade from surface structures can be accurately modelled provided the position of the sun is plotted with respect to those structures. The advantage of using the method developed is that any ground or surface obstruction can be accounted for. The specific growth patterns of trees or the inclusion of later playground structures is taken into account when the outdoor environment is surveyed. In this way detailed shading patterns can be developed for existing outdoor environments which improve upon methods that make shade predictions based upon only the largest uniform surface structures and take little account of small scale surface objects such as trees and other small scale surface objects that become part of changing outdoor environments.

The method of modelling playground exposure presented in this work required a labour intensive survey of 822 playground sites. This is a necessary step required to make an accurate estimate of the UV exposure in any real environment. A valuable extension to this work could involve automated image processing of a survey playground. A wide-angle lens, attached to a digital camera fitted to a portable computer could be used to process sky view images as they are taken. Playground surveying software could further be developed to plot measured locations and process site images for sky view and shade density to develop UV hazard charts of various playground and outdoor settings in a shorter time frame than has been required for the current study whereby image processing and playground modelling were performed post survey.

6.6.2 Model limitations

Modelled UV exposures in the playground environment have been presented as the erythemal UV incident on a horizontal plane. Predictions of horizontal plane exposure were further weighted to measurements of body surface ER to determine estimates of body surface exposure under different conditions in the playground environment. The influence of the local environment and the behaviour of students in the school playground will result in variations from the predicted body surface exposure and the actual received body surface exposure placing some limitations on any prediction made using the techniques developed for this research.

The first obvious limitation of note is caused by the measurement of body surface exposure on mannequin subjects. The movement of living human subjects is dependent on individual attitude and lifestyles. The posture of a human subject as it is related to the solar UV environment is very much dependent upon the activity undertaken by the individual. Ratios of exposure expressed relative to the horizontal plane UV will be different for students undertaking different sporting activities and will be different for students sitting and standing in the school environment. The measurements of exposure in this work were recorded on a standing upright body and headform mannequin and therefore cannot be taken to represent the body surface exposure pattern received by a student under all conditions. The upright posture was examined here primarily because students using outdoor environments are likely to be either moving between classes, engaged in sporting activity during normal class times, or using the open oval environment during recess breaks for primarily recreational and sporting activities. Some variation in exposure is therefore possible in the real school environment due particularly to a sitting posture which is most likely to affect the predicted ratios of exposure to the leg region of the body. Although the body mannequin selected for the measurement of ER was a female mannequin of 178 cm height, this mannequin cannot be taken to represent individual body shape and size for students ranging from 6 to 17 years of age. It must also therefore be expected that there will be some variation in body surface exposure distributions due to individual body surface shape and size among a school population. An examination of different body postures and the use of different sized mannequins could be used to refine predictions of exposure distribution.

Predictions of UV exposure, weighted to human body surface topography for this work are dependent only upon the ambient UV that falls onto a horizontal plane. That is, there are additional uncertainties in the predicted pattern of body surface exposure caused by variation in the albedo present in any particular area of a playground environment. For a student located near a wall that has a high albedo surface for example, the exposure pattern affecting the body surface will be different to the exposure pattern measured in an open environment. The extent to which surfaces of various albedo and orientations with respect to the horizontal plane affect patterns in body surface exposure is dependent upon the cumulative albedo of the various surfaces specific to the local area of the surrounding playground and their aspect with respect to solar position. Such effects are difficult to model in detail due to the multitude of different surfaces that may be present in any specific playground site and have not been directly included in this research. Instead, a technique to express the cumulative effect of both vertical standing and ground surfaces has been presented from broad-band measurements of surface albedo. As an approximation, albedo contributions were estimated at each of the 822 playground sites from site ground surfaces and the cumulative sum of vertical standing surfaces located within 2 m of the specific playground site. Playground albedo contributions to the total exposure received by students were determined to be less than 10% for the model school environment when weighted to site sky view. As an improvement to the approximation developed for the current research, the influence of vertical standing and ground surface contributions to body surface exposures could be determined at increasing distances from the reflecting surface. The total surface area of individual ground and standing surfaces will also influence the actual exposure received by a student population.

Measurements of ER were recorded over grass surfaces in an open field site at the University of Southern Queensland. The studied playground environment experienced variations in surface albedo from 4% for grass surfaces to 10% for concrete. Variations in the measured body ER due to variation in surface albedo found in the playground environment are likely to be greatest to the lower regions of the full sized body mannequin and lower proximities of the headform mannequin. The greatest increase in ER due to increased surface albedo found in different regions of the playground will be 6% for concrete surfaces, 2% to 3% for paved surfaces, 3% for bitumen surfaces and 4% for paving dust surfaces found in the studied playground environment. The extent to which each of these albedo differences will influence ER to the surfaces of the mannequin model is dependent on the orientation of the mannequin body site relative to the horizontal plane and will be less to mannequin surfaces orientated away from the reflecting surface normal.

In this research a model of UV_{ery} exposure was developed assuming a constant ozone concentration of 300 DU and clear sky conditions. The changing influence of stratospheric ozone will affect modelled student exposures. The horizontal plane UV model developed for this research has however included provision for various ozone concentrations and a simple model has been included in the supplied horizontal plane UV exposure software to model ozone concentrations at different longitudes and latitudes (Van Heuklon 1979). The influence of cloud as it relates to UV enhancements and more typically reductions in exposure, is dependent upon temporal cloud conditions which can change significantly during the course of a school day. A simple cloud model has been integrated into the developed horizontal plane UV exposure model (Josefsson 1986), although this has not been specifically investigated in this research. Further research into the modelled effects of cloud, particularly cloud enhancement to the ambient UV could be integrated into the developed horizontal plane model to make better predictions of UV exposure on cloudy days.

6.6.3 Increasing awareness in school populations

The developed UV exposure school environment model has been presented to demonstrate its effectiveness in making reasonable predictions of the exposures that affect school children. Models such as that developed for this research may be used to increase awareness of the local UV environment with changing season and on a day to day basis. This is seen as an important use of this research, particularly in regards to Queensland school environments which present a significant risk to children for the development of preventable solar induced diseases. Using the techniques demonstrated for the model school, other school environments could be assessed for the factors that affect solar safety including the quality and quantity of playground shade regions, sky view, and local albedo. An interesting extension of this research could include the assessment of the solar safety among different school environments. The quality of protection offered by schools of given localities could be adequately assessed to develop rankings to inform parents of the relative protection offered and similarly the relative risks of developing NMSC could be assessed between different school environments using the methods outlined. Playground specific models can be utilised by school administrators to plan for sporting events and to assess regions of the playground to make informed decisions about the local UV environment on a daily basis. Furthermore, students themselves may be given access to information about the UV in their local school environment to help them make informed decisions about their daily playground use.

CHAPTER 7 CONCLUSIONS

The outcome of this research has been the development of a playground specific UV exposure model that can be utilised to predict personal erythemally effective exposures over skin surfaces of the human body in a school environment. This is the first research to do this based on actual exposure ratio measurements which were made using miniaturised polysulphone dosimeters to allow for the high density measurement of exposure over the surface topography of the face, neck, arm, hand and leg, regions of the human body frequently exposed to ambient UV. Additional outcomes have further been developed and discussed. A summary of the specific outcomes relating to this research is given below:

7.1 Annual playground exposure

Mean playground statistics of sky view, and shade density were used to determine an estimate of the annual UV_{ery} exposure for the 202 day school calendar year. Assuming clear sky conditions and a constant ozone concentration of 300 DU, the annual HBSHS playground exposure was determined at 4210 SED. The weighted annual UV_{ery} exposure for each respective body part ER was determined to be 330 SED for the face, 300 SED for the back of the neck, 140 SED for the arm, 290 SED for the hand, and 190 SED for the leg. The ER for each of the mentioned body parts was determined as the median ER measured in the 30^o-50^o SZA range, the mean annual SZA range experienced at Hervey Bay's latitude.

7.2 Playground exposure ranges

Measurements of playground sky view, shade, and albedo contribution were utilised to provide estimates of playground surface UV_{ery} exposure. Maximum surface exposures were modelled in the school playground open environments, varying from above 20

SED and 60 SED in the 8:30am to 3:05pm school day for the winter and summer solstice respectively.

7.3 Tree shade and shading structures

The quality of tree cover in the playground environment was determined by comparing modelled UV_{ery} exposure under tree cover to open UV_{ery} playground exposures. This technique can be used to determine tree cover PF and is based on the image processing measurement of sky view and shade in the playground. The UPF of shade cloth structures was also determined in the HBSHS playground environment by determining the ratio of unprotected modelled UV_{ery} to protected UV_{ery} located underneath shade structures. The UPF of shade structures located in the model school environment varied from 1.1 to 5.3 in winter and 1.1 to 16.3 in summer.

7.4 Measurement of playground surface albedo

Playground ground and standing surface albedo was measured using a broad-band UV meter. These measurements were used to estimate playground site albedo contribution by weighting with site sky view. Regions of the school playground that made the greatest albedo contributions to the ambient UV were highlighted.

7.5 SZA ranges of body surface UV distribution

A total of 2491 measurements of body surface UV exposure were taken over a four year period in the SZA ranges 0^o-30^o, 30^o-50^o, and 50^o-80^o. This data set provides detailed information on the range of exposure distributions affecting unprotected human skin surfaces taking into account shading caused by the body itself.

7.6 Comparison of measured body ER and sites of skin cancer incidence

The patterns in solar UV exposure affecting unprotected skin surfaces of the body measured in this research were found to be in better agreement with published distributions of SCC than BCC. No direct relationship was determined between sites of facial NMSC and ER distributions measured in the 0^o-30^o, 30^o-50^o and 50^o-80^o SZA ranges.

7.7 Measured student exposure

The mean measured exposure recorded to students observing the normal school routine between February and June in the period between 8:30am and 3:05pm was 2.4 SED. Exposures measured during the school swimming carnival varied between 4.9 SED and 49.8 SED. Student location in the playground was determined to be a significant factor in increasing exposure to the face, neck, arm, hand, and leg body sites regardless of season and cloud cover. Most of the personal exposures measured in the school environment between February and June were found to exceed the occupational limit of exposure to solar UV radiation.

7.8 Activity index

The mean activity index of children using the study playground environment between 8:30am and 3:05pm was 0.2. The highest activity indices were determined for the short period before the start of school and during both meal breaks. The greatest activity index was observed during a school meal break time. It was determined that most (41%) of the student population had spent two periods outdoors during the normal school routine and most of these students spent both of their two periods outdoors during meal breaks.

7.9 Hat use

Hat use in the playground was noted at 8%. Of the hats that were worn by students most were baseball style caps.

7.10 NMSC risk

NMSC risk was determined for children using various regions of the playground environment. The risk of developing NMSC was discussed in relation to hat use in the school population. It was determined that children using open outdoor environments during both school meal breaks increased their risk of developing BCC by 1.8 and increased their risk of developing SCC by 2.2 compared to children that used well protected playground environments. Students restricted from the playground environment between 10:00am and 2:00pm were found to have a reduced risk for the development of BCC by 2.1 and 2.7 for the development of SCC. It was also determined that moving the school swimming carnival from 15 February to 15 April resulted in a reduction in the risk of developing both BCC and SCC skin cancers provided exposure received outside of school hours was low.

7.11 Recommendations of playground exposure limits

It was determined that playground exposures could be greatly reduced if students were restricted from using the playground environment between 10:00am and 2:00pm. Most of the daily cumulative exposure received by a school student in the model school playground was found to occur during the school meal break periods between 11:25am and 12:05pm and 1:15pm and 1:55pm. The active use of sun protection measures during school meal breaks is likely to have the most significant effect on reducing cumulative UV exposure. High personal exposures measured during the school swimming carnival also highlight the need to take active precautions during outdoor school events such as sports days. School administrators have both the potential and responsibility to reduce risks associated with excessive childhood UV exposures received in the school environment.

The research presented in this work was developed with the intention of providing a model that could be used to educate children, teachers and administrators of the severity of the UV climate present in Queensland school playground environments. Much of the inspiration for the research came about by observation of Queensland schools holding swimming carnival events in the early February of each year which to the author's understanding is the case largely because qualifying rounds need to be held early in the year to determine district and state championships. Continuing to follow such practices without proper consideration of the health risks inherent in the environment makes no contribution toward reducing skin cancer mortality rates, which in Queensland are recognised as the highest in the world. It is hoped that the methods presented for assessing detailed environmental and anatomical distribution patterns will make some contribution toward better understanding those very real risks presented to children by being exposed to a known carcinogen.

REFERENCES

ACCV (Anti-Cancer Council of Victoria), 1999, *SunSmart Campaign 2000-03*, Report of the Anti-Cancer Council, Melbourne.

Agar, N.S., Halliday, G.M., Barnetson, R.S., Ananthaswamy, H.N., Wheeler, M., Jones, A.M. 2004, 'The basal layer in human squamous tumors habors more UVA than UVB fingerprint mutuations: a role for UVA in human skin carcinogenesis', *Proceedings of the National Academy of Sciences of the United States of America*, vol. 101, no. 14, pp. 4954-4959.

AIHW (Australian Institute of Health and Welfare) and AACR (Australasian Association of Cancer Registries), 2007, *Cancer in Australia: an overview, 2006*, Cancer Series no. 37, Australian Government, Canberra, Available at: http://www.aihw.gov.au/publications/can/ca06/, Accessed on 14 April 2008.

Airey, D.K., Wong, J.C.F. & Fleming, R.A. 1995, 'A comparison of human- and headform- based measurements of solar ultraviolet B dose,' *Photodermatology, Photoimmunology and Photomedicine,* vol. 11, no. 4, pp. 155-158.

Armstrong, B.K. 1988, 'Epidemiology of malignant melanoma: intermittent or total accumulated exposure to the sun?,' *The Journal of Dermatologic Surgery and Oncology*, vol. 14, pp. 835-849.

Armstrong, B.K. 1994, 'Stratospheric ozone and health,' *International Journal of Epidemiology*, vol. 23. pp. 873-885.

Armstrong, B.K. & Kricker, A. 1996, 'Epidemiology of sun exposure and skin cancer', in *Skin Cancer*, vol. 26, eds I.M. Leigh, J.A. Newton Bishop & M.L. Kripke, pp. 133-154, Cold Spring Harbor Laboratory Press, Cold Spring Harbor.

ARPANSA (Australian Radiation Protection and Nuclear Safety Agency). 2006, *Radiation Protection Standard: Occupational Exposure to Ultraviolet Radiation* Radiation Protection Series Publication no. 12, Canberra: Australian Government.

Atkinson, R.J., Matthews, W.A., Newman, P.A. & Plumb, R.A. 1989, 'Evidence of the mid-latitude impact of Antarctic ozone depletion,' *Nature*, vol. 340, pp. 290-294.

Balanda, K. P., Stanton, W.R., Lowe J.B. & Purdie, J. 1999, 'Predictors of sun protective behaviors among school children,' *Behavioral Medicine,* vol. 25, pp. 28-35.

Barton, I.J. & Paltridge, G.W. 1979, 'The Australian climatology of biologically effective ultraviolet radiation,' *Australian Journal of Dermatology*, vol. 20, pp. 68-74.

Blumthaler, M. & Ambach, W. 1988, 'Solar UVB-albedo of various surfaces,' Photochemistry and Photobiology, vol. 48, no. 1, pp. 85-88.

Broadstock, M., Borland, R. & Hill, D. 1996, 'Knowledge, attitudes and reported behaviours relevant to sun protection and suntanning in adolescents,' *Psychology and Health*, vol. 11, pp. 527-539.

Brodkin, R.H., Kopf, A.W. & Andrade, R. 1969, 'Basal-cell epithelioma and elastosis: a comparison of distribution', in *The Biologic Effects of Ultraviolet Radiation: with Emphasis on the Skin*, ed. F. Urbach, pp. 581-618, Pergamon, New York..

Bruls W.A.G., Slaper, H., van der Leun, J.C. & Berrens, L. 1984, 'Transmission of human epidermis and stratum corneum as a function of thickness in the ultraviolet and visible wavelengths,' *Photochemistry and Photobiology*, vol. 40, no. 4, pp. 485-494.

Björn, L.O. 1989, 'Computer programs for estimating ultraviolet radiation in daylight', in *Radiation Measurement in Photobiology*, ed. B.L. Diffey, pp. 161-189, Academic Press, New York.

Braslau, N. & Dave, J. V. 1973, 'Effect of aerosols on the transfer of solar energy through realistic model atmospheres, Part III: Ground level Fluxes in the biologically active bands, 0.2850-0.3700 microns', IBM Research Report, RC 4308.

Buettner, P.G. & Raasch, B.A. 1998, 'Incidence rates of skin caner in Townsville, Australia,' *International Journal of Cancer*, vol. 78, no. 5, pp. 587-593.

Campbell, C., Quinn, A.G., Angus, B., Farr, P.M. & Rees, J.L. 1993. 'Wavelength specific patterns of p53 induction in human skin following exposure to UV radiation', *Cancer Research*, vol. 53, pp. 2697-2699.

CIE (International Commission on Illumination) Research Note 1987, 'A reference action spectrum for ultraviolet induced erythema in human skin,' *CIE- Journal*, vol. 6, no. 1, pp. 17-22.

CIE (International Commission on Illumination) Technical Report 1992, 'Personal dosimetry of UV radiation,' Publication no. CIE 98.

CIE (International Commission on Illumination) 1997, 'Standard erythema dose, a review,' B.L. Diffey, C.T. Jansén, F. Urbach, H.C. Wulf – CIE, Vienna, Austria.

CIE (International Commission on Illumination) 2006, 'Action spectrum for the production of previtamin D_3 in human skin,' Publication no. CIE 174.

Chapman, S. 1930. 'A theory of upper atmospheric ozone,' *Memoirs of the Royal Meteorological Society*, vol. 3, pp. 103-25.

Chuang, T.Y., Popescu, A., Su, W.P.D., & Chute, C.G. 1990, 'Basal cell carcinoma: a population-based incidence study in Rochester, Minnesota,' *Journal of the American Academy of Dermatology*, vol. 22, pp. 413-417.

Clemens, T.L., Adams, J.S., Henderson, S.L. & Holick, M.F. 1982, 'Increased skin pigment reduces the capacity of skin to synthesize vitamin D_3,' *Lancet*, vol. 1, pp. 74-76.

Coebergh, J.W.W. Neumann, H.A.M., Vrints, L.W., van der Heijden, L., Meijer, W.J. & Verhagen-Telings, M.T. 1991, 'Trends in the incidence of non-melanoma skin cancer in the SE Netherlands 1975-1988: a registry based study,' *British Journal of Dermatology*, vol. 125, pp. 353-359.

Cooke, K.R., Skegg, D.C.G. & Fraser, J. 1983, 'Trends in malignant melanoma of skin in New Zealand,' *International Journal of Cancer*, vol. 31, pp. 715-718.

Cutnell, J. D. & Johnson, K.W. 1998, *Physics: Fourth Edition*, John Wiley & Sons, New York.

Dave, J.V. & Halpern, P. 1976, 'Effects of changes in ozone amount on the ultraviolet radiation received at sea level of a model atmosphere,' *Atmospheric Environment*, vol. 10, pp. 547-555.

Davis, A., Deane, G.H.W. & Diffey, B.L. 1976, 'Possible dosimeter for ultraviolet radiation,' *Nature*, vol. 261, pp. 169-170.

deGruijl, F.R. 1982, *The dose response relationship for UV tumorigenesis*, University of Utrecht, PhD Thesis.

deGruijl, F.R. 1999, 'Skin cancer and solar UV radiation,' *European Journal of Cancer*, vol 35, no. 14, pp. 2003-2009.

Diepgen, T.L. & Mahler, V. 2002, 'The epidemiology of skin cancer,' *British Journal of Dermatology*, vol. 146, no. s61, pp. 1-6.

Diffey, B.L. 1977, 'The calculation of the spectral distribution of natural ultraviolet radiation under clear day conditions (for UV dosimeter correction),' *Physics in Medicine and Biology*, vol. 22, pp. 309-316.

Diffey, B.L., Kerwin, M. & Davis, A. 1977, 'The anatomical distribution of sunlight,' *British Journal of Dermatology*, vol. 97, no. 4, pp. 407-410.

Diffey, B.L., Tate, T.J. & Davis, A. 1979, 'Solar dosimetry of the face: the relationship of natural ultraviolet radiation exposure to basal cell carcinoma localisation,' *Physics in Medicine and Biology*, vol. 24, pp. 931-939.

Diffey, B.L. 1987, 'A comparison of dosimeters used for solar ultraviolet radiometry,' *Photochemistry and Photobiology*, vol. 46, pp. 55-60.

Diffey, B.L. 1989, ‘Ultraviolet radiation dosimetry with polysulphone film’, in *Radiation measurement in photobiology*, ed. B.L. Diffey, pp. 135-159, Academic Press, London.

Diffey, B.L. 1991, ‘Solar ultraviolet radiation effects on biological systems,’ *Physics in Medicine and Biology,* vol. 36, no. 3, pp. 299-328.

Diffey, B.L. 1992, ‘Stratospheric ozone depletion and the risk of non-melanoma skin cancer in a British population,’ *Physics in Medicine and Biology*, vol. 37, pp. 2267-2279.

Diffey, B. L. & Cheeseman, J. 1992, ‘Sun protection with hats,’ *British Journal of Dermatology*, vol. 127**,** pp. 10-12.

Diffey, B.L., Gibson, C.J., Haylock, R., McKinlay, A.F. 1996, ‘Outdoor ultraviolet exposure of children and adolescents,’ *British Journal of Dermatology*, vol. 134. no. 6, pp. 1030-1034.

Diffey, B. L., Jansen, C.T., Urbach, F. and Wulf, H.C. 1997, ‘The standard erythema dose: a new photobiological concept,’ *Photodermatology, Photoimmunology and Photomedicine*, vol. 13, pp. 64-66.

Diffey, B.L. 2002, ‘What is light?,’ *Photodermatology, Photoimmunology and Photomedicine*, vol. 18, no. 2, pp. 68-74.

Dixon, H., Borland, R. & Hill, D. 1999, ‘Sun protection and sunburn in primary school children: the influence of age, gender, and coloring,’ *Preventive Medicine*, vol. 28, pp. 119-130.

Downs, N.J., Kimlin, M.G., Parisi, A.V. & McGrath, J.J. 2001, ‘Modelling Human Facial UV Exposure,’ *Radiation Protection in Australasia*, vol. 17, no. 3, pp. 103-109.

Downs, N.J. & Parisi, A.V. 2007, ‘Three dimensional visualisation of human facial exposure to solar ultraviolet,’ *Photochemical and Photobiological Sciences*, vol.6, pp. 90-98.

Downs, N.J. & Parisi, A.V. 2008, ‘Patterns in the received facial ultraviolet exposure of school children measured at a sub-tropical latitude,’ *Photochemistry and Photobiology*, vol. 84(1), pp. 90-100.

Elwood, J.M. & Gallagher, R.P. 1998, ‘Body site distribution of cutaneous malignant melanoma in relationship to patterns in sun exposure,’ *International Journal of Cancer*, vol. 78, no. 3, pp. 276-280.

EQ (Education Queensland), 2008, *Shaping the smart state: a guide to state schools*, Queensland Government: Education Queensland, Available at: http://education.qld.gov.au/schools/about/pdfs/guide-to-state-schools.pdf, Accessed on 21 July 2008.

Estupinan, J.G., Raman, S., Crescenti, G.H., Streicher, J.J. & Barnard, W.F. 1996, ‘Effects of clouds and haze on UV-B radiation,’ *Journal of Geophysical Research*, vol. 101, no. d11, pp. 16807-16816.

Evans, R.D., Kopf, A.W., Lew, R.A., Rigel, D.S., Bart, R.S., Friedman, R.J. & Rivers, J.K. 1988, ‘Risk factors for the development of malignant melanoma-I: review of case control studies,’ *Journal of Dermatological Surge and Oncology*, vol. 14, pp. 393-408.

Farman, J.C., Gardiner, B.G. & Shaklin, J.D. 1985, ‘Large losses of total ozone in Antarctica reveal seasonal ClOx / NOx interaction,’ *Nature*, vol. 315, pp. 207-210.

Farr, P.M., Besag, J.E. & Diffey, B.L. 1988, ‘The time-course of UVB and UVC erythema,’ *Journal of Investigative Dermatology*, vol. 91, pp. 454-457.

Feister, U. 1994, ‘Measurements of chemically and biologically effective radiation reaching the ground,’ *Journal of Atmospheric Chemistry*, vol. 19, no. 3, pp. 289-315.

Feister, U. & Grewe, R. 1995, ‘Spectral albedo measurements in the UV and visible region over different types of surfaces,’ *Photochemistry and Photobiology*, vol. 62, no. 4, pp. 736-744.

Fishman, J., Watson, C.E., Larsen, J.C. & Logan, J.A. 1990, ‘Distribution of tropospheric ozone determined from satellite data,’ *Journal of Geophysical Research*, vol. 95, no. D4, pp. 3599-3617.

Fitzpatrick, T.B. 1975, ‘Soleil et peau,’ *Journal de Medicine Esthetique*, vol. 2, pp. 33-34.

Gambichler, T., Moussa, G., Tomi, N.S., Paech, V., Altmeyer, P. & Kreuter, A. 2006, ‘Reference limits for erythema-effective UV doses,’ *Photochemistry and Photobiology*, vol. 82, no. 4, pp. 1097-1102.

Garland, C.F., Garland, F.C., Gorham, E.D., Lipkin, M., Newmark, H., Holick, M.F. & Raffa, J.V. 2002, ‘Ultraviolet B, vitamin D, and their mechanisms in cancer prevention’, in *Ultraviolet Ground- and Space-based Measurements, Models, and Effects: Proceedings of SPIE*, eds. J.R. Slusser, J.R. Herman, and W. Gao, pp. 313-323, The International Society for Optical Engineering, SPIE, Bellingham.

Gasparro F.P., Mitchnick, M. & Nash, J.F. 1998, ‘A review of sunscreen safety and efficacy,’ *Photochemistry and Photobiology*, vol. 68, pp. 243-256.

Gies, P.H., Roy, C.R., Toomey, S., MacLennan, R. & Watson, M. 1995, ‘Solar UVR exposure of three groups of outdoor workers on the sunshine coast, Queensland,’ *Photochemistry and Photobiology*, vol. 62, no. 2, pp. 1015-1021.

Gies, P., Roy, S., Toomey, R., MacLennan, R. & Watson, M. 1998, 'Solar UVR exposures of primary school children at three locations in Queensland,' *Photochemistry and Photobiology*, vol. 68, pp. 78-83.

Gies, P., & Wright, J. 2003, 'Measured solar ultraviolet radiation exposures of outdoor workers in Queensland in the building and construction industry,' *Photochemistry and Photobiology*, vol. 78, no. 4, pp. 342-348.

Gies, P. & Mackay, C. 2004, 'Measurements of the solar UVR protection provided by shade structures in New Zealand primary schools,' *Photochemistry and Photobiology*, vol. 80, pp. 334-339.

Gies, P., Javorniczky, J., Roy, C. & Henderson, S. 2006, 'Measurements of the UVR protection provided by hats used at school,' *Photochemistry and Photobiology*, vol. 82, pp. 750-754.

Gilchrest, B.A., Eller, M.S., Geller, A.C. & Yaar, M. 1999, 'The pathogenesis of melanoma induced by ultraviolet radiation', *New England Journal of Medicine*, vol. 340, pp. 1341-1348.

Giles, G.G., Marks, R. & Foley, P. 1988, 'Incidence of non-melanocytic skin cancer treated in Australia,' *British Medical Journal*, vol. 296, no. 6614, pp. 13-17.

Giles-Corti, B., English, D.R., Costa, C., Milne, E., Cross, D. & Johnston, R. 2004, 'Creating SunSmart Schools,' *Health Education Research: Theory and Practice*, vol. 19, no. 1, pp. 98-109.

Girgis, A., Sanson-Fisher, R.W. & Watson, A. 1994, 'A workplace intervention for increasing outdoor workers' use of solar protection,' *American Journal of Public Health*, vol. 84, no. 1, pp. 77-81.

Glass, G.G. & Hoover, R.N. 1989, 'The emerging epidemic of melanoma and squamous cell skin cancer,' *The Journal of the American Medical Association*, vol. 262, no. 15, pp. 2097-2100.

Gorham, E.D., Garland, F.C. & Garland, C.F. 1990, 'Sunlight and breast cancer incidence in the USSR,' *International Journal of Epidemiology*, vol. 19, pp. 614-622.

Grant, R.H. 1997, 'Biologically active radiation in the vicinity of a singal tree,' *Photochemistry and Photobiology*, vol. 65, no. 6, pp. 974-982.

Grant, R.H. & Heisler, G.M. 1996, 'Solar ultraviolet-B and photosynthetically active irradiance in the urban sub-canopy: a survey of influences,' *International Journal of Biometeorology*, vol. 39, pp. 201-212.

Grant, R.H. & Heisler, G.M. 2001, 'Multi-waveband solar irradiance on tree-shaded vertical and horizontal surfaces: cloud-free and partly cloudy skies,' *Photochemistry and Photobiology*, vol 73, no.1, pp. 24-31.

Grant, R.H., Heisler, G.M. & Gao, W. 2002, 'Estimation of pedestrian level UV exposure under trees', *Photochemistry and Photobiology*, vol. 75, no. 4, pp. 369-376.

Grant, W.B. 2002, 'An estimate of premature cancer mortality in the U.S. due to inadequate doses of solar UV-B radiation,' *Cancer*, vol. 94, pp. 1867-1875.

Green, A. MacLennan, R., Youl, P. & Martin, N. 1993, 'Site distribution of cutaneous melanoma in Queensland,' *International Journal of Cancer*, vol. 53, pp. 232-236.

Green, A.E.S., Cross, K.R., & Smith, L.A. 1980, 'Improved analytic characterization of ultraviolet skylight,' *Photochemistry and Photobiology*, vol. 31, pp. 59-65.

Green, A.E.S., Sawada, T. & Shettle, E.P. 1974, 'The middle ultraviolet reaching the ground,' *Photochemistry and Photobiology*, vol. 19, pp. 251-259.

Grifoni, D, Carreras, G., Sabatini, F. & Zipoli, G. 2005, 'UV hazard on a summer's day under Mediterranean conditions, and the protective role of a beach umbrella,' *International Journal of Biometeorology*, vol. 50, no. 2, pp. 75-82.

Grifoni, D., Carreras, G. Sabatini, F. & Zipoli, G. 2006, 'UV hazard on Italian Apennines under different shading and ground cover conditions during peak tourist seasons of the year', *International Journal of Environmental Health Research*, vol. 16, no. 6, pp. 427-437.

Harris, R.B. & Alberts, D.S. 2004, 'Strategies for skin cancer prevention,' *International Journal of Dermatology*, vol. 43, pp. 243-251.

Harrison, G.I. & Young, A.R. 2002, 'Ultraviolet radiation-induced erythema in human skin,' *Methods*, vol. 28, no.1, pp. 14-19.

Hayes, C.E., Cantorna, M.T. & DeLuca, H.F., 1997, 'Vitamin D and multiple sclerosis,' *Proceedings of the Society for Experimental Biology and Medicine*, vol. 216, pp. 21-27.

Heisler, G.M & Grant, R.H. 2000, *Ultraviolet Radiation, Human Health, and the Urban Forest*, General Technical Report NE-268, United States Department of Agriculture Forest Service.

Heisler, G.M., Grant, R.H. & Gao, W. 2003, 'Individual- and scattered-tree influences on ultraviolet irradiance,' *Agricultural and Forest Meteorology*, vol. 120, pp. 113-126.

Herlihy, E., Gies, P.H., Roy, C.R. & Jones, M. 1994, 'Personal dosimetry of solar UV radiation for different outdoor activities', *Photochemistry and Photobiology*, vol. 60, no. 3 pp. 288-294.

Hess, M. & Koepke, P. 2008, ‘Modelling UV irradiances on arbitrarily orientated surfaces: effects of sky obstructions’, *Atmospheric Chemistry and Physics Discussions*, vol. 8, pp. 3357-3381.

Hill, D., White, V., Marks, R. & Borland, R. 1993, ‘Changes in sun-related attitudes and behaviours and reduced sunburn prevalence in a population at high risk of melanoma,’ *European Journal of Cancer Prevention*, vol. 2, pp. 447-456.

Hoeppe, P., Oppenrieder, A., Erianto, C., Koepke, P., Reuder, J., Seefeldner, M. & Nowak, D. 2004, ‘Visualization of UV exposure of the human body based on data from a scanning UV-measuring system,’ *International Journal of Biometeorology*, vol. 49, pp. 18-25.

Hofmann, J.S. 1987, ‘Assessing the risks of trace gases that can modify the stratosphere: Vol. 1 Executive Summary’, *EPA/400/1-87/001A*, Environmental Protection Agency, Washington.

Holick, M.F. 1997, ‘Photobiology of Vitamin D’, in *Vitamin D*, eds D. Feldman, F. H. Glorieux & J.W. Pike, pp. 33-39, Academic Press.

Holick, M.F. 2003, ‘Evolution and function of vitamin D,’ *Recent Results in Cancer Research*, vol. 164, pp. 3-28.

Holick, M.F. 2004, ‘Vitamin D: importance in the prevention of cancers, type 1 diabetes, heart disease, and osteoporosis,’ *The American Journal of Clinical Nutrition*, vol. 79, no. 3, pp. 362-371.

Holman, C.D.J., Gibson, I.M., Stephenson, M. & Armstrong, B.K. 1983, ‘Ultraviolet irradiation of human body sites in relation to occupation and outdoor activity: field studies using personal UVR dosimeters’, *Clinical and Experimental Dermatology*, vol. 8, no.3, pp. 269-277.

Huffman, R.E. 1992, *Atmospheric Ultraviolet Remote Sensing*, Academic Press, San Diego.

Hunter, D.J., Colditz, G.A. Stampfer, M.J., Rosner, B., Willet, W.C. & Speizer, F.E. 1990, ‘Risk factors for basal cell carcinoma in a prospective cohort of women,’ *Annals of Epidemiology*, vol. 1, pp. 13-23.

Hussein, M.R. 2005, ‘Ultraviolet radiation and skin cancer: molecular mechanisms,’ *Journal of Cutaneous Pathology*, vol. 32, pp. 191-205.

Hypponen, E., Laara, E., Reunanen, A., Jarvelin, M.R. & Virtanen, S.M. 2001, ‘Intake of vitamin D and risk of type 1 diabetes: a birth-cohort study,’ *Lancet*, vol. 358, pp. 1500-1503.

ICNIRP (International Commission on Non-Ionizing Radiation Protection), 1999, ‘Guidelines of limits of exposure to ultraviolet radiation of wavelengths between 180nm and 400nm (Incoherent Optical Radiation)’, in *Guidelines on Limiting Exposure to Non-Ionizing Radiation*, eds. R. Matthes, J.H. Bernhardt and A.F. McKinlay, pp. 207-226, Markl-Druck, Munich.

IRPA (International Radiation Protection Association), 1989, ‘Proposed change to the IRPA 1985 guidelines on limits of exposure to ultraviolet radiation,’ *Health Physics*, vol. 56, pp. 971-972.

Isaksen, I.S.A. & Stordal, F. 1986, ‘Ozone perturbations by enhanced levels of CFCs, N_2O, and CH_4: A two-dimensional diabatic circulation study including uncertainty estimates,’ *Journal of Geophysical Research*, vol. 91, no. D4, pp. 5249-5263.

Jokela, K., Leszczynski, K. & Visuri R. 1993, ‘Effects of Arctic ozone depletion and snow on UV exposure in Finland,’ *Photochemistry and Photobiology*, vol. 58, no. 4, pp. 559-566.

Josefsson, W. 1986, ‘Solar ultraviolet radiation in Sweden’, Reports: Meteorology and Climatology, 53, 71, Swedish Meteorological and Hydrological Institute, Norrkoping.

Katsambas, A. & Nicolaidou, E. 1996, ‘Cutaneous malignant melanoma and sun exposure. Recent developments and epidemiology,’ *Archives of Dermatology*, vol. 132, pp. 444-450.

Kerr, J.B. & McElroy, C.T. 1993, ‘Evidence for large upward trends of ultraviolet-B radiation linked to ozone depletion,’ *Science*, vol. 262, pp. 1032-1034.

Kimlin, M.G., Parisi, A.V. & Wong, J.C.F. 1998, ‘The facial distribution of erythemal ultraviolet exposure in south-east Queensland,’ *Physics in Medicine and Biology*, vol. 43. pp. 231-240.

Kimlin, M. G. & Parisi, A. V. 1999, ‘Ultraviolet protective capabilities of hats under two different atmospheric conditions,’ *Second Internet Conference on Photochemistry and Photobiology*, July 16 - September 7 1999. Available at: http://www.photobiology.com/photobiology99/contrib/kimlin/index.htm. Accessed on 20 April 2007.

Kimlin, M.G. & Parisi, A.V. 2001, ‘Usage of real-time ultraviolet data to modify the daily erythemal exposure of primary schoolchildren,’ *Photodermatology, Photimmunology and Photomedicine*, vol. 17, pp. 130-135.

Kimlin, M.G., Downs, N.J. & Parisi, A.V. 2003a, ‘Comparison of human facial UV exposure at high and low latitudes and the potential impact on dermal vitamin D production,’ *Photochemical and Photobiological Sciences*, vol. 2, no. 4, pp. 370-375.

Kimlin, M.G., Parisi, A.V. & Downs, N.J. 2003b, 'Human UVA exposures estimated from ambient UVA measurements,' *Photochemical and Photobiological Sciences*, vol. 2, no. 4, pp. 365-369.

Kimlin, M.G., Olds, W.J. & Moore, M.R. 2006, 'Location and vitamin D synthesis: Is the hypothesis validated by geophysical data?,' *Journal of Photochemistry and Photobiology B: Biology*, vol. 86, no. 3, pp. 234-239.

Koh, H.K., Kligler, B.E. & Lew, R.A. 1990, 'Sunlight and cutaneous malignant melanoma: evidence for and against causation,' *Photochemistry and Photobiology*, vol. 51, pp. 765-79.

Kollias, N., Sayre, R.M., Zeise, L. & Chedekel, M.R. 1991, 'Photoprotection by Melanin,' *Journal of Photochemistry and Photobiology B: Biology*, vol. 9, no. 2, pp. 135-60.

Konishi, E. & Yoshizawa, Y. 1985, 'Estimation of depth of basal cell layer of skin for radiation protection,' *Radiation Protection Dosimetry*, vol. 11, no.1, pp. 29-33.

Kraemer, K.H., Lee, M.M., Andrews, A.D. & Lambert, W.C. 1994, 'The role of sunlight and DNA repair in melanoma and non melanoma skin cancer. The xeroderma pigmentosum paradigm,' *Archives of Dermatology*, vol. 130, no. 8, pp. 1018-1021.

Kricker, A., English, D.R., Randell, P.L., Heenan, P.J., Clay, C.D., Delaney, T.A. and Armstrong, B.A. 1990, 'Skin cancer in Geraldton, Western Australia: a survey of incidence and prevalence,' *Medical Journal of Australia*, vol. 152, no. 8, pp. 399-407.

Kricker, A., Armstrong, B.K. & English, D.R. 1994, 'Sun exposure and non-melanocytic skin cancer,' *Cancer Causes and Control*, vol. 5, no. 4, pp. 367-392.

Kricker, A., Armstrong, B.K., English, D.R. & Heenan, P.J. 1995, 'Does intermittent sun exposure cause basal cell carcinoma? A case control study in Western Australia', *International Journal of Cancer*, vol. 60, no. 4, pp. 489-494.

Lester, R.A. & Parisi, A.V. 2002, 'Spectral ultraviolet albedo of roofing surfaces and human facial exposure', *International Journal of Environmental Health Research*, vol. 12, pp. 75-81.

Levi, F. La Vecchia, C. Te, V.C. & Mezzanotte, G. 1988, 'Descriptive epidemiology of skin cancer in the Swiss Canton of Vaud,' *International Journal of Cancer,* vol. 42, pp. 811-816.

Leyden, J.J. 1990, 'Clinical Features of ageing skin,' *British Journal of Dermatology*, vol. 122, (Suppl. 35), pp. 1-3.

Lock-Anderson, J., Wulf, H.C. & Knudstorp, N.D. 1998, 'Interdependence of eye and hair colour, skin type and skin pigmentation in Caucasian population,' *Acta Dermato-Venereologica*, vol. 78, pp. 214-219.

Loggie, B.W. & Eddy, J.A. 1988, 'Solar considerations in the development of cutaneous melanoma,' *Seminars in Oncology*, vol. 15, pp. 494-499.

Longstreth, J., de Gruijl, F.R., Kripke, M.L., Abseck, S., Arnold, F., Slaper, H.I., Velders, G., Takizawa, Y. & van der Leun, J.C. 1998, 'Health Risks,' *Journal of Photochemistry and Photobiology B: Biology*, vol. 46, pp. 20-39.

Lowe, J.B., Balanda, K.P., Gillespie, A.M., Del Mar, C.B. & Gentle, A.F. 1993, 'Sun-related attitudes and beliefs among Queensland school children: the role of gender and age,' *Australian Journal of Public Health*, vol. 17, no. 3, pp. 202-208.

Lowe, J.B., Borland, R., Stanton, W.R., Baade, P., White, V. & Balanda, K.P. 2000, 'Sun-safe behaviour among secondary school students in Australia,' *Health Education Research: Theory and Practice*, vol. 15, no. 3, pp. 271-281.

MacKie, R.M., Freudenberger, T. & Aitchison, T.C. 1989, 'Personal risk-factor chart for cutaneous melanoma,' *Lancet*, vol. 2, pp. 487-490.

MacLaughlin, J.A., & Holick, M.F. 1985, 'Ageing decreases the capacity of human skin to produce vitamin D_3,' *Journal of Clinical Investigation*, vol. 76, pp. 1536-1538.

Madronich, S. 1993, 'UV radiation in the natural and perturbed atmosphere', in *UVB Radiation and Ozone Depletion: effects on humans, animals, plants, microorganisms and materials*, ed. M. Tevini, Lewis Publishers, Boca Raton.

Madronich, S., McKenzie, R.L., Björn, L.O. & Caldwell, M.M. 1998, 'Changes in biologically active ultraviolet reaching the earth's surface', *Journal of Photochemistry and Photobiology B: Biology*, vol. 46, pp. 5-19.

Malone, K. & Tranter, P. 2003, 'Children's environmental learning and the use, design and management of schoolgrounds,' *Children, Youth and Environments*, vol. 13, no. 2, Available at: http://www.colorado.edu/journals/cye/13_2/Malone_Tranter/ChildrensEnvLearning.htm, Accessed on 21 July 2008.

Marks, R., Rennie, G. & Selwood, T. 1988, 'The relationship of basal cell carcinomas and squamous cell carcinomas to solar keratoses,' *Archives of Dermatology*, vol. 124, no. 7, pp. 1039-1042.

Matsuoka, L.Y., Wortsman, J., Hanifan, N. & Holick, M.F. 1988, 'Chronic sunscreen use decreases circulating concentration of 25-hydro vitamin D: A preliminary study,' *Archives of Dermatology*, vol. 124, pp. 1802-1804.

Matsuoka, L.Y., Wortsman, J., Dannenberg, M.J., Hollis, B.W., Lu, Z. & Holick, M.F. 1992, 'Clothing prevents ultraviolet-B radiation-dependent photosysthesis of vitamin D3,' *Journal of Clinical Endocrinol Metabolism*, vol. 75, pp. 1099-1103.

Mech, M. & Koepke, P. 2004, ‘Model for UV irradiance on arbitiarly orientated surfaces,’ *Theoretical and Applied Climatology*, vol. 77, pp. 151-158.

Meyer-Arendt, J.R. 1995, *Introduction to Classical and Modern Optics*, Prentice-Hall, New Jersey.

McCarthy, W.H. 2004, ‘The Australian experience in sun protection and screening for melanoma,’ *Journal of Surgical Oncology*, vol. 86, pp. 236-245.

McGrath, J.J. 2001, ‘Does ‘imprinting’ with low prenatal vitamin D contribute to the risk of various adult disorders?,’ *Medical Hypotheses*, vol. 56, pp. 367-371.

McKenzie, R.L. 1991, ‘Application of a simple model to calculate latitudinal and hemispheric differences in ultraviolet radiation,’ *Weather and Climate*, vol. 11, pp. 3-14.

McKenzie, R.L. Kotkamp, M. & Ireland, W. 1996, ‘Upwelling UV spectral irradiances and surface albedo measurements at Lauder, New Zealand,’ *Geophysical Research Letters*, vol. 23, pp. 1757-1760.

McKenzie, R.L., Aucamp, P.J., Bais, A.F., Björn, L.O. and Ilyas, M. 2007, ‘Changes in biologically-active ultraviolet radiation reaching the earth’s surface,’ *Photochemical and Photobiological Sciences*, vol. 6, pp. 218-231.

Mech, M. & Koepke, P. 2004, ‘Model for UV irradiance for arbitrarily orientated surfaces,’ *Theoretical and Applied Climatology*, vol. 77. nos. 3-4, pp. 151-158.

Meulmeester, J.F., van den Berg, H., Wedel, M., Boshuis, P.G., Hulshof, K.F.A.M. & Luyken, R. 1990, ‘Vitamin D status, parathyroid hormone and sunlight in Turkish, Moroccan and Caucasian children in the Netherlands,’ *European Journal of Clinical Nutrition*, vol. 44, pp. 461-470.

Michalsky, J. J. 1988 ‘The astronomical almanac's algorithm for approximate solar position (1950-2050),’ *Solar Energy*, vol. 40, pp. 227-235.

Milne, E., Corti, B., English, D.R., Cross, D., Costa, C. & Johnston, R. 1999a, ‘The use of observational methods for monitoring sun-protection activities in schools,’ *Health Education Research: Theory & Practice*, vol. 14, no.2, pp. 167-175.

Milne, E., English, D.R., Corti, B., Cross, D., Borland, R., Gies, H.P., Costa, C. & Johnston, R. 1999b, ‘Direct measurement of sun protection activities in schools,’ *Journal of Preventive Medicine*, vol. 29, pp. 45-52.

Montague, M., Borland, R. & Sinclair, C. 2001, ‘Slip! Slop! Slap! and SunSmart, 1980-2000: skin cancer control and 20 years of population-based campaigning,’ *Health Education and Behavior*, vol. 28. no. 3, pp. 209-305.

NASA (National Aeronautics and Space Administration) 1988, ‘Present state of the knowledge of the Upper Atmosphere 1988: An assessment report, NASA Reference publication 1208’, eds R.T. Watson and the ozone trends panel, M.J. Prather and ad hoc theory panel, M.J. Kurylo and the NASA panel for data evaluation, NASA Office of Space Science and Applications, Washington.

NHMRC (National Health and Medical Research Council), 1989, *Occupational Standard for Exposure to Ultraviolet Radiation*, Radiation Health Series no. 29, Canberra: Australian Government.

NHMRC (National Health and Medical Research Council), 1996, *Primary Prevention of Skin Cancer in Australia*, Report of the Sun Protection Programs Working Party, Publication No. 2120, Australian Government Publishing Service.

NRPB (National Radiological Protection Board), 1995, *Statement on effects of Ultraviolet Radiation on Human Health and Health Effects from Ultraviolet Radiation*, vol. 6, pp. 115-142.

Nguyen, T.D., Siskind, V., Green, L., Frost, C. & Green. A. 1997, ‘Ultraviolet radiation, melanocytic naevi and their dose-response relationship,’ *British Journal of Dermatology*, vol. 137, pp. 91-95.

Olson, R.L., Sayre, R.M. & Everett, M.A. 1966, ‘Effect of anatomic location and time on ultraviolet erythema,’ *Archives of Dermatology*, vol. 93, pp. 211-215.

Orphal, J. & Chance, K. 2003, ‘Ultraviolet and visible absorption cross-sections for HITRAN’, *Journal of Quantitative Spectroscopy and Radiative Transfer*, vol. 82, pp. 491-504.

Paltridge G.W. & Barton I.J. 1978, ‘Erythemal ultraviolet radiation distribution over Australia - the calculations, detailed results and input data including frequency analysis of observed Australian cloud cover,’ *Commonwealth Scientific and Industrial Research Organisation - Division of Atmospheric Physics Technical Paper*, no. 33, pp. 1-48. Australia.

Parisi, A.V. & Kimlin, M.G. 1997a, ‘Ozone and ultraviolet radiation,’ *Australasian Science*, vol. 18, no. 1, pp. 44-46.

Parisi, A.V. & Kimlin, M.G. 1997b, ‘Why do UV levels vary?,’ *Australasian Science*, vol. 18, no. 2, pp. 39-41.

Parisi, A.V., Meldrum, L.R. & Kimlin, M.G. 1998, ‘Polysulphone film thickness and its effects in ultraviolet radiation dosimetery,’ *Internet Photochemistry and Photobiology Conference*, Jan 18 - Feb 5, 1999, Available: http://www.photobiology.com/UVR98/parisi/_ [Accessed 16 January 2007].

Parisi, A.V. & Kimlin, M.G. 1999, ‘Comparison of the spectral biologically effective solar ultraviolet in adjacent tree shade and sun,’ *Physics in Medicine and Biology*, vol. 44, pp. 2071-2080.

Parisi, A.V., Kimlin, M.G., Mulheran, L., Meldrum, L.R. & Randall, C., 2000, ‘Field-based measurements of personal erythemal ultraviolet exposure through a common summer garment,’ *Photodermatology, Photoimmunology and Photomedicine*, vol. 16, no. 3, pp. 134-138.

Parisi, A.V., Kimlin, M.G., Wong, J.C.F. & Wilson, M. 2001, ‘Solar ultraviolet exposures at ground level in tree shade during summer in south east Queensland,’ *International Journal of Environmental Health Research*, vol. 11, pp. 117-127.

Parisi, A.V., Sabburg, J, Kimlin , M.G. & Downs, N. 2003, ‘Measured and modelled contributions to UV by the albedo of surfaces in an urban environment,’ *Theoretical and Applied Climatology*, vol. 76, nos. 3-4, pp. 181-188.

Parisi, A. V. & Downs, N. 2004, ‘Cloud cover and horizontal plane eye damaging solar UV exposures,’ *International Journal of Biometeorology*, vol. 49, pp. 130-136.

Parisi, A.V., Sabburg, J. & Kimlin, M.G. 2004, *Scattered and Filtered Solar UV Measurements*, Kluwer Academic Publishers, Dordrecht.

Parrish, J.A., Jaenicke, K.F. & Anderson, R.R. 1982, ‘Erythema and melanogenesis action spectra of normal human skin,’ *Photochemistry and Photobiology*, vol. 36, pp. 187-191.

Pearl, D.K. & Scott, E.L. 1986, ‘The anatomical distribution of skin cancers,’ *International Journal of Epidemiology*, vol. 15, no. 4, pp. 502-506.

Preece, M.A., Tomlinson, S., Ribot, C.A., Pietrek, J, Korn, H.T., Davies, D.M., Ford, J.A., Dunnigan, M.G. & O'Riordan, J.L.H. 1975, ‘Studies of vitamin D deficiency in man,’ *Quarterly Journal of Medicine*, vol. 44, pp. 575-589.

Raasch, B., Maclennan, R., Wronski, I. & Robertson, I. 1998, ‘Body site specific incidence of basal and squamous cell carcinoma in an exposed population, Townsville, Australia,’ *Mutation Research - Fundamental and Molecular Mechanisms of Mutagenesis*, vol. 422, pp.101-106.

Randel, W.J., Stolarski, R.S., Cunnold, D.M., Logan, J.A. & Zawodny, J.M. 1999, ‘Trends in the vertical distribution of ozone,’ *Science*, vol. 285, no. 5434, pp. 1689-1692.

Rigel, D.S., Kopf, A.W. & Friedman, R.J. 1987, ‘The rate of malignant melanoma in the United States: are we making an impact?,’ *Journal of American Academic Dermatology*, vol. 17, pp. 1050-1052.

Roberts, D.L. 1990, 'Incidence of non-melanoma skin cancer in West Glamorgan, South Wales,' *British Journal of Dermatology*, vol. 122, pp. 399-403.

Rosso, S., Zanetti, R., Pippione, M. & Sancho-Garnier, H. 1998, 'Parallel risk assessment of melanoma and basal cell carcinoma: skin characteristics and sun exposure,' *Melanoma Research*, vol. 8, no. 6, pp. 573-583.

Rottman, G. 2000, 'Variations of solar ultraviolet irradiance observed by the UARS solstice – 1991-1999,' *Space Science Reviews*, vol. 94, pp. 83-91.

Roy, C.R., Gies, H.P. & Toomey, S. 1995, 'The solar UV radiation environment: measurement techniques and results,' *Journal of Photochemistry and Photobiology B: Biology*, vol. 31, no. 1, pp. 21-27.

Rundel, R.D. 1986, 'Computation of spectral distribution and intensity of solar UVB radiation', in *Stratospheric Ozone Reduction, Solar Ultraviolet Radiation and Plant Life*, eds R.C. Worrest & M.M. Caldwell, Springer-Verlag, Berlin.

Sabburg, J.M., Parisi, A.V. & Kimlin, M.G. 2003, 'Enhanced spectral UV irradiance: a 1 year preliminary study,' *Atmospheric Research*, vol. 66, no. 4, pp. 261-272.

Schauberger, G. 1990, 'Model for the global irradiance of the solar biologically-effective ultraviolet-radiation on inclined surfaces,' *Photochemistry and Photobiology*, vol. 52, no. 5, pp. 1029-1032.

Schindell, D., Rind, D., Balachandran, N., Lean, J. & Lonergan, P. 1999, 'Solar cycle variability, ozone, and climate,' *Science*, vol. 284, no. 5412, pp. 305-308.

Schippnick, P.F. & Green, A.E.S. 1982, 'Analytical characterization of spectral actinic flux and spectral irradiance in the middle ultraviolet,' *Photochemistry and Photobiology*, vol. 35, pp. 89-101.

Schothorst, A. Slaper, H., Schouten, R. & Suurmond, D. 1985, 'UVB doses in maintenance psoriasis phototherapy versus solar UVB exposure,' *Photodermatology*, vol. 2, pp. 213-220.

Scotto, J., Fears, T.R. & Fraumeni, J.F. 1983, 'Incidence of non-melanoma skin cancer in the United States,' Bethesda MD, US Department of Health and Human Sciences, NIH Publication, no. 83-2433.

Scrivener, Y, Grosshans, E. & Cribier, B. 2002, 'Variation of basal cell carcinomas according to gender, age, location and histopathological subtype,' *British Journal of Dermatology*, vol. 147, pp. 41-47.

Setlow, R.B., Grist, E., Thompson, K. & Woodhead, A.P. 1993, 'Wavelengths effective in induction of malignant melanoma,' *Proceedings of the National Academy of Sciences*, vol. 90, pp. 6666-6670.

Siani, A.M., Casale, G.R., Diémoz, H., Kimlin, M.G., Lang, C.A. & Colosimo, A. 2008, 'Personal UV exposure in high albedo alpine sites,' *Atmospheric Chemistry and Physics*, vol. 8, pp. 3749-3760.

Siani, A.M., Casale, G.R., Sisto, R., Borra, M., Kimlin, M.G., Lang, C.A. & Colosimo, A. 2009, 'Short-term UV Exposure of Sunbathers at a Mediterranean Sea Site,' *Photochemistry and Photobiology*, vol. 85, no. 1, pp. 171-177.

Sober, A.J. 1987, 'Solar exposure in the etiology of cutaneous melanoma,' *Photodermatology*, vol. 4, pp. 23-31.

Staples, M., Marks, R. & Giles, G. 1999, 'Trends in the incidence of non-melanocytic skin cancer (NMSC) treated in Australia 1985-1995: Are primary prevention programs starting to have an effect?' *International Journal of Cancer*, vol. 78, no.2, pp.144-148.

Sterenborg, H.J.C.M. & van der Leun, J.C. 1987, 'Action spectra for tumorigenesis by ultraviolet radiation', in *Human Exposure to Ultraviolet Radiation: Risks and Regulations,* eds W.F. Passchier & B.F.M. Bosnjakovic, pp. 173-190, Elsevier, Amsterdam.

Streicher, J.J., Culverhouse, W.C., Dulberg, M.S. & Fornaro, R.J. 2004, 'Modeling the anatomical distribution of sunlight,' *Photochemistry and Photobiology*, vol. 79, no. 1, pp. 40-47.

Sze, N.D., Ko, M.K.W., Weisenstein, D.K., Rodriguez, J.M., Stolarski, R.S. & Schoeberl, M.R. 1989, 'Antarctic ozone hole: possible implications for ozone trends in the Southern Hemisphere,' *Journal of Geophysics Research*, vol. 94, no. D9, pp. 11521-11528.

Taylor, J.S. 1995, 'DNA, sunlight and skin cancer,' *Pure and Applied Chemistry*, vol. 67, no. 1, pp. 183-90.

TOMS, 2008, Total Ozone Mapping Spectrometer: Ozone Processing Team – NASA/GSFC Code 613.3, National Aeronautics and Space Administration, Available at: http://jwocky.gsfc.nasa.gov/teacher/ozone_overhead_v8.html, Accessed on 27 March 2008.

Toomey, S.J., Gies, H.P. & Roy, C.R. 1995, 'UVR protection offered by shadecloths and polycarbonates,' *Radiation Protection in Australia*, vol. 13, no.2, pp. 50-54.

Turnbull, D.J. & Parisi, A.V. 2006, 'Effective shade structures,' *Medical Journal of Australia*, vol. 184, pp. 13-15.

Turnbull, D., Parisi, A. & Downs, N. 2006, 'Effect of Clouds on the diffuse component of the solar terrestrial erythemal UV,' *Radiation Protection in Australasia*, vol. 23, pp. 2-9.

Turner, J., Parisi, A. & Turnbull, D.J. 2008, 'Reflected solar radiation from horizontal, vertical and inclined surfaces: ultraviolet and visible spectral and broadband behaviour due to solar zenith angle, orientation and surface type,' *Journal of Photochemisty and Photobiology B: Biology,* vol. 92, no. 1, pp. 29-37.

Urbach, F., Epstein, J.H. & Forbes, P.D. 1974, 'Ultraviolet carcinogenesis: experimental, global and genetic aspects', in *Sunlight and Man: Normal and Abnormal Photobiological Responses*, eds M.A. Pathak, L.C. Harber, M. Seiji & A. Kukita, pp. 259-283, University of Tokyo Press, Tokyo.

Urbach, F. 1982, 'Photocarcinogenesis', in *The Science of Photomedicine*, eds J.D. Regan & J.A. Parrish, pp. 261-92, Plenum, New York.

Urbach, F. 1993, 'Environmental risk factors for skin cancer', in *Skin Carcinogenesis in Man and in Experimental Models,* eds. E. Hecker, J.F. Marks, W. Tilgen, Springer-Verlag.

Urbach, F. 1997, 'Ultraviolet radiation and skin cancer of humans,' *Journal of Photochemistry and Photobiology B: biology*, vol. 40. no. 1, pp. 3-7.

Van Heuklon, T.K. 1979, 'Estimating atmospheric ozone for solar radiation models', *Solar Energy*, vol. 22, pp. 63-68.

Vishvakarman, D., Wong, J.C.F. and Boreham, B.W. 2001, 'Annual occupational exposure to ultraviolet radiation in central Queensland,' *Health Physics,* vol. 81, pp. 536-544.

Vishvakarman, D. & Wong, J.C.F. 2003, 'Description of the use of a risk estimation model to assess the increased risk of non-melanoma skin cancer among outdoor workers in Central Queensland, Australia,' *Photodermatology Photoimmunology and Photomedicine*, vol. 19, pp. 81-88.

Walter, S.D., King, W.D., Marrett, I.D. 1999, 'Association of cutaneous malignant melanoma with intermittent exposure to ultraviolet radiation: results of a case control study in Ontario, Canada,' *International Journal of Epidemiology*, vol. 28, pp. 418-427.

Webb, A.R., Kline, L. & Holick, M.F. 1988, 'Influence of season and latitude on the cutaneous synthesis of vitamin D_3: Exposure to winter sunlight in Boston and Edmonton will not promote vitamin D_3 synthesis in human skin,' *Journal of Clinical Endocrinol Metabolism*, vol. 67, pp. 373-378.

Webb, A.R. and Holick, M.F. 1988, 'The role of sunlight in the cutaneous production of vitamin D_3,' *Annual Reviews in Nutrition*, vol. 8, pp. 375-399.

Webb, A.R., Weihs, P. & Blumthaler, M. 1999, 'Spectral UV irradiance on vertical surfaces: a case study,' *Photochemistry and Photobiology*, vol. 69, no. 4, pp. 464-470.

Wei, Q, Lee, J.E., Gershenwald, J.E., Ross, M.I., Mansfield, P.F, Strom., S.S., Wang, L., Guo, Z., Qiao, Y., Amos, C.I., Spitz, M.R. & Duvic, M. 2003, ‘Repair of UV-light induced DNA damage and risk of cutaneous malignant melanoma,’ *Journal of the National Cancer Institute,* vol. 96, no. 4, pp. 308-315.

Weinstock, M.A. 1996, ‘Controversies in the role of sunlight in the pathogenesis of cutaneous melanoma,’ *Photochemistry and Photobiology,* vol. 63, pp. 406-410.

Whiteman, D.C., Parsons, P.G. & Green, A.C., 1998, ‘p53 expression and risk factors for cutaneous melanoma: a case-control study,’ *International Journal of Cancer,* vol. 77, no. 6, pp. 843-848.

Whitaker, C.J., Lee, W.R. and Downes, J.E. 1979, ‘Squamous cell skin cancer in the north-west of England, 1967-69, and its relation to occupation,’ *British Journal of Industrial Medicine*, vol. 36, no. 1, pp. 43-51.

WHO (World Health Organization) 1994, *Ultraviolet radiation*, Published under the joint sponsorship of the United Nations Environment Programme, the International Commission on Non-Ionization Radiation Protection and the World Health Organization, Geneva, Switzerland.

WHO (World Health Organization) 2006, *Environmental Burden of Disease Series,* No.13, eds A. Prüss-Üstün, H. Zeeb, C. Mathers, M. Repacholi, pp. 1-250, Geneva, Switzerland,.

Wlaschek, W.M.M., Tantcheva-Poór, I., Schneider, L.A., Naderi, L., Razi-Wolf, Z., Schüller, J., Scharffetter-Kochanek, K. 2008, ‘Chronological and photoageing of the fibroblasts and dermal connective tissue,’ *Clinical and Experimental Dermatology,* vol. 26, no. 7, pp. 592-599.

WMO (World Meteorological Organization) 1994, *Scientific Assessment of Ozone Depletion*, Global Ozone Research and Monitoring Project, Report No. 37, World Meteorological Organization, Geneva, Switzerland.

WMO (World Meteorological Organization) 2007, *Scientific Assessment of Ozone Depletion: 2006*, Report No. 50, Surface Ultraviolet Radiation: Past, Present and Future, Chapter 7, pp. 7.1-7.54, World Meteorological Organization, Geneva, Switzerland.

Wong, J.C.F., Toomey, S., Fleming, R.A. & Thomas, B.W. 1995, ‘UV-B radiometry and dosimetry for solar measurements,’ *Health Physics,* vol. 68, no. 2, pp. 175-184.

Wong, J.C.F., Airey, D.K. & Fleming, R.A. 1996, ‘Annual reduction of solar UV exposure to the facial area of outdoor workers in Southeast Queensland by wearing a hat,’ *Photodermatology Photoimmunology and Photomedicine*, vol. 12, pp. 131-135.

APPENDICES

Appendix A. Manufacturing polysulphone film dosimeters

The polysulphone film used in the manufacture of miniaturised dosimeters for this research was cast at the University of Southern Queensland. The casting and manufacture of polysulphone dosimeters involves:

1. Dissolving polysulphone pellets into a chloroform solvent;
2. Casting the polysulphone film solution onto a purpose built glass casting table;
3. Removing dry polysulphone sheets and inspecting for defects;
4. Cutting and adhering polysulphone film sections to dosimeter frames.

A.1 Mixing the polysulphone film solution

Polysuphone pellets are mixed into chloroform solution. A solution of 25 mL is used to cast the polysulphone film to approximately the size of an A4 sheet. The mixing process is performed in a fume cupboard and gloves are used to minimise the likelihood of the solution coming into contact with the skin. The polysulphone pellets are shaken in sealed glass containers and left to dissolve over a 24 hour period.

A.2 Casting the polysulphone film solution

The casting table used in the manufacture of polysulphone film consists of a glass base onto which the film solution is poured. The film is cast to an approximate thickness of 40 μm. To achieve uniform film thickness, an automated blade sweeps over the poured solution at a constant rate determined by a stepper motor drive. The dried film sheet is removed from the table using gloves to prevent grease and finger prints affecting the newly cast film.

A.3 Film inspection and storage

When the polysulphone film is lifted from the casting table, it is immediately dried by placing between paper towels. The film sheet is inspected for defects under a UV free light source and adhered to backing paper for storage to prevent curling. Defects that are often present in the manufactured film include:

- *thickness variation* which can result from uneven pouring of the initial solution onto the table and variations caused by blade movement over the solution;
- *Rippling and scratches* that occur from the uneven movement of the blade across the film solution and scratches that are present in the underlying glass base;
- *Dust and foreign* matter typically noticed upon inspection and observed as raised or non transparent specks in the cast film;
- *Watermarks* that are typically observed due to the presence of excess water droplets that have remained on the table during the casting process;
- *Variation in film opacity* due to the presence of cleaning agents that have not been completely removed before the film has been cast.

Defects in the cast film can result in sheets being discarded entirely before dosimeter manufacture, but more typically are regions of the sheet mostly located near the edges that are avoided when the film is cut for dosimeter manufacture. Polysulphone sheets are attached to clean backing paper with adhesive tape. The cast polysulphone sheets and backing paper are then stored in light proof envelopes prior to dosimeter manufacture.

A.4 Attaching polysulphone film to dosimeter frames

Stored sheets of polysulphone film are cut into strips of approximately 1 cm width. Regions of the cut strips that do not contain defects are then cut into further 1 cm sections. These sections then are attached to flexible card frames to complete the manufacture of the miniaturised dosimeters. The frames to which the polysulphone film sections are attached are made from thin cardboard sections that have a 6 mm diameter hole punched through a section measuring approximately 10 mm by 15 mm. The dosimeters developed for this research differ from those in previous research (Downs & Parisi 2001) which have clear apertures measuring approximately 25 mm by 25 mm and are attached to larger plastic frame holders. A smaller dosimeter was developed for this research due to the high density measurements that were required to measure UV exposure over complex skin surface topography including the face. The smaller lightweight dosimeter was also preferred for use with school children, being more comfortable to wear than the conventional sized dosimeter.

Appendix B. Calibration and uncertainty in polysulphone dosimeters

B.1 Polysulphone dosimeter calibration

Miniaturised polysulphone dosimeters were calibrated on a horizontal plane under clear sky conditions at the University of Southern Queensland's Toowoomba Campus (28^{o}S, 152^{o}E) during later summer, early autumn and late autumn. Dosimeters were calibrated to the USQ's permanently mounted outdoor scanning spectroradiometer (model DTM300, Bentham instruments, Reading UK). This instrument has a stated uncertainty of ±10%, including traceability of the system's calibration lamp. Figures B.1.1, B.1.2 and B.1.3 show the respective summer, early autumn and late autumn calibrations of miniaturised polysulphone dosimeters to the erythemally weighted UV exposure measured by the USQ 's scanning spectroradiometer.

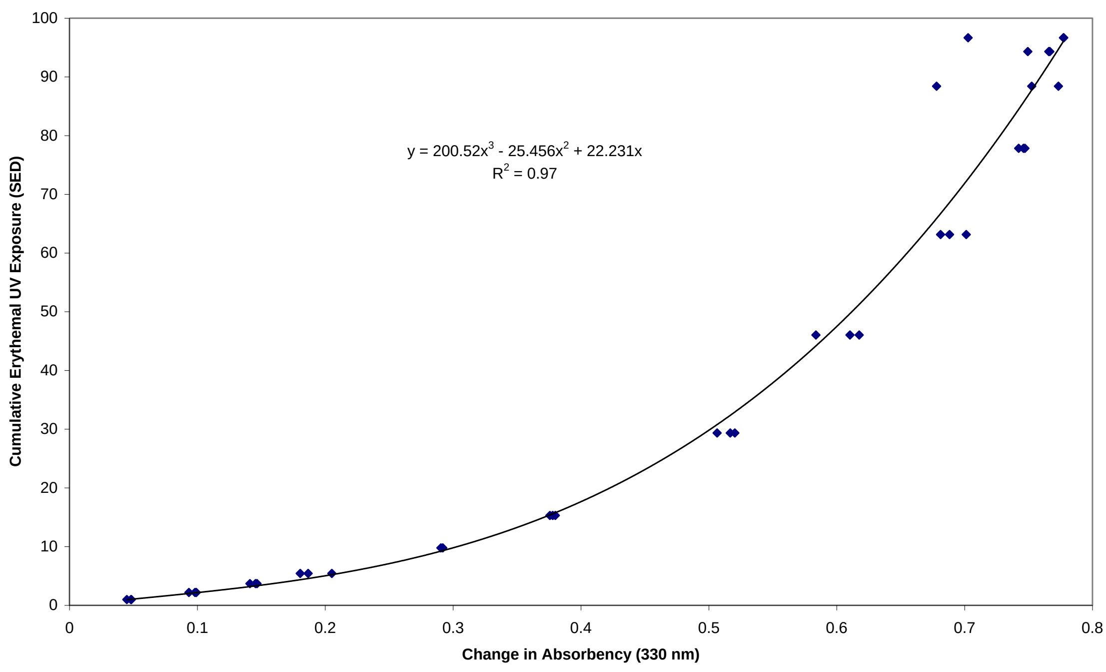

Figure B.1.1: Polysulphone dosimeter calibration for 23 February 2008.

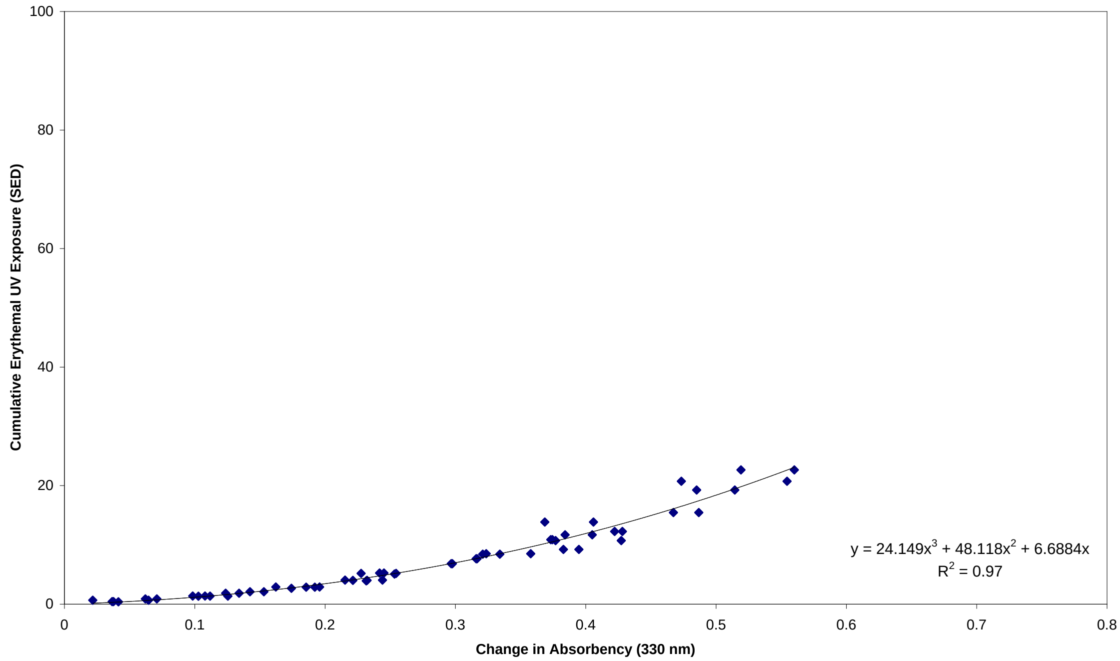

Figure B.1.2: Polysulphone dosimeter calibration for 18 April 2007.

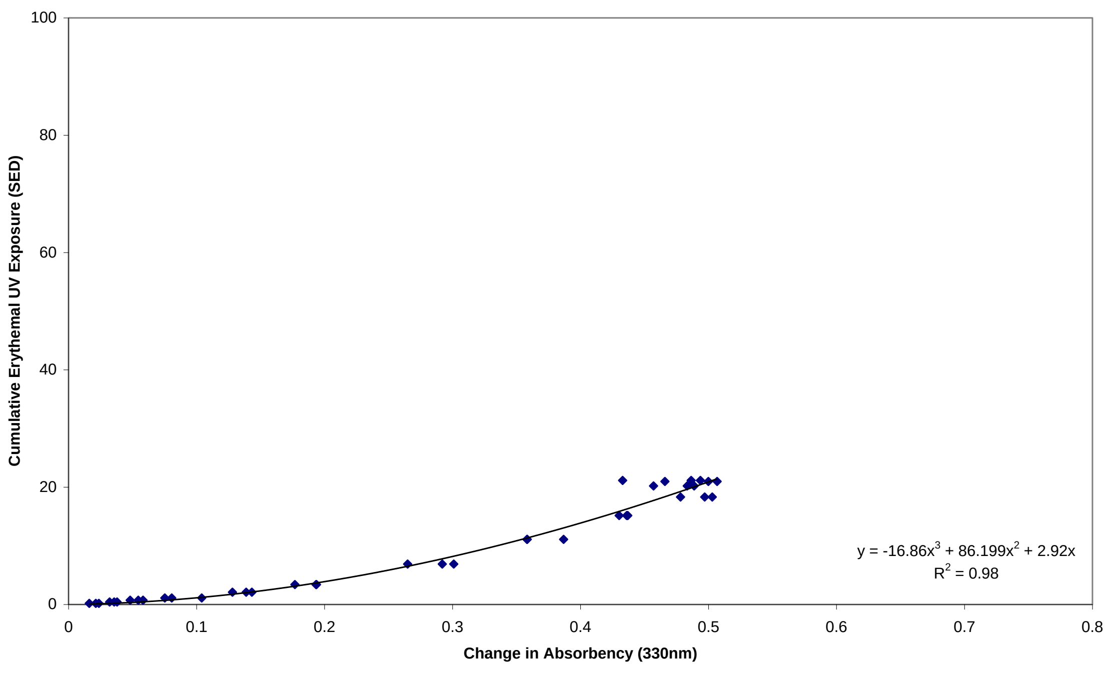

Figure B.1.3: Polysulphone dosimeter calibration for 8 May 2008.

B.2 Measurements of uncertainty in polysulphone dosimeters

The change in absorbance, ΔA measured over 46 sets of polysulphone dosimeters exposed to equivalent levels of solar UV are listed in Table B.2.1. This table was used to determine the error of the miniaturised polysulphone dosimeters used in this research. The calibration plots (Appendix B.1) were also developed from the ΔA measurements listed in Table B.2.1. The mean variation in ΔA determined from Table B.2.1 was compared to the mean ΔA measured on a horizontal plane in each of the SZA ranges 0^o-30^o, 30^o-50^o and 50^o to 80^o (Table B.2.2) to determine the uncertainty in ER in each SZA range. Table B.2.2 lists the horizontal plane ΔA measured for each mannequin headform and body field experiment.

Table B.2.1: Variation in ΔA for sets of miniaturised polysulphone dosimeters exposed to equivalent solar UV exposures. Sets are organized into separate rows in the table.

Calibration 23 February 2008

Change in absorbency at 330 nm			range
0.048	0.045	0.048	0.003
0.098	0.093	0.099	0.006
0.141	0.145	0.147	0.006
0.180	0.205	0.187	0.025
0.290	0.292	0.378	0.087
0.380	0.376		0.004
0.520	0.517	0.506	0.014
0.610	0.618	0.584	0.034
0.688	0.701	0.681	0.020
0.742	0.746	0.747	0.005
0.678	0.773	0.752	0.095
0.767	0.749	0.766	0.017
0.778	0.703	0.777	0.075

Cloud affected calibration 20 February 2008 (not plotted in Appendix B.1)

Change in absorbency at 330 nm			range
0.033	0.034	0.042	0.008
0.086	0.085	0.088	0.003
0.136	0.145	0.134	0.011
0.194	0.168	0.158	0.035
0.254	0.273	0.270	0.019
0.322	0.349	0.330	0.027
0.471	0.446	0.483	0.037

0.521	0.560	0.544					0.038
0.616	0.625	0.624					0.009
0.630	0.652	0.647					0.022

Calibration 18 April 2007

Change in absorbency at 330 nm							Range
0.070	0.082	0.094	0.057	0.098	0.089	0.092	0.045
0.136	0.139	0.128	0.146	0.123	0.127	0.127	0.024
0.206	0.183	0.184	0.189	0.195	0.191	0.182	0.023
0.221	0.215	0.229	0.228	0.229	0.226	0.259	0.045
0.247	0.263	0.252	0.224	0.247	0.281	0.283	0.059
0.296	0.301	0.333	0.332	0.298	0.294	0.311	0.039
0.335	0.378	0.288	0.324	0.308	0.288	0.338	0.090
0.302	0.328	0.368	0.366	0.366	0.358	0.330	0.066
0.393	0.378	0.411	0.381	0.355	0.373		0.057
0.374	0.403	0.341	0.403	0.414	0.342	0.379	0.072

Calibration 8 May 2008

Change in absorbency at 330 nm							Range
0.01618	0.024	0.021					0.008
0.032	0.038	0.036					0.006
0.055	0.058	0.048					0.010
0.104	0.075	0.080					0.029
0.144	0.139	0.128					0.015
0.194	0.193	0.177					0.017
0.292	0.265	0.301					0.036
0.358	0.387	0.358					0.029
0.436	0.437	0.430					0.007
0.478	0.503	0.497					0.025
0.483	0.457	0.489					0.032
0.500	0.466	0.507					0.041
0.494	0.433	0.486					0.061
						mean ΔA	0.032

Table B.2.2: Change in absorbency measured on a horizontal plane in the SZA ranges 0^o-30^o, 30^o-50^o and 50^o to 80^o.

SZA 0^o-30^o

Date	Mannequin Sites	Change in absorbency at 330 nm	Mean change in absorbency at 330 nm
01/02/2008	arm / hand / leg	0.681	
13/12/2007	Arm	0.614	
18/02/2006	Face	0.436	
12/03/2007	Face	0.411	
25/01/2008	face / neck	0.689	
14/11/2007	face / neck	0.558	
21/02/2008	face / neck	0.611	
21/11/2007	Hand	0.584	0.573

SZA 30^o-50^o

Date	Mannequin Sites	Change in absorbency at 330 nm	Mean change in absorbency at 330 nm
02/04/2008	arm / hand	0.477	
30/04/2007	arm	0.347	
16/09/2005	face	0.354	
18/12/2007	face / neck	0.290	
16/10/2007	face	0.266	
05/10/2006	face	0.363	
04/03/2008	leg	0.457	0.365

SZA 50^o-80^o

Date	Mannequin Sites	Change in absorbency at 330 nm	Mean change in absorbency at 330 nm
12/07/2007	arm	0.310	
18/07/2008	arm	0.205	
27/05/2005	face	0.178	
27/08/2007	face / neck	0.179	
16/10/2007	face	0.180	
28/02/2008	hand	0.179	
06/08/2007	leg	0.159	
02/08/2007	leg	0.226	0.202

Appendix C. Colouring body surface wireframes

Specific ER colour levels represented along exposure contours ranging from 0 to 100% are interpolated between measured dosimeter sites. Each interpolation between adjacent measurement sites consists of 5 evenly spaced coloured segments and is represented accordingly:

$$x_i = x_{i-1} + \left(\frac{A-B}{5}\right)$$

where points A and B represent the measured ER at two adjacent sites located at contour mesh intersections on the model wireframe and values x_1 through x_4 are spaced evenly in the adjacent dosimeter site interval (Figure C.1). The exposure ratio level (ER) and subsequent colour assigned to each of the 5 segments spaced between measurement sites is calculated as the average of the value assigned to each segment x_i and $x_{(i+1)}$, represented in the range x_1 through x_4.

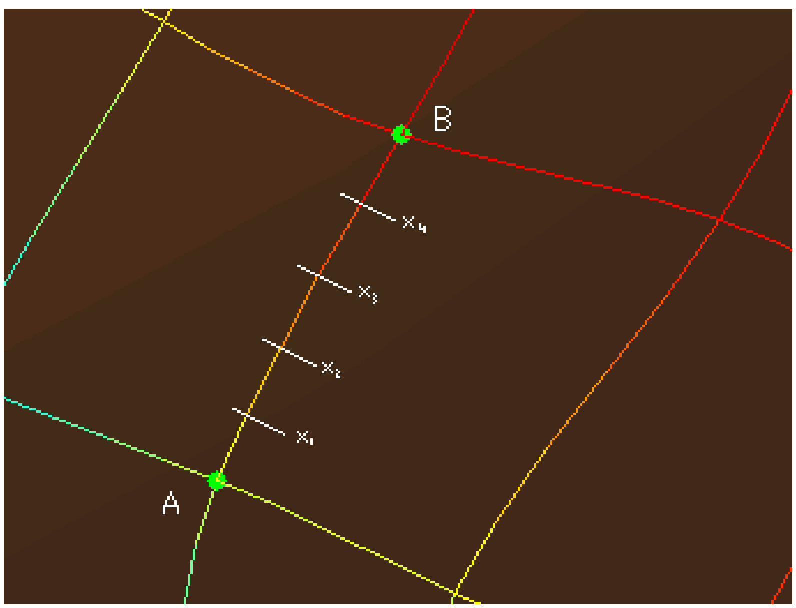

Figure C.1: Exposure contours and representative colour ER segment divisions interpolated between two adjacent measurement sites, A and B highlighted in the figure. For the case shown here, points A and B are separated by approximately 5 mm and represent ERs to the forehead. Each segment between A and B is given a specific colour level.

Using this technique, wireframe meshes of mannequin body part models can be represented as a specific colour. Measurements of exposure are represented in three dimensional space on the wireframe mesh model (Figure C.2).

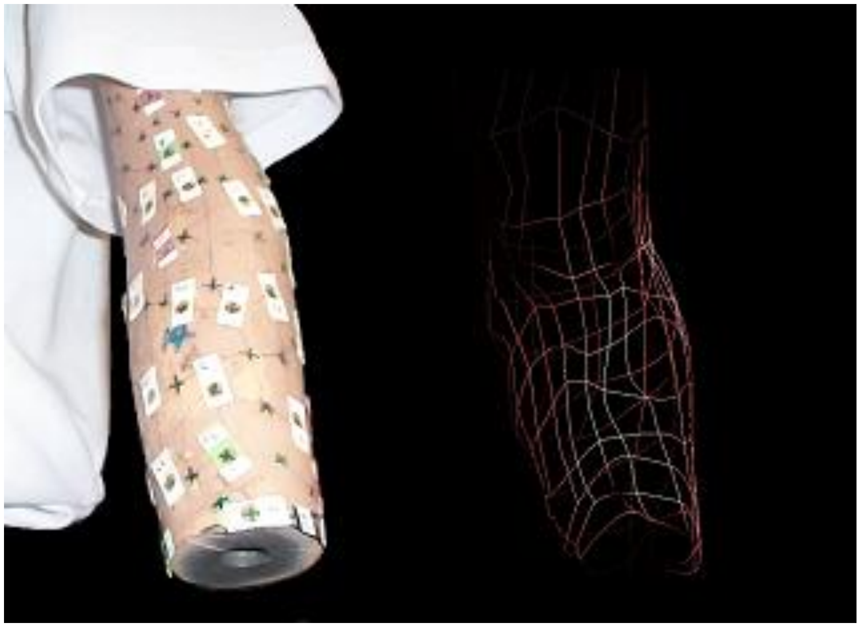

Figure C.2: Photographed mannequin arm dosimeter sites (left) and three dimensional model exposure contours (right). The ERs were measured for the arm in a vertical position alongside the mannequin as photographed.

Appendix D. Developed software and algorithms

The two main algorithms developed for this research are concerned with calculating the horizontal plane UV exposure and representing UV exposures on three dimensional body surfaces. Additional algorithms used to represent UV hot spots in the playground environment are also given. Two programming development environments were used to develop the algorithms used for this research, Microsoft Visual Basic (version 6) and Matlab (version 7.1). The code for these algorithms is given in this section of the appendices and was written and developed over the years since originally developing the horizontal plane UV irradiance model for earlier Masters research. The work is original, except for obvious exceptions including the direct and diffuse horizontal plane UV irradiance equations which are modified versions of the work presented by Rundel (1986), Green, Sawada & Shettle (1974), Green, Cross and Smith (1980), Schippnick and Green (1982), Braslau and Dave (1973), and Dave and Halpern (1976), the solar altitude and azimuth model (Michalsky 1988), the earth-sun distance and cloud models (Josefsson 1986), the global ozone model Van Heuklon's (1979) and the various biological action spectra and meteorological data included in the code.

The horizontal plane UV exposure model was developed in the Visual Basic language and has been packaged with this work as an executable file. A description of this software is given in Section D.1. The code developed and presented here has evolved from the original parent version of this software Pro3uv (version 3.0) into the current version 6.0. Readers of this work may find the inclusion of additional biological action spectra or Van Heuklon's (1979) global ozone model of some use and these are present in the packaged software although not present in the listed code. The code listing given for the horizontal plane UV exposure model is the subroutine used by the larger software package to calculate the UV irradiance on a horizontal plane. To include the entire code listing for this software would extend this work by several hundred pages, therefore the complete code listing for the horizontal UV exposure model is provided in the attached supplementary CD-ROM.

The three dimensional body surface (D.3), playground model (D.4) and skyview processing algorithm (D.5) included here were developed for use in the MATLAB processing environment. These algorithms have not been modified and are the complete code listings used in this research. While the code listings are complete and unmodified, ensuring each algorithm's integrity, some modification of the code may be necessary to ensure each algorithm's usability on different workstations or for different situations to those which were intended for this specific research application.

D.1 The horizontal plane UV exposure package

The horizontal plane UV exposure software package is a global UV irradiance modeller. It is designed to generate a single text file that lists UV exposure totals under various conditions. The generated text file lists ozone concentration (Dobson units), cloud cover (okta's), year, month, day of the month, day of the year, hour of the day, and solar zenith angle as input parameters for integrated UV irradiance totals that describe the diffuse, direct, global, and erythemally effective exposure in units of Jm^{-2}. Additional biological action spectra were also included in the software although these were not used in this research. For the developed horizontal plane UV exposure model, the diffuse, direct and global irradiances are integrated after being calculated at various solar zenith angles. The formulae for calculating the instantaneous irradiance values on the surface of the earth are based also on the extra-terrestrial spectral irradiance from 280 nm to 400 nm and are described by Green (1974). Variations in the earth-sun distance that influence the extra-terrestrial spectral irradiance are also accounted for by a factor formulated by Josefsson (1986). The varying position of the sun and therefore solar zenith angle is calculated at fixed 5 minute steps for any given latitude and longitude. This position is based on an algorithm presented in the Astronomical Almanac and is implemented as described by Michalsky (1988). Each integrated irradiance is progressively summed as the program executes and is based on a trapezoidal approximation. Although there are more sophisticated numerical integration techniques available, the trapezoidal approximation is by far the fastest and easiest method to employ in this case whereby integrations need to be done progressively and recorded to a textfile at different times. Trapezoidal errors are small, especially when integrated over larger time periods. The progressive integration applied by the developed software is always performed in 5 minute steps regardless of the selected textfile recording step.

If the horizontal plane UV exposure model is executed with no cloud input, the global exposure is simply the sum of the diffuse and direct components of the integrated UV exposure. Inputting cloud will affect the global irradiance and therefore the related responses written to the text file but will not affect the diffuse and direct components listed. The cloud model (Josefsson 1986) operates on the total clear sky global irradiance only, the differing effect on the separate diffuse and direct components are not modelled and remain in the textfile as clear sky values. A results summary is also produced that lists the input parameters and irradiance totals for the selected period from which the user can decide to create another model, erasing the previous text file or print the model summary.

A button on the main interface lists textfile options. The user can select one of the totals to decide how data is stored in the textfile, or choose not to save the file to disk. If the user wants to save the data to the disk, it will be saved to a file called "irrad.dat" and stored in the directory "c:\UV". Therefore, *it is important before operating the software to make a directory under C: called UV*. An additional button is also included on the main interface for the direct import of ozone and cloud cover data.

Pressing the Start button on the main interface will begin the UV exposure algorithm. The horizontal plane UV exposure model also incorporates a progress bar that can be used to monitor the progress of the model once it is started. If integration is to be done for a period longer than 1 year, expect the model to take a long time to calculate. (1 year takes approximately 3 minutes). When recording data for a period longer than 1 year the progress bar will move very slowly. This is to be expected as in this situation the progress bar will only update once at the end of every year as opposed to periods recorded within 1 year when the progress bar updates on a daily basis.

D.1.1 Horizontal plane UV exposure model interface

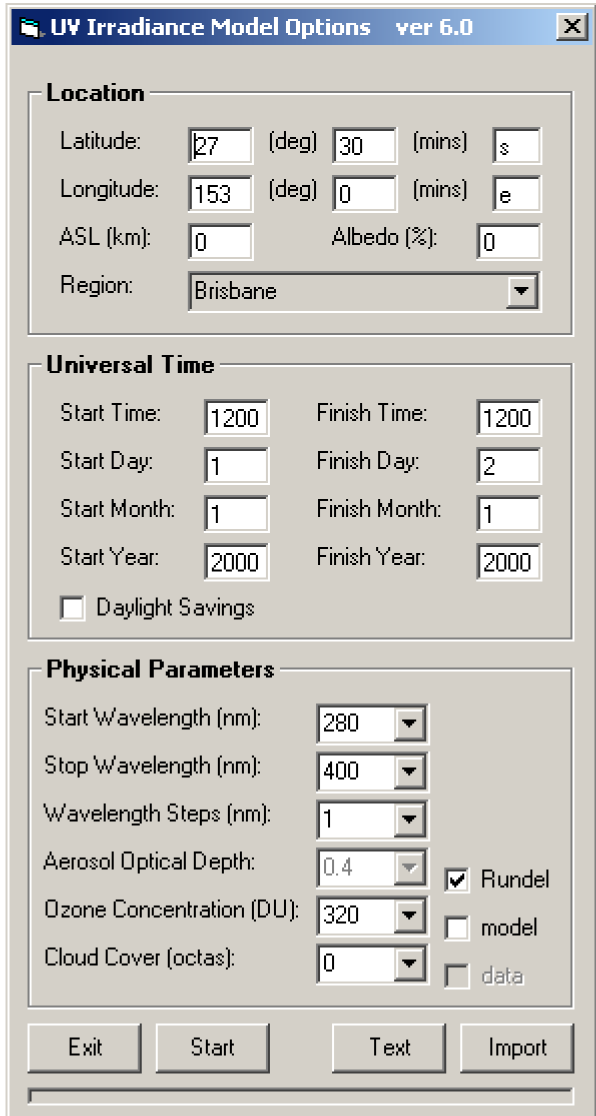

The main interface is divided into three sections:

1. Location: From here the user can either select a region already known from the Region selection box or enter the coordinates in longitude and latitude. Hemispheres of latitude and Longitude are entered in the text boxes next to respective coordinates as either n - north, s - south, e - east, w - west, and must be typed in lower case. An error is triggered if the user enters incorrect values into the main interface that disables the start model calculation button until acceptable values are entered. Any

location coordinates on earth will be acceptable model parameters. Selecting a region from the region select box will automatically input the correct coordinates into the model. Similarly, typing coordinates (in degrees only) that match a known location will highlight the region of interest in the region select dialog box.

2. Universal Time: This section of the input interface is used to determine the start and stop times for the integration process. Again the model will not operate if the user enters incorrect values for start and finish times. Start and finish times must be entered in 24 hour format with 0000 = midnight and 2359 = last allowable time that can be entered. *All times entered must be in universal time not local time*. Universal time is used to avoid confusion between the many possible local time zones that vary from country to country. Start and finish days are entered as days of the month, months are entered as numbers, not text, from 1 = January to 12 = December. The years entered should be any years after and including the year 1900. Although the model will operate for years before 1900, accuracy cannot be assured, given that the sun's position is calculated from the number of hours that have passed after 0000h 1 Jan 1900.

3. Physical Parameters: The integration of the incident spectral irradiance can be varied over a range of wavelengths. The default setup is from 280 nm to 400 nm. Very little, if any radiation gets through in the 280 nm to 290 nm band and Green's model will reflect this. The user can either select from some possible start and stop wavelengths or enter them directly in the start and stop combo boxes. *If the user enters wavelengths directly, integer values must be used.* The spectral step increment can be varied to one of the available steps (1 nm = default, 5 nm, or 10 nm). Increasing the step increment reduces the number of calculations that must be performed to calculate a total irradiance sum over the user defined bandwidth from the extra-terrestrial spectral irradiance, but reduces accuracy of the instantaneous irradiances. Cloud can be entered or selected from one of the listed integer values. If the user enters cloud cover (measured in oktas - or eighths of the sky covered), no more than the maximum of 8 eighths can be entered. Ozone concentration entered in

DU can be any real number the user wishes to try. A global ozone model option exists and should be “checked” if the user wishes to use it. The model can be used to approximate ozone concentration for any location on earth. (Van Heuklon 1979). As this is an old model, which is based on little measured data in the southern hemisphere, its validity over high southerly latitudes cannot be assured. A newer model for global ozone concentration does exist, however it requires that average ozone levels be known for the region in question (Böjrn 1989).

D.2 Horizontal plane UV exposure model code

The UV irradiance equations used to model the horizontal plane UV exposures in this research form part of the main Visual Basic code listing and are located in a subroutine called “physical” listed in the code. It is this subroutine which is present in this code listing. The complete code listing for the horizontal plane UV exposure model is included in the supplementary CD-ROM.

D.2.1 UV irradiance model subroutine

```
Sub physical()
'Generates the UV irradiance see (Green, Sawada & Shettle 1974), (Green, Cross & Smith 1980), (Schippnick & Green 1982), (Josefsson 1986) and (Rundel 1986)

Dim z2 As Double          'SZA expressed in radians
Dim woz As Double         'ozone extinction amount (g/cu.cm)
Dim koz As Double         'ozone extinction coefficient (/cu.cm)
Dim wa As Double          'air extinction amount (cu.km)
Dim ka As Double          'air extinction coefficient (/cu.km)
Dim wp As Double          'particulate extinction amount (cu.km)
Dim kp As Double          'particulate extinction coefficient (/cu.km)
Dim wchange As Double     'incremented storage array wavelength
Dim Cl As Double          'total cloudiness (average of 3 octa /24)
Dim clouds As Double      'cloud correction factor (Josefsson 1986)
Dim EarthSun As Double    'Earth Sun variability factor (Josefsson 1986)
Dim G1 As Double          'Total downward global irradiance
Dim S1 As Double          'diffuse zenith angle ratio parameter
Dim S2 As Double          'diffuse zenith angle ratio parameter
Dim M1 As Double          'diffuse/direct ratio parameter
Dim M2 As Double          'diffuse/direct ratio parameter
Dim M As Double           'Cos(z2)
Dim D0 As Double          'direct irradiance at 0 height and 0 zenith
Dim D As Double           'direct irradiance at variable height and zenith
Dim B1 As Double          'downward albedo contribution to diffuse irradiance
Dim B2 As Double          'upward albedo contrbution to diffuse irradiance
Dim qa As Double          '(Green, Sawada & Shettle 1974) air parameter
Dim qp As Double          'GSS, 1974 particulate parameter
Dim qoz As Double         'GSS, 1974 ozone parameter
Dim bdirt1 As Double      'Direct irradiance parameter
Dim bdirt2 As Double      'Direct irradiance parameter
Dim bdirt3 As Double      'Direct irradiance parameter
Dim A As Double           'Direct irradiance parameter
Dim altstore As Double    'temporary storeage for user specified altitude

Const pi = 3.141592654
woz = (wo / 1000)
koz = 10
wa = 8.42
ka = 0.145
```

```
wp = 1.58
kp = 0.26

bdir = 0       'initilize irradiances before they are summed over wavelength range
bdiff = 0
Girrad = 0
EryAction = 0
ActAction = 0
ViDAction = 0
DNAAction = 0
pcoAction = 0
pkeAction = 0
fmlAction = 0
catAction = 0
nmcAction = 0
fliAction = 0
edfAction = 0
edrAction = 0
AdfAction = 0
AdrAction = 0
VdfAction = 0
VdrAction = 0
DdfAction = 0
DdrAction = 0
pdfAction = 0
pdrAction = 0
kdfAction = 0
kdrAction = 0
fdfAction = 0
fdrAction = 0
cdfAction = 0
cdrAction = 0
ndfAction = 0
ndrAction = 0
ldfAction = 0
ldrAction = 0

z2 = z1 * ((2 * pi) / 360)  'solar zenith angle in radians


wchange = w1            'incrementing wavelength start value
i = (w1 - 280) + 1      'storage array pointer
EarthSun = 1 + 0.033 * Cos((2 * pi * dchange) / 365.25)   'Earth Sun variability factor
Cl = (3 * clcov) / 24
clouds = 1 - (0.7 * (Cl ^ 2.5))   'cloud correction factor
Do While wchange <= w2   'sum over the user specified wavelength range
  If z2 < (pi / 2) Then 'only sum over wavelength range if Sun above horizon


    B1 = 0
    B2 = 0
    M = Cos(z2)
    '*******************************************************************
    '*******************************************************************
    Rem MODIFICATION OF RUNDEL ALGORITHM (1986)

    altstore = alty       'store the user specified altitude

    If albedo <> 0 Then   'if user wants to calculate albedo contribtuion
                          'must find the global irradiance at 0 altitude first
      alty = 0

      '*******************************************************************
      Rem CALCULATES OPTICAL DEPTHS VERSUS WAVELENGTH.
      Rem 1 = RAYLEIGH SCATTERING
      Rem 2 = AEROSOL SCATTERING
      Rem 3 = OZONE ABSORPTION
      Rem 4 = AEROSOL ABSORPTION
      T1 = 1.221 * (300 / wchange) ^ 4.27
      Rem GCS EQ. 18
      Rem K3=9.9405/(0.0445+EXP((wchange-300)/7.294))
      Rem T3=woz*K3
      Rem GCS EQ.19 (USE THIS OPTION TO COMPARE WITH GCS MODEL)
      T2 = (0.08052 / 0.204) * (0.205 + (wchange - 302.5) * 0.000175)
      Rem PERSONAL COMMUNICATION FROM A.E.S. GREEN (1983)
      K3 = 9.788 * 1.0556 / (0.0556 + Exp((wchange - 300) / 6.978))
      T3 = woz * K3
      Rem PERSONAL COMMUNICATION FROM A.E.S. GREEN (1983)
      If Rundel = True Then '<------------------- Nathan Change to Rundel algorithm
        T4 = (0.034 / 0.204) * (0.08052 / 0.034) * (0.034 - (wchange - 302.5) * 0.00005)
        Rem PERSONAL COMMUNICATION FROM A.E.S GREEN (1983)
      Else
        T4 = waod * (0.034 - (wchange - 302.5) * 0.00005)
        Rem Nathan's change
      End If
      '*********************************************************************

      Rem CALCULATES RELATIVE SPECIES CONCENTRAION VS. HEIGHT
      Rem 1 = RAYLEIGH SCATTERING
      Rem 2 = AEROSOL SCATTERING
      Rem 3 = OZONE ABSORPTION
      Rem 4 = AEROSOL ABSORPTION
      N1 = 1.437 / (0.437 + Exp(alty / 6.35))
      N2 = 0.8208 / (-0.145 + Exp(alty / 0.952)) + 0.04 * (1 + Exp(-16.33 / 3.09)) / (1 + Exp((alty - 16.33) / 3.09))
```

```
        N3 = 0.13065 / (2.35 + Exp(alty / 2.66)) + 0.961 * (1 + Exp(-22.51 / 4.92)) / (1 + Exp((alty - 22.51) / 4.92))
        Rem N1, N2, N3 FROM GCS EQ. 9 AND TABLE 1
        '**********************************************************************

        Rem CALCULATES S(wchange,z2,alty) RATIO OF IRRADIANCE AT ZENITH
        Rem ANGLE z2 TO IRRADIANCE AT ZENITH ANGLE 0
        Rem     wchange = WAVELENGTH
        Rem     z2 = SOLAR ZENITH ANGLE
        Rem     alty = HEIGHT (KM)
        Rem     1 = DOWN
        Rem     2 = UP
        P1 = (1.0226 / (M ^ 2 + 0.0226)) ^ 0.5 - 1
        P2 = (1.0112 / (M ^ 2 + 0.0112)) ^ 0.5 - 1
        Rem SG EQ. 11
        F1 = 1 / (1 + 84.37 * (T3 + T4) ^ 0.6776)
        F5 = 1 / (1 + 28.8 * (T3 + T4) ^ 1.325)
        Rem SG EQ. 10
        S1 = (F1 + (1 - F1) * Exp(-T3 * N3 ^ 2.392 * P1)) * Exp(-(0.5346 * T1 * N1 ^ 0.3475 + 0.6077 * T2 * N2 ^ 0.3445) * P1)
        S2 = (F5 + (1 - F5) * Exp(-T3 * P2)) * Exp(-(0.644 * T1 * N1 ^ 0.0795 + 0.102 * T2) * P2)
        Rem SG EQ. 9
        '***********************************************************************

        Rem CALCULATES M(wchange,alty) RATIO OF DIFFUSE IRRADIANCE AT
        Rem HEIGHT alty TO DIRECT IRRADIANCE AT alty = 0
        Rem     1 = DOWN
        Rem     2 = UP
        Rem N6 =  7.389/(6.389+EXP(0.921*alty/6.35))
        Rem SG EQ. 17 FOR N1 BAR
        A1 = 1.735 - 0.346 * N1 ^ 5
        A2 = 0.8041 * T1 ^ A1 * N6
        Rem F1D(wchange,alty) FROM SG EQ. 15
        A3 = 1 / (1 + 0.3264 * woz ^ 1.223 * N3 ^ (1 + 1.7 * T3) * K3 ^ 0.7555)
        Rem G3D(wchange,alty) FOR DH MODEL FROM SG EQ. 13 (PREFERRED OPTION)
        Rem A3 = 1/(1+0.3747*koz^1.223*N3^(1+1.5*T3)*K3^0.7555
        Rem G3D(wchange,alty) FOR BD MODEL FROM SG EQ. 13
        A4 = 1 / (1 + 1.554 * T4 ^ 0.88 * N2 ^ 0.49)
        Rem G4D(wchange,alty) FROM SG EQ. 13
        A5 = (A2 * A3 + N2 ^ 0.564) * 1.437 * (T2 ^ 1.12) / A3
        Rem F2D(wchange,alty) FROM SG EQ. 13
        M1 = (A2 + A5) * A3 * A4
        Rem SG EQ. 12
        A6 = 1.1032 * T1 ^ 1.735 * (1 - N1) ^ 0.921
        Rem F1U(wchange,alty) FROM SG EQ. 14
        A7 = 2.027 * T1 ^ 1.735 * T2 ^ 1.12 * (1 - N1) ^ 0.921 + 0.4373 * T2 ^ 1.12 * (1 - N2) ^ 0.564
        Rem F2U(wchange,alty) FROM SG. 19
        A8 = 1 / (1 + 0.1983 * woz ^ 1.1181 * K3 ^ 0.7555 * N3)
        Rem G3U(wchange,alty) FOR DH FROM SG EQ. 13 (PREFERRED OPTION)
        Rem A8 = 1/(1+0.2248*koz^1.1181*K3^0.7555*N3)
        Rem G3U(wchange,alty) FOR DB FROM SG EQ. 13
        A9 = 1 / (1 + 6.2 * T4 ^ 0.88 * N2 ^ 0.356)
        Rem G4U(wchange,alty) FROM SG EQ. 13
        M2 = (A6 + A7) * A8 * A9
        Rem SG EQ. 12
        '******************************************************************

        Rem CALCULATES DIRECT IRRADIANCE
        Hla = 0.582 * (300 / wchange) ^ 5 * (Exp(9.102) - 1) / (Exp(9.102 * 300 / wchange) - 1)
        Rem UNITS OF W NM^-1 M^-2
        Rem EXTRATERRESTRIAL IRRADIANCE FROM SG TABLE 1
        Rem Hla = 1.095*(1-EXP(-0.6902*EXP((wchange-300)/23.74)))
        Rem UNITS OF W NM^-1 M^-2
        Rem EXTRATERRESTRIAL IRRADIANCE FROM GCS EQ. 17
        Hla = Hla * (1 - 0.738 * Exp(-(wchange - 279.5) ^ 2 / 2 / 2.96 ^ 2) - 0.485 * Exp(-(wchange - 286.1) ^ 2 / 2 / 1.57 ^ 2) - 0.243 * Exp(-(wchange - 300.4) ^ 2 / 2
/ 1.8 ^ 2) + 0.192 * Exp(-(wchange - 333.2) ^ 2 / 2 / 4.26 ^ 2) - 0.167 * Exp(-(wchange - 358.5) ^ 2 / 2 / 2.01 ^ 2) + 0.097 * Exp(-(wchange - 368) ^ 2 / 2 / 2.43 ^ 2))
 * EarthSun
        Rem ADD SMOOTHED FRAUNHOFER STRUCTURE
        S5 = Sqr((M * M + 0.0018) / (1 + 0.0018))
        S6 = Sqr((M * M + 0.0003) / (1 + 0.0003))
        S7 = Sqr((M * M + 0.0074) / (1 + 0.0074))
        A = T1 * N1 / S5 + T2 * N2 / S6 + T3 * N3 / S7 + T4 * N2 / S6
        Rem TOTAL OPTICAL DEPTH
        A0 = T1 + T2 + T3 + T4
        Rem TOTAL OPTICAL DEPTH FOR z2 = 0 AND alty = 0
        D = M * Hla * Exp(-A)
        Rem DIRECT IRRADIANCE FROM GCS EQ. 1
        D0 = Hla * Exp(-A0)
        Rem DIRECT IRRADIANCE FOR z2 = 0 AND alty = 0
        '*******************************************************************

        G = D + S1 * M1 * D0  '(HORIZONTAL PLANE IRRADIANCE AT SEA LEVEL AND NO ALBEDO CONTRIBUTION)
        alty = altstore   'restore local altitude to calculate local global irradiance

    End If

    '******************************************************************
    Rem CALCULATES OPTICAL DEPTHS VERSUS WAVELENGTH.
    Rem 1 = RAYLEIGH SCATTERING
    Rem 2 = AEROSOL SCATTERING
    Rem 3 = OZONE ABSORPTION
    Rem 4 = AEROSOL ABSORPTION
    T1 = 1.221 * (300 / wchange) ^ 4.27
    Rem GCS EQ. 18
    Rem K3=9.9405/(0.0445+EXP((wchange-300)/7.294))
    Rem T3=woz*K3
```

```
Rem GCS EQ.19 (USE THIS OPTION TO COMPARE WITH GCS MODEL)
T2 = (0.08052 / 0.204) * (0.205 + (wchange - 302.5) * 0.000175)
Rem PERSONAL COMMUNICATION FROM A.E.S. GREEN (1983)
K3 = 9.788 * 1.0556 / (0.0556 + Exp((wchange - 300) / 6.978))
T3 = woz * K3
Rem PERSONAL COMMUNICATION FROM A.E.S. GREEN (1983)
If Rundel = True Then '<----------------------- Nathan change to Rundel algorithm
  T4 = (0.034 / 0.204) * (0.08052 / 0.034) * (0.034 - (wchange - 302.5) * 0.00005)
  Rem PERSONAL COMMUNICATION FROM A.E.S GREEN (1983)
Else
  T4 = waod * (0.034 - (wchange - 302.5) * 0.00005)
  Rem Nathan's change
End If
'*********************************************************************

Rem CALCULATES RELATIVE SPECIES CONCENTRAION VS. HEIGHT
Rem 1 = RAYLEIGH SCATTERING
Rem 2 = AEROSOL SCATTERING
Rem 3 = OZONE ABSORPTION
Rem 4 = AEROSOL ABSORPTION
N1 = 1.437 / (0.437 + Exp(alty / 6.35))
N2 = 0.8208 / (-0.145 + Exp(alty / 0.952)) + 0.04 * (1 + Exp(-16.33 / 3.09)) / (1 + Exp((alty - 16.33) / 3.09))
N3 = 0.13065 / (2.35 + Exp(alty / 2.66)) + 0.961 * (1 + Exp(-22.51 / 4.92)) / (1 + Exp((alty - 22.51) / 4.92))
Rem N1, N2, N3 FROM GCS EQ. 9 AND TABLE 1
'*********************************************************************

Rem CALCULATES S(wchange,z2,alty) RATIO OF IRRADIANCE AT ZENITH
Rem ANGLE z2 TO IRRADIANCE AT ZENITH ANGLE 0
Rem    wchange = WAVELENGTH
Rem    z2 = SOLAR ZENITH ANGLE
Rem    alty = HEIGHT (KM)
Rem    1 = DOWN
Rem    2 = UP
P1 = (1.0226 / (M ^ 2 + 0.0226)) ^ 0.5 - 1
P2 = (1.0112 / (M ^ 2 + 0.0112)) ^ 0.5 - 1
Rem SG EQ. 11
F1 = 1 / (1 + 84.37 * (T3 + T4) ^ 0.6776)
F5 = 1 / (1 + 28.8 * (T3 + T4) ^ 1.325)
Rem SG EQ. 10
S1 = (F1 + (1 - F1) * Exp(-T3 * N3 ^ 2.392 * P1)) * Exp(-(0.5346 * T1 * N1 ^ 0.3475 + 0.6077 * T2 * N2 ^ 0.3445) * P1)
S2 = (F5 + (1 - F5) * Exp(-T3 * P2)) * Exp(-(0.644 * T1 * N1 ^ 0.0795 + 0.102 * T2) * P2)
Rem SG EQ. 9
'**********************************************************************

Rem CALCULATES M(wchange,alty) RATIO OF DIFFUSE IRRADIANCE AT
Rem HEIGHT alty TO DIRECT IRRADIANCE AT alty = 0
Rem    1 = DOWN
Rem    2 = UP
Rem N6 =  7.389/(6.389+EXP(0.921*alty/6.35))
Rem SG EQ. 17 FOR N1 BAR
A1 = 1.735 - 0.346 * N1 ^ 5
A2 = 0.8041 * T1 ^ A1 * N6
Rem F1D(wchange,alty) FROM SG EQ. 15
A3 = 1 / (1 + 0.3264 * woz ^ 1.223 * N3 ^ (1 + 1.7 * T3) * K3 ^ 0.7555)
Rem G3D(wchange,alty) FOR DH MODEL FROM SG EQ. 13 (PREFERRED OPTION)
Rem A3 = 1/(1+0.3747*koz^1.223*N3^(1+1.5*T3)*K3^0.7555
Rem G3D(wchange,alty) FOR BD MODEL FROM SG EQ. 13
A4 = 1 / (1 + 1.554 * T4 ^ 0.88 * N2 ^ 0.49)
Rem G4D(wchange,alty) FROM SG EQ. 13
A5 = (A2 * A3 + N2 ^ 0.564) * 1.437 * (T2 ^ 1.12) / A3
Rem F2D(wchange,alty) FROM SG EQ. 13
M1 = (A2 + A5) * A3 * A4
Rem SG EQ. 12
A6 = 1.1032 * T1 ^ 1.735 * (1 - N1) ^ 0.921
Rem F1U(wchange,alty) FROM SG EQ. 14
A7 = 2.027 * T1 ^ 1.735 * T2 ^ 1.12 * (1 - N1) ^ 0.921 + 0.4373 * T2 ^ 1.12 * (1 - N2) ^ 0.564
Rem F2U(wchange,alty) FROM SG. 19
A8 = 1 / (1 + 0.1983 * woz ^ 1.1181 * K3 ^ 0.7555 * N3)
Rem G3U(wchange,alty) FOR DH FROM SG EQ. 13 (PREFERRED OPTION)
Rem A8 = 1/(1+0.2248*koz^1.1181*K3^0.7555*N3)
Rem G3U(wchange,alty) FOR DB FROM SG EQ. 13
A9 = 1 / (1 + 6.2 * T4 ^ 0.88 * N2 ^ 0.356)
Rem G4U(wchange,alty) FROM SG EQ. 13
M2 = (A6 + A7) * A8 * A9
Rem SG EQ. 12
'*****************************************************************

Rem CALCULATES DIRECT IRRADIANCE
Hla = 0.582 * (300 / wchange) ^ 5 * (Exp(9.102) - 1) / (Exp(9.102 * 300 / wchange) - 1)
Rem UNITS OF W NM^-1 M^-2
Rem EXTRATERRESTRIAL IRRADIANCE FROM SG TABLE 1
Rem Hla = 1.095*(1-EXP(-0.6902*EXP((wchange-300)/23.74)))
Rem UNITS OF W NM^-1 M^-2
Rem EXTRATERRESTRIAL IRRADIANCE FROM GCS EQ. 17
Hla = Hla * (1 - 0.738 * Exp(-(wchange - 279.5) ^ 2 / 2 / 2.96 ^ 2) - 0.485 * Exp(-(wchange - 286.1) ^ 2 / 2 / 1.57 ^ 2) - 0.243 * Exp(-(wchange - 300.4) ^ 2 / 2 /
1.8 ^ 2) + 0.192 * Exp(-(wchange - 333.2) ^ 2 / 2 / 4.26 ^ 2) - 0.167 * Exp(-(wchange - 358.5) ^ 2 / 2 / 2.01 ^ 2) + 0.097 * Exp(-(wchange - 368) ^ 2 / 2 / 2.43 ^ 2))
* EarthSun
Rem ADD SMOOTHED FRAUNHOFER STRUCTURE
S5 = Sqr((M * M + 0.0018) / (1 + 0.0018))
S6 = Sqr((M * M + 0.0003) / (1 + 0.0003))
S7 = Sqr((M * M + 0.0074) / (1 + 0.0074))
A = T1 * N1 / S5 + T2 * N2 / S6 + T3 * N3 / S7 + T4 * N2 / S6
Rem TOTAL OPTICAL DEPTH
A0 = T1 + T2 + T3 + T4
```

```
Rem TOTAL OPTICAL DEPTH FOR z2 = 0 AND alty = 0
D = M * Hla * Exp(-A)
Rem DIRECT IRRADIANCE FROM GCS EQ. 1
D0 = Hla * Exp(-A0)
Rem DIRECT IRRADIANCE FOR z2 = 0 AND alty = 0
'*********************************************************************

Rem CALCULATES EFFECT OF NON-ZERO ALBEDO
Rem     1 = DOWN
Rem     2 = UP
If albedo = 0 Then GoTo 900
   Rem     B = ALBEDO
   R = (0.4424 * T1 ^ 0.5626 / (1 + 0.2797 * woz ^ 1.0132 * K3 ^ 0.8404) + 0.1 * T2 ^ 0.88) / (1 + 3.7 * T4)
   Rem SG EQ. 28, 29
   E1 = N1 * Exp(-(0.4638 * T2 * (1 - N2) + 3.5 * T3 * (1 - N3) + 0.4638 * T4 * (1 - N2)))
   E2 = Exp(-(0.4909 * T1 * (1 - N1) + 0.5658 * T2 * (1 - N2) + 2.417 * T3 * (1 - N3) + 0.5658 * T4 * (1 - N2)))
   Rem SG EQ. 32, 33
   B1 = R * albedo / (1 - R * albedo) * E1 * G
   B2 = albedo / (1 - R * albedo) * E2 * G
900   Rem ALBEDO CONTRIBUTION FROM SG EQ. 25, 27, 31
'*********************************************************************

G1 = D + S1 * M1 * D0 + B1      'Total Global downward irradiance at specified
                                'wavelength, altitude, zenith angle and albedo
'*********************************************************************
'*********************************************************************

'Diffuse solar irradiance
q1 = 1 / (Sqr(1 - ((Sin(z2) * Sin(z2)) / (1 + (311 / 6371)) ^ 2)))    'eq 7 GSS 1974 with yi = 311 (Barton 1983) or q1 = 1.10
q2 = 1 / (Sqr(1 - ((Sin(z2) * Sin(z2)) / (1.06 * (1 + 0.106 * alty)))))
bp = 7.48 / ((1 - (((Sin(z2)) ^ 4) / 1.148)) ^ 0.25)
O = 1.62 * Exp(0.24 * koz * woz - ((wchange - 300) / bp)) * q1 + (0.872 * (1 + 0.179 * alty + 0.0487 * ((T4 * N2) - 0.538) ^ 2)) * q2
bdiffw = (Hla * Exp(-O)) + B1  'diffuse irradiance including altitude and albedo contribution
If wchange < w2 Then
   bdiff = bdiff + (steps * bdiffw) 'cumulative diffuse irradiance
Else
   bdiff = bdiff + bdiffw
End If


bdirw = D
If wchange < w2 Then
   bdir = bdir + (steps * bdirw)   'cumulative direct irradiance
Else
   bdir = bdir + bdirw
End If

'Global solar irradiance
Girradw = (bdirw + bdiffw) * clouds 'global irradiance including cloud modification
If wchange < w2 Then
   Girrad = Girrad + (steps * Girradw) 'cumulative global irradiance
Else
   Girrad = Girrad + Girradw
End If

'Erythemal Action spectrum
EryActionw = Ery(i) * Girradw       'Erythemal response at specified wavelength
If wchange < w2 Then
   EryAction = EryAction + (steps * EryActionw) 'cumulative Erythemal response
Else
   EryAction = EryAction + EryActionw
End If

'Diffuse Erythemal Action Spectrum
edfActionw = Ery(i) * bdiffw       'Erythemal response at specified wavelength
If wchange < w2 Then
   edfAction = edfAction + (steps * edfActionw) 'cumulative Erythemal response
Else
   edfAction = edfAction + edfActionw
End If

'Direct Erythemal Action Spectrum
edrActionw = Ery(i) * bdirw       'Erythemal response at specified wavelength
If wchange < w2 Then
   edrAction = edrAction + (steps * edrActionw) 'cumulative Erythemal response
Else
   edrAction = edrAction + edrActionw
End If

'Actinic Action spectrum
ActActionw = Act(i) * Girradw       'Actinic response at specified wavelength
If wchange < w2 Then
   ActAction = ActAction + (steps * ActActionw) 'cumulative Actinic response
Else
   ActAction = ActAction + ActActionw
End If

'Diffuse Actinic Action spectrum
AdfActionw = Act(i) * bdiffw       'Actinic response at specified wavelength
If wchange < w2 Then
   AdfAction = AdfAction + (steps * AdfActionw) 'cumulative Actinic response
Else
   AdfAction = AdfAction + AdfActionw
End If
```

```
'Direct Actinic Action spectrum
AdrActionw = Act(i) * bdirw      'Actinic response at specified wavelength
If wchange < w2 Then
  AdrAction = AdrAction + (steps * AdrActionw) 'cumulative Actinic response
Else
  AdrAction = AdrAction + AdrActionw
End If

'Vitamin D3 Action Spectrum
ViDActionw = ViD(i) * Girradw      'Vitamin D3 response at specified wavelength
If wchange < w2 Then
  ViDAction = ViDAction + (steps * ViDActionw) 'cumulative Vitamin D3 response
Else
  ViDAction = ViDAction + ViDActionw
End If

'Vitamin D3 Diffuse Action Spectrum
VdfActionw = ViD(i) * bdiffw      'Vitamin D3 response at specified wavelength
If wchange < w2 Then
  VdfAction = VdfAction + (steps * VdfActionw) 'cumulative Vitamin D3 response
Else
  VdfAction = VdfAction + VdfActionw
End If

'Vitamin D3 Direct Action Spectrum
VdrActionw = ViD(i) * bdirw      'Vitamin D3 response at specified wavelength
If wchange < w2 Then
  VdrAction = VdrAction + (steps * VdrActionw) 'cumulative Vitamin D3 response
Else
  VdrAction = VdrAction + VdrActionw
End If

'DNA Action Spectrum
DNAActionw = DNA(i) * Girradw      'DNA response at specified wavelength
If wchange < w2 Then
  DNAAction = DNAAction + (steps * DNAActionw) 'cumulative DNA response
Else
  DNAAction = DNAAction + DNAActionw
End If

'Diffuse DNA Action Spectrum
DdfActionw = DNA(i) * bdiffw      'DNA response at specified wavelength
If wchange < w2 Then
  DdfAction = DdfAction + (steps * DdfActionw) 'cumulative DNA response
Else
  DdfAction = DdfAction + DdfActionw
End If

'Direct DNA Action Spectrum
DdrActionw = DNA(i) * bdirw      'DNA response at specified wavelength
If wchange < w2 Then
  DdrAction = DdrAction + (steps * DdrActionw) 'cumulative DNA response
Else
  DdrAction = DdrAction + DdrActionw
End If

'Photoconjuct Action Spectrum
pcoActionw = pco(i) * Girradw      'pco response at specified wavelength
If wchange < w2 Then
  pcoAction = pcoAction + (steps * pcoActionw) 'cumulative pco response
Else
  pcoAction = pcoAction + pcoActionw
End If

'Diffuse Photoconjuct Action Spectrum
pdfActionw = pco(i) * bdiffw      'pco response at specified wavelength
If wchange < w2 Then
  pdfAction = pdfAction + (steps * pdfActionw) 'cumulative pco response
Else
  pdfAction = pdfAction + pdfActionw
End If

'Direct Photoconjuct Action Spectrum
pdrActionw = pco(i) * bdirw      'pco response at specified wavelength
If wchange < w2 Then
  pdrAction = pdrAction + (steps * pdrActionw) 'cumulative pco response
Else
  pdrAction = pdrAction + pdrActionw
End If

'Photokerititis Action Spectrum
pkeActionw = pke(i) * Girradw      'pke response at specified wavelength
If wchange < w2 Then
  pkeAction = pkeAction + (steps * pkeActionw) 'cumulative pke response
Else
  pkeAction = pkeAction + pkeActionw
End If

'Diffuse Photokerititis Action Spectrum
kdfActionw = pke(i) * bdiffw      'pke response at specified wavelength
If wchange < w2 Then
  kdfAction = kdfAction + (steps * kdfActionw) 'cumulative pke response
Else
```

```
  kdfAction = kdfAction + kdfActionw
End If

'Direct Photokerititis Action Spectrum
kdrActionw = pke(i) * bdirw      'pke response at specified wavelength
If wchange < w2 Then
  kdrAction = kdrAction + (steps * kdrActionw) 'cumulative pke response
Else
  kdrAction = kdrAction + kdrActionw
End If

'Fish Melanoma Action Spectrum
fmlActionw = fml(i) * Girradw      'fml response at specified wavelength
If wchange < w2 Then
  fmlAction = fmlAction + (steps * fmlActionw) 'cumulative fml response
Else
  fmlAction = fmlAction + fmlActionw
End If

'Diffuse Fish Melanoma Action Spectrum
fdfActionw = fml(i) * bdiffw      'fml response at specified wavelength
If wchange < w2 Then
  fdfAction = fdfAction + (steps * fdfActionw) 'cumulative fml response
Else
  fdfAction = fdfAction + fdfActionw
End If

'Direct Fish Melanoma Action Spectrum
fdrActionw = fml(i) * bdirw      'fml response at specified wavelength
If wchange < w2 Then
  fdrAction = fdrAction + (steps * fdrActionw) 'cumulative fml response
Else
  fdrAction = fdrAction + fdrActionw
End If

'Cataract Action Spectrum
catActionw = cat(i) * Girradw      'cataract response at specified wavelength
If wchange < w2 Then
  catAction = catAction + (steps * catActionw) 'cumulative cataract response
Else
  catAction = catAction + catActionw
End If

'Diffuse Cataract Action Spectrum
cdfActionw = cat(i) * bdiffw      'cataract response at specified wavelength
If wchange < w2 Then
  cdfAction = cdfAction + (steps * cdfActionw) 'cumulative cataract response
Else
  cdfAction = cdfAction + cdfActionw
End If

'Direct Cataract Action Spectrum
cdrActionw = cat(i) * bdirw      'cataract response at specified wavelength
If wchange < w2 Then
  cdrAction = cdrAction + (steps * cdrActionw) 'cumulative cataract response
Else
  cdrAction = cdrAction + cdrActionw
End If

'NMSC Action Spectrum
nmcActionw = nmc(i) * Girradw      'NMSC response at specified wavelength
If wchange < w2 Then
  nmcAction = nmcAction + (steps * nmcActionw) 'cumulative NMSC response
Else
  nmcAction = nmcAction + nmcActionw
End If

'Diffuse NMSC Action Spectrum
ndfActionw = nmc(i) * bdiffw      'NMSC response at specified wavelength
If wchange < w2 Then
  ndfAction = ndfAction + (steps * ndfActionw) 'cumulative NMSC response
Else
  ndfAction = ndfAction + ndfActionw
End If

'Direct NMSC Action Spectrum
ndrActionw = nmc(i) * bdirw      'NMSC response at specified wavelength
If wchange < w2 Then
  ndrAction = ndrAction + (steps * ndrActionw) 'cumulative NMSC response
Else
  ndrAction = ndrAction + ndrActionw
End If

'Flint & Caldwell Action Spectrum
fliActionw = fli(i) * Girradw      'fli response at specified wavelength
If wchange < w2 Then
  fliAction = fliAction + (steps * fliActionw) 'cumulative fli response
Else
  fliAction = fliAction + fliActionw
End If

'Diffuse Flint & Caldwell Action Spectrum
ldfActionw = fli(i) * bdiffw      'fli response at specified wavelength
If wchange < w2 Then
```

```
      ldfAction = ldfAction + (steps * ldfActionw) 'cumulative fli response
    Else
      ldfAction = ldfAction + ldfActionw
    End If

    'Direct Flint & Caldwell Action Spectrum
    ldrActionw = fli(i) * bdirw      'fli response at specified wavelength
    If wchange < w2 Then
      ldrAction = ldrAction + (steps * ldrActionw) 'cumulative fli response
    Else
      ldrAction = ldrAction + ldrActionw
    End If

  Else
    Rem Sun is below the horizon
    Rem Don't sum over the wavelength range
    Rem All spectra are 0 for this particular SZA
    bdir = 0
    bdiff = 0
    Girrad = 0
    EryAction = 0
    ActAction = 0
    ViDAction = 0
    DNAAction = 0
    pcoAction = 0
    pkeAction = 0
    fmlAction = 0
    catAction = 0
    nmcAction = 0
    fliAction = 0
    edfAction = 0
    edrAction = 0
    AdfAction = 0
    AdrAction = 0
    VdfAction = 0
    VdrAction = 0
    DdfAction = 0
    DdrAction = 0
    pdfAction = 0
    pdrAction = 0
    kdfAction = 0
    kdrAction = 0
    fdfAction = 0
    fdrAction = 0
    cdfAction = 0
    cdrAction = 0
    ndfAction = 0
    ndrAction = 0
    ldfAction = 0
    ldrAction = 0

  End If
  Wave(i) = wchange

  wchange = wchange + steps      'increment wavelength in user defined steps
  i = i + steps
Loop


70 Rem The wavelength totals have been calculated for the given SZA

End Sub
```

D.3 Three dimensional wireframe exposure models

Three dimensional wireframe models were developed for each of the face, neck, arm, hand and leg mannequin body parts. These models were used to represent both the ER and absolute UV_{ery} exposure on the three dimensional surfaces of the studied body parts. To list each model for each respective body part would repeat much of the same code, therefore only the code used to develop the face wireframe exposure model is listed here. Each of the face, neck, arm, hand and leg algorithms are however listed in the attached supplementary data CD-ROM. The algorithm listed below was written for use with MATLAB version 7.1.

```
%MASTER PROGRAM FOR FACIAL EXPOSURE RATIOS

clear

x =
[168,142,124,115,106.5,101,98,95,92,90,87.5,84.5,82,79,76.5,74,72.5,72,72.5,72,70,65,60,52,46,41.5,43,48,52,52,51,47,47.5,50,51,48,50,53,55,53,51,50,51.5,
56,67,107,109,109.5,110.5,111.5 ...
166,140,123,112,105.5,99.5,95,92,90,87,84.5,81,79,76,73.5,70.5,70,69,70.5,72,71,65.5,62.5,56.5,45.5,41.5,43,48,51.5,51,49.5,46,46,48,49,47,47,51.5,53.5,51.
5,50,49.5,50.5,54.5,66,108,109,110,111,112 ...
166,140,125.5,114,106.5,101,96,93,89.5,87,84.5,81.5,79,76.5,74,70,69,68.5,72,75,80,78.5,73,66,62,48,46.5,53,55.5,54.5,51.5,48,47.5,49,52,47.5,48.5,53,54,52
.5,50.5,50,51.5,55,69,109.5,110.5,111,112,113 ...
167,152,127.5,115.5,108.8,101,97,93.5,90,86.5,83.5,80.5,78,75.5,73.5,70,68.5,70.5,77,80.5,84,85.5,84.5,75.5,69,66,57,52,55.5,58,55.5,52,50.5,50.5,54.5,50.5,
52,54.5,55.5,54,51.5,51,52.5,56.5,91.5,111.5,112,112.5,113.5,114.5 ...
167,157,129.5,118.5,110,103,98.5,94,91.5,87,85,81.5,79.5,76,74,70,68.5,73,80.5,82.25,86,87.5,87,83,73,69,67.5,66.5,61.5,61,59.5,57,54.5,54.5,57.5,54.5,55.5,
57.5,58.5,57,53.5,53,55,60.5,113,113.5,115,115,116.5,116.5 ...
168,161,135,121.5,112.5,106.5,100.5,96,91.5,89,86,83,80.5,78,74.5,70.5,70,77.5,80,83,84,85.5,85.5,83,75,70.5,68,67.5,66.5,64.5,62.5,61.5,60.25,60,62,61,61.
5,62.5,62.5,61,59,59.5,61.5,67,116,118,118.5,118.5,119,119.5 ...
167,142,125,117,109,104,99.5,95.5,91.5,88.5,84.5,81.5,79,75.5,72,72.5,78.5,79.5,81.5,83.5,83.5,85,84.5,77,72.5,69.5,68,67.5,67,66,64.5,63.5,63.5,65,64.5,65,
66,67,66,65.5,66.5,70,82,120,121,121.5,121.25,121.5,121.5 ...
167,155,130,120,113,107,102,98,95,91,88,84.5,81,78,73,74,79,80.5,81.5,83.5,83.5,86,85,79.5,74.5,71,69.5,69,69,69.25,68.5,67.75,67.5,67.5,69,70,72,73,73.5,
73.5,76,80,122.5,125.25,125,125,125.75,126,126 ...
166.5,139,124.75,116.5,111,106,102,100,95.25,91.75,88,84.5,79.25,74.75,76.5,80,81.5,82.5,85.5,85,87,86.5,80.25,75.5,72.5,70.75,70,70.5,71.25,71.75,71.75,7
1.75,72.75,74.5,75.5,78,79,80,81.75,85.25,100.75,130,130.75,130.5,130.5,130,130,130 ...
167,155,131,122,114.5,110.25,106,102.75,99.75,96,92.5,87.75,82.75,77.75,78,81.75,82.75,86,87.25,88.25,90.75,88.25,81.75,77.25,74.25,72.75,72.25,72.5,73.
5,75,76.25,77.5,80,81,84.25,86,86.75,89.5,91.75,107,133.75,136,136.5,136,135.75,135.5,135,135.5 ...
166,145,129.75,121.25,115,111.5,108.5,104.75,102,99.5,94.5,88.5,81.75,81,84,86,89.5,95.25,95,97,92.25,85.75,80.25,77,75.75,75.25,76.5,79,81.75,83.5,86.25
,90.5,92.75,93.5,96.75,97.5,101.75,116,141.75,143.5,144,144,143.5,143.5,143.5,143,143 ...
166.25,140.5,129.5,123,117.75,114.75,112,109,107,105,102.5,93.5,86,87.25,89.5,93,97.5,104.25,103.25,98,92.25,86,82.5,81,81.75,83.5,87.25,90.75,93.5,98.5,
102.5,105,107.25,110,125,148,150,151.75,153.75,153,154,154,155,155.25,155.25,152.75 ...
167,147,134.5,128,123.75,118.75,116.25,115,113.25,112.75,111,107.25,98,97.75,101.5,105,111.5,109,104.25,99,94.5,91.25,90,91.75,97.75,105,111.5,114.5,1
19.5,121,122.25,122.5 ...
170,151.25,139.75,132.25,129.25,126.25,124.25,122.5,122.25,123.75,122.5,123.25,123.75,124.5,121.5,119.75,117.75,113.75,111.25,108.25,108,115.25,121.5,
129,142.5,144,146.5,151 ...
168,155.5,144.5,142,139.75,138.5,136.25,136.5,136.75,137,138.25,139.25,141,142.75,142.75,145.5,149.5,151.5,151.25,148.75,148.5,149,151,150,150.75,154
...
173.25,161.75,155,154,153.75,154.25,154.75,155.5,157.25,160,164,157.5,153.75,153,155.5,163,164.25,160.25,159.25,161,158.25,155.5 ...
167,162,159,162,164,167,167.5,165.75,170.5 ...
172.75,174.25,176,176.75,176 ...
166,140,123,112,105.5,99.5,95,92,90,87,84.5,81,79,76,73.5,70.5,70,69,70.5,72,71,65.5,62.5,56.5,45.5,41.5,43,48,51.5,51,49.5,46,46,48,49,47,47,51.5,53.5,51.
5,50,49.5,50.5,54.5,66,108,109,110,111,112];


y = (-
1)*[89.61,89.61,89.61,89.61,89.61,89.61,89.61,89.61,89.61,89.61,89.61,89.61,89.61,89.61,89.61,89.61,89.61,89.61,89.61,89.61,89.61,89.61,89.61,89.61,89.61,89.61,
89.61,89.61,89.61,89.61,89.61,89.61,89.61,89.61,89.61,89.61,89.61,89.61,89.61,89.61,89.61,89.61,89.61,89.61,89.61,89.61,89.61,89.61,89.61,89.61,89.61,89.61,89.61 ...
84.21,84.21,84.21,84.21,84.21,84.21,84.21,84.21,84.21,84.21,84.21,84.21,84.21,84.21,84.21,84.21,84.21,84.21,84.21,84.21,84.21,84.21,84.21,84.21,84.21,84.21,84.
21,84.21,84.21,84.21,84.21,84.21,84.21,84.21,84.21,84.21,84.21,84.21,84.21,84.21,84.21,84.21,84.21,84.21,84.21,84.21,84.21,84.21,84.21,84.21,84.21 ...
79.22,79.22,79.22,79.22,79.22,79.22,79.22,79.22,79.22,79.22,79.22,79.22,79.22,79.22,79.22,79.22,79.22,79.22,79.22,79.22,79.22,79.22,79.22,79.22,79.22,79.22,79.
22,79.22,79.22,79.22,79.22,79.22,79.22,79.22,79.22,79.22,79.22,79.22,79.22,79.22,79.22,79.22,79.22,79.22,79.22,79.22,79.22,79.22,79.22,79.22,79.22 ...
74.22,74.22,74.22,74.22,74.22,74.22,74.22,74.22,74.22,74.22,74.22,74.22,74.22,74.22,74.22,74.22,74.22,74.22,74.22,74.22,74.22,74.22,74.22,74.22,74.22,74.22,74.
22,74.22,74.22,74.22,74.22,74.22,74.22,74.22,74.22,74.22,74.22,74.22,74.22,74.22,74.22,74.22,74.22,74.22,74.22,74.22,74.22,74.22,74.22,74.22,74.22 ...
69.22,69.22,69.22,69.22,69.22,69.22,69.22,69.22,69.22,69.22,69.22,69.22,69.22,69.22,69.22,69.22,69.22,69.22,69.22,69.22,69.22,69.22,69.22,69.22,69.22,69.22,69.
22,69.22,69.22,69.22,69.22,69.22,69.22,69.22,69.22,69.22,69.22,69.22,69.22,69.22,69.22,69.22,69.22,69.22,69.22,69.22,69.22,69.22,69.22,69.22,69.22 ...
64.22,64.22,64.22,64.22,64.22,64.22,64.22,64.22,64.22,64.22,64.22,64.22,64.22,64.22,64.22,64.22,64.22,64.22,64.22,64.22,64.22,64.22,64.22,64.22,64.22,64.22,64.
22,64.22,64.22,64.22,64.22,64.22,64.22,64.22,64.22,64.22,64.22,64.22,64.22,64.22,64.22,64.22,64.22,64.22,64.22,64.22,64.22,64.22,64.22,64.22,64.22 ...
```

```
59.22,59.22,59.22,59.22,59.22,59.22,59.22,59.22,59.22,59.22,59.22,59.22,59.22,59.22,59.22,59.22,59.22,59.22,59.22,59.22,59.22,59.22,59.22,59.22,59.22,59.
22,59.22,59.22,59.22,59.22,59.22,59.22,59.22,59.22,59.22,59.22,59.22,59.22,59.22,59.22,59.22,59.22,59.22,59.22,59.22,59.22,59.22,59.22,59.22 ...
54.22,54.22,54.22,54.22,54.22,54.22,54.22,54.22,54.22,54.22,54.22,54.22,54.22,54.22,54.22,54.22,54.22,54.22,54.22,54.22,54.22,54.22,54.22,54.22,54.22,54.
22,54.22,54.22,54.22,54.22,54.22,54.22,54.22,54.22,54.22,54.22,54.22,54.22,54.22,54.22,54.22,54.22,54.22,54.22,54.22,54.22,54.22,54.22,54.22 ...
49.22,49.22,49.22,49.22,49.22,49.22,49.22,49.22,49.22,49.22,49.22,49.22,49.22,49.22,49.22,49.22,49.22,49.22,49.22,49.22,49.22,49.22,49.22,49.22,49.22,49.
22,49.22,49.22,49.22,49.22,49.22,49.22,49.22,49.22,49.22,49.22,49.22,49.22,49.22,49.22,49.22,49.22,49.22,49.22,49.22,49.22,49.22,49.22 ...
44.22,44.22,44.22,44.22,44.22,44.22,44.22,44.22,44.22,44.22,44.22,44.22,44.22,44.22,44.22,44.22,44.22,44.22,44.22,44.22,44.22,44.22,44.22,44.22,44.22,44.
22,44.22,44.22,44.22,44.22,44.22,44.22,44.22,44.22,44.22,44.22,44.22,44.22,44.22,44.22,44.22,44.22,44.22,44.22,44.22,44.22,44.22,44.22 ...
39.22,39.22,39.22,39.22,39.22,39.22,39.22,39.22,39.22,39.22,39.22,39.22,39.22,39.22,39.22,39.22,39.22,39.22,39.22,39.22,39.22,39.22,39.22,39.22,39.22,39.
22,39.22,39.22,39.22,39.22,39.22,39.22,39.22,39.22,39.22,39.22,39.22,39.22,39.22,39.22,39.22,39.22,39.22,39.22,39.22,39.22,39.22 ...
34.22,34.22,34.22,34.22,34.22,34.22,34.22,34.22,34.22,34.22,34.22,34.22,34.22,34.22,34.22,34.22,34.22,34.22,34.22,34.22,34.22,34.22,34.22,34.22,34.22,34.
22,34.22,34.22,34.22,34.22,34.22,34.22,34.22,34.22,34.22,34.22,34.22,34.22,34.22,34.22,34.22,34.22,34.22,34.22,34.22,34.22 …
29.22,29.22,29.22,29.22,29.22,29.22,29.22,29.22,29.22,29.22,29.22,29.22,29.22,29.22,29.22,29.22,29.22,29.22,29.22,29.22,29.22,29.22,29.22,29.22,29.22,29.
22,29.22,29.22,29.22,29.22,29.22,29.22 ...
24.22,24.22,24.22,24.22,24.22,24.22,24.22,24.22,24.22,24.22,24.22,24.22,24.22,24.22,24.22,24.22,24.22,24.22,24.22,24.22,24.22,24.22,24.22,24.22,24.22,24.
22,24.22,24.22 ...
19.22,19.22,19.22,19.22,19.22,19.22,19.22,19.22,19.22,19.22,19.22,19.22,19.22,19.22,19.22,19.22,19.22,19.22,19.22,19.22,19.22,19.22,19.22,19.22,19.22,19.
22 ...
14.22,14.22,14.22,14.22,14.22,14.22,14.22,14.22,14.22,14.22,14.22,14.22,14.22,14.22,14.22,14.22,14.22,14.22,14.22,14.22,14.22,14.22 ...
9.22,9.22,9.22,9.22,9.22,9.22,9.22,9.22,9.22 ...
4.22,4.22,4.22,4.22,4.22 ...
90,90,90,90,90,90,90,90,90,90,90,90,90,90,90,90,90,90,90,90,90,90,90,90,90,90,90,90,90,90,90,90,90,90,90,90,90,90,90,90,90,90,90,90,90,90,90,90,90,90];


z = (-
1)*[77,82,87,92,97,102,107,112,117,122,127,132,137,142,147,152,157,162,167,172,177,182,187,192,197,202,207,212,217,222,227,232,237,242,247,252,257,
262,267,272,277,282,287,292,297,302,307,312,317,322 ...
77,82,87,92,97,102,107,112,117,122,127,132,137,142,147,152,157,162,167,172,177,182,187,192,197,202,207,212,217,222,227,232,237,242,247,252,257,262,
267,272,277,282,287,292,297,302,307,312,317,322 ...
77.5,82,87,92,97,102,107,112,117,122,127,132,137,142,147,152,157,162,167,172,177,182,187,192,197,202,207,212,217,222,227,232,237,242,247,252,257,26
2,267,272,277,282,287,292,297,302,307,312,317,322 ...
78.5,82,87,92,97,102,107,112,117,122,127,132,137,142,147,152,157,162,167,172,177,182,187,192,197,202,207,212,217,222,227,232,237,242,247,252,257,26
2,267,272,277,282,287,292,297,302,307,312,317,322 ...
79.5,82,87,92,97,102,107,112,117,122,127,132,137,142,147,152,157,162,167,172,177,182,187,192,197,202,207,212,217,222,227,232,237,242,247,252,257,26
2,267,272,277,282,287,292,297,302,307,312,317,322 ...
80.5,82,87,92,97,102,107,112,117,122,127,132,137,142,147,152,157,162,167,172,177,182,187,192,197,202,207,212,217,222,227,232,237,242,247,252,257,26
2,267,272,277,282,287,292,297,302,307,312,317,322 ...
82,87,92,97,102,107,112,117,122,127,132,137,142,147,152,157,162,167,172,177,182,187,192,197,202,207,212,217,222,227,232,237,242,247,252,257,262,26
7,272,277,282,287,292,297,302,307,312,317,322 ...
84,87,92,97,102,107,112,117,122,127,132,137,142,147,152,157,162,167,172,177,182,187,192,197,202,207,212,217,222,227,232,237,242,247,252,257,262,26
7,272,277,282,287,292,297,302,307,312,317,322 ...
87,92,97,102,107,112,117,122,127,132,137,142,147,152,157,162,167,172,177,182,187,192,197,202,207,212,217,222,227,232,237,242,247,252,257,262,267,2
72,277,282,287,292,297,302,307,312,317,322 ...
89.5,92,97,102,107,112,117,122,127,132,137,142,147,152,157,162,167,172,177,182,187,192,197,202,207,212,217,222,227,232,237,242,247,252,257,262,267,
272,277,282,287,292,297,302,307,312,317,322 ...
92.8,97,102,107,112,117,122,127,132,137,142,147,152,157,162,167,172,177,182,187,192,197,202,207,212,217,222,227,232,237,242,247,252,257,262,267,27
2,277,282,287,292,297,302,307,312,317,322 ...
97,102,107,112,117,122,127,132,137,142,147,152,157,162,167,172,177,182,187,192,197,202,207,212,217,222,227,232,237,242,247,252,257,262,267,272,277
,282,287,292,297,302,307,312,317,322 ...
101.8,107,112,117,122,127,132,137,142,147,152,157,162,167,172,177,182,187,192,197,202,207,212,217,222,227,232,237,242,247,252,257 ...
108.8,112,117,122,127,132,137,142,147,152,157,162,167,172,177,182,187,192,197,202,207,212,217,222,227,232,237,242 ...
117.4,122,127,132,137,142,147,152,157,162,167,172,177,182,187,192,197,202,207,212,217,222,227,232,237,242 ...
129.9,137,142,147,152,157,162,167,172,177,182,187,192,197,202,207,212,217,222,227,232,237 ...
184,187,192,197,202,207,212,217,222 ...
189,197,202,207,212 ...
77,82,87,92,97,102,107,112,117,122,127,132,137,142,147,152,157,162,167,172,177,182,187,192,197,202,207,212,217,222,227,232,237,242,247,252,257,262,
267,272,277,282,287,292,297,302,307,312,317,322];


%specifiy color maps
cmap = colormap(hsv(101));   %can't index array at 0 must start at 1
gdmap = cmap;   %grid data color map
cmap = colormap(copper(100));   %face surface map


% Original plot of Contour positions
plot3(x,y,z,'.','Markersize', 1)
axis([0 350 -350 0 -350 0])
xlabel('x-axis')
ylabel('y-axis')
zlabel('z-axis')

% Surface meshing
zm = -350:5:0;
ym = -350:5:0;
xm = 0:5:350;

[xi,yi] = meshgrid(zm,ym);
[xr,yr,zr]=griddata(z,y,x,xi,yi);
mesh(zr,yr,xr)
h = surf(zr,yr,xr,'LineStyle','none')
colormap copper
set(h,'FaceLighting','phong','Facecolor','interp','AmbientStrength',0.6);
light('Position',[-1 1 1],'Style','infinite'); %light for face background
grid off
% Axis and background Setup
set(gca,'Color','k','XColor',[0.3,0.3,0.3],'YColor',[0.3,0.3,0.3],'ZColor',[0.3,0.3,0.3])
grid off
axis([0 350 -350 0 -350 0])
xlabel('x-axis')
ylabel('y-axis')
zlabel('z-axis')
```

```
hidden off   % turn off hidden contours behind face surface
hold on
%##########################################################################################
%##########################################################################################
%##########################################################################################
%EXPOSURE RATIO CONTOURS
% CN1
x1 =
[168,142,124,115,106.5,101,98,95,92,90,87.5,84.5,82,79,76.5,74,72.5,72,72.5,72,70,65,60,52,46,41.5,43,48,52,52,51,47,47.5,50,51,48,50,53,55,53,51,50,51.5,
56,67,107,109,109.5,110.5,111.5];
y1 = (-
1)*[89.61,89.61,89.61,89.61,89.61,89.61,89.61,89.61,89.61,89.61,89.61,89.61,89.61,89.61,89.61,89.61,89.61,89.61,89.61,89.61,89.61,89.61,89.61,89.61,89.61,
89.61,89.61,89.61,89.61,89.61,89.61,89.61,89.61,89.61,89.61,89.61,89.61,89.61,89.61,89.61,89.61,89.61,89.61,89.61,89.61,89.61,89.61,89.61,89.61,89.61];
z1 = (-
1)*[77,82,87,92,97,102,107,112,117,122,127,132,137,142,147,152,157,162,167,172,177,182,187,192,197,202,207,212,217,222,227,232,237,242,247,252,257,
262,267,272,277,282,287,292,297,302,307,312,317,322];

top1 =
[100,100,96,92,88,84,82,80,79,78,80,81,82,83,82,81,69,56,57,59,75,91,95,99,86,74,47,21,36,52,67,81,53,25,47,69,47,24,48,72,64,55,36,18,18,17,17,22,26,26];

%[ex,ey,ez] = griddata(x1,y1,z1,top);
%mesh(ex,ey,ez)
for n = 1:50
  co = top1(n)/100;
  %plot3(x1(n),y1(n),z1(n),'.','Markersize', 20,'Color',[0,co,0]);
end

%CN2
x2 =
[166,140,123,112,105.5,99.5,95,92,90,87,84.5,81,79,76,73.5,70.5,70,69,70.5,72,71,65.5,62.5,56.5,45.5,41.5,43,48,51.5,51,49.5,46,46,48,49,47,47,51.5,53.5,51.
5,50,49.5,50.5,54.5,66,108,109,110,111,112];
y2 = (-
1)*[95.01,95.01,95.01,95.01,95.01,95.01,95.01,95.01,95.01,95.01,95.01,95.01,95.01,95.01,95.01,95.01,95.01,95.01,95.01,95.01,95.01,95.01,95.01,95.01,95.01,
95.01,95.01,95.01,95.01,95.01,95.01,95.01,95.01,95.01,95.01,95.01,95.01,95.01,95.01,95.01,95.01,95.01,95.01,95.01,95.01,95.01,95.01,95.01,95.01,95.01];
z2 = (-
1)*[77,82,87,92,97,102,107,112,117,122,127,132,137,142,147,152,157,162,167,172,177,182,187,192,197,202,207,212,217,222,227,232,237,242,247,252,257,
262,267,272,277,282,287,292,297,302,307,312,317,322];

top2 =
[100,100,97,93,90,86,84,82,80,78,80,82,83,84,78,72,62,51,54,56,70,84,91,98,85,73,50,27,41,56,67,78,54,29,47,65,48,30,50,70,62,53,36,19,21,22,22,26,26,26];
%interpolated data

%CN3
x3 =
[166,140,125.5,114,106.5,101,96,93,89.5,87,84.5,81.5,79,76.5,74,70,69,68.5,72,75,80,78.5,73,66,62,48,46.5,53,55.5,54.5,51.5,48,47.5,49,52,47.5,48.5,53,54,5
2.5,50.5,50,51.5,55,69,109.5,110.5,111,112,113];
y3 = (-
1)*[100,100,100,100,100,100,100,100,100,100,100,100,100,100,100,100,100,100,100,100,100,100,100,100,100,100,100,100,100,100,100,100,100,100,100,100,10
0,100,100,100,100,100,100,100,100,100,100,100,100,100];
z3 = (-
1)*[77.5,82,87,92,97,102,107,112,117,122,127,132,137,142,147,152,157,162,167,172,177,182,187,192,197,202,207,212,217,222,227,232,237,242,247,252,25
7,262,267,272,277,282,287,292,297,302,307,312,317,322];

top3 =
[100,100,97,95,91,88,85,83,80,78,80,83,84,85,74,63,55,47,50,52,65,78,87,96,84,72,53,34,46,59,67,74,54,34,48,61,49,37,52,68,59,51,36,21,24,26,26,29,26,26];

%CN4
x4 =
[167,152,127.5,115.5,108.8,101,97,93.5,90,86.5,83.5,80.5,78,75.5,73.5,70,68.5,70.5,77,80.5,84,85.5,84.5,75.5,69,66,57,52,55.5,58,55.5,52,50.5,50.5,54.5,50.5,
52,54.5,55.5,54,51.5,51,52.5,56.5,91.5,111.5,112,112.5,113.5,114.5];
y4 = (-
1)*[105,105,105,105,105,105,105,105,105,105,105,105,105,105,105,105,105,105,105,105,105,105,105,105,105,105,105,105,105,105,105,105,105,105,105,105,10
5,105,105,105,105,105,105,105,105,105,105,105,105,105];
z4 = (-
1)*[78.5,82,87,92,97,102,107,112,117,122,127,132,137,142,147,152,157,162,167,172,177,182,187,192,197,202,207,212,217,222,227,232,237,242,247,252,25
7,262,267,272,277,282,287,292,297,302,307,312,317,322];

top4 =
[100,100,98,96,93,89,87,85,81,77,81,84,85,87,70,53,48,42,46,49,61,72,84,95,83,72,56,40,51,62,67,71,55,39,48,58,51,43,54,66,57,49,36,23,27,31,31,33,26,26];

%CN5
x5 =
[167,157,129.5,118.5,110,103,98.5,94,91.5,87,85,81.5,79.5,76,74,70,68.5,73,80.5,82.25,86,87.5,87,83,73,69,67.5,66.5,61.5,61,59.5,57,54.5,54.5,57.5,54.5,55.5
,57.5,58.5,57,53.5,53,55,60.5,113,113.5,115,115,116.5,116.5];
y5 = (-
1)*[110,110,110,110,110,110,110,110,110,110,110,110,110,110,110,110,110,110,110,110,110,110,110,110,110,110,110,110,110,110,110,110,110,110,110,110,11
0,110,110,110,110,110,110,110,110,110,110,110,110,110];
z5 = (-
1)*[79.5,82,87,92,97,102,107,112,117,122,127,132,137,142,147,152,157,162,167,172,177,182,187,192,197,202,207,212,217,222,227,232,237,242,247,252,25
7,262,267,272,277,282,287,292,297,302,307,312,317,322];

top5 =
[100,100,99,97,94,91,89,86,81,77,81,85,87,88,66,44,41,37,42,46,56,66,80,94,82,71,59,47,56,66,67,68,55,43,49,54,52,50,56,63,55,47,36,24,30,35,35,37,26,26];

%CN6
x6 =
[168,161,135,121.5,112.5,106.5,100.5,96,91.5,89,86,83,80.5,78,74.5,70.5,70,77.5,80,83,84,85.5,85.5,83,75,70.5,68,67.5,66.5,64.5,62.5,61.5,60.25,60,62,61,61.
5,62.5,62.5,61,59,59.5,61.5,67,116,118,118.5,118.5,119,119.5];
y6 = (-
1)*[115,115,115,115,115,115,115,115,115,115,115,115,115,115,115,115,115,115,115,115,115,115,115,115,115,115,115,115,115,115,115,115,115,115,115,115,11
5,115,115,115,115,115,115,115,115,115,115,115,115,115];
```

```
z6 = (-
1)*[80.5,82,87,92,97,102,107,112,117,122,127,132,137,142,147,152,157,162,167,172,177,182,187,192,197,202,207,212,217,222,227,232,237,242,247,252,25
7,262,267,272,277,282,287,292,297,302,307,312,317,322];

top6
=[100,100,99,99,96,93,90,87,82,76,81,86,88,89,62,35,34,33,38,43,51,60,76,92,81,70,62,54,61,69,67,64,56,48,49,50,53,56,59,61,53,45,36,26,33,39,40,41,26,26
];

% CN7
x7=[167,142,125,117,109,104,99.5,95.5,91.5,88.5,84.5,81.5,79,75.5,72,72.5,78.5,79.5,81.5,83.5,83.5,85,84.5,77,72.5,69.5,68,67.5,67,66,64.5,63.5,63.5,65,64.5
,65,66,67,66,65.5,66.5,70,82,120,121,121.5,121.25,121.5,121.5];
y7 = (-
1)*[120,120,120,120,120,120,120,120,120,120,120,120,120,120,120,120,120,120,120,120,120,120,120,120,120,120,120,120,120,120,120,120,120,120,120,12
0,120,120,120,120,120,120,120,120,120,120,120,120,120];
z7 = (-
1)*[82,87,92,97,102,107,112,117,122,127,132,137,142,147,152,157,162,167,172,177,182,187,192,197,202,207,212,217,222,227,232,237,242,247,252,257,262
,267,272,277,282,287,292,297,302,307,312,317,322];

top7 =
[100,100,100,100,97,95,92,89,82,76,82,88,89,90,58,26,27,28,34,39,47,54,73,91,81,70,65,60,66,73,67,61,56,52,49,46,54,62,61,59,51,43,35,28,36,44,44,44,44];
%[ex,ey,ez] = griddata(x1,y1,z1,top);
%mesh(ex,ey,ez)
for n = 1:49
   co = top7(n)/100;
   %plot3(x7(n),y7(n),z7(n),'.','Markersize', 20,'Color',[0,co,0]);
end

%CN8
x8 =
[167,155,130,120,113,107,102,98,95,91,88,84.5,81,78,73,74,79,80.5,81.5,83.5,83.5,86,85,79.5,74.5,71,69.5,69,69,69.25,68.5,67.75,67.5,67.5,69,70,72,73,73.5,
73.5,76,80,122.5,125.25,125,125,125.75,126,126];
y8 = (-
1)*[125,125,125,125,125,125,125,125,125,125,125,125,125,125,125,125,125,125,125,125,125,125,125,125,125,125,125,125,125,125,125,125,125,125,125,12
5,125,125,125,125,125,125,125,125,125,125,125,125,125];
z8 = (-
1)*[84,87,92,97,102,107,112,117,122,127,132,137,142,147,152,157,162,167,172,177,182,187,192,197,202,207,212,217,222,227,232,237,242,247,252,257,262
,267,272,277,282,287,292,297,302,307,312,317,322];

top8 =
[99,99,98,98,95,91,89,86,80,74,79,84,86,87,59,31,33,35,39,43,49,54,70,86,76,67,60,54,66,73,67,61,56,52,49,46,54,62,61,59,51,43,35,28,36,44,44,44,44];


%CN9
x9 =
[166.5,139,124.75,116.5,111,106,102,100,95.25,91.75,88,84.5,79.25,74.75,76.5,80,81.5,82.5,85.5,85,87,86.5,80.25,75.5,72.5,70.75,70,70.5,71.25,71.75,71.75,
71.75,72.75,74.5,75.5,78,79,80,81.75,85.25,100.75,130,130.75,130.5,130.5,130,130,130];
y9 = (-
1)*[130,130,130,130,130,130,130,130,130,130,130,130,130,130,130,130,130,130,130,130,130,130,130,130,130,130,130,130,130,130,130,130,130,130,130,13
0,130,130,130,130,130,130,130,130,130,130,130,130];
z9 = (-
1)*[87,92,97,102,107,112,117,122,127,132,137,142,147,152,157,162,167,172,177,182,187,192,197,202,207,212,217,222,227,232,237,242,247,252,257,262,26
7,272,277,282,287,292,297,302,307,312,317,322];

top9 = [98,98,97,95,92,88,86,84,78,72,76,80,82,84,60,36,39,42,45,47,51,54,67,80,72,65,56,47,66,73,67,61,56,52,49,46,54,62,61,59,51,43,35,28,36,44,44,44];

%CN10
x10
=[167,155,131,122,114.5,110.25,106,102.75,99.75,96,92.5,87.75,82.75,77.75,78,81.75,82.75,86,87.25,88.25,90.75,88.25,81.75,77.25,74.25,72.75,72.25,72.5,7
3.5,75,76.25,77.5,80,81,84.25,86,86.75,89.5,91.75,107,133.75,136,136.5,136,135.75,135.5,135,135.5];

y10 = (-
1)*[135,135,135,135,135,135,135,135,135,135,135,135,135,135,135,135,135,135,135,135,135,135,135,135,135,135,135,135,135,135,135,135,135,135,135,13
5,135,135,135,135,135,135,135,135,135,135,135,135];
z10 = (-
1)*[89.5,92,97,102,107,112,117,122,127,132,137,142,147,152,157,162,167,172,177,182,187,192,197,202,207,212,217,222,227,232,237,242,247,252,257,262,
267,272,277,282,287,292,297,302,307,312,317,322];

top10 = [97,97,95,93,89,85,83,81,75,69,73,77,79,81,61,42,45,49,50,51,52,54,64,75,68,62,51,40,66,73,67,61,56,52,49,46,54,62,61,59,51,43,35,28,36,44,44,44];

%CN11
x11 =
[166,145,129.75,121.25,115,111.5,108.5,104.75,102,99.5,94.5,88.5,81.75,81,84,86,89.5,95.25,95,97,92.25,85.75,80.25,77,75.75,75.25,76.5,79,81.75,83.5,86.2
5,90.5,92.75,93.5,96.75,97.5,101.75,116,141.75,143.5,144,144,143.5,143.5,143.5,143,143];
y11 = (-
1)*[140,140,140,140,140,140,140,140,140,140,140,140,140,140,140,140,140,140,140,140,140,140,140,140,140,140,140,140,140,140,140,140,140,140,140,14
0,140,140,140,140,140,140,140,140,140,140,140];
z11 = (-
1)*[92.8,97,102,107,112,117,122,127,132,137,142,147,152,157,162,167,172,177,182,187,192,197,202,207,212,217,222,227,232,237,242,247,252,257,262,267
,272,277,282,287,292,297,302,307,312,317,322];

top11 = [97,97,94,91,86,82,80,78,73,67,70,73,75,77,62,47,51,56,56,55,54,54,62,69,64,59,47,34,66,73,67,61,56,52,49,46,54,62,61,59,51,43,35,28,36,44,44];

%CN12
x12 =
[166.25,140.5,129.5,123,117.75,114.75,112,109,107,105,102.5,93.5,86,87.25,89.5,93,97.5,104.25,103.25,98,92.25,86,82.5,81,81.75,83.5,87.25,90.75,93.5,98.5
,102.5,105,107.25,110,125,148,150,151.75,153.75,153,154,154,155,155.25,155.25,152.75];
y12 = (-
1)*[145,145,145,145,145,145,145,145,145,145,145,145,145,145,145,145,145,145,145,145,145,145,145,145,145,145,145,145,145,145,145,145,145,145,145,14
5,145,145,145,145,145,145,145,145,145,145];
z12 = (-
1)*[97,102,107,112,117,122,127,132,137,142,147,152,157,162,167,172,177,182,187,192,197,202,207,212,217,222,227,232,237,242,247,252,257,262,267,272,
277,282,287,292,297,302,307,312,317,322];

top12 = [96,96,92,88,83,78,77,75,70,65,67,70,72,74,63,52,58,63,61,59,56,53,59,64,60,57,42,27,66,73,67,61,56,52,49,46,54,62,61,59,51,43,35,28,36,44];
```

```
% CN13
x13 =
[167,147,134.5,128,123.75,118.75,116.25,115,113.25,112.75,111,107.25,98,97.75,101.5,105,111.5,109,104.25,99,94.5,91.25,90,91.75,97.75,105,111.5,114.5,1
19.5,121,122.25,122.5];
y13 = (-1)*[150,150,150,150,150,150,150,150,150,150,150,150,150,150,150,150,150,150,150,150,150,150,150,150,150,150,150,150,150,150,150,150];
z13 = (-1)*[101.8,107,112,117,122,127,132,137,142,147,152,157,162,167,172,177,182,187,192,197,202,207,212,217,222,227,232,237,242,247,252,257];

top13 = [95,95,90,86,80,75,74,73,68,63,65,66,68,71,64,57,64,70,67,63,58,53,56,59,56,54,37,21,66,73,67,61];

%CN14
x14
=[170,151.25,139.75,132.25,129.25,126.25,124.25,122.5,122.25,123.75,122.5,123.25,123.75,124.5,121.5,119.75,117.75,113.75,111.25,108.25,108,115.25,121.
5,129,142.5,144,146.5,151];
y14=-1*[155,155,155,155,155,155,155,155,155,155,155,155,155,155,155,155,155,155,155,155,155,155,155,155,155,155,155,155];
z14=-1*[107,112,117,122,127,132,137,142,147,152,157,162,167,172,177,182,187,192,197,202,207,212,217,222,227,232,237,242];

top14 = [94,94,89,84,78,72,71,70,66,61,62,62,65,68,65,63,70,77,72,67,60,53,53,53,52,52,33,14];
%[ex,ey,ez] = griddata(x1,y1,z1,top);
%mesh(ex,ey,ez)
for n = 1:28
  co = top14(n)/100;
  %plot3(x14(n),y14(n),z14(n),'.','Markersize', 20,'Color',[0,co,0]);
end

%CN15
x15 =
[168,155.5,144.5,142,139.75,138.5,136.25,136.5,136.75,137,138.25,139.25,141,142.75,142.75,145.5,149.5,151.5,151.25,148.75,148.5,149,151,150,150.75,154
];
y15 =(-1)*[160,160,160,160,160,160,160,160,160,160,160,160,160,160,160,160,160,160,160,160,160,160,160,160,160,160];
z15 = (-1)*[117.4,122,127,132,137,142,147,152,157,162,167,172,177,182,187,192,197,202,207,212,217,222,227,232,237,242];

top15 = [94,94,89,84,78,72,71,70,66,61,62,62,65,68,65,63,70,77,72,67,60,53,53,53,52,52];

%CN16
x16 = [173.25,161.75,155,154,153.75,154.25,154.75,155.5,157.25,160,164,157.5,153.75,153,155.5,163,164.25,160.25,159.25,161,158.25,155.5];
y16 = (-1)*[165,165,165,165,165,165,165,165,165,165,165,165,165,165,165,165,165,165,165,165,165,165];
z16 = (-1)*[129.9,137,142,147,152,157,162,167,172,177,182,187,192,197,202,207,212,217,222,227,232,237];

top16 = [94,94,89,84,78,72,71,70,66,61,62,62,65,68,65,63,70,77,72,67,60,53];

%CN17
x17 = [167,162,159,162,164,167,167.5,165.75,170.5];
y17 = (-1)*[170,170,170,170,170,170,170,170,170];
z17 = (-1)*[184,187,192,197,202,207,212,217,222];

top17 = [94,94,89,84,78,72,71,70,66];


%CN18
x18 = [172.75,174.25,176,176.75,176];
y18 = (-1)*[175,175,175,175,175];
z18 = (-1)*[189,197,202,207,212];

top18 = [94,94,89,84,78];


%##########################################################################################
%##########################################################################################
%##########################################################################################
%INTERPOLATED CONTOUR LINES
% CN1
%cn1a = plot3(x1,y1,z1,'-g');
% 1mm interpolated contour lines for CN1
cn1z = min(z1):1:max(z1);
for n = 1:length(cn1z)
  cn1y(n) = -89.61;
end
cn1xi = interp1(z1,x1,cn1z,'spline');
%cn1 = plot3(cn1xi,cn1y,cn1z,'Linewidth',0.75);

%COLOURING CONTOUR CN1
if (z1(50) < z1(1))
  st = -1;
else
  st = 1;
end
cn1z2 = z1(1):st:z1(50);
for n= 1:length(cn1z2)
  cn1y2(n) = -89.61;
end
cn1xi2 = interp1(z1,x1,cn1z2,'spline');

stp = 1;
for k = 1:49
  ncval = top1(k);   %starting point of 5 colour bands
  pcval = ncval/100;   %progressive point for each band
  ncval2 = top1(k+1);   %end point of 5 colour bands
  for j = stp:(stp+4)   %DIVIDE FIRST INTERVAL INTO 5 COLOUR BANDS
    colx(1) = cn1xi2(j);
    colx(2) = cn1xi2(j+1);
    coly(1) = cn1y2(j);
    coly(2) = cn1y2(j+1);
    colz(1) = cn1z2(j);
```

```
    colz(2) = cn1z2(j+1);
    cval = ((pcval*100)+((ncval2-ncval)/5))/100;
    cvalp = (cval+pcval)/2;   %average between two points for a colour
    cvalp = round(cvalp*100)+1;
    pcval = cval;
    plot3(colx,coly,colz,'Color',[gdmap(cvalp,1),gdmap(cvalp,2),gdmap(cvalp,3)],'Linewidth',0.75);   %[0,cvalp,0]
  end
stp = stp+5;
end
%***************************************************************

% CN2
%cn2a = plot3(x2,y2,z2,'-g');
% 1mm interpolated contour lines for CN2
cn2z = min(z2):1:max(z2);
for n = 1:length(cn2z)
  cn2y(n) = -95.01;
end
cn2xi = interp1(z2,x2,cn2z,'spline');
%cn2 = plot3(cn2xi,cn2y,cn2z,'Linewidth',0.75);

%COLOURING CONTOUR CN2
if (z2(50) < z2(1))
  st = -1;
else
  st = 1;
end
cn2z2 = z2(1):st:z2(50);
for n= 1:length(cn2z2)
  cn2y2(n) = -95.01;
end
cn2xi2 = interp1(z2,x2,cn2z2,'spline');

stp = 1;
for k = 1:49
  ncval = top2(k);   %starting point of 5 colour bands
  pcval = ncval/100;   %progressive point for each band
  ncval2 = top2(k+1);   %end point of 5 colour bands
  for j = stp:(stp+4)   %DIVIDE FIRST INTERVAL INTO 5 COLOUR BANDS
    colx(1) = cn2xi2(j);
    colx(2) = cn2xi2(j+1);
    coly(1) = cn2y2(j);
    coly(2) = cn2y2(j+1);
    colz(1) = cn2z2(j);
    colz(2) = cn2z2(j+1);
    cval = ((pcval*100)+((ncval2-ncval)/5))/100;
    cvalp = (cval+pcval)/2;   %average between two points for a colour
    cvalp = round(cvalp*100)+1;
    pcval = cval;
    plot3(colx,coly,colz,'Color',[gdmap(cvalp,1),gdmap(cvalp,2),gdmap(cvalp,3)],'Linewidth',0.75);   %[0,cvalp,0]
  end
stp = stp+5;
end
%***************************************************************

% CN3   %STARTS at -77.5 in z NOT -77
%cn3a = plot3(x3,y3,z3,'-g');
% 1mm interpolated contour lines for CN3
cn3z = min(z3):1:max(z3);
for n = 1:length(cn3z)
  cn3y(n) = -100;
end
cn3xi = interp1(z3,x3,cn3z,'spline');
%cn3 = plot3(cn3xi,cn3y,cn3z,'Linewidth',0.75);

%COLOURING CONTOUR CN3
if (z3(50) < z3(1))
  st = -1;
else
  st = 1;
end
cn3z2pre = z3(2):st:z3(50);
cn3z2(1) = -77.5;
cn3z2(2) = -78;
cn3z2(3) = -79;
cn3z2(4) = -80;
cn3z2(5) = -81;
cn3z2(6) = -82;
for padd = 7:(length(cn3z2pre)+5)
  cn3z2(padd) = cn3z2pre(padd-5);
end
for n= 1:length(cn3z2)
  cn3y2(n) = -100;
end
cn3xi2 = interp1(z3,x3,cn3z2,'spline');

stp = 1;
for k = 1:49
  ncval = top3(k);   %starting point of 5 colour bands
  pcval = ncval/100;   %progressive point for each band
  ncval2 = top3(k+1);   %end point of 5 colour bands
  for j = stp:(stp+4)   %DIVIDE FIRST INTERVAL INTO 5 COLOUR BANDS
    colx(1) = cn3xi2(j);
    colx(2) = cn3xi2(j+1);
```

```
      coly(1) = cn3y2(j);
      coly(2) = cn3y2(j+1);
      colz(1) = cn3z2(j);
      colz(2) = cn3z2(j+1);
      cval = ((pcval*100)+((ncval2-ncval)/5))/100;
      cvalp = (cval+pcval)/2;   %average between two points for a colour
      cvalp = round(cvalp*100)+1;
      pcval = cval;
      plot3(colx,coly,colz,'Color',[gdmap(cvalp,1),gdmap(cvalp,2),gdmap(cvalp,3)],'Linewidth',0.75);   %[0,cvalp,0]
   end
stp = stp+5;
end
%****************************************************************

% CN4   %STARTS at -78.5 in z NOT -77
%cn4a = plot3(x4,y4,z4,'-g');
% 1mm interpolated contour lines for CN4
cn4z = min(z4):1:max(z4);
for n = 1:length(cn4z)
   cn4y(n) = -105;
end
cn4xi = interp1(z4,x4,cn4z,'spline');
%cn4 = plot3(cn4xi,cn4y,cn4z,'Linewidth',0.75);

%COLOURING CONTOUR CN4
if (z4(50) < z4(1))
   st = -1;
else
   st = 1;
end
cn4z2pre = z4(2):st:z4(50);
cn4z2(1) = -78.5;
cn4z2(2) = -79.2;
cn4z2(3) = -79.9;
cn4z2(4) = -80.6;
cn4z2(5) = -81.3;
cn4z2(6) = -82;
for padd = 7:(length(cn4z2pre)+5)
   cn4z2(padd) = cn4z2pre(padd-5);
end
for n= 1:length(cn4z2)
   cn4y2(n) = -105;
end
cn4xi2 = interp1(z4,x4,cn4z2,'spline');

stp = 1;
for k = 1:49
   ncval = top4(k);   %starting point of 5 colour bands
   pcval = ncval/100;   %progressive point for each band
   ncval2 = top4(k+1);   %end point of 5 colour bands
   for j = stp:(stp+4)   %DIVIDE FIRST INTERVAL INTO 5 COLOUR BANDS
      colx(1) = cn4xi2(j);
      colx(2) = cn4xi2(j+1);
      coly(1) = cn4y2(j);
      coly(2) = cn4y2(j+1);
      colz(1) = cn4z2(j);
      colz(2) = cn4z2(j+1);
      cval = ((pcval*100)+((ncval2-ncval)/5))/100;
      cvalp = (cval+pcval)/2;   %average between two points for a colour
      cvalp = round(cvalp*100)+1;
      pcval = cval;
      plot3(colx,coly,colz,'Color',[gdmap(cvalp,1),gdmap(cvalp,2),gdmap(cvalp,3)],'Linewidth',0.75);   %[0,cvalp,0]
   end
stp = stp+5;
end
%****************************************************************

% CN5   %STARTS at -79.5 in z NOT -77
%cn5a = plot3(x5,y5,z5,'-g');
% 1mm interpolated contour lines for CN5
cn5z = min(z5):1:max(z5);
for n = 1:length(cn5z)
   cn5y(n) = -110;
end
cn5xi = interp1(z5,x5,cn5z,'spline');
%cn5 = plot3(cn5xi,cn5y,cn5z,'Linewidth',0.75);

%COLOURING CONTOUR CN5
if (z5(50) < z5(1))
   st = -1;
else
   st = 1;
end
cn5z2pre = z5(2):st:z5(50);
cn5z2(1) = -79.5;
cn5z2(2) = -80;
cn5z2(3) = -80.5;
cn5z2(4) = -81;
cn5z2(5) = -81.5;
cn5z2(6) = -82;
for padd = 7:(length(cn5z2pre)+5)
   cn5z2(padd) = cn5z2pre(padd-5);
end
for n= 1:length(cn5z2)
```

```
  cn5y2(n) = -110;
end
cn5xi2 = interp1(z5,x5,cn5z2,'spline');

stp = 1;
for k = 1:49
  ncval = top5(k);   %starting point of 5 colour bands
  pcval = ncval/100;   %progressive point for each band
  ncval2 = top5(k+1);   %end point of 5 colour bands
  for j = stp:(stp+4)   %DIVIDE FIRST INTERVAL INTO 5 COLOUR BANDS
    colx(1) = cn5xi2(j);
    colx(2) = cn5xi2(j+1);
    coly(1) = cn5y2(j);
    coly(2) = cn5y2(j+1);
    colz(1) = cn5z2(j);
    colz(2) = cn5z2(j+1);
    cval = ((pcval*100)+((ncval2-ncval)/5))/100;
    cvalp = (cval+pcval)/2;   %average between two points for a colour
    cvalp = round(cvalp*100)+1;
    pcval = cval;
    plot3(colx,coly,colz,'Color',[gdmap(cvalp,1),gdmap(cvalp,2),gdmap(cvalp,3)],'Linewidth',0.75);   %[0,cvalp,0]
  end
stp = stp+5;
end
%****************************************************************

% CN6   %STARTS at -80.5 in z NOT -77
%cn6a = plot3(x6,y6,z6,'-g');
% 1mm interpolated contour lines for CN6
cn6z = min(z6):1:max(z6);
for n = 1:length(cn6z)
  cn6y(n) = -115;
end
cn6xi = interp1(z6,x6,cn6z,'spline');
%cn6 = plot3(cn6xi,cn6y,cn6z,'Linewidth',0.75);

%COLOURING CONTOUR CN6
if (z6(50) < z6(1))
  st = -1;
else
  st = 1;
end
cn6z2pre = z6(2):st:z6(50);
cn6z2(1) = -80.5;
cn6z2(2) = -80.8;
cn6z2(3) = -81.1;
cn6z2(4) = -81.4;
cn6z2(5) = -81.7;
cn6z2(6) = -82;
for padd = 7:(length(cn6z2pre)+5)
  cn6z2(padd) = cn6z2pre(padd-5);
end
for n= 1:length(cn6z2)
  cn6y2(n) = -115;
end
cn6xi2 = interp1(z6,x6,cn6z2,'spline');

stp = 1;
for k = 1:49
  ncval = top6(k);   %starting point of 5 colour bands
  pcval = ncval/100;   %progressive point for each band
  ncval2 = top6(k+1);   %end point of 5 colour bands
  for j = stp:(stp+4)   %DIVIDE FIRST INTERVAL INTO 5 COLOUR BANDS
    colx(1) = cn6xi2(j);
    colx(2) = cn6xi2(j+1);
    coly(1) = cn6y2(j);
    coly(2) = cn6y2(j+1);
    colz(1) = cn6z2(j);
    colz(2) = cn6z2(j+1);
    cval = ((pcval*100)+((ncval2-ncval)/5))/100;
    cvalp = (cval+pcval)/2;   %average between two points for a colour
    cvalp = round(cvalp*100)+1;
    pcval = cval;
    plot3(colx,coly,colz,'Color',[gdmap(cvalp,1),gdmap(cvalp,2),gdmap(cvalp,3)],'Linewidth',0.75);   %[0,cvalp,0]
  end
stp = stp+5;
end
%****************************************************************

% CN7
%cn7a = plot3(x7,y7,z7,'-g');
% 1mm interpolated contour lines for CN7
cn7z = min(z7):1:max(z7);
for n = 1:length(cn7z)
  cn7y(n) = -120;
end
cn7xi = interp1(z7,x7,cn7z,'spline');
%cn7 = plot3(cn7xi,cn7y,cn7z,'Linewidth',0.75);

%COLOURING CONTOUR CN7
if (z7(49) < z7(1))
  st = -1;
else
  st = 1;
```

```
end
cn7z2 = z7(1):st:z7(49);
for n= 1:length(cn7z2)
  cn7y2(n) = -120;
end
cn7xi2 = interp1(z7,x7,cn7z2,'spline');
%cn7COL = plot3(cn7xi2,cn7y2,cn7z2,'r'); %INTERPOLATED COORDINATES BETWEEN 1ST AND 2ND POINTS IN CN7
stp = 1;
for k = 1:48
  ncval = top7(k);   %starting point of 5 colour bands
  pcval = ncval/100;   %progressive point for each band
  ncval2 = top7(k+1);   %end point of 5 colour bands
  for j = stp:(stp+4)   %DIVIDE FIRST INTERVAL INTO 5 COLOUR BANDS
    colx(1) = cn7xi2(j);
    colx(2) = cn7xi2(j+1);
    coly(1) = cn7y2(j);
    coly(2) = cn7y2(j+1);
    colz(1) = cn7z2(j);
    colz(2) = cn7z2(j+1);
    cval = ((pcval*100)+((ncval2-ncval)/5))/100;
    cvalp = (cval+pcval)/2;   %average between two points for a colour
    cvalp = round(cvalp*100)+1;
    pcval = cval;
    plot3(colx,coly,colz,'Color',[gdmap(cvalp,1),gdmap(cvalp,2),gdmap(cvalp,3)],'Linewidth',0.75);   %[0,cvalp,0]
  end
stp = stp+5;
end
%*****************************************************************

% CN8
%cn8a = plot3(x8,y8,z8,'-g');
% 1mm interpolated contour lines for CN8
cn8z = min(z8):1:max(z8);
for n = 1:length(cn8z)
  cn8y(n) = -125;
end
cn8xi = interp1(z8,x8,cn8z,'spline');
%cn8 = plot3(cn8xi,cn8y,cn8z,'Linewidth',0.75);

%COLOURING CONTOUR CN8
if (z8(49) < z8(1))
  st = -1;
else
  st = 1;
end
cn8z2pre = z8(2):st:z8(49);   %STARTS at z = -84 not -82
cn8z2(1) = -84;
cn8z2(2) = -84.6;
cn8z2(3) = -85.2;
cn8z2(4) = -85.8;
cn8z2(5) = -86.4;
cn8z2(6) = -87;
for padd = 7:(length(cn8z2pre)+5)
  cn8z2(padd) = cn8z2pre(padd-5);
end
for n= 1:length(cn8z2)
  cn8y2(n) = -125;
end
cn8xi2 = interp1(z8,x8,cn8z2,'spline');
%cn8COL = plot3(cn8xi2,cn8y2,cn8z2,'r'); %INTERPOLATED COORDINATES BETWEEN 1ST AND 2ND POINTS IN CN8
stp = 1;
for k = 1:48
  ncval = top8(k);   %starting point of 5 colour bands
  pcval = ncval/100;   %progressive point for each band
  ncval2 = top8(k+1);   %end point of 5 colour bands
  for j = stp:(stp+4)   %DIVIDE FIRST INTERVAL INTO 5 COLOUR BANDS
    colx(1) = cn8xi2(j);
    colx(2) = cn8xi2(j+1);
    coly(1) = cn8y2(j);
    coly(2) = cn8y2(j+1);
    colz(1) = cn8z2(j);
    colz(2) = cn8z2(j+1);
    cval = ((pcval*100)+((ncval2-ncval)/5))/100;
    cvalp = (cval+pcval)/2;   %average between two points for a colour
    cvalp = round(cvalp*100)+1;
    pcval = cval;
    plot3(colx,coly,colz,'Color',[gdmap(cvalp,1),gdmap(cvalp,2),gdmap(cvalp,3)],'Linewidth',0.75);   %[0,cvalp,0]
  end
stp = stp+5;
end
%*****************************************************************

% CN9
%cn9a = plot3(x9,y9,z9,'-g');
% 1mm interpolated contour lines for CN9
cn9z = min(z9):1:max(z9);
for n = 1:length(cn9z)
  cn9y(n) = -130;
end
cn9xi = interp1(z9,x9,cn9z,'spline');
%cn9 = plot3(cn9xi,cn9y,cn9z,'Linewidth',0.75);

%COLOURING CONTOUR CN9
if (z9(48) < z9(1))
```

```
  st = -1;
else
  st = 1;
end
cn9z2 = z9(1):st:z9(48);
for n= 1:length(cn9z2)
  cn9y2(n) = -130;
end
cn9xi2 = interp1(z9,x9,cn9z2,'spline');
%cn9COL = plot3(cn9xi2,cn9y2,cn9z2,'r'); %INTERPOLATED COORDINATES BETWEEN 1ST AND 2ND POINTS IN CN7
stp = 1;
for k = 1:47
  ncval = top9(k);   %starting point of 5 colour bands
  pcval = ncval/100;   %progressive point for each band
  ncval2 = top9(k+1);   %end point of 5 colour bands
  for j = stp:(stp+4)   %DIVIDE FIRST INTERVAL INTO 5 COLOUR BANDS
    colx(1) = cn9xi2(j);
    colx(2) = cn9xi2(j+1);
    coly(1) = cn9y2(j);
    coly(2) = cn9y2(j+1);
    colz(1) = cn9z2(j);
    colz(2) = cn9z2(j+1);
    cval = ((pcval*100)+((ncval2-ncval)/5))/100;
    cvalp = (cval+pcval)/2;   %average between two points for a colour
    cvalp = round(cvalp*100)+1;
    pcval = cval;
    plot3(colx,coly,colz,'Color',[gdmap(cvalp,1),gdmap(cvalp,2),gdmap(cvalp,3)],'Linewidth',0.75);   %[0,cvalp,0]
  end
stp = stp+5;
end
%**************************************************************

% CN10
%cn10a = plot3(x10,y10,z10,'-g');
% 1mm interpolated contour lines for CN10
cn10z = min(z10):1:max(z10);
for n = 1:length(cn10z)
  cn10y(n) = -135;
end
cn10xi = interp1(z10,x10,cn10z,'spline');
%cn10 = plot3(cn10xi,cn10y,cn10z,'Linewidth',0.75);

%COLOURING CONTOUR CN10
if (z10(48) < z10(1))
  st = -1;
else
  st = 1;
end
cn10z2pre = z10(2):st:z10(48);
cn10z2(1) = -89.5;
cn10z2(2) = -90;
cn10z2(3) = -90.5;
cn10z2(4) = -91;
cn10z2(5) = -91.5;
cn10z2(6) = -92;
for padd = 7:(length(cn10z2pre)+5)
  cn10z2(padd) = cn10z2pre(padd-5);
end
for n= 1:length(cn10z2)
  cn10y2(n) = -135;
end
cn10xi2 = interp1(z10,x10,cn10z2,'spline');
%cn10COL = plot3(cn10xi2,cn10y2,cn10z2,'r'); %INTERPOLATED COORDINATES BETWEEN 1ST AND 2ND POINTS IN CN7
stp = 1;
for k = 1:47
  ncval = top10(k);   %starting point of 5 colour bands
  pcval = ncval/100;   %progressive point for each band
  ncval2 = top10(k+1);   %end point of 5 colour bands
  for j = stp:(stp+4)   %DIVIDE FIRST INTERVAL INTO 5 COLOUR BANDS
    colx(1) = cn10xi2(j);
    colx(2) = cn10xi2(j+1);
    coly(1) = cn10y2(j);
    coly(2) = cn10y2(j+1);
    colz(1) = cn10z2(j);
    colz(2) = cn10z2(j+1);
    cval = ((pcval*100)+((ncval2-ncval)/5))/100;
    cvalp = (cval+pcval)/2;   %average between two points for a colour
    cvalp = round(cvalp*100)+1;
    pcval = cval;
    plot3(colx,coly,colz,'Color',[gdmap(cvalp,1),gdmap(cvalp,2),gdmap(cvalp,3)],'Linewidth',0.75);   %[0,cvalp,0]
  end
stp = stp+5;
end
%**************************************************************

% CN11
%cn11a = plot3(x11,y11,z11,'-g');
% 1mm interpolated contour lines for CN11
cn11z = min(z11):1:max(z11);
for n = 1:length(cn11z)
  cn11y(n) = -140;
end
cn11xi = interp1(z11,x11,cn11z,'spline');
%cn11 = plot3(cn11xi,cn11y,cn11z,'Linewidth',0.75);
```

```
%COLOURING CONTOUR CN11
if (z11(47) < z11(1))
  st = -1;
else
  st = 1;
end
cn11z2pre = z11(2):st:z11(47);
cn11z2(1) = -92.8;
cn11z2(2) = -93.64;
cn11z2(3) = -94.48;
cn11z2(4) = -95.32;
cn11z2(5) = -96.16;
cn11z2(6) = -97;
for padd = 7:(length(cn11z2pre)+5)
  cn11z2(padd) = cn11z2pre(padd-5);
end
for n= 1:length(cn11z2)
  cn11y2(n) = -140;
end
cn11xi2 = interp1(z11,x11,cn11z2,'spline');
%cn11COL = plot3(cn11xi2,cn11y2,cn11z2,'r'); %INTERPOLATED COORDINATES BETWEEN 1ST AND 2ND POINTS IN CN7
stp = 1;
for k = 1:46
  ncval = top11(k);   %starting point of 5 colour bands
  pcval = ncval/100;   %progressive point for each band
  ncval2 = top11(k+1);   %end point of 5 colour bands
  for j = stp:(stp+4)   %DIVIDE FIRST INTERVAL INTO 5 COLOUR BANDS
    colx(1) = cn11xi2(j);
    colx(2) = cn11xi2(j+1);
    coly(1) = cn11y2(j);
    coly(2) = cn11y2(j+1);
    colz(1) = cn11z2(j);
    colz(2) = cn11z2(j+1);
    cval = ((pcval*100)+((ncval2-ncval)/5))/100;
    cvalp = (cval+pcval)/2;   %average between two points for a colour
    cvalp = round(cvalp*100)+1;
    pcval = cval;
    plot3(colx,coly,colz,'Color',[gdmap(cvalp,1),gdmap(cvalp,2),gdmap(cvalp,3)],'Linewidth',0.75);   %[0,cvalp,0]
  end
stp = stp+5;
end
%****************************************************************

% CN12
%cn12a = plot3(x12,y12,z12,'-g');
% 1mm interpolated contour lines for CN12
cn12z = min(z12):1:max(z12);
for n = 1:length(cn12z)
  cn12y(n) = -145;
end
cn12xi = interp1(z12,x12,cn12z,'spline');
%cn12 = plot3(cn12xi,cn12y,cn12z,'Linewidth',0.75);

%COLOURING CONTOUR CN12
if (z12(46) < z12(1))
  st = -1;
else
  st = 1;
end
cn12z2 = z12(1):st:z12(46);
for n= 1:length(cn12z2)
  cn12y2(n) = -145;
end
cn12xi2 = interp1(z12,x12,cn12z2,'spline');
%cn12COL = plot3(cn12xi2,cn12y2,cn12z2,'r'); %INTERPOLATED COORDINATES BETWEEN 1ST AND 2ND POINTS IN CN7
stp = 1;
for k = 1:45
  ncval = top12(k);   %starting point of 5 colour bands
  pcval = ncval/100;   %progressive point for each band
  ncval2 = top12(k+1);   %end point of 5 colour bands
  for j = stp:(stp+4)   %DIVIDE FIRST INTERVAL INTO 5 COLOUR BANDS
    colx(1) = cn12xi2(j);
    colx(2) = cn12xi2(j+1);
    coly(1) = cn12y2(j);
    coly(2) = cn12y2(j+1);
    colz(1) = cn12z2(j);
    colz(2) = cn12z2(j+1);
    cval = ((pcval*100)+((ncval2-ncval)/5))/100;
    cvalp = (cval+pcval)/2;   %average between two points for a colour
    cvalp = round(cvalp*100)+1;
    pcval = cval;
    plot3(colx,coly,colz,'Color',[gdmap(cvalp,1),gdmap(cvalp,2),gdmap(cvalp,3)],'Linewidth',0.75);   %[0,cvalp,0]
  end
stp = stp+5;
end
%****************************************************************

% CN13
%cn13a = plot3(x13,y13,z13,'-g');
% 1mm interpolated contour lines for CN13
cn13z = min(z13):1:max(z13);
for n = 1:length(cn13z)
  cn13y(n) = -150;
```

```
end
cn13xi = interp1(z13,x13,cn13z,'spline');
%cn13 = plot3(cn13xi,cn13y,cn13z,'Linewidth',0.75);

%COLOURING CONTOUR CN13
if (z13(32) < z13(1))
  st = -1;
else
  st = 1;
end
cn13z2pre = z13(2):st:z13(32);
cn13z2(1) = -101.8;
cn13z2(2) = -102.84;
cn13z2(3) = -103.88;
cn13z2(4) = -104.92;
cn13z2(5) = -105.96;
cn13z2(6) = -107;
for padd = 7:(length(cn13z2pre)+5)
  cn13z2(padd) = cn13z2pre(padd-5);
end
for n= 1:length(cn13z2)
  cn13y2(n) = -150;
end
cn13xi2 = interp1(z13,x13,cn13z2,'spline');
%cn13COL = plot3(cn13xi2,cn13y2,cn12z2,'r'); %INTERPOLATED COORDINATES BETWEEN 1ST AND 2ND POINTS IN CN7
stp = 1;
for k = 1:31
  ncval = top13(k);   %starting point of 5 colour bands
  pcval = ncval/100;   %progressive point for each band
  ncval2 = top13(k+1);   %end point of 5 colour bands
  for j = stp:(stp+4)   %DIVIDE FIRST INTERVAL INTO 5 COLOUR BANDS
    colx(1) = cn13xi2(j);
    colx(2) = cn13xi2(j+1);
    coly(1) = cn13y2(j);
    coly(2) = cn13y2(j+1);
    colz(1) = cn13z2(j);
    colz(2) = cn13z2(j+1);
    cval = ((pcval*100)+((ncval2-ncval)/5))/100;
    cvalp = (cval+pcval)/2;   %average between two points for a colour
    cvalp = round(cvalp*100)+1;
    pcval = cval;
    plot3(colx,coly,colz,'Color',[gdmap(cvalp,1),gdmap(cvalp,2),gdmap(cvalp,3)],'Linewidth',0.75);   %[0,cvalp,0]
  end
stp = stp+5;
end
%**************************************************************

% CN14
%cn14a = plot3(x14,y14,z14,'-g');
% 1mm interpolated contour lines for CN14
cn14z = min(z14):1:max(z14);
for n = 1:length(cn14z)
  cn14y(n) = -155;
end
cn14xi = interp1(z14,x14,cn14z,'spline');
%cn14 = plot3(cn14xi,cn14y,cn14z,'Linewidth',0.75);

%COLOURING CONTOUR CN14
if (z14(28) < z14(1))
  st = -1;
else
  st = 1;
end
cn14z2 = z14(1):st:z14(28);
for n= 1:length(cn14z2)
  cn14y2(n) = -155;
end
cn14xi2 = interp1(z14,x14,cn14z2,'spline');
stp = 1;
for k = 1:27
  ncval = top14(k);   %starting point of 5 colour bands
  pcval = ncval/100;   %progressive point for each band
  ncval2 = top14(k+1);   %end point of 5 colour bands
  for j = stp:(stp+4)   %DIVIDE FIRST INTERVAL INTO 5 COLOUR BANDS
    colx(1) = cn14xi2(j);
    colx(2) = cn14xi2(j+1);
    coly(1) = cn14y2(j);
    coly(2) = cn14y2(j+1);
    colz(1) = cn14z2(j);
    colz(2) = cn14z2(j+1);
    cval = ((pcval*100)+((ncval2-ncval)/5))/100;
    cvalp = (cval+pcval)/2;   %average between two points for a colour
    cvalp = round(cvalp*100)+1;
    pcval = cval;
    plot3(colx,coly,colz,'Color',[gdmap(cvalp,1),gdmap(cvalp,2),gdmap(cvalp,3)],'Linewidth',0.75);   %[0,cvalp,0]
  end
stp = stp+5;
end
%**************************************************************

% CN15
%cn15a = plot3(x15,y15,z15,'-g');
% 1mm interpolated contour lines for CN15
cn15z = min(z15):1:max(z15);
```

```
for n = 1:length(cn15z)
  cn15y(n) = -160;
end
cn15xi = interp1(z15,x15,cn15z,'spline');
%cn15 = plot3(cn15xi,cn15y,cn15z,'Linewidth',0.75);

%COLOURING CONTOUR CN15
if (z15(26) < z15(1))
  st = -1;
else
  st = 1;
end
cn15z2pre = z15(2):st:z15(26);
cn15z2(1) = -117.4;
cn15z2(2) = -118.32;
cn15z2(3) = -119.24;
cn15z2(4) = -120.16;
cn15z2(5) = -121.08;
cn15z2(6) = -122;
for padd = 7:(length(cn15z2pre)+5)
  cn15z2(padd) = cn15z2pre(padd-5);
end
for n= 1:length(cn15z2)
  cn15y2(n) = -160;
end
cn15xi2 = interp1(z15,x15,cn15z2,'spline');
stp = 1;
for k = 1:25
  ncval = top15(k);   %starting point of 5 colour bands
  pcval = ncval/100;   %progressive point for each band
  ncval2 = top15(k+1);   %end point of 5 colour bands
  for j = stp:(stp+4)   %DIVIDE FIRST INTERVAL INTO 5 COLOUR BANDS
    colx(1) = cn15xi2(j);
    colx(2) = cn15xi2(j+1);
    coly(1) = cn15y2(j);
    coly(2) = cn15y2(j+1);
    colz(1) = cn15z2(j);
    colz(2) = cn15z2(j+1);
    cval = ((pcval*100)+((ncval2-ncval)/5))/100;
    cvalp = (cval+pcval)/2;   %average between two points for a colour
    cvalp = round(cvalp*100)+1;
    pcval = cval;
    plot3(colx,coly,colz,'Color',[gdmap(cvalp,1),gdmap(cvalp,2),gdmap(cvalp,3)],'Linewidth',0.75);   %[0,cvalp,0]
  end
stp = stp+5;
end
%*****************************************************************

% CN16
%cn16a = plot3(x16,y16,z16,'-g');
% 1mm interpolated contour lines for CN16
cn16z = min(z16):1:max(z16);
for n = 1:length(cn16z)
  cn16y(n) = -165;
end
cn16xi = interp1(z16,x16,cn16z,'spline');
%cn16 = plot3(cn16xi,cn16y,cn16z,'Linewidth',0.75);

%COLOURING CONTOUR CN16
if (z16(22) < z16(1))
  st = -1;
else
  st = 1;
end
cn16z2pre = z16(2):st:z16(22);
cn16z2(1) = -129.9;
cn16z2(2) = -131.32;
cn16z2(3) = -132.74;
cn16z2(4) = -134.16;
cn16z2(5) = -135.58;
cn16z2(6) = -137;
for padd = 7:(length(cn16z2pre)+5)
  cn16z2(padd) = cn16z2pre(padd-5);
end
for n= 1:length(cn16z2)
  cn16y2(n) = -165;
end
cn16xi2 = interp1(z16,x16,cn16z2,'spline');
stp = 1;
for k = 1:21
  ncval = top16(k);   %starting point of 5 colour bands
  pcval = ncval/100;   %progressive point for each band
  ncval2 = top16(k+1);   %end point of 5 colour bands
  for j = stp:(stp+4)   %DIVIDE FIRST INTERVAL INTO 5 COLOUR BANDS
    colx(1) = cn16xi2(j);
    colx(2) = cn16xi2(j+1);
    coly(1) = cn16y2(j);
    coly(2) = cn16y2(j+1);
    colz(1) = cn16z2(j);
    colz(2) = cn16z2(j+1);
    cval = ((pcval*100)+((ncval2-ncval)/5))/100;
    cvalp = (cval+pcval)/2;   %average between two points for a colour
    cvalp = round(cvalp*100)+1;
    pcval = cval;
```

```
    plot3(colx,coly,colz,'Color',[gdmap(cvalp,1),gdmap(cvalp,2),gdmap(cvalp,3)],'Linewidth',0.75);   %[0,cvalp,0]
  end
stp = stp+5;
end
%****************************************************************

% CN17
%cn17a = plot3(x17,y17,z17,'-g');
% 1mm interpolated contour lines for CN17
cn17z = min(z17):1:max(z17);
for n = 1:length(cn17z)
  cn17y(n) = -170;
end
cn17xi = interp1(z17,x17,cn17z,'spline');
%cn17 = plot3(cn17xi,cn17y,cn17z,'Linewidth',0.75);

%COLOURING CONTOUR CN17
if (z17(9) < z17(1))
  st = -1;
else
  st = 1;
end
cn17z2pre = z17(2):st:z17(9);
cn17z2(1) = -184;
cn17z2(2) = -184.6;
cn17z2(3) = -185.2;
cn17z2(4) = -185.8;
cn17z2(5) = -186.4;
cn17z2(6) = -187;
for padd = 7:(length(cn17z2pre)+5)
  cn17z2(padd) = cn17z2pre(padd-5);
end
for n= 1:length(cn17z2)
  cn17y2(n) = -170;
end
cn17xi2 = interp1(z17,x17,cn17z2,'spline');
stp = 1;
for k = 1:8
  ncval = top17(k);   %starting point of 5 colour bands
  pcval = ncval/100;   %progressive point for each band
  ncval2 = top17(k+1);   %end point of 5 colour bands
  for j = stp:(stp+4)   %DIVIDE FIRST INTERVAL INTO 5 COLOUR BANDS
    colx(1) = cn17xi2(j);
    colx(2) = cn17xi2(j+1);
    coly(1) = cn17y2(j);
    coly(2) = cn17y2(j+1);
    colz(1) = cn17z2(j);
    colz(2) = cn17z2(j+1);
    cval = ((pcval*100)+((ncval2-ncval)/5))/100;
    cvalp = (cval+pcval)/2;   %average between two points for a colour
    cvalp = round(cvalp*100)+1;
    pcval = cval;
    plot3(colx,coly,colz,'Color',[gdmap(cvalp,1),gdmap(cvalp,2),gdmap(cvalp,3)],'Linewidth',0.75);   %[0,cvalp,0]
  end
stp = stp+5;
end
%****************************************************************

% CN18
%cn18a = plot3(x18,y18,z18,'-g');
% 1mm interpolated contour lines for CN18
cn18z = min(z18):1:max(z18);
for n = 1:length(cn18z)
  cn18y(n) = -175;
end
cn18xi = interp1(z18,x18,cn18z,'spline');
%cn18 = plot3(cn18xi,cn18y,cn18z,'Linewidth',0.75);

%COLOURING CONTOUR CN18
if (z18(5) < z18(1))
  st = -1;
else
  st = 1;
end
cn18z2pre = z18(2):st:z18(5);
cn18z2(1) = -189;
cn18z2(2) = -190.6;
cn18z2(3) = -192.2;
cn18z2(4) = -193.8;
cn18z2(5) = -195.4;
cn18z2(6) = -197;
for padd = 7:(length(cn18z2pre)+5)
  cn18z2(padd) = cn18z2pre(padd-5);
end
for n= 1:length(cn18z2)
  cn18y2(n) = -175;
end
cn18xi2 = interp1(z18,x18,cn18z2,'spline');
stp = 1;
for k = 1:4
  ncval = top18(k);   %starting point of 5 colour bands
  pcval = ncval/100;   %progressive point for each band
  ncval2 = top18(k+1);   %end point of 5 colour bands
  for j = stp:(stp+4)   %DIVIDE FIRST INTERVAL INTO 5 COLOUR BANDS
```

```
    colx(1) = cn18xi2(j);
    colx(2) = cn18xi2(j+1);
    coly(1) = cn18y2(j);
    coly(2) = cn18y2(j+1);
    colz(1) = cn18z2(j);
    colz(2) = cn18z2(j+1);
    cval = ((pcval*100)+((ncval2-ncval)/5))/100;
    cvalp = (cval+pcval)/2;   %average between two points for a colour
    cvalp = round(cvalp*100)+1;
    pcval = cval;
    plot3(colx,coly,colz,'Color',[gdmap(cvalp,1),gdmap(cvalp,2),gdmap(cvalp,3)],'Linewidth',0.75);   %[0,cvalp,0]
  end
stp = stp+5;
end
%****************************************************************

%###########################################################################
%###########################################################################
%###########################################################################
% HORIZONTAL CONTOURS
%FIRST COLUMN------------------------------------------------------------------------------------------------------------------------
%CX1
xx1 = [x1(2),x2(2),x3(2),x4(2),x5(2),x6(2),x7(1)];
yx1 = [y1(2),y2(2),y3(2),y4(2),y5(2),y6(2),y7(1)];
zx1 = [z1(2),z2(2),z3(2),z4(2),z5(2),z6(2),z7(1)];

topx1 = [top7(1),top6(2),top5(2),top4(2),top3(2),top2(2),top1(2)];
for n = 1:7
  co = top1(n)/100;
  %plot3(xx1(n),yx1(n),zx1(n),'.','Markersize', 20,'Color',[0,co,0]);
end

%INTERPOLATED CONTOUR CX1
% 1mm interpolated contour lines for CX1
cn1yx = min(yx1):1:max(yx1);
for n = 1:length(cn1yx)
  cn1zx(n) = zx1(1);
end
cn1xxi = interp1(yx1,xx1,cn1yx,'spline');
%cn1x = plot3(cn1xxi,cn1yx,cn1zx,'Linewidth',0.75);

stp = 1;
for k = 1:6
  ncval = topx1(k);   %starting point of 5 colour bands
  pcval = ncval/100;   %progressive point for each band
  ncval2 = topx1(k+1);   %end point of 5 colour bands
  for j = stp:(stp+4)   %DIVIDE FIRST INTERVAL INTO 5 COLOUR BANDS
    colx(1) = cn1xxi(j);
    colx(2) = cn1xxi(j+1);
    coly(1) = cn1yx(j);
    coly(2) = cn1yx(j+1);
    colz(1) = cn1zx(j);
    colz(2) = cn1zx(j+1);
    cval = ((pcval*100)+((ncval2-ncval)/5))/100;
    cvalp = (cval+pcval)/2;   %average between two points for a colour
    cvalp = round(cvalp*100)+1;
    pcval = cval;
    plot3(colx,coly,colz,'Color',[gdmap(cvalp,1),gdmap(cvalp,2),gdmap(cvalp,3)],'Linewidth',0.75);   %[0,cvalp,0]
  end
stp = stp+5;
end

%CX2
xx2 = [x1(3),x2(3),x3(3),x4(3),x5(3),x6(3),x7(2),x8(2),x9(1)];
yx2 = [y1(3),y2(3),y3(3),y4(3),y5(3),y6(3),y7(2),y8(2),y9(1)];
zx2 = [z1(3),z2(3),z3(3),z4(3),z5(3),z6(3),z7(2),z8(2),z9(1)];

topx2 = [top9(1),top8(2),top7(2),top6(3),top5(3),top4(3),top3(3),top2(3),top1(3)];
for n = 1:9
  co = top1(n)/100;
  %plot3(xx2(n),yx2(n),zx2(n),'.','Markersize', 20,'Color',[0,co,0]);
end

%INTERPOLATED CONTOUR CX2
% 1mm interpolated contour lines for CX2
cn2yx = min(yx2):1:max(yx2);
for n = 1:length(cn2yx)
  cn2zx(n) = zx2(1);
end
cn2xxi = interp1(yx2,xx2,cn2yx,'spline');
%cn2x = plot3(cn2xxi,cn2yx,cn2zx,'Linewidth',0.75);

stp = 1;
for k = 1:8
  ncval = topx2(k);   %starting point of 5 colour bands
  pcval = ncval/100;   %progressive point for each band
  ncval2 = topx2(k+1);   %end point of 5 colour bands
  for j = stp:(stp+4)   %DIVIDE FIRST INTERVAL INTO 5 COLOUR BANDS
    colx(1) = cn2xxi(j);
    colx(2) = cn2xxi(j+1);
    coly(1) = cn2yx(j);
    coly(2) = cn2yx(j+1);
    colz(1) = cn2zx(j);
    colz(2) = cn2zx(j+1);
```

```
    cval = ((pcval*100)+((ncval2-ncval)/5))/100;
    cvalp = (cval+pcval)/2;   %average between two points for a colour
    cvalp = round(cvalp*100)+1;
    pcval = cval;
    plot3(colx,coly,colz,'Color',[gdmap(cvalp,1),gdmap(cvalp,2),gdmap(cvalp,3)],'Linewidth',0.75);   %[0,cvalp,0]
  end
stp = stp+5;
end

%CX3
xx3 = [x1(4),x2(4),x3(4),x4(4),x5(4),x6(4),x7(3),x8(3),x9(2),x10(2),x11(1)];
yx3 = [y1(4),y2(4),y3(4),y4(4),y5(4),y6(4),y7(3),y8(3),y9(2),y10(2),y11(1)];
zx3 = [z1(4),z2(4),z3(4),z4(4),z5(4),z6(4),z7(3),z8(3),z9(2),z10(2),z11(1)];

topx3 = [top11(1),top10(2),top9(2),top8(3),top7(3),top6(4),top5(4),top4(4),top3(4),top2(4),top1(4)];
for n = 1:11
  co = top1(n)/100;
  %plot3(xx3(n),yx3(n),zx3(n),'.','Markersize', 20,'Color',[0,co,0]);
end

%INTERPOLATED CONTOUR CX3
% 1mm interpolated contour lines for CX3
cn3yx = min(yx3):1:max(yx3);
for n = 1:length(cn3yx)
  cn3zx(n) = zx3(1);
end
cn3xxi = interp1(yx3,xx3,cn3yx,'spline');
%cn3x = plot3(cn3xxi,cn3yx,cn3zx,'Linewidth',0.75);

stp = 1;
for k = 1:10
  ncval = topx3(k);   %starting point of 5 colour bands
  pcval = ncval/100;   %progressive point for each band
  ncval2 = topx3(k+1);   %end point of 5 colour bands
  for j = stp:(stp+4)   %DIVIDE FIRST INTERVAL INTO 5 COLOUR BANDS
    colx(1) = cn3xxi(j);
    colx(2) = cn3xxi(j+1);
    coly(1) = cn3yx(j);
    coly(2) = cn3yx(j+1);
    colz(1) = cn3zx(j);
    colz(2) = cn3zx(j+1);
    cval = ((pcval*100)+((ncval2-ncval)/5))/100;
    cvalp = (cval+pcval)/2;   %average between two points for a colour
    cvalp = round(cvalp*100)+1;
    pcval = cval;
    plot3(colx,coly,colz,'Color',[gdmap(cvalp,1),gdmap(cvalp,2),gdmap(cvalp,3)],'Linewidth',0.75);   %[0,cvalp,0]
  end
stp = stp+5;
end

%CX4
xx4 = [x1(5),x2(5),x3(5),x4(5),x5(5),x6(5),x7(4),x8(4),x9(3),x10(3),x11(2),x12(1)];
yx4 = [y1(5),y2(5),y3(5),y4(5),y5(5),y6(5),y7(4),y8(4),y9(3),y10(3),y11(2),y12(1)];
zx4 = [z1(5),z2(5),z3(5),z4(5),z5(5),z6(5),z7(4),z8(4),z9(3),z10(3),z11(2),z12(1)];

topx4 = [top12(1),top11(2),top10(3),top9(3),top8(4),top7(4),top6(5),top5(5),top4(5),top3(5),top2(5),top1(5)];
for n = 1:12
  co = top1(n)/100;
  %plot3(xx4(n),yx4(n),zx4(n),'.','Markersize', 20,'Color',[0,co,0]);
end

%INTERPOLATED CONTOUR CX4
% 1mm interpolated contour lines for CX4
cn4yx = min(yx4):1:max(yx4);
for n = 1:length(cn4yx)
  cn4zx(n) = zx4(1);
end
cn4xxi = interp1(yx4,xx4,cn4yx,'spline');
%cn4x = plot3(cn4xxi,cn4yx,cn4zx,'Linewidth',0.75);

stp = 1;
for k = 1:11
  ncval = topx4(k);   %starting point of 5 colour bands
  pcval = ncval/100;   %progressive point for each band
  ncval2 = topx4(k+1);   %end point of 5 colour bands
  for j = stp:(stp+4)   %DIVIDE FIRST INTERVAL INTO 5 COLOUR BANDS
    colx(1) = cn4xxi(j);
    colx(2) = cn4xxi(j+1);
    coly(1) = cn4yx(j);
    coly(2) = cn4yx(j+1);
    colz(1) = cn4zx(j);
    colz(2) = cn4zx(j+1);
    cval = ((pcval*100)+((ncval2-ncval)/5))/100;
    cvalp = (cval+pcval)/2;   %average between two points for a colour
    cvalp = round(cvalp*100)+1;
    pcval = cval;
    plot3(colx,coly,colz,'Color',[gdmap(cvalp,1),gdmap(cvalp,2),gdmap(cvalp,3)],'Linewidth',0.75);   %[0,cvalp,0]
  end
stp = stp+5;
end

%CX5
xx5 = [x1(6),x2(6),x3(6),x4(6),x5(6),x6(6),x7(5),x8(5),x9(4),x10(4),x11(3),x12(2),x13(1)];
yx5 = [y1(6),y2(6),y3(6),y4(6),y5(6),y6(6),y7(5),y8(5),y9(4),y10(4),y11(3),y12(2),y13(1)];
```

```
zx5 = [z1(6),z2(6),z3(6),z4(6),z5(6),z6(6),z7(5),z8(5),z9(4),z10(4),z11(3),z12(2),z13(1)];

topx5 = [top13(1),top12(2),top11(3),top10(4),top9(4),top8(5),top7(5),top6(6),top5(6),top4(6),top3(6),top2(6),top1(6)];
for n = 1:13
  co = top1(n)/100;
  %plot3(xx5(n),yx5(n),zx5(n),'.','Markersize', 20,'Color',[0,co,0]);
end

%INTERPOLATED CONTOUR CX5
% 1mm interpolated contour lines for CX5
cn5yx = min(yx5):1:max(yx5);
for n = 1:length(cn5yx)
  cn5zx(n) = zx5(1);
end
cn5xxi = interp1(yx5,xx5,cn5yx,'spline');
%cn5x = plot3(cn5xxi,cn5yx,cn5zx,'Linewidth',0.75);

stp = 1;
for k = 1:12
  ncval = topx5(k);   %starting point of 5 colour bands
  pcval = ncval/100;   %progressive point for each band
  ncval2 = topx5(k+1);   %end point of 5 colour bands
  for j = stp:(stp+4)   %DIVIDE FIRST INTERVAL INTO 5 COLOUR BANDS
    colx(1) = cn5xxi(j);
    colx(2) = cn5xxi(j+1);
    coly(1) = cn5yx(j);
    coly(2) = cn5yx(j+1);
    colz(1) = cn5zx(j);
    colz(2) = cn5zx(j+1);
    cval = ((pcval*100)+((ncval2-ncval)/5))/100;
    cvalp = (cval+pcval)/2;   %average between two points for a colour
    cvalp = round(cvalp*100)+1;
    pcval = cval;
    plot3(colx,coly,colz,'Color',[gdmap(cvalp,1),gdmap(cvalp,2),gdmap(cvalp,3)],'Linewidth',0.75);   %[0,cvalp,0]
  end
stp = stp+5;
end

%CX6
xx6 = [x1(7),x2(7),x3(7),x4(7),x5(7),x6(7),x7(6),x8(6),x9(5),x10(5),x11(4),x12(3),x13(2),x14(1)];
yx6 = [y1(7),y2(7),y3(7),y4(7),y5(7),y6(7),y7(6),y8(6),y9(5),y10(5),y11(4),y12(3),y13(2),y14(1)];
zx6 = [z1(7),z2(7),z3(7),z4(7),z5(7),z6(7),z7(6),z8(6),z9(5),z10(5),z11(4),z12(3),z13(2),z14(1)];

topx6 = [top14(1),top13(2),top12(3),top11(4),top10(5),top9(5),top8(6),top7(6),top6(7),top5(7),top4(7),top3(7),top2(7),top1(7)];
for n = 1:14
  co = top1(n)/100;
  %plot3(xx6(n),yx6(n),zx6(n),'.','Markersize', 20,'Color',[0,co,0]);
end

%INTERPOLATED CONTOUR CX6
% 1mm interpolated contour lines for CX6
cn6yx = min(yx6):1:max(yx6);
for n = 1:length(cn6yx)
  cn6zx(n) = zx6(1);
end
cn6xxi = interp1(yx6,xx6,cn6yx,'spline');
%cn6x = plot3(cn6xxi,cn6yx,cn6zx,'Linewidth',0.75);

stp = 1;
for k = 1:13
  ncval = topx6(k);   %starting point of 5 colour bands
  pcval = ncval/100;   %progressive point for each band
  ncval2 = topx6(k+1);   %end point of 5 colour bands
  for j = stp:(stp+4)   %DIVIDE FIRST INTERVAL INTO 5 COLOUR BANDS
    colx(1) = cn6xxi(j);
    colx(2) = cn6xxi(j+1);
    coly(1) = cn6yx(j);
    coly(2) = cn6yx(j+1);
    colz(1) = cn6zx(j);
    colz(2) = cn6zx(j+1);
    cval = ((pcval*100)+((ncval2-ncval)/5))/100;
    cvalp = (cval+pcval)/2;   %average between two points for a colour
    cvalp = round(cvalp*100)+1;
    pcval = cval;
    plot3(colx,coly,colz,'Color',[gdmap(cvalp,1),gdmap(cvalp,2),gdmap(cvalp,3)],'Linewidth',0.75);   %[0,cvalp,0]
  end
stp = stp+5;
end

%CX7
xx7 = [x1(8),x2(8),x3(8),x4(8),x5(8),x6(8),x7(7),x8(7),x9(6),x10(6),x11(5),x12(4),x13(3),x14(2)];
yx7 = [y1(8),y2(8),y3(8),y4(8),y5(8),y6(8),y7(7),y8(7),y9(6),y10(6),y11(5),y12(4),y13(3),y14(2)];
zx7 = [z1(8),z2(8),z3(8),z4(8),z5(8),z6(8),z7(7),z8(7),z9(6),z10(6),z11(5),z12(4),z13(3),z14(2)];

topx7 = [top14(2),top13(3),top12(4),top11(5),top10(6),top9(6),top8(7),top7(7),top6(8),top5(8),top4(8),top3(8),top2(8),top1(8)];
for n = 1:14
  co = top1(n)/100;
  %plot3(xx7(n),yx7(n),zx7(n),'.','Markersize', 20,'Color',[0,co,0]);
end

%INTERPOLATED CONTOUR CX7
% 1mm interpolated contour lines for CX7
cn7yx = min(yx7):1:max(yx7);
for n = 1:length(cn7yx)
```

```
  cn7zx(n) = zx7(1);
end
cn7xxi = interp1(yx7,xx7,cn7yx,'spline');
%cn7x = plot3(cn7xxi,cn7yx,cn7zx,'Linewidth',0.75);

stp = 1;
for k = 1:13
  ncval = topx7(k);   %starting point of 5 colour bands
  pcval = ncval/100;   %progressive point for each band
  ncval2 = topx7(k+1);   %end point of 5 colour bands
  for j = stp:(stp+4)   %DIVIDE FIRST INTERVAL INTO 5 COLOUR BANDS
    colx(1) = cn7xxi(j);
    colx(2) = cn7xxi(j+1);
    coly(1) = cn7yx(j);
    coly(2) = cn7yx(j+1);
    colz(1) = cn7zx(j);
    colz(2) = cn7zx(j+1);
    cval = ((pcval*100)+((ncval2-ncval)/5))/100;
    cvalp = (cval+pcval)/2;   %average between two points for a colour
    cvalp = round(cvalp*100)+1;
    pcval = cval;
    plot3(colx,coly,colz,'Color',[gdmap(cvalp,1),gdmap(cvalp,2),gdmap(cvalp,3)],'Linewidth',0.75);   %[0,cvalp,0]
  end
stp = stp+5;
end

%CX8
xx8 = [x1(9),x2(9),x3(9),x4(9),x5(9),x6(9),x7(8),x8(8),x9(7),x10(7),x11(6),x12(5),x13(4),x14(3),x15(1)];
yx8 = [y1(9),y2(9),y3(9),y4(9),y5(9),y6(9),y7(8),y8(8),y9(7),y10(7),y11(6),y12(5),y13(4),y14(3),y15(1)];
zx8 = [z1(9),z2(9),z3(9),z4(9),z5(9),z6(9),z7(8),z8(8),z9(7),z10(7),z11(6),z12(5),z13(4),z14(3),z15(1)];

topx8 = [top15(1),top14(3),top13(4),top12(5),top11(6),top10(7),top9(7),top8(8),top7(8),top6(9),top5(9),top4(9),top3(9),top2(9),top1(9)];
for n = 1:15
  co = top1(n)/100;
  %plot3(xx8(n),yx8(n),zx8(n),'.','Markersize', 20,'Color',[0,co,0]);
end

%INTERPOLATED CONTOUR CX8
% 1mm interpolated contour lines for CX8
cn8yx = min(yx8):1:max(yx8);
for n = 1:length(cn8yx)
  cn8zx(n) = zx8(1);
end
cn8xxi = interp1(yx8,xx8,cn8yx,'spline');
%cn8x = plot3(cn8xxi,cn8yx,cn8zx,'Linewidth',0.75);

stp = 1;
for k = 1:14
  ncval = topx8(k);   %starting point of 5 colour bands
  pcval = ncval/100;   %progressive point for each band
  ncval2 = topx8(k+1);   %end point of 5 colour bands
  for j = stp:(stp+4)   %DIVIDE FIRST INTERVAL INTO 5 COLOUR BANDS
    colx(1) = cn8xxi(j);
    colx(2) = cn8xxi(j+1);
    coly(1) = cn8yx(j);
    coly(2) = cn8yx(j+1);
    colz(1) = cn8zx(j);
    colz(2) = cn8zx(j+1);
    cval = ((pcval*100)+((ncval2-ncval)/5))/100;
    cvalp = (cval+pcval)/2;   %average between two points for a colour
    cvalp = round(cvalp*100)+1;
    pcval = cval;
    plot3(colx,coly,colz,'Color',[gdmap(cvalp,1),gdmap(cvalp,2),gdmap(cvalp,3)],'Linewidth',0.75);   %[0,cvalp,0]
  end
stp = stp+5;
end

%CX9
xx9 = [x1(10),x2(10),x3(10),x4(10),x5(10),x6(10),x7(9),x8(9),x9(8),x10(8),x11(7),x12(6),x13(5),x14(4),x15(2)];
yx9 = [y1(10),y2(10),y3(10),y4(10),y5(10),y6(10),y7(9),y8(9),y9(8),y10(8),y11(7),y12(6),y13(5),y14(4),y15(2)];
zx9 = [z1(10),z2(10),z3(10),z4(10),z5(10),z6(10),z7(9),z8(9),z9(8),z10(8),z11(7),z12(6),z13(5),z14(4),z15(2)];

topx9 = [top15(2),top14(4),top13(5),top12(6),top11(7),top10(8),top9(8),top8(9),top7(9),top6(10),top5(10),top4(10),top3(10),top2(10),top1(10)];
for n = 1:15
  co = top1(n)/100;
  %plot3(xx9(n),yx9(n),zx9(n),'.','Markersize', 20,'Color',[0,co,0]);
end

%INTERPOLATED CONTOUR CX9
% 1mm interpolated contour lines for CX9
cn9yx = min(yx9):1:max(yx9);
for n = 1:length(cn9yx)
  cn9zx(n) = zx9(1);
end
cn9xxi = interp1(yx9,xx9,cn9yx,'spline');
%cn9x = plot3(cn9xxi,cn9yx,cn9zx,'Linewidth',0.75);

stp = 1;
for k = 1:14
  ncval = topx9(k);   %starting point of 5 colour bands
  pcval = ncval/100;   %progressive point for each band
  ncval2 = topx9(k+1);   %end point of 5 colour bands
  for j = stp:(stp+4)   %DIVIDE FIRST INTERVAL INTO 5 COLOUR BANDS
    colx(1) = cn9xxi(j);
```

```
    colx(2) = cn9xxi(j+1);
    coly(1) = cn9yx(j);
    coly(2) = cn9yx(j+1);
    colz(1) = cn9zx(j);
    colz(2) = cn9zx(j+1);
    cval = ((pcval*100)+((ncval2-ncval)/5))/100;
    cvalp = (cval+pcval)/2;   %average between two points for a colour
    cvalp = round(cvalp*100)+1;
    pcval = cval;
    plot3(colx,coly,colz,'Color',[gdmap(cvalp,1),gdmap(cvalp,2),gdmap(cvalp,3)],'Linewidth',0.75);   %[0,cvalp,0]
  end
stp = stp+5;
end

%CX10
xx10 = [x1(11),x2(11),x3(11),x4(11),x5(11),x6(11),x7(10),x8(10),x9(9),x10(9),x11(8),x12(7),x13(6),x14(5),x15(3)];
yx10 = [y1(11),y2(11),y3(11),y4(11),y5(11),y6(11),y7(10),y8(10),y9(9),y10(9),y11(8),y12(7),y13(6),y14(5),y15(3)];
zx10 = [z1(11),z2(11),z3(11),z4(11),z5(11),z6(11),z7(10),z8(10),z9(9),z10(9),z11(8),z12(7),z13(6),z14(5),z15(3)];

topx10 = [top15(3),top14(5),top13(6),top12(7),top11(8),top10(9),top9(9),top8(10),top7(10),top6(11),top5(11),top4(11),top3(11),top2(11),top1(11)];
for n = 1:15
  co = top1(n)/100;
  %plot3(xx10(n),yx10(n),zx10(n),'.','Markersize', 20,'Color',[0,co,0]);
end

%INTERPOLATED CONTOUR CX10
% 1mm interpolated contour lines for CX10
cn10yx = min(yx10):1:max(yx10);
for n = 1:length(cn10yx)
  cn10zx(n) = zx10(1);
end
cn10xxi = interp1(yx10,xx10,cn10yx,'spline');
%cn10x = plot3(cn10xxi,cn10yx,cn10zx,'Linewidth',0.75);

stp = 1;
for k = 1:14
  ncval = topx10(k);   %starting point of 5 colour bands
  pcval = ncval/100;   %progressive point for each band
  ncval2 = topx10(k+1);   %end point of 5 colour bands
  for j = stp:(stp+4)   %DIVIDE FIRST INTERVAL INTO 5 COLOUR BANDS
    colx(1) = cn10xxi(j);
    colx(2) = cn10xxi(j+1);
    coly(1) = cn10yx(j);
    coly(2) = cn10yx(j+1);
    colz(1) = cn10zx(j);
    colz(2) = cn10zx(j+1);
    cval = ((pcval*100)+((ncval2-ncval)/5))/100;
    cvalp = (cval+pcval)/2;   %average between two points for a colour
    cvalp = round(cvalp*100)+1;
    pcval = cval;
    plot3(colx,coly,colz,'Color',[gdmap(cvalp,1),gdmap(cvalp,2),gdmap(cvalp,3)],'Linewidth',0.75);   %[0,cvalp,0]
  end
stp = stp+5;
end

%CX11
xx11 = [x1(12),x2(12),x3(12),x4(12),x5(12),x6(12),x7(11),x8(11),x9(10),x10(10),x11(9),x12(8),x13(7),x14(6),x15(4),x16(1)];
yx11 = [y1(12),y2(12),y3(12),y4(12),y5(12),y6(12),y7(11),y8(11),y9(10),y10(10),y11(9),y12(8),y13(7),y14(6),y15(4),y16(1)];
zx11 = [z1(12),z2(12),z3(12),z4(12),z5(12),z6(12),z7(11),z8(11),z9(10),z10(10),z11(9),z12(8),z13(7),z14(6),z15(4),z16(1)];

topx11 = [top16(1),top15(4),top14(6),top13(7),top12(8),top11(9),top10(10),top9(10),top8(11),top7(11),top6(12),top5(12),top4(12),top3(12),top2(12),top1(12)];
for n = 1:16
  co = top1(n)/100;
  %plot3(xx11(n),yx11(n),zx11(n),'.','Markersize', 20,'Color',[0,co,0]);
end

%INTERPOLATED CONTOUR CX11
% 1mm interpolated contour lines for CX11
cn11yx = min(yx11):1:max(yx11);
for n = 1:length(cn11yx)
  cn11zx(n) = zx11(1);
end
cn11xxi = interp1(yx11,xx11,cn11yx,'spline');
%cn11x = plot3(cn11xxi,cn11yx,cn11zx,'Linewidth',0.75);

stp = 1;
for k = 1:15
  ncval = topx11(k);   %starting point of 5 colour bands
  pcval = ncval/100;   %progressive point for each band
  ncval2 = topx11(k+1);   %end point of 5 colour bands
  for j = stp:(stp+4)   %DIVIDE FIRST INTERVAL INTO 5 COLOUR BANDS
    colx(1) = cn11xxi(j);
    colx(2) = cn11xxi(j+1);
    coly(1) = cn11yx(j);
    coly(2) = cn11yx(j+1);
    colz(1) = cn11zx(j);
    colz(2) = cn11zx(j+1);
    cval = ((pcval*100)+((ncval2-ncval)/5))/100;
    cvalp = (cval+pcval)/2;   %average between two points for a colour
    cvalp = round(cvalp*100)+1;
    pcval = cval;
    plot3(colx,coly,colz,'Color',[gdmap(cvalp,1),gdmap(cvalp,2),gdmap(cvalp,3)],'Linewidth',0.75);   %[0,cvalp,0]
  end
stp = stp+5;
```

```
end

%CX12
xx12 = [x1(13),x2(13),x3(13),x4(13),x5(13),x6(13),x7(12),x8(12),x9(11),x10(11),x11(10),x12(9),x13(8),x14(7),x15(5),x16(2)];
yx12 = [y1(13),y2(13),y3(13),y4(13),y5(13),y6(13),y7(12),y8(12),y9(11),y10(11),y11(10),y12(9),y13(8),y14(7),y15(5),y16(2)];
zx12 = [z1(13),z2(13),z3(13),z4(13),z5(13),z6(13),z7(12),z8(12),z9(11),z10(11),z11(10),z12(9),z13(8),z14(7),z15(5),z16(2)];

topx12 = [top16(2),top15(5),top14(7),top13(8),top12(9),top11(10),top10(11),top9(11),top8(12),top7(12),top6(13),top5(13),top4(13),top3(13),top2(13),top1(13)];
for n = 1:16
  co = top1(n)/100;
  %plot3(xx12(n),yx12(n),zx12(n),'.','Markersize', 20,'Color',[0,co,0]);
end

%INTERPOLATED CONTOUR CX12
% 1mm interpolated contour lines for CX12
cn12yx = min(yx12):1:max(yx12);
for n = 1:length(cn12yx)
  cn12zx(n) = zx12(1);
end
cn12xxi = interp1(yx12,xx12,cn12yx,'spline');
%cn12x = plot3(cn12xxi,cn12yx,cn12zx,'Linewidth',0.75);

stp = 1;
for k = 1:15
  ncval = topx12(k);   %starting point of 5 colour bands
  pcval = ncval/100;   %progressive point for each band
  ncval2 = topx12(k+1);   %end point of 5 colour bands
  for j = stp:(stp+4)   %DIVIDE FIRST INTERVAL INTO 5 COLOUR BANDS
    colx(1) = cn12xxi(j);
    colx(2) = cn12xxi(j+1);
    coly(1) = cn12yx(j);
    coly(2) = cn12yx(j+1);
    colz(1) = cn12zx(j);
    colz(2) = cn12zx(j+1);
    cval = ((pcval*100)+((ncval2-ncval)/5))/100;
    cvalp = (cval+pcval)/2;   %average between two points for a colour
    cvalp = round(cvalp*100)+1;
    pcval = cval;
    plot3(colx,coly,colz,'Color',[gdmap(cvalp,1),gdmap(cvalp,2),gdmap(cvalp,3)],'Linewidth',0.75);   %[0,cvalp,0]
  end
stp = stp+5;
end

%CX13
xx13 = [x1(14),x2(14),x3(14),x4(14),x5(14),x6(14),x7(13),x8(13),x9(12),x10(12),x11(11),x12(10),x13(9),x14(8),x15(6),x16(3)];
yx13 = [y1(14),y2(14),y3(14),y4(14),y5(14),y6(14),y7(13),y8(13),y9(12),y10(12),y11(11),y12(10),y13(9),y14(8),y15(6),y16(3)];
zx13 = [z1(14),z2(14),z3(14),z4(14),z5(14),z6(14),z7(13),z8(13),z9(12),z10(12),z11(11),z12(10),z13(9),z14(8),z15(6),z16(3)];

topx13 = [top16(3),top15(6),top14(8),top13(9),top12(10),top11(11),top10(12),top9(12),top8(13),top7(13),top6(14),top5(14),top4(14),top3(14),top2(14),top1(14)];
for n = 1:16
  co = top1(n)/100;
  %plot3(xx13(n),yx13(n),zx13(n),'.','Markersize', 20,'Color',[0,co,0]);
end

%INTERPOLATED CONTOUR CX13
% 1mm interpolated contour lines for CX13
cn13yx = min(yx13):1:max(yx13);
for n = 1:length(cn13yx)
  cn13zx(n) = zx13(1);
end
cn13xxi = interp1(yx13,xx13,cn13yx,'spline');
%cn13x = plot3(cn13xxi,cn13yx,cn13zx,'Linewidth',0.75);

stp = 1;
for k = 1:15
  ncval = topx13(k);   %starting point of 5 colour bands
  pcval = ncval/100;   %progressive point for each band
  ncval2 = topx13(k+1);   %end point of 5 colour bands
  for j = stp:(stp+4)   %DIVIDE FIRST INTERVAL INTO 5 COLOUR BANDS
    colx(1) = cn13xxi(j);
    colx(2) = cn13xxi(j+1);
    coly(1) = cn13yx(j);
    coly(2) = cn13yx(j+1);
    colz(1) = cn13zx(j);
    colz(2) = cn13zx(j+1);
    cval = ((pcval*100)+((ncval2-ncval)/5))/100;
    cvalp = (cval+pcval)/2;   %average between two points for a colour
    cvalp = round(cvalp*100)+1;
    pcval = cval;
    plot3(colx,coly,colz,'Color',[gdmap(cvalp,1),gdmap(cvalp,2),gdmap(cvalp,3)],'Linewidth',0.75);   %[0,cvalp,0]
  end
stp = stp+5;
end

%CX14
xx14 = [x1(15),x2(15),x3(15),x4(15),x5(15),x6(15),x7(14),x8(14),x9(13),x10(13),x11(12),x12(11),x13(10),x14(9),x15(7),x16(4)];
yx14 = [y1(15),y2(15),y3(15),y4(15),y5(15),y6(15),y7(14),y8(14),y9(13),y10(13),y11(12),y12(11),y13(10),y14(9),y15(7),y16(4)];
zx14 = [z1(15),z2(15),z3(15),z4(15),z5(15),z6(15),z7(14),z8(14),z9(13),z10(13),z11(12),z12(11),z13(10),z14(9),z15(7),z16(4)];

topx14 = [top16(4),top15(7),top14(9),top13(10),top12(11),top11(12),top10(13),top9(13),top8(14),top7(14),top6(15),top5(15),top4(15),top3(15),top2(15),top1(15)];
for n = 1:16
  co = top1(n)/100;
  %plot3(xx14(n),yx14(n),zx14(n),'.','Markersize', 20,'Color',[0,co,0]);
end
```

```
%INTERPOLATED CONTOUR CX14
% 1mm interpolated contour lines for CX14
cn14yx = min(yx14):1:max(yx14);
for n = 1:length(cn14yx)
  cn14zx(n) = zx14(1);
end
cn14xxi = interp1(yx14,xx14,cn14yx,'spline');
%cn14x = plot3(cn14xxi,cn14yx,cn14zx,'Linewidth',0.75);

stp = 1;
for k = 1:15
  ncval = topx14(k);   %starting point of 5 colour bands
  pcval = ncval/100;   %progressive point for each band
  ncval2 = topx14(k+1);   %end point of 5 colour bands
  for j = stp:(stp+4)   %DIVIDE FIRST INTERVAL INTO 5 COLOUR BANDS
    colx(1) = cn14xxi(j);
    colx(2) = cn14xxi(j+1);
    coly(1) = cn14yx(j);
    coly(2) = cn14yx(j+1);
    colz(1) = cn14zx(j);
    colz(2) = cn14zx(j+1);
    cval = ((pcval*100)+((ncval2-ncval)/5))/100;
    cvalp = (cval+pcval)/2;   %average between two points for a colour
    cvalp = round(cvalp*100)+1;
    pcval = cval;
    plot3(colx,coly,colz,'Color',[gdmap(cvalp,1),gdmap(cvalp,2),gdmap(cvalp,3)],'Linewidth',0.75);   %[0,cvalp,0]
  end
stp = stp+5;
end

%CX15
xx15 = [x1(16),x2(16),x3(16),x4(16),x5(16),x6(16),x7(15),x8(15),x9(14),x10(14),x11(13),x12(12),x13(11),x14(10),x15(8),x16(5)];
yx15 = [y1(16),y2(16),y3(16),y4(16),y5(16),y6(16),y7(15),y8(15),y9(14),y10(14),y11(13),y12(12),y13(11),y14(10),y15(8),y16(5)];
zx15 = [z1(16),z2(16),z3(16),z4(16),z5(16),z6(16),z7(15),z8(15),z9(14),z10(14),z11(13),z12(12),z13(11),z14(10),z15(8),z16(5)];

topx15 =
[top16(5),top15(8),top14(10),top13(11),top12(12),top11(13),top10(14),top9(14),top8(15),top7(15),top6(16),top5(16),top4(16),top3(16),top2(16),top1(16)];
for n = 1:16
  co = top1(n)/100;
  %plot3(xx15(n),yx15(n),zx15(n),'.','Markersize', 20,'Color',[0,co,0]);
end

%INTERPOLATED CONTOUR CX15
% 1mm interpolated contour lines for CX15
cn15yx = min(yx15):1:max(yx15);
for n = 1:length(cn15yx)
  cn15zx(n) = zx15(1);
end
cn15xxi = interp1(yx15,xx15,cn15yx,'spline');
%cn15x = plot3(cn15xxi,cn15yx,cn15zx,'Linewidth',0.75);

stp = 1;
for k = 1:15
  ncval = topx15(k);   %starting point of 5 colour bands
  pcval = ncval/100;   %progressive point for each band
  ncval2 = topx15(k+1);   %end point of 5 colour bands
  for j = stp:(stp+4)   %DIVIDE FIRST INTERVAL INTO 5 COLOUR BANDS
    colx(1) = cn15xxi(j);
    colx(2) = cn15xxi(j+1);
    coly(1) = cn15yx(j);
    coly(2) = cn15yx(j+1);
    colz(1) = cn15zx(j);
    colz(2) = cn15zx(j+1);
    cval = ((pcval*100)+((ncval2-ncval)/5))/100;
    cvalp = (cval+pcval)/2;   %average between two points for a colour
    cvalp = round(cvalp*100)+1;
    pcval = cval;
    plot3(colx,coly,colz,'Color',[gdmap(cvalp,1),gdmap(cvalp,2),gdmap(cvalp,3)],'Linewidth',0.75);   %[0,cvalp,0]
  end
stp = stp+5;
end

%CX16
xx16 = [x1(17),x2(17),x3(17),x4(17),x5(17),x6(17),x7(16),x8(16),x9(15),x10(15),x11(14),x12(13),x13(12),x14(11),x15(9),x16(6)];
yx16 = [y1(17),y2(17),y3(17),y4(17),y5(17),y6(17),y7(16),y8(16),y9(15),y10(15),y11(14),y12(13),y13(12),y14(11),y15(9),y16(6)];
zx16 = [z1(17),z2(17),z3(17),z4(17),z5(17),z6(17),z7(16),z8(16),z9(15),z10(15),z11(14),z12(13),z13(12),z14(11),z15(9),z16(6)];

topx16 =
[top16(6),top15(9),top14(11),top13(12),top12(13),top11(14),top10(15),top9(15),top8(16),top7(16),top6(17),top5(17),top4(17),top3(17),top2(17),top1(17)];
for n = 1:16
  co = top1(n)/100;
  %plot3(xx16(n),yx16(n),zx16(n),'.','Markersize', 20,'Color',[0,co,0]);
end

%INTERPOLATED CONTOUR CX16
% 1mm interpolated contour lines for CX16
cn16yx = min(yx16):1:max(yx16);
for n = 1:length(cn16yx)
  cn16zx(n) = zx16(1);
end
cn16xxi = interp1(yx16,xx16,cn16yx,'spline');
%cn16x = plot3(cn16xxi,cn16yx,cn16zx,'Linewidth',0.75);
```

```
stp = 1;
for k = 1:15
   ncval = topx16(k);   %starting point of 5 colour bands
   pcval = ncval/100;   %progressive point for each band
   ncval2 = topx16(k+1);   %end point of 5 colour bands
   for j = stp:(stp+4)   %DIVIDE FIRST INTERVAL INTO 5 COLOUR BANDS
      colx(1) = cn16xxi(j);
      colx(2) = cn16xxi(j+1);
      coly(1) = cn16yx(j);
      coly(2) = cn16yx(j+1);
      colz(1) = cn16zx(j);
      colz(2) = cn16zx(j+1);
      cval = ((pcval*100)+((ncval2-ncval)/5))/100;
      cvalp = (cval+pcval)/2;   %average between two points for a colour
      cvalp = round(cvalp*100)+1;
      pcval = cval;
      plot3(colx,coly,colz,'Color',[gdmap(cvalp,1),gdmap(cvalp,2),gdmap(cvalp,3)],'Linewidth',0.75);   %[0,cvalp,0]
   end
stp = stp+5;
end

%CX17
xx17 = [x1(18),x2(18),x3(18),x4(18),x5(18),x6(18),x7(17),x8(17),x9(16),x10(16),x11(15),x12(14),x13(13),x14(12),x15(10),x16(7)];
yx17 = [y1(18),y2(18),y3(18),y4(18),y5(18),y6(18),y7(17),y8(17),y9(16),y10(16),y11(15),y12(14),y13(13),y14(12),y15(10),y16(7)];
zx17 = [z1(18),z2(18),z3(18),z4(18),z5(18),z6(18),z7(17),z8(17),z9(16),z10(16),z11(15),z12(14),z13(13),z14(12),z15(10),z16(7)];

topx17 =
[top16(7),top15(10),top14(12),top13(13),top12(14),top11(15),top10(16),top9(16),top8(17),top7(17),top6(18),top5(18),top4(18),top3(18),top2(18),top1(18)];
for n = 1:16
   co = top1(n)/100;
   %plot3(xx17(n),yx17(n),zx17(n),'.','Markersize', 20,'Color',[0,co,0]);
end

%INTERPOLATED CONTOUR CX17
% 1mm interpolated contour lines for CX17
cn17yx = min(yx17):1:max(yx17);
for n = 1:length(cn17yx)
   cn17zx(n) = zx17(1);
end
cn17xxi = interp1(yx17,xx17,cn17yx,'spline');
%cn17x = plot3(cn17xxi,cn17yx,cn17zx,'Linewidth',0.75);

stp = 1;
for k = 1:15
   ncval = topx17(k);   %starting point of 5 colour bands
   pcval = ncval/100;   %progressive point for each band
   ncval2 = topx17(k+1);   %end point of 5 colour bands
   for j = stp:(stp+4)   %DIVIDE FIRST INTERVAL INTO 5 COLOUR BANDS
      colx(1) = cn17xxi(j);
      colx(2) = cn17xxi(j+1);
      coly(1) = cn17yx(j);
      coly(2) = cn17yx(j+1);
      colz(1) = cn17zx(j);
      colz(2) = cn17zx(j+1);
      cval = ((pcval*100)+((ncval2-ncval)/5))/100;
      cvalp = (cval+pcval)/2;   %average between two points for a colour
      cvalp = round(cvalp*100)+1;
      pcval = cval;
      plot3(colx,coly,colz,'Color',[gdmap(cvalp,1),gdmap(cvalp,2),gdmap(cvalp,3)],'Linewidth',0.75);   %[0,cvalp,0]
   end
stp = stp+5;
end

%CX18
xx18 = [x1(19),x2(19),x3(19),x4(19),x5(19),x6(19),x7(18),x8(18),x9(17),x10(17),x11(16),x12(15),x13(14),x14(13),x15(11),x16(8)];
yx18 = [y1(19),y2(19),y3(19),y4(19),y5(19),y6(19),y7(18),y8(18),y9(17),y10(17),y11(16),y12(15),y13(14),y14(13),y15(11),y16(8)];
zx18 = [z1(19),z2(19),z3(19),z4(19),z5(19),z6(19),z7(18),z8(18),z9(17),z10(17),z11(16),z12(15),z13(14),z14(13),z15(11),z16(8)];

topx18 =
[top16(8),top15(11),top14(13),top13(14),top12(15),top11(16),top10(17),top9(17),top8(18),top7(18),top6(19),top5(19),top4(19),top3(19),top2(19),top1(19)];
for n = 1:16
   co = top1(n)/100;
   %plot3(xx18(n),yx18(n),zx18(n),'.','Markersize', 20,'Color',[0,co,0]);
end

%INTERPOLATED CONTOUR CX18
% 1mm interpolated contour lines for CX18
cn18yx = min(yx18):1:max(yx18);
for n = 1:length(cn18yx)
   cn18zx(n) = zx18(1);
end
cn18xxi = interp1(yx18,xx18,cn18yx,'spline');
%cn18x = plot3(cn18xxi,cn18yx,cn18zx,'Linewidth',0.75);

stp = 1;
for k = 1:15
   ncval = topx18(k);   %starting point of 5 colour bands
   pcval = ncval/100;   %progressive point for each band
   ncval2 = topx18(k+1);   %end point of 5 colour bands
   for j = stp:(stp+4)   %DIVIDE FIRST INTERVAL INTO 5 COLOUR BANDS
      colx(1) = cn18xxi(j);
      colx(2) = cn18xxi(j+1);
      coly(1) = cn18yx(j);
      coly(2) = cn18yx(j+1);
```

```
    colz(1) = cn18zx(j);
    colz(2) = cn18zx(j+1);
    cval = ((pcval*100)+((ncval2-ncval)/5))/100;
    cvalp = (cval+pcval)/2;   %average between two points for a colour
    cvalp = round(cvalp*100)+1;
    pcval = cval;
    plot3(colx,coly,colz,'Color',[gdmap(cvalp,1),gdmap(cvalp,2),gdmap(cvalp,3)],'Linewidth',0.75);   %[0,cvalp,0]
  end
stp = stp+5;
end

%CX19
xx19 = [x1(20),x2(20),x3(20),x4(20),x5(20),x6(20),x7(19),x8(19),x9(18),x10(18),x11(17),x12(16),x13(15),x14(14),x15(12),x16(9)];
yx19 = [y1(20),y2(20),y3(20),y4(20),y5(20),y6(20),y7(19),y8(19),y9(18),y10(18),y11(17),y12(16),y13(15),y14(14),y15(12),y16(9)];
zx19 = [z1(20),z2(20),z3(20),z4(20),z5(20),z6(20),z7(19),z8(19),z9(18),z10(18),z11(17),z12(16),z13(15),z14(14),z15(12),z16(9)];

topx19 =
[top16(9),top15(12),top14(14),top13(15),top12(16),top11(17),top10(18),top9(18),top8(19),top7(19),top6(20),top5(20),top4(20),top3(20),top2(20),top1(20)];
for n = 1:16
  co = top1(n)/100;
  %plot3(xx19(n),yx19(n),zx19(n),'.','Markersize', 20,'Color',[0,co,0]);
end

%INTERPOLATED CONTOUR CX19
% 1mm interpolated contour lines for CX19
cn19yx = min(yx19):1:max(yx19);
for n = 1:length(cn19yx)
  cn19zx(n) = zx19(1);
end
cn19xxi = interp1(yx19,xx19,cn19yx,'spline');
%cn19x = plot3(cn19xxi,cn19yx,cn19zx,'Linewidth',0.75);

stp = 1;
for k = 1:15
  ncval = topx19(k);   %starting point of 5 colour bands
  pcval = ncval/100;   %progressive point for each band
  ncval2 = topx19(k+1);   %end point of 5 colour bands
  for j = stp:(stp+4)   %DIVIDE FIRST INTERVAL INTO 5 COLOUR BANDS
    colx(1) = cn19xxi(j);
    colx(2) = cn19xxi(j+1);
    coly(1) = cn19yx(j);
    coly(2) = cn19yx(j+1);
    colz(1) = cn19zx(j);
    colz(2) = cn19zx(j+1);
    cval = ((pcval*100)+((ncval2-ncval)/5))/100;
    cvalp = (cval+pcval)/2;   %average between two points for a colour
    cvalp = round(cvalp*100)+1;
    pcval = cval;
    plot3(colx,coly,colz,'Color',[gdmap(cvalp,1),gdmap(cvalp,2),gdmap(cvalp,3)],'Linewidth',0.75);   %[0,cvalp,0]
  end
stp = stp+5;
end

%CX20
xx20 = [x1(21),x2(21),x3(21),x4(21),x5(21),x6(21),x7(20),x8(20),x9(19),x10(19),x11(18),x12(17),x13(16),x14(15),x15(13),x16(10)];
yx20 = [y1(21),y2(21),y3(21),y4(21),y5(21),y6(21),y7(20),y8(20),y9(19),y10(19),y11(18),y12(17),y13(16),y14(15),y15(13),y16(10)];
zx20 = [z1(21),z2(21),z3(21),z4(21),z5(21),z6(21),z7(20),z8(20),z9(19),z10(19),z11(18),z12(17),z13(16),z14(15),z15(13),z16(10)];

topx20 =
[top16(10),top15(13),top14(15),top13(16),top12(17),top11(18),top10(19),top9(19),top8(20),top7(20),top6(21),top5(21),top4(21),top3(21),top2(21),top1(21)];
for n = 1:16
  co = top1(n)/100;
  %plot3(xx20(n),yx20(n),zx20(n),'.','Markersize', 20,'Color',[0,co,0]);
end

%INTERPOLATED CONTOUR CX20
% 1mm interpolated contour lines for CX20
cn20yx = min(yx20):1:max(yx20);
for n = 1:length(cn20yx)
  cn20zx(n) = zx20(1);
end
cn20xxi = interp1(yx20,xx20,cn20yx,'spline');
%cn20x = plot3(cn20xxi,cn20yx,cn20zx,'Linewidth',0.75);

stp = 1;
for k = 1:15
  ncval = topx20(k);   %starting point of 5 colour bands
  pcval = ncval/100;   %progressive point for each band
  ncval2 = topx20(k+1);   %end point of 5 colour bands
  for j = stp:(stp+4)   %DIVIDE FIRST INTERVAL INTO 5 COLOUR BANDS
    colx(1) = cn20xxi(j);
    colx(2) = cn20xxi(j+1);
    coly(1) = cn20yx(j);
    coly(2) = cn20yx(j+1);
    colz(1) = cn20zx(j);
    colz(2) = cn20zx(j+1);
    cval = ((pcval*100)+((ncval2-ncval)/5))/100;
    cvalp = (cval+pcval)/2;   %average between two points for a colour
    cvalp = round(cvalp*100)+1;
    pcval = cval;
    plot3(colx,coly,colz,'Color',[gdmap(cvalp,1),gdmap(cvalp,2),gdmap(cvalp,3)],'Linewidth',0.75);   %[0,cvalp,0]
  end
stp = stp+5;
end
```

```
%CX21
xx21 = [x1(22),x2(22),x3(22),x4(22),x5(22),x6(22),x7(21),x8(21),x9(20),x10(20),x11(19),x12(18),x13(17),x14(16),x15(14),x16(11)];
yx21 = [y1(22),y2(22),y3(22),y4(22),y5(22),y6(22),y7(21),y8(21),y9(20),y10(20),y11(19),y12(18),y13(17),y14(16),y15(14),y16(11)];
zx21 = [z1(22),z2(22),z3(22),z4(22),z5(22),z6(22),z7(21),z8(21),z9(20),z10(20),z11(19),z12(18),z13(17),z14(16),z15(14),z16(11)];

topx21 =
[top16(11),top15(14),top14(16),top13(17),top12(18),top11(19),top10(20),top9(20),top8(21),top7(21),top6(22),top5(22),top4(22),top3(22),top2(22),top1(22)];
for n = 1:16
  co = top1(n)/100;
  %plot3(xx21(n),yx21(n),zx21(n),'.','Markersize', 20,'Color',[0,co,0]);
end

%INTERPOLATED CONTOUR CX21
% 1mm interpolated contour lines for CX21
cn21yx = min(yx21):1:max(yx21);
for n = 1:length(cn21yx)
  cn21zx(n) = zx21(1);
end
cn21xxi = interp1(yx21,xx21,cn21yx,'spline');
%cn21x = plot3(cn21xxi,cn21yx,cn21zx,'Linewidth',0.75);

stp = 1;
for k = 1:15
  ncval = topx21(k);   %starting point of 5 colour bands
  pcval = ncval/100;   %progressive point for each band
  ncval2 = topx21(k+1);   %end point of 5 colour bands
  for j = stp:(stp+4)   %DIVIDE FIRST INTERVAL INTO 5 COLOUR BANDS
    colx(1) = cn21xxi(j);
    colx(2) = cn21xxi(j+1);
    coly(1) = cn21yx(j);
    coly(2) = cn21yx(j+1);
    colz(1) = cn21zx(j);
    colz(2) = cn21zx(j+1);
    cval = ((pcval*100)+((ncval2-ncval)/5))/100;
    cvalp = (cval+pcval)/2;   %average between two points for a colour
    cvalp = round(cvalp*100)+1;
    pcval = cval;
    plot3(colx,coly,colz,'Color',[gdmap(cvalp,1),gdmap(cvalp,2),gdmap(cvalp,3)],'Linewidth',0.75);   %[0,cvalp,0]
  end
stp = stp+5;
end

%CX22
xx22 = [x1(23),x2(23),x3(23),x4(23),x5(23),x6(23),x7(22),x8(22),x9(21),x10(21),x11(20),x12(19),x13(18),x14(17),x15(15),x16(12),x17(2)];
yx22 = [y1(23),y2(23),y3(23),y4(23),y5(23),y6(23),y7(22),y8(22),y9(21),y10(21),y11(20),y12(19),y13(18),y14(17),y15(15),y16(12),y17(2)];
zx22 = [z1(23),z2(23),z3(23),z4(23),z5(23),z6(23),z7(22),z8(22),z9(21),z10(21),z11(20),z12(19),z13(18),z14(17),z15(15),z16(12),z17(2)];

topx22 =
[top17(2),top16(12),top15(15),top14(17),top13(18),top12(19),top11(20),top10(21),top9(21),top8(22),top7(22),top6(23),top5(23),top4(23),top3(23),top2(23),top1(2
3)];
for n = 1:17
  co = top1(n)/100;
  %plot3(xx22(n),yx22(n),zx22(n),'.','Markersize', 20,'Color',[0,co,0]);
end

%INTERPOLATED CONTOUR CX22
% 1mm interpolated contour lines for CX22
cn22yx = min(yx22):1:max(yx22);
for n = 1:length(cn22yx)
  cn22zx(n) = zx22(1);
end
cn22xxi = interp1(yx22,xx22,cn22yx,'spline');
%cn22x = plot3(cn22xxi,cn22yx,cn22zx,'Linewidth',0.75);

stp = 1;
for k = 1:16
  ncval = topx22(k);   %starting point of 5 colour bands
  pcval = ncval/100;   %progressive point for each band
  ncval2 = topx22(k+1);   %end point of 5 colour bands
  for j = stp:(stp+4)   %DIVIDE FIRST INTERVAL INTO 5 COLOUR BANDS
    colx(1) = cn22xxi(j);
    colx(2) = cn22xxi(j+1);
    coly(1) = cn22yx(j);
    coly(2) = cn22yx(j+1);
    colz(1) = cn22zx(j);
    colz(2) = cn22zx(j+1);
    cval = ((pcval*100)+((ncval2-ncval)/5))/100;
    cvalp = (cval+pcval)/2;   %average between two points for a colour
    cvalp = round(cvalp*100)+1;
    pcval = cval;
    plot3(colx,coly,colz,'Color',[gdmap(cvalp,1),gdmap(cvalp,2),gdmap(cvalp,3)],'Linewidth',0.75);   %[0,cvalp,0]
  end
stp = stp+5;
end

%CX23
xx23 = [x1(24),x2(24),x3(24),x4(24),x5(24),x6(24),x7(23),x8(23),x9(22),x10(22),x11(21),x12(20),x13(19),x14(18),x15(16),x16(13),x17(3)];
yx23 = [y1(24),y2(24),y3(24),y4(24),y5(24),y6(24),y7(23),y8(23),y9(22),y10(22),y11(21),y12(20),y13(19),y14(18),y15(16),y16(13),y17(3)];
zx23 = [z1(24),z2(24),z3(24),z4(24),z5(24),z6(24),z7(23),z8(23),z9(22),z10(22),z11(21),z12(20),z13(19),z14(18),z15(16),z16(13),z17(3)];

topx23 =
[top17(3),top16(13),top15(16),top14(18),top13(19),top12(20),top11(21),top10(22),top9(22),top8(23),top7(23),top6(24),top5(24),top4(24),top3(24),top2(24),top1(2
4)];
```

```
for n = 1:17
  co = top1(n)/100;
  %plot3(xx23(n),yx23(n),zx23(n),'.','Markersize', 20,'Color',[0,co,0]);
end

%INTERPOLATED CONTOUR CX23
% 1mm interpolated contour lines for CX23
cn23yx = min(yx23):1:max(yx23);
for n = 1:length(cn23yx)
  cn23zx(n) = zx23(1);
end
cn23xxi = interp1(yx23,xx23,cn23yx,'spline');
%cn23x = plot3(cn23xxi,cn23yx,cn23zx,'Linewidth',0.75);

stp = 1;
for k = 1:16
  ncval = topx23(k);   %starting point of 5 colour bands
  pcval = ncval/100;   %progressive point for each band
  ncval2 = topx23(k+1);   %end point of 5 colour bands
  for j = stp:(stp+4)   %DIVIDE FIRST INTERVAL INTO 5 COLOUR BANDS
    colx(1) = cn23xxi(j);
    colx(2) = cn23xxi(j+1);
    coly(1) = cn23yx(j);
    coly(2) = cn23yx(j+1);
    colz(1) = cn23zx(j);
    colz(2) = cn23zx(j+1);
    cval = ((pcval*100)+((ncval2-ncval)/5))/100;
    cvalp = (cval+pcval)/2;   %average between two points for a colour
    cvalp = round(cvalp*100)+1;
    pcval = cval;
    plot3(colx,coly,colz,'Color',[gdmap(cvalp,1),gdmap(cvalp,2),gdmap(cvalp,3)],'Linewidth',0.75);   %[0,cvalp,0]
  end
stp = stp+5;
end

%CX24
xx24 = [x1(25),x2(25),x3(25),x4(25),x5(25),x6(25),x7(24),x8(24),x9(23),x10(23),x11(22),x12(21),x13(20),x14(19),x15(17),x16(14),x17(4),x18(2)];
yx24 = [y1(25),y2(25),y3(25),y4(25),y5(25),y6(25),y7(24),y8(24),y9(23),y10(23),y11(22),y12(21),y13(20),y14(19),y15(17),y16(14),y17(4),y18(2)];
zx24 = [z1(25),z2(25),z3(25),z4(25),z5(25),z6(25),z7(24),z8(24),z9(23),z10(23),z11(22),z12(21),z13(20),z14(19),z15(17),z16(14),z17(4),z18(2)];

topx24 =
[top18(2),top17(4),top16(14),top15(17),top14(19),top13(20),top12(21),top11(22),top10(23),top9(23),top8(24),top7(24),top6(25),top5(25),top4(25),top3(25),top2(2
5),top1(25)];
for n = 1:18
  co = top1(n)/100;
  %plot3(xx24(n),yx24(n),zx24(n),'.','Markersize', 20,'Color',[0,co,0]);
end

%INTERPOLATED CONTOUR CX24
% 1mm interpolated contour lines for CX24
cn24yx = min(yx24):1:max(yx24);
for n = 1:length(cn24yx)
  cn24zx(n) = zx24(1);
end
cn24xxi = interp1(yx24,xx24,cn24yx,'spline');
%cn24x = plot3(cn24xxi,cn24yx,cn24zx,'Linewidth',0.75);

stp = 1;
for k = 1:17
  ncval = topx24(k);   %starting point of 5 colour bands
  pcval = ncval/100;   %progressive point for each band
  ncval2 = topx24(k+1);   %end point of 5 colour bands
  for j = stp:(stp+4)   %DIVIDE FIRST INTERVAL INTO 5 COLOUR BANDS
    colx(1) = cn24xxi(j);
    colx(2) = cn24xxi(j+1);
    coly(1) = cn24yx(j);
    coly(2) = cn24yx(j+1);
    colz(1) = cn24zx(j);
    colz(2) = cn24zx(j+1);
    cval = ((pcval*100)+((ncval2-ncval)/5))/100;
    cvalp = (cval+pcval)/2;   %average between two points for a colour
    cvalp = round(cvalp*100)+1;
    pcval = cval;
    plot3(colx,coly,colz,'Color',[gdmap(cvalp,1),gdmap(cvalp,2),gdmap(cvalp,3)],'Linewidth',0.75);   %[0,cvalp,0]
  end
stp = stp+5;
end

%CX25
xx25 = [x1(26),x2(26),x3(26),x4(26),x5(26),x6(26),x7(25),x8(25),x9(24),x10(24),x11(23),x12(22),x13(21),x14(20),x15(18),x16(15),x17(5),x18(3)];
yx25 = [y1(26),y2(26),y3(26),y4(26),y5(26),y6(26),y7(25),y8(25),y9(24),y10(24),y11(23),y12(22),y13(21),y14(20),y15(18),y16(15),y17(5),y18(3)];
zx25 = [z1(26),z2(26),z3(26),z4(26),z5(26),z6(26),z7(25),z8(25),z9(24),z10(24),z11(23),z12(22),z13(21),z14(20),z15(18),z16(15),z17(5),z18(3)];

topx25 =
[top18(3),top17(5),top16(15),top15(18),top14(20),top13(21),top12(22),top11(23),top10(24),top9(24),top8(25),top7(25),top6(26),top5(26),top4(26),top3(26),top2(2
6),top1(26)];
for n = 1:18
  co = top1(n)/100;
  %plot3(xx25(n),yx25(n),zx25(n),'.','Markersize', 20,'Color',[0,co,0]);
end

%INTERPOLATED CONTOUR CX25
% 1mm interpolated contour lines for CX25
cn25yx = min(yx25):1:max(yx25);
```

```
for n = 1:length(cn25yx)
   cn25zx(n) = zx25(1);
end
cn25xxi = interp1(yx25,xx25,cn25yx,'spline');
%cn25x = plot3(cn25xxi,cn25yx,cn25zx,'Linewidth',0.75);

stp = 1;
for k = 1:17
   ncval = topx25(k);   %starting point of 5 colour bands
   pcval = ncval/100;   %progressive point for each band
   ncval2 = topx25(k+1);   %end point of 5 colour bands
   for j = stp:(stp+4)   %DIVIDE FIRST INTERVAL INTO 5 COLOUR BANDS
      colx(1) = cn25xxi(j);
      colx(2) = cn25xxi(j+1);
      coly(1) = cn25yx(j);
      coly(2) = cn25yx(j+1);
      colz(1) = cn25zx(j);
      colz(2) = cn25zx(j+1);
      cval = ((pcval*100)+((ncval2-ncval)/5))/100;
      cvalp = (cval+pcval)/2;   %average between two points for a colour
      cvalp = round(cvalp*100)+1;
      pcval = cval;
      plot3(colx,coly,colz,'Color',[gdmap(cvalp,1),gdmap(cvalp,2),gdmap(cvalp,3)],'Linewidth',0.75);   %[0,cvalp,0]
   end
stp = stp+5;
end

%CX26
xx26 = [x1(27),x2(27),x3(27),x4(27),x5(27),x6(27),x7(26),x8(26),x9(25),x10(25),x11(24),x12(23),x13(22),x14(21),x15(19),x16(16),x17(6),x18(4)];
yx26 = [y1(27),y2(27),y3(27),y4(27),y5(27),y6(27),y7(26),y8(26),y9(25),y10(25),y11(24),y12(23),y13(22),y14(21),y15(19),y16(16),y17(6),y18(4)];
zx26 = [z1(27),z2(27),z3(27),z4(27),z5(27),z6(27),z7(26),z8(26),z9(25),z10(25),z11(24),z12(23),z13(22),z14(21),z15(19),z16(16),z17(6),z18(4)];

topx26 =
[top18(4),top17(6),top16(16),top15(19),top14(21),top13(22),top12(23),top11(24),top10(25),top9(25),top8(26),top7(26),top6(27),top5(27),top4(27),top3(27),top2(2
7),top1(27)];
for n = 1:18
   co = top1(n)/100;
   %plot3(xx26(n),yx26(n),zx26(n),'.','Markersize', 20,'Color',[0,co,0]);
end

%INTERPOLATED CONTOUR CX26
% 1mm interpolated contour lines for CX26
cn26yx = min(yx26):1:max(yx26);
for n = 1:length(cn26yx)
   cn26zx(n) = zx26(1);
end
cn26xxi = interp1(yx26,xx26,cn26yx,'spline');
%cn26x = plot3(cn26xxi,cn26yx,cn26zx,'Linewidth',0.75);

stp = 1;
for k = 1:17
   ncval = topx26(k);   %starting point of 5 colour bands
   pcval = ncval/100;   %progressive point for each band
   ncval2 = topx26(k+1);   %end point of 5 colour bands
   for j = stp:(stp+4)   %DIVIDE FIRST INTERVAL INTO 5 COLOUR BANDS
      colx(1) = cn26xxi(j);
      colx(2) = cn26xxi(j+1);
      coly(1) = cn26yx(j);
      coly(2) = cn26yx(j+1);
      colz(1) = cn26zx(j);
      colz(2) = cn26zx(j+1);
      cval = ((pcval*100)+((ncval2-ncval)/5))/100;
      cvalp = (cval+pcval)/2;   %average between two points for a colour
      cvalp = round(cvalp*100)+1;
      pcval = cval;
      plot3(colx,coly,colz,'Color',[gdmap(cvalp,1),gdmap(cvalp,2),gdmap(cvalp,3)],'Linewidth',0.75);   %[0,cvalp,0]
   end
stp = stp+5;
end

%CX27
xx27 = [x1(28),x2(28),x3(28),x4(28),x5(28),x6(28),x7(27),x8(27),x9(26),x10(26),x11(25),x12(24),x13(23),x14(22),x15(20),x16(17),x17(7),x18(5)];
yx27 = [y1(28),y2(28),y3(28),y4(28),y5(28),y6(28),y7(27),y8(27),y9(26),y10(26),y11(25),y12(24),y13(23),y14(22),y15(20),y16(17),y17(7),y18(5)];
zx27 = [z1(28),z2(28),z3(28),z4(28),z5(28),z6(28),z7(27),z8(27),z9(26),z10(26),z11(25),z12(24),z13(23),z14(22),z15(20),z16(17),z17(7),z18(5)];

topx27 =
[top18(5),top17(7),top16(17),top15(20),top14(22),top13(23),top12(24),top11(25),top10(26),top9(26),top8(27),top7(27),top6(28),top5(28),top4(28),top3(28),top2(2
8),top1(28)];
for n = 1:18
   co = top1(n)/100;
   %plot3(xx27(n),yx27(n),zx27(n),'.','Markersize', 20,'Color',[0,co,0]);
end

%INTERPOLATED CONTOUR CX27
% 1mm interpolated contour lines for CX27
cn27yx = min(yx27):1:max(yx27);
for n = 1:length(cn27yx)
   cn27zx(n) = zx27(1);
end
cn27xxi = interp1(yx27,xx27,cn27yx,'spline');
%cn27x = plot3(cn27xxi,cn27yx,cn27zx,'Linewidth',0.75);

stp = 1;
for k = 1:17
```

```
  ncval = topx27(k);   %starting point of 5 colour bands
  pcval = ncval/100;   %progressive point for each band
  ncval2 = topx27(k+1);   %end point of 5 colour bands
  for j = stp:(stp+4)   %DIVIDE FIRST INTERVAL INTO 5 COLOUR BANDS
    colx(1) = cn27xxi(j);
    colx(2) = cn27xxi(j+1);
    coly(1) = cn27yx(j);
    coly(2) = cn27yx(j+1);
    colz(1) = cn27zx(j);
    colz(2) = cn27zx(j+1);
    cval = ((pcval*100)+((ncval2-ncval)/5))/100;
    cvalp = (cval+pcval)/2;   %average between two points for a colour
    cvalp = round(cvalp*100)+1;
    pcval = cval;
    plot3(colx,coly,colz,'Color',[gdmap(cvalp,1),gdmap(cvalp,2),gdmap(cvalp,3)],'Linewidth',0.75);   %[0,cvalp,0]
  end
stp = stp+5;
end

%CX28
xx28 = [x1(29),x2(29),x3(29),x4(29),x5(29),x6(29),x7(28),x8(28),x9(27),x10(27),x11(26),x12(25),x13(24),x14(23),x15(21),x16(18),x17(8)];
yx28 = [y1(29),y2(29),y3(29),y4(29),y5(29),y6(29),y7(28),y8(28),y9(27),y10(27),y11(26),y12(25),y13(24),y14(23),y15(21),y16(18),y17(8)];
zx28 = [z1(29),z2(29),z3(29),z4(29),z5(29),z6(29),z7(28),z8(28),z9(27),z10(27),z11(26),z12(25),z13(24),z14(23),z15(21),z16(18),z17(8)];

topx28 =
[top17(8),top16(18),top15(21),top14(23),top13(24),top12(25),top11(26),top10(27),top9(27),top8(28),top7(28),top6(29),top5(29),top4(29),top3(29),top2(29),top1(2
9)];
for n = 1:17
  co = top1(n)/100;
  %plot3(xx28(n),yx28(n),zx28(n),'.','Markersize', 20,'Color',[0,co,0]);
end

%INTERPOLATED CONTOUR CX28
% 1mm interpolated contour lines for CX28
cn28yx = min(yx28):1:max(yx28);
for n = 1:length(cn28yx)
  cn28zx(n) = zx28(1);
end
cn28xxi = interp1(yx28,xx28,cn28yx,'spline');
%cn28x = plot3(cn28xxi,cn28yx,cn28zx,'Linewidth',0.75);

stp = 1;
for k = 1:16
  ncval = topx28(k);   %starting point of 5 colour bands
  pcval = ncval/100;   %progressive point for each band
  ncval2 = topx28(k+1);   %end point of 5 colour bands
  for j = stp:(stp+4)   %DIVIDE FIRST INTERVAL INTO 5 COLOUR BANDS
    colx(1) = cn28xxi(j);
    colx(2) = cn28xxi(j+1);
    coly(1) = cn28yx(j);
    coly(2) = cn28yx(j+1);
    colz(1) = cn28zx(j);
    colz(2) = cn28zx(j+1);
    cval = ((pcval*100)+((ncval2-ncval)/5))/100;
    cvalp = (cval+pcval)/2;   %average between two points for a colour
    cvalp = round(cvalp*100)+1;
    pcval = cval;
    plot3(colx,coly,colz,'Color',[gdmap(cvalp,1),gdmap(cvalp,2),gdmap(cvalp,3)],'Linewidth',0.75);   %[0,cvalp,0]
  end
stp = stp+5;
end

%CX29
xx29 = [x1(30),x2(30),x3(30),x4(30),x5(30),x6(30),x7(29),x8(29),x9(28),x10(28),x11(27),x12(26),x13(25),x14(24),x15(22),x16(19),x17(9)];
yx29 = [y1(30),y2(30),y3(30),y4(30),y5(30),y6(30),y7(29),y8(29),y9(28),y10(28),y11(27),y12(26),y13(25),y14(24),y15(22),y16(19),y17(9)];
zx29 = [z1(30),z2(30),z3(30),z4(30),z5(30),z6(30),z7(29),z8(29),z9(28),z10(28),z11(27),z12(26),z13(25),z14(24),z15(22),z16(19),z17(9)];

topx29 =
[top17(9),top16(19),top15(22),top14(24),top13(25),top12(26),top11(27),top10(28),top9(28),top8(29),top7(29),top6(30),top5(30),top4(30),top3(30),top2(30),top1(3
0)];
for n = 1:17
  co = top1(n)/100;
  %plot3(xx29(n),yx29(n),zx29(n),'.','Markersize', 20,'Color',[0,co,0]);
end

%INTERPOLATED CONTOUR CX29
% 1mm interpolated contour lines for CX29
cn29yx = min(yx29):1:max(yx29);
for n = 1:length(cn29yx)
  cn29zx(n) = zx29(1);
end
cn29xxi = interp1(yx29,xx29,cn29yx,'spline');
%cn29x = plot3(cn29xxi,cn29yx,cn29zx,'Linewidth',0.75);

stp = 1;
for k = 1:16
  ncval = topx29(k);   %starting point of 5 colour bands
  pcval = ncval/100;   %progressive point for each band
  ncval2 = topx29(k+1);   %end point of 5 colour bands
  for j = stp:(stp+4)   %DIVIDE FIRST INTERVAL INTO 5 COLOUR BANDS
    colx(1) = cn29xxi(j);
    colx(2) = cn29xxi(j+1);
    coly(1) = cn29yx(j);
    coly(2) = cn29yx(j+1);
```

```
      colz(1) = cn29zx(j);
      colz(2) = cn29zx(j+1);
      cval = ((pcval*100)+((ncval2-ncval)/5))/100;
      cvalp = (cval+pcval)/2;   %average between two points for a colour
      cvalp = round(cvalp*100)+1;
      pcval = cval;
      plot3(colx,coly,colz,'Color',[gdmap(cvalp,1),gdmap(cvalp,2),gdmap(cvalp,3)],'Linewidth',0.75);   %[0,cvalp,0]
   end
stp = stp+5;
end

%CX30
xx30 = [x1(31),x2(31),x3(31),x4(31),x5(31),x6(31),x7(30),x8(30),x9(29),x10(29),x11(28),x12(27),x13(26),x14(25),x15(23),x16(20)];
yx30 = [y1(31),y2(31),y3(31),y4(31),y5(31),y6(31),y7(30),y8(30),y9(29),y10(29),y11(28),y12(27),y13(26),y14(25),y15(23),y16(20)];
zx30 = [z1(31),z2(31),z3(31),z4(31),z5(31),z6(31),z7(30),z8(30),z9(29),z10(29),z11(28),z12(27),z13(26),z14(25),z15(23),z16(20)];

topx30 =
[top16(20),top15(23),top14(25),top13(26),top12(27),top11(28),top10(29),top9(29),top8(30),top7(30),top6(31),top5(31),top4(31),top3(31),top2(31),top1(31)];
for n = 1:16
   co = top1(n)/100;
   %plot3(xx30(n),yx30(n),zx30(n),'.','Markersize', 20,'Color',[0,co,0]);
end

%INTERPOLATED CONTOUR CX30
% 1mm interpolated contour lines for CX30
cn30yx = min(yx30):1:max(yx30);
for n = 1:length(cn30yx)
   cn30zx(n) = zx30(1);
end
cn30xxi = interp1(yx30,xx30,cn30yx,'spline');
%cn30x = plot3(cn30xxi,cn30yx,cn30zx,'Linewidth',0.75);

stp = 1;
for k = 1:15
   ncval = topx30(k);   %starting point of 5 colour bands
   pcval = ncval/100;   %progressive point for each band
   ncval2 = topx30(k+1);   %end point of 5 colour bands
   for j = stp:(stp+4)   %DIVIDE FIRST INTERVAL INTO 5 COLOUR BANDS
      colx(1) = cn30xxi(j);
      colx(2) = cn30xxi(j+1);
      coly(1) = cn30yx(j);
      coly(2) = cn30yx(j+1);
      colz(1) = cn30zx(j);
      colz(2) = cn30zx(j+1);
      cval = ((pcval*100)+((ncval2-ncval)/5))/100;
      cvalp = (cval+pcval)/2;   %average between two points for a colour
      cvalp = round(cvalp*100)+1;
      pcval = cval;
      plot3(colx,coly,colz,'Color',[gdmap(cvalp,1),gdmap(cvalp,2),gdmap(cvalp,3)],'Linewidth',0.75);   %[0,cvalp,0]
   end
stp = stp+5;
end

%CX31
xx31 = [x1(32),x2(32),x3(32),x4(32),x5(32),x6(32),x7(31),x8(31),x9(30),x10(30),x11(29),x12(28),x13(27),x14(26),x15(24),x16(21)];
yx31 = [y1(32),y2(32),y3(32),y4(32),y5(32),y6(32),y7(31),y8(31),y9(30),y10(30),y11(29),y12(28),y13(27),y14(26),y15(24),y16(21)];
zx31 = [z1(32),z2(32),z3(32),z4(32),z5(32),z6(32),z7(31),z8(31),z9(30),z10(30),z11(29),z12(28),z13(27),z14(26),z15(24),z16(21)];

topx31 =
[top16(21),top15(24),top14(26),top13(27),top12(28),top11(29),top10(30),top9(30),top8(31),top7(31),top6(32),top5(32),top4(32),top3(32),top2(32),top1(32)];
for n = 1:16
   co = top1(n)/100;
   %plot3(xx31(n),yx31(n),zx31(n),'.','Markersize', 20,'Color',[0,co,0]);
end

%INTERPOLATED CONTOUR CX31
% 1mm interpolated contour lines for CX31
cn31yx = min(yx31):1:max(yx31);
for n = 1:length(cn31yx)
   cn31zx(n) = zx31(1);
end
cn31xxi = interp1(yx31,xx31,cn31yx,'spline');
%cn31x = plot3(cn31xxi,cn31yx,cn31zx,'Linewidth',0.75);

stp = 1;
for k = 1:15
   ncval = topx31(k);   %starting point of 5 colour bands
   pcval = ncval/100;   %progressive point for each band
   ncval2 = topx31(k+1);   %end point of 5 colour bands
   for j = stp:(stp+4)   %DIVIDE FIRST INTERVAL INTO 5 COLOUR BANDS
      colx(1) = cn31xxi(j);
      colx(2) = cn31xxi(j+1);
      coly(1) = cn31yx(j);
      coly(2) = cn31yx(j+1);
      colz(1) = cn31zx(j);
      colz(2) = cn31zx(j+1);
      cval = ((pcval*100)+((ncval2-ncval)/5))/100;
      cvalp = (cval+pcval)/2;   %average between two points for a colour
      cvalp = round(cvalp*100)+1;
      pcval = cval;
      plot3(colx,coly,colz,'Color',[gdmap(cvalp,1),gdmap(cvalp,2),gdmap(cvalp,3)],'Linewidth',0.75);   %[0,cvalp,0]
   end
stp = stp+5;
end
```

```
%CX32
xx32 = [x1(33),x2(33),x3(33),x4(33),x5(33),x6(33),x7(32),x8(32),x9(31),x10(31),x11(30),x12(29),x13(28),x14(27),x15(25),x16(22)];
yx32 = [y1(33),y2(33),y3(33),y4(33),y5(33),y6(33),y7(32),y8(32),y9(31),y10(31),y11(30),y12(29),y13(28),y14(27),y15(25),y16(22)];
zx32 = [z1(33),z2(33),z3(33),z4(33),z5(33),z6(33),z7(32),z8(32),z9(31),z10(31),z11(30),z12(29),z13(28),z14(27),z15(25),z16(22)];

topx32 =
[top16(22),top15(25),top14(27),top13(28),top12(29),top11(30),top10(31),top9(31),top8(32),top7(32),top6(33),top5(33),top4(33),top3(33),top2(33),top1(33)];
for n = 1:16
  co = top1(n)/100;
  %plot3(xx32(n),yx32(n),zx32(n),'.','Markersize', 20,'Color',[0,co,0]);
end

%INTERPOLATED CONTOUR CX32
% 1mm interpolated contour lines for CX32
cn32yx = min(yx32):1:max(yx32);
for n = 1:length(cn32yx)
  cn32zx(n) = zx32(1);
end
cn32xxi = interp1(yx32,xx32,cn32yx,'spline');
%cn32x = plot3(cn32xxi,cn32yx,cn32zx,'Linewidth',0.75);

stp = 1;
for k = 1:15
  ncval = topx32(k);   %starting point of 5 colour bands
  pcval = ncval/100;   %progressive point for each band
  ncval2 = topx32(k+1);   %end point of 5 colour bands
  for j = stp:(stp+4)   %DIVIDE FIRST INTERVAL INTO 5 COLOUR BANDS
    colx(1) = cn32xxi(j);
    colx(2) = cn32xxi(j+1);
    coly(1) = cn32yx(j);
    coly(2) = cn32yx(j+1);
    colz(1) = cn32zx(j);
    colz(2) = cn32zx(j+1);
    cval = ((pcval*100)+((ncval2-ncval)/5))/100;
    cvalp = (cval+pcval)/2;   %average between two points for a colour
    cvalp = round(cvalp*100)+1;
    pcval = cval;
    plot3(colx,coly,colz,'Color',[gdmap(cvalp,1),gdmap(cvalp,2),gdmap(cvalp,3)],'Linewidth',0.75);   %[0,cvalp,0]
  end
stp = stp+5;
end

%CX33
xx33 = [x1(34),x2(34),x3(34),x4(34),x5(34),x6(34),x7(33),x8(33),x9(32),x10(32),x11(31),x12(30),x13(29),x14(28),x15(26)];
yx33 = [y1(34),y2(34),y3(34),y4(34),y5(34),y6(34),y7(33),y8(33),y9(32),y10(32),y11(31),y12(30),y13(29),y14(28),y15(26)];
zx33 = [z1(34),z2(34),z3(34),z4(34),z5(34),z6(34),z7(33),z8(33),z9(32),z10(32),z11(31),z12(30),z13(29),z14(28),z15(26)];

topx33 = [top15(26),top14(28),top13(29),top12(30),top11(31),top10(32),top9(32),top8(33),top7(33),top6(34),top5(34),top4(34),top3(34),top2(34),top1(34)];
for n = 1:15
  co = top1(n)/100;
  %plot3(xx33(n),yx33(n),zx33(n),'.','Markersize', 20,'Color',[0,co,0]);
end

%INTERPOLATED CONTOUR CX33
% 1mm interpolated contour lines for CX33
cn33yx = min(yx33):1:max(yx33);
for n = 1:length(cn33yx)
  cn33zx(n) = zx33(1);
end
cn33xxi = interp1(yx33,xx33,cn33yx,'spline');
%cn33x = plot3(cn33xxi,cn33yx,cn33zx,'Linewidth',0.75);

stp = 1;
for k = 1:14
  ncval = topx33(k);   %starting point of 5 colour bands
  pcval = ncval/100;   %progressive point for each band
  ncval2 = topx33(k+1);   %end point of 5 colour bands
  for j = stp:(stp+4)   %DIVIDE FIRST INTERVAL INTO 5 COLOUR BANDS
    colx(1) = cn33xxi(j);
    colx(2) = cn33xxi(j+1);
    coly(1) = cn33yx(j);
    coly(2) = cn33yx(j+1);
    colz(1) = cn33zx(j);
    colz(2) = cn33zx(j+1);
    cval = ((pcval*100)+((ncval2-ncval)/5))/100;
    cvalp = (cval+pcval)/2;   %average between two points for a colour
    cvalp = round(cvalp*100)+1;
    pcval = cval;
    plot3(colx,coly,colz,'Color',[gdmap(cvalp,1),gdmap(cvalp,2),gdmap(cvalp,3)],'Linewidth',0.75);   %[0,cvalp,0]
  end
stp = stp+5;
end


%CX34
xx34 = [x1(35),x2(35),x3(35),x4(35),x5(35),x6(35),x7(34),x8(34),x9(33),x10(33),x11(32),x12(31),x13(30)];
yx34 = [y1(35),y2(35),y3(35),y4(35),y5(35),y6(35),y7(34),y8(34),y9(33),y10(33),y11(32),y12(31),y13(30)];
zx34 = [z1(35),z2(35),z3(35),z4(35),z5(35),z6(35),z7(34),z8(34),z9(33),z10(33),z11(32),z12(31),z13(30)];

topx34 = [top13(30),top12(31),top11(32),top10(33),top9(33),top8(34),top7(34),top6(35),top5(35),top4(35),top3(35),top2(35),top1(35)];
for n = 1:13
  co = top1(n)/100;
  %plot3(xx34(n),yx34(n),zx34(n),'.','Markersize', 20,'Color',[0,co,0]);
```

```
end

%INTERPOLATED CONTOUR CX34
% 1mm interpolated contour lines for CX34
cn34yx = min(yx34):1:max(yx34);
for n = 1:length(cn34yx)
  cn34zx(n) = zx34(1);
end
cn34xxi = interp1(yx34,xx34,cn34yx,'spline');
%cn34x = plot3(cn34xxi,cn34yx,cn34zx,'Linewidth',0.75);

stp = 1;
for k = 1:12
  ncval = topx34(k);   %starting point of 5 colour bands
  pcval = ncval/100;   %progressive point for each band
  ncval2 = topx34(k+1);   %end point of 5 colour bands
  for j = stp:(stp+4)   %DIVIDE FIRST INTERVAL INTO 5 COLOUR BANDS
    colx(1) = cn34xxi(j);
    colx(2) = cn34xxi(j+1);
    coly(1) = cn34yx(j);
    coly(2) = cn34yx(j+1);
    colz(1) = cn34zx(j);
    colz(2) = cn34zx(j+1);
    cval = ((pcval*100)+((ncval2-ncval)/5))/100;
    cvalp = (cval+pcval)/2;   %average between two points for a colour
    cvalp = round(cvalp*100)+1;
    pcval = cval;
    plot3(colx,coly,colz,'Color',[gdmap(cvalp,1),gdmap(cvalp,2),gdmap(cvalp,3)],'Linewidth',0.75);   %[0,cvalp,0]
  end
stp = stp+5;
end

%CX35
xx35 = [x1(36),x2(36),x3(36),x4(36),x5(36),x6(36),x7(35),x8(35),x9(34),x10(34),x11(33),x12(32),x13(31)];
yx35 = [y1(36),y2(36),y3(36),y4(36),y5(36),y6(36),y7(35),y8(35),y9(34),y10(34),y11(33),y12(32),y13(31)];
zx35 = [z1(36),z2(36),z3(36),z4(36),z5(36),z6(36),z7(35),z8(35),z9(34),z10(34),z11(33),z12(32),z13(31)];

topx35 = [top13(31),top12(32),top11(33),top10(34),top9(34),top8(35),top7(35),top6(36),top5(36),top4(36),top3(36),top2(36),top1(36)];
for n = 1:13
  co = top1(n)/100;
  %plot3(xx35(n),yx35(n),zx35(n),'.','Markersize', 20,'Color',[0,co,0]);
end

%INTERPOLATED CONTOUR CX35
% 1mm interpolated contour lines for CX35
cn35yx = min(yx35):1:max(yx35);
for n = 1:length(cn35yx)
  cn35zx(n) = zx35(1);
end
cn35xxi = interp1(yx35,xx35,cn35yx,'spline');
%cn35x = plot3(cn35xxi,cn35yx,cn35zx,'Linewidth',0.75);

stp = 1;
for k = 1:12
  ncval = topx35(k);   %starting point of 5 colour bands
  pcval = ncval/100;   %progressive point for each band
  ncval2 = topx35(k+1);   %end point of 5 colour bands
  for j = stp:(stp+4)   %DIVIDE FIRST INTERVAL INTO 5 COLOUR BANDS
    colx(1) = cn35xxi(j);
    colx(2) = cn35xxi(j+1);
    coly(1) = cn35yx(j);
    coly(2) = cn35yx(j+1);
    colz(1) = cn35zx(j);
    colz(2) = cn35zx(j+1);
    cval = ((pcval*100)+((ncval2-ncval)/5))/100;
    cvalp = (cval+pcval)/2;   %average between two points for a colour
    cvalp = round(cvalp*100)+1;
    pcval = cval;
    plot3(colx,coly,colz,'Color',[gdmap(cvalp,1),gdmap(cvalp,2),gdmap(cvalp,3)],'Linewidth',0.75);   %[0,cvalp,0]
  end
stp = stp+5;
end

%CX36
xx36 = [x1(37),x2(37),x3(37),x4(37),x5(37),x6(37),x7(36),x8(36),x9(35),x10(35),x11(34),x12(33),x13(32)];
yx36 = [y1(37),y2(37),y3(37),y4(37),y5(37),y6(37),y7(36),y8(36),y9(35),y10(35),y11(34),y12(33),y13(32)];
zx36 = [z1(37),z2(37),z3(37),z4(37),z5(37),z6(37),z7(36),z8(36),z9(35),z10(35),z11(34),z12(33),z13(32)];

topx36 = [top13(32),top12(33),top11(34),top10(35),top9(35),top8(36),top7(36),top6(37),top5(37),top4(37),top3(37),top2(37),top1(37)];
for n = 1:13
  co = top1(n)/100;
  %plot3(xx36(n),yx36(n),zx36(n),'.','Markersize', 20,'Color',[0,co,0]);
end

%INTERPOLATED CONTOUR CX36
% 1mm interpolated contour lines for CX36
cn36yx = min(yx36):1:max(yx36);
for n = 1:length(cn36yx)
  cn36zx(n) = zx36(1);
end
cn36xxi = interp1(yx36,xx36,cn36yx,'spline');
%cn36x = plot3(cn36xxi,cn36yx,cn36zx,'Linewidth',0.75);

stp = 1;
```

```
for k = 1:12
  ncval = topx36(k);   %starting point of 5 colour bands
  pcval = ncval/100;   %progressive point for each band
  ncval2 = topx36(k+1);   %end point of 5 colour bands
  for j = stp:(stp+4)   %DIVIDE FIRST INTERVAL INTO 5 COLOUR BANDS
    colx(1) = cn36xxi(j);
    colx(2) = cn36xxi(j+1);
    coly(1) = cn36yx(j);
    coly(2) = cn36yx(j+1);
    colz(1) = cn36zx(j);
    colz(2) = cn36zx(j+1);
    cval = ((pcval*100)+((ncval2-ncval)/5))/100;
    cvalp = (cval+pcval)/2;   %average between two points for a colour
    cvalp = round(cvalp*100)+1;
    pcval = cval;
    plot3(colx,coly,colz,'Color',[gdmap(cvalp,1),gdmap(cvalp,2),gdmap(cvalp,3)],'Linewidth',0.75);   %[0,cvalp,0]
  end
stp = stp+5;
end

%CX37
xx37 = [x1(38),x2(38),x3(38),x4(38),x5(38),x6(38),x7(37),x8(37),x9(36),x10(36),x11(35),x12(34)];
yx37 = [y1(38),y2(38),y3(38),y4(38),y5(38),y6(38),y7(37),y8(37),y9(36),y10(36),y11(35),y12(34)];
zx37 = [z1(38),z2(38),z3(38),z4(38),z5(38),z6(38),z7(37),z8(37),z9(36),z10(36),z11(35),z12(34)];

topx37 = [top12(34),top11(35),top10(36),top9(36),top8(37),top7(37),top6(38),top5(38),top4(38),top3(38),top2(38),top1(38)];
for n = 1:12
  co = top1(n)/100;
  %plot3(xx37(n),yx37(n),zx37(n),'.','Markersize', 20,'Color',[0,co,0]);
end

%INTERPOLATED CONTOUR CX37
% 1mm interpolated contour lines for CX37
cn37yx = min(yx37):1:max(yx37);
for n = 1:length(cn37yx)
  cn37zx(n) = zx37(1);
end
cn37xxi = interp1(yx37,xx37,cn37yx,'spline');
%cn37x = plot3(cn37xxi,cn37yx,cn37zx,'Linewidth',0.75);

stp = 1;
for k = 1:11
  ncval = topx37(k);   %starting point of 5 colour bands
  pcval = ncval/100;   %progressive point for each band
  ncval2 = topx37(k+1);   %end point of 5 colour bands
  for j = stp:(stp+4)   %DIVIDE FIRST INTERVAL INTO 5 COLOUR BANDS
    colx(1) = cn37xxi(j);
    colx(2) = cn37xxi(j+1);
    coly(1) = cn37yx(j);
    coly(2) = cn37yx(j+1);
    colz(1) = cn37zx(j);
    colz(2) = cn37zx(j+1);
    cval = ((pcval*100)+((ncval2-ncval)/5))/100;
    cvalp = (cval+pcval)/2;   %average between two points for a colour
    cvalp = round(cvalp*100)+1;
    pcval = cval;
    plot3(colx,coly,colz,'Color',[gdmap(cvalp,1),gdmap(cvalp,2),gdmap(cvalp,3)],'Linewidth',0.75);   %[0,cvalp,0]
  end
stp = stp+5;
end

%CX38
xx38 = [x1(39),x2(39),x3(39),x4(39),x5(39),x6(39),x7(38),x8(38),x9(37),x10(37),x11(36),x12(35)];
yx38 = [y1(39),y2(39),y3(39),y4(39),y5(39),y6(39),y7(38),y8(38),y9(37),y10(37),y11(36),y12(35)];
zx38 = [z1(39),z2(39),z3(39),z4(39),z5(39),z6(39),z7(38),z8(38),z9(37),z10(37),z11(36),z12(35)];

topx38 = [top12(35),top11(36),top10(37),top9(37),top8(38),top7(38),top6(39),top5(39),top4(39),top3(39),top2(39),top1(39)];
for n = 1:12
  co = top1(n)/100;
  %plot3(xx38(n),yx38(n),zx38(n),'.','Markersize', 20,'Color',[0,co,0]);
end

%INTERPOLATED CONTOUR CX38
% 1mm interpolated contour lines for CX38
cn38yx = min(yx38):1:max(yx38);
for n = 1:length(cn38yx)
  cn38zx(n) = zx38(1);
end
cn38xxi = interp1(yx38,xx38,cn38yx,'spline');
%cn38x = plot3(cn38xxi,cn38yx,cn38zx,'Linewidth',0.75);

stp = 1;
for k = 1:11
  ncval = topx38(k);   %starting point of 5 colour bands
  pcval = ncval/100;   %progressive point for each band
  ncval2 = topx38(k+1);   %end point of 5 colour bands
  for j = stp:(stp+4)   %DIVIDE FIRST INTERVAL INTO 5 COLOUR BANDS
    colx(1) = cn38xxi(j);
    colx(2) = cn38xxi(j+1);
    coly(1) = cn38yx(j);
    coly(2) = cn38yx(j+1);
    colz(1) = cn38zx(j);
    colz(2) = cn38zx(j+1);
    cval = ((pcval*100)+((ncval2-ncval)/5))/100;
```

```
    cvalp = (cval+pcval)/2;   %average between two points for a colour
    cvalp = round(cvalp*100)+1;
    pcval = cval;
    plot3(colx,coly,colz,'Color',[gdmap(cvalp,1),gdmap(cvalp,2),gdmap(cvalp,3)],'Linewidth',0.75);   %[0,cvalp,0]
  end
stp = stp+5;
end

%CX39
xx39 = [x1(40),x2(40),x3(40),x4(40),x5(40),x6(40),x7(39),x8(39),x9(38),x10(38),x11(37),x12(36)];
yx39 = [y1(40),y2(40),y3(40),y4(40),y5(40),y6(40),y7(39),y8(39),y9(38),y10(38),y11(37),y12(36)];
zx39 = [z1(40),z2(40),z3(40),z4(40),z5(40),z6(40),z7(39),z8(39),z9(38),z10(38),z11(37),z12(36)];

topx39 = [top12(36),top11(37),top10(38),top9(38),top8(39),top7(39),top6(40),top5(40),top4(40),top3(40),top2(40),top1(40)];
for n = 1:12
  co = top1(n)/100;
  %plot3(xx39(n),yx39(n),zx39(n),'.','Markersize', 20,'Color',[0,co,0]);
end

%INTERPOLATED CONTOUR CX39
% 1mm interpolated contour lines for CX39
cn39yx = min(yx39):1:max(yx39);
for n = 1:length(cn39yx)
  cn39zx(n) = zx39(1);
end
cn39xxi = interp1(yx39,xx39,cn39yx,'spline');
%cn39x = plot3(cn39xxi,cn39yx,cn39zx,'Linewidth',0.75);

stp = 1;
for k = 1:11
  ncval = topx39(k);   %starting point of 5 colour bands
  pcval = ncval/100;   %progressive point for each band
  ncval2 = topx39(k+1);   %end point of 5 colour bands
  for j = stp:(stp+4)   %DIVIDE FIRST INTERVAL INTO 5 COLOUR BANDS
    colx(1) = cn39xxi(j);
    colx(2) = cn39xxi(j+1);
    coly(1) = cn39yx(j);
    coly(2) = cn39yx(j+1);
    colz(1) = cn39zx(j);
    colz(2) = cn39zx(j+1);
    cval = ((pcval*100)+((ncval2-ncval)/5))/100;
    cvalp = (cval+pcval)/2;   %average between two points for a colour
    cvalp = round(cvalp*100)+1;
    pcval = cval;
    plot3(colx,coly,colz,'Color',[gdmap(cvalp,1),gdmap(cvalp,2),gdmap(cvalp,3)],'Linewidth',0.75);   %[0,cvalp,0]
  end
stp = stp+5;
end

%CX40
xx40 = [x1(41),x2(41),x3(41),x4(41),x5(41),x6(41),x7(40),x8(40),x9(39),x10(39),x11(38),x12(37)];
yx40 = [y1(41),y2(41),y3(41),y4(41),y5(41),y6(41),y7(40),y8(40),y9(39),y10(39),y11(38),y12(37)];
zx40 = [z1(41),z2(41),z3(41),z4(41),z5(41),z6(41),z7(40),z8(40),z9(39),z10(39),z11(38),z12(37)];

topx40 = [top12(37),top11(38),top10(39),top9(39),top8(40),top7(40),top6(41),top5(41),top4(41),top3(41),top2(41),top1(41)];
for n = 1:12
  co = top1(n)/100;
  %plot3(xx40(n),yx40(n),zx40(n),'.','Markersize', 20,'Color',[0,co,0]);
end

%INTERPOLATED CONTOUR CX40
% 1mm interpolated contour lines for CX40
cn40yx = min(yx40):1:max(yx40);
for n = 1:length(cn40yx)
  cn40zx(n) = zx40(1);
end
cn40xxi = interp1(yx40,xx40,cn40yx,'spline');
%cn40x = plot3(cn40xxi,cn40yx,cn40zx,'Linewidth',0.75);

stp = 1;
for k = 1:11
  ncval = topx40(k);   %starting point of 5 colour bands
  pcval = ncval/100;   %progressive point for each band
  ncval2 = topx40(k+1);   %end point of 5 colour bands
  for j = stp:(stp+4)   %DIVIDE FIRST INTERVAL INTO 5 COLOUR BANDS
    colx(1) = cn40xxi(j);
    colx(2) = cn40xxi(j+1);
    coly(1) = cn40yx(j);
    coly(2) = cn40yx(j+1);
    colz(1) = cn40zx(j);
    colz(2) = cn40zx(j+1);
    cval = ((pcval*100)+((ncval2-ncval)/5))/100;
    cvalp = (cval+pcval)/2;   %average between two points for a colour
    cvalp = round(cvalp*100)+1;
    pcval = cval;
    plot3(colx,coly,colz,'Color',[gdmap(cvalp,1),gdmap(cvalp,2),gdmap(cvalp,3)],'Linewidth',0.75);   %[0,cvalp,0]
  end
stp = stp+5;
end

%CX41
xx41 = [x1(42),x2(42),x3(42),x4(42),x5(42),x6(42),x7(41),x8(41),x9(40),x10(40),x11(39),x12(38)];
yx41 = [y1(42),y2(42),y3(42),y4(42),y5(42),y6(42),y7(41),y8(41),y9(40),y10(40),y11(39),y12(38)];
zx41 = [z1(42),z2(42),z3(42),z4(42),z5(42),z6(42),z7(41),z8(41),z9(40),z10(40),z11(39),z12(38)];
```

```
topx41 = [top12(38),top11(39),top10(40),top9(40),top8(41),top7(41),top6(42),top5(42),top4(42),top3(42),top2(42),top1(42)];
for n = 1:12
  co = top1(n)/100;
  %plot3(xx41(n),yx41(n),zx41(n),'.','Markersize', 20,'Color',[0,co,0]);
end

%INTERPOLATED CONTOUR CX41
% 1mm interpolated contour lines for CX41
cn41yx = min(yx41):1:max(yx41);
for n = 1:length(cn41yx)
  cn41zx(n) = zx41(1);
end
cn41xxi = interp1(yx41,xx41,cn41yx,'spline');
%cn41x = plot3(cn41xxi,cn41yx,cn41zx,'Linewidth',0.75);

stp = 1;
for k = 1:11
  ncval = topx41(k);   %starting point of 5 colour bands
  pcval = ncval/100;   %progressive point for each band
  ncval2 = topx41(k+1);   %end point of 5 colour bands
  for j = stp:(stp+4)   %DIVIDE FIRST INTERVAL INTO 5 COLOUR BANDS
    colx(1) = cn41xxi(j);
    colx(2) = cn41xxi(j+1);
    coly(1) = cn41yx(j);
    coly(2) = cn41yx(j+1);
    colz(1) = cn41zx(j);
    colz(2) = cn41zx(j+1);
    cval = ((pcval*100)+((ncval2-ncval)/5))/100;
    cvalp = (cval+pcval)/2;   %average between two points for a colour
    cvalp = round(cvalp*100)+1;
    pcval = cval;
    plot3(colx,coly,colz,'Color',[gdmap(cvalp,1),gdmap(cvalp,2),gdmap(cvalp,3)],'Linewidth',0.75);   %[0,cvalp,0]
  end
stp = stp+5;
end

%CX42
xx42 = [x1(43),x2(43),x3(43),x4(43),x5(43),x6(43),x7(42),x8(42),x9(41),x10(41),x11(40),x12(39)];
yx42 = [y1(43),y2(43),y3(43),y4(43),y5(43),y6(43),y7(42),y8(42),y9(41),y10(41),y11(40),y12(39)];
zx42 = [z1(43),z2(43),z3(43),z4(43),z5(43),z6(43),z7(42),z8(42),z9(41),z10(41),z11(40),z12(39)];

topx42 = [top12(39),top11(40),top10(41),top9(41),top8(42),top7(42),top6(43),top5(43),top4(43),top3(43),top2(43),top1(43)];
for n = 1:12
  co = top1(n)/100;
  %plot3(xx42(n),yx42(n),zx42(n),'.','Markersize', 20,'Color',[0,co,0]);
end

%INTERPOLATED CONTOUR CX42
% 1mm interpolated contour lines for CX42
cn42yx = min(yx42):1:max(yx42);
for n = 1:length(cn42yx)
  cn42zx(n) = zx42(1);
end
cn42xxi = interp1(yx42,xx42,cn42yx,'spline');
%cn42x = plot3(cn42xxi,cn42yx,cn42zx,'Linewidth',0.75);

stp = 1;
for k = 1:11
  ncval = topx42(k);   %starting point of 5 colour bands
  pcval = ncval/100;   %progressive point for each band
  ncval2 = topx42(k+1);   %end point of 5 colour bands
  for j = stp:(stp+4)   %DIVIDE FIRST INTERVAL INTO 5 COLOUR BANDS
    colx(1) = cn42xxi(j);
    colx(2) = cn42xxi(j+1);
    coly(1) = cn42yx(j);
    coly(2) = cn42yx(j+1);
    colz(1) = cn42zx(j);
    colz(2) = cn42zx(j+1);
    cval = ((pcval*100)+((ncval2-ncval)/5))/100;
    cvalp = (cval+pcval)/2;   %average between two points for a colour
    cvalp = round(cvalp*100)+1;
    pcval = cval;
    plot3(colx,coly,colz,'Color',[gdmap(cvalp,1),gdmap(cvalp,2),gdmap(cvalp,3)],'Linewidth',0.75);   %[0,cvalp,0]
  end
stp = stp+5;
end

%CX43
xx43 = [x1(44),x2(44),x3(44),x4(44),x5(44),x6(44),x7(43),x8(43),x9(42),x10(42),x11(41),x12(40)];
yx43 = [y1(44),y2(44),y3(44),y4(44),y5(44),y6(44),y7(43),y8(43),y9(42),y10(42),y11(41),y12(40)];
zx43 = [z1(44),z2(44),z3(44),z4(44),z5(44),z6(44),z7(43),z8(43),z9(42),z10(42),z11(41),z12(40)];

topx43 = [top12(40),top11(41),top10(42),top9(42),top8(43),top7(43),top6(44),top5(44),top4(44),top3(44),top2(44),top1(44)];
for n = 1:12
  co = top1(n)/100;
  %plot3(xx43(n),yx43(n),zx43(n),'.','Markersize', 20,'Color',[0,co,0]);
end

%INTERPOLATED CONTOUR CX43
% 1mm interpolated contour lines for CX43
cn43yx = min(yx43):1:max(yx43);
for n = 1:length(cn43yx)
  cn43zx(n) = zx43(1);
```

```
end
cn43xxi = interp1(yx43,xx43,cn43yx,'spline');
%cn43x = plot3(cn43xxi,cn43yx,cn43zx,'Linewidth',0.75);

stp = 1;
for k = 1:11
  ncval = topx43(k);   %starting point of 5 colour bands
  pcval = ncval/100;   %progressive point for each band
  ncval2 = topx43(k+1);   %end point of 5 colour bands
  for j = stp:(stp+4)   %DIVIDE FIRST INTERVAL INTO 5 COLOUR BANDS
    colx(1) = cn43xxi(j);
    colx(2) = cn43xxi(j+1);
    coly(1) = cn43yx(j);
    coly(2) = cn43yx(j+1);
    colz(1) = cn43zx(j);
    colz(2) = cn43zx(j+1);
    cval = ((pcval*100)+((ncval2-ncval)/5))/100;
    cvalp = (cval+pcval)/2;   %average between two points for a colour
    cvalp = round(cvalp*100)+1;
    pcval = cval;
    plot3(colx,coly,colz,'Color',[gdmap(cvalp,1),gdmap(cvalp,2),gdmap(cvalp,3)],'Linewidth',0.75);   %[0,cvalp,0]
  end
stp = stp+5;
end

%CX44
xx44 = [x1(45),x2(45),x3(45),x4(45),x5(45),x6(45),x7(44),x8(44),x9(43),x10(43),x11(42),x12(41)];
yx44 = [y1(45),y2(45),y3(45),y4(45),y5(45),y6(45),y7(44),y8(44),y9(43),y10(43),y11(42),y12(41)];
zx44 = [z1(45),z2(45),z3(45),z4(45),z5(45),z6(45),z7(44),z8(44),z9(43),z10(43),z11(42),z12(41)];

topx44 = [top12(41),top11(42),top10(43),top9(43),top8(44),top7(44),top6(45),top5(45),top4(45),top3(45),top2(45),top1(45)];
for n = 1:12
  co = top1(n)/100;
  %plot3(xx44(n),yx44(n),zx44(n),'.','Markersize', 20,'Color',[0,co,0]);
end

%INTERPOLATED CONTOUR CX44
% 1mm interpolated contour lines for CX44
cn44yx = min(yx44):1:max(yx44);
for n = 1:length(cn44yx)
  cn44zx(n) = zx44(1);
end
cn44xxi = interp1(yx44,xx44,cn44yx,'spline');
%cn44x = plot3(cn44xxi,cn44yx,cn44zx,'Linewidth',0.75);

stp = 1;
for k = 1:11
  ncval = topx44(k);   %starting point of 5 colour bands
  pcval = ncval/100;   %progressive point for each band
  ncval2 = topx44(k+1);   %end point of 5 colour bands
  for j = stp:(stp+4)   %DIVIDE FIRST INTERVAL INTO 5 COLOUR BANDS
    colx(1) = cn44xxi(j);
    colx(2) = cn44xxi(j+1);
    coly(1) = cn44yx(j);
    coly(2) = cn44yx(j+1);
    colz(1) = cn44zx(j);
    colz(2) = cn44zx(j+1);
    cval = ((pcval*100)+((ncval2-ncval)/5))/100;
    cvalp = (cval+pcval)/2;   %average between two points for a colour
    cvalp = round(cvalp*100)+1;
    pcval = cval;
    plot3(colx,coly,colz,'Color',[gdmap(cvalp,1),gdmap(cvalp,2),gdmap(cvalp,3)],'Linewidth',0.75);   %[0,cvalp,0]
  end
stp = stp+5;
end

%CX45
xx45 = [x1(46),x2(46),x3(46),x4(46),x5(46),x6(46),x7(45),x8(45),x9(44),x10(44),x11(43),x12(42)];
yx45 = [y1(46),y2(46),y3(46),y4(46),y5(46),y6(46),y7(45),y8(45),y9(44),y10(44),y11(43),y12(42)];
zx45 = [z1(46),z2(46),z3(46),z4(46),z5(46),z6(46),z7(45),z8(45),z9(44),z10(44),z11(43),z12(42)];

topx45 = [top12(42),top11(43),top10(44),top9(44),top8(45),top7(45),top6(46),top5(46),top4(46),top3(46),top2(46),top1(46)];
for n = 1:12
  co = top1(n)/100;
  %plot3(xx45(n),yx45(n),zx45(n),'.','Markersize', 20,'Color',[0,co,0]);
end

%INTERPOLATED CONTOUR CX45
% 1mm interpolated contour lines for CX45
cn45yx = min(yx45):1:max(yx45);
for n = 1:length(cn45yx)
  cn45zx(n) = zx45(1);
end
cn45xxi = interp1(yx45,xx45,cn45yx,'spline');
%cn45x = plot3(cn45xxi,cn45yx,cn45zx,'Linewidth',0.75);

stp = 1;
for k = 1:11
  ncval = topx45(k);   %starting point of 5 colour bands
  pcval = ncval/100;   %progressive point for each band
  ncval2 = topx45(k+1);   %end point of 5 colour bands
  for j = stp:(stp+4)   %DIVIDE FIRST INTERVAL INTO 5 COLOUR BANDS
    colx(1) = cn45xxi(j);
    colx(2) = cn45xxi(j+1);
```

```
      coly(1) = cn45yx(j);
      coly(2) = cn45yx(j+1);
      colz(1) = cn45zx(j);
      colz(2) = cn45zx(j+1);
      cval = ((pcval*100)+((ncval2-ncval)/5))/100;
      cvalp = (cval+pcval)/2;   %average between two points for a colour
      cvalp = round(cvalp*100)+1;
      pcval = cval;
      plot3(colx,coly,colz,'Color',[gdmap(cvalp,1),gdmap(cvalp,2),gdmap(cvalp,3)],'Linewidth',0.75);   %[0,cvalp,0]
   end
stp = stp+5;
end

%CX46
xx46 = [x1(47),x2(47),x3(47),x4(47),x5(47),x6(47),x7(46),x8(46),x9(45),x10(45),x11(44),x12(43)];
yx46 = [y1(47),y2(47),y3(47),y4(47),y5(47),y6(47),y7(46),y8(46),y9(45),y10(45),y11(44),y12(43)];
zx46 = [z1(47),z2(47),z3(47),z4(47),z5(47),z6(47),z7(46),z8(46),z9(45),z10(45),z11(44),z12(43)];

topx46 = [top12(43),top11(44),top10(45),top9(45),top8(46),top7(46),top6(47),top5(47),top4(47),top3(47),top2(47),top1(47)];
for n = 1:12
   co = top1(n)/100;
   %plot3(xx46(n),yx46(n),zx46(n),'.','Markersize', 20,'Color',[0,co,0]);
end

%INTERPOLATED CONTOUR CX46
% 1mm interpolated contour lines for CX46
cn46yx = min(yx46):1:max(yx46);
for n = 1:length(cn46yx)
   cn46zx(n) = zx46(1);
end
cn46xxi = interp1(yx46,xx46,cn46yx,'spline');
%cn46x = plot3(cn46xxi,cn46yx,cn46zx,'Linewidth',0.75);

stp = 1;
for k = 1:11
   ncval = topx46(k);   %starting point of 5 colour bands
   pcval = ncval/100;   %progressive point for each band
   ncval2 = topx46(k+1);   %end point of 5 colour bands
   for j = stp:(stp+4)   %DIVIDE FIRST INTERVAL INTO 5 COLOUR BANDS
      colx(1) = cn46xxi(j);
      colx(2) = cn46xxi(j+1);
      coly(1) = cn46yx(j);
      coly(2) = cn46yx(j+1);
      colz(1) = cn46zx(j);
      colz(2) = cn46zx(j+1);
      cval = ((pcval*100)+((ncval2-ncval)/5))/100;
      cvalp = (cval+pcval)/2;   %average between two points for a colour
      cvalp = round(cvalp*100)+1;
      pcval = cval;
      plot3(colx,coly,colz,'Color',[gdmap(cvalp,1),gdmap(cvalp,2),gdmap(cvalp,3)],'Linewidth',0.75);   %[0,cvalp,0]
   end
stp = stp+5;
end

%CX47
xx47 = [x1(48),x2(48),x3(48),x4(48),x5(48),x6(48),x7(47),x8(47),x9(46),x10(46),x11(45),x12(44)];
yx47 = [y1(48),y2(48),y3(48),y4(48),y5(48),y6(48),y7(47),y8(47),y9(46),y10(46),y11(45),y12(44)];
zx47 = [z1(48),z2(48),z3(48),z4(48),z5(48),z6(48),z7(47),z8(47),z9(46),z10(46),z11(45),z12(44)];

topx47 = [top12(44),top11(45),top10(46),top9(46),top8(47),top7(47),top6(48),top5(48),top4(48),top3(48),top2(48),top1(48)];
for n = 1:12
   co = top1(n)/100;
   %plot3(xx47(n),yx47(n),zx47(n),'.','Markersize', 20,'Color',[0,co,0]);
end

%INTERPOLATED CONTOUR CX47
% 1mm interpolated contour lines for CX47
cn47yx = min(yx47):1:max(yx47);
for n = 1:length(cn47yx)
   cn47zx(n) = zx47(1);
end
cn47xxi = interp1(yx47,xx47,cn47yx,'spline');
%cn47x = plot3(cn47xxi,cn47yx,cn47zx,'Linewidth',0.75);

stp = 1;
for k = 1:11
   ncval = topx47(k);   %starting point of 5 colour bands
   pcval = ncval/100;   %progressive point for each band
   ncval2 = topx47(k+1);   %end point of 5 colour bands
   for j = stp:(stp+4)   %DIVIDE FIRST INTERVAL INTO 5 COLOUR BANDS
      colx(1) = cn47xxi(j);
      colx(2) = cn47xxi(j+1);
      coly(1) = cn47yx(j);
      coly(2) = cn47yx(j+1);
      colz(1) = cn47zx(j);
      colz(2) = cn47zx(j+1);
      cval = ((pcval*100)+((ncval2-ncval)/5))/100;
      cvalp = (cval+pcval)/2;   %average between two points for a colour
      cvalp = round(cvalp*100)+1;
      pcval = cval;
      plot3(colx,coly,colz,'Color',[gdmap(cvalp,1),gdmap(cvalp,2),gdmap(cvalp,3)],'Linewidth',0.75);   %[0,cvalp,0]
   end
stp = stp+5;
end
```

```
%CX48
xx48 = [x1(49),x2(49),x3(49),x4(49),x5(49),x6(49),x7(48),x8(48),x9(47),x10(47),x11(46),x12(45)];
yx48 = [y1(49),y2(49),y3(49),y4(49),y5(49),y6(49),y7(48),y8(48),y9(47),y10(47),y11(46),y12(45)];
zx48 = [z1(49),z2(49),z3(49),z4(49),z5(49),z6(49),z7(48),z8(48),z9(47),z10(47),z11(46),z12(45)];

topx48 = [top12(45),top11(46),top10(47),top9(47),top8(48),top7(48),top6(49),top5(49),top4(49),top3(49),top2(49),top1(49)];
for n = 1:12
  co = top1(n)/100;
  %plot3(xx48(n),yx48(n),zx48(n),'.','Markersize', 20,'Color',[0,co,0]);
end

%INTERPOLATED CONTOUR CX48
% 1mm interpolated contour lines for CX48
cn48yx = min(yx48):1:max(yx48);
for n = 1:length(cn48yx)
  cn48zx(n) = zx48(1);
end
cn48xxi = interp1(yx48,xx48,cn48yx,'spline');
%cn48x = plot3(cn48xxi,cn48yx,cn48zx,'Linewidth',0.75);

stp = 1;
for k = 1:11
  ncval = topx48(k);   %starting point of 5 colour bands
  pcval = ncval/100;   %progressive point for each band
  ncval2 = topx48(k+1);   %end point of 5 colour bands
  for j = stp:(stp+4)   %DIVIDE FIRST INTERVAL INTO 5 COLOUR BANDS
    colx(1) = cn48xxi(j);
    colx(2) = cn48xxi(j+1);
    coly(1) = cn48yx(j);
    coly(2) = cn48yx(j+1);
    colz(1) = cn48zx(j);
    colz(2) = cn48zx(j+1);
    cval = ((pcval*100)+((ncval2-ncval)/5))/100;
    cvalp = (cval+pcval)/2;   %average between two points for a colour
    cvalp = round(cvalp*100)+1;
    pcval = cval;
    plot3(colx,coly,colz,'Color',[gdmap(cvalp,1),gdmap(cvalp,2),gdmap(cvalp,3)],'Linewidth',0.75);   %[0,cvalp,0]
  end
stp = stp+5;
end

%CX49
xx49 = [x1(50),x2(50),x3(50),x4(50),x5(50),x6(50),x7(49),x8(49),x9(48),x10(48),x11(47),x12(46)];
yx49 = [y1(50),y2(50),y3(50),y4(50),y5(50),y6(50),y7(49),y8(49),y9(48),y10(48),y11(47),y12(46)];
zx49 = [z1(50),z2(50),z3(50),z4(50),z5(50),z6(50),z7(49),z8(49),z9(48),z10(48),z11(47),z12(46)];

topx49 = [top12(46),top11(47),top10(48),top9(48),top8(49),top7(49),top6(50),top5(50),top4(50),top3(50),top2(50),top1(50)];
for n = 1:12
  co = top1(n)/100;
  %plot3(xx49(n),yx49(n),zx49(n),'.','Markersize', 20,'Color',[0,co,0]);
end

%INTERPOLATED CONTOUR CX49
% 1mm interpolated contour lines for CX49
cn49yx = min(yx49):1:max(yx49);
for n = 1:length(cn49yx)
  cn49zx(n) = zx49(1);
end
cn49xxi = interp1(yx49,xx49,cn49yx,'spline');
%cn49x = plot3(cn49xxi,cn49yx,cn49zx,'Linewidth',0.75);

stp = 1;
for k = 1:11
  ncval = topx49(k);   %starting point of 5 colour bands
  pcval = ncval/100;   %progressive point for each band
  ncval2 = topx49(k+1);   %end point of 5 colour bands
  for j = stp:(stp+4)   %DIVIDE FIRST INTERVAL INTO 5 COLOUR BANDS
    colx(1) = cn49xxi(j);
    colx(2) = cn49xxi(j+1);
    coly(1) = cn49yx(j);
    coly(2) = cn49yx(j+1);
    colz(1) = cn49zx(j);
    colz(2) = cn49zx(j+1);
    cval = ((pcval*100)+((ncval2-ncval)/5))/100;
    cvalp = (cval+pcval)/2;   %average between two points for a colour
    cvalp = round(cvalp*100)+1;
    pcval = cval;
    plot3(colx,coly,colz,'Color',[gdmap(cvalp,1),gdmap(cvalp,2),gdmap(cvalp,3)],'Linewidth',0.75);   %[0,cvalp,0]
  end
stp = stp+5;
end

%%plot3(x13,y13,z13,'-b',x13,y13,z13,'*b','markersize',3);
%colorbar
```

D.4 Playground exposure model

As for the exposure model presented for the face above, only one of several playground exposure models is presented in this code listing. The code below is the HBSHS playground sky view model. Albedo, winter and summer solstice shade density and UV exposure models are provided in the attached supplementary data CD-ROM. The algorithm was developed for use with MATLAB version 7.1.

```
%HBSHS grounds and buildings

clear

% Axis and background Setup
set(gca,'Color',[1,1,1],'XColor',[0.3,0.3,0.3],'YColor',[0.3,0.3,0.3],'ZColor',[0.3,0.3,0.3])
axis([-5 217.5 -5 173 0 310])
xlabel('x-axis')
ylabel('y-axis')
zlabel('z-axis')
grid off
hold on

%front and east fence
x = 0:0.1:212.5;
for c = 1:2126;
   xl(c) = 0;
   xl2(c) = 304.4;
end
line(x,xl)
line(x,xl2)

%side fences
y = 0:0.1:304.4;
for c = 1:3045;
   yl2(c) = 0;
   yl3(c) = 212.5;
end
line(yl2,y)
line(yl3,y)

%pool fence
x2 = 168.3:0.1:212.5;
for c = 1:443;
   x2l(c) = 35.8;
end
line(x2,x2l)
xx  = 0:0.1:35.8;
for c = 1:359;
   xxl(c) = 168.3;
end
line(xxl,xx)

%admin
a = 8.8:0.1:24;
for c = 1:153;
      al(c) = 44.5;
      al2(c) = 79.5;
end
line (al,a)
line (al2,a)
a2 = 24:0.1:26.5;
for c = 1:26;
   a2l(c) = 55;
   a2l2(c) = 79.5;
end
line(a2l,a2)
line(a2l2,a2)
ax = 44.5:0.1:79.5;
for c = 1:351
   axl(c) = 8.8;
   axl2(c) = 24; %30
end
line (ax,axl)
line (ax,axl2)
ax2 = 55:0.1:79.5;
for c = 1:246;
   ax2l(c) = 26.5;
end
```

```
line(ax2,ax2l)

%library
l = 11.9:0.1:43.8;
for c = 1:320
   ll(c) = 105.2;
   ll2(c) = 128.6;
end
line (ll,l)
line (ll2,l)

lx = 105.2:0.1:128.6;
for c = 1:235
   lxl(c) = 11.9;
   lxl2(c) = 43.8;
end
line (lx,lxl)
line (lx,lxl2)

%C Block
c1 = 30:0.1:74.4;
for c = 1:445;
   cl(c) = 53.6;
   cl2(c) = 43.5;
end
c2 = 30:0.1:33;
for c = 1:31;
   cl3(c) = 46.5;
end
line(cl3,c2)
c3 = 44:0.1:74.4;
for c = 1:305;
   cl4(c) = 46.5; %45.1
end
line(cl4,c3)
c4 = 76.9:0.1:91.9;
for c = 1:151;
   c4l2(c) = 46.5;
end
line(c4l2,c4)
c5 = 74.4:0.1:91.9;
for c = 1:176;
   c5l(c) = 43.5;
   c5l2(c) = 53.6;
end
line(c5l,c5)
line(c5l2,c5)

cx2 = 46.5:0.1:53.6;
for c = 1:72;
   cxl3(c) = 33;
   cxl4(c) = 44;
end
line(cx2,cxl3)
line(cx2,cxl4)

line(cl,c1)
line(cl2,c1)
cx1 = 43.5:0.1:53.6;
for c = 1:102;
   cxl(c) = 30;
   cxl2(c) = 91.9;
end
line(cx1,cxl)
line(cx1,cxl2)
cx3 = 46.5:0.1:53.6;
for c = 1:72;
   cx3l(c) = 74.4;
   cx3l2(c) = 76.9;
end
line(cx3,cx3l)
line(cx3,cx3l2)

%E block
e = 34:0.1:61.5;
for c = 1:276;
   el(c) = 28.5;
   el2(c) = 16.1;
end
line(el,e)
line(el2,e)
ex = 16.1:0.1:28.5;
for c = 1:125;
   ex1(c) = 34;
   ex2(c) = 61.5;
end
line(ex,ex1)
line(ex,ex2)

%B block
b = 33:0.1:92.6;
for c = 1:597;
   bl(c) = 89.5;
   bl2(c) = 77.5;
```

```
end
line(bl,b)
line(bl2,b)
b2 = 33:0.1:73.4;
for c = 1:405;
   bl4(c) = 80.7;
end
line(bl4,b2)
b3 = 77:0.1:80.3;
for c = 1:34;
  bl3(c) = 80.7;
end
line(bl3,b3)
b5 = 83.8:0.1:92.6;
for c = 1:89;
   b5l(c) = 80.7;
end
line(b5l,b5)
bx = 77.5:0.1:89.5;
for c = 1:121
   bx1(c) = 33;
   bx2(c) = 92.6;
end
line(bx,bx1)
line(bx,bx2)
bx2 = 80.7:0.1:89.5;
for c = 1:89;
   bx2l(c) = 73.4;
   bx2l2(c) = 77;
   bx2l3(c) = 83.8;
   bx2l4(c) = 80.3;
end
line(bx2,bx2l)
line(bx2,bx2l2)
line(bx2,bx2l3)
line(bx2,bx2l4)

%great hall
h = 14.1:0.1:22; %38
for c = 1:80
   hl(c) = 158.6;
end
h2 = 18.1:0.1:54;
for c = 1:360
   h2l(c) = 138.6;
end
hx5 = 22:0.1:47.5;
for c = 1:256;
   hx5l(c) = 160.8;
end
line (hx5l,hx5)
hx6 = 158.6:0.1:160.8;
for c = 1:23
   hx6l(c) = 22;
end
line(hx6,hx6l)
hx7 = 159.3:0.1:160.8;
for c = 1:16
   hx7l(c) = 47.5;
end
line(hx7,hx7l)

h5 = 47.5:0.1:54;
for c = 1:66;
   h5l(c) = 159.3;
end
line(h5l,h5)

line (hl,h)
line (h2l,h2)
hx = 138.6:0.1:159.3;
for c = 1:208;
   hxl(c) = 54;
end
line (hx,hxl)
hx2 = 138.6:0.1:141.1;
for c = 1:26
   hx2l(c) = 18.1;
end
line (hx2,hx2l)
h3 = 12.4:0.1:18.1;
for c = 1:58
   h3l(c) = 141.1;
end
line (h3l,h3)
hx3 = 141.1:0.1:145;
for c = 1:40
   hx3l(c) = 12.4;
end
line (hx3,hx3l)
h4 = 12.4:0.1:14.1;
for c = 1:18
   h4l(c) = 145;
end
```

```
line (h4l,h4)
hx4 = 145:0.1:158.6;
for c = 1:137
   hx4l(c) = 14.1;
end
line (hx4,hx4l)

%Art
t = 58.7:0.1:74.4;
for c = 1:158;
   tl(c) = 138.2;
end
t2 = 62.4:0.1:74.4;
for c = 1:121;
   tl2(c) = 135.8;
   tl5(c) = 156.3;
   tl6(c) = 158.2;
end
t3 = 58.7:0.1:62.4;
for c = 1:38;
   tl3(c) = 140.3;
end

line(tl,t)
line(tl2,t2)
line(tl3,t3)
line(tl5,t2)
line(tl6,t2)
tx = 135.8:0.1:138.2;
for c = 1:25;
   txl(c) = 62.4;
end
line(tx,txl)
tx2 = 138.2:0.1:140.3;
for c = 1:22;
   tx2l(c) = 58.7;
end
line(tx2,tx2l)
tx4 = 135.8:0.1:158.2;
for c = 1:225;
   txl4(c) = 74.4;
end
line(tx4,txl4)
tx8 = 140.3:0.1:158.2;
for c = 1:180;
   tx8l(c) = 62.4;
end
line(tx8,tx8l)

%D Block
d = 55.3:0.1:93;
for c = 1:378;
   dl(c) = 113.9;
   dl2(c) = 101.5;
end
line(dl,d)
line(dl2,d)
d2 = 77.2:0.1:84.2;
for c = 1:71;
   d2l(c) = 107.9;
end
line(d2l,d2)
dx = 101.5:0.1:113.9;   %102.3
for c = 1:125;
   dxl(c) = 55.3;
   dxl3(c) = 93;
end
line(dx,dxl)
line(dx,dxl3)
dx2 = 107.9:0.1:113.9;
for c = 1:61;
   dx2l(c) = 84.2;
   dx2l2(c) = 77.2;
end
line(dx2,dx2l)
line(dx2,dx2l2)

%man arts
m = 49:0.1:74.4;
for c = 1:255;
   ml(c) = 195.2;
end
line(ml,m)
m2 = 47.5:0.1:74.4;
for c = 1:270;
   m2l(c) = 172.9;
end
line(m2l,m2)
m3 = 39:0.1:47.5;
for c = 1:86;
   m3l(c) = 169.3;
end
line(m3l,m3)
m4 = 39:0.1:49;
```

```
for c = 1:101;
   m4l(c) = 199.5;
end
line(m4l,m4)
mx = 169.3:0.1:172.9;
for c = 1:37;
   mxl(c) = 47.5;
end
line(mx,mxl)
mx2 = 195.2:0.1:199.5;
for c = 1:44;
   mx2l(c) = 49;
end
line(mx2,mx2l)
mx3 = 169.3:0.1:199.5;
for c = 1:303;
   mx3l(c) = 39;
end
line(mx3,mx3l)
mx4 = 172.9:0.1:195.2;
for c = 1:224;
   mx4l(c) = 74.4;
end
line(mx4,mx4l)

%fence shed
f = 45.5:0.1:58.5;
for c = 1:131;
   fl(c) = 207;
   fl2(c) = 211.5;
end
line(fl,f)
line(fl2,f)
fx = 207:0.1:211.5;
for c = 1:46;
   fxl(c) = 45.5;
   fxl2(c) = 58.5;
end
line(fx,fxl)
line(fx,fxl2)

%man arts shed
s = 39:0.1:43.8;
for c = 1:49;
   sl(c) = 200;
   sl2(c) = 208;
end
line(sl,s)
line(sl2,s)
sx = 200:0.1:208;
for c = 1:81;
   sxl(c) = 39;
   sxl2(c) = 43.8;
end
line(sx,sxl)
line(sx,sxl2)

%pool toilet
l8 = 12:0.1:23;
for c = 1:111;
   ll8(c)= 172;
end
line(ll8,l8)
l8x = 168.3:0.1:172;
for c = 1:38;
   l8xl(c) = 12;
   l9xl(c) = 23;
end
line(l8x,l8xl)
line(l8x,l9xl)

%pool canteen
pc = 1:0.1:6;
for c = 1:51;
   pcl(c) = 171;
   pcl2(c) = 176;
end
line(pcl,pc)
line(pcl2,pc)
pcx = 171:0.1:176;
for c = 1:51;
   pcxl(c) = 1;
   pcxl2(c) = 6;
end
line(pcx,pcxl)
line(pcx,pcxl2)

%pool shed
ps = 25.9:0.1:34.3;
for c = 1:85;
   psl(c) = 201.9;
   psl2(c) = 211;
end
line(psl,ps)
```

```
line(psl2,ps)
psx = 201.9:0.1:211;
for c = 1:92;
   psxl(c) = 25.9;
   psxl2(c) = 34.3;
end
line(psx,psxl)
line(psx,psxl2)

%pool
p = 11:0.1:22.5;
for c = 1:116;
   pl(c) = 176.5;
   pl2(c) = 201.5;
end
line(pl,p)
line(pl2,p)
px = 176.5:0.1:201.5;
for c = 1:251;
   pxl(c) = 11;
   pxl2(c) = 22.5;
end
line(px,pxl)
line(px,pxl2)

%H Block
h = 84.2:0.1:110.4;
for c = 1:263;
   hl(c) = 185.6;
   hl2(c) = 182.8;
   hl3(c) = 197.8;
end
line(hl,h)
line(hl2,h)
line(hl3,h)
hxx = 182.8:0.1:197.8;
for c = 1:151;
   hxxl(c) = 84.2;
   hxxl2(c) = 110.4;
end
line(hxx,hxxl)
line(hxx,hxxl2)

%G Block
g = 77.2:0.1:83.5;
for c = 1:64;
   gl(c) = 142.3;
   gl2(c) = 172.5;
   gl3(c) = 169.9;
   gl4(c) = 140;
end
line(gl,g)
line(gl2,g)
line(gl3,g)
line(gl4,g)
g2 = 77.2:0.1:92.4;
for c = 1:153;
   g2l(c) = 150.2;
   g2l2(c) = 164.6;
   g2l3(c) = 152.2;
   g2l4(c) = 162.6;
end
line(g2l,g2)
line(g2l2,g2)
line(g2l3,g2)
line(g2l4,g2)
g3 = 83.5:0.1:100.6;
for c = 1:172;
   g3l(c) = 140;
   g3l2(c) = 172.5;
end
line(g3l,g3)
line(g3l2,g3)
g4 = 93:0.1:100.6;
for c  = 1:77;
   g4l(c) = 142.3;
   g4l2(c) = 170.3;
end
line(g4l,g4)
line(g4l2,g4)
g6 = 100.6:0.1:102.7;
for c = 1:22;
   g6l(c) = 147.8;
end
line(g6l,g6)
g7 = 102.7:0.1:107.5;
for c = 1:49;
   g7l(c) = 144.9;
end
line(g7l,g7)
g9 = 100.6:0.1:107.5;
for c = 1:70;
   g9l(c) = 165.6;
end
```

```
line(g9l,g9)
gx = 140:0.1:152.2;
for c = 1:123
   gxl(c) = 77.2;
end
line(gx,gxl)
gx2 = 150.2:0.1:164.6;
for c = 1:145;
   gx2l(c) = 92.4;
end
line(gx2,gx2l)
gx3 = 162.6:0.1:172.5;
for c = 1:100;
   gx3l(c) = 77.2;
end
line(gx3,gx3l)
gx4 = 140:0.1:142.3;
for c = 1:24;
   gx4l(c) = 83.5;
end
line(gx4,gx4l)
gx5 = 169.9:0.1:172.5;
for c = 1:27;
   gx5l(c) = 83.5;
end
line(gx5,gx5l)
gx6 = 140:0.1:142.3;
for c = 1:24;
   gx6l(c) = 93;
end
line(gx6,gx6l)
gx7 = 170.3:0.1:172.5;
for c = 1:23;
   gx7l(c) = 93;
end
line(gx7,gx7l)
gx8 = 140:0.1:147.8;
for c = 1:79;
   gx8l(c) = 100.6;
end
line(gx8,gx8l)
gx9 = 144.9:0.1:147.8;
for c = 1:30
   gx9l(c) = 102.7;
end
line(gx9,gx9l)
gx10 = 165.6:0.1:172.5;
for c = 1:70;
   gx10l(c) = 100.6;
end
line(gx10,gx10l)
gx11 = 144.9:0.1:165.6;
for c = 1:208;
   gx11l(c) = 107.5;
end
line(gx11,gx11l)

%L Block
j = 77.2:0.1:114.2;
for c = 1:371;
   jl(c) = 23.5;
   jl2(c) = 25.6;
   jl3(c) = 34.4;
end
line(jl,j)
line(jl2,j)
line(jl3,j)
jx = 23.5:0.1:34.4;
for c = 1:110;
   jxl(c) = 77.2;
   jxl2(c) = 114.2;
end
line(jx,jxl)
line(jx,jxl2)

%tuckshop
k = 68.1:0.1:80.3;
for c = 1:123;
   kl(c) = 58.2;
   kl2(c) = 72.6;
end
line(kl,k)
line(kl2,k)
kx = 58.2:0.1:72.6;
for c = 1:145;
   kxl(c) = 68.1;
   kxl2(c) = 73;
   kxl3(c) = 80.3;
end
line(kx,kxl)
line(kx,kxl2)
line(kx,kxl3)

%toilet
```

```
w = 98.3:0.1:108;
for c = 1:98;
   wl(c) = 104.9;
   wl2(c) = 125.8;
end
line(wl,w)
line(wl2,w)
w2 = 98.3:0.1:99.9;
for c = 1:17;
   w2l(c) = 112.6;
   w2l2(c) = 119.3;
end
line(w2l,w2)
line(w2l2,w2)
wx = 104.9:0.1:112.6;
for c = 1:78;
   wxl(c) = 98.3;
end
line(wx,wxl)
wx2 = 119.3:0.1:125.8;
for c = 1:66;
   wx2l(c) = 98.3;
end
line(wx2,wx2l)
wx3 = 104.9:0.1:125.8;
for c = 1:210;
   wx3l(c) = 108;
end
line(wx3,wx3l)
wx4 = 112.6:0.1:119.3;
for c = 1:68;
   wx4l(c) = 99.9;
end
line(wx4,wx4l)

%m block
i = 106.4:0.1:140.6;
for c = 1:343;
   il(c) = 5.4;
   il2(c) = 14.5;
   il3(c) = 16.9;
end
line(il,i)
line(il2,i)
line(il3,i)
ix = 5.4:0.1:16.9;
for c = 1:116;
   ixl(c) = 106.4;
   ixl2(c) = 140.6;
end
line(ix,ixl)
line(ix,ixl2)

%marine shed
o = 199:0.1:214;
for c = 1:151;
   ol(c) = 196.2;
   ol2(c) = 205.7;
end
line(ol,o)
line(ol2,o)
ox = 196.2:0.1:205.7;
for c = 1:96;
   oxl(c) = 199;
   oxl2(c) = 214;
end
line(ox,oxl)
line(ox,oxl2)

%external staircases
v = 42.5:0.1:52;
for c = 1:96;
   vl(c) = 75.5;
end
line(vl,v)
vx = 75.5:0.1:77.5;
for c = 1:21;
   vxl(c) = 42.5;
   vxl2(c) = 52;
end
line(vx,vxl)
line(vx,vxl2)
v2 = 53.3:0.1:55.3;
for c =1:21;
   v2l(c) = 103.3;
   v2l2(c) = 101.8;
end
line(v2l,v2)
line(v2l2,v2)
vx2 = 101.8:0.1:103.3;
for c = 1:16;
   vx2l(c) = 53.3;
end
line(vx2,vx2l)
```

```
v3 = 43.8:0.1:46.3;
for c = 1:26;
   v3l(c) = 39.6;
end
line(v3l,v3)
vx3 = 39.6:0.1:43.5;
for c = 1:40;
   vx3l(c) = 43.8;
   vx3l2(c) = 46.3;
end
line(vx3,vx3l)
line(vx3,vx3l2)


sitex =
[173,178,183,188,193,198,203,208,5,10,15,20,25,37.64,42.64,47.64,53.64,58.64,63.64,68.64,73.64,78.64,83.64,88.64,93.64,98.64,103.64,108.64,113.64,118.6
4,123.64,128.64,133.64,138.64,143.64,148.64,153.64,158.64,163.64 ...
208,203,198,193,188,183,178,174.5,163.64,158.64,153.64,148.64,143.64,138.64,133.64,128.64,123.64,118.64,113.64,108.64,103.64,98.64,93.64,88.64,83.64,
43.2,38.2,33.2,28.2,23.2,18.2,13.2,8.2,5 ...
5,10,15,20,25,30,35,40,82.79,87.79,92.79,97.79,102.79,133.44,138.44,163.29,174.5,203,209 ...
209,203,174.5,163.29,133.44,102.79,97.79,91.79,86.79,81.79,40,35,30,25,20,16,9,5 ...
208,203,198,193,188,183,178,174.5,169.5,163.29,137.44,133.44,102.79,97.79,82.79,74.49,69.49,64.49,59.49,40,35,30,25,20,15,10,5 ...
198.5,193.5,188.5,183.5,178.5,174.5,169.5,163.29,137.44,133.44,102.79,97.79,92.79,87.79,82.79,77.79,64.49,54.49,44.49,39.49,34.49,30,25,20,15,10,5 ...
198.5,193.5,188.5,183.5,178.5,174.5,169.5,163.29,137.44,133.44,99.79,92.79,79.79,64.49,54.49,49.49,44.49,39.49,34.49,29.79,15,10,5 ...
5,10,15,29.79,34.79,39.79,44.79,49.79,54.79,59.79,64.79,69.79,74.79,79.79,92.79,97.89,100.11,133.44,137.44,163.29,209.5 ...
206.5,201.5,163.29,137.44,133.44,128.44,123.44,118.44,113.64,100.11,95.11,90.11,79.79,74.79,69.79,59.79,54.79,44.79,39.05,34.35,29.35,15,10,5 ...
5,10,15,29.35,34.35,39.35,44.35,54.79,59.79,64.79,69.29,79.79,90.11,95.11,100.11,105.11,110.11,115.11,120.11,125.11,130.11,135.11,137.8,163.29,168.29,1
97,202,206.5 ...
206.5,202,197,168.29,163.29,158.29,153.29,148.29,143.29,138.79,133.79,127.79,123.79,118.79,113.79,108.79,103.79,98.79,93.99,89.79,79.79,74.79,69.79,64
.79,61.19,54.79,44.35,39.35,34.35,29.35,15,10,5 ...
5,10,15,29.35,34.35,39.35,44.35,54.79,60.79,65.79,70.79,75.79,79.79,90.35,95.35,100.35,105.35,110.35,115.35,120.35,125.35,130.35,135.35,143.29,158.29,1
63.29,168.29,196.9,201.6,205.2 ...
207.5,202.5,197.5,168.29,163.29,158.29,135.35,130.35,125.35,120.35,115.35,110.35,105.35,100.35,95.35,90.35,79.79,74.79,69.79,64.79,59.79,54.79,44.35,39
.35,34.35,29.35,24.35,19.35,14.35,9.9,5.5 ...
6,10,15,20,25,30,35,40,45,54.6,59.6,64.6,69.6,74.6,79.79,90.3,95.3,100.3,106.3,110.3,115.3,124.3,129.3,134.3,158.4,163.4,168.4,197.5,202.5,207.5 ...
207.5,203.8,198.8,193.8,188.8,183.8,178.8,173.8,168.8,163.8,158.8,153.8,148.8,143.8,138.8,133.8,128.8,123.8,118.8,113.8,108.8,103.8,98.8,93.8,88.8,83.8,78
.8,73.8,56.9,51.9,46.9,44.9,39.9,34.9,29.9,24.9,19.9,14.9,9.9,5.4 ...
5.9,9.9,14.9,19.9,24.54,39.6,44.8,55.1,73.8,79.8,84.8,89.8,94.8,99.8,104.8,118.9,123.9,128.9,133.9,138.9,155.18,160.18,174.9,180.4,184.9,188.9,195.5,201.5,2
06.5 ...
206.53,201.53,184.85,179.85,174.85,163,158,152.8,138.9,133.9,128.9,123.9,118.9,113.9,108.9,103.9,98.9,93.9,79.3,74.3,69.3,64.3,59.3,54.3,45.4,39.9,34.9,24
.3,19.3,14.3,9.3,4.3 ...
4.3,9.3,14.3,19.3,24.8,34.9,39.9,45.3,55.4,60.4,65.4,70.4,75.4,78.6,92.7,97.7,103.2,108.2,113.2,118.2,123.2,128.2,133.2,138.2,151.7,157.7,160.7,173.4,178.4,1
83.4,201.5,206.5 ...
206.5,201.5,183.4,176.4,173.4,137.3,132.3,127.3,122.3,115.1,110.1,105.1,100.1,95.1,90.1,85.1,80.1,73.6,70.1,65.1,60.1,55.6,50.1,45.1,40.1,35.1,24.3,19.3,14.
3,9.3,4.3 ...
4.3,9.3,14.3,19.3,25,35.1,40.1,45.1,50.1,55.1,60.1,65.1,70.1,75.1,80.1,85.1,90.1,95.1,100.1,127.3,132.3,137.3,142.3,146.3,173.4,178.4,183.4,201.5,206.5 ...
206.5,201.5,183.6,178.6,173.6,168.6,142.3,137.3,132.3,127.8,100.1,95.1,90.1,85.1,80.1,75.1,70.1,65.1,60.1,55.1,50.1,45.1,40.1,35.1,25,20,14.9,9.8,4.7 ...
4.5,15.76,20.76,24.66,35.13,40.13,45.13,50.13,55.13,60.13,65.13,70.13,75.13,80.13,85.13,90.13,95.13,100.13,105.13,110.23,115.33,120.43,125.53,130.63,135
.73,140.83,145.93,151.03,156.13,161.23,166.33,171.43,176.53,181.63,186.73,191.83,196.93,202.03,207.13 ...
207.13,202.03,196.93,191.83,186.73,181.63,176.53,156.53,136.53,116.53,96.53,76.53,56.53,36.53,31.53,26.53,21.53,16.63,4.5 ...
4.5,16.63,21.63,26.63,31.63,36.63 ...
4.5,16.63,21.63,26.63,31.63,36.63 ...
4.5,16.63,22.63,26.63,31.63,36.63 ...
4.5,16.63,21.63,26.63,31.63,36.63,56.53,76.53,96.53,116.53,136.53,156.53,176.53,196.53,207.53 ...
4.5,9.5,14.5,19.5,22.9,26.9,31.9,36.9 ...
4.5,9.5,14.5,18.5,22.9,26.9,31.9,36.9 ...
4.5,9.5,14.5,19.5,22.9,26.9,31.9,36.9 ...
4.5,9.5,14.5,19.5,22.9,26.9,31.9,36.9,56.53,76.13,95.73,115.33,134.93,154.53,174.13,193.73,208.23 ...
208.23,193.73,174.13,154.53,134.93,115.33,95.73,76.13,56.53,36.9,19.5,4.5 ...
4.5,19.5,36.9,56.53,76.13,95.73,115.33,134.93,154.53,174.13,193.73,208.23 ...
208.23,193.73,174.13,154.53,134.93,115.33,95.73,76.13,56.53,36.9,19.5,4.5 ...
4.5,19.5,36.9,56.53,76.13,95.73,115.33,134.93,154.53,174.13,193.73,208.73 ...
208.73,193.73,174.13,154.53,134.93,115.33,95.73,76.13,56.53,36.9,19.5,4.5 ...
4.5,19.5,36.9,56.5,76.1,95.7,115.3,134.9,154.5,174.1,193.7,208.7 ...
208.7,193.7,174.1,154.5,134.9,115.3,95.7,76.1,56.5,36.9,19.5,4.5];

sitey = [5,5,5,5,5,5,5,5,5,5,5,5,5,5,5,5,5,5,5,5,5,5,5,5,5,5,5,5,5,5,6.5,6.5,6.5,6.5,6.5,5,5,5,5,5,5,5,5 ...
10,10,10,10,10,10,10,10,10,10,10,10,10,10,10,10,10,10,10,10,10,10,10,10,10,11,10,10,10,10,10,10,10,10 ...
15,15,15,15,15,15,15,15,15,15,15,15,15,15,15,15,15,15,15 ...
20,20,20,20,20,20,20,20,20,20,20,20,20,20,20,20,20,20 ...
25,25,25,25,25,25,25,25,25,25,25,25,25,25,25,25,25,25,25,25,25,25,25,25,25,25,25 ...
30,30,30,30,30,30,30,30,30,30,30,30,30,30,30,30,30,30,30,30,30,30,30,30,30,30,30 ...
34.5,34.5,34.5,34.5,34.5,34.5,34.5,35,35,35,35,35,35,35,35,35,35,35,35,35,35,35,35,35 ...
40,40,40,40,40,40,40,40,40,40,40,40,40,40,40,40,40,40,40,40,42 ...
45,45,45,45,45,45,45,45,45,45,45,45,45,45,45,45,45,45,45,45,45,45,45,45,45 ...
50,50,50,50,50,50,50,50,50,50,50,50,50,50,50,50,50,50,50,50,50,50,50,50,50,50,50,50 ...
55,55,55,55,55,55,55,55,55,55,55,55,55,55,55,55,55,55,55,55,55,55,55,55,55,55,55,55,55,55,55,55,55 ...
60,60,60,60,60,60,60,60,60,60,60,60,60,60,60,60,60,60,60,60,60,60,60,60,60,60,60,60,60,60 ...
65,65,65,65,65,65,65,65,65,65,65,65,65,65,65,65,65,65,65,65,65,65,65,65,65,65,65,65,65,65,65 ...
70,70,69,70,70,70,70,70,70,70,70,70,70,70,70,70,70,70,70,70,70,70,70,70,70,70,70,70.7,70,70,70 ...
76,76,76,76,76,76,76,76,76,76,76,76,76,76,76,76,76,76,76,76,76,76,76,76,76,76,76,76,76,76,76,76,75,75,75,75,75,75,75,75,75 ...
80,80,80,80,80,80,80,80.4,81,81,81,81,81,81,81,81,81,81,81,81,79.9,79.9,81,81,81,81,81,81,81 ...
86,86,86,86,86,86,87.3,86,86,86,86,86,86,86,86,86,86,86,86,86.5,86.5,86.5,86.5,86.5,86.5,86.5,86.5,86,86,86,86,86 ...
91,91,91,91,91,91.5,91.5,91.5,91.5,91.5,91.5,91.5,91.5,91.5,91.5,91.5,91.5,91.5,91.5,91.5,91.5,91,91,91,91,91,91,91,91,91,91,91 ...
96,96,96,96,96,96,96,96,96,96,96,96,96,96,96,96,96,96,96,96,96,96,96,96,96,96,96,96,96,96,96 ...
101,101,101,101,101,101,101,101,101,101,101,101,101,101,101,101,101,101,101,101,101,101,101.7,101.7,101,101,101,101,101 ...
106,106,106,106,106,106,105.3,105.3,105.3,105.3,106,106,106,106,106,106,106,106,106,106,106,106,106,106,106,106,106,106 ...
111,111,111,111,111,111,111,111,111,111,111,111,111,111,111,111,111,111,111,111,111,111,111,111,111,111,111,111,111,111,111,111,111,111,111,111,111,11
1,111,111 ...
116,116,116,116,116,116,116,116,116,116,116,116,116,116,116,116,116,116,116 ...
121,121,121,121,121,121 ...
126,126,126,126,126,126 ...
131,131,131,131,131,131 ...
136,136,136,136,136,136,136,136,136,136,136,136,136,136,136 ...
```

```
141,141,141,141,141,141,141,141 ...
146,146,146,146,146,146,146,146 ...
151,151,151,151,151,151,151,151 ...
156,156,156,156,156,156,156,156,156,156,156,156,156,156,156,156,156 ...
176,176,176,176,176,176,176,176,176,176,176,176 ...
196,196,196,196,196,196,196,196,196,196,196,196 ...
216,216,216,216,216,216,216,216,216,216,216,216 ...
236,236,236,236,236,236,236,236,236,236,236,236 ...
256,256,256,256,256,256,256,256,256,256,256,256 ...
276,276,276,276,276,276,276,276,276,276,276,276 ...
296,296,296,296,296,296,296,296,296,296,296,296];

sitez = [0,0,0,0,0,0,0,0,0,0,0,0,0,0,0,0,0,0,0,0,0,0,0,0,0,0,0,0,0,0,0,0,0,0,0,0,0,0,0 ...
0,0,0,0,0,0,0,0,0,0,0,0,0,0,0,0,0,0,0,0,0,0,0,0,0,0,0,0,0,0,0,0,0,0 ...
0,0,0,0,0,0,0,0,0,0,0,0,0,0,0,0,0,0,0 ...
0,0,0,0,0,0,0,0,0,0,0,0,0,0,0,0,0,0 ...
0,0,0,0,0,0,0,0,0,0,0,0,0,0,0,0,0,0,0,0,0,0,0,0,0,0,0 ...
0,0,0,0,0,0,0,0,0,0,0,0,0,0,0,0,0,0,0,0,0,0,0,0,0,0,0 ...
0,0,0,0,0,0,0,0,0,0,0,0,0,0,0,0,0,0,0,0,0,0,0 ...
0,0,0,0,0,0,0,0,0,0,0,0,0,0,0,0,0,0,0,0,0 ...
0,0,0,0,0,0,0,0,0,0,0,0,0,0,0,0,0,0,0,0,0,0,0,0 ...
0,0,0,0,0,0,0,0,0,0,0,0,0,0,0,0,0,0,0,0,0,0,0,0,0,0,0,0 ...
0,0,0,0,0,0,0,0,0,0,0,0,0,0,0,0,0,0,0,0,0,0,0,0,0,0,0,0,0,0,0,0,0 ...
0,0,0,0,0,0,0,0,0,0,0,0,0,0,0,0,0,0,0,0,0,0,0,0,0,0,0,0,0,0 ...
0,0,0,0,0,0,0,0,0,0,0,0,0,0,0,0,0,0,0,0,0,0,0,0,0,0,0,0,0,0,0 ...
0,0,0,0,0,0,0,0,0,0,0,0,0,0,0,0,0,0,0,0,0,0,0,0,0,0,0,0,0,0 ...
0,0,0,0,0,0,0,0,0,0,0,0,0,0,0,0,0,0,0,0,0,0,0,0,0,0,0,0,0,0,0,0,0,0,0,0,0,0,0,0 ...
0,0,0,0,0,0,0,0,0,0,0,0,0,0,0,0,0,0,0,0,0,0,0,0,0,0,0,0,0 ...
0,0,0,0,0,0,0,0,0,0,0,0,0,0,0,0,0,0,0,0,0,0,0,0,0,0,0,0,0,0,0,0 ...
0,0,0,0,0,0,0,0,0,0,0,0,0,0,0,0,0,0,0,0,0,0,0,0,0,0,0,0,0,0,0,0 ...
0,0,0,0,0,0,0,0,0,0,0,0,0,0,0,0,0,0,0,0,0,0,0,0,0,0,0,0,0,0,0 ...
0,0,0,0,0,0,0,0,0,0,0,0,0,0,0,0,0,0,0,0,0,0,0,0,0,0,0,0,0 ...
0,0,0,0,0,0,0,0,0,0,0,0,0,0,0,0,0,0,0,0,0,0,0,0,0,0,0,0,0 ...
0,0,0,0,0,0,0,0,0,0,0,0,0,0,0,0,0,0,0,0,0,0,0,0,0,0,0,0,0,0,0,0,0,0,0,0,0,0,0 ...
0,0,0,0,0,0,0,0,0,0,0,0,0,0,0,0,0,0,0 ...
0,0,0,0,0,0 ...
0,0,0,0,0,0 ...
0,0,0,0,0,0 ...
0,0,0,0,0,0,0,0,0,0,0,0,0,0,0 ...
0,0,0,0,0,0,0,0 ...
0,0,0,0,0,0,0,0 ...
0,0,0,0,0,0,0,0 ...
0,0,0,0,0,0,0,0,0,0,0,0,0,0,0,0,0 ...
0,0,0,0,0,0,0,0,0,0,0,0 ...
0,0,0,0,0,0,0,0,0,0,0,0 ...
0,0,0,0,0,0,0,0,0,0,0,0 ...
0,0,0,0,0,0,0,0,0,0,0,0 ...
0,0,0,0,0,0,0,0,0,0,0,0 ...
0,0,0,0,0,0,0,0,0,0,0,0 ...
0,0,0,0,0,0,0,0,0,0,0,0];



sx =
[5,10,15,20,25,37.64,42.64,47.64,53.64,58.64,63.64,68.64,73.64,78.64,83.64,88.64,93.64,98.64,103.64,108.64,113.64,118.64,123.64,128.64,133.64,138.64,143
.64,148.64,153.64,158.64,163.64,173,178,183,188,193,198,203,208 ...
5,8.2,13.2,18.2,23.2,28.2,33.2,38.2,43.2,83.64,88.64,93.64,98.64,103.64,108.64,113.64,118.64,123.64,128.64,133.64,138.64,143.64,148.64,153.64,158.64,163.
64,174.5,178,183,188,193,198,203,208 ...
5,10,15,20,25,30,35,40,82.79,87.79,92.79,97.79,102.79,133.44,138.44,163.29,174.5,203,209 ...
5,9,16,20,25,30,35,40,81.79,86.79,91.79,97.79,102.79,133.44,163.29,174.5,203,209 ...
5,10,15,20,25,30,35,40,59.49,64.49,69.49,74.49,82.79,97.79,102.79,133.44,137.44,163.29,169.5,174.5,178,183,188,193,198,203,208 ...
5,10,15,20,25,30,34.49,39.49,44.49,54.49,64.49,77.79,82.79,87.79,92.79,97.79,102.79,133.44,137.44,163.29,169.5,174.5,178.5,183.5,188.5,193.5,198.5 ...
5,10,15,29.79,34.49,39.49,44.49,49.49,54.49,64.49,79.79,92.79,99.79,133.44,137.44,163.29,169.5,174.5,178.5,183.5,188.5,193.5,198.5 ...
5,10,15,29.79,34.79,39.79,44.79,49.79,54.79,59.79,64.79,69.79,74.79,79.79,92.79,97.89,100.11,133.44,137.44,163.29,209.5 ...
5,10,15,29.35,34.35,39.05,44.79,54.79,59.79,69.79,74.79,79.79,90.11,95.11,100.11,113.64,118.44,123.44,128.44,133.44,137.44,163.29,201.5,206.5 ...
5,10,15,29.35,34.35,39.35,44.35,54.79,59.79,64.79,69.29,79.79,90.11,95.11,100.11,105.11,110.11,115.11,120.11,125.11,130.11,135.11,137.8,163.29,168.29,1
97,202,206.5 ...
5,10,15,29.35,34.35,39.35,44.35,54.79,61.19,64.79,69.79,74.79,79.79,89.79,93.99,98.79,103.79,108.79,113.79,118.79,123.79,127.79,133.79,138.79,143.29,14
8.29,153.29,158.29,163.29,168.29,197,202,206.5 ...
5,10,15,29.35,34.35,39.35,44.35,54.79,60.79,65.79,70.79,75.79,79.79,90.35,95.35,100.35,105.35,110.35,115.35,120.35,125.35,130.35,135.35,143.29,158.29,1
63.29,168.29,196.9,201.6,205.2 ...
5.5,9.9,14.35,19.35,24.35,29.35,34.35,39.35,44.35,54.79,59.79,64.79,69.79,74.79,79.79,90.35,95.35,100.35,105.35,110.35,115.35,120.35,125.35,130.35,135.3
5,158.29,163.29,168.29,197.5,202.5,207.5 ...
6,10,15,20,25,30,35,40,45,54.6,59.6,64.6,69.6,74.6,79.79,90.3,95.3,100.3,106.3,110.3,115.3,124.3,129.3,134.3,158.4,163.4,168.4,197.5,202.5,207.5 ...
5.4,9.9,14.9,19.9,24.9,29.9,34.9,39.9,44.9,46.9,51.9,56.9,73.8,78.8,83.8,88.8,93.8,98.8,103.8,108.8,113.8,118.8,123.8,128.8,133.8,138.8,143.8,148.8,153.8,158
.8,163.8,168.8,173.8,178.8,183.8,188.8,193.8,198.8,203.8,207.5 ...
5.9,9.9,14.9,19.9,24.54,39.6,44.8,55.1,73.8,79.8,84.8,89.8,94.8,99.8,104.8,118.9,123.9,128.9,133.9,138.9,155.18,160.18,174.9,180.4,184.9,188.9,195.5,201.5,2
06.5 ...
4.3,9.3,14.3,19.3,24.3,34.9,39.9,45.4,54.3,59.3,64.3,69.3,74.3,79.3,93.9,98.9,103.9,108.9,113.9,118.9,123.9,128.9,133.9,138.9,152.8,158,163,174.85,179.85,18
4.85,201.53,206.53 ...
4.3,9.3,14.3,19.3,24.8,34.9,39.9,45.3,55.4,60.4,65.4,70.4,75.4,78.6,92.7,97.7,103.2,108.2,113.2,118.2,123.2,128.2,133.2,138.2,151.7,157.7,160.7,173.4,178.4,1
83.4,201.5,206.5 ...
4.3,9.3,14.3,19.3,24.3,35.1,40.1,45.1,50.1,55.6,60.1,65.1,70.1,73.6,80.1,85.1,90.1,95.1,100.1,105.1,110.1,115.1,122.3,127.3,132.3,137.3,173.4,176.4,183.4,201
.5,206.5 ...
4.3,9.3,14.3,19.3,25,35.1,40.1,45.1,50.1,55.1,60.1,65.1,70.1,75.1,80.1,85.1,90.1,95.1,100.1,127.3,132.3,137.3,142.3,146.3,173.4,178.4,183.4,201.5,206.5 ...
4.7,9.8,14.9,20,25,35.1,40.1,45.1,50.1,55.1,60.1,65.1,70.1,75.1,80.1,85.1,90.1,95.1,100.1,127.8,132.3,137.3,142.3,168.6,173.6,178.6,183.6,201.5,206.5 ...
4.5,15.76,20.76,24.66,35.13,40.13,45.13,50.13,55.13,60.13,65.13,70.13,75.13,80.13,85.13,90.13,95.13,100.13,105.13,110.23,115.33,120.43,125.53,130.63,135
.73,140.83,145.93,151.03,156.13,161.23,166.33,171.43,176.53,181.63,186.73,191.83,196.93,202.03,207.13 ...
4.5,16.63,21.53,26.53,31.53,36.53,56.53,76.53,96.53,116.53,136.53,156.53,176.53,181.63,186.73,191.83,196.93,202.03,207.13 ...
4.5,16.63,21.63,26.63,31.63,36.63 ...
4.5,16.63,21.63,26.63,31.63,36.63 ...
4.5,16.63,22.63,26.63,31.63,36.63 ...
4.5,16.63,21.63,26.63,31.63,36.63,56.53,76.53,96.53,116.53,136.53,156.53,176.53,196.53,207.53 ...
4.5,9.5,14.5,19.5,22.9,26.9,31.9,36.9 ...
```

```
4.5,9.5,14.5,18.5,22.9,26.9,31.9,36.9 ...
4.5,9.5,14.5,19.5,22.9,26.9,31.9,36.9 ...
4.5,9.5,14.5,19.5,22.9,26.9,31.9,36.9,56.53,76.13,95.73,115.33,134.93,154.53,174.13,193.73,208.23 ...
4.5,19.5,36.9,56.53,76.13,95.73,115.33,134.93,154.53,174.13,193.73,208.23 ...
4.5,19.5,36.9,56.53,76.13,95.73,115.33,134.93,154.53,174.13,193.73,208.23 ...
4.5,19.5,36.9,56.53,76.13,95.73,115.33,134.93,154.53,174.13,193.73,208.23 ...
4.5,19.5,36.9,56.53,76.13,95.73,115.33,134.93,154.53,174.13,193.73,208.73 ...
4.5,19.5,36.9,56.53,76.13,95.73,115.33,134.93,154.53,174.13,193.73,208.73 ...
4.5,19.5,36.9,56.5,76.1,95.7,115.3,134.9,154.5,174.1,193.7,208.7 ...
4.5,19.5,36.9,56.5,76.1,95.7,115.3,134.9,154.5,174.1,193.7,208.7];

sy = [5,5,5,5,5,5,5,5,5,5,5,5,5,5,5,5,5,5,5,6.5,6.5,6.5,6.5,6.5,5,5,5,5,5,5,5,5,5,5,5,5,5,5,5 ...
10,10,10,10,10,10,10,10,11,10,10,10,10,10,10,10,10,10,10,10,10,10,10,10,10,10,10,10,10,10,10,10,10 ...
15,15,15,15,15,15,15,15,15,15,15,15,15,15,15,15,15,15,15 ...
20,20,20,20,20,20,20,20,20,20,20,20,20,20,20,20,20,20 ...
25,25,25,25,25,25,25,25,25,25,25,25,25,25,25,25,25,25,25,25,25,25,25,25,25,25,25 ...
30,30,30,30,30,30,30,30,30,30,30,30,30,30,30,30,30,30,30,30,30,30,30,30,30,30,30 ...
35,35,35,35,35,35,35,35,35,35,35,35,35,35,35,35,34.5,34.5,34.5,34.5,34.5,34.5,34.5 ...
40,40,40,40,40,40,40,40,40,40,40,40,40,40,40,40,40,40,40,40,42 ...
45,45,45,45,45,45,45,45,45,45,45,45,45,45,45,45,45,45,45,45,45,45,45,45 ...
50,50,50,50,50,50,50,50,50,50,50,50,50,50,50,50,50,50,50,50,50,50,50,50,50,50,50 ...
55,55,55,55,55,55,55,55,55,55,55,55,55,55,55,55,55,55,55,55,55,55,55,55,55,55,55,55,55,55,55,55 ...
60,60,60,60,60,60,60,60,60,60,60,60,60,60,60,60,60,60,60,60,60,60,60,60,60,60,60,60,60,60 ...
65,65,65,65,65,65,65,65,65,65,65,65,65,65,65,65,65,65,65,65,65,65,65,65,65,65,65,65,65,65,65 ...
70,70,69,70,70,70,70,70,70,70,70,70,70,70,70,70,70,70,70,70,70,70,70,70,70,70,70,70.7,70,70,70 ...
75,75,75,75,75,75,75,75,75,76,76,76,76,76,76,76,76,76,76,76,76,76,76,76,76,76,76,76,76,76,76,76,76,76,76,76,76,76,76 ...
80,80,80,80,80,80,80,80.4,81,81,81,81,81,81,81,81,81,81,81,81,79.9,79.9,81,81,81,81,81,81,81 ...
86,86,86,86,86,86.5,86.5,86.5,86.5,86.5,86.5,86.5,86.5,86,86,86,86,86,86,86,86,86,86,86,86,87.3,86,86,86,86,86,86 ...
91,91,91,91,91,91.5,91.5,91.5,91.5,91.5,91.5,91.5,91.5,91.5,91.5,91.5,91.5,91.5,91.5,91.5,91.5,91,91,91,91,91,91,91,91,91,91,91 ...
96,96,96,96,96,96,96,96,96,96,96,96,96,96,96,96,96,96,96,96,96,96,96,96,96,96,96,96,96,96,96 ...
101,101,101,101,101,101,101,101,101,101,101,101,101,101,101,101,101,101,101,101,101,101,101.7,101.7,101,101,101,101,101 ...
106,106,106,106,106,106,106,106,106,106,106,106,106,106,106,106,106,106,106,105.3,105.3,105.3,105.3,106,106,106,106,106,106 ...
111,111,111,111,111,111,111,111,111,111,111,111,111,111,111,111,111,111,111,111,111,111,111,111,111,111,111,111,111,111,111,111,111,111,111,111,11
1,111,111 ...
116,116,116,116,116,116,116,116,116,116,116,116,116,116,116,116,116,116,116 ...
121,121,121,121,121,121 ...
126,126,126,126,126,126 ...
131,131,131,131,131,131 ...
136,136,136,136,136,136,136,136,136,136,136,136,136,136,136 ...
141,141,141,141,141,141,141,141 ...
146,146,146,146,146,146,146,146 ...
151,151,151,151,151,151,151,151 ...
156,156,156,156,156,156,156,156,156,156,156,156,156,156,156,156,156 ...
176,176,176,176,176,176,176,176,176,176,176,176 ...
196,196,196,196,196,196,196,196,196,196,196,196 ...
216,216,216,216,216,216,216,216,216,216,216,216 ...
236,236,236,236,236,236,236,236,236,236,236,236 ...
256,256,256,256,256,256,256,256,256,256,256,256 ...
276,276,276,276,276,276,276,276,276,276,276,276 ...
296,296,296,296,296,296,296,296,296,296,296,296];

skyvw = [73,30,39,85,90,88,85,82,80,76,79,77,76,70,65,49,52,49,42,40,50,56,59,54,58,73,82,86,87,88,87,44,68,50,36,48,46,35,49 ...
75,69,61,74,83,88,85,85,73,59,58,57,58,56,37,37,40,43,42,61,66,69,52,75,80,79,64,76,70,69,69,67,63,56 ...
73,59,74,82,83,86,85,77,59,40,57,64,60,64,48,67,63,70,27 ...
67,60,74,83,79,85,86,78,54,65,56,66,63,63,53,68,73,17 ...
74,69,73,75,79,83,82,74,7,6,7,17,58,64,64,59,13,43,35,70,80,84,86,86,81,59,59 ...
83,80,72,69,70,77,79,73,53,37,53,14,15,17,17,17,15,58,14,27,56,70,78,82,83,82,78 ...
80,77,54,48,75,68,37,4,35,64,24,33,5,58,14,24,46,61,67,70,73,74,75 ...
81,76,40,41,73,62,28,5,34,52,56,66,64,29,37,30,10,59,13,42,69 ...
77,75,48,41,73,59,15,28,31,62,46,6,30,51,10,30,43,56,54,46,10,43,64,70 ...
73,72,35,40,71,62,31,19,48,55,28,27,29,46,9,46,52,58,57,49,29,25,21,48,36,33,77,73 ...
64,64,34,40,71,65,35,16,54,52,38,53,30,27,42,11,33,36,41,29,9,4,39,28,31,30,30,39,51,41,46,79,62 ...
63,62,28,43,71,64,33,19,45,8,29,59,33,28,47,29,3,4,7,11,8,18,45,43,55,61,55,52,82,79  ...
55,57,43,51,60,67,72,60,10,32,48,24,40,59,33,27,37,32,3,1,9,8,8,4,7,32,66,65,44,81,85 ...
47,58,45,59,68,72,70,56,26,17,1,0,1,40,19,26,34,24,0,2,24,12,17,27,26,38,55,37,73,83 ...
51,59,49,12,4,9,5,10,5,2,3,0,1,1,1,2,3,4,1,1,4,2,4,5,6,0,0,0,5,5,1,8,3,1,7,31,63,69,78,80 ...
48,51,49,35,4,34,14,19,36,17,1,2,3,3,1,8,15,9,31,26,47,46,60,64,28,67,73,79,83 ...
39,40,37,49,14,13,33,6,30,53,62,61,53,18,6,6,4,2,17,17,7,16,22,14,29,54,14,40,70,17,69,81 ...
40,38,32,39,4,13,39,32,40,52,66,66,59,45,26,26,24,6,10,12,26,25,27,10,7,44,13,41,56,28,68,82 ...
41,39,38,34,14,24,51,51,38,40,39,43,66,59,52,56,52,50,61,55,41,12,35,42,46,19,45,73,37,69,78 ...
51,40,45,37,5,32,63,67,60,52,61,69,74,60,76,75,76,75,72,40,57,57,43,13,78,80,40,69,75 ...
52,22,27,26,8,35,66,66,62,64,72,78,81,82,83,84,82,82,82,43,60,69,59,72,79,79,43,70,82 ...
38,5,24,3,32,66,71,65,66,77,81,84,85,87,87,86,86,86,83,75,72,72,69,38,36,35,31,31,30,30,34,39,44,74,56,40,51,81,85 ...
47,7,69,69,67,55,73,83,87,84,82,82,84,84,83,84,84,85,90 ...
47,33,75,79,79,74 ...
48,34,76,83,84,84 ...
48,31,73,85,86,86 ...
39,31,74,86,88,88,92,93,94,94,94,94,93,89,80 ...
59,24,32,74,78,88,90,90 ...
80,52,63,81,88,89,91,91 ...
90,88,89,91,92,91,92,92 ...
94,94,93,94,94,93,94,93,94,94,94,95,94,94,93,90,63 ...
92,94,92,91,90,91,91,91,90,94,91,88 ...
97,96,92,44,71,68,74,85,80,84,88,89 ...
94,95,94,89,86,84,85,89,85,87,89,90 ...
95,96,96,96,95,94,94,94,95,95,95,94 ...
95,96,97,96,96,96,96,96,96,96,96,96 ...
95,96,96,97,96,95,95,94,93,93,94,95 ...
90,95,95,96,94,70,86,84,56,59,83,93];



v = [5,10,15,20,25,30,35,40,45,50,55,60,65,70,75,80,85,90,95];
```

```
figure(1)
whitebg('w');
% Surface meshing
xm = 0:0.5:215;
ym = 0:0.5:310;
zm = 0:0.5:100;


[xi,yi] = meshgrid(xm,ym);
[xr,yr,zr]=griddata(sx,sy,skyvw,xi,yi);
%mesh(xr,yr,zr);
h = contourf(xr,yr,zr,v,'LineStyle','none'); %surfc(xr,yr,zr,'LineStyle','none')
colormap jet(19)
grid off




axis equal tight
axis([-5 217.5 -5 310 0 0.1])
%plot3(sitex,sitey,sitez,'r+','MarkerSize', 2,'MarkerFacecolor', 'r')
xlabel('western fence (m)')
ylabel('northern fence (m)')
zlabel('')
view([0 0 20]);
```

D.5 Playground sky view image processing algorithm

Each of the 822 playground survey site composite images were run through the following algorithm to determine sky view up to 32^{o} in ZA. The code was developed in MATLAB version 7.1. The following algorithm requires the MATLAB image processing toolbox to run correctly.

```
% Image processing algorithm to estimate sky view

clear

    for T = 1:1
    IMname = 'site808'                  %image name to process
    IMpathI = 'C:\nathan\phD\photos\skyview\HBSHS\proco\cloudaff'
    IMnameM = 'mask'                    %image name SZA mask
    IMpath = 'C:\nathan\phD\photos\skyview\HBSHS\proco'
    jpg = fullfile(IMpathI,[IMname,'.jpg','']);
    png = fullfile(IMpath,[IMnameM,'.bmp','']);


    RGB = imread(jpg);
    [X,map] = rgb2ind(RGB,256);
    [Z,map2] = imread(png);
    K = Z ;
    [m,n] = size(X);
    [levels, colpart] = size(map);   %determine the number of colour levels

    redmap = zeros(256,3);
    greenmap = zeros(256,3);
    bluemap = zeros(256,3);
    cloudmapBR = zeros(256,3);

    %*****************************************************************
    % ADD GROUND MASK TO IMAGE
    maskCNT = 0;    %no. of masked pixels
    for y = 1:m
      for i = 1:n
        mapval = (Z(y,i));
        mapval = mapval +1;
        if mapval == 1   %if part of black image mask
          X(y,i) = map2(1); %mask ground view
          maskCNT = maskCNT +1;
        end
      end
    end
    %*****************************************************************

    %*****************************************************************
    %algorithm for splitting the image into its R G B levels and pixel transitions (texture)
    maxcloudBR = 0;   %initilise greatest cloud value  in cloud map (blue - red)

    diff = 0;
    olddiff = 0;
    transition = 0;
    trans1 = 0;
    trans2 = 0;
    trans3 = 0;
    trans4 = 0;
    trans5 = 0;
    Bmask = 0;
    pixCNT = 0;
    skyCNT = 0;

    for y = 1:m
      for i = 1:n
        pixCNT = pixCNT +1;
        mapval = double(X(y,i));
        mapval = mapval + 1;
        redmap(mapval,1) = map(mapval,1);            %JPEG map starts at 0 MATLAB map starts at 1
        greenmap(mapval,2) = map(mapval,2);
        bluemap(mapval,3) = map(mapval,3);

       diff = abs(map(mapval,3) - map(mapval,1));   %look at changes in pixel level (texture) [Blue - Red]
          if double(X(y,i)) == 0
          %don't count as a valid transition between pixels
          olddiff = diff;
          Bmask =1;
        else
          if Bmask == 0
```

```
        transition = diff-olddiff;
        if transition < 0.05
          trans1 = trans1+1;      %increment level 1 texture change
        end
        if transition <= 0.1 & transition > 0.05
          trans2 = trans2+1;      %increment level 2 texture change
        end
        if transition <= 0.15 & transition > 0.1
          trans3 = trans3+1;      %increment level 3 texture change
        end
        if transition <= 0.2 & transition > 0.15
          trans4 = trans4+1;      %increment level 4 of texture change
        end
        if transition <= 1 & transition > 0.2
          trans5 = trans5+1;      %increment level 5 of texture change
        end
      end
      Bmask =0;
      olddiff = diff;
    end

    if map(mapval,3) - map(mapval,1) < 0             %blue - red
      cloudmapBR(mapval,1) = 0;
      cloudmapBR(mapval,2) = 0;
      cloudmapBR(mapval,3) = 0;
     else
      cloudmapBR(mapval,1) = map(mapval,3) - map(mapval,1);
      cloudmapBR(mapval,2) = map(mapval,3) - map(mapval,1);
      cloudmapBR(mapval,3) = map(mapval,3) - map(mapval,1);
      if cloudmapBR(mapval,1) > maxcloudBR   % assign maxcloudBR as the brightest blue sky pixel in image (greatest level of blue-red)
        maxcloudBR = cloudmapBR(mapval,1);
      end
     end
     % if map(mapval,3) - map(mapval,1) == 0 then must be a masked pixel OR a BLACK image pixel

  end
end
pixCNT = pixCNT - maskCNT;   %total no. of potential sky pixels in the 90o tp 32.3o SZA range photographed (64% of total skyview)
%*****************************************************************

%*****************************************************************
% increase contrast in cloud map (scale max cloud value as 1,1,1 - white)
imsum = 0;         %cumulative sum of BR image pixels (less mask)
bluesum = 0;      %cumulative sum of sky pixels
dullsum = 0;       %cumulative sum of image pixels (less mask)
skypixCNT = 0;   %counter for sky pixels
for v = 1:256
  imdev(v,1) = 2;      %ALL IMAGE PIXELS
  bluedev(v,1) = 2;   %ONLY SKY PIXELS
  dulldev(v,1) = 2;    %RED LEVEL OF ALL PIXEL
end

if maxcloudBR > 0.4
  thres = 0.9;   %threshold for cloud determination in Bright sky
else
 % if opaque(T) > 0.8
    thres = 0.4;   %threshold for cloud determination in Dull sky with > 80% cloud cover
  %end
end

for j = 1:256
  cloudmapBR(j,1) = 1- (cloudmapBR(j,1)/maxcloudBR);   %cloud is white 1,1,1, sky is less with the MAXIMUM SKY BLUE ASSIGNED 0,0,0
  cloudmapBR(j,2) = 1- (cloudmapBR(j,2)/maxcloudBR);
  cloudmapBR(j,3) = 1- (cloudmapBR(j,3)/maxcloudBR);
  imdev(j,1) = cloudmapBR(j,1);
  dulldev(j,1) = map(j,1);     %measure image brightness in red

  if cloudmapBR(j,1) < thres    %threshold for sky OR cloud CLASSIFICATION
      bluedev(j,1) = cloudmapBR(j,1);
      skypixCNT = skypixCNT + 1;   %COLOUR MAP SKY VALUES NOT PIXELS
      cloudmapBR(j,1) = 0;
      cloudmapBR(j,2) = 0;
      cloudmapBR(j,3) = 1;
  else
      cloudmapBR(j,1) = 1;
      cloudmapBR(j,2) = 1;
      cloudmapBR(j,3) = 1;
  end
end

imSD = std(imdev);
for q = 1:256
  if bluedev(q,1) ~= 2      %ONLY COUNT AS A SKY PIXEL IF BELOW THRESHOLD
    bluesum = bluesum + bluedev(q,1);
  end
  imsum = imsum + imdev(q,1);
  dullsum = dullsum + dulldev(q,1);
end
imaverage = imsum/256;
dullaverage = dullsum/256;
blueaverage = bluesum/skypixCNT;   %average blueness of those pixels classified as sky pixels
blueSD = std(bluedev);
%*****************************************************************
```

```
    for mapval = 1:256
        if cloudmapBR(mapval, 1) == 0
          if cloudmapBR(mapval, 3) == 1   %markad as blue for sky
            for y = 1:m
              for i = 1:n
                test = X(y,i);   %get pixel value
                test = test +1;   %JPEG reference starts at colour 0 not 1
                if test == mapval
                  skyCNT = skyCNT+1;   %pixel value is marked as a sky colour
                  %cloudmapBR(mapval ,1) = 1;
                  %cloudmapBR(mapval, 2) = 0;
                  %cloudmapBR(mapval, 3) = 0;
                end
              end
            end
          end
        end
    end

    PCENTsky = (skyCNT/pixCNT)*64   % PERCENTAGE of skyview (up to 64% max for photographic range of 32.3oSZA)

    figure(1)
    imshow(X,map)    %<---------------------------------------------------------------------------------------------------

    figure(2)
    imshow(X,cloudmapBR)
    imwrite(X,cloudmapBR,'C:\nathan\phD\photos\skyview\HBSHS\sets\PROCSSDsite808.png','png')


end
```

Appendix E. Measured UV transmission of playground shade cloths

Table E.1: Percentage UV transmission measured under playground shade cloth structures. Protected measurements were made approximately 0.5 m directly underneath the shade cloth using a broadband meter (Solar Light Co., model 3D, Philadelphia, PA 19126). UV transmission estimates include the meter measurement uncertainty of ±17%. Protection Factors for shade cloth structures were calculated as the ratio of unprotected modelled UV_{ery} exposure located at sites in proximity to each respective structure for both the winter solstice (21 June 2008) and summer solstice (21 December 2008) to modelled UV_{ery} at sites located underneath the shade cloth structures. The modelled UV_{ery} for protected sites located underneath their respective structures were dependent upon the total sky view at those sites. Therefore while some playground shade structures were covered with low UV transmission shade cloths, their overall shape and region of the sky covered at the modelled sites protected by the structure influenced the listed seasonal PF resulting often in lower than expected PF for some structures. Figures E.1 through to E.8 depict each shade cloth structure found in the HBSHS playground.

Shade structure	Unprotected UV (med/hr)	Protected UV (med/hr)	UV transmission (%)	PF winter / summer
Bus shelter (blue)	2.55	0.27	11 ± 2	3.0 / 3.0
Oval steps (red)	3.36	0.17	5 ± 1	2.8 / 2.2
Quadrangle (plastic)	2.09	0.05	2 ± 0	5.3 / 16.3
H Block (green)	3.35	0.25	7 ± 1	1.2 / 1.7
H block (dark green)	3.47	0.27	8 ± 1	1.4 / 1.6
M Block (red)	2.83	0.19	7 ± 1	2.1 / 2.1
C Block (green)	0.36	2.53	14 ± 2	1.1 / 1.1
Art (green)	0.20	3.04	7 ± 1	1.9 / 2.4

Figure E.1: Bus shelter shade cloth structure.

Figure E.2: Oval steps shade cloth structure.

Figure E.3: Quadrangle plastic shelter structure.

Figure E.4: H Block shade cloth sails (light green).

Figure E.5: H block shade cloth sails (dark green).

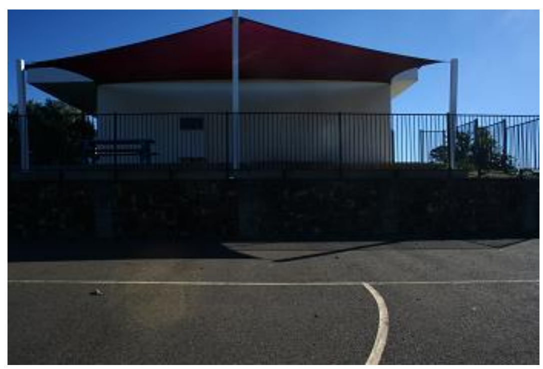

Figure E.6: M Block shade cloth sail.

Figure E.7: C Block shade cloth sail.

Figure E.8: Art block shade cloth sail.

Appendix F. Student diaries

Attached are copies of student diaries for each of the face, neck, arm, hand and leg. Students were asked to mark on the respective body part model in each diary where dosimeters were worn. Dosimeter sites were however limited to a selected number of regions on the body. A map of the school region was also included with each student diary. This map is also included here.

Personal Diary HBSHS - face

School Region List (refer to school map):

Region 1 - Indoors or Classroom

Region 2 - Under Building or Covered Area – M block (Maths/Science)
Region 3 - Under Building or Covered Area – L block (Music)
Region 4 - Under Building or Covered Area – C block (Home Ec)
Region 5 - Under Building or Covered Area – B block (Computers)
Region 6 - Under Building or Covered Area – D block (Chinese)
Region 7 - Under Building or Covered Area – G block (First Year Centre)
Region 8 - Under Building or Covered Area – G block (Art)
Region 9 - Under Building or Covered Area – F block (Manual Arts)
Region 10 - Under Building or Covered Area – H block (Manual Arts / Drama)
Region 11 - Under Building or Covered Area – Agriculture
Region 12 - Under Building or Covered Area – Canteen
Region 13 - Under Building or Covered Area – Library
Region 14 - Under Building or Covered Area – Office

Region 15 – Near Buildings Science / Music / Maths / C Block
Region 16 – Near Buildings C Block / B Block / Canteen / Office
Region 17 – Near buildings B Block / D block / Library
Region 18 – Near buildings D block / Fist year Centre / Art / Toilet Block
Region 19 – Near buildings Manual Arts / Drama / First Year Centre
Region 20 – Near buildings Library / Great Hall / Office front

Region 21 – Pool
Region 22 – Oval
Region 23 – Tree line
Region 24 – Basketball / Netball courts
Region 25 – Agriculture

<table>
<tr><td>Date:</td><td rowspan="4">Dosimeter Location (approx. position):
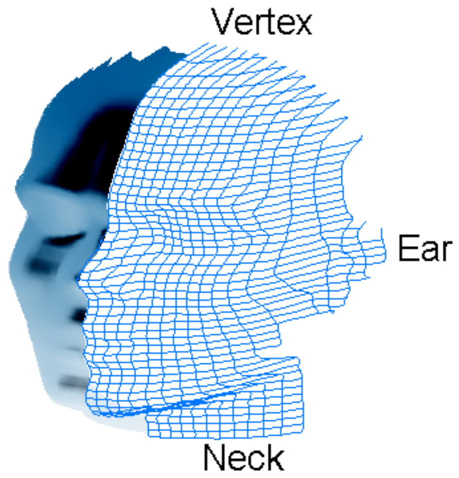
</td></tr>
<tr><td>Weather:</td></tr>
<tr><td>School locations (1-25):
Before School:

Period 1:

Period 2:

First Recess:

Period 3:

Second Recess:

Period 4:</td></tr>
<tr><td>Hat use:
❑ No hat
❑ Cap
❑ Broadbrim
❑ Legionaries</td></tr>
</table>

Personal Diary HBSHS - neck

School Region List (refer to school map):

Region 1 - Indoors or Classroom

Region 2 - Under Building or Covered Area – M block (Maths/Science)
Region 3 - Under Building or Covered Area – L block (Music)
Region 4 - Under Building or Covered Area – C block (Home Ec)
Region 5 - Under Building or Covered Area – B block (Computers)
Region 6 - Under Building or Covered Area – D block (Chinese)
Region 7 - Under Building or Covered Area – G block (First Year Centre)
Region 8 - Under Building or Covered Area – G block (Art)
Region 9 - Under Building or Covered Area – F block (Manual Arts)
Region 10 - Under Building or Covered Area – H block (Manual Arts / Drama)
Region 11 - Under Building or Covered Area – Agriculture
Region 12 - Under Building or Covered Area – Canteen
Region 13 - Under Building or Covered Area – Library
Region 14 - Under Building or Covered Area – Office

Region 15 – Near Buildings Science / Music / Maths / C Block
Region 16 – Near Buildings C Block / B Block / Canteen / Office
Region 17 – Near buildings B Block / D block / Library
Region 18 – Near buildings D block / Fist year Centre / Art / Toilet Block
Region 19 – Near buildings Manual Arts / Drama / First Year Centre
Region 20 – Near buildings Library / Great Hall / Office front

Region 21 – Pool
Region 22 – Oval
Region 23 – Tree line
Region 24 – Basketball / Netball courts
Region 25 – Agriculture

<table>
<tr><td>Date:</td><td rowspan="4">Dosimeter Location (approx. position):
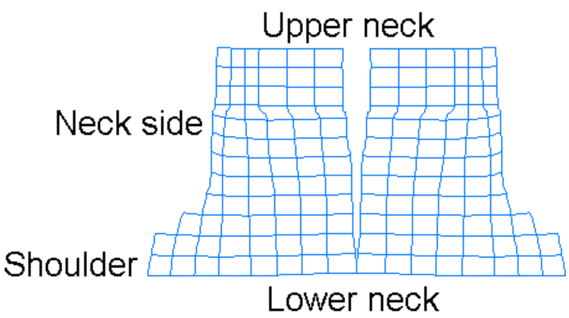
</td></tr>
<tr><td>Weather:</td></tr>
<tr><td>School locations (1-25):
Before School:

Period 1:

Period 2:

First Recess:

Period 3:

Second Recess:

Period 4:</td></tr>
<tr><td>Hat use:
❑ No hat
❑ Cap
❑ Broadbrim
❑ Legionaries</td></tr>
</table>

Personal Diary HBSHS - arm

School Region List (refer to school map):

Region 1 - Indoors or Classroom

Region 2 - Under Building or Covered Area – M block (Maths/Science)
Region 3 - Under Building or Covered Area – L block (Music)
Region 4 - Under Building or Covered Area – C block (Home Ec)
Region 5 - Under Building or Covered Area – B block (Computers)
Region 6 - Under Building or Covered Area – D block (Chinese)
Region 7 - Under Building or Covered Area – G block (First Year Centre)
Region 8 - Under Building or Covered Area – G block (Art)
Region 9 - Under Building or Covered Area – F block (Manual Arts)
Region 10 - Under Building or Covered Area – H block (Manual Arts / Drama)
Region 11 - Under Building or Covered Area – Agriculture
Region 12 - Under Building or Covered Area – Canteen
Region 13 - Under Building or Covered Area – Library
Region 14 - Under Building or Covered Area – Office

Region 15 – Near Buildings Science / Music / Maths / C Block
Region 16 – Near Buildings C Block / B Block / Canteen / Office
Region 17 – Near buildings B Block / D block / Library
Region 18 – Near buildings D block / Fist year Centre / Art / Toilet Block
Region 19 – Near buildings Manual Arts / Drama / First Year Centre
Region 20 – Near buildings Library / Great Hall / Office front

Region 21 – Pool
Region 22 – Oval
Region 23 – Tree line
Region 24 – Basketball / Netball courts
Region 25 – Agriculture

<table>
<tr><td>Date:</td><td colspan="2" rowspan="2">Dosimeter Location (approx. position):</td></tr>
<tr><td>Weather:</td></tr>
<tr><td>School locations (1-25):
Before School:

Period 1:

Period 2:

First Recess:

Period 3:

Second Recess:

Period 4:</td><td rowspan="2">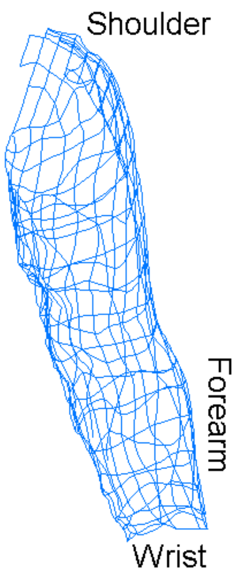
</td><td rowspan="2">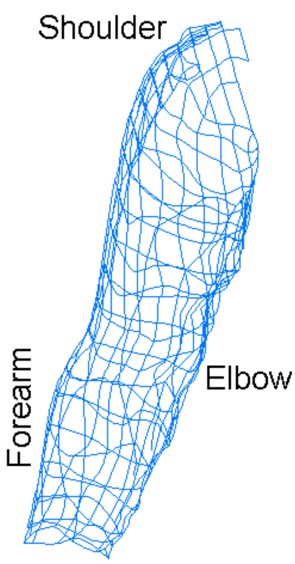
</td></tr>
<tr><td>Hat use:
❑ No hat
❑ Cap
❑ Broadbrim
❑ Legionaries</td></tr>
</table>

Personal Diary HBSHS - hand

School Region List (refer to school map):

Region 1 - Indoors or Classroom

Region 2 - Under Building or Covered Area – M block (Maths/Science)
Region 3 - Under Building or Covered Area – L block (Music)
Region 4 - Under Building or Covered Area – C block (Home Ec)
Region 5 - Under Building or Covered Area – B block (Computers)
Region 6 - Under Building or Covered Area – D block (Chinese)
Region 7 - Under Building or Covered Area – G block (First Year Centre)
Region 8 - Under Building or Covered Area – G block (Art)
Region 9 - Under Building or Covered Area – F block (Manual Arts)
Region 10 - Under Building or Covered Area – H block (Manual Arts / Drama)
Region 11 - Under Building or Covered Area – Agriculture
Region 12 - Under Building or Covered Area – Canteen
Region 13 - Under Building or Covered Area – Library
Region 14 - Under Building or Covered Area – Office

Region 15 – Near Buildings Science / Music / Maths / C Block
Region 16 – Near Buildings C Block / B Block / Canteen / Office
Region 17 – Near buildings B Block / D block / Library
Region 18 – Near buildings D block / Fist year Centre / Art / Toilet Block
Region 19 – Near buildings Manual Arts / Drama / First Year Centre
Region 20 – Near buildings Library / Great Hall / Office front

Region 21 – Pool
Region 22 – Oval
Region 23 – Tree line
Region 24 – Basketball / Netball courts
Region 25 – Agriculture

<table>
<tr><td>Date:</td><td rowspan="2">Dosimeter Location (approx. position):</td></tr>
<tr><td>Weather:</td></tr>
<tr><td>School locations (1-25):
Before School:

Period 1:

Period 2:

First Recess:

Period 3:

Second Recess:

Period 4:</td><td rowspan="2">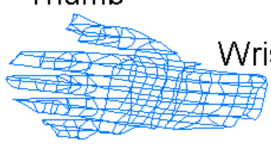

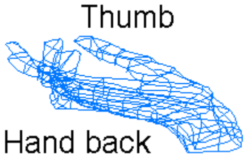

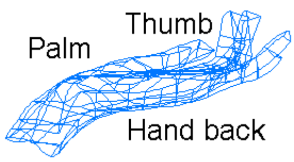
</td></tr>
<tr><td>Hat use:
❑ No hat
❑ Cap
❑ Broadbrim
❑ Legionaries</td></tr>
</table>

Personal Diary HBSHS - leg

School Region List (refer to school map):

Region 1 - Indoors or Classroom

Region 2 - Under Building or Covered Area – M block (Maths/Science)
Region 3 - Under Building or Covered Area – L block (Music)
Region 4 - Under Building or Covered Area – C block (Home Ec)
Region 5 - Under Building or Covered Area – B block (Computers)
Region 6 - Under Building or Covered Area – D block (Chinese)
Region 7 - Under Building or Covered Area – G block (First Year Centre)
Region 8 - Under Building or Covered Area – G block (Art)
Region 9 - Under Building or Covered Area – F block (Manual Arts)
Region 10 - Under Building or Covered Area – H block (Manual Arts / Drama)
Region 11 - Under Building or Covered Area – Agriculture
Region 12 - Under Building or Covered Area – Canteen
Region 13 - Under Building or Covered Area – Library
Region 14 - Under Building or Covered Area – Office

Region 15 – Near Buildings Science / Music / Maths / C Block
Region 16 – Near Buildings C Block / B Block / Canteen / Office
Region 17 – Near buildings B Block / D block / Library
Region 18 – Near buildings D block / Fist year Centre / Art / Toilet Block
Region 19 – Near buildings Manual Arts / Drama / First Year Centre
Region 20 – Near buildings Library / Great Hall / Office front

Region 21 – Pool
Region 22 – Oval
Region 23 – Tree line
Region 24 – Basketball / Netball courts
Region 25 – Agriculture

<table>
<tr><td>Date:</td><td colspan="2" rowspan="2">Dosimeter Location (approx. position):</td></tr>
<tr><td>Weather:</td></tr>
<tr><td>School locations (1-25):
Before School:

Period 1:

Period 2:

First Recess:

Period 3:

Second Recess:

Period 4:</td><td rowspan="2">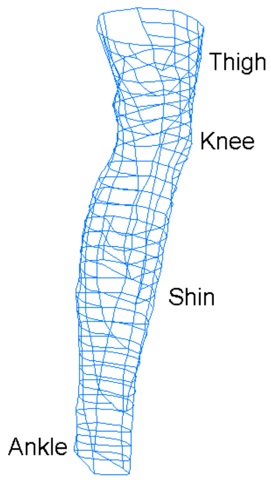
</td><td rowspan="2">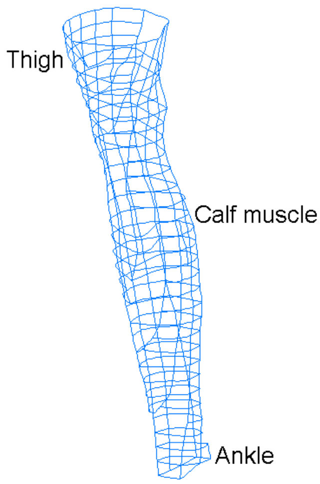
</td></tr>
<tr><td>Hat use:
❑ No hat
❑ Cap
❑ Broadbrim
❑ Legionaries</td></tr>
</table>

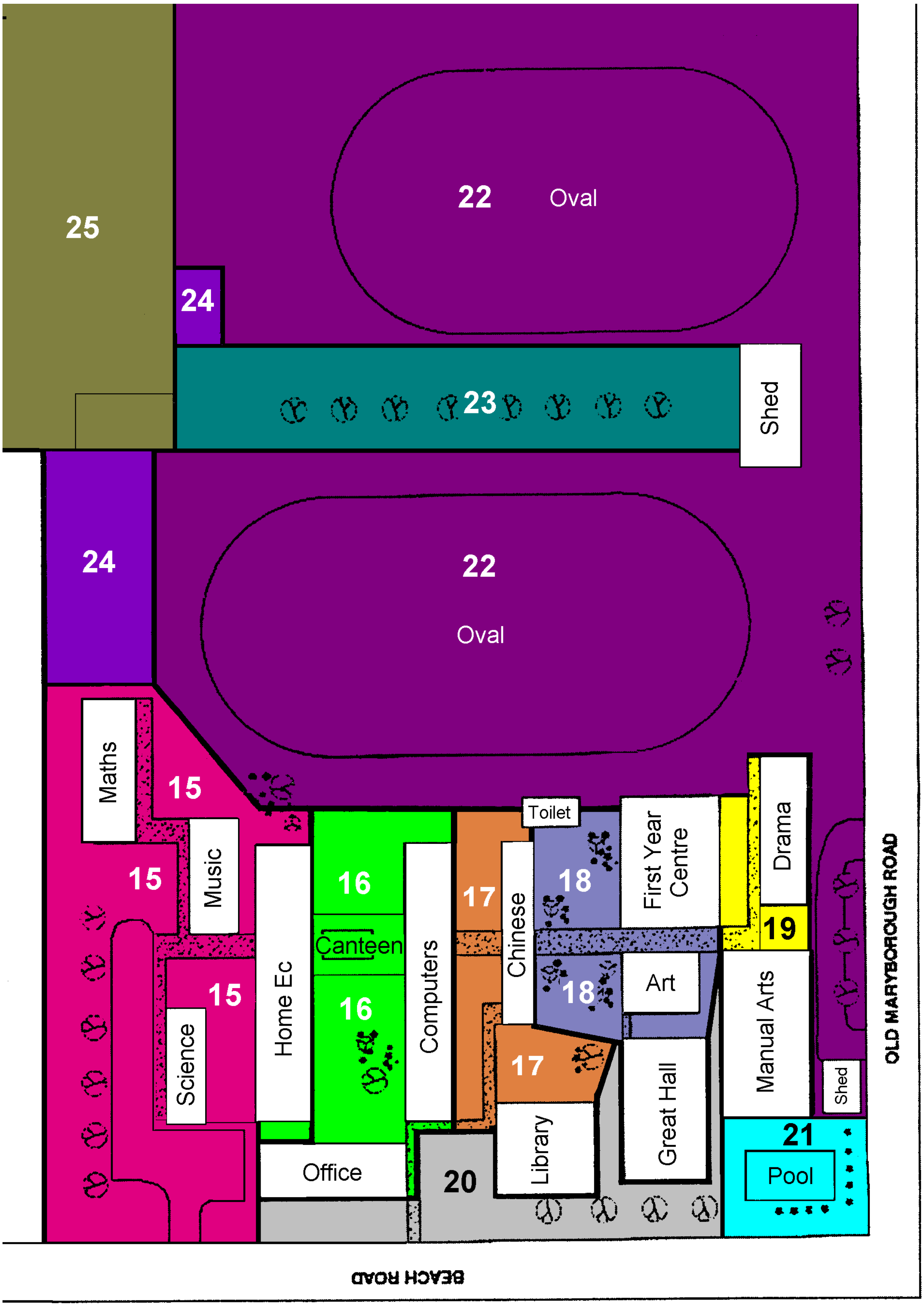
25
24
22
Oval
23
Shed
24
22
Oval
Maths
15
15
Music
15
Science
Home Ec
16
Canteen
16
Computers
17
Toilet
Chinese
18
First Year Centre
Drama
19
18
Art
17
Library
Great Hall
Manual Arts
Shed
21
Pool
Office
20
OLD MARYBOROUGH ROAD
BEACH ROAD

Appendix G. Measurements of body surface exposure ratio listed by individual trial

G.1 Facial exposure ratios

Table G.1.1: 18 February 2006, SZA 0^o-30^o, 4/8 cumulus.

	Cn1	Cn2	Cn3	Cn4	Cn5	Cn6	Cn7	Cn8	Cn9	Cn10	Cn11	Cn12	Cn13	Cn14	Cn15	Cn16	Cn17	Cn18
	100				100													
Cx1																		
Cx2	82				98													
Cx3											66							
Cx4	64				78													
Cx5											59							
Cx6	46				55													
Cx7											42							
Cx8	58				54													
Cx9											34							
Cx10	44				54													
Cx11											38							
Cx12	42				49													
Cx13											36							
Cx14	46				56													
Cx15											45							
Cx16	28				22													
Cx17											9							
Cx18					5													
Cx19											7							
Cx20					5													
Cx21											10						58	
Cx22																		
Cx23											34							
Cx24	46				42												18	
Cx25											45							
Cx26																	11	
Cx27											24							
Cx28	6				24												17	
Cx29											13							
Cx30	29				36													
Cx31											12							
Cx32	13				23													
Cx33											13							
Cx34	33				25													
Cx35											12							
Cx36	7				10													
Cx37											16							
Cx38					25													
Cx39											12							
Cx40	29																	
Cx41											12							
Cx42	8				9													
Cx43											19							
Cx44	2																	
Cx45											19							
Cx46	3				8													
Cx47											20							
Cx48	6				11													
Cx49											25							

Table G.1.2: 12 March 2007, SZA 0^o-30^o, 1/8 cirrus.

	Cn1	Cn2	Cn3	Cn4	Cn5	Cn6	Cn7	Cn8	Cn9	Cn10	Cn11	Cn12	Cn13	Cn14	Cn15	Cn16	Cn17	Cn18
Cx1	64		73	100	100													
Cx2																		
Cx3	87		78		87				84	74	89							
Cx4																		
Cx5																		
Cx6																		
Cx7																		
Cx8																		
Cx9																		
Cx10																		
Cx11																		
Cx12																		
Cx13																		
Cx14																		
Cx15																		
Cx16																		
Cx17																		
Cx18																		
Cx19																		
Cx20																		
Cx21																	69	
Cx22																		
Cx23																		
Cx24																		
Cx25																		
Cx26																		
Cx27															25			
Cx28														14				
Cx29													14					
Cx30	28		37		32				19		14	12						
Cx31																		
Cx32																		
Cx33																		
Cx34																		
Cx35																		
Cx36																		
Cx37																		
Cx38																		
Cx39																		
Cx40																		
Cx41																		
Cx42																		
Cx43																		
Cx44																		
Cx45																		
Cx46																		
Cx47																		
Cx48																		
Cx49																		

Table G.1.3: 21 February 2008, SZA 0^o-30^o, 4/8-2/8 cumulus.

	Cn1	Cn2	Cn3	Cn4	Cn5	Cn6	Cn7	Cn8	Cn9	Cn10	Cn11	Cn12	Cn13	Cn14	Cn15	Cn16	Cn17	Cn18
	100		82		77													
Cx1	70		94		89		100											
Cx2			80		85		57		70									
Cx3			90				87		58		55							
Cx4			74		78				46		74							
Cx5							79						65					
Cx6			53								28		40	54				
Cx7					47				49			42		50				
Cx8			58										38	48	34			
Cx9							45				42				43			
Cx10			52		50				54					36				
Cx11										45						36		
Cx12			45				49				29	33	29	27	36	34		
Cx13									54									
Cx14			34						69						29			
Cx15					43		42					48		22		22		
Cx16			27						4				35					
Cx17					3							14		22		23		
Cx18			6				10								19			
Cx19					8						9		15	26				
Cx20	59		11													18		
Cx21					7			14			8			25	14		60	
Cx22	70																	
Cx23	59		32			31		35			40		29		21			
Cx24			34		52			34						17		19		27
Cx25	27		47					43			47		22					
Cx26				42										25	20		13	19
Cx27			8		30			35			29		24					9
Cx28														16	12	24		
Cx29			19					28			17			17			8	
Cx30					36		35						17					
Cx31			46					26			10			15		17		
Cx32																		
Cx33			8					23			14	15	13	6				
Cx34					27													
Cx35			28					14			18	17	15					
Cx36						12												
Cx37			7						16		19	16						
Cx38					15		27	19				11						
Cx39			29								12	13						
Cx40					36					11	7							
Cx41			16						11			20						
Cx42						10	8	7	3	10								
Cx43			5									20						
Cx44	1		1	35	2		5			17								
Cx45			3									23						
Cx46							9			18								
Cx47			7									25						
Cx48							14			14								
Cx49			9		11							30						

Table G.1.4: 25 January 2008, SZA 0^o-30^o, 2/8-5/8 cumulus / altocumulus.

	Cn1	Cn2	Cn3	Cn4	Cn5	Cn6	Cn7	Cn8	Cn9	Cn10	Cn11	Cn12	Cn13	Cn14	Cn15	Cn16	Cn17	Cn18
		100		85		96												
Cx1		100		90				58										
Cx2		100		77			71			86								
Cx3		80			64			68		87								
Cx4		78			100					94		69						
Cx5					56					41		79						
Cx6		70												55				
Cx7					50			56		67		49		53				
Cx8		38												48	50			
Cx9					58					62					51			
Cx10		51													31			
Cx11					88			84		45				45		45		
Cx12		30																
Cx13					50					69					46	40		
Cx14		56								60								
Cx15					59					43				28				
Cx16		32														23		
Cx17					5					7					29			
Cx18		17			8									27		22		
Cx19										16								
Cx20		23			7									32	23	20		
Cx21								15		21								
Cx22		55	42		17										21		75	
Cx23		40								31				32				
Cx24		55			55					40							22	35
Cx25		19			44			53										
Cx26				38						29				26			12	31
Cx27		5												18	31			
Cx28					25					24				19			26	
Cx29		12						26						18				
Cx30					45					15		12		15		24		
Cx31		40																
Cx32					33					20		13		8		12		
Cx33		5						18										
Cx34					25					19		16						
Cx35		25																
Cx36					16					21								
Cx37		7						26				17						
Cx38					23					18		11						
Cx39		33										18						
Cx40					40			19		18								
Cx41		21								5		17						
Cx42					6		3	6		11								
Cx43		4				4		8				29						
Cx44		1			3					28								
Cx45				2								32						
Cx46					7			15		17								
Cx47												33						
Cx48					13					19								
Cx49								18				27						

Table G.1.5: 14 November 2007, SZA 0^o-30^o, 1/8-3/8 cumulus.

	Cn1	Cn2	Cn3	Cn4	Cn5	Cn6	Cn7	Cn8	Cn9	Cn10	Cn11	Cn12	Cn13	Cn14	Cn15	Cn16	Cn17	Cn18
Cx1																		
Cx2																		
Cx3																		
Cx4																		
Cx5																		
Cx6																		
Cx7																		
Cx8																		
Cx9																		
Cx10															27			
Cx11																28		
Cx12															22	18		
Cx13																		
Cx14												29			14	17		
Cx15																		
Cx16												23			13			
Cx17																12		
Cx18															14			
Cx19												9						
Cx20														18	14			
Cx21												8						
Cx22															15	31		
Cx23												21		18				
Cx24																		
Cx25												34						
Cx26																7		
Cx27												18		10				
Cx28																16		
Cx29												9		10				
Cx30																15		
Cx31												9						
Cx32																8		
Cx33												9						
Cx34																		
Cx35												12						
Cx36																		
Cx37												9						
Cx38												8						
Cx39												9						
Cx40																		
Cx41																		
Cx42																		
Cx43																		
Cx44																		
Cx45																		
Cx46																		
Cx47																		
Cx48																		
Cx49																		

Table G.1.6: 19 June 2006, SZA 30°-50°, 8/8 cumulonimbus / altocumulus.

	Cn1	Cn2	Cn3	Cn4	Cn5	Cn6	Cn7	Cn8	Cn9	Cn10	Cn11	Cn12	Cn13	Cn14	Cn15	Cn16	Cn17	Cn18
	100																	
Cx1																		
Cx2	62																	
Cx3											72							
Cx4	54																	
Cx5																		
Cx6																		
Cx7																		
Cx8	48																	
Cx9																		
Cx10																		
Cx11																		
Cx12	45																	
Cx13											53							
Cx14																		
Cx15																		
Cx16	49																	
Cx17																		
Cx18											24							
Cx19																		
Cx20	60																	
Cx21																	58	
Cx22																		
Cx23																		
Cx24	61										63							
Cx25																		
Cx26																	36	
Cx27																		
Cx28	18										30							
Cx29																		
Cx30																		
Cx31	48																	
Cx32																		
Cx33																		
Cx34											20							
Cx35																		
Cx36	18																	
Cx37																		
Cx38																		
Cx39																		
Cx40											14							
Cx41	54																	
Cx42																		
Cx43											35							
Cx44																		
Cx45	2																	
Cx46																		
Cx47	22																	
Cx48																		
Cx49											36							

Table G.1.7: 22 June 2006, SZA 30^{o}-50^{o}, 7/8-8/8 cumulonimbus.

	Cn1	Cn2	Cn3	Cn4	Cn5	Cn6	Cn7	Cn8	Cn9	Cn10	Cn11	Cn12	Cn13	Cn14	Cn15	Cn16	Cn17	Cn18
	100																	
Cx1																		
Cx2																		
Cx3	88										45							
Cx4																		
Cx5																		
Cx6	60										54							
Cx7																		
Cx8																		
Cx9																		
Cx10											47							
Cx11																		
Cx12	68																	
Cx13																		
Cx14																		
Cx15											59							
Cx16																		
Cx17																		
Cx18																		
Cx19	34										21							
Cx20																		
Cx21																	50	
Cx22	69																	
Cx23											35							
Cx24																		
Cx25	51																	39
Cx26																		
Cx27											43							
Cx28																	29	
Cx29																		
Cx30	54																	
Cx31											27							
Cx32																		
Cx33																		
Cx34	55						33											
Cx35											31							
Cx36																		
Cx37																		
Cx38	32																	
Cx39											26							
Cx40																		
Cx41	52										21							
Cx42																		
Cx43																		
Cx44	3																	
Cx45											39							
Cx46	7																	
Cx47																		
Cx48																		
Cx49	17										30							

Table G.1.8: 16 September 2005, SZA 30^o-50^o.

	Cn1	Cn2	Cn3	Cn4	Cn5	Cn6	Cn7	Cn8	Cn9	Cn10	Cn11	Cn12	Cn13	Cn14	Cn15	Cn16	Cn17	Cn18
Cx1	100																	
Cx2							100											
Cx3																		
Cx4							100											
Cx5	71																	
Cx6							90											
Cx7	65													88				
Cx8							79											
Cx9	62													70				
Cx10							58											
Cx11	66													53				
Cx12							77											
Cx13	69													51				
Cx14							82											
Cx15	66													40				
Cx16							12											
Cx17	35													42				
Cx18							13											
Cx19	38													48				
Cx20							21											
Cx21	82													42				
Cx22							33											
Cx23	98													60				
Cx24							83											
Cx25	56													47				
Cx26							51											
Cx27	9													32				
Cx28							39											
Cx29	31													32				
Cx30							54											
Cx31	67													31				
Cx32							40											
Cx33	12													6				
Cx34							31											
Cx35	50																	
Cx36							26											
Cx37	11																	
Cx38							42											
Cx39	54																	
Cx40							38											
Cx41	34																	
Cx42																		
Cx43	8																	
Cx44							13											
Cx45																		
Cx46	8						24											
Cx47																		
Cx48	12						25											
Cx49																		

Table G.1.9: 5 October 2006, SZA 30°-50°, 3/8 cumulus.

	Cn1	Cn2	Cn3	Cn4	Cn5	Cn6	Cn7	Cn8	Cn9	Cn10	Cn11	Cn12	Cn13	Cn14	Cn15	Cn16	Cn17	Cn18
Cx1																		
Cx2																		
Cx3																		
Cx4																		
Cx5		66		70		70		67		75	66	75	48					
Cx6																		
Cx7																		
Cx8																		
Cx9																		
Cx10																		
Cx11																		
Cx12																		
Cx13																		
Cx14		16		48		54				59		47	33	29	33	32		
Cx15																		
Cx16																		
Cx17																		
Cx18																		
Cx19																		
Cx20																		
Cx21																		
Cx22																		
Cx23																		
Cx24		47		53		57		58		58		52	43	36	28		20	24
Cx25																		
Cx26																		
Cx27																		
Cx28																		
Cx29																		
Cx30																		
Cx31		44		45		39		30		19		18	20	19		20		
Cx32																		
Cx33																		
Cx34																		
Cx35																		
Cx36																		
Cx37																		
Cx38																		
Cx39																		
Cx40																		
Cx41		16		16		19		14										
Cx42																		
Cx43																		
Cx44																		
Cx45																		
Cx46																		
Cx47																		
Cx48																		
Cx49																		

Table G.1.10: 18 December 2007, SZA 30°-50°, 7/8-8/8 cumulonimbus / stratus.

	Cn1	Cn2	Cn3	Cn4	Cn5	Cn6	Cn7	Cn8	Cn9	Cn10	Cn11	Cn12	Cn13	Cn14	Cn15	Cn16	Cn17	Cn18
Cx1																		
Cx2										92								
Cx3										76								
Cx4							100			59		71						
Cx5												63						
Cx6							48			48		60		62				
Cx7														51				
Cx8										85		67						
Cx9							50							35				
Cx10										48		38						
Cx11							38									38		
Cx12										51		36		35		37		
Cx13							52											
Cx14										75		34		27		31		
Cx15							65											
Cx16										16				27		28		
Cx17												27						
Cx18		21								13				26		41		
Cx19												19						
Cx20		23								19				31				
Cx21							19					25						
Cx22		36								30				37		46		
Cx23		37										46						77
Cx24		73								44				34				
Cx25												47				18		30
Cx26		19								42				24				
Cx27												28						31
Cx28										29				25		32		
Cx29							34					22		25				
Cx30										22				28		25		
Cx31							44					18						
Cx32										22						14		
Cx33							29					16						
Cx34										31								
Cx35							31					35						
Cx36										24								
Cx37							23					22						
Cx38										26		19						
Cx39							29					22						
Cx40										18								
Cx41							23			10		26						
Cx42																		
Cx43							5			19		29						
Cx44																		
Cx45							14			24		30						
Cx46																		
Cx47							17			24		47						
Cx48																		
Cx49							21			25		35						

Table G.1.11: 16 October 2007, SZA 30^o-50^o, clear.

	Cn1	Cn2	Cn3	Cn4	Cn5	Cn6	Cn7	Cn8	Cn9	Cn10	Cn11	Cn12	Cn13	Cn14	Cn15	Cn16	Cn17	Cn18
			69															
Cx1			97					70										
Cx2																		
Cx3			69					63										
Cx4													65					
Cx5								60										
Cx6			61										56					
Cx7																		
Cx8			45					55										
Cx9													39		46			
Cx10																		
Cx11								60							46			
Cx12													32					
Cx13																		
Cx14								57										
Cx15								49					37					
Cx16															32			
Cx17																		
Cx18								9					26					
Cx19																		
Cx20								16										
Cx21			27										44					
Cx22																		
Cx23			46					37										
Cx24													38					
Cx25			36					49							17			
Cx26																		
Cx27															31			
Cx28			16					34					22					
Cx29																		
Cx30															30			
Cx31			35					30					21					
Cx32																		
Cx33			8										15					
Cx34								24										
Cx35			37										18					
Cx36																		
Cx37								19										
Cx38			18															
Cx39								21										
Cx40			35															
Cx41																		
Cx42			17					8										
Cx43																		
Cx44								11										
Cx45																		
Cx46								21										
Cx47																		
Cx48																		
Cx49								26										

Table G.1.12: 16 October 2007, SZA 50^{o}-80^{o}, clear.

	Cn1	Cn2	Cn3	Cn4	Cn5	Cn6	Cn7	Cn8	Cn9	Cn10	Cn11	Cn12	Cn13	Cn14	Cn15	Cn16	Cn17	Cn18
			81		100													
Cx1								74										
Cx2																		
Cx3																		
Cx4											63	77						
Cx5												88						
Cx6														90				
Cx7														72				
Cx8											66		78					
Cx9																		
Cx10								39					48		66			
Cx11											74					70		
Cx12								55						53				
Cx13											60					62		
Cx14								54					52		53			
Cx15																54		
Cx16								18				53	32					
Cx17														43		26		
Cx18													45		31			
Cx19										18						29		
Cx20													11	49				
Cx21								25							23	52		
Cx22			30							38								
Cx23														49	49			60
Cx24								83					52			31		
Cx25			46					51			82						16	46
Cx26														50				
Cx27								37					51		49			40
Cx28											47			40				
Cx29													22		34		25	
Cx30								40			33							
Cx31													28	27		37		
Cx32								56			33							
Cx33													24	8				
Cx34											22							
Cx35								39					41					
Cx36											45							
Cx37								37										
Cx38											36	25						
Cx39						45						23						
Cx40								24			18							
Cx41						47						38						
Cx42																		
Cx43										43		36						
Cx44							14											
Cx45										35		27						
Cx46							14											
Cx47										46		58						
Cx48							32											
Cx49										33		43						

Table G.1.13: 27 May 2005, SZA 50^o-80^o.

	Cn1	Cn2	Cn3	Cn4	Cn5	Cn6	Cn7	Cn8	Cn9	Cn10	Cn11	Cn12	Cn13	Cn14	Cn15	Cn16	Cn17	Cn18
	100																	
Cx1							73											
Cx2	100																	
Cx3							100											
Cx4	100																	
Cx5							84											
Cx6	78													75				
Cx7							80											
Cx8	94													63				
Cx9							90											
Cx10	88													100				
Cx11							75											
Cx12	88													68				
Cx13							83											
Cx14	92													53				
Cx15							82											
Cx16	56													34				
Cx17							11											
Cx18	41													94				
Cx19							34											
Cx20	67													37				
Cx21							42											
Cx22	100													77				
Cx23							59											
Cx24	33													44				
Cx25							79											
Cx26	25													43				
Cx27							56											
Cx28	21													61				
Cx29							52											
Cx30	65													30				
Cx31							59											
Cx32	39													34				
Cx33							45											
Cx34	64																	
Cx35							39											
Cx36	22																	
Cx37							41											
Cx38	36																	
Cx39							63											
Cx40	62																	
Cx41							25											
Cx42	29																	
Cx43							8											
Cx44	7																	
Cx45	1																	
Cx46																		
Cx47	13						16											
Cx48																		
Cx49	28						37											

Table G.1.14: 27 August 2007, SZA 50^o-80^o, 1/8 cumulus.

	Cn1	Cn2	Cn3	Cn4	Cn5	Cn6	Cn7	Cn8	Cn9	Cn10	Cn11	Cn12	Cn13	Cn14	Cn15	Cn16	Cn17	Cn18
		100		83														
Cx1		100		100														
Cx2		96							100									
Cx3									79									
Cx4		94																
Cx5									92				97					
Cx6		73																
Cx7									94				72					
Cx8		73																
Cx9									86									
Cx10		78											76					
Cx11									79							65		
Cx12		65																
Cx13									66				56			59		
Cx14		77																
Cx15									77									
Cx16		58											57			57		
Cx17									28									
Cx18		29																
Cx19									39				54			43		
Cx20		61																
Cx21									39									
Cx22		53										58						
Cx23																		69
Cx24		75							64			83						
Cx25																		48
Cx26		26							73									
Cx27																		34
Cx28		15										23						
Cx29									51									
Cx30		63																
Cx31																37		
Cx32		39							44			33						
Cx33																		
Cx34		72																
Cx35									30			38						
Cx36																		
Cx37		15																
Cx38									35			32						
Cx39		66																
Cx40												44						
Cx41		33				38			22									
Cx42									0									
Cx43		10							28									
Cx44		0																
Cx45		1							40									
Cx46																		
Cx47																		
Cx48									52									
Cx49		16																

G.2 Neck exposure ratios

Table G.2.1: 14 November 2007, 0^o-30^o, 1/8-3/8 cumulus.

	Cn1	Cn2	Cn3	Cn4	Cn5	Cn6	Cn7	Cn8	Cn9
Cx1	5		4	17	6	16	7		
Cx2	6		9		11		10		
Cx3	9		11		9		10		
Cx4	13		12		13		11		
Cx5	13		10		16		15		
Cx6	12		12		16		15		
Cx7	14		15		17		17		
Cx8	15		15		17		21		
Cx9	15		17		21		23		
Cx10	16		18		22		34		
Cx11	21		19		26		28		44
Cx12	18		20		25		30		39
Cx13	16		21		21		31		33

Table G.2.3: 25 January 2008, 0^o-30^o, 2/8-5/8 cumulus / altocumulus.

	Cn1	Cn2	Cn3	Cn4	Cn5	Cn6	Cn7	Cn8	Cn9
Cx1		11		10		14			
Cx2		17		15		18			
Cx3		33		23		22			
Cx4		23		26		27			
Cx5		26		33		29	32		
Cx6		28		37		28	24		
Cx7		24		33		54	36		
Cx8		19		33		39	48		
Cx9		28		34		51			
Cx10		52		25		55		53	
Cx11		47		47		39		51	67
Cx12		32		35		49		50	
Cx13		32		39		41		43	

Table G.2.4: 18 December 2007, 30^o-50^o, 7/8-8/8 cumulonimbus / stratus.

	Cn1	Cn2	Cn3	Cn4	Cn5	Cn6	Cn7	Cn8	Cn9
Cx1		14		13		13			
Cx2		21		21		16			
Cx3		24		23		23			
Cx4		32		30		27			
Cx5		38		35		32			
Cx6		33		37		35			
Cx7		56		33		35			
Cx8		35		32		47			
Cx9		37		38		44			
Cx10		33		44		44		62	
Cx11		40		30		40		49	53
Cx12		43		69		42		59	
Cx13		38		42		44		48	

Table G.2.5: 27 August 2007, 50^{o}-80^{o}, 1/8 cumulus.

	Cn1	Cn2	Cn3	Cn4	Cn5	Cn6	Cn7	Cn8	Cn9
Cx1	19								
Cx2									
Cx3	43								
Cx4									
Cx5	49				47		48		
Cx6			49						
Cx7	59				62		57		
Cx8			48						
Cx9	58				66		69		
Cx10			56						
Cx11	45				63		77		86
Cx12			60						
Cx13	62				68		68		73

G.3 Arm exposure ratios

Table G.3.1: 13 December 2007, 0^o-30^o, 5/8-7/8 cumulonimbus / altocumulus / cirrus.

	Cn1	Cn2	Cn3	Cn4	Cn5	Cn6	Cn7	Cn8	Cn9	Cn10	Cn11	Cn12	Cn13	Cn14	Cn15	Cn20	Cn21	Cn22	Cn23
Cx1																			
Cx2																			
Cx3																			
Cx4																			
Cx5																			
Cx6																			
Cx7																			
Cx8																			
Cx9																			
Cx10																			
Cx11																			5
Cx12						3	1	1										4	7
Cx13	9	5	5	5	3	2			1	1	0						2	14	22
Cx14	25	22	20	14	30	5	24	18	6	7	3		0				6		19
Cx15	25	31	33	31	43	24	31	25	16	19	13			3		5	7	16	10
Cx16	21	26	37	41	47	34	34	29	23	16	17		4	4				9	13
Cx17	19	23	32	39	35	38	37	28	24	20	14	6	a				4	9	13
Cx18	12	21	27	32	31	38	39	29	22	19	12	12	6	4	3			8	9
Cx19	10	17	25	28	29	37	36	36	21	21		8	7	4			5		
Cx20	10	16	19	28	32	34	36	55	27			7	7	5				6	
Cx21				26	6	38	46		29				5	5					
Cx22						39							4		7				
Cx23						33								4	8				
Cx24													5	4	5				
Cx25															5				
Cx26													7		6				
Cx27													8	4					
Cx28															4				

Table G.3.2: 1 February 2008, 0^{o}-30^{o}, 3/8-5/8 cumulus.

	Cn1	Cn2	Cn3	Cn4	Cn5	Cn6	Cn7	Cn8	Cn9	Cn10	Cn11	Cn12	Cn13	Cn14	Cn15	Cn20	Cn21	Cn22	Cn23
Cx1																			
Cx2																			
Cx3																			
Cx4																			
Cx5																			
Cx6																			
Cx7																			
Cx8																			
Cx9																			
Cx10																			
Cx11																			
Cx12																			
Cx13																		5	9
Cx14	18	9	6	7	21	5	20	15		8								8	13
Cx15	25	43	43	31	54	23	35	31	13	17	13					3	4	9	10
Cx16	13	23	38	39	61	49	37	32	20	23	17				3		3	6	7
Cx17	12	19	29	30	54	60	40	a	27	21	19	8	4	3					7
Cx18	8	13	19	27	38	36	44	42	23	22	13	13			3			5	6
Cx19	6	10	19	29	31	40	43	36	25	23		11	8	5			3	5	
Cx20	5	9	13	23	30	41	39	a	a			10	6	4	4				
Cx21				18	29	43	a		40				6	3	4				
Cx22						35							5	4	4				
Cx23						27							5		6				
Cx24													7	3	4				
Cx25															3				
Cx26														4					
Cx27													8		3				
Cx28														4					

Table G.3.3: 30 April 2007, 30^o-50^o, clear.

	Cn1	Cn2	Cn3	Cn4	Cn5	Cn6	Cn7	Cn8	Cn9	Cn10	Cn11	Cn12	Cn13	Cn14	Cn15	Cn20	Cn21	Cn22	Cn23
Cx1																			
Cx2					0														
Cx3							0			0									
Cx4												0							
Cx5					0		0												
Cx6	0									0					0				
Cx7					0														
Cx8										0		0				0		0	
Cx9	0		0		0		0												
Cx10								0	0	a				0				0	
Cx11	0		0		0	0						0				0			
Cx12							15											5	
Cx13	19		0		13				13	7				0				5	13
Cx14	16		25		43		0			0		0							10
Cx15	21						35		28		16	5		2		0			5
Cx16	17		21		38			47	23	25									
Cx17			0		39	17		51											
Cx18	3						37					24						2	
Cx19									46			17	13		0				
Cx20	0					33	39		0			14		4					
Cx21							0		29										
Cx22														1					
Cx23																			
Cx24																			
Cx25																			
Cx26																			
Cx27													12	2					
Cx28																			

Table G.3.4: 2 April 2008, 30^{o}-50^{o}, 1/8-2/8 cumulus.

	Cn1	Cn2	Cn3	Cn4	Cn5	Cn6	Cn7	Cn8	Cn9	Cn10	Cn11	Cn12	Cn13	Cn14	Cn15	Cn20	Cn21	Cn22	Cn23
Cx1																			
Cx2																			
Cx3																			
Cx4																			
Cx5																			
Cx6																			
Cx7																			
Cx8																			
Cx9																			
Cx10																			
Cx11																			
Cx12							2		1									1	1
Cx13	1	0	1	1	1			8	1	1								10	13
Cx14	19	1	14	8	33	5	26		11	11	5						6		17
Cx15	23	28	30	44	49	31	42	40	21	25	18				3		7	15	14
Cx16	19	25	37	51	54	47	45	45	35	30	25	7	5		4			8	9
Cx17	17	23	38	40	46	48	49	35	36	32	20			3	4		6	6	8
Cx18	10	17	33	41	45	45	37	35	34	22	17	19	11						8
Cx19	8	20	29	33	48	49	37	55	36	28		14		7	5		6	7	
Cx20	8		20	24	42	51	51		34			13	10	6					
Cx21				23	39	47	38		47				9	5	6				
Cx22						39							7	5					
Cx23						30									7				
Cx24															6				
Cx25													11	4					
Cx26																			
Cx27													10	6	5				
Cx28													15						

Table G.3.5: 18 July 2007, 50^o-80^o, clear.

	Cn1	Cn2	Cn3	Cn4	Cn5	Cn6	Cn7	Cn8	Cn9	Cn10	Cn11	Cn12	Cn13	Cn14	Cn15	Cn20	Cn21	Cn22	Cn23
Cx1																			
Cx2																			
Cx3																			
Cx4																			
Cx5																			
Cx6																			
Cx7																			
Cx8																			
Cx9																			
Cx10																			
Cx11														2					
Cx12																			20
Cx13										25									24
Cx14	27		39				66		43		46		13						23
Cx15	32										65				13	12		14	
Cx16		48	47		67			87	76	66			23						
Cx17	19			55		59	74	65		54								11	19
Cx18	19	21	41		54		71	60			49	41	37		13				
Cx19	12	11	32		52	51	63	88	57			43							
Cx20	11	25		38		55	58		66			48	33	18					
Cx21				25		52	65						35						
Cx22														12					
Cx23																			
Cx24														12					
Cx25																			
Cx26														20					
Cx27																			
Cx28														21					

Table G.3.6: 12 July 2007, 50^o-80^o, clear.

	Cn1	Cn2	Cn3	Cn4	Cn5	Cn6	Cn7	Cn8	Cn9	Cn10	Cn11	Cn12	Cn13	Cn14	Cn15	Cn20	Cn21	Cn22	Cn23
Cx1																			
Cx2																			
Cx3																			
Cx4																			
Cx5																			
Cx6																			
Cx7																			
Cx8																			
Cx9																			
Cx10																			
Cx11																			
Cx12								11											
Cx13						6													
Cx14		20		31				64											
Cx15						61		71		49									
Cx16		33		62							49								
Cx17		26			51	56	70	57	63			24		16					
Cx18		25		55				77		60									
Cx19		16		47		68		75		44				26					
Cx20		18		34				56					24						
Cx21				33	43	56							24						
Cx22													19						
Cx23						45													
Cx24																			
Cx25													29						
Cx26																			
Cx27																			
Cx28													46						

G.4 Hand exposure ratios

Table G.4.1: 21 November 2007, 0^o-30^o, 2/8-3/8 cumulus.

	Cn1	Cn2	Cn3	Cn4	Cn5	Cn6	Cn7	Cn8	Cn9	C10	C11	C12	C13	C14	C15	C16	C17	C18	C19	C20	C21	C22	C23
Cx1																	4			4			
Cx2						22													4				
Cx3							42									8		3			13		
Cx4					11	31	45									6			3				
Cx5					37	49	48	37	35	30	27					7			3		14		
Cx6						65		35	34	24	15					5							
Cx7					52	76		62		44	26					2							
Cx8				20	69			52		46	30	11				2					3		
Cx9			16		76	73		73		50	42	34		2	5							5	
C10		29		57	66	75		72		48	52	53	6	2	2		1			2		3	10
C11		42	69	51	57	75		71		61	56	53				1				2	1		6
C12			31	63	47	65		63		56		38						2				1	6
C13	32	65	29	10	42		33	70		40		23				3			2				3
C14		26	22		37	67	9	62		61	8				2			5		8			
C15			17		30	65			10							5							
C16					41	54	3	58		29	28							8	3				
C17					37	17		41		14													
C18					46			11		7													
C19					41			11		9													
C20								9															

Table G.4.2: 1 February 2008, 0^o-30^o, 3/8-5/8 cumulus.

	Cn1	Cn2	Cn3	Cn4	Cn5	Cn6	Cn7	Cn8	Cn9	C10	C11	C12	C13	C14	C15	C16	C17	C18	C19	C20	C21	C22	C23
Cx1																							
Cx2																9		4	4		12		
Cx3						31										9					12		
Cx4					32	42	49									9					16		
Cx5					51	58	51	41	37	37	24					6		4	5		20		
Cx6					56		63	37	42	35	14					6					15		
Cx7					62		64		48	38						3			4				
Cx8											31	15	9		14	2					7		
Cx9			21	40	63		69	66		50				2	6					2		9	
C10					61						49	50	10		2		2			3		5	
C11		48	66	65		74	65	58	52	58						2		2				2	11
C12		64	54	67	51						56	36								4			8
C13		62	37	11	52	54	30	56	32	40													3
C14		21	17		33	59	25	59	14	44	43					5		8					3
C15			14			60	8			42	47												
C16					39	54	7	51	4		34						2		5				
C17					50	28		41		20								22					
C18					53			16		9													
C19					48			11		12													
C20																							

Table G.4.3: 2 April 2008, 30^o-50^o, 1/8-2/8 cumulus.

	Cn1	Cn2	Cn3	Cn4	Cn5	Cn6	Cn7	Cn8	Cn9	C10	C11	C12	C13	C14	C15	C16	C17	C18	C19	C20	C21	C22	C23
Cx1																		6			15		
Cx2						31										12			6				
Cx3																		5		12	20		
Cx4					21	46	57									10	5				22		
Cx5					50			45	42	44	33							5					
Cx6					61	62	70	53	45		18								6				
Cx7					64	74			56		32					5	4			6			
Cx8				35				61	55	53	41	25	10		20			2					
Cx9			34		52	76	70	70		58		34		3	7	2		1				10	
C10		47		61	67	66			58		52								3		3		20
C11			66					71		51	53	58				3		3					13
C12	39		64	67	53	70	60	46	53	56				4						11		5	
C13		69	31	10			37			51	32	33											9
C14		47			52	72		60	10							8				15			
C15			16		48	68				60					4			17					
C16						60	15	61	11														
C17					51	31		45		20													
C18					60			24															
C19					57			15		14													
C20								15															

Table G.4.4: 28 August 2007, 50^o-80^o, 4/8-5/8 cirrus.

	Cn1	Cn2	Cn3	Cn4	Cn5	Cn6	Cn7	Cn8	Cn9	C10	C11	C12	C13	C14	C15	C16	C17	C18	C19	C20	C21	C22	C23
Cx1																							
Cx2																			3				
Cx3						60											3						
Cx4							60									17			7		39		
Cx5					58		71		60		41												
Cx6						57			53		27						7		10				
Cx7								71		45											0		
Cx8					53	84				68		35	17		17	0		0					
Cx9						75		80		58				0			0		0		3		
C10				58		73		42		59					0		0		0				41
C11			67			60		66		56				5		2				6			
C12				70	52	58		78		63													20
C13				10		68		62		53		34								20			
C14		42	31		40	72	7	77								15		12					
C15						60		73		60													
C16					76	67	20																
C17						34		61										26					
C18					65					8													
C19								36															
C20																							

G.5 Leg exposure ratios

Table G.5.1: 13 November 2007, 0^o-30^o, 2/8 cumulus.

	Cn3	Cn4	Cn5	Cn6	Cn7	Cn8	Cn9	Cn10	Cn11	Cn12	Cn13	Cn14	Cn15
Cx1						7	6	9					
Cx2						6	6	22					
Cx3					1	9	5						
Cx4		0	0	1	3	10	5		0	0	0	0	0
Cx5	0	3	2	2	4	11				0	0	0	0
Cx6	1	6	4	4	5	10			0	0	0	0	0
Cx7	6	8	8	6	8	9			7	12	13	9	1
Cx8		11	12	10	11	9			10	13	16	13	7
Cx9		13	15	14	15	10			10	10	15	12	9
Cx10		15	19	17	18	9			8	8	11	11	19
Cx11		14	19	19	19	10			8	6	7	11	17
Cx12		20	23	19	16	7			7	6	6	13	15
Cx13		23	20	21	16	12			6	8	8	15	15
Cx14		21	21	20	14	12			7	7	9	16	13
Cx15		20	20	19	14	14			9	8	9	14	16
Cx16		20	19	18	14	13			9	8	9	13	
Cx17			16	16	14	16			11	10	9	12	
Cx18			16	18	15	17			9	9	9	12	
Cx19			15	15	15	24			8	10	9	11	
Cx20			13	15	15				7	8	9	10	
Cx21			15	16	17				6	10	9	8	
Cx22				16	17				7	9	10	11	
Cx23				17	16				7	9	10	11	
Cx24				18	17				6	10	9	12	
Cx25				14	16				8	9	10	13	
Cx26				14	19				8	10	11	14	
Cx27					24				8	11	10	13	
Cx28					16				7	11	11	12	
Cx29									9	10	12		
Cx30									10	10	12		
Cx31									10	11	16		
Cx32									9	10	13		
Cx33										10	12		

Table G.5.2: 1 February 2008, 0^{o}-30^{o}, 3/8-5/8 cumulus.

	Cn3	Cn4	Cn5	Cn6	Cn7	Cn8	Cn9	Cn10	Cn11	Cn12	Cn13	Cn14	Cn15
Cx1													
Cx2													
Cx3													
Cx4		14	12										
Cx5		17	16										
Cx6		17	16										
Cx7		19	22										
Cx8		24	29										
Cx9		25	32										
Cx10		11	37	30									
Cx11		34	39										
Cx12		35	34										
Cx13		34	39										
Cx14		33	33										
Cx15		28	33										
Cx16		27	30										
Cx17			24										
Cx18			31										
Cx19			28										
Cx20			23										
Cx21			26										
Cx22													
Cx23													
Cx24													
Cx25													
Cx26													
Cx27													
Cx28													
Cx29													
Cx30													
Cx31													
Cx32													
Cx33													

Table G.5.3: 4 March 2008, 30^o-50^o, 3/8-2/8 cumulus.

	Cn3	Cn4	Cn5	Cn6	Cn7	Cn8	Cn9	Cn10	Cn11	Cn12	Cn13	Cn14	Cn15
Cx1						17	13	18					
Cx2					4	21	11	35					
Cx3		4	5	6	9	23	11						
Cx4	6	11	9	8	12	25	10						
Cx5	13	15	13	13	13	31			14	20	17		9
Cx6	21	22	18	15	20	25			16	22	25	37	19
Cx7	25	28	29	21	25	21			17	22	28	38	30
Cx8		34	33	18	38	22			17	20	26	22	29
Cx9		37	34	29	43	23			14	17	25	44	30
Cx10		52	29	38	38	23			14	10	a	44	42
Cx11		43	45	31	42	22			11	12	a	42	45
Cx12		44	44	38	33	27			13	13	21	43	31
Cx13		37	47	36	33	28			10	13	21	48	35
Cx14		33	39	44	36	35			12	12	a	46	33
Cx15		39	32	28	33	30			18	15	a	40	33
Cx16		36	32	32	30	40			14	14	a	36	
Cx17			27	31	34	35			14	14	21	35	
Cx18			29	35	35	46			14	14	20	22	
Cx19			34	31	45	41			13	14	15	26	
Cx20			21	28	41				12	13	16	27	
Cx21			32	38	48				11	15	16	26	
Cx22				38	39				11	14	17	23	
Cx23				32	36				14	16	18	29	
Cx24				26	36				11	15	19	32	
Cx25				33	37				13	15	24	29	
Cx26				26	39				16	16	19	33	
Cx27					43				13	18	23	26	
Cx28					44				15	17	25	25	
Cx29									15	18	23		
Cx30									16	19	23		
Cx31									14	21	22		
Cx32									15	19	28		
Cx33										14	25		

Table G.5.4: 6 August 2007, 50^o-80^o, clear.

	Cn3	Cn4	Cn5	Cn6	Cn7	Cn8	Cn9	Cn10	Cn11	Cn12	Cn13	Cn14	Cn15
Cx1													
Cx2					12								
Cx3					19								
Cx4					22								
Cx5				35									
Cx6	43		42		40								
Cx7	50			36									
Cx8		47	15		58								
Cx9		63											
Cx10			42	58	48								
Cx11		64			55								
Cx12			70										
Cx13		62			46								
Cx14			53										
Cx15		43		59	40								
Cx16		62	60										
Cx17					44								
Cx18			56	59									
Cx19					57								
Cx20			46	51									
Cx21					57								
Cx22				65									
Cx23				54	60								
Cx24				49									
Cx25					58								
Cx26				51									
Cx27					61								
Cx28					50								
Cx29													
Cx30													
Cx31													
Cx32													
Cx33													

Table G.5.5: 2 August 2008, 50^o-80^o, clear.

	Cn3	Cn4	Cn5	Cn6	Cn7	Cn8	Cn9	Cn10	Cn11	Cn12	Cn13	Cn14	Cn15
Cx1						33	24						
Cx2													
Cx3						36							
Cx4													
Cx5		35									47		
Cx6													
Cx7			38						32		50	36	51
Cx8		42											38
Cx9			70	41					34	37	51	56	
Cx10		62			82						37		77
Cx11			62	65					24	25		40	
Cx12		71			52						31		48
Cx13			75						27	25			
Cx14		60			56						35		47
Cx15			59						39	25		61	52
Cx16					45						27		
Cx17			53							27		57	
Cx18					51						41		
Cx19			55							33		42	
Cx20											45		
Cx21			49							24			
Cx22				51							32		
Cx23										33		37	
Cx24				52							26		
Cx25				52								53	
Cx26					53						42		
Cx27												45	
Cx28											49		
Cx29													
Cx30											41		
Cx31													
Cx32											40		
Cx33													

Appendix H. Surface model contour assignments

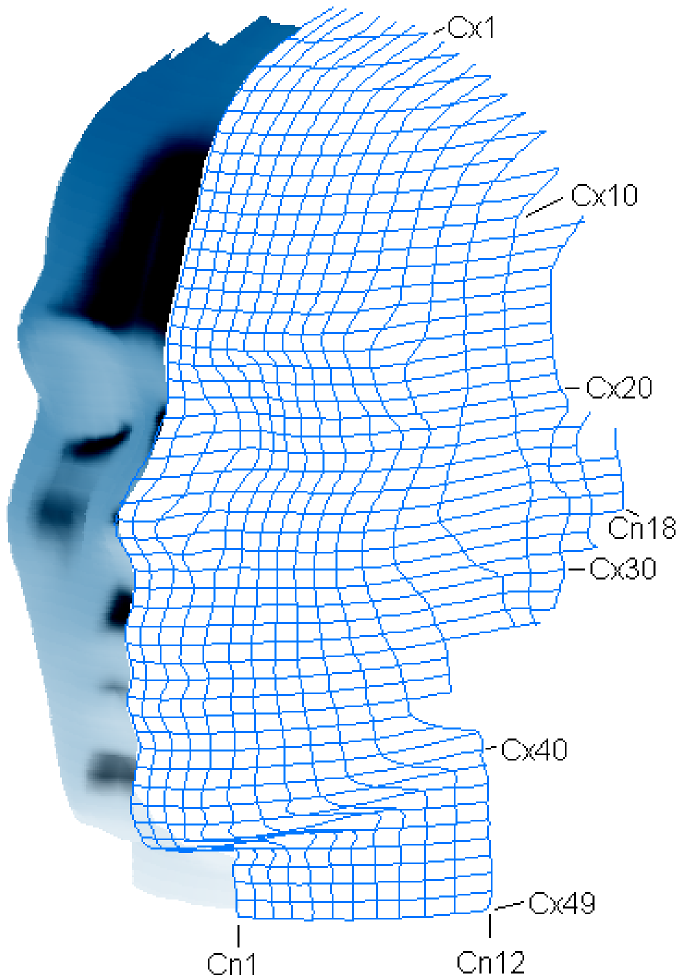

Figure H.1: Horizontal (Cx) and vertical (Cn) facial contour assignments.

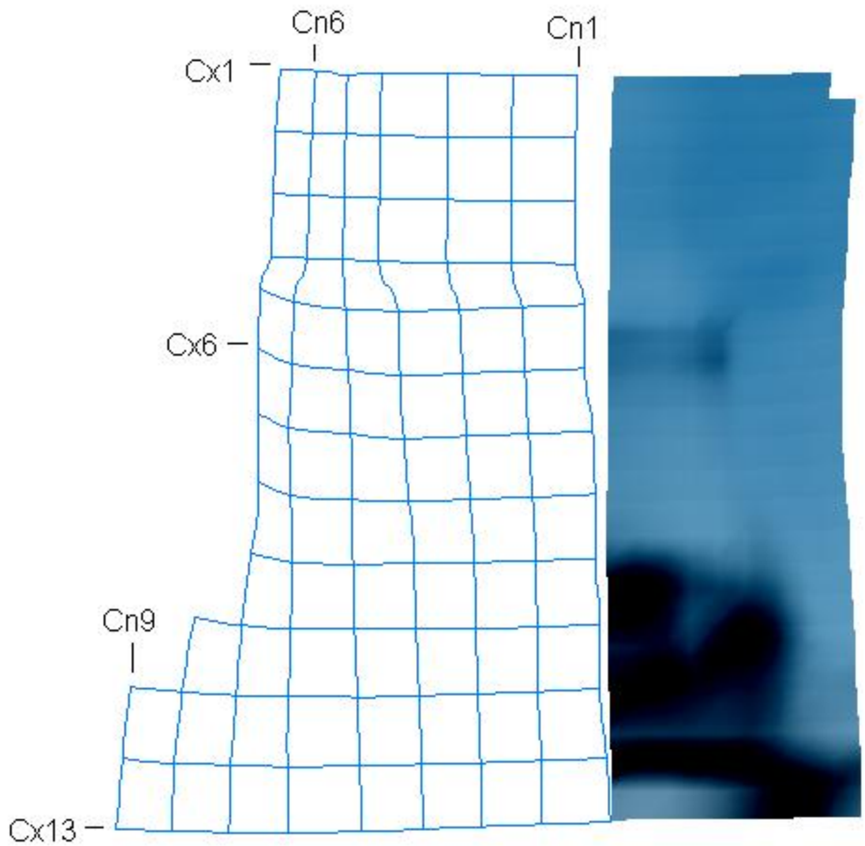

Figure H.2: Horizontal (Cx) and vertical (Cn) neck contour assignments.

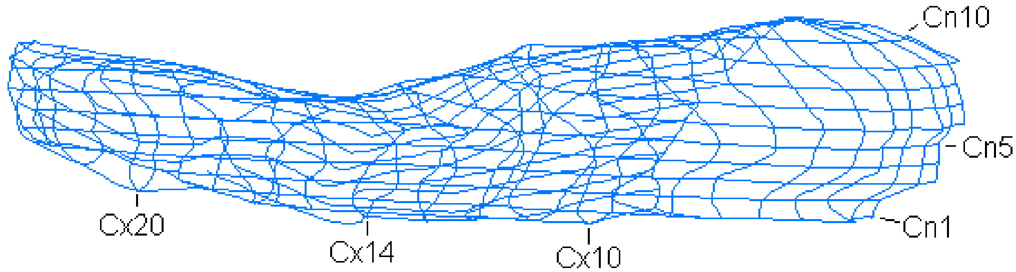

Figure H.3: View of three dimensional arm surface from behind the shoulder. Contours marked Cn1 through Cn23 are oriented along the arm's longitudinal axis. Contours Cn1, Cn5 and Cn10 are shown. Contours marked Cx10, Cx14 and Cx20 are also shown in the diagram. These contours formed complete bands around the arm surface and were numbered from the shoulder (figure right) to the wrist (figure left).

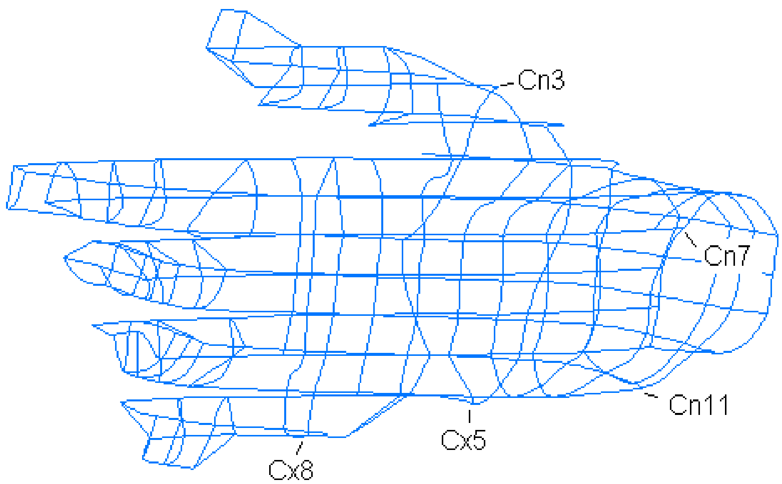

Figure H.4: Contours marked Cn1 through Cn23 represent the longitudinal contours extending from the wrist to the finger tips of the three dimensional hand surface. These contours start and end on the thumb. Contours banded about the hand surface and individual fingers start from the wrist and extend to the finger tip bands. Contours Cx5 and Cx8 are shown in the figure.

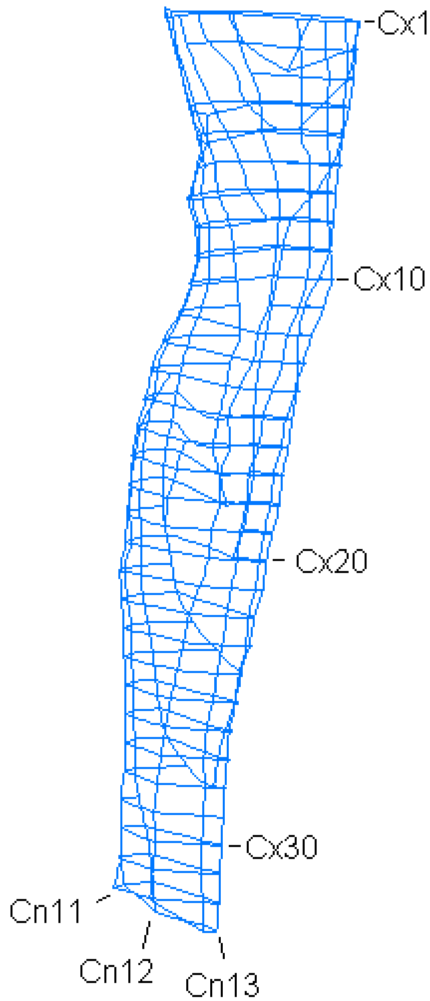

Figure H.5: Longitudinal leg contours extending from the upper thigh to the ankle start at Cn0 and end at Cn16. Contours Cn11 through Cn13 are shown in the figure for a forward facing view of the leg model showing the knee positioned to the upper right. Banded contours Cx1, Cx10, Cx20 and Cx30 show the thigh to ankle order in which these contours were labeled.

Appendix I. Polynomial coefficients for facial horizontal contours

Table I.1: Equation 3.1 Coefficients β_1 through β_9 for the SZA range 0^o-30^o.

Cx	β_1	β_2	β_3	β_4	β_5	β_6	β_7
Cx1	-1.26018370309002E-19	7.74841918351686E-18	2.56933786459068E-15	-4.75242471965701E-13	3.91399886422726E-11	-1.97762417771912E-09	6.76149618367300E-08
Cx2	-1.76786996960371E-19	6.34255098176379E-17	-1.03979548720293E-14	1.03130444214024E-12	-6.90550094090475E-11	3.29805449252062E-09	-1.15714963797726E-07
Cx3	3.23253235143603E-21	-1.49807827877126E-18	3.17711733454850E-16	-4.08494191848433E-14	3.55608832982661E-12	-2.21714027310808E-10	1.02139599887044E-08
Cx4	-1.92958876824599E-21	9.40148906190649E-19	-2.09646449830958E-16	2.83513912988723E-14	-2.59741230367796E-12	1.70568845015939E-10	-8.28537138433333E-09
Cx5	-5.13960434153612E-23	2.67401164815220E-20	-6.35043475760039E-18	9.11336842769909E-16	-8.81889822796553E-14	6.08206703545792E-12	-3.08213329351485E-10
Cx6	-5.73672256116784E-23	3.59436153026322E-20	-1.02665050871653E-17	1.77236542140447E-15	-2.06694561579329E-13	1.72382474939177E-11	-1.06157725502477E-09
Cx7	-6.09420183281925E-23	3.76182174499130E-20	-1.06003792153762E-17	1.80696959086181E-15	-2.08152094535847E-13	1.71444369847199E-11	-1.04191905000255E-09
Cx8	-3.34939280855552E-23	2.03226198258984E-20	-5.62424149968268E-18	9.39811399678183E-16	-1.05791577080774E-13	8.47402816983674E-12	-4.97338518792889E-10
Cx9	-4.75296367717211E-23	2.96726148788336E-20	-8.47474757508879E-18	1.46674446360350E-15	-1.71759690193709E-13	1.43909867887760E-11	-8.89651573693804E-10
Cx10	-4.65137809422664E-23	2.92884658385785E-20	-8.44357264647979E-18	1.47638939749881E-15	-1.74851964454794E-13	1.48349200791013E-11	-9.30069184702916E-10
Cx11	1.67433610017152E-24	-1.33785732337546E-21	4.87636210898657E-19	-1.07478317570640E-16	1.60040323789313E-14	-1.70325663146915E-12	1.33648003546348E-10
Cx12	8.98332782679973E-24	-6.18371062788157E-21	1.95171016292515E-18	-3.74266602285382E-16	4.87112340997749E-14	-4.55257893695589E-12	3.15275852533254E-10
Cx13	9.18350544178758E-24	-6.34065380513282E-21	2.00351462338897E-18	-3.83814049032393E-16	4.97832982037798E-14	-4.62438088442417E-12	3.17342457771217E-10
Cx14	3.13463943656397E-24	-2.04435527587301E-21	6.06433856674738E-19	-1.08237985117596E-16	1.29559041163820E-14	-1.09711438827062E-12	6.75375410681880E-11
Cx15	1.38405061711471E-23	-9.31547674762272E-21	2.86996238020524E-18	-5.36192254635880E-16	6.78454556743743E-14	-6.14988631116181E-12	4.11977983770200E-10
Cx16	5.89656543156420E-24	-4.15510233158562E-21	1.34004970593938E-18	-2.62017548833661E-16	3.46851544542358E-14	-3.28771997790682E-12	2.30163952802120E-10
Cx17	-6.23146541673040E-24	4.17928179127543E-21	-1.28464639869391E-18	2.39841950157917E-16	-3.03854436803958E-14	2.76424555421454E-12	-1.86372024407328E-10
Cx18	-1.89806232688923E-24	1.27807130899342E-21	-3.93454829928534E-19	7.33570277263668E-17	-9.25013124818617E-15	8.34444619507626E-13	-5.55573340836344E-11
Cx19	1.92089956012460E-24	-1.26694314269758E-21	3.82523426869504E-19	-7.00447234452108E-17	8.68747407534955E-15	-7.71947082356197E-13	5.06912321566473E-11
Cx20	1.24960425273325E-24	-8.20683530858806E-22	2.45686297684421E-19	-4.43647330289592E-17	5.38858009123962E-15	-4.64756486038153E-13	2.92870486158853E-11
Cx21	2.09358061046873E-24	-1.39099170702758E-21	4.21634160064765E-19	-7.71863692005385E-17	9.52175231654218E-15	-8.36331357339466E-13	5.38881896371942E-11
Cx22	-2.06047284644551E-26	-7.78818364057198E-24	1.01487313351404E-20	-3.57768294007133E-18	7.00415996725743E-16	-8.97649940004537E-14	8.08960363521222E-12
Cx23	7.92697944900869E-25	-6.51734346200187E-22	2.43091591291141E-19	-5.45976871522620E-17	8.25819792955846E-15	-8.90786761615079E-13	7.07509009528238E-11
Cx24	5.14121952514994E-25	-3.91838210409161E-22	1.36576714668199E-19	-2.88270491520854E-17	4.11192852094176E-15	-4.18868440382919E-13	3.13936041227382E-11
Cx25	1.64359279642609E-24	-1.29280234929177E-21	4.66143818392984E-19	-1.02074308158586E-16	1.51599576621629E-14	-1.61523014814493E-12	1.27350310926925E-10
Cx26	8.71115445124443E-25	-6.86709348127093E-22	2.48038348902336E-19	-5.43845822835481E-17	8.08416617788538E-15	-8.61785940746579E-13	6.79675006555803E-11
Cx27	-1.91207550236309E-26	2.09636631927032E-23	-9.73092906282102E-21	2.62615992044114E-18	-4.68681269857608E-16	5.91414962798110E-14	-5.48162635212407E-12
Cx28	5.08323795650393E-25	-3.85563598426353E-22	1.33668026635742E-19	-2.80603528612058E-17	3.98349544683858E-15	-4.04483572914550E-13	3.03010939927536E-11
Cx29	1.05930465015785E-24	-7.68361968200197E-22	2.55169843379860E-19	-5.13975152397234E-17	7.01222146712109E-15	-6.85360755777524E-13	4.94984641972260E-11
Cx30	4.42731749176608E-25	-3.69569777301787E-22	1.37720485664847E-19	-3.05719060395994E-17	4.53660974975340E-15	-4.77637628465153E-13	3.69027027243384E-11
Cx31	1.39670929995387E-24	-9.70606296547513E-22	3.08582600815311E-19	-5.94602688872650E-17	7.75517227807942E-15	-7.24245777841871E-13	4.99693964669893E-11
Cx32	3.15832722472878E-24	-2.15589832063969E-21	6.73525116835991E-19	-1.27570830928872E-16	1.63593358701288E-14	-1.50228253900881E-12	1.01905253174881E-10
Cx33	1.37825199695799E-23	-8.86536866576811E-21	2.61523354829100E-18	-4.68729441226116E-16	5.70023476750305E-14	-4.97467807257537E-12	3.21346190652992E-10
Cx34	-1.48481202794048E-22	8.06308461112913E-20	-2.00403669900136E-17	3.01972296686671E-15	-3.08020929407281E-13	2.24922037818397E-11	-1.21260476668455E-09
Cx35	-1.62124339044466E-22	8.78470704065911E-20	-2.17774653851143E-17	3.27176661207699E-15	-3.32636669880122E-13	2.42045585643587E-11	-1.30023567774841E-09
Cx36	-3.48210909487753E-22	1.90210076072934E-19	-4.75777279416577E-17	7.21879058602185E-15	-7.41890920385789E-13	5.46192379962376E-11	-2.97099787256247E-09
Cx37	-2.34444971762485E-22	1.24973445175252E-19	-3.05713743872624E-17	4.54604776342873E-15	-4.58840890998142E-13	3.32389876992669E-11	-1.78203338133859E-09
Cx38	1.60199622153761E-22	-6.22753741461689E-20	9.90313934291133E-18	-7.28555001783814E-16	3.33028139731728E-15	4.49549404160791E-12	-4.76907580601662E-10
Cx39	-1.67555335990350E-22	1.03544030691382E-19	-2.86228376864376E-17	4.72004585493130E-15	-5.20818386899005E-13	4.07953353223076E-11	-2.34501511393214E-09
Cx40	-4.83015163868803E-22	2.61621178930879E-19	-6.49332827554276E-17	9.78586596931402E-15	-1.00028229801965E-12	7.33613670241652E-11	-3.98249507764154E-09
Cx41	2.23780236830610E-22	-9.84289037142033E-20	1.92507174241877E-17	-2.18633235484520E-15	1.56607795530752E-13	-7.00353095836880E-12	1.58173251893030E-10
Cx42	-2.83455895354777E-22	1.33123550996526E-19	-2.84355819158924E-17	3.65542851804461E-15	-3.15362212511260E-13	1.92767779086720E-11	-8.59127432472519E-10
Cx43	-7.80786190088163E-23	3.74289209478168E-20	-8.18517170952919E-18	1.08119683418811E-15	-9.62774315829374E-14	6.10812833317068E-12	-2.84506884611791E-10
Cx44	-6.59248512566818E-23	3.12370440053111E-20	-6.73765157073522E-18	8.75406071900619E-16	-7.63995391402392E-14	4.72781601691219E-12	-2.13421024060996E-10
Cx45	-2.14229630759495E-22	1.06801790272618E-19	-2.44208594822776E-17	3.39399696829560E-15	-3.20290879315512E-13	2.17156183408534E-11	-1.09143696930828E-09
Cx46	-2.89486091253581E-22	1.46736129167388E-19	-3.41637465304405E-17	4.84136338150619E-15	-4.66447090910099E-13	3.23216904070144E-11	-1.66158326480618E-09
Cx47	-4.28559764351628E-22	2.20404624334861E-19	-5.20724149020984E-17	7.48828687502258E-15	-7.32070582625333E-13	5.14622731850337E-11	-2.68296897233032E-09
Cx48	-5.31745750708848E-22	2.73924302742926E-19	-6.48310976002550E-17	9.34052269260316E-15	-9.14956008352480E-13	6.44523195692908E-11	-3.36752279390287E-09
Cx49	-4.76979138015997E-22	2.45598343308759E-19	-5.81060716806892E-17	8.36932385067433E-15	-8.19649235824916E-13	5.77279491187825E-11	-3.01552593021316E-09

Table I.2: Equation 3.1 Coefficients β_8 through β_{14} for the SZA range 0^o-30^o.

Cx	β_8	β_9	β_{10}	β_{11}	β_{12}	β_{13}	β_{14}
Cx1	-1.63099162180164E-06	2.82346525183224E-05	-3.51761671876862E-04	3.13418287105349E-03	-1.97634645746950E-02	8.74706668323634E-02	-2.70759314402299E-01
Cx2	3.02629545302704E-06	-5.92294923397922E-05	8.63096983930746E-04	-9.23154526505422E-03	7.06684395289166E-02	-3.71937857644736E-01	1.26295611942048E+00
Cx3	-3.53628245591070E-07	9.27028149391212E-06	-1.84023538410660E-04	2.74830699752556E-03	-3.04712462837074E-02	2.45510690320386E-01	-1.39182322069813E+00
Cx4	3.02869554828917E-07	-8.39569383870242E-06	1.76524010031897E-04	-2.79686264843394E-03	3.29473677121780E-02	-2.82403534804228E-01	1.70491039778105E+00
Cx5	1.16715457727893E-08	-3.33095593945042E-07	7.18807105166047E-06	-1.17321204625896E-04	1.44538183335380E-03	-1.33472702844352E-02	9.04532440374509E-02
Cx6	4.91421780256289E-08	-1.72436899375811E-06	4.59077466301514E-05	-9.21885257190797E-04	1.37815028369228E-02	-1.50020546047989E-01	1.14896036665289E+00
Cx7	4.75321992837485E-08	-1.64027567788375E-06	4.28282206135550E-05	-8.40706383433164E-04	1.22437954304321E-02	-1.29543313768737E-01	9.65481554903466E-01
Cx8	2.16913183132122E-08	-7.05402041567358E-07	1.69999037981838E-05	-2.98769805824233E-04	3.72210527710328E-03	-3.14152682050476E-02	1.67774052764705E-01
Cx9	4.12499414740812E-08	-1.44410448088364E-06	3.81368429540009E-05	-7.53883142755577E-04	1.09935249895453E-02	-1.15665228220988E-01	8.50992480457967E-01
Cx10	4.38149154757834E-08	-1.56205085422913E-06	4.21287509264288E-05	-8.53513798644613E-04	1.28104421975053E-02	-1.39381069590152E-01	1.06491617455865E+00
Cx11	-7.86060726567255E-09	3.48854227618470E-07	-1.16681068060943E-05	2.91659125800330E-04	-5.36234378804920E-03	7.07439384083824E-02	-6.45833632139855E-01
Cx12	-1.64563267187657E-08	6.52184959027968E-07	-1.96172501174462E-05	4.44479042341150E-04	-7.47084909658262E-03	9.08750983215129E-02	-7.70411016775176E-01
Cx13	-1.63603442154589E-08	6.38172994306002E-07	-1.88259316670519E-05	4.16883015107086E-04	-6.82794349204493E-03	8.07882983483470E-02	-6.66620715378450E-01
Cx14	-3.05552629589378E-09	1.01363377841599E-07	-2.42460392455258E-06	4.02189978191293E-05	-4.23585076039564E-04	2.13836023433558E-03	4.88236951520776E-03
Cx15	-2.07417166596295E-08	7.90490136946525E-07	-2.27964738496642E-05	4.93894383716924E-04	-7.92546598003264E-03	9.21231646875212E-02	-7.50826239936938E-01
Cx16	-1.21007005582546E-08	4.81134897874825E-07	-1.44601805527717E-05	3.26064671787490E-04	-5.43589793535943E-03	6.54459379424064E-02	-5.49277587386775E-01
Cx17	9.47580467040812E-09	-3.66152374532899E-07	1.07558547600882E-05	-2.38649636930986E-04	3.94646361498522E-03	-4.76194782870999E-02	4.06460303058242E-01
Cx18	2.77708336575520E-09	-1.05020428957098E-07	3.00619260625064E-06	-6.47612103909004E-05	1.03741241823948E-03	-1.21250764634648E-02	1.00595814865681E-01
Cx19	-2.50125224308129E-09	9.33783556757510E-08	-2.63514693803705E-06	5.57548632068333E-05	-8.70300864885095E-04	9.76127864643024E-03	-7.54489271051547E-02
Cx20	-1.36649157562813E-09	4.73187428285051E-08	-1.20714691608149E-06	2.22842233090790E-05	-2.88131440434137E-04	2.45767151845892E-03	-1.20411618395845E-02
Cx21	-2.58681946401946E-09	9.30469404122719E-08	-2.50380637416354E-06	5.00038528326179E-05	-7.30703839570901E-04	7.64458960731637E-03	-5.53372779700500E-02
Cx22	-5.31994194545929E-10	2.60280488894348E-08	-9.54927547551187E-07	2.62422569859220E-05	-5.34840424526770E-04	7.92353964915430E-03	-8.25311703954456E-02
Cx23	-4.21078101670946E-09	1.89243971021709E-07	-6.42303763679738E-06	1.63510855621899E-04	-3.07876062140346E-03	4.19337150384447E-02	-3.99694895704309E-01
Cx24	-1.75747024944500E-09	7.38540319392003E-08	-2.32267434599259E-06	5.41319613829856E-05	-9.20683744662010E-04	1.12291764187596E-02	-9.70168834723945E-02
Cx25	-7.55489548737361E-09	3.39563993165124E-07	-1.15537867777051E-05	2.95239438512423E-04	-5.57800088104195E-03	7.59925919146181E-02	-7.18834019484660E-01
Cx26	-4.03341646056238E-09	1.81415793783993E-07	-6.18301968145983E-06	1.58550532419520E-04	-3.01542699779204E-03	4.15607576152733E-02	-4.00695492548023E-01
Cx27	3.81324365879930E-10	-2.01177208917881E-08	8.06339244611864E-07	-2.44044709294853E-05	5.49924033969026E-04	-9.01287100307001E-03	1.03713661743046E-01
Cx28	-1.70268791503599E-09	7.22545493693507E-08	-2.31291688901005E-06	5.53720049520454E-05	-9.74815739174836E-04	1.22768469857880E-02	-1.05947188975633E-01
Cx29	-2.68592928493070E-09	1.10258952423952E-07	-3.42102705893300E-06	7.95714458298775E-05	-1.36508902469620E-03	1.68220889887683E-02	-1.42914195745377E-01
Cx30	-2.13206154858483E-09	9.29305840074434E-08	-3.05866361003173E-06	7.55304310610714E-05	-1.37924642141494E-03	1.81711560296791E-02	-1.66087302005870E-01
Cx31	-2.59118605438754E-09	1.01772166242679E-07	-3.02885221069044E-06	6.78782774975189E-05	-1.13015167937482E-03	1.36669247164439E-02	-1.15844336303576E-01
Cx32	-5.19268390093453E-09	2.00201168414315E-07	-5.83846749999887E-06	1.27884876111013E-04	-2.07425962819782E-03	2.43519827973627E-02	-1.99909384596931E-01
Cx33	-1.56205314046306E-08	5.75258963821579E-07	-1.60337146068879E-05	3.35468545660953E-04	-5.18618149461226E-03	5.77786278810626E-02	-4.46913116460016E-01
Cx34	4.90698724388122E-08	-1.50070487271258E-06	3.46613341745867E-05	-6.00013084164552E-04	7.67047008197715E-03	-7.07536253582966E-02	4.55112358704764E-01
Cx35	5.24335175850110E-08	-1.59867918818968E-06	3.68408147983781E-05	-6.37092970697553E-04	8.14992542532904E-03	-7.53737284484754E-02	4.86966046305666E-01
Cx36	1.21395013802231E-07	-3.75168088975735E-06	8.76313081519705E-05	-1.53525611027099E-03	1.98764087577513E-02	-1.85772181262924E-01	1.21089310887638E+00
Cx37	7.18681058721841E-08	-2.19464401038839E-06	5.06964146320334E-05	-8.79109064646219E-04	1.12797991808759E-02	-1.04756003308438E-01	6.82102713395853E-01
Cx38	2.80614137465836E-08	-1.10746646214268E-06	3.09877007106433E-05	-6.25587633049813E-04	9.10244922737972E-03	-9.40502019360395E-02	6.70200883783974E-01

Cx39	1.00753131695417E-07	-3.26258148092728E-06	7.96652981470487E-05	-1.45725407100859E-03	1.96934859778042E-02	-1.92202225783928E-01	1.30824502584789E+00
Cx40	1.62728863506891E-07	-5.04036466159933E-06	1.18281916803706E-04	-2.08752506508527E-03	2.73097353592791E-02	-2.58834235136735E-01	1.71701405853681E+00
Cx41	1.80462724838439E-09	-2.89270222033717E-07	1.17907449625605E-05	-2.89230544400948E-04	4.77006828287522E-03	-5.40186158242271E-02	4.13922015974922E-01
Cx42	2.82996461101664E-08	-6.90932312763917E-07	1.24224695207122E-05	-1.61796058759179E-04	1.48149181826227E-03	-9.02373943434196E-03	3.21232068535859E-02
Cx43	9.87937233574444E-09	-2.57028793428205E-07	4.99100805683067E-06	-7.13989509879409E-05	7.34112257976654E-04	-5.19950356471920E-03	2.35314206534108E-02
Cx44	7.11954523920001E-09	-1.75790584426894E-07	3.18414618531658E-06	-4.14208142116401E-05	3.71837595155543E-04	-2.13039797106118E-03	6.34163124375731E-03
Cx45	4.13570327653732E-08	-1.18970617056249E-06	2.59534311871308E-05	-4.25632033861749E-04	5.15936778248186E-03	-4.50010652204131E-02	2.71478048046600E-01
Cx46	6.44235340565421E-08	-1.89611035793773E-06	4.22906687952428E-05	-7.08111580594730E-04	8.74427984259814E-03	-7.74570495262747E-02	4.72611272947404E-01
Cx47	1.05449462266097E-07	-3.14448468026754E-06	7.10237782876681E-05	-1.20389457891929E-03	1.50505639030390E-02	-1.35066088367092E-01	8.36481917355885E-01
Cx48	1.32656712726667E-07	-3.96529698195156E-06	8.97922576995545E-05	-1.52627399499256E-03	1.91410697382181E-02	-1.72422889840868E-01	1.07293780089007E+00
Cx49	1.18749391680499E-07	-3.54738975302720E-06	8.02389061421187E-05	-1.36118144367614E-03	1.70122551489175E-02	-1.52365230723995E-01	9.39201824963427E-01

Table I.3: Equation 3.1 Coefficients β_{15} through β_{19} for the SZA range 0^o-30^o.

Cx	β_{15}	β_{16}	β_{17}	β_{18}	β_{19}
Cx1	5.80906034555732E-01	-8.68846070389097E-01	2.25672271899842E-02	1.06988141993277E+01	6.70183340304313E+01
Cx2	-2.47664736171691E+00	2.14407176575916E+00	-6.21700496637760E-01	7.57092399027650E+00	7.71648147628635E+01
Cx3	5.28535913357688E+00	-1.24377769423931E+01	1.61283495806766E+01	-1.10860644068219E+01	8.80269205843525E+01
Cx4	-6.90309839862168E+00	1.73640449440084E+01	-2.38168101966121E+01	1.24269501672393E+01	8.32038618307148E+01
Cx5	-4.27444359476805E-01	1.28078152176811E+00	-2.10762214625942E+00	-3.37679279202110E-01	8.37854607225382E+01
Cx6	-5.87316482951376E+00	1.84749166538006E+01	-3.14828933625439E+01	2.08619514715416E+01	7.84311700423514E+01
Cx7	-4.84620844686137E+00	1.52593882416178E+01	-2.59511465758906E+01	1.15863788876756E+01	7.68681885193850E+01
Cx8	-5.20278035137783E-01	8.97769461279082E-01	1.75316818281798E-01	-1.33535620402435E+01	7.89524037805045E+01
Cx9	-4.19244860991787E+00	1.29334387007999E+01	-2.12489666562557E+01	5.58959062809962E+00	7.44843146062547E+01
Cx10	-5.45367784342304E+00	1.73999544389891E+01	-2.98913208626570E+01	1.51386081840655E+01	7.14155448666315E+01
Cx11	3.86945529028647E+00	-1.40802299253934E+01	2.84050883395227E+01	-3.39189386733974E+01	7.85959040450542E+01
Cx12	4.30104731480695E+00	-1.45464548689279E+01	2.73988394009383E+01	-3.42019098208628E+01	7.56497540042315E+01
Cx13	3.64059081143993E+00	-1.21723936504021E+01	2.25566933046190E+01	-2.53064991877276E+01	7.42005027992384E+01
Cx14	-1.20444125818937E-01	5.13443182028137E-01	-7.99375252482940E-01	-1.66131815437724E+00	6.92483568813007E+01
Cx15	4.09214490902496E+00	-1.38619084907461E+01	2.59404201098272E+01	-2.58410465563547E+01	7.07845420559507E+01
Cx16	3.04824663434877E+00	-1.03406915970865E+01	1.95645477927913E+01	-2.46413238740747E+01	6.88639972674985E+01
Cx17	-2.34509356242187E+00	8.49077235542378E+00	-1.62603670028736E+01	3.52226980051100E+00	6.14651163584451E+01
Cx18	-5.69329887770431E-01	2.04203360794048E+00	-3.32716348923995E+00	-8.91827041774747E+00	6.16214647303229E+01
Cx19	3.75605770442550E-01	-1.09196959942725E+00	2.22982951511399E+00	-1.19910105817158E+01	6.13218009589387E+01
Cx20	1.68559156658743E-02	1.24065013441319E-01	-8.77100787532080E-02	-8.63933469987276E+00	5.89842474315046E+01
Cx21	2.61501451093952E-01	-7.34532550445072E-01	1.32285067891459E+00	-6.86309559364764E+00	6.51316795056087E+01
Cx22	5.73860748657050E-01	-2.45877051163707E+00	5.71629639747439E+00	-8.47416972050004E+00	7.12480025374600E+01
Cx23	2.53807642150344E+00	-9.95299775854715E+00	2.14484351201060E+01	-2.40474068730441E+01	6.30736775187257E+01
Cx24	5.92932267010363E-01	-2.48249501097061E+00	5.59563787331643E+00	-1.58098624808613E+00	4.47684153340595E+01
Cx25	4.46099579861084E+00	-1.66915836431241E+01	3.35593940842551E+01	-3.12593053102971E+01	3.18883956266696E+01
Cx26	2.56092475362328E+00	-1.00085753543611E+01	2.16207058849671E+01	-2.45665006156425E+01	3.07746734659988E+01
Cx27	-7.94968702867610E-01	3.72315111784584E+00	-8.70116741623480E+00	2.31550730655071E+00	2.50348095646653E+01
Cx28	5.85944253970093E-01	-1.88876039804778E+00	3.61822126222650E+00	-8.44997049828784E+00	2.84564541665642E+01
Cx29	7.85395756183382E-01	-2.54295310779887E+00	4.69044274268340E+00	-8.34690670739172E+00	2.84800835273793E+01
Cx30	9.90425926012007E-01	-3.50493647503006E+00	6.51636318122218E+00	-5.66758785895852E+00	2.86840591225687E+01
Cx31	6.51567748056256E-01	-2.23613138198828E+00	3.94835898219167E+00	2.86903802260208E-01	2.64925675591890E+01
Cx32	1.08883298819214E+00	-3.62519938528642E+00	6.51963547622624E+00	-5.29638782251859E+00	2.47640054765047E+01
Cx33	2.27092743364006E+00	-6.98203478803683E+00	1.18526061369900E+01	-1.34200597534851E+01	2.33290151542318E+01
Cx34	-1.94275916542184E+00	5.10717744490293E+00	-7.14407618087967E+00	2.67232079937544E+00	1.94193757413914E+01
Cx35	-2.08902949071630E+00	5.50767370762293E+00	-7.92931149119247E+00	6.45128780512599E+00	1.73591923333329E+01
Cx36	-5.23234634814103E+00	1.38809074695458E+01	-1.99166561197516E+01	1.21041563719811E+01	1.43906192688675E+01
Cx37	-2.97322123711151E+00	8.07624490546923E+00	-1.18985518539609E+01	5.25136816790716E+00	1.39616083542010E+01
Cx38	-3.13759880886016E+00	8.92471238316954E+00	-1.37371745949210E+01	1.09346939990095E+01	1.17751227405944E+01
Cx39	-5.88614569746990E+00	1.61058576757813E+01	-2.39863394505641E+01	2.13437732839651E+01	9.01443011850178E+00
Cx40	-7.56574094051570E+00	2.04135704058595E+01	-3.00007370353833E+01	2.38240362359301E+01	6.54037916253368E+00
Cx41	-2.05310856761011E+00	6.08575464886078E+00	-9.83067341796405E+00	1.07457033718306E+01	6.11249438591749E+00
Cx42	-3.44732510861013E-02	-1.96092486960658E-01	5.60534515623717E-01	1.82502432918537E+00	5.11808486292043E+00
Cx43	-5.81652807867101E-02	4.24538330183567E-02	9.28880788822688E-02	3.57312301833465E-02	3.03018719846670E+00
Cx44	2.90940227508950E-05	-5.97651953464475E-02	1.54176755237428E-01	-1.26328596122831E-01	1.02041588789409E+00
Cx45	-1.07037605392283E+00	2.54332291191945E+00	-3.20251995485424E+00	1.67110274646053E+00	8.16560247013864E-01
Cx46	-1.87512244088366E+00	4.45754779418530E+00	-5.57959518795032E+00	2.87282088161673E+00	6.92439432983708E-01
Cx47	-3.38044548995641E+00	8.22880774961962E+00	-1.06229679574918E+01	5.69616302598150E+00	3.52712069630538E-01
Cx48	-4.36334810650141E+00	1.07090568671737E+01	-1.39690398974517E+01	7.58648430649223E+00	1.23269323268032E-01
Cx49	-3.76304453545913E+00	9.03636614530995E+00	-1.14407261075861E+01	5.97484260112901E+00	3.46599488253276E-01

Table I.4: Equation 3.1 Coefficients β_1 through β_9 for the SZA range 30^o-50^o.

Cx	β_1	β_2	β_3	β_4	β_5	β_6	β_7
Cx1	8.90102607497261E-18	-2.26665936795583E-15	2.60261824167473E-13	-1.77558380259758E-11	7.97171209172970E-10	-2.45685476261508E-08	5.22315251641399E-07
Cx2	1.70331064501020E-19	-6.49949206272372E-17	1.13445779556786E-14	-1.20023759816611E-12	8.59771538580671E-11	-4.41164125724937E-09	1.67298677487453E-07
Cx3	5.33893012093240E-21	-2.49906594221873E-18	5.35310354992221E-16	-6.95213506284663E-14	6.11412798902004E-12	-3.85209563598551E-10	1.79387631170514E-08
Cx4	5.54321351636734E-22	-2.50730087067411E-19	5.12234962345538E-17	-6.23953116190176E-15	5.03473283363149E-13	-2.82372348290061E-11	1.12006479928252E-09
Cx5	-5.23142718445267E-22	2.84973734833385E-19	-7.10820696711963E-17	1.07545886191553E-14	-1.10213392291021E-12	8.09122928724687E-11	-4.38930345311106E-09
Cx6	-2.40272516034886E-23	1.22274982393741E-20	-2.73526247794297E-18	3.47817404991278E-16	-2.65982745229493E-14	1.08793710587844E-12	8.12994606866355E-13
Cx7	-1.56354470620423E-23	7.49295853496845E-21	-1.52104840807566E-18	1.60708712806317E-16	-7.31218208106268E-15	-3.11618518818081E-13	7.39938964725985E-11
Cx8	9.15842194567633E-24	-6.41131479723837E-21	2.03189782469892E-18	-3.86628538922208E-16	4.93557706816565E-14	-4.47155950224587E-12	2.96491956461549E-10
Cx9	-2.58572612230634E-24	1.19062497569016E-21	-2.22512336123047E-19	1.91151393728371E-17	-1.31534746753903E-16	-1.45852437340283E-13	1.70192065007426E-11
Cx10	-1.55326272572587E-23	9.69400580450985E-21	-2.78265654157455E-18	4.87201157603648E-16	-5.81724054197215E-14	5.01645043188636E-12	-3.22700128593761E-10
Cx11	7.36878553594077E-24	-4.77789597963795E-21	1.41230269828344E-18	-2.51882519003916E-16	3.02309965354218E-14	-2.57801905218343E-12	1.60730423073887E-10
Cx12	1.13282057030542E-23	-7.42485061439778E-21	2.22147440901366E-18	-4.01684038820987E-16	4.89791050148540E-14	-4.25489247918132E-12	2.71223852990053E-10
Cx13	1.40101192075777E-23	-9.23692963575063E-21	2.78234111474411E-18	-5.07034932581168E-16	6.23904805075941E-14	-5.47871256130638E-12	3.53795368993954E-10
Cx14	1.25010002577375E-23	-8.43501172229155E-21	2.60518873719725E-18	-4.87872745985357E-16	6.18586204544727E-14	-5.61592337807799E-12	3.76506883822383E-10
Cx15	9.53194604769944E-25	-4.99984555788531E-22	1.06279082719208E-19	-1.00299078603381E-17	-1.08190396515472E-16	1.48922192480613E-13	-2.04184558435153E-11
Cx16	-7.72662239060769E-24	5.31680346420078E-21	-1.67657664147574E-18	3.20985739794936E-16	-4.16722839226778E-14	3.88089764269676E-12	-2.67484047372875E-10
Cx17	-1.71401896535617E-25	7.83508247414654E-23	-9.59533838906074E-21	-1.63180307915083E-18	7.47763897099825E-16	-1.28654160957963E-13	1.36489903001998E-11
Cx18	2.97392881984743E-24	-1.86978892399509E-21	5.33861915705974E-19	-9.15414814093427E-17	1.05023601080909E-14	-8.49852976242541E-13	4.97881260246874E-11
Cx19	5.04160807408248E-24	-3.27640582034135E-21	9.73090491833341E-19	-1.74962767931273E-16	2.12668175487025E-14	-1.84818261709205E-12	1.18439536737883E-10
Cx20	3.76891382902068E-24	-2.47257289169679E-21	7.41828943802536E-19	-1.34818035956351E-16	1.65703225618064E-14	-1.45626417326318E-12	9.43366994026565E-11
Cx21	1.99643631468378E-24	-1.25462519868616E-21	3.57238165754056E-19	-6.08662930939247E-17	6.89780783634371E-15	-5.45918807956888E-13	3.07376918251041E-11
Cx22	-1.98436378814641E-24	1.43818997995534E-21	-4.78010435379084E-19	9.65560085529615E-17	-1.32429134967288E-14	1.30503281999662E-12	-9.53706582391635E-11
Cx23	-4.18228196202486E-24	3.06337833164961E-21	-1.02971698965284E-18	2.10494000456539E-16	-2.92325345697231E-14	2.91808305026847E-12	-2.16042679915849E-10
Cx24	-9.48102034746159E-25	7.55077878241094E-22	-2.75988692939030E-19	6.13399507262893E-17	-9.25873264194994E-15	1.00393739947547E-12	-8.06670216487457E-11
Cx25	-2.23650969811101E-25	1.84969099622409E-22	-7.04119738717052E-20	1.63285588671818E-17	-2.57353716572026E-15	2.91265094834772E-13	-2.43884171898832E-11
Cx26	-3.12631364759070E-25	2.43905826561401E-22	-8.74823747845657E-20	1.91105159203469E-17	-2.83911380688282E-15	3.03301582253820E-13	-2.40200433653344E-11
Cx27	-7.38667539946217E-25	5.68517671194349E-22	-2.00575009414963E-19	4.29754607037838E-17	-6.24525686231210E-15	6.51041149031500E-13	-5.02109223444818E-11
Cx28	-2.53952742222392E-24	1.87814295447151E-21	-6.37369672438972E-19	1.31519124061423E-16	-1.84330206376231E-14	1.85648448255481E-12	-1.38630605336414E-10
Cx29	-2.20791213478821E-24	1.65036954478908E-21	-5.66365289411192E-19	1.18249593210825E-16	-1.67798245274368E-14	1.71220137707746E-12	-1.29628127169297E-10
Cx30	4.86264046480054E-24	-3.14724975396215E-21	9.25854378696721E-19	-1.63636160203335E-16	1.93424853369892E-14	-1.60964990253420E-12	9.65543358806181E-11
Cx31	2.48718566674882E-24	-1.59494835891851E-21	4.63734110315375E-19	-8.07139057698685E-17	9.34399561089141E-15	-7.54852701918384E-13	4.32886819082587E-11
Cx32	-1.67569816687007E-24	1.22950644281726E-21	-4.15419727469502E-19	8.56390239760206E-17	-1.20307904071384E-14	1.21825606303280E-12	-9.17208671646095E-11
Cx33	6.88282503833339E-24	-4.04517934973417E-21	1.07102966880866E-18	-1.68025543717693E-16	1.72301866381085E-14	-1.19340850522117E-12	5.46380649649329E-11
Cx34	7.23090987408674E-23	-4.02337495847702E-20	1.02658343697258E-17	-1.59089040550786E-15	1.67152941806948E-13	-1.25862834058879E-11	6.99903642316928E-10
Cx35	-7.30410834884548E-23	3.95051069807484E-20	-9.77921971793164E-18	1.46774148132385E-15	-1.49158837615527E-13	1.08562065423692E-11	-5.83787014648601E-10
Cx36	-4.76389503598254E-23	2.58906150542297E-20	-6.43986601544033E-18	9.70981976483683E-16	-9.90803075839960E-14	7.23466758880221E-12	-3.89764166036763E-10
Cx37	2.56421544396566E-22	-1.16015353610271E-19	2.36816321653816E-17	-2.87677642149838E-15	2.30741924982405E-13	-1.27890681149227E-11	4.95763191875525E-10
Cx38	5.11628773376607E-22	-2.36386819129361E-19	4.95581834674727E-17	-6.23357167928455E-15	5.23981982582934E-13	-3.10173815184829E-11	1.32632870250761E-09
Cx39	2.87674751175497E-22	-1.22185488381685E-19	2.27990630492273E-17	-2.41549721851597E-15	1.53400081701305E-13	-5.13150978303514E-12	-1.61927590912416E-11
Cx40	-1.89019461903838E-22	1.24311732956656E-19	-3.57119764060914E-17	6.03144396738389E-15	-6.74885313026363E-13	5.32170224940193E-11	-3.06173892904308E-09
Cx41	-2.36296067089273E-22	1.47494172525094E-19	-4.09043104747005E-17	6.73390030478278E-15	-7.38804276640133E-13	5.73349537474803E-11	-3.25391613183671E-09
Cx42	3.33011139382469E-22	-1.45945400666326E-19	2.84999256486295E-17	-3.24536192976219E-15	2.35283545651817E-13	-1.09276509077086E-11	2.87682117442014E-10
Cx43	-1.35069968210494E-22	6.68045116427305E-20	-1.51486731070396E-17	2.08743234500018E-15	-1.95309374905288E-13	1.31324045447885E-11	-6.55022052835564E-10
Cx44	9.54128066972098E-24	1.56740153176725E-21	-1.88475569565366E-18	4.84806835814571E-16	-6.77124869642894E-14	6.13411907666654E-12	-3.88014239115965E-10
Cx45	-3.84621588783914E-23	1.87519654655388E-20	-4.17642574203446E-18	5.62662519031325E-16	-5.11768789205374E-14	3.32107380708313E-12	-1.58417956063114E-10
Cx46	3.09532859001063E-23	-6.42278830527858E-21	-7.11423114345550E-19	4.17988446164691E-16	-7.09708698513403E-14	7.03277721723610E-12	-4.68479985307469E-10
Cx47	-7.42753922574821E-23	4.30338360323789E-20	-1.13227600759269E-17	1.79487449005129E-15	-1.91628062829427E-13	1.45843180376833E-11	-8.16508352276746E-10
Cx48	-3.81401159611805E-23	2.40698146424946E-20	-6.74103117836029E-18	1.12021675864566E-15	-1.24066184351812E-13	9.72230797604700E-12	-5.57463311894665E-10
Cx49	-6.46036817754600E-23	3.70530335017763E-20	-9.65660468113228E-18	1.51730455252877E-15	-1.60703858645568E-13	1.21452021910187E-11	-6.75969832268572E-10

Table I.5: Equation 3.1 Coefficients β_8 through β_{14} for the SZA range 30^o-50^o.

Cx	β_8	β_9	β_{10}	β_{11}	β_{12}	β_{13}	β_{14}
Cx1	-7.33573934996983E-06	5.59679688937685E-05	8.79566796906517E-05	-7.90492297959423E-03	1.01483540850358E-01	-7.28461005180423E-01	3.26430334937267E+00
Cx2	-4.76871820933651E-06	1.02909158955823E-04	-1.68056474184858E-03	2.06150751220595E-02	-1.87184115462002E-01	1.22922421471134E+00	-5.64085264355265E+00
Cx3	-6.28085089006147E-07	1.66573582546921E-05	-3.34589273272571E-04	5.05470465087902E-03	-5.66179300726465E-02	4.59529300698768E-01	-2.61119765581491E+00
Cx4	-3.11189294812744E-08	5.72679816812324E-07	-5.55647809996109E-06	-2.16276666453233E-05	1.64639603584450E-03	-2.71335715406777E-02	2.50616007194817E-01
Cx5	1.78913951808553E-07	-5.51918299021203E-06	1.28818122868541E-04	-2.25914918474071E-03	2.93611332508671E-02	-2.76624766492598E-01	1.82782861444850E+00
Cx6	-3.08954563415986E-09	2.11581362696875E-07	-8.23204922852916E-06	2.13307841755655E-04	-3.82256650124491E-03	4.74098504152691E-02	-3.98845813457820E-01
Cx7	-5.85508306655756E-09	2.85637071111299E-07	-9.54980484094633E-06	2.25619194227099E-04	-3.77842895863597E-03	4.42755795679480E-02	-3.53622244915886E-01
Cx8	-1.46196699848930E-08	5.39202275493103E-07	-1.48397039099257E-05	3.01759603171925E-04	-4.45470873420462E-03	4.65193345130189E-02	-3.31815343937319E-01
Cx9	-1.05208096599144E-09	4.08907501961877E-08	-1.00422151576031E-06	1.35741935074688E-05	-1.69578840669288E-05	-2.85846806168600E-03	5.20482327399539E-02
Cx10	1.57671422354072E-08	-5.89984063359541E-07	1.69133709217076E-05	-3.68870865149244E-04	6.02862373382390E-03	-7.20106998368413E-02	6.04985999158401E-01
Cx11	-7.42318906000068E-09	2.54398417749753E-07	-6.41316673649124E-06	1.16479516176720E-04	-1.46744839032297E-03	1.19652111458636E-02	-5.43090856331555E-02
Cx12	-1.28727866597629E-08	4.56793832927428E-07	-1.20634726407035E-05	2.34000284735229E-04	-3.25913662435516E-03	3.14966254734737E-02	-2.01189426834231E-01
Cx13	-1.70611070439093E-08	6.17624199382531E-07	-1.67357922588038E-05	3.35918336670390E-04	-4.90396422726918E-03	5.06866176621120E-02	-3.57606734530982E-01
Cx14	-1.89505734595659E-08	7.20970397094362E-07	-2.07143804706565E-05	4.45878757054157E-04	-7.07842130065418E-03	8.07898643488409E-02	-6.36999955326890E-01
Cx15	1.61985586729517E-09	-8.72041012223273E-08	3.34407770613053E-06	-9.26143474731804E-05	1.84324293712684E-03	-2.58333758590151E-02	2.45669489556421E-01
Cx16	1.38771437181457E-08	-5.45898221389329E-07	1.62781263837558E-05	-3.65254138955271E-04	6.07571702237246E-03	-7.31194923719276E-02	6.13363825540651E-01
Cx17	-9.97990744851200E-10	5.24895550392426E-08	-2.01880774278935E-06	5.68616528228167E-05	-1.16091119351276E-03	1.68090681655818E-02	-1.66567060739191E-01
Cx18	-2.13075284315542E-09	6.62026183715491E-08	-1.45446383979936E-06	2.10795855480194E-05	-1.58333736727261E-04	-4.68157806215204E-04	2.54358028150404E-02
Cx19	-5.69029360804683E-09	2.06339870218107E-07	-5.64096826543750E-06	1.15268478975151E-04	-1.73081669593783E-03	1.85656047228504E-02	-1.35956460726414E-01
Cx20	-4.57588579901433E-09	1.67098114815328E-07	-4.57845369445730E-06	9.29602437358616E-05	-1.36498009552190E-03	1.38741464623526E-02	-8.96904867746460E-02
Cx21	-1.22263893947891E-09	3.27944363863042E-08	-4.99439057760150E-07	-4.84041917655005E-08	1.95846359268109E-04	-4.75993403305307E-03	5.97771191355316E-02
Cx22	5.25901975455053E-09	-2.20536998357878E-07	7.03539206847249E-06	-1.69635250286729E-04	3.04958636211741E-03	-3.99730578993259E-02	3.69191633746605E-01
Cx23	1.20658030893796E-08	-5.12004969206703E-07	1.64988791006539E-05	-4.00631425804973E-04	7.21894662860270E-03	-9.41809756726868E-02	8.57435485514809E-01
Cx24	4.88379263172473E-09	-2.24330824234022E-07	7.81154608525177E-06	-2.04585927635759E-04	3.96882633510715E-03	-5.56760538178542E-02	5.45193720804118E-01
Cx25	1.53418735757095E-09	-7.28964849767045E-08	2.60907221748508E-06	-6.96097584286572E-05	1.35820938712161E-03	-1.88084748809760E-02	1.76702154525486E-01
Cx26	1.43260023618191E-09	-6.47053502020117E-08	2.20684449726107E-06	-5.62067488268398E-05	1.04723068298039E-03	-1.38090026254295E-02	1.22408225899670E-01
Cx27	2.91214011147674E-09	-1.27820448163894E-07	4.23817846996275E-06	-1.05143290040367E-04	1.91635572414558E-03	-2.49231524873758E-02	2.21321421991624E-01
Cx28	7.80623459172837E-09	-3.33834968081273E-07	1.08349543561094E-05	-2.64755957993306E-04	4.79359195486504E-03	-6.26801040571112E-02	5.69469604998294E-01
Cx29	7.40568933949065E-09	-3.21544099580388E-07	1.06025168792160E-05	-2.63378450621234E-04	4.85119014380566E-03	-6.45909385523170E-02	5.98460779708135E-01
Cx30	-4.19233501706890E-09	1.29645306065028E-07	-2.71205756329637E-06	3.26119600297866E-05	-3.65464541344966E-05	-5.97265293118852E-03	1.04881241494372E-01
Cx31	-1.74466401511667E-09	4.67606917220967E-08	-6.70818851623932E-07	-2.87565700505166E-06	3.73663979825224E-04	-8.70973538497611E-03	1.10257599261915E-01
Cx32	5.21999421747869E-09	-2.26072795845482E-07	7.44174275116148E-06	-1.84587956316899E-04	3.39315900707524E-03	-4.50183512064547E-02	4.14370408731671E-01
Cx33	-1.42165037108419E-09	4.51233485514083E-10	1.65418286828183E-06	-7.50817214662534E-05	1.88987061080096E-03	-3.05123716586122E-02	3.20498576359845E-01
Cx34	-2.91838955542110E-08	9.16848072229898E-07	-2.16173602977686E-05	3.77767292238392E-04	-4.78476828914093E-03	4.24180024083770E-02	-2.49747099374630E-01
Cx35	2.35893227747465E-08	-7.21543991827529E-07	1.67067235798833E-05	-2.90886007280402E-04	3.75760130075460E-03	-3.52435247507096E-02	2.32289101576174E-01
Cx36	1.57463958904279E-08	-4.80150276654428E-07	1.10385159084371E-05	-1.89824024804502E-04	2.40590903548664E-03	-2.19709937581249E-02	1.39854352819658E-01
Cx37	-1.31343939383284E-08	2.14581441096305E-07	-1.13505858196452E-06	-3.90683755087184E-05	1.17116968088986E-03	-1.64214452238112E-02	1.38992303842548E-01
Cx38	-4.12801147249365E-08	9.26213419072475E-07	-1.44543591871165E-05	1.41341075627037E-04	-5.11853210175212E-04	-6.83563404569782E-03	1.19246329530909E-01
Cx39	1.12853332909572E-08	-6.38076559784567E-07	2.08804725053041E-05	-4.59173471430991E-04	7.03853255731298E-03	-7.52508460292040E-02	5.49315928604601E-01
Cx40	1.31015701264643E-07	-4.20632049812754E-06	1.01373942693891E-04	-1.82135764634681E-03	2.40427160766874E-02	-2.27780094073970E-01	1.49589566300442E+00
Cx41	1.37524551129644E-07	-4.36263700691825E-06	1.03840219205700E-04	-1.84000809337934E-03	2.38940386129603E-02	-2.21821755570754E-01	1.42008572567779E+00
Cx42	-7.27750278063569E-10	-2.76822467695538E-07	1.26025665588824E-05	-3.15288283728741E-04	5.16243621261522E-03	-5.72577751269552E-02	4.26441110834720E-01
Cx43	2.46620068306487E-08	-7.06346944239660E-07	1.53894689506554E-05	-2.53232157446410E-04	3.10050578888290E-03	-2.75726254979029E-02	1.71740681051595E-01
Cx44	1.77801129160117E-08	-6.01055789287200E-07	1.50865496030879E-05	-2.80452515612742E-04	3.81977772170950E-03	-3.73695375555190E-02	2.54484942452612E-01
Cx45	5.63727075431713E-09	-1.50216498682292E-07	2.97820831960917E-06	-4.31082099942982E-05	4.38050897399617E-04	-2.87354663370160E-03	9.51274940447385E-03

Cx46	2.22020126102527E-08	-7.68395657871824E-07	1.96190594935826E-05	-3.69280740329937E-04	5.07314947827541E-03	-4.98768288903957E-02	3.39987547002542E-01
Cx47	3.41962987380915E-08	-1.07869590313074E-06	2.55982702285769E-05	-4.53093153638141E-04	5.88423794805952E-03	-5.46440203330983E-02	3.49473651741971E-01
Cx48	2.38217212408637E-08	-7.64800178332367E-07	1.84471254250957E-05	-3.31824140054685E-04	4.38504014734261E-03	-4.15711137237177E-02	2.73006659002593E-01
Cx49	2.81829202410828E-08	-8.86482505108171E-07	2.10214433272337E-05	-3.72846333144013E-04	4.87069285556032E-03	-4.57489460138222E-02	2.98264607147215E-01

Table I.6: Equation 3.1 Coefficients β_{15} through β_{19} for the SZA range 30^o-50^o.

Cx	β_{15}	β_{16}	β_{17}	β_{18}	β_{19}
Cx1	-9.10621043652760E+00	1.49500852189392E+01	-1.28470468183070E+01	4.39757021102360E+00	9.96976022004871E+01
Cx2	1.71936610820933E+01	-3.22008825836157E+01	3.25384801396282E+01	-1.46830936965180E+01	9.42104634581734E+01
Cx3	9.87331805567662E+00	-2.29931238406555E+01	2.90306842677919E+01	-1.72219308875385E+01	8.77945247947520E+01
Cx4	-1.40236631852648E+00	4.58111854746920E+00	-7.82343193963670E+00	4.43422479172173E+00	7.71626280024777E+01
Cx5	-8.06033166059294E+00	2.19634113687618E+01	-3.24719041676640E+01	1.92302554580187E+01	6.81811695088754E+01
Cx6	2.18780064604054E+00	-7.31447883456757E+00	1.31976557619261E+01	-1.06121302631463E+01	6.97609554843342E+01
Cx7	1.84763747649166E+00	-5.91461639653962E+00	1.03130504495326E+01	-8.81631252485183E+00	6.63204547894656E+01
Cx8	1.54543738850387E+00	-4.41659410161971E+00	6.97067732352878E+00	-6.72886474774478E+00	6.47927667129006E+01
Cx9	-4.38898126749350E-01	1.90582116727443E+00	-3.99187231802767E+00	1.63182662201800E+00	6.14552840345691E+01
Cx10	-3.37547529804289E+00	1.14872677647629E+01	-2.08972540930483E+01	1.39228106219806E+01	6.13446232720807E+01
Cx11	7.18159876283164E-02	3.82404779558776E-01	-1.49598960026170E+00	-9.00152750907779E-01	6.57160171419323E+01
Cx12	7.95415557829884E-01	-1.77650565526895E+00	1.92043035833456E+00	-3.48215821062379E+00	6.80172455330306E+01
Cx13	1.64280377911393E+00	-4.60405216269997E+00	6.99903914569764E+00	-7.21295554427432E+00	6.96929447742130E+01
Cx14	3.25683381457479E+00	-9.79971980338901E+00	1.64360632274263E+01	-2.66754676945502E+01	6.92710942400946E+01
Cx15	-1.49474167295523E+00	5.33556230514559E+00	-9.83284473721530E+00	4.68012071498659E+00	6.48726279326555E+01
Cx16	-3.39104245895946E+00	1.13598390839789E+01	-2.01762400628302E+01	1.31469024786786E+01	4.86415239726332E+01
Cx17	1.07051604265509E+00	-4.12123614167156E+00	8.37322879131111E+00	-7.25475934568328E+00	3.63229655852971E+01
Cx18	-2.80138750517245E-01	1.52361392922768E+00	-3.66040830376774E+00	-1.03700066309228E+00	3.62328509423050E+01
Cx19	6.31081237861808E-01	-1.64792592096046E+00	2.36077187049122E+00	-6.20156269210225E+00	3.81300191800347E+01
Cx20	2.98161557144693E-01	-9.63814075980025E-02	-1.00229624702728E+00	-9.30036313232856E+00	5.95279963642815E+01
Cx21	-4.30195438440388E-01	1.71050590067549E+00	-3.45338061039724E+00	-1.98082800126908E+00	8.15282943791795E+01
Cx22	-2.28122208557006E+00	8.71215858510519E+00	-1.81192343483092E+01	1.11859654020747E+01	8.67444285339835E+01
Cx23	-5.15902374982399E+00	1.89307893520143E+01	-3.73767209701692E+01	2.66148715131626E+01	9.20919533681896E+01
Cx24	-3.53930834333996E+00	1.40804157645026E+01	-2.96661139983861E+01	1.89216172128105E+01	7.16099044435658E+01
Cx25	-1.05308840020773E+00	3.60781466612291E+00	-6.10036110941318E+00	1.96345105411740E+00	5.56660034693603E+01
Cx26	-6.72913744238641E-01	2.01273898068918E+00	-2.52124722366111E+00	3.01122763605960E-03	3.33949976645065E+01
Cx27	-1.25690995877442E+00	4.14298104448143E+00	-6.77684118729168E+00	5.33092614810385E+00	8.63195667427898E+00
Cx28	-3.39598394639901E+00	1.22278514955044E+01	-2.33179750272812E+01	1.80927277067188E+01	1.68091556037339E+01
Cx29	-3.64959319348921E+00	1.34995235089644E+01	-2.66546468790150E+01	2.14184115870104E+01	2.69433777265003E+01
Cx30	-8.75212519467623E-01	3.86513949105526E+00	-8.46109613484651E+00	5.63349244995099E+00	4.75879286701921E+01
Cx31	-8.22894531688934E-01	3.50129328344143E+00	-7.37806739921534E+00	1.08794454013312E+00	6.57222533336726E+01
Cx32	-2.49724073917863E+00	9.06000998673815E+00	-1.73889069121129E+01	1.22468530231397E+01	3.75746797621207E+01
Cx33	-2.11779932801955E+00	8.20683776707868E+00	-1.65131089456972E+01	1.32550337030242E+01	9.56051967698836E+00
Cx34	9.01883485970289E-01	-1.74795227264938E+00	1.34033289163079E+00	-6.90468221378888E-01	3.08601764490281E+01
Cx35	-1.02336324009725E+00	2.78463809744362E+00	-4.13178684847563E+00	1.58813546267021E+00	4.96550163656225E+01
Cx36	-5.90598574232561E-01	1.53147428819967E+00	-2.14091734773356E+00	1.43833003934831E+00	1.78401769075476E+01
Cx37	-7.27290818428125E-01	2.24686930696252E+00	-3.67503114479430E+00	3.84233745759650E+00	1.06288311473455E+01
Cx38	-8.45133801966107E-01	3.14410455508885E+00	-5.81821671490039E+00	2.81624668754650E+00	3.23097408499033E+01
Cx39	-2.62148551656150E+00	7.59320978567322E+00	-1.17604093696302E+01	5.03912848593752E+00	5.29242309110120E+01
Cx40	-6.47281046456228E+00	1.70890252329674E+01	-2.42731045820735E+01	1.38705122948608E+01	4.21233265490814E+01
Cx41	-5.96004775833770E+00	1.52378815500966E+01	-2.04848746913850E+01	6.01142183204719E+00	3.24692088396955E+01
Cx42	-2.05536795897913E+00	5.98144215489123E+00	-9.29792523462192E+00	5.70254891539100E+00	2.01388523743560E+01
Cx43	-7.09858898874785E-01	1.79354903062217E+00	-2.44750235423461E+00	1.68207756804931E+00	7.82684751092830E+00
Cx44	-1.14944136485236E+00	3.19170394449988E+00	-4.79723179692883E+00	3.05440142015571E+00	1.57319120534249E+00
Cx45	6.61875337665719E-03	-1.63405519135120E-01	4.56419941774205E-01	-4.09318870332561E-01	2.07160336683950E+00
Cx46	-1.53009584181509E+00	4.21072555006248E+00	-6.25877247695867E+00	4.20724054071509E+00	7.46090908786306E+00
Cx47	-1.45900484374474E+00	3.68298351881020E+00	-4.97021849611265E+00	2.82253460518731E+00	8.65161691023054E+00
Cx48	-1.18063674252525E+00	3.11564180509997E+00	-4.43973769300035E+00	3.29066843975674E+00	1.16530173491765E+01
Cx49	-1.28273100592904E+00	3.37109703300139E+00	-4.78784255876506E+00	3.49256769827267E+00	1.16274060537057E+01

Table I.7: Equation 3.1 Coefficients β_1 through β_9 for the SZA range 50^o-80^o.

Cx	β_1	β_2	β_3	β_4	β_5	β_6	β_7
Cx1	-6.51104076416401E-19	1.87496431895462E-16	-2.47909721330226E-14	1.99705371733207E-12	-1.09686442415836E-10	4.35584389142960E-09	-1.29394689146134E-07
Cx2	-4.75150160221520E-21	1.90680104957772E-18	-3.46739816601049E-16	3.79220750183651E-14	-2.79004575346969E-12	1.46256523853147E-10	-5.64193342327957E-09
Cx3	3.64694872818833E-22	-1.67107185516345E-19	3.51771815602492E-17	-4.50714100881997E-15	3.92555886400443E-13	-2.45839973262423E-11	1.14205157129311E-09
Cx4	1.56711467289525E-22	-7.39778355985225E-20	1.59118664161011E-17	-2.06435320034744E-15	1.80253476995834E-13	-1.11932520652017E-11	5.09326165549693E-10
Cx5	-4.02361639726682E-24	1.00313191107260E-21	4.16352018444652E-20	-5.00018064141675E-17	9.58720140339665E-15	-1.03297520262047E-12	7.41331233458469E-11
Cx6	-7.26950448686496E-24	4.03301692549786E-21	-1.01885916190416E-18	1.55214859542430E-16	-1.59191022197809E-14	1.16239911288357E-12	-6.23334254228075E-11
Cx7	4.97431039984709E-25	-6.13973807352882E-22	2.53663595867228E-19	-5.60327624539073E-17	7.81757043201794E-15	-7.46574528733522E-13	5.09763501902651E-11
Cx8	9.94229484002091E-24	-6.21919632902462E-21	1.78166944088237E-18	-3.09677675805913E-16	3.64710848057207E-14	-3.07830104311965E-12	1.92079781028480E-10
Cx9	2.34917012776363E-24	-1.64162251779440E-21	5.20333227330995E-19	-9.92416046063892E-17	1.27334571292014E-14	-1.16352006031905E-12	7.81531606562979E-11
Cx10	5.39437226466843E-23	-3.46542588321369E-20	1.01894506607319E-17	-1.81648827756593E-15	2.19246151274412E-13	-1.89487497317651E-11	1.20957021642555E-09
Cx11	8.96054973992133E-24	-5.75695097954597E-21	1.68370674026907E-18	-2.96594462838948E-16	3.50860132705968E-14	-2.94152614945639E-12	1.79718231097538E-10
Cx12	5.30409993811664E-24	-3.41586558365512E-21	1.00070235333234E-18	-1.76400402659620E-16	2.08519531818449E-14	-1.74322963131176E-12	1.05873031364707E-10
Cx13	5.13358396712481E-24	-3.33197527701394E-21	9.84661058892768E-19	-1.75287117220445E-16	2.09555294646554E-14	-1.77526688413386E-12	1.09564135635508E-10
Cx14	5.95626019314930E-24	-3.84864156755011E-21	1.13177930152461E-18	-2.00388728487324E-16	2.38119589536250E-14	-2.00344090053352E-12	1.22662214278128E-10
Cx15	8.26832814335403E-24	-5.27966502459547E-21	1.52992461047676E-18	-2.65900967062570E-16	3.08511213672295E-14	-2.51516409643767E-12	1.47504983262444E-10
Cx16	4.44589602697987E-24	-2.80171915154251E-21	7.97980725057089E-19	-1.35531075010758E-16	1.52360061142084E-14	-1.18737428143933E-12	6.50361731364348E-11
Cx17	5.06634715576856E-25	-2.93766826320561E-22	7.58436696448548E-20	-1.14368560175956E-17	1.10646586020259E-15	-7.03729066359085E-14	2.81361610768809E-12
Cx18	1.67953967707070E-23	-1.10239691517374E-20	3.31224592262473E-18	-6.03665547142065E-16	7.45521512379295E-14	-6.60155615480343E-12	4.32552399094864E-10
Cx19	2.17460910263207E-25	8.52507463049356E-23	-9.96551354980969E-20	3.26946514102039E-17	-5.96162161461614E-15	7.09479787472050E-13	-5.90829630820828E-11
Cx20	9.02091711179192E-24	-5.74017943223136E-21	1.66493863528064E-18	-2.91513220064242E-16	3.43960612438739E-14	-2.89165238183477E-12	1.78597528215747E-10
Cx21	6.46709978495496E-24	-4.11436615084280E-21	1.19097944916031E-18	-2.07558042874635E-16	2.42823704731744E-14	-2.01278397085567E-12	1.21572218238804E-10
Cx22	-4.70272803928249E-24	3.36976712807588E-21	-1.10660475439562E-18	2.20690800057977E-16	-2.98586432022315E-14	2.89976659804398E-12	-2.08597175564691E-10
Cx23	3.44665484863041E-26	1.02189173129342E-23	-1.60683851118473E-20	6.02525352898315E-18	-1.24123536569128E-15	1.66867979223748E-13	-1.57413385098701E-11
Cx24	-3.41484167976622E-25	2.54903812037772E-22	-8.74502760285147E-20	1.82958069669039E-17	-2.61146598768887E-15	2.69478186396009E-13	-2.07711257717480E-11
Cx25	-9.06288842138347E-25	7.04776127615994E-22	-2.51339799076672E-19	5.44562748920530E-17	-8.00505332332794E-15	8.44375949442783E-13	-6.59122043654810E-11
Cx26	-9.31301783597357E-25	7.25790160328905E-22	-2.59105856289159E-19	5.61280222993798E-17	-8.23781405962504E-15	8.66252928325044E-13	-6.73035182327521E-11
Cx27	-5.90502749013497E-25	4.69162744383645E-22	-1.70584970273195E-19	3.75943827498797E-17	-5.60685007266649E-15	5.98346562631931E-13	-4.71126134117526E-11
Cx28	-1.37718939739057E-24	1.00343405261386E-21	-3.35835337687003E-19	6.84154963017399E-17	-9.47572612000495E-15	9.43838814000422E-13	-6.97380090745980E-11
Cx29	-2.35116359679648E-24	1.70570299296002E-21	-5.67326317470951E-19	1.14633325074467E-16	-1.57183069430626E-14	1.54736487324408E-12	-1.12841336558740E-10
Cx30	3.95351393401107E-24	-2.55983773525179E-21	7.55130983761441E-19	-1.34316529582715E-16	1.60675916644513E-14	-1.36500632767461E-12	8.47622503045615E-11
Cx31	2.91212223425705E-24	-1.94416746988813E-21	5.93490882678670E-19	-1.09724687832296E-16	1.37172717219713E-14	-1.22618505780282E-12	8.08214525111170E-11
Cx32	2.59429705019504E-24	-1.76617524340446E-21	5.52297773370926E-19	-1.05146178660241E-16	1.36169403279906E-14	-1.26945945040317E-12	8.79242628090767E-11
Cx33	-1.22863002906085E-23	7.74683211622250E-21	-2.23715503738258E-18	3.92028432870282E-16	-4.65583126869990E-14	3.96417953941952E-12	-2.49651313024915E-10
Cx34	1.75178724450659E-22	-9.59059260811851E-20	2.40202028563875E-17	-3.64589964226832E-15	3.74525782857059E-13	-2.75398612987009E-11	1.49525957797917E-09
Cx35	1.16525482355897E-22	-6.27892876804298E-20	1.54744032515682E-17	-2.31046780347337E-15	2.33377617298542E-13	-1.68659380991731E-11	8.99487003729445E-10
Cx36	2.76890965030689E-23	-1.40146296855467E-20	3.22319053838587E-18	-4.45340828956243E-16	4.11691645701066E-14	-2.68290291862018E-12	1.26413061765269E-10
Cx37	-6.24755507593486E-23	3.35093704903888E-20	-8.23709467467072E-18	1.22879656058275E-15	-1.24166979603686E-13	8.98284532070088E-12	-4.79511111487634E-10
Cx38	3.14627419340237E-22	-1.42482814393413E-19	2.91060222339736E-17	-3.53720584995961E-15	2.83668564270137E-13	-1.57028279977798E-11	6.06569930145617E-10
Cx39	7.96250556719701E-22	-3.53143071466379E-19	7.01200945651495E-17	-8.18479204888099E-15	6.17647036266868E-13	-3.09224663469278E-11	9.83787069595946E-10
Cx40	5.74960671905989E-22	-2.69079547739827E-19	5.73081923601215E-17	-7.35153397502013E-15	6.33616736162449E-13	-3.87527885761412E-11	1.73177425015894E-09
Cx41	-2.75392978393749E-22	1.21778428724871E-19	-2.40453658852573E-17	2.77807676031439E-15	-2.05638029420182E-13	9.89291169577306E-12	-2.83628478616773E-10
Cx42	-1.52741108898012E-22	7.41251150363403E-20	-1.64700877732222E-17	2.22038467719204E-15	-2.02899976017588E-13	1.32979998446697E-11	-6.45032681300501E-10
Cx43	-5.50888070678418E-22	2.64828075103087E-19	-5.81568160165438E-17	7.72753915783890E-15	-6.93696916493128E-13	4.44901043469990E-11	-2.10234919053330E-09
Cx44	-2.32423553081621E-22	1.13113340866203E-19	-2.51570987922691E-17	3.38680684022874E-15	-3.08167510429584E-13	2.00410583315221E-11	-9.60629221228803E-10
Cx45	-1.84561121822049E-24	4.77937190877324E-21	-1.98369549081101E-18	3.99627303890563E-16	-4.93036118687137E-14	4.11250353907255E-12	-2.44070202077565E-10
Cx46	1.37270466559028E-23	-3.58940306169709E-21	1.03553033208947E-19	8.00443153000845E-17	-1.58217158086773E-14	1.57943632996980E-12	-1.01665961560773E-10
Cx47	-7.04964379069883E-23	3.48186005447464E-20	-7.80703822911619E-18	1.05069797667095E-15	-9.45454021504949E-14	5.99582371572963E-12	-2.75097945689674E-10
Cx48	3.77565334163765E-22	-1.81293233445801E-19	3.98114112596106E-17	-5.29830734634427E-15	4.77431680753758E-13	-3.08275659428150E-11	1.47243530343562E-09
Cx49	7.93065040023392E-23	-3.82401300605404E-20	8.43438435930240E-18	-1.12830682272531E-15	1.02368318352406E-13	-6.67488094953981E-12	3.23498013359086E-10

Table I.8: Equation 3.1 Coefficients β_8 through β_{14} for the SZA range 50^o-80^o.

Cx	β_8	β_9	β_{10}	β_{11}	β_{12}	β_{13}	β_{14}
Cx1	2.93251610976187E-06	-5.11814568934431E-05	6.87988688577352E-04	-7.05468742241052E-03	5.40629495202368E-02	-2.99652723094407E-01	1.14701099158153E+00
Cx2	1.63055822613881E-07	-3.55984984907857E-06	5.87510515326780E-05	-7.28419403341756E-04	6.69314263313765E-03	-4.45659370583229E-02	2.07775563626199E-01
Cx3	-4.00282752017597E-08	1.06648995821422E-06	-2.16048874825790E-05	3.30681619614187E-04	-3.77389908396688E-03	3.14198044929137E-02	-1.84352649026255E-01
Cx4	-1.72475004318977E-08	4.37167044308178E-07	-8.27913740941206E-06	1.16154426614260E-04	-1.18831971458559E-03	8.63298586306805E-03	-4.23737072134175E-02
Cx5	-3.77630936245482E-09	1.40508790466439E-07	-3.86169164431435E-06	7.83515963965445E-05	-1.16101025889539E-03	1.22912938158255E-02	-8.96061117732939E-02
Cx6	2.49671756398408E-09	-7.52604953768174E-08	1.70765864733159E-06	-2.89807450320875E-05	3.63208596782994E-04	-3.30041031855811E-03	2.13232115080966E-02
Cx7	-2.54853003475650E-09	9.43327444011676E-08	-2.58891962042275E-06	5.22897346948454E-05	-7.63648573343375E-04	7.80938160631511E-03	-5.27979027750138E-02
Cx8	-9.00990532405295E-09	3.19940683132063E-07	-8.59439375413430E-06	1.73257335951605E-04	-2.57953823426960E-03	2.76247782912603E-02	-2.04094747422390E-01
Cx9	-3.92590945944238E-09	1.48576226678045E-07	-4.23396178951251E-06	9.01336327646501E-05	-1.41044536125879E-03	1.57956491761437E-02	-1.21344378550502E-01
Cx10	-5.79863838312711E-08	2.10246297770500E-06	-5.76277000632419E-05	1.18539789272571E-03	-1.80368105740036E-02	1.98410606748440E-01	-1.52476321641844E+00
Cx11	-8.09921717598549E-09	2.69192248658679E-07	-6.51556430314708E-06	1.11409175887967E-04	-1.25883383599063E-03	7.75867107670665E-03	1.22895441413492E-04
Cx12	-4.71984223049927E-09	1.53924023584976E-07	-3.60122964218444E-06	5.76196728038697E-05	-5.53886302397216E-04	1.49779827997341E-03	3.48363808632332E-02
Cx13	-4.98457735570879E-09	1.67054795177940E-07	-4.06863189980131E-06	6.97050624713564E-05	-7.80526552365537E-04	4.54522214563453E-03	6.07256092279837E-03
Cx14	-5.52703601884141E-09	1.82990753085180E-07	-4.38299488994640E-06	7.31726660357891E-05	-7.79215410484797E-04	3.83063948167185E-03	1.78144147491262E-02
Cx15	-6.24855586778750E-09	1.88077877646940E-07	-3.81454010184355E-06	4.38182458371113E-05	-1.03156493232501E-05	-8.82141805237505E-03	1.52551418690633E-01
Cx16	-2.45802810997126E-09	5.89331313274768E-08	-5.82295158646494E-07	-1.43159243730356E-05	7.09285201560691E-04	-1.44057721645338E-02	1.72465986337900E-01
Cx17	-5.35694538904701E-11	-9.21999121506015E-10	9.73760702621401E-08	-3.24624283010687E-06	6.25247727277809E-05	-7.36136190422101E-04	4.90589164251490E-03
Cx18	-2.13372887936369E-08	7.98530639507540E-07	-2.26765769790749E-05	4.85399969149330E-04	-7.72352523967743E-03	8.93104662934428E-02	-7.25220784901475E-01
Cx19	3.56714150699915E-09	-1.58929572779452E-07	5.25840755854262E-06	-1.28874331101523E-04	2.31464137445201E-03	-2.98731170406524E-02	2.68644223082776E-01
Cx20	-8.23703908551809E-09	2.85557232318161E-07	-7.43316485614801E-06	1.44108370270011E-04	-2.04872538215514E-03	2.08417154287409E-02	-1.46304790395056E-01
Cx21	-5.41675273061622E-09	1.78056000066716E-07	-4.26486492987481E-06	7.22171630889789E-05	-8.07829279963295E-04	4.87987442981688E-03	2.04230360270750E-03
Cx22	1.13068729538037E-08	-4.65270856792200E-07	1.45319626458290E-05	-3.42035537320515E-04	5.97825797803474E-03	-7.57803615704188E-02	6.72286046091355E-01
Cx23	1.08043259727165E-09	-5.49045441174762E-08	2.07595556637077E-06	-5.80857836636249E-05	1.18355103913825E-03	-1.70556223124542E-02	1.65620762585540E-01
Cx24	1.21727734045879E-09	-5.46097867799571E-08	1.87006156109327E-06	-4.82446791980060E-05	9.13746222931662E-04	-1.21508738476197E-02	1.04868286612929E-01
Cx25	3.87063958930362E-09	-1.72124423039292E-07	5.78890150259029E-06	-1.45992737616119E-04	2.71601891648073E-03	-3.63168630655170E-02	3.35617602523791E-01
Cx26	3.92735557416498E-09	-1.73265991944345E-07	5.77346731988524E-06	-1.44152826326952E-04	2.65658471431655E-03	-3.53017646416228E-02	3.26955066812092E-01
Cx27	2.78186711537248E-09	-1.23992040325018E-07	4.16721574639686E-06	-1.04773078163042E-04	1.94136634213054E-03	-2.59065810504838E-02	2.40805862931770E-01
Cx28	3.88599100418401E-09	-1.64400425667010E-07	5.27501098368659E-06	-1.27344821298798E-04	2.27821995274319E-03	-2.95088632444370E-02	2.67597245109733E-01
Cx29	6.20030194088386E-09	-2.58593079303426E-07	8.18443533027640E-06	-1.95195516667468E-04	3.45887590430728E-03	-4.45326604586071E-02	4.03011719429850E-01
Cx30	-3.90021998698581E-09	1.33336616818810E-07	-3.36235115979689E-06	6.13968744448295E-05	-7.83886417489776E-04	6.53905694144502E-03	-3.01321930645388E-02
Cx31	-3.99308695903615E-09	1.48878009946373E-07	-4.18526707361642E-06	8.80263892026266E-05	-1.36442918653530E-03	1.52168660998455E-02	-1.17755090305924E-01
Cx32	-4.60267786347350E-09	1.83469350100078E-07	-5.56770283844259E-06	1.27706650068620E-04	-2.18195898667743E-03	2.71291346952382E-02	-2.36995493557491E-01
Cx33	1.18273349749342E-08	-4.24613235589150E-07	1.15499411083888E-05	-2.36385808267075E-04	3.58920285474591E-03	-3.95235681488670E-02	3.04960529061570E-01
Cx34	-6.09534340262942E-08	1.87870592346970E-06	-4.37567396295793E-05	7.64333927312826E-04	-9.86582912857136E-03	9.19245927139872E-02	-5.97357381650127E-01
Cx35	-3.59951087324689E-08	1.08844551794163E-06	-2.48578803982572E-05	4.25638970608007E-04	-5.38677779756210E-03	4.92798162605104E-02	-3.15668854466373E-01
Cx36	-4.34033066541607E-09	1.07723751005524E-07	-1.87694951905945E-06	2.13260996236057E-05	-1.23871066566794E-04	-2.31928748152933E-04	9.35273653458749E-03
Cx37	1.91832540950136E-08	-5.78353733156940E-07	1.31072249923808E-05	-2.21051408187107E-04	2.72473660149659E-03	-2.39009040050278E-02	1.44031930109632E-01
Cx38	-1.59245126147681E-08	2.52875525846121E-07	-1.02644542516716E-06	-5.68313866428348E-05	1.58879059457281E-03	-2.19563496014874E-02	1.85134293480171E-01
Cx39	-1.50706511734401E-08	-2.17680983608439E-07	1.91511107670705E-05	-5.53624588091041E-04	9.68910871048796E-03	-1.11894149975170E-01	8.57078939678447E-01
Cx40	-5.73586970357375E-08	1.41328359389310E-06	-2.57622202951875E-05	3.42081630782736E-04	-3.21329213787946E-03	2.02193265880973E-02	-7.54167594831222E-02
Cx41	2.31326710198579E-09	1.84669231456711E-07	-9.68258708775692E-06	2.54708404661414E-04	-4.30617661746202E-03	4.90099627503852E-02	-3.72988957709539E-01
Cx42	2.35540129907762E-08	-6.52216649373010E-07	1.36887742951190E-05	-2.16142491086276E-04	2.53036869902029E-03	-2.14778368857692E-02	1.28154948754701E-01

Cx43	7.44112940799791E-08	-1.98602271322411E-06	3.99316523093826E-05	-6.00002503414499E-04	6.63477719136129E-03	-5.27326339074460E-02	2.91422611881418E-01
Cx44	3.44979131608071E-08	-9.34234207193642E-07	1.90515806647158E-05	-2.89983131547585E-04	3.23941298419243E-03	-2.58741081390387E-02	1.42429768726867E-01
Cx45	1.05941302295969E-08	-3.40808751565512E-07	8.14801925937172E-06	-1.43839709607697E-04	1.84496297638712E-03	-1.67241647639955E-02	1.02637621520781E-01
Cx46	4.56036111849250E-09	-1.47288547539449E-07	3.46638170627430E-06	-5.93438517090554E-05	7.28802007990146E-04	-6.24412544592396E-03	3.56348449193593E-02
Cx47	9.21874621598892E-09	-2.24559646924053E-07	3.88874367365758E-06	-4.53164272270136E-05	3.03594663295734E-04	-3.06408204116480E-04	-1.36134317172727E-02
Cx48	-5.29561137719730E-08	1.44629361347903E-06	-3.00367346917417E-05	4.72029731229356E-04	-5.54896847318041E-03	4.78391103241274E-02	-2.92847634032969E-01
Cx49	-1.18910371168775E-08	3.35320767956905E-07	-7.28776104858843E-06	1.21813155925326E-04	-1.54965548026851E-03	1.46733623639778E-02	-9.92558956452748E-02

Table I.9: Equation 3.1 Coefficients β_{15} through β_{19} for the SZA range 50^o-80^o.

Cx	β_{15}	β_{16}	β_{17}	β_{18}	β_{19}
Cx1	-2.85214424080768E+00	4.23339241270116E+00	-3.28175601535287E+00	1.02543022316111E+00	9.99401106581239E+01
Cx2	-6.44468967586559E-01	1.23145383378299E+00	-1.24410501520985E+00	-3.68107215620365E-01	9.99504304539794E+01
Cx3	7.20955045877184E-01	-1.71536772996416E+00	2.26411172826267E+00	-2.70348986927948E+00	1.00136836033653E+02
Cx4	1.24794855182908E-01	-1.46654054780163E-01	-1.17924124886270E-02	-1.51628902172452E+00	9.99550107059646E+01
Cx5	4.23987404334402E-01	-1.18820896044364E+00	1.82650576478466E+00	-2.57084094581797E+00	8.91658059181360E+01
Cx6	-9.70297391660795E-02	3.05853906636672E-01	-4.53090857227484E-01	-1.18560470212099E+00	7.79225035047620E+01
Cx7	2.10636112639638E-01	-3.78080300357467E-01	3.01310949150427E-01	-3.62922284507242E+00	8.59348252799968E+01
Cx8	9.73269675547708E-01	-2.70577168034521E+00	4.27193663225557E+00	-8.79611819894550E+00	9.43930994358033E+01
Cx9	5.97628845312800E-01	-1.70290423271108E+00	2.77968498111654E+00	-6.17972802652497E+00	9.12585961456030E+01
Cx10	7.77888604213175E+00	-2.43702552131107E+01	4.15156260128766E+01	-3.28925866571444E+01	9.28378960404893E+01
Cx11	-3.94717400192226E-01	2.83921580557948E+00	-7.90040794946460E+00	3.94680131105166E+00	8.60808507301643E+01
Cx12	-4.95744274274894E-01	2.90343837100292E+00	-7.35337105113215E+00	9.09496379268228E-01	8.63010793613184E+01
Cx13	-3.11797714475486E-01	2.16085679580652E+00	-5.81195049351315E+00	6.96467950761575E-01	8.85945559241109E+01
Cx14	-4.07817342352737E-01	2.58859401353424E+00	-6.89636803806906E+00	2.97395954688713E+00	9.03553065017480E+01
Cx15	-1.31380892516917E+00	6.20667563085732E+00	-1.47709357451284E+01	1.26885135611659E+01	7.08292911124598E+01
Cx16	-1.26296128699928E+00	5.41968871824028E+00	-1.22889491143527E+01	1.22456840208484E+01	5.35859792606086E+01
Cx17	-1.21728433765279E-02	-4.59314587159565E-02	2.83215881153986E-01	-1.21558093601362E+00	4.91584852682642E+01
Cx18	3.92824405169250E+00	-1.31284065914963E+01	2.41047552498314E+01	-2.21768337291629E+01	4.43754965741874E+01
Cx19	-1.60623806622770E+00	5.92669385039241E+00	-1.17405074896216E+01	7.67265608334503E+00	5.20892005117507E+01
Cx20	6.71489074884432E-01	-1.85390718922590E+00	2.68795506928345E+00	-2.70978129939654E+00	6.71674004993942E+01
Cx21	-2.78845312716769E-01	2.00826030812247E+00	-5.39416162494373E+00	-1.46728188190031E+00	8.26994125246891E+01
Cx22	-3.95996339798237E+00	1.43066487239216E+01	-2.74824917859551E+01	1.20567957201460E+01	9.57427905692140E+01
Cx23	-1.00098234479992E+00	3.30202693301375E+00	-4.94930576628235E+00	1.94157666718052E+00	6.71414854951858E+01
Cx24	-5.00596218265433E-01	8.22095065352346E-01	1.01548995796139E-01	1.07778493700442E+01	3.46174010583113E+01
Cx25	-2.02212296950058E+00	7.30682366766044E+00	-1.45415448058364E+01	1.84912875197139E+01	2.68266708361827E+01
Cx26	-2.00958448867272E+00	7.61617285172148E+00	-1.56746429673782E+01	1.38444533817906E+01	2.22408814565744E+01
Cx27	-1.48596636580908E+00	5.65973751188158E+00	-1.16383802535132E+01	9.49952452229357E+00	2.08395488953647E+01
Cx28	-1.61912844438753E+00	6.07143267543810E+00	-1.22015654110359E+01	8.54472541616946E+00	1.87768808638551E+01
Cx29	-2.44122245397437E+00	9.17575758230783E+00	-1.87147390564707E+01	1.51388390045399E+01	3.96797353087730E+01
Cx30	2.42990550412346E-02	4.39210146889902E-01	-1.84264185608818E+00	1.90316202471678E+00	6.43949871453163E+01
Cx31	5.98328717536525E-01	-1.83188907488388E+00	2.98573036045919E+00	-2.33087275090230E+00	5.22275508903819E+01
Cx32	1.38013190438135E+00	-4.93989349413642E+00	9.54408047445878E+00	-7.81599107172068E+00	4.04388618450765E+01
Cx33	-1.56492025567354E+00	4.92835236753652E+00	-8.49387233803741E+00	7.44123642395162E+00	5.10479286750595E+01
Cx34	2.57641734755927E+00	-6.84877398959587E+00	9.65649814559911E+00	-3.23960764273494E+00	6.48366594284011E+01
Cx35	1.35474524892342E+00	-3.64816756892349E+00	5.21837378156938E+00	-2.60794056487231E-01	4.34758512915249E+01
Cx36	-5.85868820347877E-02	1.13920471594063E-01	-1.43040300934263E-01	3.23314292030919E+00	2.20214678065030E+01
Cx37	-5.73301042419372E-01	1.44524292604461E+00	-1.74140301706415E+00	-3.29063593037854E+00	2.88439306785994E+01
Cx38	-9.67447105330606E-01	2.97821218974307E+00	-4.87230001503456E+00	4.46799798363280E+00	3.55192674013255E+01
Cx39	-4.21021588972203E+00	1.23571259764726E+01	-1.95781699514000E+01	1.79507350150139E+01	4.71997267264467E+01
Cx40	9.97701993069893E-02	3.43484424075757E-01	-1.24564330359987E+00	-1.85424408036949E+00	6.17505802594285E+01
Cx41	1.82281935917594E+00	-5.29659327915854E+00	8.37065563062064E+00	-9.28486015769019E+00	4.67458407513863E+01
Cx42	-5.16349861023430E-01	1.32684198678003E+00	-1.82621324381224E+00	-7.25237337224396E-01	2.88450515134513E+01
Cx43	-1.07217482962428E+00	2.47677231119309E+00	-3.06814854596593E+00	-6.00848281582010E-01	1.78096357871568E+01
Cx44	-5.15691842961005E-01	1.16062570001801E+00	-1.29964273529730E+00	-1.46518029194435E+00	6.92160459846392E+00
Cx45	-4.00298469164902E-01	9.08919249321628E-01	-1.05048920118429E+00	4.78834247169152E-01	9.58061421085633E-01
Cx46	-1.26120558844665E-01	2.47706985506183E-01	-1.47844416901593E-01	-7.08023085269094E-01	7.00139393856773E+00
Cx47	1.19847999114358E-01	-4.47864812649495E-01	8.63034972420541E-01	-1.81005117345009E+00	1.30874766080719E+01
Cx48	1.20630366185164E+00	-3.05976338697308E+00	4.38188443838154E+00	-5.33311642500665E+00	2.13168669538738E+01
Cx49	4.46215295675014E-01	-1.18679134004512E+00	1.89317644563176E+00	-4.80294270501822E+00	2.81260465487304E+01

Appendix J. Photographs of ground and standing surfaces located in the model playground.

Table J.1: Sample ground surface images.

Ground surface	
Light coloured pavers	
Dark coloured pavers	
Concrete	

Bitumen

Blue metal paving dust

Grass

Table J.2: Sample vertical standing surface images.

Standing surface	
White fibreboard	
Light coloured brick	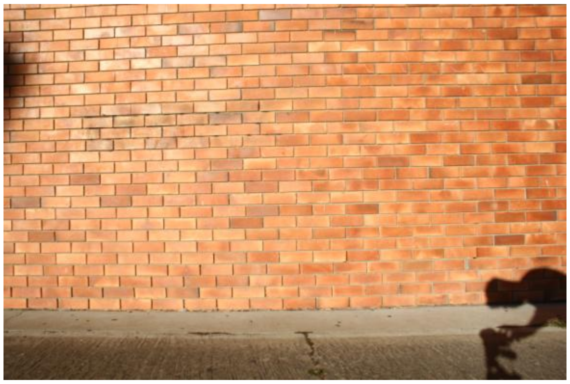
Dark coloured brick	

White painted brick

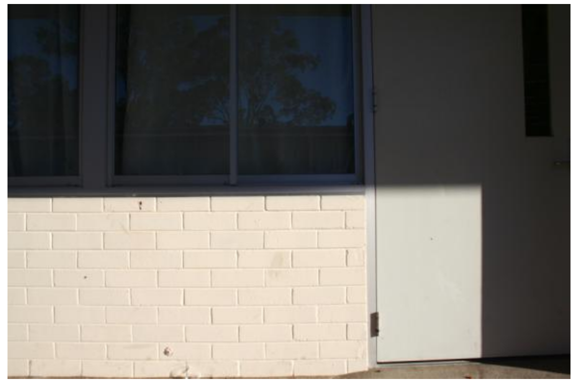

Brown painted paling

White painted paling

Glass

White painted blocks

White painted weatherboard

Yellow painted sleepers

Stone work

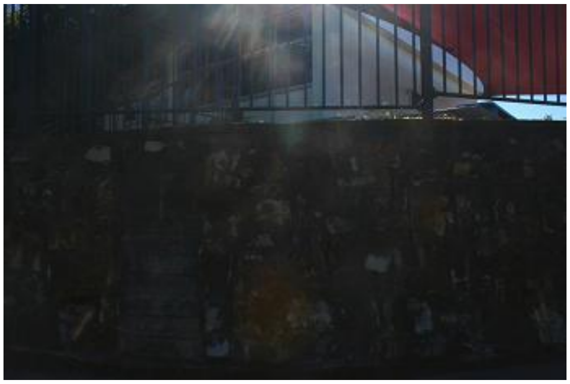

Light coloured garden block

Dark coloured garden block

Thick vegetation

Appendix K. Playground buildings

Table K.1: School buildings in the model school playground.

Building	
Administration	
E block	
M Block	

L Block

C Block

Canteen

B Block

D Block

Toilet Block

Library

G Block

Art Block

Great Hall

H Block

Manual arts workshops

Manual arts storage sheds

Oval storage shed

Pool storage

Pool toilet block

Pool Canteen

Appendix L. Playground sky view image set

L.1 Processed sky view

Table L.1: Hervey Bay State High School playground sky view site locations, sky/cloud threshold (blue-red pixel threshold), and site sky view estimate listed as a percentage. Site sky view was determined from each site location processed image up to 32.3^o in ZA and estimated by ground observation above 32.3^o in ZA. Estimates of sky view for playground sites covered by shade cloths were determined from the measured UV transmission of each playground shade cloth (Appendix E). Site locations listed in the table refer to playground locations where the sky view was surveyed (Figure L.1). Site locations were sorted into survey (traverse) lines according to position from the western fence. Each survey line was separated by 5 m when located near buildings and 20 m over the school's open playground environment. Each site location listed in each survey line starts from the northern fence and ends at the southern fence with site locations being separated by approximately 5 m and 20 m. Variations in site locations from separations of 5 m and 20 m were due to playground obstructions and are shown in Figure L.1.

Survey line 1 (5 m from western fence line)					Survey line 2 (10 m from western fence line)				
Site	sky/cld threshold	processed sky-view <ZA32.3^o (%)	estimated sky-view >ZA32.3^o (%)	site sky-view (%)	Site	Sky/cld threshold	processed sky-view <ZA32.3^o (%)	estimated sky-view >ZA32.3^o (%)	site sky-view (%)
0	0.65	37	36	73	56	0.8	45	30	75
1	0.85	25	5	30	55	0.7	40	29	69
2	0.85	34	5	39	54	0.7	37	24	61
3	0.85	49	36	85	53	0.8	44	30	74
4	0.85	54	36	90	52	0.8	49	34	83
5	0.8	52	36	88	51	0.8	52	36	88
6	0.8	49	36	85	50	0.7	49	36	85
7	0.8	46	36	82	49	0.8	49	36	85
8	0.8	44	36	80	48	0.8	39	34	73
9	0.8	40	36	76	47	0.8	26	33	59
10	0.8	43	36	79	46	0.8	26	32	58
11	0.8	41	36	77	45	0.8	25	32	57
12	0.8	40	36	76	44	0.8	25	33	58
13	0.8	35	35	70	43	0.8	24	32	56
14	0.8	30	35	65	42	0.8	11	26	37
15	0.8	14	35	49	41	0.8	11	26	37
16	0.8	19	33	52	40	0.8	14	26	40
17	0.8	19	30	49	39	0.8	16	27	43
18	0.8	12	30	42	38	0.8	12	30	42
19	0.9	10	30	40	37	0.8	28	33	61
20	0.8	19	31	50	36	0.8	32	34	66
21	0.8	25	31	56	35	0.8	33	36	69

22	0.8	27	32	59
23	0.8	23	31	54
24	0.8	26	32	58
25	0.8	39	34	73
26	0.8	46	36	82
27	0.8	50	36	86
28	0.8	51	36	87
29	0.8	52	36	88
30	0.8	51	36	87
325	0.6	24	20	44
326	0.65	32	36	68
327	0.65	16	34	50
328	0.65	10	26	36
329	0.65	18	30	48
330	0.65	16	30	46
331	0.65	10	25	35
332	0.8	25	24	49

34	0.8	32	20	52
33	0.8	39	36	75
32	0.8	44	36	80
31	0.8	43	36	79
340	0.7	32	32	64
339	0.7	39	37	76
338	0.7	34	36	70
337	0.7	33	36	69
336	0.7	33	36	69
335	0.7	31	36	67
334	0.7	28	35	63
333	0.8	28	28	56

Survey line 3 (15 m from western fence line)

site	Sky/cld threshold	processed sky-view <ZA32.3º (%)	estimated sky-view >ZA32.3º (%)	site sky-view (%)
57	0.7	41	32	73
58	0.7	37	22	59
59	0.7	44	30	74
60	0.7	47	35	82
61	0.7	48	35	83
62	0.8	50	36	86
63	0.8	49	36	85
64	0.8	41	36	77
65	0.8	25	34	59
66	0.8	16	24	40
67	0.8	29	28	57
68	0.8	28	36	64
69	0.8	24	36	60
70	0.8	28	36	64
71	0.8	20	28	48
72	0.8	31	36	67
341	0.65	30	33	63
352	0.65	33	37	70
353	0.75	11	16	27

Survey line 4 (20 m from western fence line)

Site	Sky/cld threshold	processed sky-view <ZA32.3º (%)	estimated sky-view >ZA32.3º (%)	site sky-view (%)
104x	0.8	40	27	67
105x	0.8	37	23	60
103x	0.8	43	31	74
134	0.95	50	33	83
83	0.8	46	33	79
82	0.9	51	34	85
81	0.9	50	36	86
80	0.9	42	36	78
79	0.9	20	34	54
78	0.9	30	35	65
77	0.9	21	35	56
76	0.8	30	36	66
75	0.8	27	36	63
74	0.8	27	36	63
73	0.8	22	31	53
342	0.8	33	35	68
351	0.7	36	37	73
354	0.7	9	8	17

Survey line 5 (25 m from western fence line)

Site	sky/cld threshold	processed sky-view <ZA32.3º (%)	estimated sky-view >ZA32.3º (%)	site sky-view (%)
133x	0.85	46	28	74
132x	0.85	43	26	69
111	0.8	46	27	73
110	0.8	46	29	75
109	0.8	47	32	79
108	0.75	47	36	83
107	0.75	46	36	82
106	0.75	38	36	74
93	0.75	7	0	7
92	0.75	6	0	6
91	0.75	7	0	7
90	0.75	6	11	17
89	0.75	22	36	58
88	0.8	28	36	64
87	0.8	28	36	64
85	0.9	24	35	59
86	0.8	13	0	13
84	0.9	22	21	43
344	0.8	17	18	35
343	0.8	35	35	70
345	0.8	44	36	80
346	0.8	48	36	84
347	0.8	50	36	86
348	0.8	50	36	86

Survey line 6 (30 m from western fence line)

Site	sky/cld threshold	processed sky-view <ZA32.3º (%)	estimated sky-view >ZA32.3º (%)	site sky-view (%)
142	0.8	48	35	83
141	0.8	35	35	80
140	0.8	38	34	72
139	0.8	34	35	69
138	0.8	34	36	70
137r	0.8	41	36	77
137	0.8	43	36	79
136	0.8	37	36	73
135	0.8	28	25	53
119x	0.8	17	20	37
102x	0.8	20	33	53
101x	0.8	10	4	14
100	0.8	12	3	15
99x	0.8	15	2	17
98x	0.8	15	2	17
97x	0.8	16	1	17
96x	0.8	14	1	15
95	0.8	22	36	58
96	0.8	14	0	14
94	0.8	16	11	27
362	0.8	30	26	56
361	0.8	37	33	70
360	0.8	42	36	78
359	0.8	46	36	82

349	0.8	45	36	81	358	0.7	47	36	83
350	0.75	28	31	59	357	0.7	46	36	82
355	0.75	25	34	59	356	0.7	42	36	78
Survey line 7 (35 m from western fence line)					Survey line 8 (40 m from western fence line)				
Site	Sky/cld threshold	processed sky-view <ZA32.3° (%)	estimated sky-view >ZA32.3° (%)	site sky-view (%)	Site	Sky/cld threshold	processed sky-view <ZA32.3° (%)	estimated sky-view >ZA32.3° (%)	site sky-view (%)
128x	0.75	44	36	80	129x	0.85	45	36	81
127x	0.8	41	36	77	130x	0.8	40	36	76
126x	0.8	27	27	54	131x	0.8	22	18	40
125x	0.8	29	19	48	143	0.8	23	18	41
124x	0.8	39	36	75	144	0.85	37	36	73
123x	0.8	32	36	68	145	0.85	27	35	62
122x	0.8	21	16	37	146	0.8	17	11	28
121x	0.8	4	0	4	147	0.8	5	0	5
120x	0.8	18	17	35	148	0.8	17	17	34
118x	0.8	28	36	64	149	0.8	18	34	52
117x	0.8	14	10	24	150	0.8	22	34	56
116x	0.8	16	17	33	151	0.8	30	36	66
115x	0.8	5	0	5	152	0.8	28	36	64
113x	0.8	23	35	58	153	0.8	13	16	29
114x	0.8	14	0	14	154	0.8	13	24	37
112x	0.8	14	10	24	155	0.8	8	22	30
363	0.8	20	26	46	156	0.8	9	1	10
364	0.8	28	33	61	158	0.8	24	35	59
365	0.8	31	36	67	159	0.8	13	0	13
366	0.8	34	36	70	157	0.8	12	30	42
367	0.8	37	36	73	381	0.8	34	35	69
368	0.8	38	36	74					
369	0.8	39	36	75					
Survey line 9 (45 m from western fence line)					Survey line 10 (50 m from western fence line)				
Site	Sky/cld threshold	processed sky-view <ZA32.3° (%)	estimated sky-view >ZA32.3° (%)	site sky-view (%)	Site	Sky/cld threshold	processed sky-view <ZA32.3° (%)	estimated sky-view >ZA32.3° (%)	site sky-view (%)
181	0.8	43	34	77	182	0.8	41	32	73
180	0.8	39	36	75	183	0.8	37	35	72
179	0.8	21	27	48	184	0.8	17	18	35
178	0.8	23	18	41	185	0.8	22	18	40
177	0.8	37	36	73	186	0.8	35	36	71
176	0.8	29	30	59	87	0.8	27	35	62
175	0.8	15	0	15	188	0.8	17	14	31
174	0.8	13	15	28	189	0.8	12	7	19
173	0.8	8	23	31	190	0.8	17	31	48
172	0.8	27	35	62	191	0.8	20	35	55
171	0.8	14	32	46	192	0.8	10	18	28
170	0.8	5	1	6	193	0.8	13	14	27
169	0.8	13	17	30	194	0.8	14	15	29
168	0.8	18	33	51	195	0.8	19	27	46
167	0.8	10	0	10	196	0.8	9	0	9
166	0.8	12	18	30	197	0.8	12	34	46
165	0.8	20	23	43	198	0.8	16	36	52
164	0.8	20	36	56	199	0.75	22	36	58
163	0.8	20	34	54	200	0.8	22	35	57
162	0.8	19	27	46	201	0.8	23	26	49
161	0.8	10	0	10	202	0.8	19	10	29
160	0.8	17	26	43	203	0.8	11	14	25
380	0.8	28	36	64	204	0.8	8	13	21
379	0.8	36	34	70	205	0.8	22	26	48
					206	0.8	16	20	36
					376	0.8	15	18	33
					377	0.8	41	36	77
					378	0.8	37	36	73
Survey line 11 (55 m from western fence line)					Survey line 12 (60 m from western fence line)				
Site	Sky/cld threshold	processed sky-view <ZA32.3° (%)	estimated sky-view >ZA32.3° (%)	site sky-view (%)	Site	Sky/cld threshold	processed sky-view <ZA32.3° (%)	estimated sky-view >ZA32.3° (%)	site sky-view (%)
236	0.8	37	27	64	236x	0.8	34	29	63

235	0.8	37	27	64
234	0.8	18	16	34
233	0.8	22	18	40
232	0.8	35	36	71
231	0.8	29	36	65
230	0.8	20	15	35
229	0.8	9	7	16
228	0.8	20	34	54
227	0.8	17	35	52
226	0.8	14	24	38
225	0.8	18	35	53
224	0.8	16	14	30
223	0.8	12	15	27
222	0.8	17	25	42
221	0.8	10	1	11
220	0.8	16	17	33
219	0.8	19	17	36
218	0.8	19	22	41
217	0.8	18	11	29
216	0.8	8	1	9
215	0.8	3	1	4
214	0.8	15	24	39
213	0.8	14	14	28
212	0.75	13	18	31
211	0.75	13	17	30
210	0.75	12	18	30
209	0.8	19	20	39
208	0.8	24	27	51
207	0.8	21	20	41
375	0.7	20	26	46
374	0.8	43	36	79
373	0.8	27	35	62

237x	0.8	33	29	62
238x	0.8	17	11	28
239x	0.8	25	18	43
240x	0.8	35	36	71
241x	0.8	29	35	64
242x	0.8	18	15	33
243x	0.8	11	8	19
244x	0.8	15	30	45
245x	0.8	7	1	8
246x	0.8	15	14	29
247x	0.8	24	35	59
248x	0.8	18	15	33
249x	0.8	12	16	28
250x	0.8	15	32	47
251x	0.8	9	20	29
252x	0.8	3	0	3
253x	0.8	4	0	4
254x	0.8	3	4	7
256	0.8	7	4	11
257	0.8	4	4	8
258	0.8	8	10	18
259	0.85	14	31	45
260	0.8	8	35	43
261	0.8	20	35	55
262	0.8	30	31	61
263	0.8	25	30	55
372	0.8	29	23	52
371	0.8	46	36	82
370	0.8	43	36	79

Survey line 13 (65 m from western fence line)

Site	Sky/cld threshold	processed sky-view <ZA32.3° (%)	estimated sky-view >ZA32.3° (%)	site sky-view (%)
291	0.8	30	25	55
290	0.8	34	23	57
289	0.8	16	27	43
288	0.8	18	33	51
287	0.8	24	36	60
286	0.8	31	36	67
285	0.8	36	36	72
284	0.8	25	35	60
283	0.9	7	3	10
282	0.8	16	16	32
281	0.8	14	34	48
280	0.8	10	14	24
279	0.8	17	23	40
278	0.8	24	35	59
277	0.8	19	14	33
276	0.8	11	16	27
275	0.8	13	24	37
274	0.8	11	21	32
273	0.8	3	0	3
272	0.8	1	0	1
271	0.8	5	4	9
270	0.8	5	3	8
269	0.8	5	3	8
268	0.8	2	2	4
267	0.8	6	1	7
266	0.8	16	16	32
265	0.8	30	36	66
264	0.8	29	36	65
324	0.8	21	23	44
323	0.8	45	36	81
322	0.8	49	36	85

Survey line 14 (70 m from western fence line)

Site	Sky/cld threshold	processed sky-view <ZA32.3° (%)	estimated sky-view >ZA32.3° (%)	site sky-view (%)
292	0.8	27	20	47
293	0.8	31	27	58
294	0.8	18	27	45
295	0.8	27	32	59
296	0.8	32	36	68
297	0.8	36	36	72
298	0.8	24	36	70
299	0.8	22	34	56
300	0.8	10	16	26
301	0.8	8	9	17
302	0.8	1	0	1
303	0.8	0	0	0
304	0.8	1	0	1
305	0.8	11	29	40
306	0.8	10	9	19
307	0.8	9	17	26
308	0.8	11	23	34
309	0.8	7	17	24
310	0.8	0	0	0
311	0.8	2	0	2
312	0.8	6	18	24
313	0.8	6	6	12
314	0.8	10	7	17
315	0.8	9	18	27
318	0.8	8	18	26
317	0.8	22	16	38
316	0.8	22	33	55
321	0.8	17	20	37
320	0.8	39	34	73
319	0.8	47	36	83

Survey line 15 (76 m from western fence line)

Site	sky/cld threshold	processed sky-view <ZA32.3° (%)	estimated sky-view >ZA32.3° (%)	site sky-view (%)
421	0.8	27	24	51
420	0.8	30	29	59
419	0.8	20	29	49
418	0.8	11	1	12
417	0.8	4	0	4
416	0.8	9	0	9
415	0.8	5	0	5
414	0.8	10	0	10
413	0.8	5	0	5
412	0.8	2	0	2
411	0.8	3	0	3
410	0.9	0	0	0
409	0.8	1	0	1
408	0.8	1	0	1
407	0.8	1	0	1
406	0.8	2	0	2
405	0.8	3	0	3
404	0.9	4	0	4
403	0.9	1	0	1
402	0.9	1	0	1
401	0.8	3	1	4
400	0.8	2	0	2
399	0.8	3	1	4
398	0.8	5	0	5
397	0.8	6	0	6
396	0.8	0	0	0
395	0.8	0	0	0
394	0.8	0	0	0
393	0.8	5	0	5
392	0.8	5	0	5
391	0.8	1	0	1
390	0.9	8	0	8
389	0.8	3	0	3
388	0.8	1	0	1
387	0.8	7	0	7
386	0.8	17	14	31
385	0.8	29	34	63
384	0.8	34	35	69
383	0.8	42	36	78
382	0.8	44	36	80

Survey line 16 (81 m from western fence line)

Site	sky/cld threshold	processed sky-view <ZA32.3° (%)	estimated sky-view >ZA32.3° (%)	site sky-view (%)
422	0.8	24	24	48
423	0.8	27	24	51
424	0.8	27	22	49
425	0.8	14	21	35
426	0.8	1	3	4
427	0.8	10	24	34
428	0.8	5	9	14
429	0.8	7	12	19
430	0.8	12	24	36
431	0.8	7	10	17
432	0.8	1	0	1
433	0.8	2	0	2
434	0.8	3	0	3
435	0.8	3	0	3
436	0.8	1	0	1
437	0.9	1	7	8
438	0.9	7	8	15
439	0.8	4	5	9
440	0.8	13	18	31
441	0.8	6	20	26
442	0.8	13	34	47
443	0.8	12	34	46
444	0.8	25	35	60
445	0.8	29	35	60
446	0.8	20	8	28
447	0.8	31	36	67
448	0.8	37	36	73
449	0.8	43	36	79
450	0.8	47	36	83

Survey line 17 (86 m from western fence line)

Site	Sky/cld threshold	processed sky-view <ZA32.3° (%)	estimated sky-view >ZA32.3° (%)	site sky-view (%)
482	0.8	17	22	39
481	0.8	18	22	40
480	0.8	17	20	37
479	0.9	25	24	49
478	0.9	5	9	14
477	0.8	6	7	13
476	0.8	10	23	33
475	0.8	6	0	6
474	0.8	12	18	30
473	0.8	19	34	53
472	0.8	26	36	62
471	0.85	26	35	61
470	0.85	21	32	53
469	0.8	11	7	18
468	0.8	6	0	6
467	0.8	6	0	6
466	0.8	4	0	4
465	0.8	2	0	2
464	0.8	6	11	17
463	0.8	6	11	17

Survey line 18 (91 m from western fence line)

Site	Sky/cld threshold	processed sky-view <ZA32.3° (%)	estimated sky-view >ZA32.3° (%)	site sky-view (%)
483	0.8	18	22	40
484	0.8	19	19	38
485	0.8	14	18	32
486	0.8	16	23	39
487	0.8	1	3	4
488	0.8	6	7	13
489	0.8	16	23	39
489x	0.8	16	16	32
490	0.8	17	23	40
491	0.8	23	29	52
492	0.8	30	36	66
493	0.8	30	36	66
494	0.8	24	35	59
495	0.8	24	21	45
496	0.8	16	10	26
497	0.8	17	9	26
498	0.8	15	9	24
499	0.8	6	0	6
500	0.8	6	4	10
501	0.8	8	4	12

462	0.8	4	3	7	502	0.8	8	18	26
461	0.8	8	8	16	503	0.8	11	14	25
460	0.8	9	13	22	504	0.8	13	14	27
459	0.8	5	9	14	505	0.8	5	5	10
458	0.8	11	18	29	506	0.8	6	1	7
457	0.8	19	35	54	507	0.8	13	31	44
456	0.8	7	7	14	508	0.8	6	7	13
455	0.8	29	11	40	509	0.8	21	20	41
454	0.8	34	36	70	510	0.8	27	29	56
453	0.8	16	1	17	511	0.8	14	14	28
452	0.8	34	35	69	512	0.8	33	35	68
451	0.8	46	35	81	513	0.8	47	35	82
Survey line 19 (96 m from western fence line)					Survey line 20 (101 m from western fence line)				
Site	Sky/cld threshold	processed sky-view <ZA32.3^o (%)	estimated sky-view >ZA32.3^o (%)	site sky-view (%)	Site	Sky/cld threshold	processed sky-view <ZA32.3^o (%)	estimated sky-view >ZA32.3^o (%)	site sky-view (%)
514	0.8	19	22	41	546	0.8	25	26	51
515	0.8	21	18	39	547	0.8	19	21	40
516	0.8	19	19	38	548	0.8	20	25	45
517	0.8	13	21	34	549	0.8	14	23	37
518	0.8	4	10	14	550	0.8	3	2	5
519	0.8	11	13	24	551	0.8	14	18	32
520	0.8	22	29	51	552	0.8	27	36	63
521	0.8	23	28	51	553	0.9	32	35	67
523	0.8	18	20	38	554	0.8	27	33	60
524	0.8	20	20	40	555	0.8	30	22	52
525	0.8	23	16	39	556	0.8	34	27	61
526	0.8	26	17	43	557	0.8	36	33	69
527	0.8	31	35	66	558	0.8	39	35	74
528	0.8	28	31	59	559	0.8	34	26	60
529	0.8	22	30	52	560	0.9	40	36	76
530	0.8	23	33	56	561	0.8	39	36	75
531	0.8	19	33	52	562	0.8	41	35	76
532	0.8	18	32	50	563	0.8	40	35	75
533	0.8	26	35	61	564	0.8	36	36	72
534	0.8	24	31	55	565	0.8	16	24	40
535	0.8	12	29	41	566	0.8	30	27	57
536	0.8	6	6	12	567	0.8	25	32	57
537	0.8	6	29	35	568	0.8	20	23	43
538	0.8	18	24	42	569	0.8	5	8	13
539	0.8	23	23	46	570	0.8	42	36	78
540	0.8	10	9	19	571	0.8	44	36	80
541	0.8	26	19	45	572	0.8	24	16	40
542	0.8	37	36	73	573	0.8	34	35	69
543	0.8	20	17	37	574	0.9	43	32	75
544	0.8	34	35	69					
545	0.8	48	30	78					
Survey line 21 (106 m from western fence line)					Survey line 22 (111 m from western fence line)				
Site	Sky/cld threshold	processed sky-view <ZA32.3^o (%)	estimated sky-view >ZA32.3^o (%)	site sky-view (%)	Site	Sky/cld threshold	processed sky-view <ZA32.3^o (%)	estimated sky-view >ZA32.3^o (%)	site sky-view (%)
603	0.8	25	27	52	604	0.8	21	17	38
602	0.8	8	14	22	605	0.8	4	1	5
601	0.8	11	16	27	606	0.8	6	18	24
600	0.8	8	18	26	607	0.8	3	0	3
599	0.8	3	5	8	608	0.8	16	16	32
598	0.8	17	18	35	609	0.8	31	35	66
597	0.8	30	36	66	610	0.8	36	35	71
596	0.8	32	34	66	611	0.8	38	27	65
595	0.8	32	30	62	612	0.8	39	27	66
594	0.8	35	29	64	613	0.8	42	35	77
593	0.8	38	34	72	614	0.8	45	36	81
592	0.8	42	36	78	615	0.8	48	36	84
591	0.8	45	36	81	616	0.8	49	36	85
590	0.8	46	36	82	617	0.8	51	36	87
589	0.8	47	36	83	618	0.8	51	36	87
588	0.8	48	36	84	619	0.8	50	36	86
587	0.8	46	36	82	620	0.8	50	36	86

586	0.8	46	36	82
585	0.8	46	36	82
584	0.8	26	17	43
583	0.8	33	27	60
582	0.8	34	35	69
581	0.8	24	35	59
580	0.8	36	36	72
579	0.8	43	36	79
578	0.8	43	36	79
577	0.8	26	17	43
576	0.8	34	36	70
575	0.8	47	35	82

621	0.8	50	36	86
622	0.8	47	36	83
623	0.8	39	36	75
624	0.8	36	36	72
625	0.8	37	35	72
626	0.8	34	35	69
627	0.8	32	6	38
628	0.8	30	6	36
629	0.8	29	6	35
630	0.8	25	6	31
631	0.8	25	6	31
632	0.8	24	6	30
633	0.8	24	6	30
634	0.8	28	6	34
635	0.8	33	6	39
636	0.8	38	6	44
637	0.8	38	36	74
638	0.8	36	20	56
639	0.8	26	14	40
640	0.8	33	18	51
641	0.8	45	36	81
642	0.8	49	36	85

Survey line 23 (116 m from western fence line)

Site	Sky/cld threshold	processed sky-view <ZA32.3° (%)	estimated sky-view >ZA32.3° (%)	site sky-view (%)
662	0.8	29	18	47
661	0.8	4	3	7
660	0.8	33	36	69
659	0.8	33	36	69
658	0.8	32	35	67
657	0.8	34	21	55
656	0.9	38	35	73
655	0.9	47	36	83
654	0.9	51	36	87
653	0.9	48	36	84
652	0.9	46	36	82
651	0.9	46	36	82
650	0.9	48	36	84
649	0.9	48	36	84
648	0.9	47	36	83
647	0.9	48	36	84
646	0.9	48	36	84
645	0.9	49	36	85
643	0.9	54	36	90

Survey line 24 (121 m from western fence line)

Site	sky/cld threshold	processed sky-view <ZA32.3° (%)	estimated sky-view >ZA32.3° (%)	site sky-view (%)
663	0.8	29	18	47
664	0.8	21	12	33
665	0.8	39	36	75
666	0.8	43	36	79
667	0.8	44	35	79
668	0.8	44	30	74

Survey line 25 (126 m from western fence line)

Site	Sky/cld threshold	processed sky-view <ZA32.3° (%)	estimated sky-view >ZA32.3° (%)	site sky-view (%)
674	0.8	30	18	48
673	0.8	21	13	34
672	0.8	40	36	76
671	0.8	47	36	83
670	0.8	48	36	84
669	0.8	48	36	84

Survey line 26 (131 m from western fence line)

Site	sky/cld threshold	processed sky-view <ZA32.3° (%)	estimated sky-view >ZA32.3° (%)	site sky-view (%)
675	0.8	30	18	48
676	0.8	18	13	31
677	0.8	38	35	73
678	0.8	49	36	85
679	0.8	50	36	86
680	0.8	50	36	86

Survey line 27 (136 m from western fence line)

Site	sky/cld threshold	processed sky-view <ZA32.3° (%)	estimated sky-view >ZA32.3° (%)	site sky-view (%)
681	0.8	25	14	39
682	0.8	17	14	31
683	0.8	38	36	74
684	0.8	50	36	86
685	0.8	52	36	88
686	0.8	52	36	88
687	0.8	56	36	92
688	0.8	57	36	93

Survey line 28 (141 m from western fence line)

Site	sky/cld threshold	processed sky-view <ZA32.3° (%)	estimated sky-view >ZA32.3° (%)	site sky-view (%)
696	0.8	36	23	59
697	0.8	14	10	24
698	0.8	22	10	32
699	0.8	40	34	74
700	0.8	42	36	78
701	0.8	52	36	88
702	0.8	54	36	90
703	0.8	54	36	90

689	0.8	58	36	94
690	0.8	58	36	94
691	08.	58	36	94
692	0.8	58	36	94
693	0.8	57	36	93
694	0.8	53	36	89
695	08	45	35	80

Survey line 29 (146 m from western fence line)

Site	Sky/cld threshold	processed sky-view <ZA32.3^{o} (%)	estimated sky-view >ZA32.3^{o} (%)	site sky-view (%)
704	0.8	44	36	80
705	0.8	33	19	52
706	0.8	37	26	63
707	0.8	45	36	81
708	0.8	52	36	88
709	0.8	53	36	89
710	0.8	55	36	91
711	0.8	55	36	91

Survey line 30 (151 m from western fence line)

Site	sky/cld threshold	processed sky-view <ZA32.3^{o} (%)	estimated sky-view >ZA32.3^{o} (%)	site sky-view (%)
712	0.8	54	36	90
713	0.8	52	36	88
714	0.8	53	36	89
715	0.8	55	36	91
176	0.8	56	36	92
717	0.8	55	36	91
718	0.8	56	36	92
719	0.8	56	36	92

Survey line 31 (156 m from western fence line)

Site	sky/cld threshold	processed sky-view <ZA32.3^{o} (%)	estimated sky-view >ZA32.3^{o} (%)	site sky-view (%)
720	0.8	58	36	94
721	0.8	58	36	94
722	0.8	57	36	93
723	0.8	58	36	94
724	0.8	58	36	94
725	0.8	57	36	93
726	0.8	58	36	94
727	0.8	57	36	93
728	0.8	58	36	94
729	0.8	58	36	94
730	0.8	58	36	94
731	0.8	59	36	95
732	0.8	58	36	94
733	0.8	58	36	94
734	0.8	57	36	93
735	0.8	54	36	90
736	0.8	37	26	63

Survey line 32 (176 m from western fence line)

Site	sky/cld threshold	processed sky-view <ZA32.3^{o} (%)	estimated sky-view >ZA32.3^{o} (%)	site sky-view (%)
737	0.9	56	36	92
738	0.9	58	36	94
739	0.9	56	36	92
740	0.9	55	36	91
741	0.9	54	36	90
742	0.9	55	36	91
743	0.9	55	36	91
744	0.9	55	36	91
745	0.9	54	36	90
746	0.9	58	36	94
747	0.8	55	36	91
748	0.8	52	36	88

Survey line 33 (196 m from western fence line)

Site	sky/cld threshold	processed sky-view <ZA32.3^{o} (%)	estimated sky-view >ZA32.3^{o} (%)	site sky-view (%)
749	0.8	61	36	97
750	0.8	60	36	96
751	0.8	56	36	92
752	0.8	28	16	44
752x	0.8	36	35	71
753	0.8	34	34	68
754	0.8	40	34	74
755	0.8	49	36	85
756	0.8	47	33	80
757	0.8	50	34	84
758	0.8	52	36	88
759	0.8	53	36	89

Survey line 34 (216 m from western fence line)

Site	Sky/cld threshold	processed sky-view <ZA32.3^{o} (%)	estimated sky-view >ZA32.3^{o} (%)	site sky-view (%)
771	0.8	58	36	94
770	0.8	59	36	95
769	0.8	58	36	94
768	0.8	53	36	89
767	0.8	50	36	86
766	0.8	48	36	84
765	0.8	49	36	85
764	0.8	53	36	89
763	0.8	50	35	85
762	0.8	51	36	87
761	0.8	53	36	89
760	0.8	54	36	90

Survey line 35 (236 m from western fence line)

Site	sky/cld threshold	processed sky-view <ZA32.3^{o} (%)	estimated sky-view >ZA32.3^{o} (%)	site sky-view (%)
772	0.8	59	36	95
773	0.38	60	36	96
774	0.9	60	36	96
775	0.9	60	36	96
776	0.9	59	36	95
777	0.9	58	36	94

Survey line 36 (256 m from western fence line)

Site	Sky/cld threshold	processed sky-view <ZA32.3^{o} (%)	estimated sky-view >ZA32.3^{o} (%)	site sky-view (%)
795	0.9	59	36	95
794	0.9	60	36	96
793	0.9	61	36	97
792	0.9	60	36	96
791	0.9	60	36	96
790	0.9	60	36	96

778	0.8	58	36	94	789	0.9	60	36	96
779	0.8	58	36	94	788	0.9	60	36	96
780	0.9	59	36	95	787	0.9	60	36	96
781	0.9	59	36	95	786	0.9	60	36	96
782	0.9	59	36	95	785	0.9	60	36	96
783	0.9	58	36	94	784	0.9	60	36	96
Survey line 37 (276 m from western fence line)					Survey line 38 (296 m from western fence line)				
Site	Sky/cld threshold	processed sky-view <ZA32.3º (%)	estimated sky-view >ZA32.3º (%)	site sky-view (%)	Site	sky/cld threshold	processed sky-view <ZA32.3º (%)	estimated sky-view >ZA32.3º (%)	site sky-view (%)
796	0.9	59	36	95	819	0.9	54	36	90
797	0.9	60	36	96	818	0.9	59	36	95
798	0.9	60	36	96	817	0.9	59	36	95
799	0.9	61	36	97	816	0.9	60	36	96
800	0.9	60	36	96	815	0.9	58	36	94
801	0.9	59	36	95	814	0.9	40	30	70
802	0.9	59	36	95	813	0.9	51	35	86
803	0.9	58	36	94	812	0.9	49	35	84
804	0.9	57	36	93	811	0.9	31	25	56
805	0.9	57	36	93	810	0.9	34	25	59
806	0.9	58	36	94	809	0.9	47	36	83
807	0.9	59	36	95	808	0.9	57	36	93

L.2 Playground sky view site locations

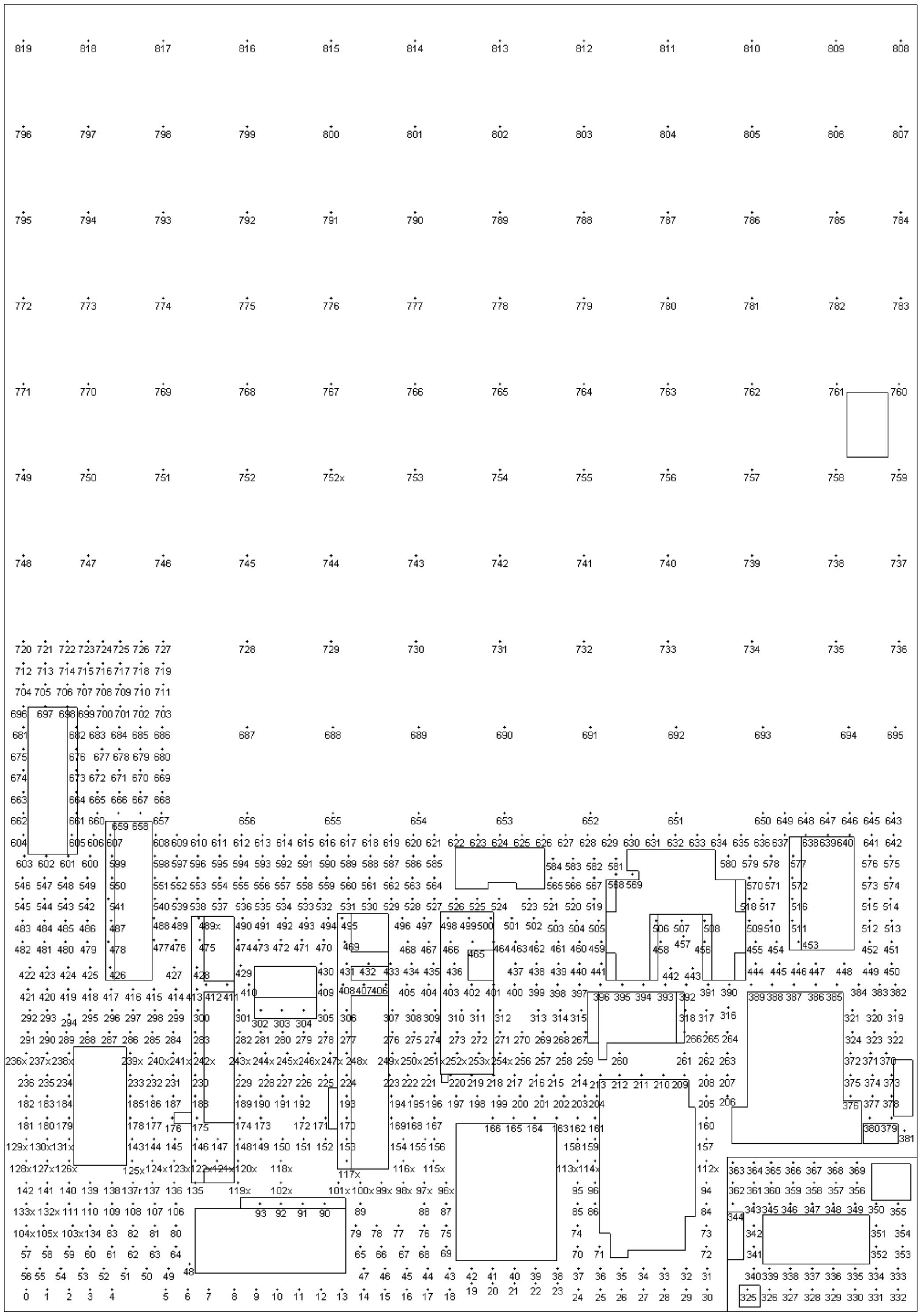

Figure L.1: Hervey Bay State High School identifier codes for sky view survey sites.

L.3 Sky view survey images

Table L.2: Unprocessed images (upper part) and processed sky view (lower part) listed according to site identifier codes (Figure L.1). Processed images include the horizon mask (black).

Survey line 1 (5 m from western fence line)

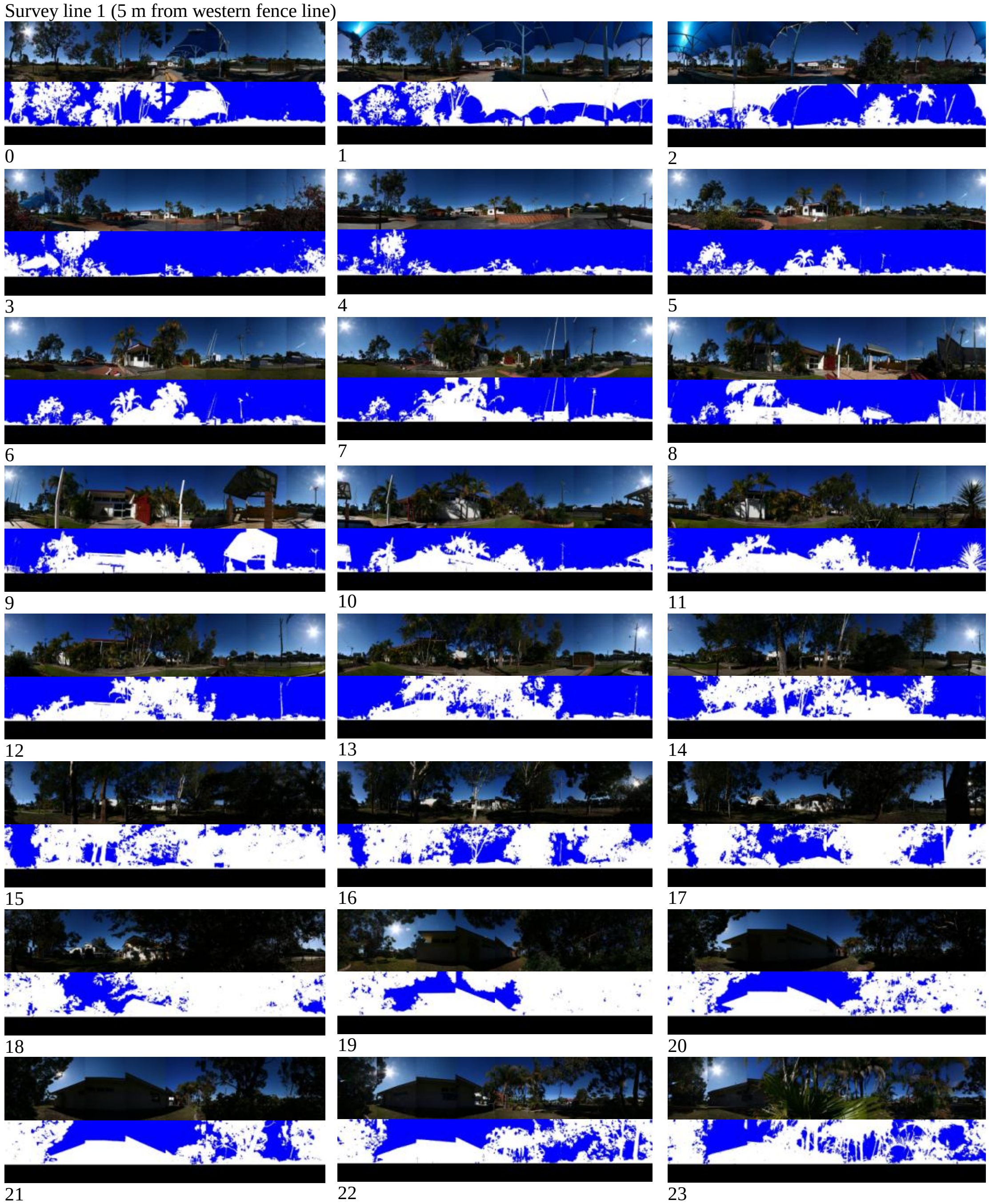


24
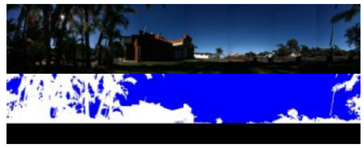
25

26
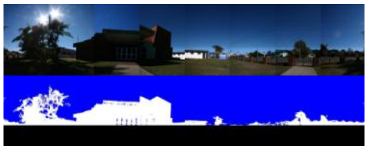
27
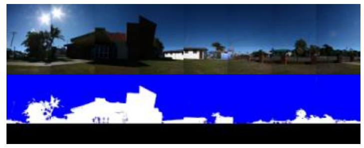
28
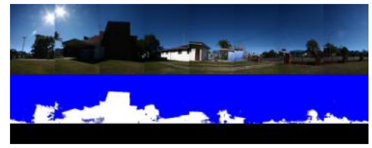
29
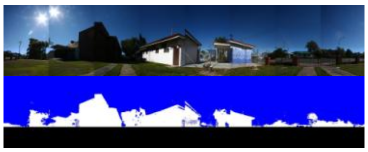
30

325

326
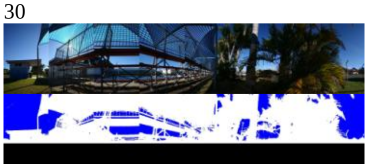
327
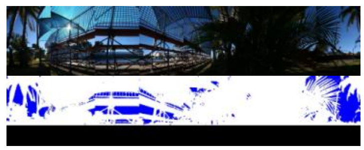
328

329
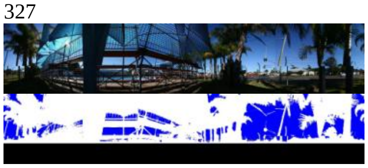
330

331

332

Survey line 2 (10 m from western fence line)

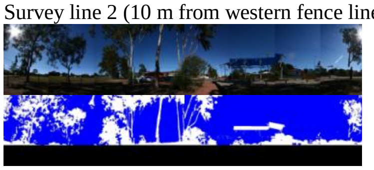
56
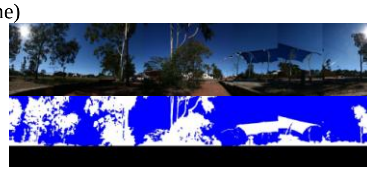
55
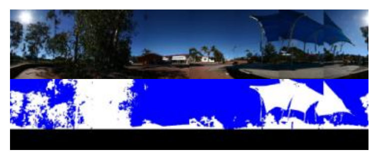
54
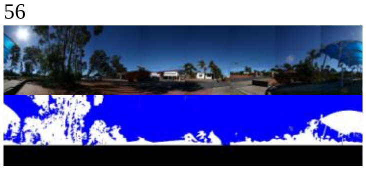
53
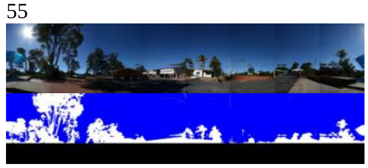
52

51

50

49

48

47
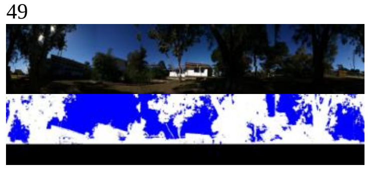
46

45

44

43
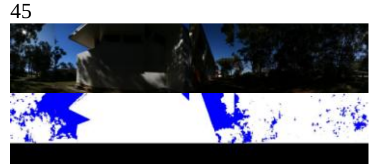
42

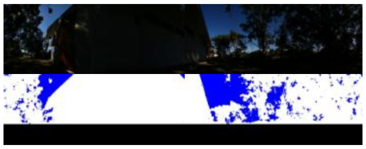
41

40

39

38

37

36
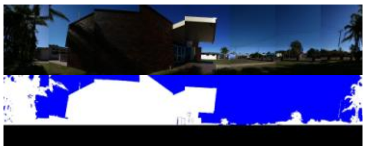
35

34
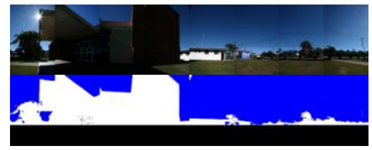
33
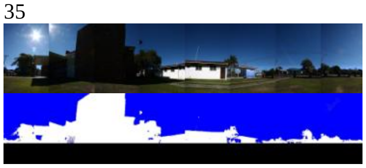
32
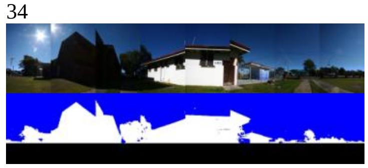
31
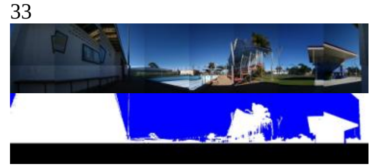
340
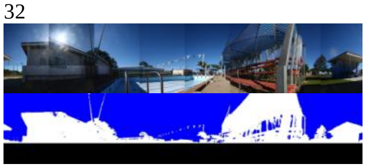
339

338

337
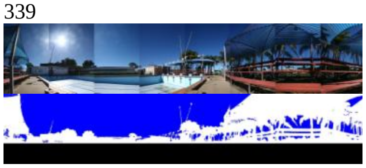
336

335

334

333

Survey line 3 (15 m from western fence line)

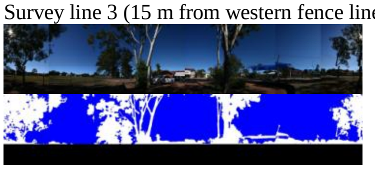
57

58

59

60
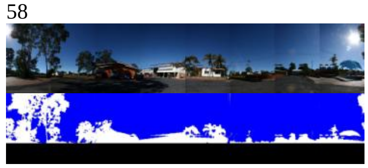
61

62

63

64

65

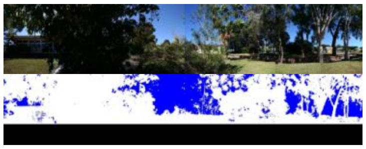
66

67
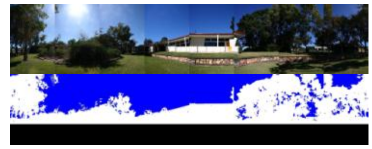
68

69

70

71
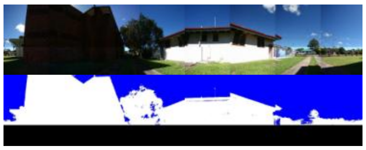
72
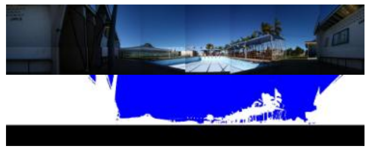
341

352

353

Survey line 4 (20 m from western fence line)

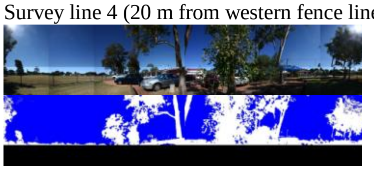
104x

105x

103x

134

83

82

81

80

79

78

77
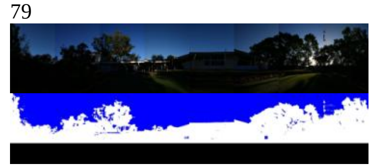
76

75
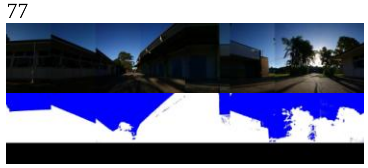
74
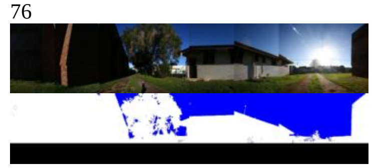
73
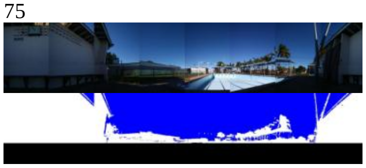
342
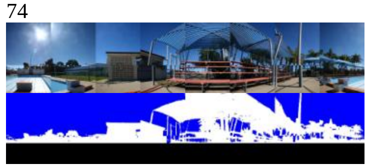
351

354

Survey line 5 (25 m from western fence line)

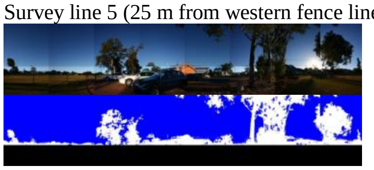
133x


132x

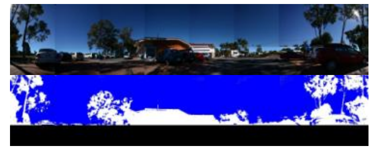
111


110


109


108


107


106


93

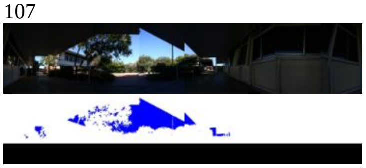
92

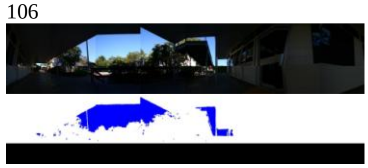
91

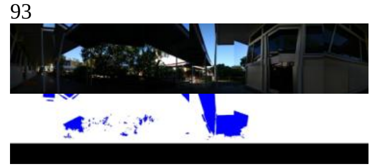
90


89


88


87


85

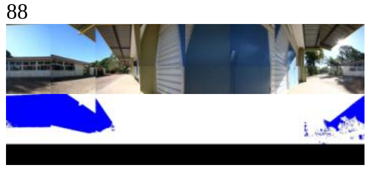
86


84

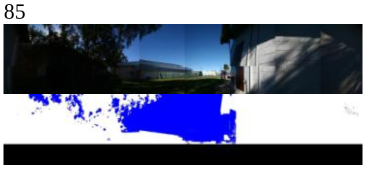
344

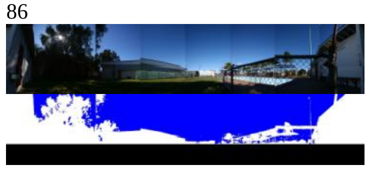
343


345

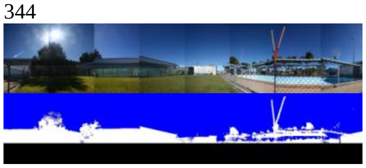
346


347

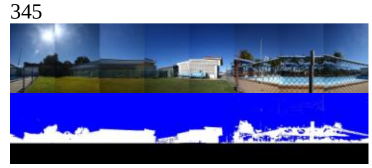
348


349


350


355

Survey line 6 (30 m from western fence line)

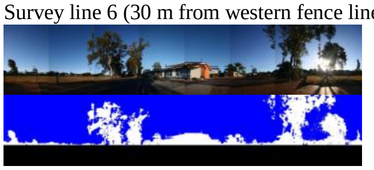
142

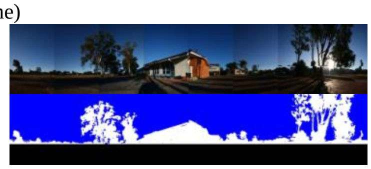
141


140


139

138

137r

137
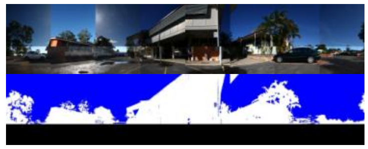
136

135

119x

102x

101x

100x

99x

98x

97x

96x

95
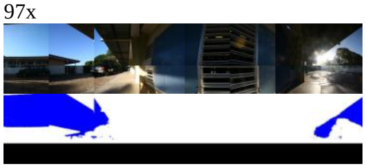
96

94
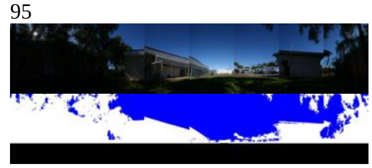
362
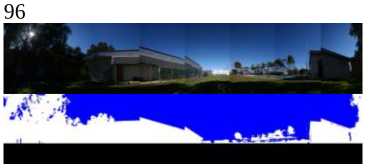
361

360

359

358

357

356

Survey line 7 (35 m from western fence line)

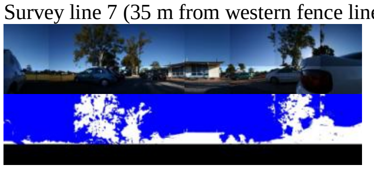
128x
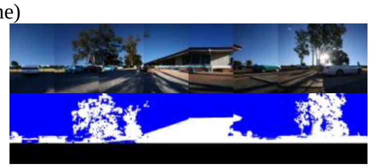
127x

126x
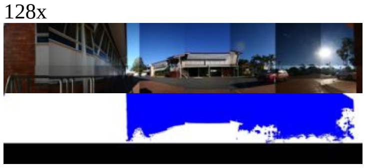
125x

124x

123x


122x

121x

120x
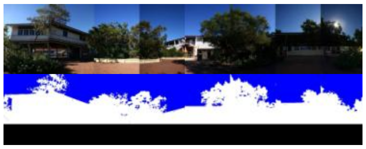
118x

117x

116x

115x

113x
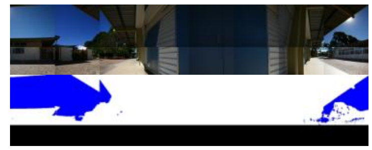
114x

112x

363

364
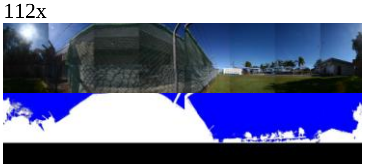
365
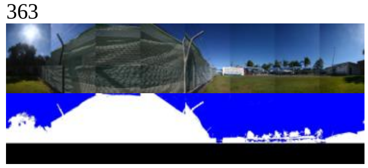
366
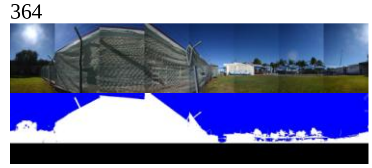
367

368

369

Survey line 8 (40 m from western fence line)

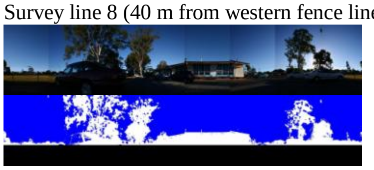
129x

130x

131x
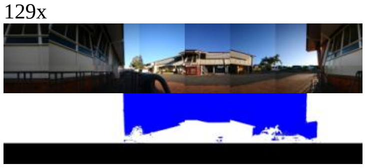
143

144

145

146
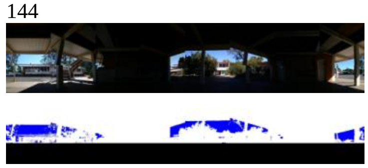
147
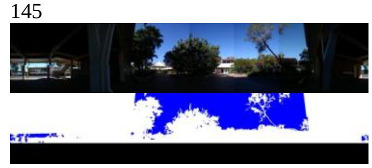
148
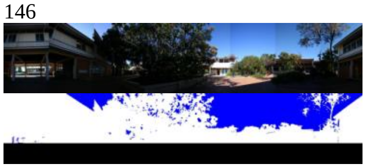
149

150

151


152
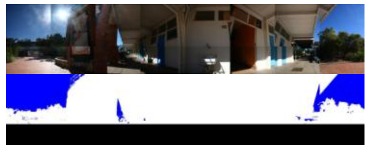
153
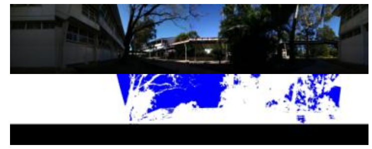
154

155
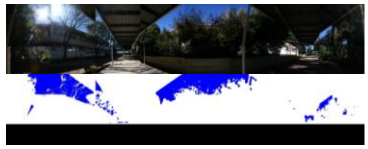
156

158
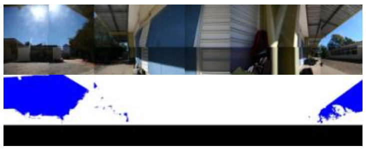
159
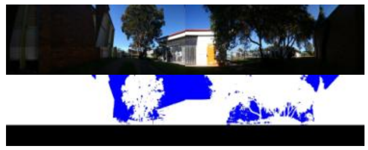
157

381

Survey line 9 (45 m from western fence line)

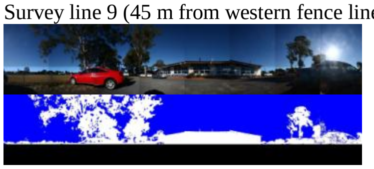
181

180

179

178

177

176

175

174
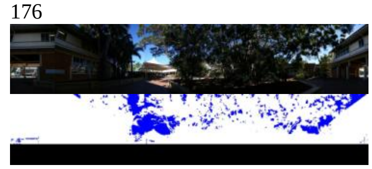
173

172

171

170
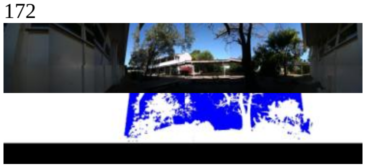
169

168
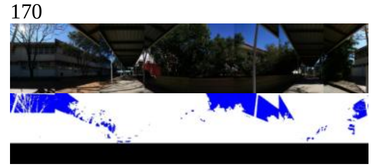
167

166

165
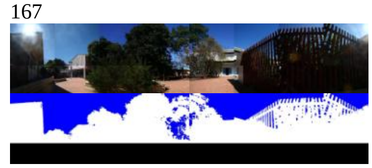
164

163

162

161

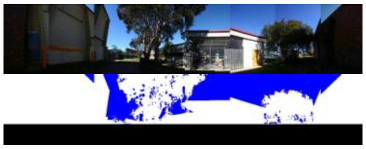
160
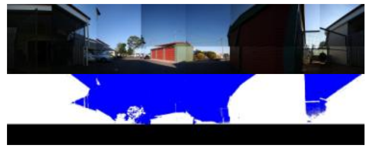
380
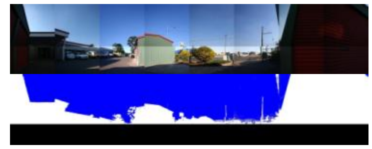
379

Survey line 10 (50 m from western fence line)

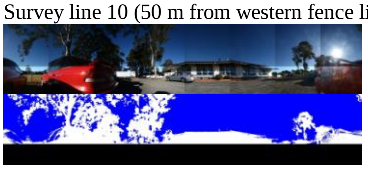
182

183

184

185

186

187

188

189

190
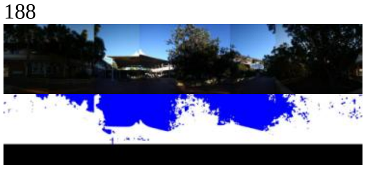
191

192

193

194
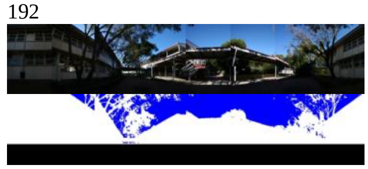
195

196

197

198

199

200

201
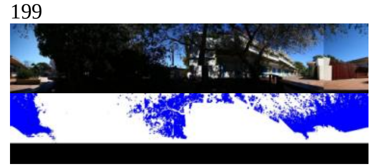
202
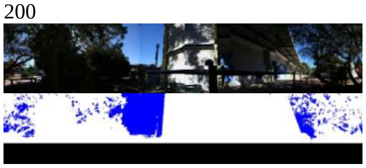
203
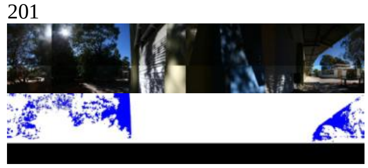
204

205
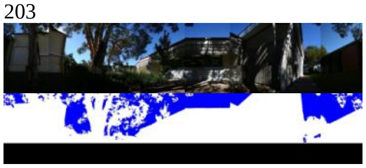
206

376

377

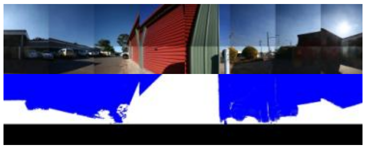
378

Survey line 11 (55 m from western fence line)

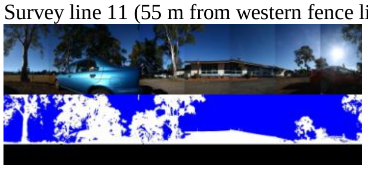
236


235


234


233


232


231


230


229


228


227


226


225


224

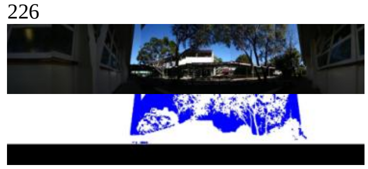
223


222

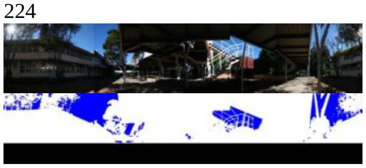
221


220


219


218


217

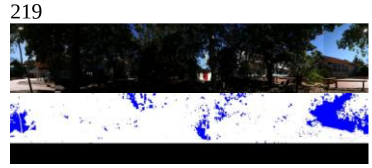
216


215

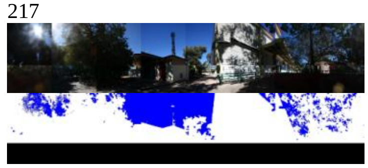
214


213


212


211


210

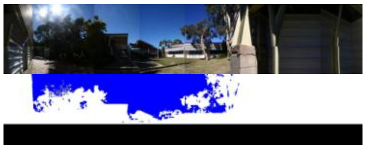
209

208

207

375

374

373

Survey line 12 (60 m from western fence line)

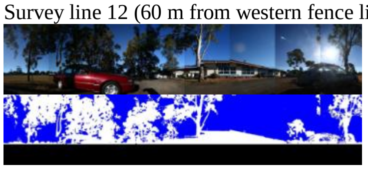
236x

237x

238x

239x

240x

241x

242x

243x

244x

245x

246x

247x

248x
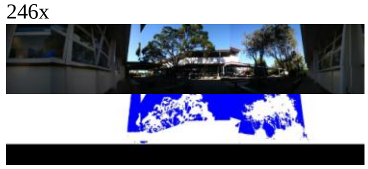
249x

250x

251x

252x
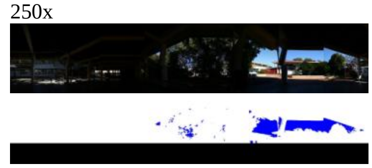
253x

254x
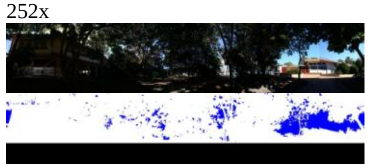
256

257

258

259

260


261
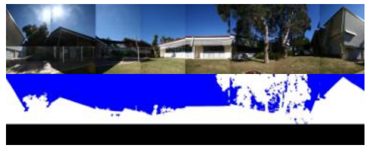
262

263

272

371
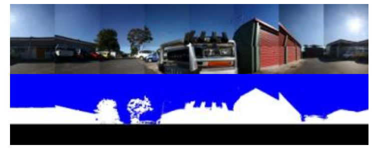
370

Survey line 13 (65 m from western fence line)

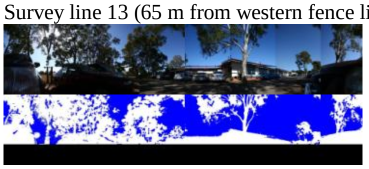
291

290

289
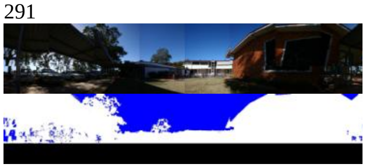
288
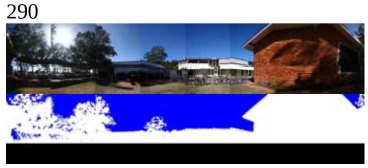
287

286

285

284

283

282

281

280

279

278

277

276

275

274
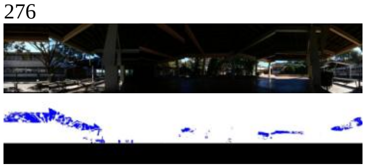
273
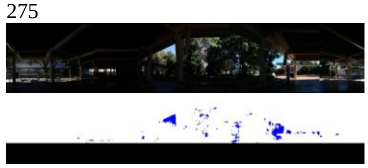
272
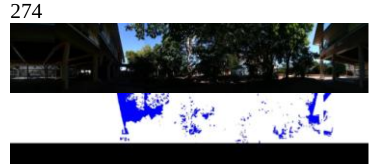
271
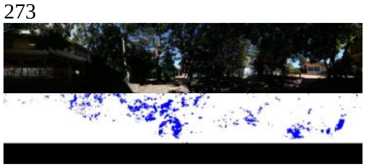
270
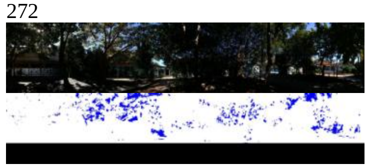
269

268


267

266

265

264

324

323

322

Survey line 14 (70 m from western fence line)

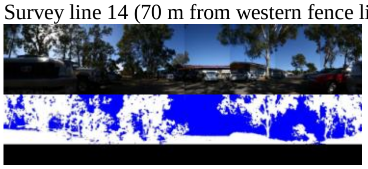
292

293

294
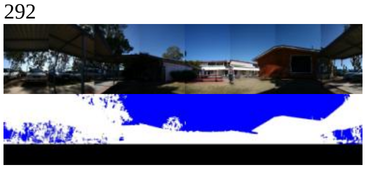
295

296

297

298

299

300

301

302

303

304

305
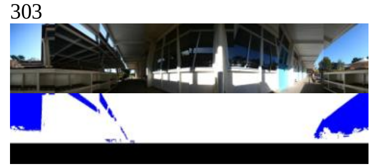
306

307

308
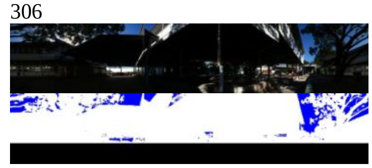
309

310
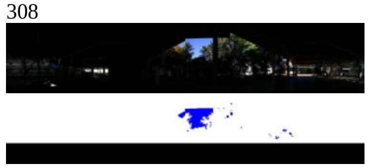
311
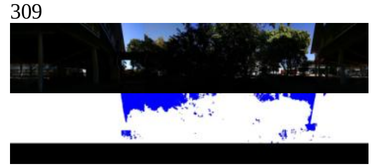
312

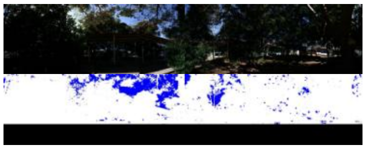
313
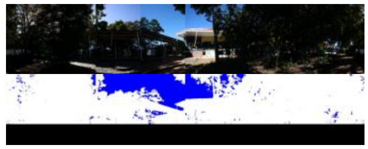
314

315

318

317

316

321

320

319

Survey line 15 (76 m from western fence line)

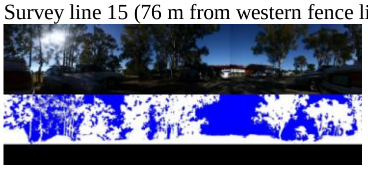
421

420

419

418

417

416

415

414
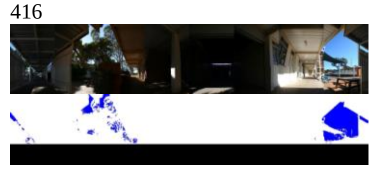
413
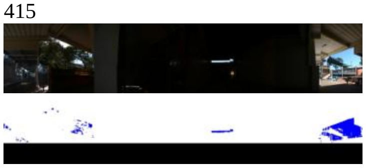
412

411
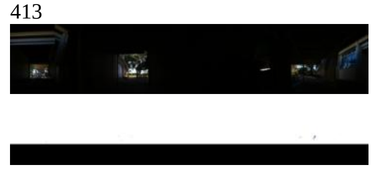
410

409

408
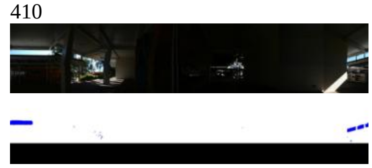
407

406

405

404
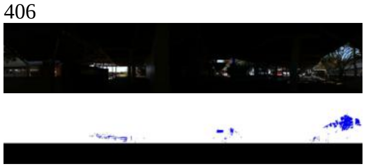
403

402
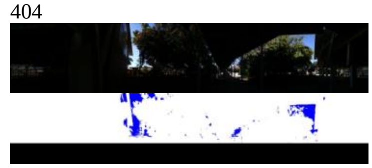
401

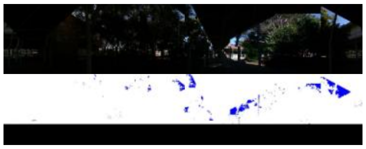
400
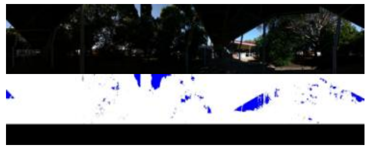
399

398

397

396

395

394

393

392

391

390

389

388

387

386
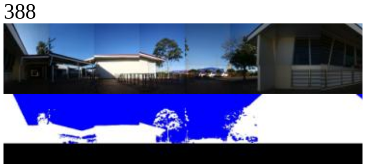
385

384

383

382

Survey line 16 (81 m from western fence line)

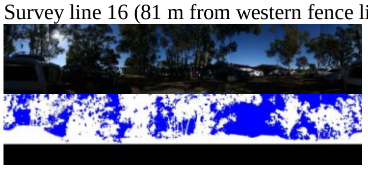
422
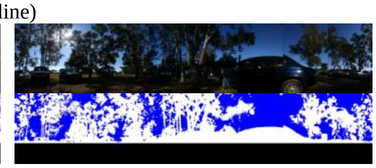
423

424
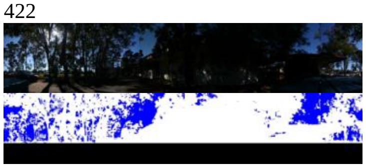
425

426

427

428
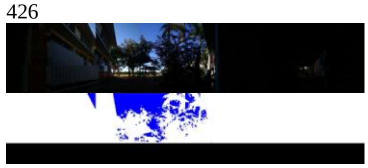
429

430


431
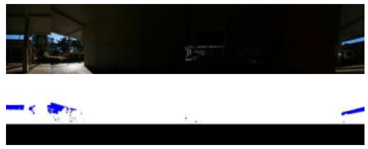
432

433

434

435
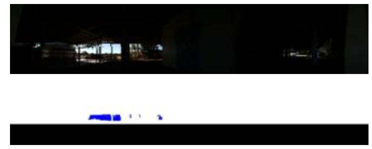
436
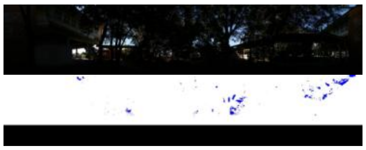
437
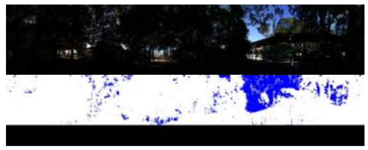
438
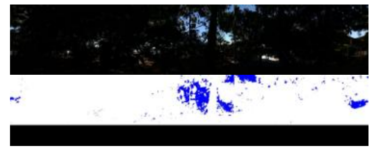
439

440
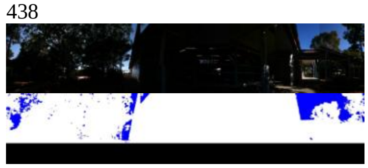
441

442

443

444

445

446

447

448
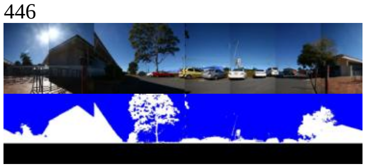
449

450

Survey line 17 (86 m from western fence line)

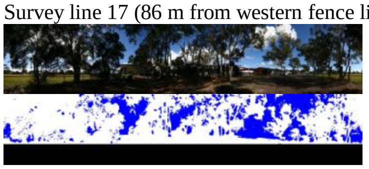
482
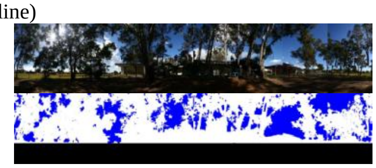
481
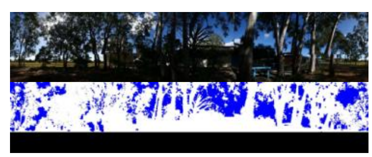
480

479

478

477

476

475

474


473


472


471


470


469


468


467


466


465

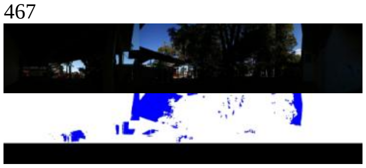
464


463

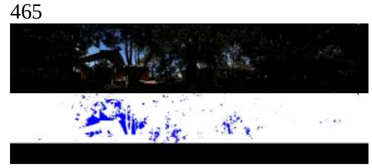
462

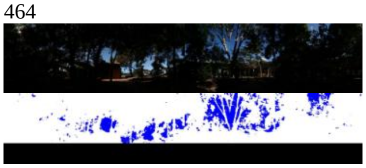
461


460


459


458


457


456


455

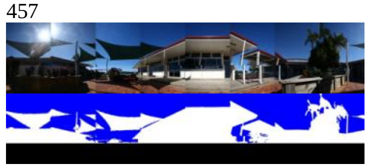
454

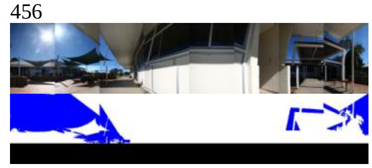
453

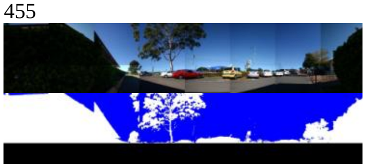
452


451

Survey line 18 (91 m from western fence line)

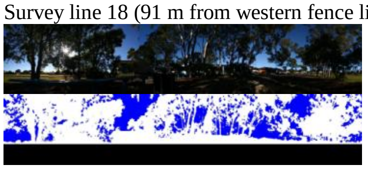
483


484

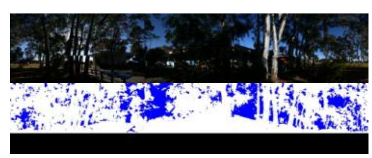
485


486


487

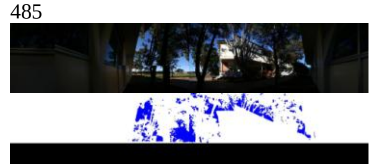
488


489

489x

490

491

492

493

494
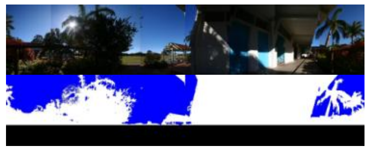
495

496

497

498

499

500

501

502
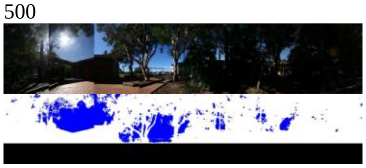
503

504

505
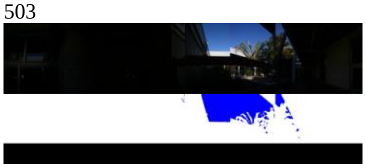
506

507

508
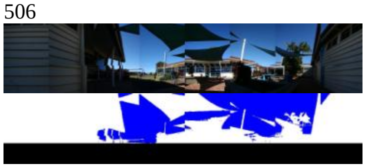
509

510

511

512

513

Survey line 19 (96 m from western fence line)

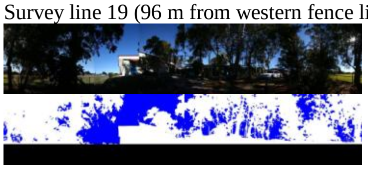
545

544
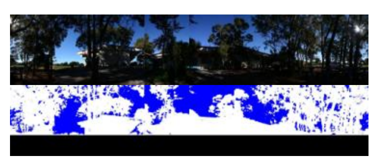
543

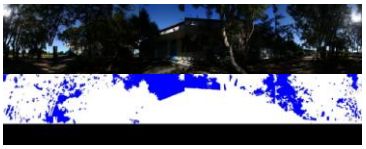
542
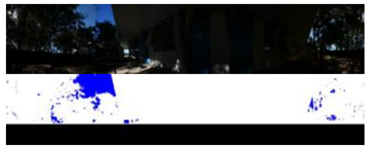
541
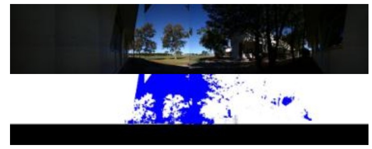
540
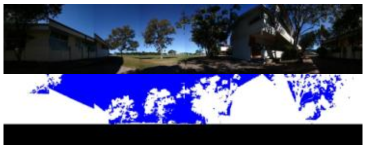
539
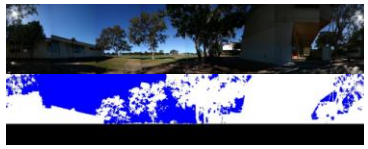
538
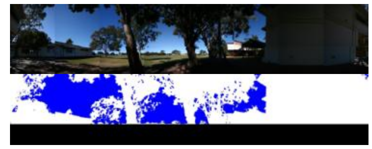
537

536

535

534

533

532

531

530

529

528

527

526

525

524

523

521
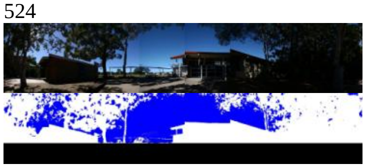
520

519

518

517

516
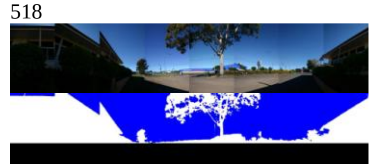
515
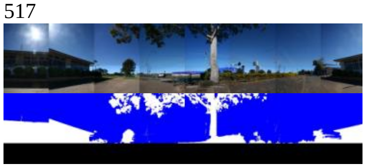
514

Survey line 20 (101 m from western fence line)

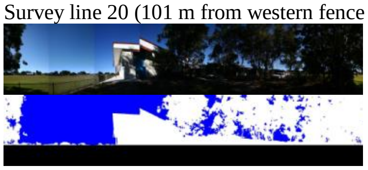
546
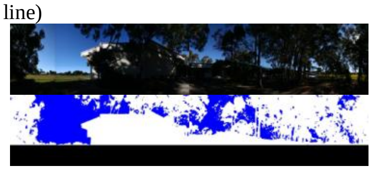
547

548

549
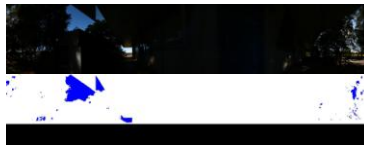
550

551
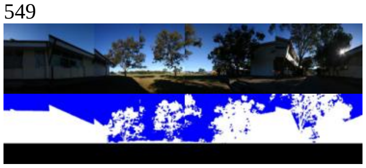
552
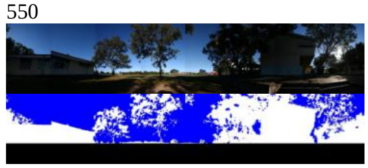
553
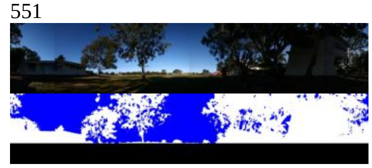
554
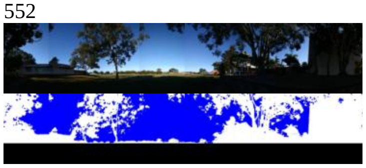
555
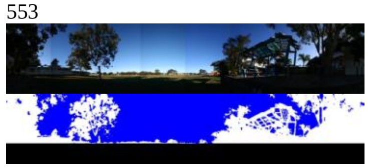
556

557

558
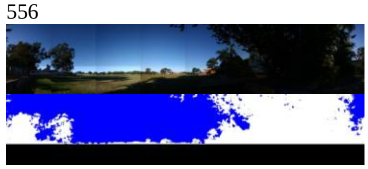
559

560

561

562

563
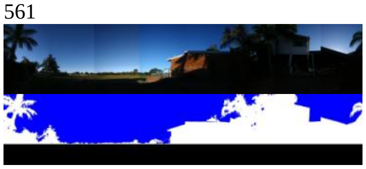
564

565
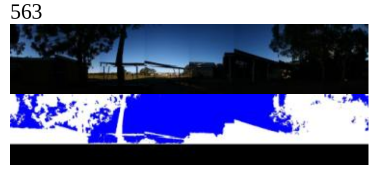
566
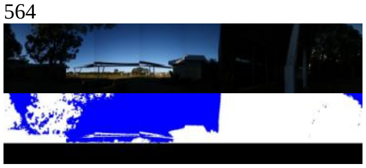
567

568

569

570

571

572

573
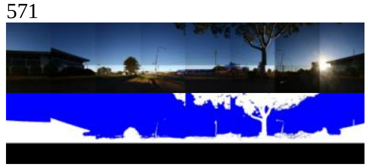
574

Survey line 21 (106 m from western fence line)

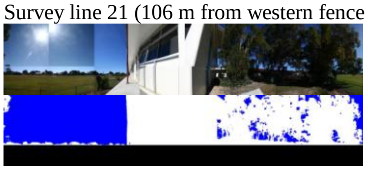
603


602


601


600


599

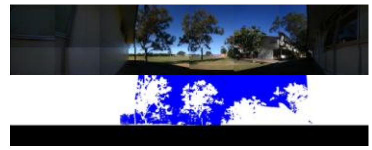
598

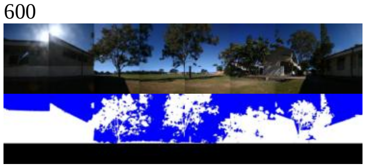
597

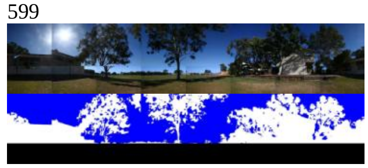
596


595


594

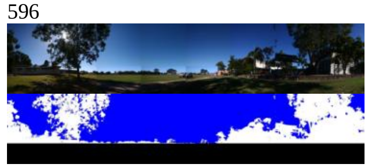
593


592


591


590


589


588


587


586


585


584


583


582


581


580


579


578


577

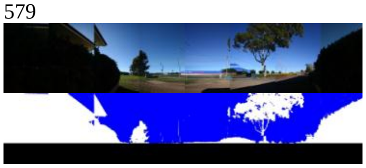
576

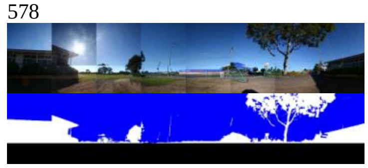
575

Survey line 22 (111 m from western fence line)

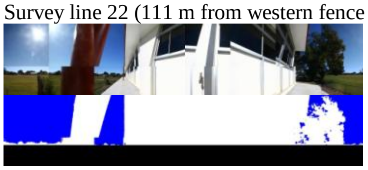
604

605

606

607
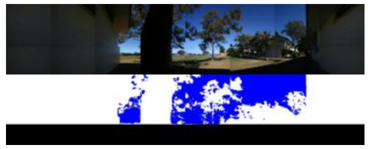
608

609
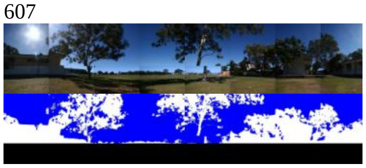
610
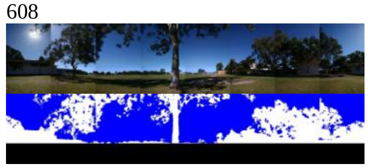
611

612

613

614

615

616

617

618

619

620

621
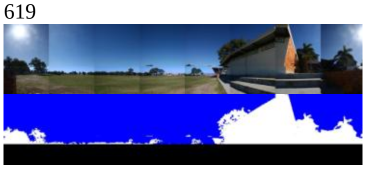
622

623
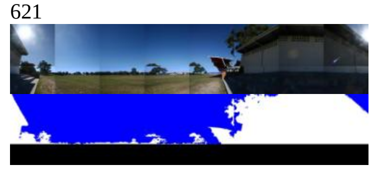
624

625

626

627
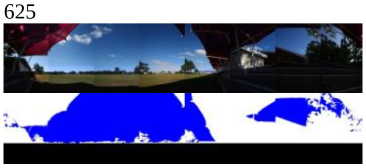
628
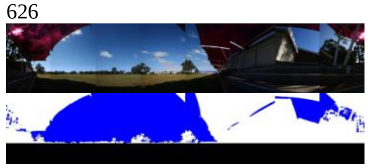
629

630
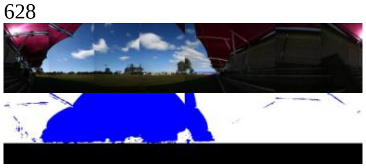
631
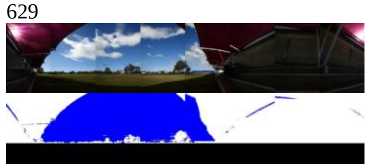
632
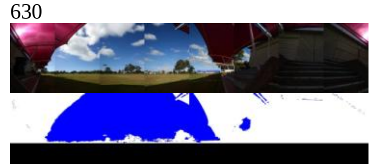
633

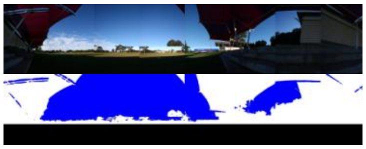
634
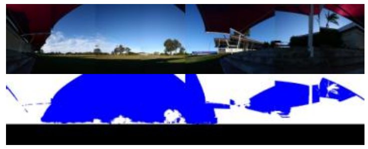
635
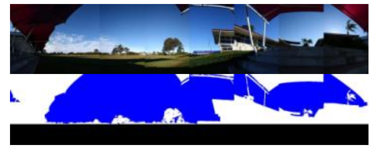
636
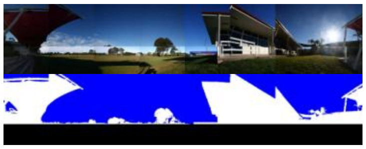
637

638
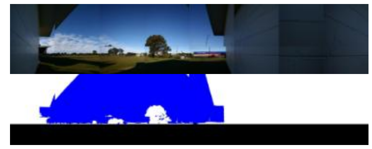
639
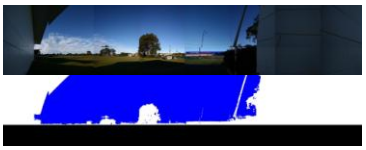
640
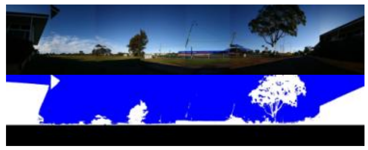
641
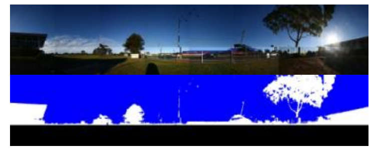
642

Survey line 23 (116 m from western fence line)

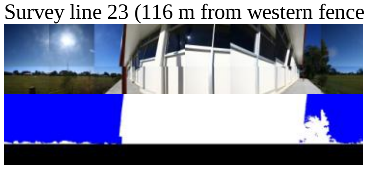
662

661
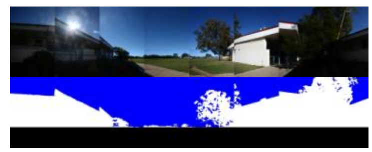
660

659

658

657

656
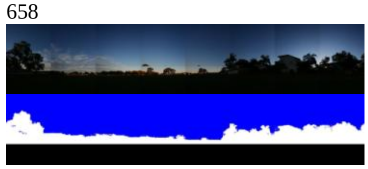
655

654

653
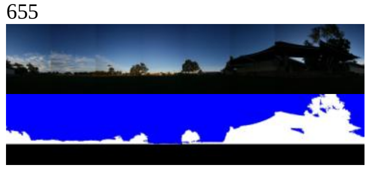
652

651
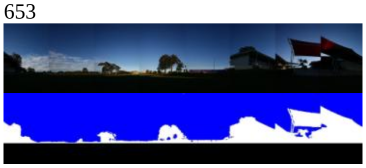
650

649
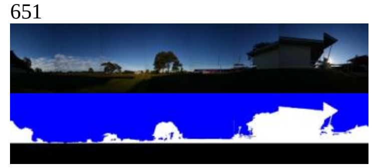
648
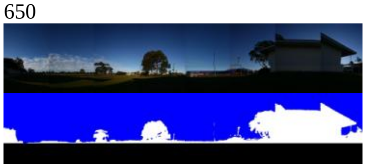
647
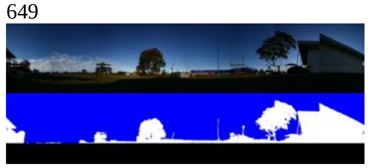
646
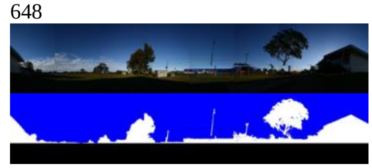
645

643

Survey line 24 (121 m from western fence line)

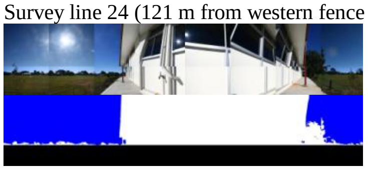
663

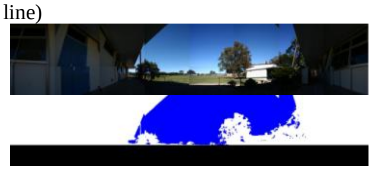
664

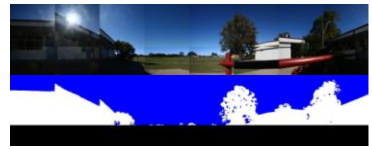
665

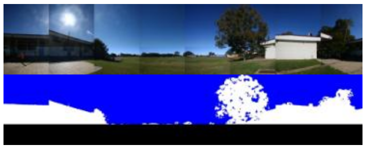
666

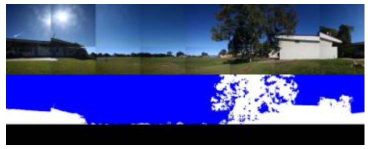
667


668

Survey line 25 (126 m from western fence line)

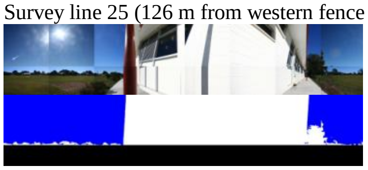
674

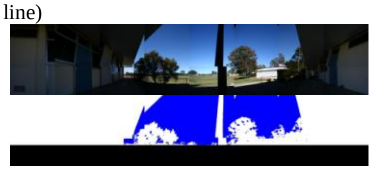
673

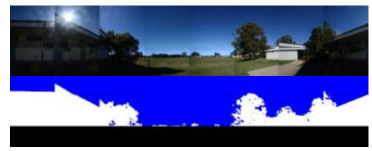
672


671


670

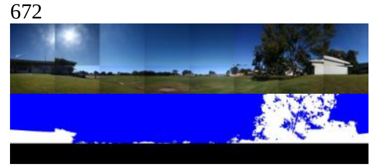
669

Survey line 26 (131 m from western fence line)

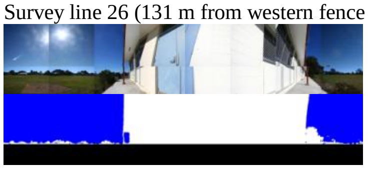
675

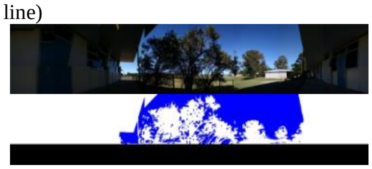
676

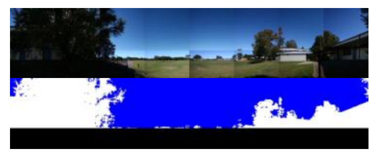
677

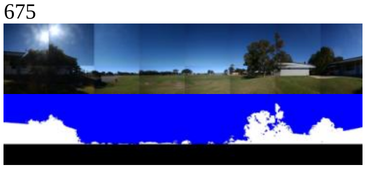
678

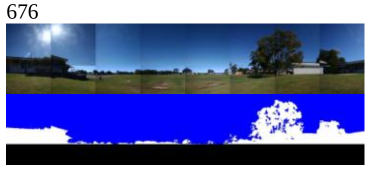
679

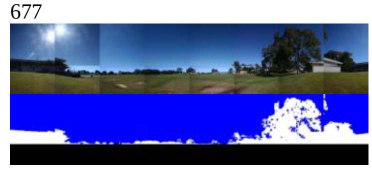
680

Survey line 27 (136 m from western fence line)

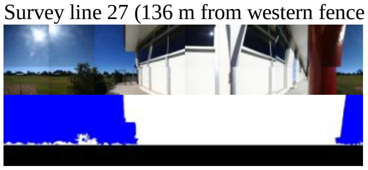
681

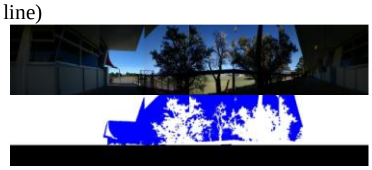
682


683

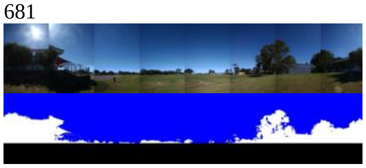
684

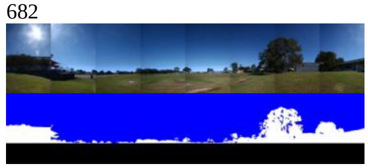
685

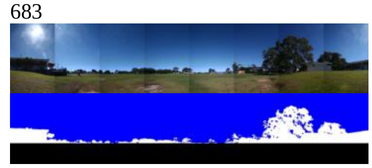
686

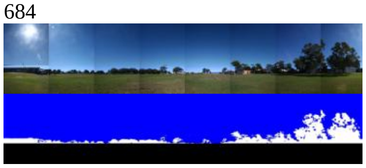
687

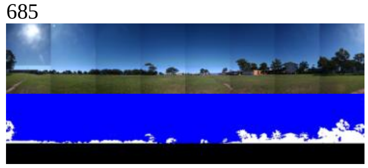
688

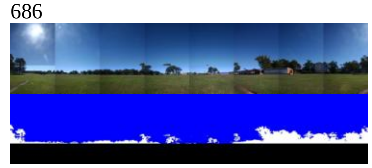
689

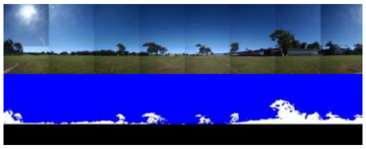
690

691
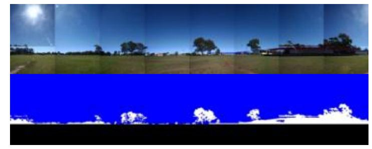
692
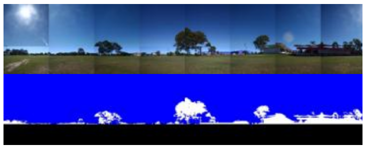
693
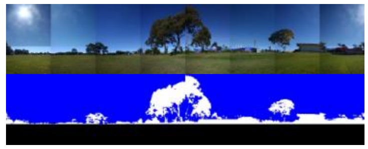
694
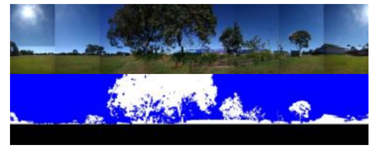
695

Survey line 28 (141 m from western fence line)

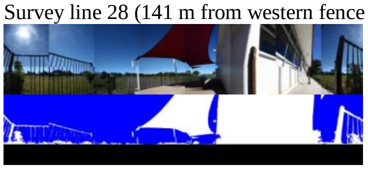
696

697

698

699
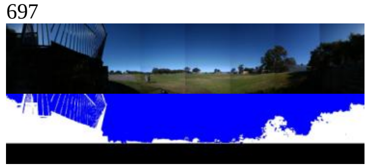
700
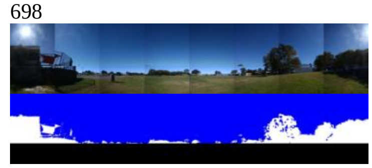
701

702
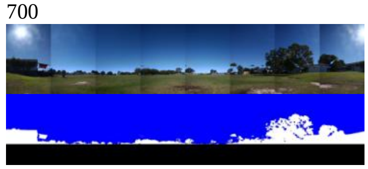
703

Survey line 29 (146 m from western fence line)

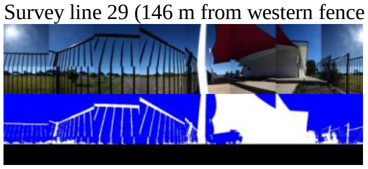
704
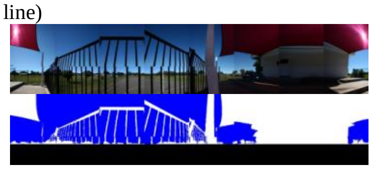
705

706

707
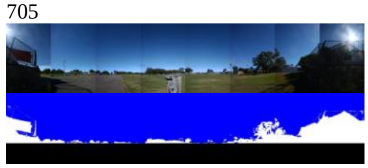
708
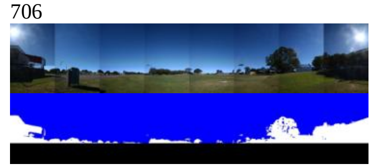
709
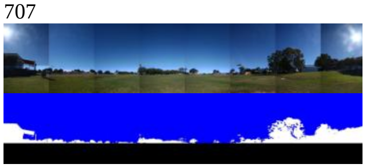
710
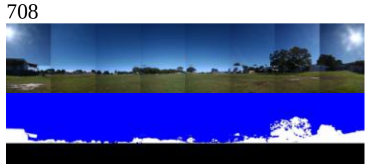
711

Survey line 30 (151 m from western fence line)

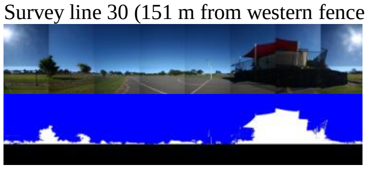
712
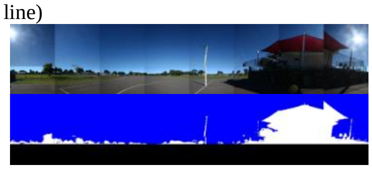
713

714
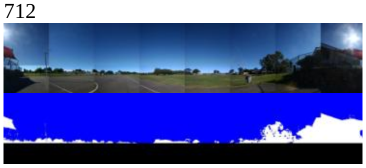
715

716
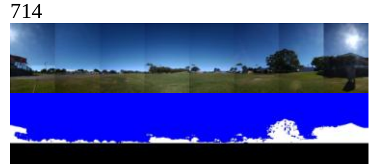
717

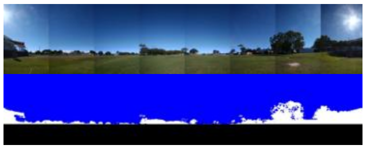
718
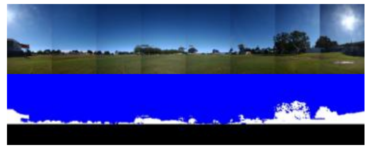
719

Survey line 31 (156 m from western fence line)

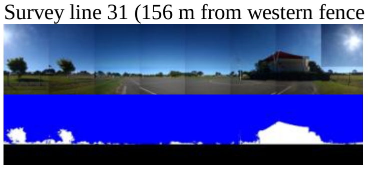
720
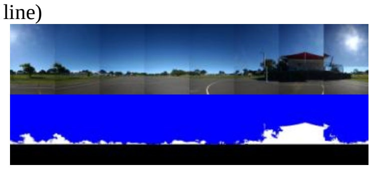
721
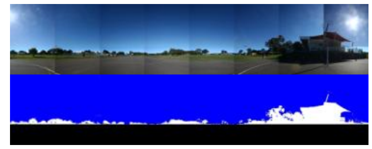
722
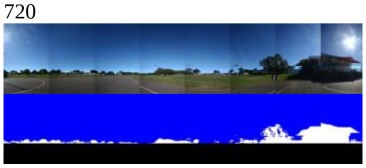
723

724
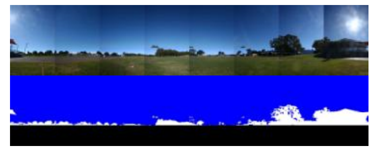
725
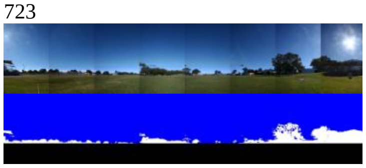
726
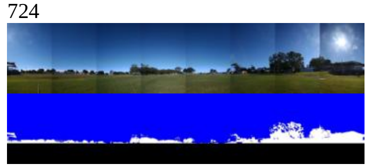
727
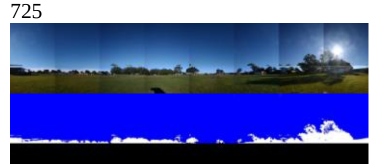
728
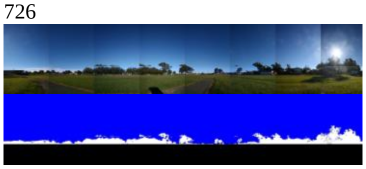
729
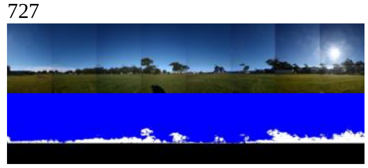
730

731
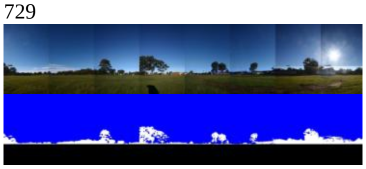
732
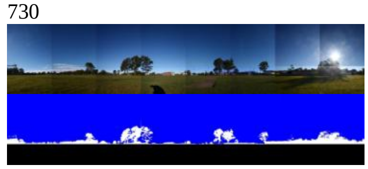
733
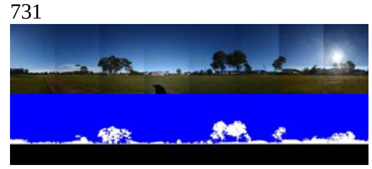
734
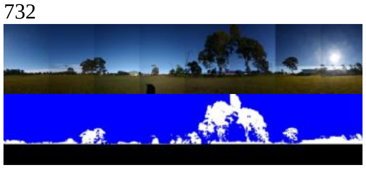
735

736

Survey line 32 (176 m from western fence line)

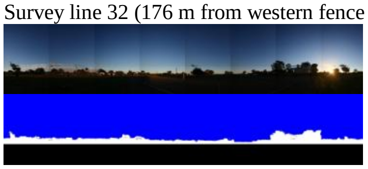
748
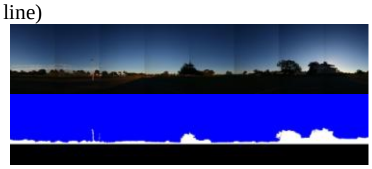
747

746
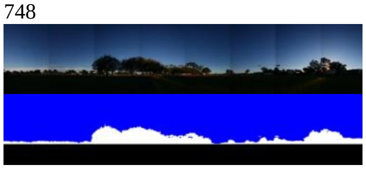
745
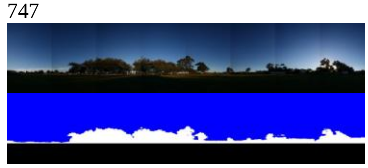
744

743

742
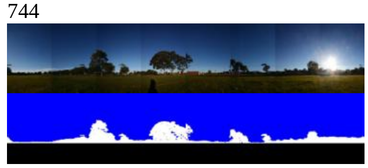
741
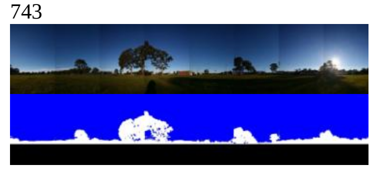
740

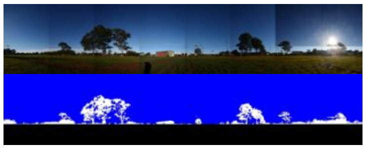
739
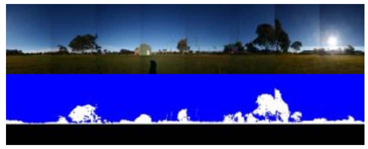
738
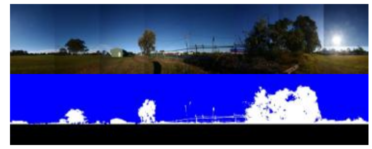
737

Survey line 33 (196 m from western fence line)

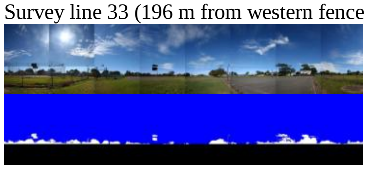
749
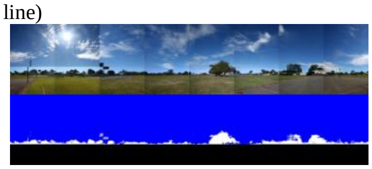
750
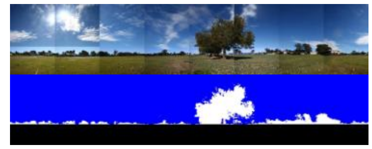
751

752

752x
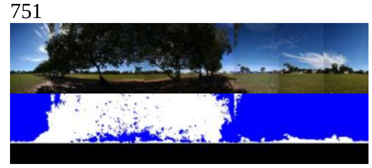
753
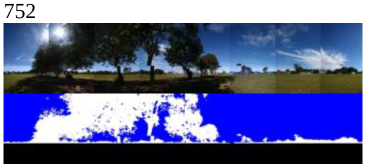
754
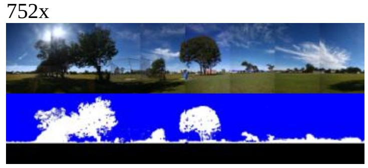
755

756

757
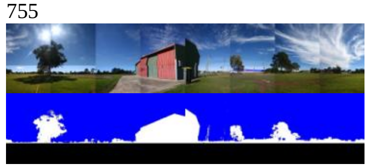
758

759

Survey line 34 (216 m from western fence line)

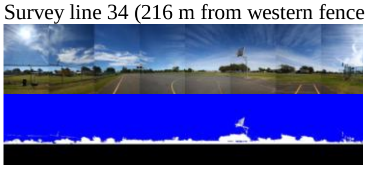
771

770

769

768

767
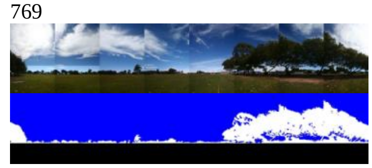
766
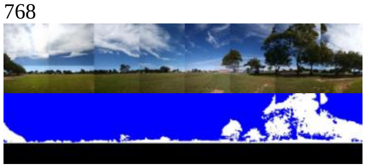
765
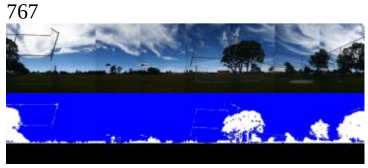
764
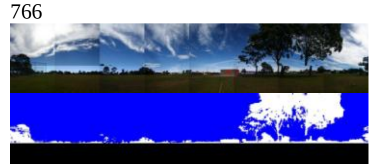
763
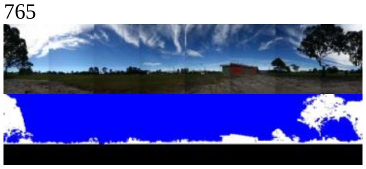
762

761
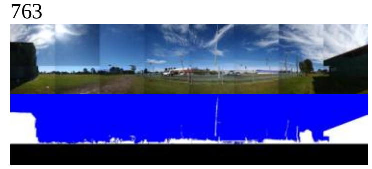
760

Survey line 35 (236 m from western fence line)

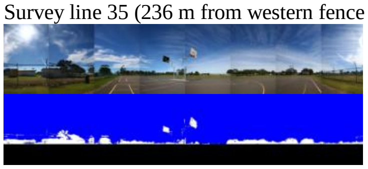
772

773

774

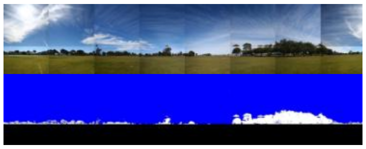
775

776
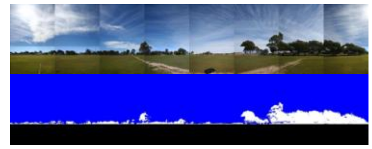
777
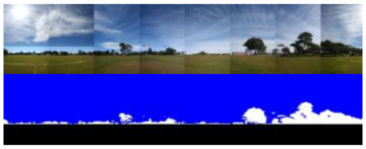
778
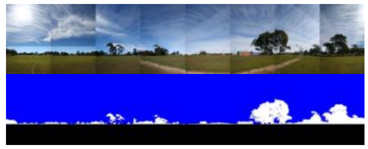
779

780

781
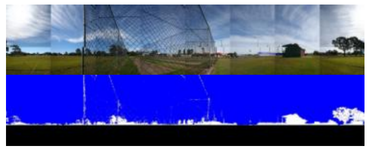
782
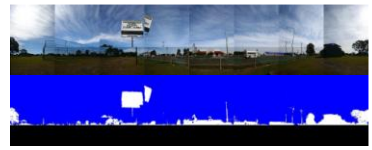
783

Survey line 36 (256 m from western fence line)

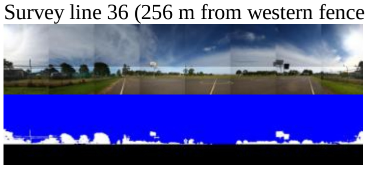
795
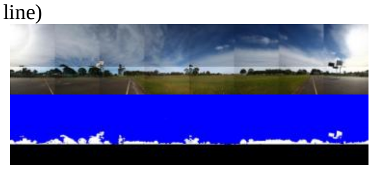
794

793
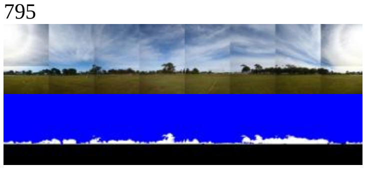
792
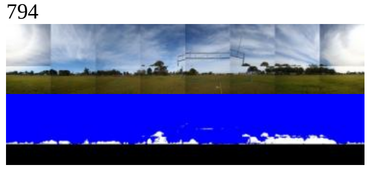
791
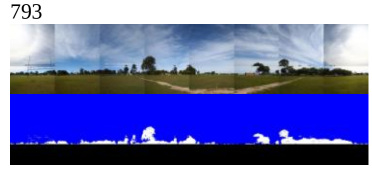
790

789

788
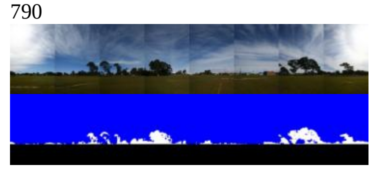
787

786

785

784

Survey line 37 (276 m from western fence line)

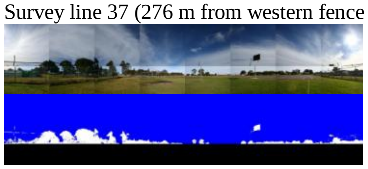
796

797

798

799

800

801

802

803

804


805

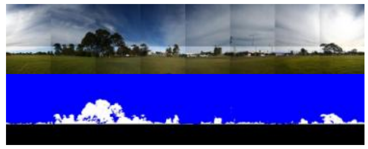
806

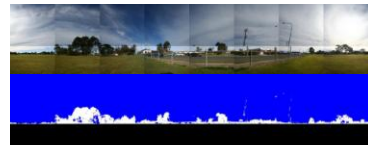
807

Survey line 38 (296 m from western fence line)

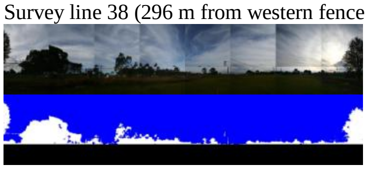
819

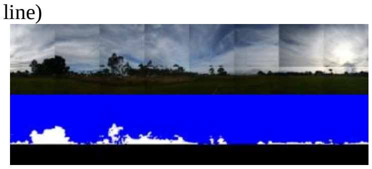
818

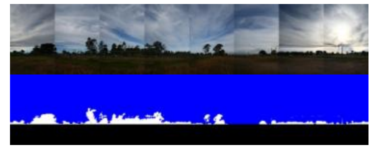
817

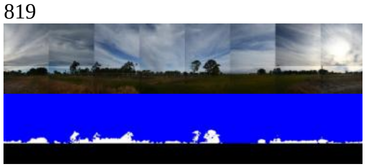
816


815


814

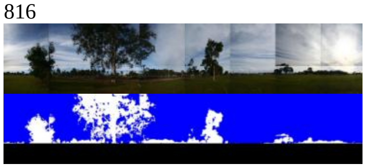
813


812

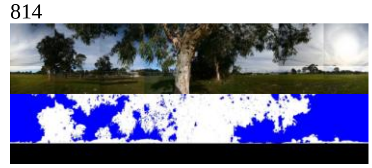
811


810


809


808

Appendix M. Shade density templates

Figure M.1.1 and Figure M.1.2 are the shade density templates compared with each playground survey site to determine playground shade density for the winter solstice, 21 June 2008 and summer solstice, 21 December 2008 respectively. Tables M.1.1 and M.1.2 list the SZA and azimuth position of the sun (Michalsky 1988) and pixel positions used to plot the respective solar position onto each template in Figures M.1.1 and M.1.2.

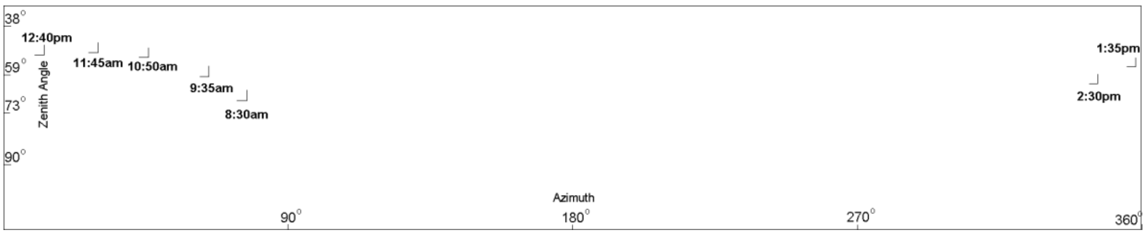

Figure M.1.1: Shade template for 21 June 2008 (arrows show solar position).

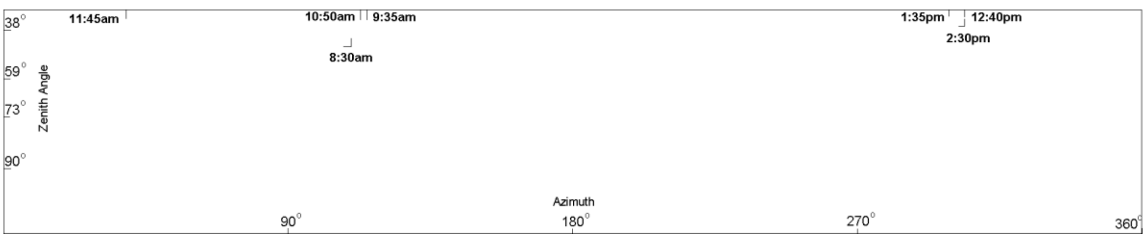

Figure M.1.2: Shade template for 21 December 2008 (arrows show solar position, lines show solar azimuth position only at the respective times).

Table M.1.1: SZA, azimuth and pixel positions used to develop 21 June 2008 shade template.

Time	SZA(^{o})	Pixels from top	Azimuth (^{o})	Pixels from left
8:30am	69	162	49	415
9:35am	59	121	37	350
10:50am	51	88	18	247
11:45am	49	80	2	161
12:40pm	50	84	345	69
1:35pm	55	104	330	1932
2:30pm	62	133	318	1867

Table M.1.2: SZA, azimuth and pixel positions used to develop 21 December 2008 shade template.

Time	SZA(^{o})	Pixels from top	Azimuth (^{o})	Pixels from left
8:30am	45	63	82	593
9:35am	30	outside limit	87	620
10:50am	13	outside limit	85	609
11:45am	2	outside limit	11	209
12:40pm	12	outside limit	276	1640
1:35pm	25	outside limit	271	1613
2:30pm	37	28	276	1640

Appendix N. Ozone concentrations for Hervey Bay

Table N.1: OMI (TOMS 2008) ozone concentrations listed for Hervey Bay (25^{o}S, 153^{o}E), June 2007 and December 2007.

June 2007	Ozone concentration (DU)	December 2007	Ozone concentration (DU)
1	250	1	297
2	255	2	292
3	259	3	287
4	na	4	289
5	250	5	278
6	268	6	278
7	286	7	278
8	293	8	280
9	303	9	283
10	286	10	280
11	274	11	277
12	261	12	280
13	256	13	na
14	268	14	286
15	273	15	280
16	269	16	272
17	259	17	277
18	262	18	283
19	265	19	270
20	254	20	269
21	259	21	270
22	269	22	264
23	284	23	266
24	284	24	261
25	275	25	268
26	258	26	256
27	282	27	264
28	301	28	265
29	286	29	275
30	281	30	263
		31	267

Appendix O. Playground site albedo, shade and UV exposure data

Table O.1: The table presents playground site data used to produce Figures 4.4, 4.7, 4.8, 4.9 and 4.10 for playground survey lines 1 through 37. Data is arranged in each survey line from sites located on the playground northern fenceline to sites located on the southern fenceline. Figure L.1 gives playground site codes referred to in the table.

Survey line 1 (5 m from western fence line)

Site	Ground Albedo (%)	Standing Albedo (%)	Winter shade density	Summer shade density	Winter UV (SED)	Summer UV (SED)
0	10	0	3	2	10.6	45.4
1	6	0	4.89	5.67	3.7	17.1
2	6	0	5.67	5.34	4.5	17.8
3	10	1.5	2	0	13.9	58.9
4	7	0	1	0	13.7	59.9
5	4	0	0	0	14.5	58.9
6	4	0	0	0	14.2	57.9
7	4	0	0	0	13.9	56.9
8	4	0	1	2	13.3	47.3
9	7	0	2	0	11.9	55.1
10	4	0	1	0	12.5	55.8
11	4	0	2	1	12.8	52.1
12	4	0	1	0	12.2	54.8
13	4	0	1	2	12.3	43.9
14	4	0	3	3	9.5	36.9
15	4	1.5	4	4	8.4	30.2
16	4	0	6	5	6.5	27.8
17	4	0	7	3	5.0	36.3
18	4	3.25	7	4	4.3	29.0
19	4	6.5	4	5	5.8	23.2
20	4	6	6	4	5.5	32.2
21	4	0	5	3	7.2	34.7
22	4	0	4	4	7.6	34.4
23	4	4	4	3	8.3	35.4
24	10	1.75	4	2	7.7	43.1
25	4	0	6	4	7.6	34.3
26	4	0	3	0	10.4	56.9
27	10	0	1	0	13.2	58.8
28	4	0	0	0	14.4	58.6
29	4	0	0	0	14.5	58.9
30	10	0	1	0	14.1	59.2
325	10	1.5	6	4	5.7	29.8
326	4	0	3	0	11.4	52.0
327	4	1.5	2	1	9.2	43.0
328	4	1.5	3.89	2	5.5	33.5
329	4	0	4.78	1	6.1	40.6
330	4	0	3.78	2	6.0	36.6
331	4	1.5	5.78	3	4.0	31.8
332	4	0	5	6	6.5	18.2

Survey line 2 (10 m from western fence line)

Site	Ground Albedo (%)	Standing Albedo (%)	Winter shade density	Summer shade density	Winter UV (SED)	Summer UV (SED)
56	4	0	4	2	9.8	45.6
55	7	0	4	3	8.6	38.5
54	7	0	4	3	8.6	35.7
53	7	0	3.78	1	11.0	49.0
52	10	0	1	0	13.0	57.8
51	7	0	2	0	12.3	59.2
50	7	0	2	0	11.9	58.2
49	7	0	1	0	13.1	58.2
48	7	0	0	1	13.0	51.0
47	4	0	4	3	8.0	35.8
46	4	0	4	4	7.5	34.1
45	4	0	5	7	7.3	19.6
44	4	0	5	2	7.4	40.8
43	4	0	3	3	8.9	38.7
42	4	2.75	4	6	7.3	18.2
41	4	2.75	6	6	5.0	18.2
40	4	2.75	6	6	5.3	19.2
39	4	2.75	6	4	5.6	28.3
38	4	7	5	4	6.8	26.5
37	4	0	5	2	7.7	45.4
36	4	0	6	2	7.1	41.5
35	4	0	6	1	8.2	49.4
34	10	0	2	3	9.4	32.8
33	4	0	4	0	9.3	54.4
32	4	0	1	2	13.3	47.3
31	10	0	2	0	12.2	56.4
340	10	0.75	6	0	6.8	51.3
339	10	0	2	0	11.8	55.3
338	10	0	2.67	2.67	11.3	45.0
337	10	0	2.67	2.67	11.2	44.7
336	10	0	2.78	2.67	11.1	44.7
335	10	0	2.67	2.67	11.0	44.0
334	10	0	2.78	2.67	10.5	42.6
333	10	0	1	4.67	11.1	31.1

Survey line 3 (15 m from western fence line)

Site	Ground Albedo (%)	Standing Albedo (%)	Winter shade density	Summer shade density	Winter UV (SED)	Summer UV (SED)
57	4	0	5	3	8.9	39.6
58	7	1.75	5	2	8.5	38.9
59	7	0.5	3	2	10.9	44.6
60	7	0	2	1	11.5	51.8
61	7	0	3	0	11.5	57.5
62	7	0	4	0	10.7	58.5

Survey line 4 (20 m from western fence line)

Site	Ground Albedo (%)	Standing Albedo (%)	Winter shade density	Summer shade density	Winter UV (SED)	Summer UV (SED)
104x	4	1.75	2	1	11.7	48.9
105x	7	1.5	5	4	8.5	35.2
103x	7	0	4	2	10.0	47.7
134	7	0	2	1	11.7	52.2
83	7	0	5	0	9.4	56.1
82	7	0	2	0	12.9	58.2

63	7	0	2	0	11.9	58.2
64	7	0	2	0	11.0	55.4
65	4	0	5	2	8.2	44.3
66	4	2.25	7	4	4.1	27.2
67	4	0	3	3	9.7	39.1
68	4	0	3	1	10.4	49.3
69	4	0	4	2	8.8	44.7
70	10	0	6	1	7.9	49.8
71	10	3.25	3	3	8.9	35.9
72	10	0	4	0	8.6	52.2
341	10	0.75	7	1	6.5	47.9
352	10	0	0	0	12.7	53.2
353	4	1.75	4	5.34	5.4	15.5

81	7	0	1	0	13.4	58.5
80	7	0	0	0	13.5	55.8
79	4	1.75	7	1	5.5	46.4
78	10	2	5	1	9.1	50.7
77	10	3.25	1	2	11.3	44.7
76	4	0	4	1	10.2	48.3
75	4	0	4	0	9.9	50.3
74	10	0	4	0	9.2	50.8
73	10	0	7	0	5.5	47.3
342	10	0.75	7	0	7.1	52.7
351	10	0	0	0	13.0	54.3
354	4	1.75	5	6.23	4.0	9.0

Survey line 5 (25 m from western fence line)

Site	Ground Albedo (%)	Standing Albedo (%)	Winter shade density	Summer shade density	Winter UV (SED)	Summer UV (SED)
133x	4	0	1	2	12.9	46.3
132x	7	0	4	3	9.7	41.4
111	7	0	2	2	11.9	47.3
110	7	0	3	0	11.1	54.7
109	7	0	5	0	10.4	56.1
108	7	0	5	0	10.8	57.5
107	7	0	2	0	12.6	57.1
106	7	0	2	0	11.8	54.4
93	10	0.5	6	6	1.9	5.5
92	10	2	6	7	1.0	2.1
91	10	2	6	6	1.1	5.5
90	10	0.5	7	6	1.8	11.3
89	4	0	4	0	9.3	48.6
88	4	0	2	2	11.5	41.8
87	4	0	3	0	10.4	50.7
85	6	0	4	0	8.8	49.1
86	10	1.5	1	7	6.7	4.6
84	10	0	7	2	4.5	34.9
344	4	2	7	5	3.6	22.1
343	4	0	6	0	8.4	52.7
345	4	0	2	0	11.4	56.2
346	4	0	0	0	14.1	57.5
347	4	0	0	0	14.3	58.2
348	4	0	0	0	14.3	58.2
349	4	0	0	0	13.8	56.5
350	10	2.75	2	3	10.3	35.6
355	10	2.75	3	4.78	9.1	31.4

Survey line 6 (30 m from western fence line)

Site	Ground Albedo (%)	Standing Albedo (%)	Winter shade density	Summer shade density	Winter UV (SED)	Summer UV (SED)
142	7	0	0	3	14.0	49.8
141	7	0	1	1	13.4	55.1
140	7	0	2	0	12.2	53.7
139	7	0	5	1	9.5	49.6
138	7	0	5	2	9.6	44.1
137r	7	0	5	1	10.3	52.4
137	7	0	3	0	11.6	56.1
136	7	0	2	0	12.1	54.0
135	10	0	0	3	11.0	33.1
119x	10	0.5	4	5	5.5	18.9
102x	7	0	5	2	7.5	40.4
101x	10	0	7	6	1.5	10.2
100	10	0	7	4	1.6	14.5
99x	10	0	4	4	3.4	15.2
98x	10	0	5	4	3.3	15.2
97x	10	0	4	4	3.4	15.2
96x	10	0	6	3	2.1	17.5
95	6	0	3	0	8.8	48.7
96	10	1.5	0	7	7.0	4.9
94	10	0	7	5	2.8	17.8
362	4	0	7	5	5.7	28.1
361	4	0	5	0	8.4	52.7
360	4	0	4	0	9.8	55.5
359	4	0	1	0	13.5	56.9
358	4	0	1	0	13.6	57.2
357	4	0	0	0	13.9	56.9
356	4	0	0	0	13.4	55.5

Survey line 7 (35 m from western fence line)

Site	Ground Albedo (%)	Standing Albedo (%)	Winter shade density	Summer shade density	Winter UV (SED)	Summer UV (SED)
128x	8	0	1	1	13.4	53.5
127x	8	0	2	1	12.0	54.1
126x	7	1.5	3	1	9.5	44.5
125x	7	0.75	7	4	5.0	25.9
124x	7	0	5	0	9.9	54.7
123x	7	0	2	0	12.0	52.3
122x	10	0	1	6	8.9	18.3
121x	10	1.5	7	7	0.4	1.4
120x	10	0	7	7	3.6	12.3
118x	7	0	4	0	8.2	50.9
117x	10	1	3	5	6.4	16.8
116x	7	0	6	6	3.6	16.8
115x	10	1.75	6	7	0.7	1.8
113x	6	0	1	0	10.3	48.7
114x	10	1.5	0	7	7.0	4.9
112x	10	0	7	3	2.5	27.9
363	4	0	6	6	5.9	21.6
364	4	0	6	1	7.4	46.6
365	4	0	4	1	9.4	48.7
366	4	0	2	1	11.2	49.7

Survey line 8 (40 m from western fence line)

Site	Ground Albedo (%)	Standing Albedo (%)	Winter shade density	Summer shade density	Winter UV (SED)	Summer UV (SED)
129x	8	0	1	0	12.7	56.9
130x	8	0	2	1	11.9	53.8
131x	7	1.5	2	2	8.2	36.6
143	7	0.75	7	6	4.2	17.5
144	7	0	4	0	10.2	54.0
145	7	0	2	0	11.3	50.2
146	10	0	0	6	8.4	15.1
147	10	0	7	7	0.5	1.8
148	10	0	7	7	3.5	11.9
149	7	2.25	7	3	5.4	36.9
150	7	2.25	6	2	7.0	39.7
151	7	0	4	1	8.4	48.6
152	7	0	0	0	12.1	50.9
153	10	1	2	6	7.1	15.5
154	7	0	7	4	3.8	28.5
155	4	2	7	4	3.1	24.7
156	10	1.75	6	6	2.3	8.9
158	6	0	1	1	11.2	46.1
159	10	1.5	1	7	6.5	4.6
157	10	0	7	0	4.4	43.4

367	4	0	2	1	11.5	50.7
368	4	0	2	1	11.6	51.1
369	4	0	1	1	12.8	51.4

381	7	0	7	0	7.1	52.6

Survey line 9 (45 m from western fence line)

Site	Ground Albedo (%)	Standing Albedo (%)	Winter shade density	Summer shade density	Winter UV (SED)	Summer UV (SED)
181	8	0	3	3	10.8	41.3
180	8	0	3	0	10.6	54.8
179	7	1.5	3	5	7.8	27.4
178	7	0.75	7	7	4.2	14.2
177	7	0	4	0	10.2	54.0
176	7	1.75	1	0	10.5	49.7
175	10	0	4	6	3.2	8.3
174	10	0.5	7	7	2.9	9.8
173	7	1.75	7	5	3.2	21.6
172	7	0.5	7	0	6.4	50.3
171	4	2.25	4	3	7.1	30.7
170	10	1.5	7	6	0.6	7.5
169	10	0.75	7	7	3.1	10.5
168	7	0	7	3	5.3	36.2
167	10	1.75	5	7	2.8	3.5
166	4	2.5	6	3	4.3	30.3
165	4	2	4	3	7.9	34.6
164	7	1.5	4	1	8.4	47.2
163	7	2	3	2	10.1	43.5
162	7	2.25	4	4	6.4	25.4
161	10	1.5	3	7	3.9	3.5
160	10	0	7	1	4.5	37.9
380	7	0	6	0	7.0	50.9
379	7	0	3	2	11.0	48.3

Survey line 10 (50 m from western fence line)

Site	Ground Albedo (%)	Standing Albedo (%)	Winter shade density	Summer shade density	Winter UV (SED)	Summer UV (SED)
182	8	0	3	4	10.4	34.6
183	8	0	4	1	9.3	47.9
184	7	1.5	4	6	5.3	17.5
185	7	0.75	7	7	4.1	13.9
186	7	0	3	0	10.2	53.3
87	7	0	2	1	10.3	48.9
188	10	1.75	0	6	8.8	16.3
189	10	0.5	7	7	2.0	6.7
190	7	0	7	3	5.0	31.2
191	7	0	7	2	5.7	43.1
192	7	4	7	5	2.9	20.0
193	10	1.5	4	6	4.3	14.9
194	10	0.75	7	7	3.0	10.2
195	7	0	7	5	4.7	25.9
196	10	1.75	4	7	2.6	3.2
197	7	1.5	5	3	6.2	37.3
198	7	1.5	4	2	8.9	42.7
199	7	0	2	2	10.0	40.0
200	7	0	2	2	9.9	39.6
201	7	0	2	3	9.1	31.5
202	4	2.25	4	7	4.6	10.0
203	4	0	7	6	2.6	13.9
204	10	1.5	7	4	2.2	24.1
205	10	0	7	0	5.0	45.5
206	6	2.25	6	5	4.8	17.2
376	7	0	7	5	3.4	22.6
377	7	0	3	0	11.8	55.4
378	7	0	0	0	13.0	54.0

Survey line 11 (55 m from western fence line)

Site	Ground Albedo (%)	Standing Albedo (%)	Winter shade density	Summer shade density	Winter UV (SED)	Summer UV (SED)
236	8	0	5	1	7.9	45.7
235	8	0	5	2	7.7	39.8
234	7	1.5	6	6	3.7	17.2
233	7	0.75	7	7	4.1	13.9
232	7	0	2	0	11.3	53.3
231	7	0	2	0	10.6	51.2
230	10	1.75	1	5	8.8	20.8
229	10	0.5	7	7	1.7	5.6
228	7	0	7	1	5.6	44.4
227	7	0	6	1.96	5.5	38.0
226	7	1.5	4.96	4.96	6.1	24.1
225	7	1.5	4.96	2	7.9	42.8
224	10	1.5	3	6	7.0	15.9
223	10	0.75	7	7	2.8	9.5
222	7	0	7	5	4.3	22.9
221	10	0	6	5	2.3	14.5
220	7	0	6	5	3.6	21.3
219	7	0	4	3	6.4	27.0
218	7	0	3	3	7.1	28.8
217	7	0	4	4	4.6	19.3
216	7	1.75	6	7	1.1	3.1
215	4	4	7	7	0.4	1.4
214	6	0	7	5	4.0	24.6
213	6	2	6	3	4.1	29.6
212	6	2	7	3	3.2	30.6
211	6	2	4	5	5.8	21.2
210	6	2	6	4	4.3	27.2
209	6	2	5	3	6.4	33.4

Survey line 12 (60 m from western fence line)

Site	Ground Albedo (%)	Standing Albedo (%)	Winter shade density	Summer shade density	Winter UV (SED)	Summer UV (SED)
236x	8	0	5	2	7.6	42.3
237x	8	0	5	0	7.5	50.3
238x	7	1.75	6	5	3.0	15.7
239x	7	0.75	7	6	4.4	18.0
240x	7	0	3	0	10.1	53.3
241x	7	0	2	0	10.5	50.9
242x	10	1.75	1	6	8.6	17.0
243x	10	0.5	7	7	2.0	6.7
244x	7	0	7	2	4.6	37.6
245x	7	0	6	6.86	1.9	3.3
246x	7	0	5.88	6.86	3.3	10.6
247x	7	0	0	0	11.5	49.2
248x	10	1.5	0	6	9.0	17.0
249x	10	0.75	7	7	2.9	9.8
250x	6	0	7	2	4.8	40.3
251x	6	0	4	4	6.2	23.2
252x	10	0	7	7	0.3	1.1
253x	10	0	7	7	0.4	1.4
254x	10	1.5	7	4	0.7	16.8
256	4	0	7	7	1.1	3.8
257	6	0	7	7	0.8	2.8
258	6	0.5	7	5	1.9	14.1
259	6	0	6	2	5.6	39.9
260	4	1.75	6	2	5.4	39.5
261	6	0	7	2	5.7	43.3
262	4	0	3	0	9.8	49.6
263	4	0	2	3	10.4	38.4
372	7	0	7	2	5.4	38.4

208	4	0	4	2	8.0	41.6
207	4	1.5	4	7	6.9	14.1
375	7	0	7	2	4.7	36.3
374	7	0	0	0	13.6	56.1
373	7	0	0	0	11.9	50.2

371	7	0	0	0	13.9	57.1
370	7	0	0	0	13.6	56.1

Survey line 13 (65 m from western fence line)

Site	Ground Albedo (%)	Standing Albedo (%)	Winter shade density	Summer shade density	Winter UV (SED)	Summer UV (SED)
291	8	0	6	1	6.2	42.5
290	8	0	6	2	6.4	42.2
289	8	0	6	3	5.5	29.5
288	4	0	7	2	5.2	41.8
287	4	0	7	1	6.1	47.9
286	7	0	6	1	8.1	50.6
285	7	0	4	0	10.1	53.7
284	7	0	1	0	11.3	49.5
283	10	2.25	6.86	7	1.1	3.5
282	10	0.5	7	7	3.3	11.2
281	7	0	7	0	5.0	45.3
280	7	0	5.98	3.92	3.6	22.8
279	7	0	4.92	3.92	6.4	28.3
278	7	0	1.98	0	10.0	49.2
277	10	1.5	0	6	9.0	17.0
276	10	0.75	7	7	2.8	9.5
275	6	0	7	2	3.8	32.6
274	6	0	4	5	5.2	17.4
273	10	0	6	7	1.5	1.1
272	10	0	7	7	0.1	0.4
271	10	0	7	2	0.9	25.2
270	4	0	7	7	0.8	2.7
269	7	1.75	7	6	0.8	4.2
268	4	5.5	7	7	0.4	1.4
267	10	0	7	6	0.7	3.8
266	10	0.75	7	7	3.3	11.2
265	6	0	0.93	0	11.9	51.5
264	4	0	0	0	12.1	51.0
324	7	0	7	1	4.5	38.6
323	7	0	1	0	13.5	56.8
322	7	0	1	0	13.9	58.2

Survey line 14 (70 m from western fence line)

Site	Ground Albedo (%)	Standing Albedo (%)	Winter shade density	Summer shade density	Winter UV (SED)	Summer UV (SED)
292	8	0	6	4	6.1	30.5
293	8	0	5	5	8.3	30.8
294	8	0	6	3	5.6	30.2
295	4	0	7	1	6.0	43.1
296	4	0	5	0	8.3	52.0
297	7	0	4	0	10.0	53.7
298	7	0	3	0	10.3	53.0
299	7	0	2	0	9.0	48.1
300	10	1.75	3.58	5	5.6	17.6
301	10	0.5	7	7	1.8	6.0
302	10	0	7	7	0.1	0.4
303	10	0	7	7	0.0	0.0
304	10	0	7	7	0.1	0.4
305	7	0	7	3	4.1	28.4
306	10	1.5	3	6	4.9	12.1
307	10	0.75	7	7	2.7	9.1
308	6	0	7	4	3.5	23.0
309	6	0	3	4	5.2	22.7
310	10	0	7	7	0.0	0.0
311	10	0	7	7	0.2	0.7
312	10	0	7	2	2.5	28.8
313	4	2.25	7	5	1.2	13.2
314	7	1.5	7	4	1.8	20.3
315	10	0	6	3	3.9	29.0
318	10	0.5	7	7	2.7	9.1
317	6	0	4.65	5.58	5.6	18.0
316	4	0	1	2	10.7	42.9
321	7	2.25	7	3	3.8	27.7
320	7	0	4	1	9.2	51.0
319	7	0	1	0	12.9	57.5

Survey line 15 (76 m from western fence line)

Site	Ground Albedo (%)	Standing Albedo (%)	Winter shade density	Summer shade density	Winter UV (SED)	Summer UV (SED)
421	8	0	5	1	7.6	41.1
420	8	0	6	3	7.3	39.0
419	8	0	6	4	5.6	30.2
418	10	2.25	7	7	1.2	4.2
417	10	1.5	7	7	0.4	1.4
416	10	2.75	7	7	0.9	3.2
415	10	2	6	7	0.7	1.8
414	10	0	6	7	1.2	3.5
413	10	0	6	7	0.7	1.8
412	10	1.75	6	7	1.3	0.7
411	10	3.25	7	7	0.3	1.1
410	10	1.25	7	7	0.0	0.0
409	10	0.5	7	7	0.1	0.4
408	10	0	7	7	0.1	0.4
407	10	4.75	7	7	0.1	0.4
406	10	4.75	7	7	0.2	0.7
405	10	0	7	7	0.3	1.1
404	10	0	7	7	0.4	1.4
403	10	0	7	7	0.1	0.4
402	10	0.5	7	7	0.1	0.4
401	10	0	7	7	0.4	1.4
400	10	0	7	7	0.2	0.7
399	10	0	7	7	0.4	1.4
398	10	0	7	7	0.5	1.8

Survey line 16 (81 m from western fence line)

Site	Ground Albedo (%)	Standing Albedo (%)	Winter shade density	Summer shade density	Winter UV (SED)	Summer UV (SED)
422	8	0	7	2	5.0	34.2
423	8	0	7	2	5.3	37.6
424	6	0	6	3	6.0	31.5
425	6	0	5	4	5.1	21.3
426	10	1.5	7	7	0.4	1.4
427	7	0	4	6	5.8	17.1
428	10	1.25	7	6	1.5	10.3
429	10	1.25	7	4	2.0	21.0
430	7	0	7	4	3.7	26.7
431	10	0	5	4	3.2	19.6
432	10	4.75	7	7	0.1	0.4
433	10	2	7	7	0.2	0.7
434	10	0	7	7	0.3	1.1
435	10	0	7	7	0.3	1.1
436	10	1.75	7	7	0.1	0.4
437	4	0	7	7	0.8	2.7
438	4	0	7	7	1.5	5.2
439	4	1.75	7	7	0.9	3.1
440	7	0	7	4	3.2	20.0
441	10	0	7	4	2.7	18.3
442	6	0	7	2	4.8	36.1
443	6	2.25	4	3	7.5	30.8
444	7	0	7	2	6.2	44.9
445	7	0	3	0	10.4	50.9

397	10	0	7	7	0.6	2.1
396	10	1.5	7	7	0.0	0.0
395	10	3.75	7	7	0.0	0.0
394	10	3.75	7	7	0.0	0.0
393	10	1.5	7	6	0.5	4.8
392	10	0	7	7	0.5	1.8
391	10	2	7	7	0.1	0.4
390	10	3	6	6	1.0	4.2
389	10	2	6	7	0.5	1.1
388	10	3.5	7	7	0.1	0.4
387	10	0	7	6	0.7	5.5
386	10	0	7	6	3.2	15.4
385	10	0	3	2	10.4	46.1
384	10	0	3	2	11.0	48.2
383	7	0	3	0	11.9	55.8
382	7	0	2	0	12.2	56.4

446	10	0	6	7	4.1	9.8
447	7	0	3	1	10.4	48.9
448	7	0	2	1	11.5	51.0
449	7	0	2	0	12.2	56.1
450	7	0	0	0	14.0	57.5

Survey line 17 (86 m from western fence line)

Site	Ground Albedo (%)	Standing Albedo (%)	Winter shade density	Summer shade density	Winter UV (SED)	Summer UV (SED)
482	8	0.5	7	2	4.0	34.0
481	8	0	7	3	4.1	28.5
480	4	0	5	6	5.1	18.0
479	6	0	5	5	6.4	24.8
478	10	1.75	7	7	1.5	4.9
477	4	0.75	7	7	1.3	4.5
476	7	1.75	6	5	4.6	19.9
475	10	1.25	6	7	1.8	2.1
474	6	0.5	7	3	3.1	22.7
473	7	0	7	3	5.5	39.4
472	4	0	3	1	10.2	48.6
471	4	0	4	2	9.6	45.0
470	7	1.75	5	2	7.9	42.9
469	10	1	3	6	5.7	11.7
468	10	0	7	7	0.6	2.1
467	10	0	6	7	1.0	2.1
466	10	0	7	7	0.4	1.4
465	10	2	7	7	0.2	0.7
464	10	2	7	7	1.8	6.0
463	4	1.75	7	3	1.7	25.7
462	4	2	7	6	0.7	5.5
461	4	1.5	7	4	1.6	14.8
460	7	2.25	7	5	2.3	12.4
459	10	2.25	7	4	1.5	14.3
458	10	0.5	7	4	3.0	19.4
457	6	0	5	3	7.7	38.2
456	10	1	5	6	3.7	10.3
455	7	0.75	7	2.76	4.1	28.7
454	7	0	1.84	0	11.3	53.0
453	10	1.5	1	7	7.2	6.0
452	7	0.5	7	0	7.1	52.8
451	7	0	0	2	13.8	47.9

Survey line 18 (91 m from western fence line)

Site	Ground Albedo (%)	Standing Albedo (%)	Winter shade density	Summer shade density	Winter UV (SED)	Summer UV (SED)
483	4	0	6	2	4.2	34.1
484	4	0	7	6	3.9	18.4
485	4	0	5	7	4.6	11.0
486	6	0	6	5	4.4	24.6
487	10	1.5	7	7	0.4	1.4
488	4	0.75	7	7	1.3	4.5
489	7	0	6	2	4.2	34.4
489x	10	1.25	3	4	6.6	25.6
490	6	0	7	3	4.1	28.4
491	6	0	7	3	5.4	32.5
492	4	0	3	1	9.6	48.3
493	4	0	3	0	9.6	51.4
494	7	1.75	1	2	10.5	40.6
495	10	1	3	3	8.6	35.5
496	10	0	6	4	3.8	23.3
497	10	0	5	5	4.2	20.3
498	10	0	6	4	3.6	22.6
499	10	0	5	7	2.1	2.1
500	10	0	7	7	1.0	3.5
501	10	0	7	5	1.2	11.8
502	4	1.75	7	5	2.7	17.4
503	7	1.75	4	5	5.2	20.0
504	4	3.75	6	7	3.1	9.3
505	10	2.25	7	6	1.0	8.2
506	10	0.5	7	7	0.7	2.5
507	4	0.25	6	2	5.7	35.0
508	10	1	4	6	4.1	9.9
509	7	0.75	7	3	4.2	29.4
510	7	0	0.92	2.76	10.2	33.0
511	10	1	5.68	3.92	3.4	24.6
512	7	0	7	0	7.0	52.3
513	7	0	0	1	13.9	51.3

Survey line 19 (96 m from western fence line)

Site	Ground Albedo (%)	Standing Albedo (%)	Winter shade density	Summer shade density	Winter UV (SED)	Summer UV (SED)
514	4	2	7	4	4.2	27.5
515	6	0	5	4	5.5	29.9
516	6	0	6	5	5.0	22.3
517	6	0	7	4	3.5	25.7
518	10	1.75	7	6	1.5	10.3
519	4	0.75	7	7	2.5	8.2
520	7	0	6	3	6.4	37.2
521	7	0	3	2	9.1	41.8
523	4	0	4	4	6.5	26.0
524	4	0	7	5	4.1	21.6
525	7	0	7	4	4.0	21.2
526	7	0	4	3	6.1	29.4

Survey line 20 (101 m from western fence line)

Site	Ground Albedo (%)	Standing Albedo (%)	Winter shade density	Summer shade density	Winter UV (SED)	Summer UV (SED)
546	4	0	3	3	9.0	37.0
547	6	0	5	6	6.4	19.2
548	6	0	6	5	5.8	25.5
549	6	0	7	3	3.8	32.3
550	10	1.75	6	7	1.6	1.8
551	10	0.75	7	7	3.3	11.2
552	4	0	3	2	9.3	45.7
553	4	0	2	1	11.6	50.3
554	4	0	3	5	10.6	31.2
555	4	0	4	5	8.8	28.5
556	4	0	5	4	8.5	37.4
557	4	0	6	0	8.2	52.4

527	4	0	4	1	8.4	48.3
528	4	2.25	3	1	8.9	43.6
529	4	0.5	6	4	5.5	31.1
530	7	0	2	2	9.9	43.5
531	7	0	5	4	7.7	33.2
532	7	2.25	4	2	8.7	39.9
533	7	0	4	1	8.8	48.5
534	7	0	3	2	8.6	43.1
535	7	3.25	5	4	6.6	29.9
536	10	0	7	6	1.2	9.5
537	7	1.75	7	4	3.6	27.6
538	7	0	4	5	7.6	25.2
539	10	0	6	7	6.0	16.1
540	10	0	7	4	2.0	20.3
541	4	0	7	4	4.6	24.7
542	4	0	2	0.92	11.5	52.5
543	10	1.5	2.84	3	7.8	32.8
544	7	0.5	7	0	7.1	52.8
545	7	0	0	2	13.5	46.9

558	4	0	6	0	7.9	54.1
559	4	1.5	1	3	11.5	40.4
560	10	0	3	0	11.7	55.3
561	4	0	0	0	13.1	54.4
562	4	0	1	0	13.1	54.8
563	4	0	1	1	13.0	53.1
564	4	0	2	0	11.3	53.4
565	7	0.5	7	5	4.1	23.8
566	7	0	6	5	6.8	29.7
567	6	0	5	2	7.2	43.8
568	10	1.5	6	2	4.8	39.5
569	4	1.75	5	4	3.7	19.9
570	4	0	4	0	10.6	55.5
571	4	0	0	0	13.7	56.2
572	10	1	0	5	9.7	22.5
573	4	0.5	7	0	7.1	52.5
574	7	0	0	1	13.2	51.4

Survey line 21 (106 m from western fence line)

Site	Ground Albedo (%)	Standing Albedo (%)	Winter shade density	Summer shade density	Winter UV (SED)	Summer UV (SED)
603	10	0	1	1	10.7	45.6
602	10	2.75	7	6	2.3	12.4
601	10	2.75	7	5	2.8	17.5
600	6	1.5	7	3	2.7	23.7
599	10	1.5	6	6	2.0	8.2
598	10	0.75	7	7	3.6	12.3
597	4	0	4	1	9.4	48.3
596	4	0	1	1	11.9	48.3
595	4	0	3	3	10.2	39.8
594	4	0	3	4	10.4	35.2
593	4	0	5	2	9.5	48.8
592	4	0	5	0	9.5	55.5
591	4	0	4	0	10.9	56.5
590	4	0	1	0	12.7	56.9
589	4	0	0	0	14.0	57.2
588	4	0	0	0	14.1	57.5
587	4	0	0	0	13.9	56.9
586	4	0	0	0	13.9	56.9
585	4	0	1	0	13.7	56.9
584	6	0.5	7	5	4.4	23.8
583	6	0	5	3	7.6	36.3
582	6	0	4.95	0	9.4	52.6
581	6	1.75	3	0	9.1	49.6
580	4	1.5	6	0	7.7	53.8
579	4	0	2	0	12.6	55.8
578	4	0	0.92	0	13.2	55.8
577	10	1.5	0	3	10.0	34.9
576	4	0.5	7	0	7.2	52.9
575	4	0	0	2	13.9	52.2

Survey line 22 (111 m from western fence line)

Site	Ground Albedo (%)	Standing Albedo (%)	Winter shade density	Summer shade density	Winter UV (SED)	Summer UV (SED)
604	10	1.5	1	1	9.1	39.1
605	10	0.75	7	7	0.5	1.8
606	4	1.75	7	7	2.5	8.2
607	10	1.5	7	7	0.3	1.1
608	10	0.75	7	6	3.3	14.5
609	4	0	3	2	9.6	42.5
610	4	0	1	2	12.4	44.2
611	4	0	2	2	10.7	39.9
612	4	0	3	4	8.8	31.9
613	4	0	5	1	9.4	53.8
614	4	0	3	0	11.2	56.5
615	4	0	3	0	11.5	57.5
616	4	0	0	0	14.2	57.9
617	4	0	0	0	14.4	58.6
618	4	0	0	0	14.4	58.6
619	4	0	0	0	14.3	58.2
620	4	0	0	0	14.3	58.2
621	4	0	0	0	14.3	58.2
622	4	0	0	0	14.0	57.2
623	4	2	1	1	13.1	53.6
624	4	2	2	1	12.2	52.6
625	4	2	2	2	12.2	49.3
626	4	0	1	2	12.4	47.8
627	4	0	4	3.8	6.5	27.9
628	4	0	3.85	2.85	5.5	28.5
629	4	0	4.85	3.8	5.2	26.9
630	4	0.25	3.8	3.85	5.0	25.5
631	4	0.25	4.8	3.85	4.8	25.5
632	4	0.25	4.85	3.85	4.7	25.2
633	4	0.25	4.8	3.85	4.7	25.2
634	4	0.25	4.8	3.85	5.1	26.5
635	4	0	4.85	3.8	5.6	28.3
636	4	0	3.8	3.8	6.3	30.0
637	4	0	4.8	0	9.2	54.1
638	4	0	0	3	11.2	38.7
639	4	2	5	4	5.6	28.2
640	4	2	5	4	6.7	32.0
641	4	0	4	0	10.9	56.5
642	4	0	0	1	14.2	56.5

Survey line 23 (116 m from western fence line)

Site	Ground Albedo (%)	Standing Albedo (%)	Winter shade density	Summer shade density	Winter UV (SED)	Summer UV (SED)
662	10	1.5	0	1	10.4	42.3
661	10	1.5	7	7	0.7	2.5

Survey line 24 (121 m from western fence line)

Site	Ground Albedo (%)	Standing Albedo (%)	Winter shade density	Summer shade density	Winter UV (SED)	Summer UV (SED)
663	10	1.5	0	1	10.4	42.3
664	10	0.75	7	7	3.4	11.6

660	6	0	3	1	9.9	51.2	665	6	0	5	0	9.5	54.6
659	4	0	2	0	11.8	52.4	666	4	0	0	0	13.6	55.8
658	4	0	2	0	11.6	51.7	667	4	0	1	0	13.4	55.8
657	10	0	3	5	8.9	23.7	668	4	0	0	3	13.0	44.9
656	4	0	5	1	8.9	52.4							
655	4	0	0	0	14.0	57.2							
654	4	0	0	0	14.4	58.6							
653	4	0	0	0	14.1	57.5							
652	4	0	0	0	13.9	56.9							
651	4	0	0	0	13.9	56.9							
650	4	0	0	0	14.1	57.5							
649	4	0	0	0	14.1	57.5							
648	4	0	0	0	14.0	57.2							
647	4	0	0	0	14.1	57.5							
646	4	0	1	0	13.9	57.5							
645	4	0	1	0	14.0	57.9							
643	4	0	0	0	14.7	59.6							

Survey line 25 (126 m from western fence line)

Site	Ground Albedo (%)	Standing Albedo (%)	Winter shade density	Summer shade density	Winter UV (SED)	Summer UV (SED)
674	10	1.75	0	1	10.5	42.7
673	10	0.75	7	7	3.5	11.9
672	4	0	6	0	9.0	54.8
671	4	0	0	0	14.0	57.2
670	4	0	0	0	14.1	57.5
669	4	0	0	2	14.1	52.9

Survey line 26 (131 m from western fence line)

Site	Ground Albedo (%)	Standing Albedo (%)	Winter shade density	Summer shade density	Winter UV (SED)	Summer UV (SED)
675	10	1.75	0	1	10.5	42.7
676	10	0.75	7	7	3.2	10.9
677	4	0.5	5	1	8.2	50.9
678	4	0	0	0	14.2	57.9
679	4	0	0	0	14.3	58.2
680	4	0	0	0	14.3	58.2

Survey line 27 (136 m from western fence line)

Site	Ground Albedo (%)	Standing Albedo (%)	Winter shade density	Summer shade density	Winter UV (SED)	Summer UV (SED)
681	10	1.5	0	3	9.6	33.5
682	10	2.5	7	7	3.2	10.9
683	4	0	7	0	7.6	54.1
684	4	0	0	0	14.3	58.2
685	4	0	0	0	14.5	58.9
686	4	0	0	0	14.5	58.9
687	4	0	1	0	14.7	60.3
688	4	0	0	0	15.0	60.6
689	4	0	0	0	15.1	61.0
690	4	0	0	0	15.1	61.0
691	4	0	0	0	15.1	61.0
692	4	0	0	0	15.1	61.0
693	4	0	0	0	15.0	60.6
694	4	0	0	0	14.6	59.3
695	4	0	0	1	13.7	53.1

Survey line 28 (141 m from western fence line)

Site	Ground Albedo (%)	Standing Albedo (%)	Winter shade density	Summer shade density	Winter UV (SED)	Summer UV (SED)
696	10	1.5	0	3	11.7	40.5
697	10	2	5.79	5.79	3.9	14.9
698	10	2	5.86	5.79	4.6	17.7
699	4	0	3	0	11.4	54.1
700	4	1	5	0	10.3	55.8
701	4	0	0	0	14.5	58.9
702	4	0	0	0	14.7	59.6
703	4	0	0	0	14.7	59.6

Survey line 29 (146 m from western fence line)

Site	Ground Albedo (%)	Standing Albedo (%)	Winter shade density	Summer shade density	Winter UV (SED)	Summer UV (SED)
704	4	0	0	1	13.7	53.1
705	10	0	2.79	2.79	9.3	38.4
706	10	0	3.79	2.79	9.4	42.2
707	4	0	1	0	13.6	56.5
708	4	0	2	0	13.8	58.9
709	4	0	0	0	14.6	59.3
710	4	0	0	0	14.8	59.9
711	4	0	0	0	14.8	59.9

Survey line 30 (151 m from western fence line)

Site	Ground Albedo (%)	Standing Albedo (%)	Winter shade density	Summer shade density	Winter UV (SED)	Summer UV (SED)
712	7	0	0	0	14.7	59.9
713	7	0	0	0	14.5	59.2
714	7	0	1.93	0	14.1	59.6
715	7	0	1	0	14.7	60.3
176	4	0	0	0	14.9	60.3
717	4	0	0	0	14.8	59.9
718	4	0	0	0	14.9	60.3
719	4	0	0	0	14.9	60.3

Survey line 31 (156 m from western fence line)

Site	Ground Albedo (%)	Standing Albedo (%)	Winter shade density	Summer shade density	Winter UV (SED)	Summer UV (SED)
720	7	0	0	0	15.2	61.3
721	7	0	0	0	15.2	61.3
722	7	0	0	0	15.1	61.0
723	7	0	0	0	15.2	61.3

Survey line 32 (176 m from western fence line)

Site	Ground Albedo (%)	Standing Albedo (%)	Winter shade density	Summer shade density	Winter UV (SED)	Summer UV (SED)
737	7	0	0	0	15.0	60.6
738	7	0	0	0	15.2	61.3
739	4	0	0	0	14.9	60.3
740	4	0	0	0	14.8	59.9

724	4	0	0	0	15.1	61.0
725	4	0	0	0	15.0	60.6
726	4	0	0	0	15.1	61.0
727	4	0	0	0	15.0	60.6
728	4	0	0	0	15.1	61.0
729	4	0	0	0	15.1	61.0
730	4	0	0	0	15.1	61.0
731	4	0	0	0	15.2	61.3
732	4	0	0	0	15.1	61.0
733	4	0	0	0	15.1	61.0
734	4	0	0	0	15.0	60.6
735	4	0	0	0	14.7	59.6
736	4	1.75	0	4	12.0	37.1

741	4	0	0	0	14.7	59.6
742	4	0	0	0	14.8	59.9
743	4	0	0	0	14.8	59.9
744	4	0	0	0	14.8	59.9
745	4	0	0	0	14.7	59.6
746	4	0	0	0	15.1	61.0
747	4	0	0	0	14.8	59.9
748	4	0	0	0	14.5	58.9

Survey line 33 (196 m from western fence line)

Site	Ground Albedo (%)	Standing Albedo (%)	Winter shade density	Summer shade density	Winter UV (SED)	Summer UV (SED)
749	4	0	0	0	15.4	62.0
750	4	0	0	0	15.3	61.7
751	4	0	0	0	14.9	60.3
752	4	2.25	4	4	6.1	22.9
752x	4	0	3	2	10.1	44.2
753	4	0	3	2	9.8	43.2
754	4	0	2	2	11.6	45.2
755	4	0	2	0	12.6	57.9
756	4	0	2	3	12.2	42.0
757	4	0	3	3	11.4	43.4
758	4	0	0	0	14.5	58.9
759	4	0	1	0	14.2	59.3

Survey line 34 (216 m from western fence line)

Site	Ground Albedo (%)	Standing Albedo (%)	Winter shade density	Summer shade density	Winter UV (SED)	Summer UV (SED)
771	7	0	0	0	15.2	61.3
770	7	0	0	0	15.3	61.7
769	4	0	0	0	15.1	61.0
768	4	0	0	0	14.6	59.3
767	4	0	1	0	14.1	58.2
766	4	0	0	0	14.1	57.5
765	4	0	0	1	14.2	56.5
764	4	0	1	0	14.4	59.3
763	4	0	0	2	14.2	53.2
762	4	0	3	1	12.7	57.2
761	4	0	0	0	14.6	59.3
760	4	0	0	0	14.7	59.6

Survey line 35 (236 m from western fence line)

Site	Ground Albedo (%)	Standing Albedo (%)	Winter shade density	Summer shade density	Winter UV (SED)	Summer UV (SED)
772	7	0	0	0	15.3	61.7
773	7	0	0	0	15.4	62.0
774	4	0	0	0	15.3	61.7
775	4	0	0	0	15.3	61.7
776	4	0	0	0	15.2	61.3
777	4	0	0	0	15.1	61.0
778	4	0	0	0	15.1	61.0
779	4	0	0	0	15.1	61.0
780	4	0	0	0	15.2	61.3
781	4	0	0	0	15.2	61.3
782	4	0	0	0	15.2	61.3
783	4	0	0	0	15.1	61.0

Survey line 36 (256 m from western fence line)

Site	Ground Albedo (%)	Standing Albedo (%)	Winter shade density	Summer shade density	Winter UV (SED)	Summer UV (SED)
795	7	0	0	0	15.3	61.7
794	7	0	0	0	15.4	62.0
793	4	0	0	0	15.4	62.0
792	4	0	0	0	15.3	61.7
791	4	0	0	0	15.3	61.7
790	4	0	0	0	15.3	61.7
789	4	0	0	0	15.3	61.7
788	4	0	0	0	15.3	61.7
787	4	0	0	0	15.3	61.7
786	4	0	0	0	15.3	61.7
785	4	0	0	0	15.3	61.7
784	4	0	0	0	15.3	61.7

Survey line 37 (276 m from western fence line)

Site	Ground Albedo (%)	Standing Albedo (%)	Winter shade density	Summer shade density	Winter UV (SED)	Summer UV (SED)
796	4	0	0	0	15.2	61.3
797	4	0	0	0	15.3	61.7
798	4	0	0	0	15.3	61.7
799	4	0	0	0	15.4	62.0
800	4	0	0	0	15.3	61.7
801	4	0	0	0	15.2	61.3
802	4	0	0	0	15.2	61.3
803	4	0	1	0	14.7	61.0
804	4	0	0	0	15.0	60.6
805	4	0	0	0	15.0	60.6
806	4	0	0	0	15.1	61.0
807	4	0	0	0	15.2	61.3

Survey line 38 (296 m from western fence line)

Site	Ground Albedo (%)	Standing Albedo (%)	Winter shade density	Summer shade density	Winter UV (SED)	Summer UV (SED)
819	4	0	2	0	14.0	59.6
818	4	0	0	0	15.2	61.3
817	4	0	0	0	15.2	61.3
816	4	0	0	0	15.3	61.7
815	4	0	0	0	15.1	61.0
814	4	0	3	1	9.2	46.9
813	4	0	0	2	14.3	49.4
812	4	0	2	0	11.8	57.5
811	4	3	1	2	10.2	37.3
810	4	0.5	3	4	8.9	29.5
809	4	0	3	1	11.3	51.4
808	4	0	0	0	15.0	60.6

Appendix P. Additional facial UV exposures measured in the student population

Table P.1: Facial site exposure (SED) measured to students wearing (protected) and not wearing (unprotected) broad brimmed hats in region 24 (basketball courts) and region 22 (school oval) (Downs & Parisi 2008). The error given in the Table, t, is the 95% C.I.

Trial 1 - 29.03.2007, SZA 29-35°, 253 DU, Clear, Basketball

	Protected		$\bar{x}$	$\pm$ t	ER %	Unprotected								$\bar{x}$	$\pm$ t	ER %
Vertex						9.0	6.5							**7.8**	**11.2**	**85**
Forehead						4.4								**4.4**		**47**
Cheek	1.1		**1.1**		**13**	2.4	2.9							**2.7**	**2.2**	**30**
Chin						1.9								**1.9**		**22**
Side	1.0	0.7	**0.9**	**1.3**	**10**	1.0								**1.0**		**11**

Trial 2 - 30.03.2007, SZA 30-36°, 257 DU, Clear, Basketball

	Protected		$\bar{x}$	$\pm$ t	ER %	Unprotected								$\bar{x}$	$\pm$ t	ER %
Vertex						7.8								**7.8**		**100**
Cheek						2.4								**2.4**		**31**
Side						2.6								**2.6**		**34**

Trial 3 - 10.11.2006, SZA 9-17°, 300 DU, 6-7/8 Cumulonimbus, Basketball

	Protected		$\bar{x}$	$\pm$ t	ER %	Unprotected								$\bar{x}$	$\pm$ t	ER %
Vertex						7.1								**7.1**		**100**
Forehead						1.5	4.8	1.9						**2.7**	**3.7**	**40**
Cheek						1.5	1.6							**1.6**	**0.4**	**24**
Side	1.5		**1.5**		**23**	1.9								**1.9**		**28**

Trail 4 - 15.08.2006, SZA 40-45°, 269 DU, Clear, Soccer

	Protected		$\bar{x}$	$\pm$ t	ER %	Unprotected								$\bar{x}$	$\pm$ t	ER %
Vertex						5.6	4.3							**5.0**	**5.8**	**89**
Forehead						2.4	1.2							**1.8**	**5.4**	**34**
Nose	1.9		**1.9**		**35**											
Cheek	1.0	0.9	**1.0**	**0.4**	**19**	2.2	0.7	0.5	1.4	1.3	1.7	1.0	1.2	**1.2**	**0.4**	**23**
Side						1.3	1.3	0.7	0.7	0.7				**0.8**	**0.3**	**17**

Trail 5 - 23.02.2007, SZA 17-27°, 255 DU, 5-7/8 Cumulus, Soccer

	Protected		$\bar{x}$	$\pm$ t	ER %	Unprotected								$\bar{x}$	$\pm$ t	ER %
Vertex						3.1	4.3	4.6						**4.0**	**1.6**	**87**
Forehead						3.2	1.3							**2.3**	**8.5**	**51**
Nose	1.3		**1.3**		**29**	1.0	1.3							**1.1**	**1.3**	**26**
Cheek						0.6								**0.6**		**12**
Chin	0.5		**0.5**		**8**	1.1	1.3							**1.2**	**0.9**	**28**

Trial 6 - 29.03.2007, SZA 43-55°, 253 DU, Clear, Soccer

	Protected		$\bar{x}$	$\pm$ t	ER %	Unprotected								$\bar{x}$	$\pm$ t	ER %
Vertex						4.6	4.3	4.6						**4.5**	**0.4**	**98**
Nose	1.4		**1.4**		**32**											
Cheek	1.0		**1.0**		**22**	1.4	1.9	1.7	1.8					**1.7**	**0.4**	**39**
Chin	1.1		**1.1**		**26**											
Side						1.6	0.8							**1.2**	**3.6**	**28**

Trial 7 - 22.06.2006, SZA 50-53°, 264 DU, 7-8/8 Cumulonimbus, Soccer

	Protected		$\bar{x}$	$\pm$ t	ER %	Unprotected								$\bar{x}$	$\pm$ t	ER %
Vertex						1.9	2.1	1.4	2.1	2.5				**2.0**	**0.4**	**92**
Forehead	0.7		**0.7**		**33**											
Nose						1.7								**1.7**		**81**

Cheek	0.5	0.6	**0.6**	**0.4**	**22**	0.7	1.0	0.7			**0.8**	**0.4**	**37**
Chin						0.6	0.9				**0.8**	**1.3**	**35**
Side						0.6	0.7				**0.7**	**0.4**	**30**

Trial 8 - 19.06.2006, SZA 49-52^{o}, 262 DU, 6-8/8 Cumulonimbus, Basketball

	Protected		$\bar{x}$	$\pm$ **t**	ER %	Unprotected					$\bar{x}$	$\pm$ **t**	ER %
Vertex						1.8	1.8	1.6	2.0	2.2	**1.9**	**0.2**	**85**
Forehead	0.7	0.7	**0.7**	**0**	**30**	1.0	1.8	0.8	1.1	0.9	**1.1**	**0.4**	**51**
Nose	1.0		**1.0**		**44**	1.2	1.0				**1.1**	**0.9**	**51**
Chin	1.2		**1.2**		**54**	0.9	0.6				**0.8**	**1.3**	**32**

Trial 9 - 10.11.2006, SZA 35-49^{o}, 300 DU, 2-3/8 Cumulonimbus, Soccer

	Protected		$\bar{x}$	$\pm$ **t**	ER %	Unprotected					$\bar{x}$	$\pm$ **t**	ER %
Vertex						0.8	1.1				**0.9**	**1.3**	**65**
Forehead						0.7					**0.7**		**44**
Cheek	1.0		**1.0**		**72**	1.0	1.2	0.7	1.4	0.8	**1.0**	**0.3**	**73**
Chin						1.0					**1.0**		**69**

Appendix Q. Comparison of facial site incidence of BCC and SK to ER

Table Q.1: Measurements of facial exposure ratio and the density of facial basal cell carcinoma (BCC) and solar keratosis (SK).

Facial site			Facial site ER				Observed Incidence	
Diffey et al. 1979 facial sites	Study facial sites	Site description	Measured 0^o-30^o (%)	Measured 30^o-50^o (%)	Measured 50^o-80^o (%)	Diffey et al. 1979 (%)	BCC tumor density (Brodkin et al. 1969) (tumors/cm^2)	SK facial incidence (Nguyen et al. 1998)
7	cn1 / cx11	forehead		66		58	0.96	5
34	cn1 / cx14	lower forehead			92	34	2.9	
37	cn2 / cx16	between eyebrows	32		58	26	0.96	
32	cn1 / cx18	nose top bridge			41	24	0.2	
28	cn3 /cx22	upper nose lateral	42		30	42	8.13	
25	cn2/cx23	nose lateral surface	40			51	8.13	4
35	cn1 /cx21	nose apical ridge		82		66	10.36	24
33	cn1 /cx25	nose tip	27	56		64	8.52	6
22	cn4 / cx26	nose nostril	40			54	3.34	
23	cn3 / cx 25	above nostril	47	36	46	62	3.34	
36	cn4 /cx24	nose alar		53		59	0.96	
21	cn5/cx29	perialar				10	12.57	0
34	cn5/ cx24	maxillary	54			34	2.9	38
15	cn6 /cx31	nasolabial fold		39		31	0.83	0
20	cn1/cx29	philtrum		31		2	2.9	
	cn1/cx32	upper lip			39			0
24	cn5 / cx 33	outer upper lip				61	8.13	
19	cn1/cx36	lower lip			22	1	0.36	23
18	cn4 / cx36	outer lower lip				1	0.36	
17	cn1 /cx41	chin		34		34	0.62	
16	cn6 / cx41	chin side		41	43	28	0.62	
6	cn12 / cx14	above outer eybrow	29	47		41	0.96	
8	cn7 / cx15	above inner eyebrow	42		82	56	0.96	
31	cn3 / cx 19	below inner eyebrow				2	0.2	
30	cn3 / cx20	inner eye socket	11			14	0.55	
10	cn12 /cx18	outer eyesocket				39	1.48	
11	cn12 / cx24	lower eye socket		52	83	14	1.48	
39	cn12 / cx26	below eye socket				29	1.48	
29	cn 8 / cx20	eye		16		46		
17	cn10 / cx24	outer infraperiorbital	40	58		34	0.62	
26	cn5 /cx23	inner infraorbital				19	1.48	
27	cn8/cx23	infraorbital	35	37		8	8.14	10
40	cn7/cx25	cheek			79	48	1.48	175
14	cn6 / cx26	inner cheek				50	1.48	
13	cn11 / cx26	outer cheek				38	1.48	
9	cn11/ cx 29	lower cheek	17			49	0.96	
41	cn14 / cx33	upper mandibular	6	6	8	23	0.59	9
3	cn 13 / cx33	mid mandibular	13		24	27	0.59	
4	cn11 / cx40	submandibular	7		18	9	0.03	2
5	cn 9 / cx 37	inner mandibular	16			19	0.59	
	cn18 / cx25	ear			47			67
3	cn15/cx25	preauricular		17		27	0.59	
2	cn13 /cx 31	face side		20	28	33	2.79	7

Appendix R. Comparison of mannequin to human facial site measurements of ER

Mannequin facial site data was compared to student facial site data of ER collected in the HBSHS student population. Table R.1 summarises the mean ER of human and mannequin facial site data collected and presented by Downs & Parisi (2008). The mean variation between mannequin and human facial site ER is 6% and is greatest at the nose and cheek sites. The vertical upright position of the mannequin headform compared to the tilted position of the human face measured while playing sport is a likely explanation for the greater difference between nose and cheek site ER.

Table R.1. A comparison of mannequin and human ER (%) measured in the HBSHS population (Downs & Parisi 2008).

	Human ER (%)	Mannequin ER (%)
Vertex	88	91
Forehead	45	47
Nose	47	61
Cheek	37	51
Chin	35	34
Side of face	23	27

Appendix S. Publications resulting from this research

Refereed Journal Papers

Downs, N. & Parisi, A. 2009, "Measurements of the anatomical distribution of erythemal ultraviolet: a study comparing exposure distribution to the site incidence of solar keratoses, basal cell carcinoma and squamous cell carcinoma", *Photochemical and Photobiological Sciences*, DOI:10.1039/b901741k.

Downs, N.J. & Parisi, A.V. 2009, "Ultraviolet exposures in different playground settings: a cohort study of measurements made in a school population", *Photodermatology, Photoimmunology and Photomedicine*, vol. 25, pp. 196-201.

Downs, N., Parisi, A., Turner, J. & Turnbull, D. 2008, "Modelling ultraviolet exposures in a school environment", *Photochemical and Photobiological Sciences*, vol. 7, no. 6, pp. 700-710.

Downs, N. & Parisi, A. 2008, "Patterns in the received facial ultraviolet exposure of school children measured at a sub-tropical latitude", *Photochemistry and Photobiology*, vol. 84, no. 1, pp. 90-100.

Downs, N. & Parisi, A. 2007, "Three dimensional visualisation of human facial exposure to solar ultraviolet", *Photochemical and Photobiological Sciences*, vol.6, pp. 90-98.

Conference Presentations / Proceedings

Downs, N.J. & Parisi, A.V. 2008, "Modelling the erythemally effective UV to students in a school environment", Proceedings of the Australian Institute of Physics 18th National Congress, 30 November - 5 December, 2008, Adelaide.

Downs, N.J. & Parisi, A.V. 2008, "Modelling personal UV exposure in a school playground", The Australian Health and Medical Research Congress, 16-21 November, 2008, Brisbane.

Downs, N.J. & Parisi, A.V. 2007, "Contoured exposure assessment of biologically effective solar ultraviolet radiation", 32nd annual Australasian Radiation Protection Society conference, 21-24 October, 2007, Brisbane.

Downs, N.J. & Parisi, A.V. 2007, "Patterns in surface distribution of human exposure to solar ultraviolet", Physikalisch-Meteorologisches Observatorium Davos World Radiation Center: A conference celebrating one century of UV radiation research, 18-20 September 2007, Davos, Switzerland, pp.155-156.

Downs, N.J. & Parisi, A.V. 2006, "Comparing variations in the UV facial exposure received by school children in south-east Queensland", 17th National Congress of the Australian Institute of Physics, 3-8 December 2006, Brisbane.

Downs, N.J. & Parisi, A.V. 2006, "Mapping of the solar ultraviolet exposures to the human face", 31st annual Australasian Radiation Protection Society conference, 26-29 November, 2006, Sydney.